ACTA CHIMICA

ACADEMIAE SCIENTIARUM HUNGARICAE

TOMUS 100 FASCICULI 1–4

AKADÉMIAI KIADÓ, BUDAPEST

1979

ACTA CHIM. ACAD. SCI. HUNG. ACASA2 100 (1–4) 1–498 (1979)

ACTA CHIMICA

A MAGYAR TUDOMÁNYOS AKADÉMIA KÉMIAI TUDOMÁNYOK OSZTÁLYÁNAK IDEGEN NYELVŰ KÖZLEMÉNYEI

Acta Chimica is a journal for the publication of papers on all aspects of chemistry in English, German, French and Russian.

Acta Chimica is published in 4 volumes per year. Each volume consists of 4 issues of varying size.

Manuscripts should be sent to

Acta Chimica
Budapest, P.O. Box 67, H-1450, Hungary

Correspondence with the editors should be sent to the same address. Manuscripts are not returned to the authors.

Subscription: $36.00 per volume.

Hungarian subscribers should order from Akadémiai Kiadó, 1363 Budapest, P.O. Box 24. Account No. 215 11488.

Orders from other countries are to be sent to "Kultura" Foreign Trading Company (H-1389 Budapest 62, P.O. Box 149. Account No. 218 10990) or its representatives abroad.

ACTA CHIMICA

ACADEMIAE SCIENTIARUM HUNGARICAE

TOMUS 100

AKADÉMIAI KIADÓ, BUDAPEST

1979

ACTA CHIMICA

TOMUS 100

Fasciculi 1—4

INDEX

INDEX

ORGANIC CHEMISTRY

CHEMICAL TECHNOLOGY

Acta Chimica Academiae Scientiarum Hungaricae, Tomus 100 (1—4), pp. 5—13 (1979)

PREFACE TO VOLUME 100

THE HISTORY OF CHEMICAL PUBLICATIONS IN HUNGARY

B. LENGYEL and F. SZABADVÁRY

The present festive tome is the hundredth volume of "Acta Chimica", a number unattained so far by any of the chemical journals published in Hungary. This jubilee offers a good incentive to outline the history of chemical publications in Hungary. In doing so, it seems indispensable, however, to survey briefly the international status and development in this field.

The year 1665 was of great importance in the history of sciences. This was actually the year in which the first periodicals of natural sciences, "Philosophical Transactions" of the Royal Society, London, and "Journal des Savants" of the Academie des Sciences, Paris, were founded. Scientific communication and information were extremely accelerated by these journals. From this time onward there was no need to write a complete book for making known accomplishments; partial results could be quickly, published in the form of papers. Knowledge made rapidly public in this way stimulated other researchers, and this led to new results and new publications. Indeed, this trend has continued up to our days; research is done to gain new knowledge, and the results obtained are published in periodicals to make them known to others. This is the way how science has developed during the last three hundred years. Apparently, this kind of development seems to have come rather to a deadlock nowadays. Ever so many people do research work and publish. It seems sometimes that publication has become lately the main goal of research, as the number of publications of a scientific worker or scientific institution has everywhere mystic importance because of scientific-bureaucratic reasons. This places the researcher in the center of an insurmountable torrent of publications, impossible to follow. Evidently, a new method of scientific communication would be needed — yet it has not been found. Therefore, periodicals have still remained the most important sources of scientific information.

The route from the two journals mentioned, up to the countless, strictly specialized periodicals of our days was long. "Philosophical Transactions" and "Journal des Savants" were open for all sciences. The same applied to the periodicals appearing in the next century. From the middle of the eighteenth century, several attempts were made to found specialized scientific journals.

The first attempts brought mostly shortlived results; examples are, in the field of chemistry, "Chymische Experimente einer Gesellschaft im Erzgebirge" (Berlin, 1753—1759), "Kurelle Chemische Versuche und Erfahrungen" (Berlin, 1756), "Chymische Nebenstunden (Saint Petersburg, 1762—1768) [1].

The first successful journal dedicated to chemistry was the "Chemisches Journal" of Lorenz CRELL, started in 1778, to which, after several changes of title, the name "Chemische Annalen" was given in 1784. It is usually cited as Crells Annalen. This journal was followed in 1789 by "Annales de Chimie" of LAVOISIER and his friends. with the aim to give the contents of Crells Annalen in French, but later they changed over to the publishing of original papers. This journal appeared at regular intervals and also exists today. In the next century numerous chemical journals were then founded. All the countries existing at that time had at least one chemical journal, the larger countries even more. They covered the total field of chemistry. For a long time the German language territory predominated. Journals featuring in their title the word chemistry (not always alone, but sometimes linked with other disciplines, such as physics, pharmacy, mineralogy, *etc.*) were registered before 1841. Of the 74 journals, 38 were published in German, 8 each appeared in Great Britain, France and Italy, 5 in the Netherlands, 3 in Belgium, 2 in America, and 1 each in Sweden and Russia [2].

A further spezialization within the field of chemistry began in the last third of the past century. The "Zeitschrift für analytische Chemie" of Regigius FRESENIUS (1862) seems to be the first journal dedicated to a narrower branch of chemistry.

In Hungary, the first branch of natural science in which not only educational work but independent research was also reported, was chemistry.

Since 1526 the King of Hungary was at the same time the Hapsburg Emperor, so that the Kingdom of Hungary was closely linked with the Hapsburg hereditary provinces. From the middle of the sixteenth century till the end of the seventeenth century, the major part of Hungary, together with its present capital Budapest, belonged to the Turkish Empire, the western part constituted the Kingdom, while in the East the independent Grand Duchy of Transylvania was established. In the eighteenth century, after the driving out of the Turks, a great economical and cultural development ensued. Several schools were founded, among them the renowned Mining College in Selmecbánya (1763), the Institutum Polytechnicum-Hydrotechnicum (1782) in Buda, and the sole university of Hungary was transferred from Nagyszombat (Trnava) to Buda and complemented with a Medical Faculty (1769—1777). The first chemical department of the country was established at the Mining College of Selmecbánya in 1763, the second at the Medical Faculty of the University in 1769. Both Institutes were engaged, besides the teaching of chemistry, also in research work,and results of international importance were

attained [3]. The papers were published in foreign countries, mainly in "Crells Annalen", in the "Physikalischen Arbeiten" of Ignaz BORN in Vienna, and in SCHERER—GEHLEN's "Allgemeines Journal der Chemie".

There did not exist yet a scientific journal in Hungary, nor even a scientific language. Though Hungarian literary texts from the Middle Ages are known, and as early as the eighteenth and nineteenth centuries considerable literature unfolded, the national language played but a subordinate role. Up to the nineteenth century Latin was the official language of the Diet, of the counties and of jurisdiction. Similarly, lectures were held in Latin at the University, while at the Mining Academy the language of teaching was German.

The end of the eighteenth century gave birth to the so called "Reform-Period" in Hungary, the primary aim of which was to reinstate the Hungarian language into its own rights everywhere. Not incidentally, this movement also had the intention to counteract the attempts of forced Germanization by Joseph the Second. In the literature this period is manifested by the movement called language reforming. Artificial words were constructed to enrich the language. This movement was rapidly extended to the domain of sciences, where neologism was even more needed than elsewhere. Since natural science in Hungarian did not exist at all up to that time, words to express scientific concepts were also missing. The first authors who tried to write a book in Hungarian in the various branches of science were confronted with these problems. The first book in Hungarian on a chemical subject was published in 1800 Kolozsvár (Cluj) in Transylvania. The author was Ferenc NYULAS, and the book dealt with the analysis of Transylvanian medicinal waters [4]. Among others the following may be read in the preface: "Wherever we turn in the Hungarian description of a science, we meet with difficulties as if advancing through a jungle. One must break one's own way through it. Indeed, I had more trouble in this work with the expression of technical terms, than with the decomposition of the waters. Nobody has analyzed water in Hungarian, even the word chemistry is new in our language, so that I had to invent several expressions myself ...". In an Appendix NYULAS gave a Hungarian-Latin dictionary of about 250 Hungarian words coined by him, many of which have been permanently introduced in the professional language. These concern mainly the names of laboratory equipment, operations and processes, but not the names of elements and compounds, for which he retained the international names. In the next years this way was followed up. Other authors too created new words, some of which remained in use, while others became obsolate. Greek and particularly Latin words can be ranged rather easily and harmoniously with Hungarian words.

However, if reforming begins somewhere, it mostly does not stop where it would be advisable. In the twenties of the last century, studious scientists

were of the opinion that the nomenclature of chemical elements and compounds also ought to have been Hungarized. They took up diligently this work, suiting well general nationalistic mentality. Much inventiveness was put to play to find nice names for the elements, indicative also of their properties. After various propositions, finally a unified system of "Hungarian" elements was worked out, on the basis of which the names of the compounds were also formed. This nomenclature was then used in books and in the early publications in Hungarian journals. These publications are incomprehensible for the Hungarian chemist of today, because this language, fortunately, disappeared. Why did it disappear? Presumably because Hungary lost its war of independence of 1848—49. During the following 15 years of oppression lectures were held in German at the higher schools; German textbooks were used, and the mannered nomenclature was forgotten. When the winds of the approaching compromise with Austria began to blow, and Hungarian was introduced again as a lecturing language, the young professors appointed to the chairs of natural sciences had a background of education in German. The Hungarian nomenclature was unknown to them, they were accustomed to the international names, so they used these in their Hungarian lectures and publications. Some attempts were made by old gentlemen at reviving the Hungarian nomenclature, but they were of no avail.

The first newspaper was published in 1705 in Hungary in Latin. It was called "Mercurius hungaricus" and appeared quite irregularly; it existed for five years. "Nova Posoniensia" published in Pozsony (Bratislava) from 1721 on, similarly in Latin, appeared more regularly and lasted longer. "Wochentlich zweymal neu ankommender Mercurius" (in short "Ofnerischer Mercurius") was published from 1730 on in Buda in German. The first newspaper in Hungarian was "Magyar Hírmondó" (Hungarian Herald) published in Pozsony. It appeared first in 1780 and existed for 9 years. "Mindenes Gyűjtemény" (General Collection) was a scientific-cultural weekly in Hungarian, published from 1789 to 1792. The journals "Erdélyi Múzeum" (Transylvanian Museum) (1814—1818) and "Tudományos Gyüjtemény" (Scientific Collection) (Pest, 1817—1841) were founded already with a definite scientific aim, and published original papers. The latter was published by a bookseller and it soon became the leading journal. It covered the whole spectrum of sciences. Natural sciences were rarely represented on its pages; even more seldom were treatises on chemical subject. [5]

Simultaneously with the appearance of the first Hungarian scientific journals, the Hungarian scientist was confronted with a still existing problem: if one publishes in a small national language, it is not to be expected that the results published will become known to the international scientific world. If one wishes to surmount the language barrier one must write in a world-wide language. This is a great disadvantage of small countries!

To make acquainted the results of Hungarian authors also in foreign countries, Lajos SCHEDIUS founded first the "Litterarischen Anzeiger für Ungarn" (1797—1799), then the "Zeitschrift von und für Ungarn" (1801—1804). The latter published time and again also mineralogical-analytical communications. Owing to financial reasons, both journals were rather short-lived. In the first half of the last century, not only these journals in foreign language, but also Hungarian journals failed because of this same reason. They were called into existence by optimistic private initiatives and failed because of want of money. Hungary did not have yet appropriate scientific organisations or institutions to bear the burdens.

It was not till 1825 that the Hungarican Academy of Science was founded. In contrast to the large European academies, the Hungarian Academy was not created by royal favour, but by public collection. Though this is an origin to be proud of, it had the disadvantage that the financial situation of the new institution was insecure for a rather long period of time. Nevertheless, as soon as from 1833 on, the Academy was able to publish twice a year "Tudománytár" (Scientific Archives), which mainly reported, in Hungarian, scientific events from foreign sources. The first journal of the Hungarian Academy of Sciences, dedicated exclusively to natural sciences was "Mathematikai és Természettudományi Közlemények" (Communications of Mathematics and Natural Sciences). Its publication began rather irregularly in 1861. In 1882 the name of the journal was changed to "Mathematikai és Természettudományi Értesítő" (Bulletin of Mathematics and Natural Sciences) and was edited and published at regular periods by the Third Class (of Mathematical and Natural Sciences) of the Hungarian Academy of Sciences. The publishing of "Mathematische und naturwissenschaftliche Berichte aus Ungarn" started at the same time. In this journal, works of Hungarian scientists were published in German, seldom also in French. Though publications were not taken over automatically from one journal to the other, these journals mostly contain the same works, the one in Hungarian, the other in foreign language. From this time on, bilingual publication became general practice with Hungarian natural scientists up to our days. Up to 1942 for the mentioned Hungarian periodical and up to 1933 for the German the Academy of Sciences was able to provide for the publication of these parallel journals. The chemist members of the Academy frequently published in these organs, almost all their work in Hungarian, while the version in foreign language was often sent to a German and sometimes to a French journal (Berichte, Bulletin, Zeitschrift für anorganische Chemie, Zeitschrift für analytische Chemie, *etc.*). In the edition of "Berichte aus Ungarn" financial support was given to the Academy by the fairly rich Royal Hungarian Society of Natural Sciences, founded in 1841. Obviously, this Society rested on a broader basis of natural scientists, in view of the fact that here members had only to join, while in the Academy they were elected. Events

organized by the Society played an important role in the scientific life of the country. Publication of their monthly "Természettudományi Közlöny" (Journal of Natural Sciences) started in 1860, with the aim to propagate and popularize natural sciences, and achieved a decisively high level. [By the way, this journal appears also today under the changed title "Természet Világa" (World of Nature)].

At the end of the last century, the need for a scientific journal dedicated exclusively to chemistry was felt. The first journal including the word chemistry in its title was "Vegyészet és Gyógyszerészet" (Chemistry and Pharmacy). The publisher and owner was Emil FELLETÁR, a renowned chemist, first leader of the Hungarian Institute of Forensic Chemistry, engaged mainly in toxicological analysis. The first issue of his journal, published bi-weekly in Buda, appeared on January 1st, 1863, with scientific objectives. Notwithstanding the efforts of the editor, the first attempt to found an at least semi-chemical journal failed as soon as after nine months, because of financial reasons [6].

The next attempt, undertaken by Rudolf FABINYI, young professor of chemistry at the newly founded University of Kolozsvár in Transylvania, similarly at his own initiative and risk, had a somewhat longer lasting success. The journal called "Vegytani Lapok" (Chemical Papers) was published monthly in Kolozsvár, the first copy in 1882. It seemed that "Vegytani Lapok" would successfully fulfil its objective. The journal published original papers of significance, and received manuscripts from leading chemists of the country, also from those active in the capital, Budapest. In spite of this, the journal was discontinued after seven years without any comment; it cannot be established whether for financial or personal reasons.

It took again eight years until the next Hungarian chemical journal was founded. This third attempt remained successful. The initiator was the chemical-minerological Section of the Royal Hungarian Society of Natural Sciences mentioned already, and personally its president of that time, Károly THAN, professor of chemistry at the University of Budapest, a leading personality of Hungarian scientific life in those days and also a contributor financially, with a gift of 1000 Florins. The first copy of "Magyar Chemiai Folyóirat" (Hungarian Chemical Journal) was published in 1895 in the edition of the Society. This journal appears also today, and is highly esteemed among our already numerous chemical journals. As supplement, a monograph was yearly published, dealing with a selected field of chemistry, in continuations, which could be assembled into a book. The authors of these monographs include the most illustrious chemists of Hungary. The publication of these monographs ceased under the difficult conditions after the First World War.

The journal "Vegyészeti Lapok" (Chemical Papers) (1906—1919) was started as the organ of the Association of Hungarian Chemical Manufacturers,

and was mainly concerned with technology, process practice and chemical economy.

The Hungarian Chemical Society was founded in 1907, not so much as a scientific organization, but rather as a business federation of the already numerous Hungarian chemists, mainly in state or industrial employment. The Society founded in 1910 its monthly "Magyar Chemikusok Lapja" (Journal of Hungarian Chemists); according to its title-page, a scientific, social and technical chemical journal.

After losing the First World War, the ensuing shrinking of Hungarian territory and inflation gave rise to difficulties everywhere. A substantial part of the funds of the Academy and of the Society of Natural Sciences got lost or depreciated. Nevertheless, sparing no effort, they continued with the publication of the two journals mentioned, while the journal of the Chemical Society had to be discontinued. The Society could start again only in 1930 with a new journal under the title "Technikai Kurir" (Technical Messenger), which was discontinued in 1938. From 1940 the "Kémikusok Lapja" was then published again, and up to our days it remained the publishing organ of the Hungarian Chemical Society under the original title "Magyar Kémikusok Lapja" (only written according to modern orthography).

In the first period after World War II, scientific societies functioned as before, and they could also provide for the publication of their journals. Only the situation of the Academy became problematic. Social transformation beginning in 1948 had a large impact on the scientific life of the country. Reorganizations accompanied by an unparalleled upswing of scientific research took place.

In this development the major field of participation of the Academy, reorganized in 1949, was fundamental research. As a radical change in contrast with earlier times, this involved the development of a research network of its own, in which chemistry was represented by several institutes. A further impetus to this development were steadily extending research work at the universities and the foundation of a series of industrial research institutes, engaged mainly in applied research and development.

Under these circumstances the need for new possibilities of publication became more compelling from day to day, as the journals already existing could by no means satisfy demand. At the beginning of the fifties the situation became even more critical, as at that time there was scarcely any possibility for publication in foreign periodicals and, as it has been mentioned, the scientific journals in foreign language of the Academy had been discontinued before the war. This induced the Academy to found journals in foreign languages, making thereby possible for Hungarian scientists active in various branches of science to acquaint the international scientific world with their results. For chemistry, as a first attempt, the "Hungarica Chimica Acta" was published from 1947 to

1949 in five volumes. These can be considered as a precoursor of the present "Acta Chimica Academiae Scientiarum Hungaricae" which founded in 1952, being a representative publishing organ of Hungarian chemical science, became rapidly known and recognized.

The Hungarian journal of the Academy "Kémiai Közlemények" (Chemical Communications) has been published since the same year, which, however, in its present frame does not bring original works, but publishes, as the journal of the Class of Chemical Sciences, the best papers presented at the sessions of the Class, particularly those of foreign visiting scientists, surveys, reports on the internal life of the Class, *etc.*

In the course of time, however, it has become evident that speedy development of chemical research work all over the world requires new possibilities of publication. International journals devoted to more and more specific fields of chemistry were needed. The Hungarian Academy of Sciences and its Publishing House, Akadémiai Kiadó, also contributed to the satisfying of this demand, particularly in fields where Hungarian research work has had the highest international reputation.

The importance of these journals has been hall-marked also by the fact that foreign publishers willingly participate in joint editions. Thus, Akadémiai Kiadó has published jointly with Heyden, London, since 1969 the "Journal of Thermal Analysis"; with Elsevier, Amsterdam, since 1967 the "Journal of Radioanalytical Chemistry"; since 1972, similarly jointly with Elsevier, the "Radiochemical and Radioanalytical Letters". Another type of international co-operation is represented by "Reaction Kinetics and Catalysis Letters", published since 1974 in collaboration by the Hungarian and Soviet Academies in the care of Akadémiai Kiadó, Budapest. "Acta Alimentaria", started in 1972, offers good publication possiblities for research in food chemistry, the importance of the journal being emphasized also by the fact that Hungary is a large exporter of agricultural products.

In all these journals a transit time as short as possible is aimed at, as it is obviously essential today in the transmission of scientific information.

In addition to the periodicals mentioned above, a series of Cummunications, Annales, Acta, *etc.* are independently published by Hungarian universities and research institutes, which, however, are not comparable as regards to contents and publicity to the journals mentioned above.

Two of these should nevertheless be mentioned: the periodicals of the Technical Universities of Budapest and Veszprém. The first of these has been published since 1957, under the collective title "Periodica Polytechnica"; it contains papers of various sections, corresponding to the different Faculties. "Section Chimica" consists of papers whose authors are mostly on the staff of the Faculty for Chemistry. The University of Chemical Industries, Veszprém, has founded in 1972, jointly with the three research institutes active in Veszp-

rém, the "Hungarian Journal of Industrial Chemistry", creating thereby a forum of publication which had been missing up to that date, to report chemical-technological research in Hungary.

It should be mentioned finally that besides the journals discussed above appearing predominantly in foreign language, there are numerous publishing organs issuing chemical publications regularly or irregularly in Hungarian; these are not discussed here.

In summary, it can be seen from the aforesaid that the development and present status of our periodicals permit Hungary to occupy a honourable place in this field of international contest, a place which is suited to its situation and circumstances.

REFERENCES

[1] KROMINCK, D.: A History of Scientific and Technical Periodicals (1665—1790), p. 129. New York, 1961.
[2] YAGELLO, V.: J. Chem. Education **45,** 420 (1968)
[3] PROSZT, J.: Die Schemnitzer Bergakademie als Geburtsstätte chemisch-wissenschaftlichen Forschung in Ungarn. Sopron, 1938.
SZABADVÁRY, F.: Periodica Polytechnica, Chem. Eng. **7,** 127 (1963); J. Chem. Education **39,** 266 (1962)
[4] NYULAS, F.: Az erdélyországi orvosi vizeknek bontásáról közönségesen. (On the analysis of medicinal waters of Transsylvania, in general) Kolozsvár, 1800
[5] DEZSÉNYI, B., NEMES, Gy.: A magyar sajtó 250 éve (250 years of the Hungarian press). Budapest, 1954
[6] GRABARITS, I.: Magyar Kémikusok Lapja **32,** 266 (1977)

Béla LENGYEL H-1088 Budapest, Múzeum krt. 6—8.
Ferenc SZABADVÁRY H-1521 Budapest, Műegyetem

Acta Chimica Academiae Scientiarum Hungaricae, Tomus 100 (1—4), pp. 15—18 (1979)

EINWIRKUNG VON LITHIUMMETALL AUF DAS GEFÜGE VON OXIDISCH DOTIERTEN WOLFRAMDRÄHTE**

R. GROH*, T. MILLNER and L. BARTHA

(Forschungsinstitut für Technische Physik der Ungarischen Academie der Wissenschaften, Budapest)

Eingegangen am 2. November, 1977
Zur Veröffentlichung angenommen am 7. Dezember, 1977

Metallographische Schliffbilder, Vickers Härtezahlen, Zerreißfestigkeitswerte und Restwiderstandsmessungen weisen darauf hin, daß die primäre Rekristallisation von KSiAl-gedopten Wolframdrähten mit Durchmessern von 0,6 mm durch die aus flüssigem Lithiummetall bei 1100 °C im Verlaufe von 100 Stunden eindiffundierenden Li-Atome wesentlich erleichtert wird.

Man findet in der Literatur für die Konzentration der Fremdstoffspuren verschiedener Wolframdrahtsorten [1—6], insbesondere der KSiAl-gedopten Wolframdrähte [7] annehmbare Zahlenwerte. Über den Sauerstoffgehalt der Drähte wird man aber in Ungewißheit gelassen entweder, weil die Sauerstoffbestimmungsmethoden unzulänglich sind, oder aber, weil bis jetzt den Sauerstoffspuren — hinsichtlich ihrer die Drahteigenschaften bestimmenden Rolle — keine entsprechende Aufmerksamkeit gewidmet wurde. Laut Literaturangaben können z.B. KSiAl-dotierte Drähte neben 71 ppm K auch 9 ppm O enthalten [7]. Es bleibt dabei ungeklärt, ob dieser Sauerstoff an K-, Si- oder Al-Atome gebunden ist oder "ungebunden", d.h. allein an W-Atome gebunden im Draht vorliegt. Man bleibt auch darüber im Unklaren, ob sich die O-Atome in Kristallgitter, oder z.B. bevorzugt an den Fasergrenzen befinden. Dabei ist auch zu beachten, daß in KSiAl-gedopten Drähten — wie dies von A. KELE *(et al.)*, in einer weiteren Mitteilung gezeigt wurde [8] — durch Erhitzen in verschieden oxidierenden Atmosphären oxidische Phasen reversibel entstehen oder verschwinden.

Wie bekannt [9, 10] diffundieren im Wolframgitter Li-Atome bei z.B. 1100 °C interstiziell ebenso schnell wie z.B. C-, N- und O-Atome. Da außerdem Sauerstoffatome in Li_2O mit 72 Kcal (301 kJ) je Valenzbindung viel stärker gebunden werden als in K_2O (43 Kcal bzw. 180 kJ), SiO_2 (51 Kcal bzw. 214 kJ) und Al_2O_3 (63—65 Kcal, bzw. 264—272 kJ), versuchten wir die O-Atome des gezogenen Drahtes aus ihrer die Drahteigenschaften bestimmenden — noch

* 1325 Budapest, Postfach 76, Ungarn.
** Vortrag, gehalten im Rahmen des 9. Plansee Seminars (Reutte, 1977);
The Influence of Lithium Metal on the Structure of Oxidic Doped Tungsten Wires.

unbekannten — Verknüpfung und Rolle mittels eindiffundierter Li Atome zu entziehen, um dadurch über ihre Lage und Rolle etwas zu erfahren.

Zu diesem Zweck haben wir gezogene, gereinigte, KSiAl-gedopte Versuchs-Wolframdrähte von 0,6 mm Durchmesser mit gereinigter Oberfläche vorbereitet. Etwa 10 Drahtstücke wurden in eine mit Lithiummetall beschickte Molybdänmetall-Hülse gegeben und mittels einer Elektronenstrahl-Schweißeinrichtung in diese vakuumdicht eingeschlossen. Diese Röhre wurde mit weiteren 10 Drahtstücken in einer evakuierten abgeschmolzenen Quarzampulle 100 Stunden bei 1100 °C erhitzt. Zwischen den zwei Sorten von Drahtstücken ließen sich folgende Unterschiede feststellen.

1. Chemisch-analytische Atomabsorptionswerte der Li-Verteilung in den Drähten zeigten, daß in die äussere Zone (d.h. zwischen $d_1 = 0{,}6$ mm und $d_2 = 0{,}55$ mm) rund 35 ppm Li eingedrungen waren. Zwischen $d_2 = 0{,}55$ mm und $d_3 = 0{,}44$ mm konnte noch etwa 1 ppm Li, weiter im Drahtinneren jedoch kein Li mehr nachgewiesen werden.

2. Beide Sorten ließen im metallographischen Shliffbild (z.B. im Lichtmikroskop) eine ausgeprägte, aus primär völlig rekristalliserten Fasern bestehende »Faserstruktur« erkennen (Bild 1). Längs des Drahtdurchmessers war die Zahl der Fasern der mit Li behandelten Drähte um etwa 20% kleiner als die der nur im Vakuum erhitzten Drähte. Augenscheinlich wurden gewisse Hindernisse des radialen (seitlichen) Wachstums der Faser durch Li behoben, und zwar im ganzen Querschnitt!

3. Auch die Vickers-Härtezahlen der zwei Drahtsorten wiesen auf eine, die primäre Rekristallisation fördernde Wirkung der Li-Diffusion hin. Die nur im Vakuum erhitzten Drahtstücke zeigten HV-Werte zwischen 487—504, die mit Li behandelten zwischen 429—444.

4. Die beobachteten Zerreißfestigkeitswerte der unbehandelten Drähte ($\sigma_B = 216$ kg/mm^2), der nur im Vakuum erhitzten Drähte ($\sigma_B = 176—180$) und der mit Li behandelten Drähte ($\sigma_B = 156—166$) sind im Einklang mit den Punkten 1., 2. und 3.

5. Die Restwiderstandswerte der zwei Sorten unterschieden sich voneinander um einen erheblichen, eindeutigen Betrag. In Bild 2 ist der Zusammenhang

$$\delta(T) = \frac{\Delta\varrho(T)}{\varrho(T_2)}$$

dargestellt. $\Delta\varrho(T)$ ist der Widerstandsbetrag, um welchen sich der bei irgendeiner tiefen Temperatur (z.B. bei 77 °K) gemessene Widerstand $\varrho(T_2)$ unterscheidet. Die bei tiefen Temperaturen bestimmten $\delta(T)$-Werte dürfen als Restwiderstandswerte gedeutet werden. Wären im Draht die Li-Atome als gelöste Atome (also als Streuzentren) vorhanden, so müßte man eine Erhöhung der $\delta(T)$-Werte durch Li erwarten. Es wurde jedoch eine Verminderung der

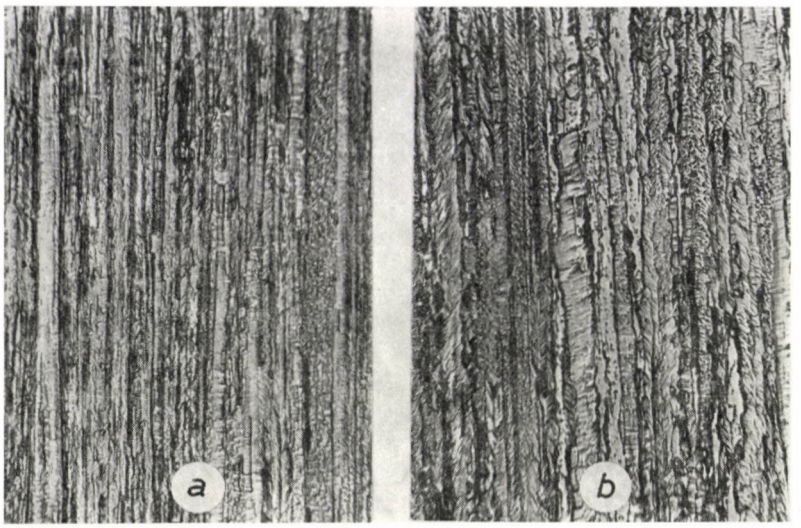

Bild 1. Textur gedopter KSiAl-Wolframdrähte; *a)* ohne Lithium, 100 St. bei 1100 °C in Vakuum erhitzt; *b)* in Berührung mit flüssigem Lithiummetall, 100 St. bei 1100 °C erhitzt (Verg. 1000×)

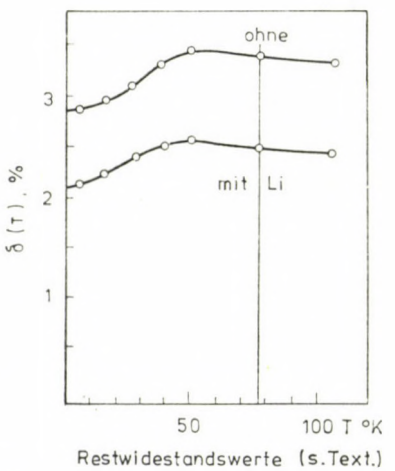

Bild. 2. Restwiderstandswerte von bei 1100 °C 100 St. mit und ohne flüssigem Lithium erhitzten, gedopten KSiAl-Wolframdrähten

$\delta(T)$-Werte beobachtet was einerseits auf die Bildung von ungelöstem Li_2O, also auf den Verbrauch von (gelösten) O-Atomen durch gelöste Li-Atome, andererseits auf die durch diesen Vorgang verursachte Verminderung der Zahl der Fasergrenzen (als Fehlstellen) zurückgeführt werden kann. Die Restwiderstandswerte sind größenordnungsmäßig mit der relativen Faserzahl der Schliffbilder im Einklang.

Diese Beobachtungen stehen mit unserer Annahme, daß die eindringenden Li-Atome mit den O-Atomen des gezogenen Drahtes reagieren, dann in Übereinstimmung, wenn wir eine Sauerstoffdiffusion aus dem Drahtinneren nach der Drahtoberfläche, also entgegen der Litiumdiffusion mit in Betracht ziehen.

Es ist leicht möglich, daß die aus ihrer ursprünglichen Lage durch Li-Atome entzogenen O-Atome hauptsächlich von den ursprünglichen Faseroberflächen des gezogenen Drahtes stammen. Diese Frage ist aber noch Gegenstand weiterer Untersuchungen, welche das Fasergleiten bei der Kontraktion gezogener Drähte zum Gegenstande haben.

*

Herrn Dr. L. URAY danken wir für die Restwiderstandsmessungen, den Herren G. GÁSPÁR und J. MILLNER für die Elektronenstrahlschweißarbeiten und Herrn Dr. L. VARGA für die mech. technischen Untersuchungen.

LITERATUR

[1] OREHOTSKY, J. L., STEINITZ, R.: Trans. Met. Soc. AIME **224,** 556—560 (1962)
[2] FRIEDMAN, S., BRETT, J.: Metallurg. Trans. **1,** 3225—3231 (1970)
[3] FARRELL, K., SCHAFFHAUSER, A. C. HOUSTON, J. T.: Metallurg. Trans. **1,** 2899—2900 (1970)
[4] BERLEC, J.: Metallurg. Trans. **1,** 2677—2683 (1970)
[5] BRETT, J., FRIEDMANN, S.: Metallurg. Trans. **3,** 769—778 (1972)
[6] YAMAZAKI, S., KOSEKI, J., OGURA, S., AKIYAMA, R.: 8. Plansee Seminar, Reutte 1974., Preprints I. Paper 7. Pp 5 and 15.
[7] SELL, H. G., STEIN, D. F., STICKLER, R., JOHSI, A., BERKEY, E.: J. Inst. Metals **100,** 275—288 (1972)
[8] KELE, A., MENYHARD, M., URAY, L., GAÁL, I.: Mitteilung D2 aus dem »Vorabdrucke, Bd. I.« des 9. Plansee Seminars, 1977.
[9] MCCRACKEN, G. M., LOVE, H. M.: Phys. Rev. Letters **5** (1960)
[10] LOVE, H. M., MCCRACKEN, G. M.: Canadian J. Physics **41,** 83—89 (1963)

Rezső GROH
Tivadar MILLNER
László BARTHA
1325 Budapest, Postfach 76, Ungarn

Acta Chimica Academiae Scientiarum Hungaricae, Tomus 100 (1—4), pp. 19—36 (1979)

SYNTHESIS OF BENZO[*a*]QUINOLIZIDINE DERIVATIVES SHOWING ANTIINFLAMMATORY ACTIVITY WITHOUT ULCEROGEN SIDE EFFECT

L. SZABÓ,[1] K. NÓGRÁDI,[1] I. TÓTH,[2] Cs. SZÁNTAY,[2] L. RADICS,[2] S. VIRÁG[3] and E. KANYÓ[3]

([1] Institute of Organic Chemistry, Technical University, Budapest, [2] Central Research Institute of Chemistry of the Hungarian Academy of Sciences, Budapest, [3] Chinoin Pharmaceutical and Chemical Works, Budapest.)

Received May 2, 1978

Accepted for publication August 3, 1978

A novel synthesis has been developed for the preparation of the benzo[*a*]quinolizidine derivatives **3b—o**, and the stereochemistry of these compounds has been studied by ^{1}H and ^{13}C—NMR spectroscopy. The structures of the alcohols **5a—f** and **6a—f**, obtained by the sodium borohydride reduction of the ketones **3b—d** and **3h—j**, have been established. Some of the compounds studied have high antiflammatory activity without ulcerogenic side effects.

A. Novel methods for the synthesis of benzo[a]quinolizidine derivatives 3b-o

The synthesis of the iodomethylates **1a, b** of the Mannich bases **2a, b** has been described in our previous papers [1, 2]. These iodomethylates react with 3,4-dihydro-6,7-dimethoxyisoquinoline to give the ketones **3b** or **3h** in good yields [1]. On the basis of WHITTAKER's results [3], we have shown that the hydrochlorides of 3,4-dihydroisoquinolines can also be made to react directly with the Mannich bases **2a, b** in aqueous methanol solution when the ketones **3b—d** and **3h—j** are formed conveniently and in excellent yields.

As some of the resulting compounds had been found to possess high antiinflammatory activity (see Section D), the preparation of further derivatives was necessary for studying the structure-activity relationship. The pyrrolidine enamine, obtained in a good yield from the ketone **3a** [4], was allowed to react with electrophilic alkenes, *e.g.* acrylonitrile [5]. Under appropriate reaction conditions certain regioselectivity was observed. From the reaction of the enamine **4a** with acrylonitrile at room temperature in anhydrous benzene, a single product, the ketonitrile **3e**, alkylated in position 1 was isolated in a yield of 28%, in addition to the unchanged ketone **3a**. In polar solvents, such as boiling ethanol, with a nearly equivalent amount of acrylonitrile, compound **3b** alkylated in position 3 was obtained as the main product. On processing the

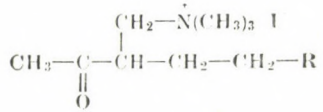

1

1, 2	R
a	CN
b	CO_2CH_3

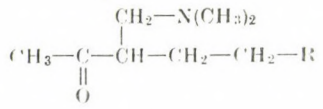

2

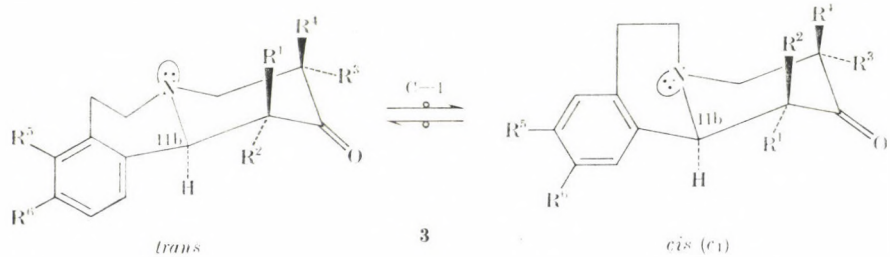

trans **3** *cis* (c_1)

3	R^1	R^2	R^3	R^4	R^5, R^6	B/C ring
a	H	H	H	H	OCH_3	*trans*
b	H	H	CH_2CH_2CN	H	OCH_3	*trans*
c	H	H	CH_2CH_2CN	H	OC_2H_5	*trans*
d	H	H	CH_2CH_2CN	H	$-OCH_2O-$	*trans*
e	CH_2CH_2CN	H	H	H	OCH_3	*trans*
f	CH_2CH_2CN	H	CH_2CH_2CN	H	OCH_3	*trans*
g	H	H	CH_2CH_2CN	CH_2CH_2CN	OCH_3	*trans*
h	H	H	$CH_2CH_2CO_2CH_3$	H	OCH_3	*trans*
i	H	H	$CH_2CH_2CO_2CH_3$	H	OC_2H_5	*trans*
j	H	H	$CH_2CH_2CO_2CH_3$	H	$-OCH_2O-$	*trans*
k	$CH_2CH_2CO_2C_2H_5$	H	H	H	OCH_3	*cis* (c_1)
l	$CH_2CH_2CO_2C_2H_5$	H	H	H	OCH_3	*trans*
m	$CH_2CH_2CO_2CH_3$	H	$CH_2CH_2CO_2CH_3$	H	OCH_3	*cis* (c_1)
n	$CH_2CH_2CO_2CH_3$	H	$CH_2CH_2CO_2CH_3$	H	OCH_3	*trans*
o	H	H	$CH_2CH_2CO_2CH_3$	$CH_2CH_2CO_2CH_3$	OCH_3	*trans*

reaction product, small amounts of the isomer 3e and the 3,3-disubstituted derivative 3g were isolated besides the starting substance 3a. Compound 3g was the main product when the enamine 4a was alkylated in boiling ethanol with a large excess of acrylonitrile, or when the enamine 4c was made to react with acrylonitrile (43%). When, however, enamine 4b was treated under similar conditions, the 1,3-disubstituted compound 3f was obtained in a yield of *ca.* 33%, presumably for steric reasons.

The structures of the ketones **3b, h**, obtained from the reaction of 6,7-dimethoxy-3,4-dihydroisoquinoline with the iodomethylates **1a, b** or the Mannich bases **2a, b**, were proved by chemical methods, and these compounds were used to prepare tetracyclic yohimbine [1] and reserpine analogues [6].

The mass spectra provided important clues in the structure elucidation of the new compounds prepared by the alkylation of the enamines **4a—c** with acrylonitrile. The mass spectra of all compounds studied in which the alkyl group is in position 1 (**3e, l**) contain an *M*-56 fragment, supporting the structure, whereas the compounds with one or two alkyl groups in position 3 (**3b, g, h, o**) produce a characteristic *M*-43 fragment. The mass spectra of the 1,3-disubstituted derivatives (**3f, m, n**) contain neither of these fragments.

We intended to convert nitriles **3b, g** and **3e, f** into the corresponding esters by boiling in methanol or ethanol in the presence of sulfuric acid.

As expected, the 3-substituted compounds (**3b, g**) uniformly produced the methyl esters **3h** and **3o**. When, however, 1-substituted (**3e**) or 1,3-disubstituted nitriles (**3f**) were refluxed in ethanol or methanol in the presence of sulfuric acid, two isomeric pairs (**3k, l** and **3m, n**) could be isolated in each case by means of preparative layer chromatography, instead of the single products expected. By interrupting the reaction after a short period (1 h), we have found that first, in a kinetically controlled reaction, compounds **3k** and **3m** are formed, which are converted into isomers **3l** and **3n** on prolonged boiling. The members of the compound pairs are in equilibrium (**3k** $\rightleftharpoons$ **l**, **3m** $\rightleftharpoons$ **n**) which is shifted by acids or bases in the direction of the upper arrow, toward the thermodynamically more stable forms (**3l, n**).

Induced by this interesting phenomenon, we have investigated the configuration and conformation of the above compounds by ^{1}H- and ^{13}C-NMR spectroscopy.

B. Stereochemical studies of the ketones 3e, f, h, k-n by means of ^{1}H- and ^{13}C-NMR spectroscopy

Displayed in Table I are the ^{1}H-NMR parameters (chemical shifts and vicinal couplings) of the angular proton, C-11bH; Table II summarizes the carbon-13 chemical shifts. By systematic ^{13}C-NMR studies of related benzo- and indoloquinolizidines [7, 8] it has been established that the ^{13}C shift value of the angular C-11b carbon reflects its actual configuration. Within the formulation used in this paper, β-configuration is characterized by C-11b resonance occurring between 54 and 57 ppm, whereas larger values, ranging from 60 to 64 ppm, indicate B/C ring fusion with α-oriented C-11b. According to data in Table II, the latter is the case for molecules **3b** and **3h**, and further increase of the C-11b shift value in the C-1 substituted derivatives is obviously due to β-substitution effects. The ^{1}H chemical shift and vicinal couplings of the angu-

Table I

Chemical Shifts[a] *(ppm) and* $^1H-^1H$ *Coupling Constants (Hz) of C-11bH*

	3b	*3e*	*3f*	*3h*	*3k*	*3l*	*3m*	*3n*
δ	3.58	3.64	3.55	3.52	3.82	3.55	3.67	3.55
$^3J_{aa}$	11	—	—	11	10	—	10	—
$^3J_{ae}$	3	3.5	3.5	3	—	3.5	—	3.5

[a] In $CDCl_3$, relative to internal TMS

lar proton in **3b** and **3h** (see Table I) are characteristic of benzo- and indoloquinolizidines with highly preferred *trans* conformation [9, 10], in which C-11bH is *axially* oriented with respect to ring C. Both of these two couplings are seen to occur also in the spectra of the C-1 substituted derivatives (see Table I). This finding suggests that the substituent at C-1 assumes *axial* orientation in **3e**, **3f**, **3l**, **3n** and *equatorial* orientation in **3k** and **3m**, *i.e.* molecules **3m** and **3n**, as well as **3k** and **3l** are epimeric pairs. While the angular proton chemical shift in derivatives with *axially* oriented C-1 substituent practically coincides with the values found for **3b** and **3h**, there are marked downfield shifts in **3k** and **3m**, suggesting a displacement of the conformational equilibrium in the latter molecules toward the preference of the *cis* (c_1) form with *axially* oriented C-11bH. This conclusion is fully supported by the ^{13}C-NMR data in Table II. Comparative carbon-13 studies on related systems show [7, 8, 11—14] that the chemical shift of C-6 and C-11 are sensitive to conformational changes of the quinolizidine moiety. Typically, a value of 50 to 52 ppm for C-6 chemical shift is expected with preferentially *trans*, and a value of 44 to 46 ppm with preferentially *cis* benzoquinolizidines. The respective values for C-11 are 108 and 112 ppm. It will be noted that the carbon-13 data also reflect the change of the C-1 substituent orientation. In particular, this can be seen from the resonances due to C-1, and C-2, which exhibit orientation-dependent α- and β-substituent effects.

(For other resonances originated by carbons near the site of substitution, these effects are masked by effects of conformational changes.)

The above results are also supported by the strong Bohlmann bands appearing in the infrared spectra of *trans*-quinolizidine derivatives, which cannot be observed in the spectra of the compounds with *cis* (c_1) conformation (**3k, m**).

In agreement with the available literature data [15, 16], the experimental results can be summarized as follows. All the 3-monosubstituted compounds (**3b—d, 3h—j**) have *trans*-quinolizidine conformation, and the substituent in position 3 is α-*equatorial*. These compounds are thermodynamically stable, and under the influence of acids or bases they retain the conformation of both the

Table II

Carbon-13 Chemical Shifts (ppm)[a]

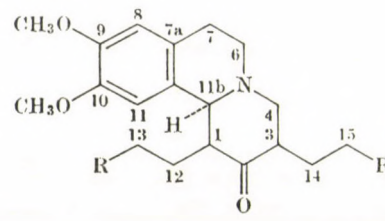

R = CN, CO_2CH_3, $CO_2C_2H_5$

	3b	3e	3f	3h	3k	3l	3m	3n
C-11b	62.21	64.54	65.41	62.41	65.68	65.19	67.14	65.86
C-6	49.99	51.27	50.96	50.31	46.55	51.44	44.86	51.51
C-7	29.38	29.51	29.53	29.42	27.72	29.58	28.96	29.56
C-7a	126.19	125.70	125.30	126.21	126.14	126.40	126.07	126.20
C-8	111.69	111.74	111.88	111.74	111.24	111.61	111.88	111.63
C-9	147.96[b]	148.16[b]	148.31[b]	148.01[b]	148.41	147.93[b]	148.54	147.91[b]
C-10	147.61[b]	147.91[b]	148.16[b]	147.67[b]	146.96	147.76[b]	146.51	147.77[b]
C-11	108.26	107.26	107.33	108.25	111.98	107.82	112.22	107.76
C-11a	128.33	128.03	128.04	128.58	127.16	128.04	126.57	127.97
C-1	47.35	54.54	55.17	47.60	52.40	55.34	51.77	55.45
C-2	208.37	210.50	210.85	209.02	209.60	211.80	209.90	212.64
C-3	47.84	38.52	45.41	48.69	38.80	38.74	46.68	45.81
C-4	60.56	54.90	60.97	61.06	52.61	55.17	61.50	61.56
C-12	—	22.95	22.74[c]	—	23.69	21.80	22.00[c]	22.02[c]
C-13	—	15.11	15.33[d]	—	32.19	31.41	31.48[d]	31.29[d]
C-14	22.80	—	23.09[c]	21.86	—	—	21.75[c]	21.91[c]
C-15	15.20	—	15.33[d]	31.68	—	—	31.98[d]	31.66[d]
CN	119.46	119.04	118.83	—	—	—	—	—
			119.23					
COOR	—	—	—	173.64	173.10	172.64	173.65	173.05
							173.68	173.74
COOR	—	—	—	51.52	14.20	14.17	51.32	51.17
					60.26	60.20	51.46	51.17
OMe	55.99	55.99	56.14	56.04	56.19	55.99	56.08	56.04
	55.84	55.84	55.94	55.94	55.94	55.82	55.88	55.84

[a] In $CDCl_3$, relative to internal TMS
[b,c,d] Assignments may be reversed within the same vertical column

ring system and the substituent in position 3. With the ketonitriles **3e** and **3f**, which also have *trans* conformation, but where the substituent is *β-axial* in position 1, the 1, 11b bond of the C ring is opened upon boiling in alcohols in the presence of sulfuric acid, and in a kinetically controlled reaction the ring is closed to form esters **3k** or **3m** with *cis* (c_1)conformation and *α-equatorial* substituent. On further acidic or alkaline treatment, the conformation of these compounds is reversed, and epimerization takes place on carbon 1 to yield the thermodynamically more stable esters **3l** or **3n** of *trans* conformation.

C. The sodium borohydride reduction of the ketones 3b-d and 3h-j

The sodium borohydride reduction of the ketonitriles **3b—d** yields *equatorial* alcohols **5a—c** as the main product, along with minor amounts of the *axial* isomers **6a—c**. The alcohols **5a—c** precipitate from the methanol solution directly during the reduction, whereas compounds **6a—c** can be isolated by preparative layer chromatography. The structures of the resulting alcohols were determined unambigously from the ^{1}H-NMR spectra of their acetyl derivatives **5g—i** and **6g—i** formed by acetylation, on the basis of the chemical shift and coupling constants of proton 2.

Similarly, reduction of the ketoesters **3h—j** yields equatorial alcohols **5d—f** as the main product along with the *axial* isomers **6d—f**. In some cases (**5d, f**) reduction of the ketoesters **3h, j** led to spontaneous ring closure, in which lactones **7a, b** were formed *via* methanol elimination. The structure of the lactones were confirmed by the mass spectra. The stereochemistry of the alcohols was again determined from the ^{1}H-NMR spectra of their acetyl derivatives (**5j—l** and **6j—l**).

D. Pharmacological tests

According to tests on various known experimental inflammation models, the investigated benzo[*a*]quinolizidine derivatives of general formula **3** have antiinflammatory activity equal to, or greater than, that of phenylbutazone (Table III). It is of particular interest that on the serotonin oedema model the tested benzo[*a*]quinolizidine derivatives proved to be several times more active than phenylbutazone or indomethacin (Table III).

Some of the benzo[*a*]quinolizidine derivatives investigated have considerable antipyretic effect as well. In the case of experimentally induced fever, their antipyretic activity exceeds that of amidazophen (Table IV).

Hot-plate and writhing syndrome tests have shown that the analgetic effect of these compounds exceed that of phenylbutazone (Tables V and VI).

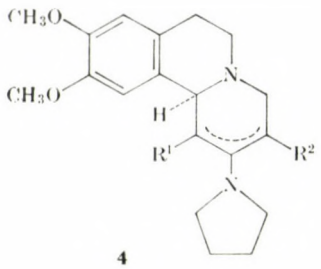

4

4	R^1	R^2
a	H	H
b	CH_2CH_2CN	H
c	H	CH_2CH_2CN

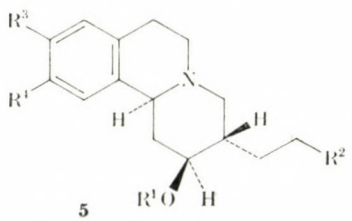

5

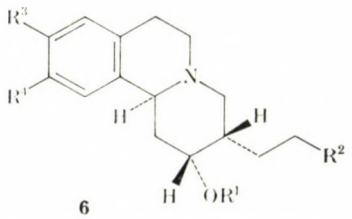

6

5, 6	R^1	R^2	R^3, R^4
a	H	CN	OCH_3
b	H	CN	OC_2H_5
c	H	CN	$-OCH_2O-$
d	H	CO_2CH_3	OCH_3
e	H	CO_2CH_3	OC_2H_5
f	H	CO_2CH_3	$-OCH_2O-$
g	$COCH_3$	CN	OCH_3
h	$COCH_3$	CN	OC_2H_5
i	$COCH_3$	CN	$-OCH_2O-$
j	$COCH_3$	CO_2CH_3	OCH_3
k	$COCH_3$	CO_2CH_3	OC_2H_5
l	$COCH_3$	CO_2CH_3	$-OCH_2O-$

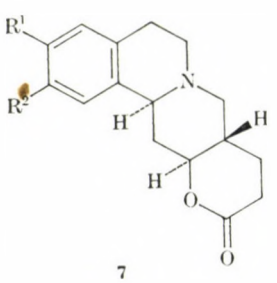

7

7	R^1, R^2
a	OCH_3
b	$-OCH_2O-$

In addition to the antiinflammatory, antipyretic and analgetic effects, benzo[*a*]quinolizidine derivatives also show a CNS sedative effect.

According to the toxicity tests, the toxicities of the majority of the compounds investigated are similar in magnitude to that of phenylbutazone (in acute experiments, peroral administration on rats; see Table VII).

Table III

Antiinflammatory effect of **3b—d** *and* **3h** *in kaolin, carragenin, serotonin oedema and Cotton-granuloma tests*

Compound	Dose, mg/kg, *per os*	Inhibition of oedema and granuloma, in % of controls			
		Kaolin 2 h	Carragenin 1.5 h	Serotonin 1 h	Cotton
3b	25	20.5[a]	—	—	—
	50	21.4[a]	24.2[a]	22.4[e]	—
	75	24.8[a]	25.7[a]	—	—
	100	47.8[b]	37.7[b]	57.8[c]	—
3c	25	17.3[a]	25.1[a]	—	—
	50	19.4[a]	41.5[b]	36.2[c]	—
	75	48.9[b]	—	—	—
	100	45.9[b]	53.7[b]	47.0[c]	—
3d	25	18.1[a]	22.0[a]	28.5[c]	—
	50	27.5[a]	30.6[b]	42.1[c]	26.4[a]
	75	43.7[b]	47.7[b]	48.7[c]	—
	100	53.4[b]	52.7[b]	—	—
3h	25	5.8	—	—	—
	50	21.4[a]	14.3	—	—
	75	24.7[a]	2.8	—	—
	100	—	17.0	16.0	—
Phenylbutazone	50	27.5[b]	24.3[a]	—	19.6[b]
	100	—	—	10.2	—
Indomethacin	10	27.2[b]	26.7[a]	—	—
	25	—	—	1.4	—
Na-salicylate	100	10.5	16.2	—	25.5[b]

[a] $p = 0.01$
[b] $p = 0.05$
[c] $p = 0.001$ (significance was calculated by means of Studient's "t" test)
[d] Inbred, genetically uniform rats of Long-Ewans strain; 10 animals in a sex ratio of 1 : 1 were used

In contrast with indomethacin, known to have ulcerogenic effect, the compounds investigated show no such effect in subacute toxicity tests, and have no adverse effect on the haematopoietic organs (Table VIII).

As a further advantage, the therapeutic indices of the compounds of general formula **3** are much higher than that of indomethacin (Table IX).

Accordingly, this group of compounds can be applied primarily for the treatment of arthritis and the inflammatory diseases of skeletal muscles, as antiinflammatory and analgetic drugs.

Table IV

Antipyretic effect on experimentally induced fever

Compound	Dose, mg/kg *per os*	Changes in body temperature, °C at		
		1 h	2 h	3 h
3d	25	-1.67^{c}	-1.81^{c}	-1.60^{b}
	50	-2.75^{c}	-3.34^{c}	-4.03^{c}
Phenylbutazone	25	-0.82^{b}	-0.84^{b}	-0.73^{a}
	50	-1.05^{b}	-1.07^{b}	-0.76^{a}
Amidazophen	25	-1.17^{c}	-0.97^{b}	-0.95^{a}

[a] $p = 0.05$
[b] $p = 0.01$
[c] $p = 0.001$

Table V

Hoot plate test

Compound	Dose mg/kg, *per os*	Effect (%) at 2 h
3c	50	33.9
3d	50	61.2
3h	50	26.4

Remark: As it is known, indomethacin and phenylbutazone do not elicit evaluable effects at a dose of 50 mg/kg given orally.

Table VI

Writhing syndrome

Compound	Dose, mg/kg, *per os*	Effect (%) at 2 h
3d	50	41.8
Phenylbutazone	100	17.6

Remark: The effect on writhes observed in the test and control animals were calculated and the difference was expressed in per cent

The absence of ulcerogenic effect or any adverse effect on the haematopoietic organs is considered advantageous, since prolonged treatment becomes possible, which is an important therapeutic factor with diseases of this kind. Some of the compounds also exhibit substantial secretion inhibiting effect.

Alcohols of general formula **5** show even more favourable effects than compounds of type **3**. Their pharmacological data will be published separately.

Table VII

Acute toxicity

Compound	LD_{50}, mg/kg orally[a]
3b	620
3c	780
3d	1407
Na-salicylate	1700
Phenylbutazone	1181
Indomethacin	12

[a] The values of LD_{50} were determined by the Litchfield—Wilcoxon method on CFY rats

Table VIII

Study of ulcer formation

Compound	Ulcer		Erosion	
	Male	Female	Male	Female
3d	0/10	1/10	0/10	1/10
Control	0/10	0/10	0/10	0/10
Indomethacin	3/10	3/10	1/10	1/10

Table IX

Therapeutic index

Compound	LD_{50}/ED_{50}	
	Kaolin oedema	Carragenin oedema
3b	12.4	6.7
3c	15.0	19.8
3d	29.2	22.6
Indomethacin	2.3	1.3

Experimental

IR spectra were recorded in KBr with a Spectromom 2000 spectrophotometer. ^1H- and ^{13}C—NMR spectra were obtained at 100 and 25.2 MHz, respectively, using a Varian XL-100/15—124XL 16 Fourier transform spectrometer. The assignments of ^{13}C resonances to the individual carbons in the molecules are based on spectral comparison, and single-frequency selective ^{13}C—^1H decouplings. Chemical shifts are reported in ppm (δ) downfield from TMS. Mass spectra (MS) were recorded with AEI MS 902 and JEOL-01SG-2 instruments (70 eV, ion source temp. 150 °C, direct insertion).

5-oxo-dimethylaminocapronitrile (2a)

This compound was synthesized by the method described in Ref. [2], and purified by distillation. B.p. 110 °C/1 mm; $n_D^{20} = 1.4453$.
IR(film): 1710 cm^{-1} (CO).

Methyl-(5-oxo-4-dimethylamino)hexanoate (2b)

The compound was obtained by the method described in Ref. [3], and purified by distillation. B.p. 104—106 °C/4 mm; $n_D^{20} = 1.4450$.
IR(film): 1725 cm^{-1} (ester CO).

General method for the preparation of the ketones 3b-d and 3h-i

To a solution of the appropriate isoquinoline hydrochloride (4.95 mmol) in 3 ml of water there was added, with stirring, a solution of **2a** (5.90 mmol) or **2b** (4.98 mmol) in 1 ml of methanol. Stirring was continued for 24 h at room temperature. The separated crystalline product was filtered off, washed with ethanol and water, and recrystallized from methanol (see Table X).

General method for the preparation of the enamines 4a-c

A solution of the ketone **3a—c** (5.36 mmol) in a mixture of pyrrolidine (10.5 ml) and *abs.* benzene (22.0 ml) was distilled for 5 h under magnetic stirring in nitrogen atmosphere. The volume of the solution was continuously maintained by adding 10% pyrrolidine containing benzene. The solvent was evaporated in vacuum, and the rest of pyrrolidine was removed by repeated distillation of benzene (3×20 ml). The crude enamines were used for the next step without purification. The structures of the enamines were confirmed by IR spectroscopy.
4a IR(KBr): 2750 (Bohlmann bands), 1650 cm^{-1} (C=C).
4b IR(KBr): 2805, 2750 (Bohlmann bands), 2310 (CN), 1658 cm^{-1} (C=C).
4c IR(KBr): 2805 (Bohlmann bands), 2310 (CN), 1650 cm^{-1} (C=C).

3-[9,10-Dimethoxy-2-oxo-1,3,4,6,7,11bα-hexahydro-2*H*-benzo[a]quinolizin-(1β)-yl]propionitrile (3e)

To a solution of the enamine **4a** (0.53 g; 1.70 mmol) in dry benzene (7 ml), acrylonitrile (90 mg; 1.70 mmol) was added, and the reaction mixture was allowed to stand at room temperature for 4 days. The solution was poured into water (4 ml), the organic layer was dried over $MgSO_4$ and the solvent evaporated in vacuum. The residue was separated by preparative TLC [silica gel, benzene-MeOH (14 : 3), R_f **3e** > **3a**, elution with acetone] to give the starting material **3a** (0.21 g; 39.3%) and **3e** (80 mg; 15%) m.p. 182 °C (from methanol).

IR(KBr): 2805, 2750 (Bohlmann bands), 2260 (CN), 1710 cm^{-1} (CO).
^1H—NMR($CDCl_3$): 6.25, 6.17 (2H, s, aromatic), 3.85 (6H, s, OCH_3), 3.64 (1H, d, J = = 3.5 Hz, 11b—H).
MS *m/e* (%): 314 (M^+, 11), 313 (5), 286 (2), 274 (100), 258 (3), 218 (2), 205 (1).
$C_{18}H_{22}N_2O_3$ (314.38). Calcd. C 68.76; H 7.05; N 8.91. Found C 68.44; H 7.13; N 9.22%.

3-[9,10-Dimethoxy-2-oxo-1,3,4,6,7,11bα-hexahydro-2*H*-benzo[a]quinolizin-(3β)-yl]propionitrile (3b)

The enamine **4a** (1.20 g; 3.82 mmol) and acrylonitrile 0.35 g; 0.65 mmol) were refluxed in ethanol (10 ml) for 8 h. The reaction mixture was poured into water, and extracted with ether (3×10 ml). After removal of the solvent the residue was treated with methanol to yield 81 mg (6.7%) of **3e**. The water phase was extracted with dichloromethane (3×10 ml). After drying ($MgSO_4$) the solvent was evaporated in vacuum. The residue was crystallized from methanol to give **3b** (185 mg; 15.8%), m.p. 129—131 °C (*lit.* [1] m.p. 130—131 °C). (For ^1H—NMR data of **3b**, see Table X).

Table X

Physical data of ketones **3b—d** *and* **3h—j**

Comp.	M.p., °C	Yield, %	Formula	Analyses	IR(KBr) ν max, cm^{-1}	^1H—NMR($CDCl_3$) δ(ppm), J (Hz)
3b	130—31	62	a)	a)	a)	6.63, 6.54 (2 H, s, aromatic); 3.84, 3.82 (6 H, s, OCH_3); 3.58 (1 H, 11.3, 11b-H).
3c	135—36	89	$C_{20}H_{26}N_2O_2$	C, H, N	2800, 2750 2300, 1710	6.44, 6.36 (2 H, s, aromatic); 3.95 (4 H, q, 6.6, CH_2CH_3); 3.52 (1 H, 10.5, 3.2, 11b-H); 1.40 (6 H, t, 6.6, CH_2CH_3).
3d	154—55	64	$C_{17}H_{18}N_2O_3$	C, H, N	2800, 2750 2380, 1715	6.52, 6.47 (2 H, s, aromatic); 5.82 (2 H, s, OCH_2O); 3.55 (1 H, 10.6, 3, 11b-H).
3h	131	95	a)	a)	a)	6.62, 6.55 (2 H, s, aromatic); 3.84, 3.82 (6 H, s, OCH_3); 3.67 (3 H, s, CO_2CH_3); 3.52 (1 H, 11, 3, 11b-H).
3i	130—32	94	$C_{21}H_{29}NO_5$	C, H, N	2800, 2750 1730, 1715	6.60, 6.54 (2 H, s, aromatic); 4.02 (4 H, q, 6.6, CH_2CH_3); 3.66 (3 H, s, CO_2CH_3); 3.35 (1 H, 10.5, 3, 11b-H); 1.42 (6 H, t, 6.6, CH_2CH_3).
3j	123—24	92	$C_{18}H_{21}NO_5$	C, H, N	2800, 2750 1750, 1740	6.62, 6.58 (2 H, s, aromatic); 5.90 (2 H, s, OCH_2O); 3.70 (3 H, s, CO_2CH_3); 3.64 (1 H, 10.7, 3, 11b-H).

a) See Ref. [1] 3-[9,10-Dimethoxy- (**3b**), -diethoxy- (**3c**) and -methylenedioxy-2-oxo-1,3,4,6,7,11bα-hexahydro-2*H*-benzo[*a*]quinolizinyl-(3α)]propionitrile (**3d**).

Methyl 3-[9,10-dimethoxy- (**3h**), -diethoxy- (**3i**) and -methylenedioxy-2-oxo-1,3,4,6,7,11bα-hexahydro-2*H*-benzo[*a*]quinolizinyl-(3α)]propionate (**3j**)

9,10-Dimethoxy-2-oxo-3,3-bis(2-cyanoethyl)-1,3,4,6,7,11bα-hexahydro-2H-benzo[a]quinolizine (3g)

(*A*) A solution of the enamine **4a** in ethanol (8 ml) was refluxed with acrylonitrile (0.45 g; 8.58 mmol) for 4 h. After cooling, the crystals were filtered off and washed with methanol to obtain 0.28 g (26.5%) of the title compound, m.p. 182—183 °C (from dichloromethane-methanol).

IR(KBr): 2300 (CN), 1715 cm^{-1} (CO).

^1H—NMR($CDCl_3$): 6.75, 6.63 (2H, s, aromatic), 3.94, 3.91 (6H, s, OCH_3).

MS *m/e* (%): 367 (M^+, 20); 366 (25); 351 (3); 336 (1); 327 (22); 324 (12); 274 (100); 205 (30).

$C_{21}H_{25}N_3O_3$ (367.44). Calcd. C 68.64; H 6.86; N 11.43. Found C 68.44; H 6.82; N 11.50%.

(*B*) The enamine **4c** (1.80 g; 4.94 mmol) and acrylonitrile (0.39 g; 7.42 mmol) were refluxed in ethanol (13 ml) for 4 h. After cooling, the separated crystals were collected and recrystallized from methanol to give 0.75 g (43%) of **3g**.

9,10-Dimethoxy-2-oxo-1β,3α-bis(2-cyanoethyl)-1,3,4,6,7,11bα-hexahydro-2H-benzo[a]quinolizine (3f)

A solution of the enamine **4b** (1.80 g; 4.94 mmol) in ethanol (13 ml) was refluxed with acrylonitrile (0.39 g; 7.42 mmol) for 48 h. The hot reaction mixture was filtered, and the crystalline product was washed wite methanol to obtain 0.60 g (33.4%) of **3f**, m.p. 202—203 °C (from dichlorometane-methanol).

IR(KBr): 2800, 2760 (Bohlmann bands), 2255 (CN), 1705 cm^{-1} (CO).

^1H—NMR($CDCl_3$): 7.37, 6.82 (2H, s, aromatic), 3.88 (6H, s, OCH_3), 3.55 (1H, d, J = = 3.5 Hz, 11bH).

MS *m/e* (%): 367 (M^+, 30); 327 (100); 314 (5); 313 (3); 274 (7); 271 (12); 266 (20); 261 (3); 260 (2); 232 (6); 205 (8).

$C_{21}H_{25}N_3O_3$ (367.44). Calcd. C 68.64; H 6.85; N 11.44. Found C 68.44; H 6.79; N 11.60%.

Methyl 3-[9,10-dimethoxy-2-oxo-1,3,4,6,7,11bα--hexahydro-2H-benzo[a]quinolizin-(3α)-yl]-propionate (3h)

3b (1.00 g; 3.20 mmol) was refluxed in a mixture of *abs.* methanol (4.78 ml) and *conc.* sulfuric acid (1.58 ml) for 3 h. The reaction mixture was poured into ice-water, made alkaline with *conc.* ammonium hydroxide (pH 9), and extracted with dichloromethane (3×5 ml). The organic layer was dried ($MgSO_4$) and evaporated to dryness in vacuum. Crystallization from methanol gave 0.42 g (37.5%) of **3h**, m.p. 130—132 °C (lit. [1] m.p. 130—129 °C). (For ^1H—NMR data, see Table X.)

Ethyl 3-[9,10-dimethoxy-2-oxo-1,3,4,6,7,11bα-hexahydro-2H-benzo[a]quinolizin-(1β)-yl]-propionate (3l) and ethyl 3-[9,10-dimethoxy-2-oxo-1,3,4,6,7,11bα-hexahydro-2H-benzo[a]quinolizin-(1α)-yl]propionate (3k)

(*A*) The ketonitrile **3e** (0.20 g; 0.63 mmol) was boiled in a mixture of ethanol (4.7 ml) and *conc.* sulfuric acid (1.58 ml) for 1 h. The solution was poured into ice-water, made alkaline with *conc.* ammonium hydroxide, and extracted with dichloromethane (3×5 ml). The organic phase was dried ($MgSO_4$) and the solvent removed in vacuum. The residue was separated by preparative TLC (silica gel, benzene-methanol 14 : 3, R_f **3l** > **3e** > **3k**, elution with acetone) to yield 30 mg (15%) of **3e**, 40 mg (20%) of **3l**, and 70 mg (35%) of **3k**.

3l, m.p. 125—127 °C (from ethanol).

IR(KBr): 2820, 2760 (Bohlmann bands), 1727 (ester CO), 1706 cm^{-1} (CO).

^1H—NMR($CDCl_3$): 7.16 (2H, s, aromatic), 4 15 (2H, q, J = 7.2 Hz, CH_2CH_3), 3.72 (6H, s, OCH_3), 3.55 (1H, d, J = 3.5 Hz, 11b—H), 1.2 (3H, t, CH_2CH_3).

MS *m/e* (%): 361 (M^+, 25), 274 (100).

3k, m.p. 140—142 °C (from methanol).

IR(KBr): 1720 (ester CO), 1700 cm^{-1} (CO).

^1H—NMR($CDCl_3$): 7.21 (2H, s, aromatic), 4.20 (2H, q, J = 7.2 Hz, CH_2CH_3), 3.85 (6H, s, OCH_3), 3.83 (1H, d, J = 10 Hz, 11b—H), 1.23 (3H, t, CH_2CH_3).

MS *m/e* (%): 361 (M^+, 25), 274 (100).

(*B*) The reaction mixture described above was refluxed for 6 h. The work-up followed procedure (*A*). The crude product was recrystallized from methanol to yield 80 mg (35%) of **31**. The methanolic mother liquor was separated by preparative TLC to give further 25 mg of **3l** (total yield 40.9%), and 20 mg (8.7%) of **3k**.

9,10-Dimethoxy-2-oxo-1β,3α-bis(2-methoxycarbonil-ethyl)-1,3,4,6,7,11bα-hexahydro-2H-benzo[a]quinolizine (3n), and 9,10-dimethoxy-2-oxo-1α,3α-bis(2-methoxycarbonylethyl)-1,3,4,6,7,11bα-hexahydro-2H-benzo[a]quinolizine (3m)

(*A*) The nitrile **3f** (0.20 g; 0.54 mmol) was refluxed in a mixture of methanol (4.7 ml) and *conc.* sulfuric acid (1.58 ml) for 1 h. After cooling, the reaction mixture was poured into ice-water, made alkaline with *conc.* ammonium hydroxide, and extracted with dichloromethane. The organic layer was dried ($MgSO_4$) and the solvent evaporated in vacuum. The remaining crude product was separated by preparative TLC (silica gel, benzene-methanol 14 : 3, R_f **3n** > **3m**, elution with acetone) to give **3n** (45 mg; 19.8%) and **3m** (85 mg; 39.5%).

3n, m.p. 105—107 °C (from methanol).

IR(KBr): 2810, 2760 (Bohlmann bands), 1736 (ester CO), 1695 cm^{-1} (CO).

^{1}H—NMR($CDCl_3$): 6.62, 6.58 (2H, s, aromatic), 3.86 (6H, s, OCH_3), 3.68, 3.62 (6H, s, CO_2CH_3), 3.55 (1H, d, J = 3.5 Hz, 11b—H).

MS *m/e* (%): 433 (M^+, 50), 432 (40); 418 (1); 402 (30), 374 (2); 361 (20); 360 (100); 347 (8); 346 (8); 304 (40); 261 (10); 260 (9); 246 (2); 232 (6); 230 (2); 218 (7); 205 (25).

3m, m.p. 129—130 °C (from methanol).

IR(KBr): 1734 (ester CO), 1690 cm^{-1} (CO).

^{1}H—NMR($CDCl_3$): 7.30, 7.10 (2H, s, aromatic), 3.86 (6H, s, OCH_3), 3.70, 3.60 (6H, s, CO_2CH_3), 3.67 (1H, d, J = 10 Hz, 11b—H).

MS *m/e* (%): 433 (M^+, 40), 432 (35); 418 (1); 402 (25); 374 (2); 361 (25); 360 (100); 347 (8); 346 (8); 304 (40); 261 (15); 260 (10); 246 (15); 232 (6); 230 (2); 218 (7); 205 (25).

(*B*) When the reaction mixture described above was boiled for 2 h, work-up according to procedure (*A*) gave 110 mg (46.6%) of **3n** and 20 mg (8.4%) of **3m**.

9,10-Dimethoxy-2-oxo-3,3-bis(2-methoxycarbonylethyl)-1,3,4,6,7,11bα-hexahydro-2H-benzo[a]quinolizine (3o)

The ketonitrile **3g** (0.50 g; 1.37 mmol) was refluxed in a mixture of methanol (4.7 ml) and *conc.* sulfuric acid (1.58 ml) for 6 h. After the usual work-up and recrystallization from methanol 0.14 g (28.8%) of **3o** was isolated, m.p. 128—130 °C.

IR(KBr): 2805, 2740 (Bohlmann bands), 1725 (ester CO), 1695 cm^{-1} (CO).

^{1}H—NMR ($CDCl_3$): 6.76, 6.66 (2H, s, aromatic), 3.99, 3.95 (6H, s, OCH_3), 3.82, 3.76 (6H, s, CO_2CH_3).

MS *m/e* (%): 433 (M^+, 32), 432 (30); 418 (6); 402 (30); 390 (28); 360 (25); 347 (25); 346 (22); 330 (5); 318 (7); 274 (100).

General prescription for the preparation of the alcohols 5a-f and 6a-f

To a stirred suspension of the appropriate ketonitrile (**3b—d, 3h—j**, 2.92 mmol) in methanol (15 ml) there gradually was added 0.12 g of sodium borohydride at 0 °C. After stirring at 0 °C for 30 min, the starting material dissolved and the alcohols **5a—f** began to separate.

Table XI

Physical data of the alcohols **5a—c** *and* **6a—c**

Compd.	M.p., °C	Yield, %	Formula[a]	IR(KBr) cm^{-1}	MS, *m/e* (M^+, %)
5a	160 234[b]	55	$C_{18}H_{24}N_2O_3$	3100 2310	316 (100)
6a	145 219[b]	23		3350 2300	316 (35)
5b	136 210[b]	67	$C_{20}H_{29}N_2O_3Cl$[b]	3100, 2770 2270	344 (75)
6b	204—206[b]	22		3200, 2800 2200	344 (30)
5c	185	68	$C_{17}H_{20}N_2O_3$	3510 2360	300 (85)
6c	136—138	9.0		3500 2360	300 (38)

[a] All compounds were analyzed for C, H and N; [b] Data of the hydrochlorides

3-[9,10-Dimethoxy- (**5a**), -diethoxy- (**5b**), and -methylenedioxy-2β-hydroxy-1,3,4,6,7,11bαH-hexahydro-2*H*-benzo[*a*]quinolizin-(3α)-yl]propionitrile (**5c**)

3-[9,10-Dimethoxy- (**6a**), -diethoxy- (**6b**), and -methylenedioxy-2α-hydroxy-1,3,4,6,7,11bαH-hexahydro-2*H*-benzo[*a*]quinolizin-(3α)-yl]propionitrile (**6c**).

The crystalline product (**5a—f**) was filtered off washed with methanol and water, and recrystallized from methanol. The pH of the methanolic mother liquor was adjusted to 7 with acetic acid, and the solvent was removed under reduced pressure. The residue was treated with 5% sodium hydrocarbonate (20 ml) and extracted with dichloromethane (3 × 10 ml). The combined extracts were washed with water, dried ($MgSO_4$), and evaporated to dryness in vacuum. Crystallization of the residue from methanol gave a further amount of the **5a—f** isomers. The isomers **6a—f** were isolated from the methanolic mother liquor by preparative TLC (silica gel, benzene-methanol 14 : 3, R_f **5a—f** > **6a—f**, elution with acetone), and recrystallized from methanol or purified as hydrochlorides. For physical data **5a—f** and **6a—f** see Tables XI and XII.

Table XII

Physical data of the alcohols **5d—f** *and* **6d—f**

Comp.	M.p. °C	Yield, %	Formula[a]	IR(KBr), cm^{-1}	MS, *m/e* (M^+, %)	^1H—NMR($CDCl_3$) δ(ppm)
5d	115 214[b]	60	$C_{19}H_{27}NO_5$	3400, 2750 1738	349 (23)	6.57, 6.66 (2 H, s, aromatic); 3.82 (9 H, s, CH_3O, CO_2CH_3).
6d	121	23		3450, 2760 1740	349 (20)	6.79, 6.71 (2 H, s, aromatic); 3.98 (6 H, s, OCH_3); 3.85 (3 H, s, CO_2CH_3).
5e	179[b]	58	$C_{21}H_{32}NO_5Cl$[b]	3400, 1740	377 (53)	6.72, 6.62 (2 H, s, aromatic); 4.09 (4 H, q, CH_2CH_3); 3.71 (3 H, s, CO_2CH_3); 1.47 (6 H, t, CH_2CH_3).
6e	210[b]	5		3320, 1740	377 (30)	6.70, 6.60 (2 H, s, aromatic); 5.04 (4 H, q, CH_2CH_3); 4.70 (3 H, s, CO_2CH_3); 1.43 (6 H, t, CH_2CH_3).
5f	163		$C_{18}H_{23}NO_5$	3200, 1710	333 (72)	
6f[c]						

[a] All compounds were analyzed for C, H and N. [b] Data of the hydrochlorides.
[c] Isolated as the *O*-acetyl derivative

Methyl [9,10-dimethoxy- (**5d**), -diethoxy- (**5e**) and -methylenedioxy-2β-hydroxy-1,3,4,6,7,11bαH-hexahydrobenzo[*a*]quinolizin-(3α)-yl]propionate (**5f**)

Methyl [9,10-dimethoxy- (**6d**), -diethoxy- (**6e**) and -methylenedioxy-2α-hydroxy-1,3,4,6,7,11bαH-hexahydrobenzo[*a*]quinolizin-(3α)-yl]propionate (**6f**)

General method of preparation of the O-acetyl derivatives 5g-l and 6g-l

(*A*) A mixture of the alcohols (**5a—f**, **6a—f**, 2.86 mmol), anhydrous pyridine (7.5 ml) and acetic anhydride (7.5 ml) was allowed to stand at room temperature for 24 h. The solvents were removed under reduced pressure, the residue was treated with water, and made alkaline with *conc.* ammonium hydroxide. The solid which separated was removed by filtration and washed with water. Crystallization from methanol gave compounds **5g—l** and **6g—l**. Physical data of these compounds are listed in Tables XIII and XIV.

(*B*) A stirred suspension of the ketones **3b—d** and **3h—j** (2.92 mmol) in methanol (15 ml) was treated with sodium borohydride (0.12 g), added in small portions at 0 °C. After a total reaction time of 30 min the reaction mixture was neutralized with acetic acid, and the

solvent was removed in vacuum. The residue was treated with 5% sodium hydrocarbonate (20 ml) and extracted with dichloromethane (3×15 ml). The organic layer was dried ($MgSO_4$) and evaporated to dryness in vacuum. The isomeric mixture of **5a—f** and **6a—f** was acetylated by procedure (*A*), and the crude products were recrystallized from methanol to yield the isomers **5g—l**. The methanolic mother liquor was separated by preparative TLC (silica gel, benzene-methanol 14 : 3, R_f **5g—l** > **6g—l**, elution with acetone) to give the isomers **6g—l**.

Isolation of the lactones 7a-b

A solution of **5d** or **5f** (0.20 g) in dichloromethane (5 ml) was allowed to stand at room temperature for 2 days. The solution was separated by preparative TLC (silica gel, benzene-methanol 14 : 3, R_f **7a** > **5d**; **7b** > **5f**, elution with acetone).

7a (63 mg; 35%), m.p. 198—200 °C (from methanol).

IR(KBr): 2800, 2750 (Bohlmann bands), 1730 cm^{-1} (lactone CO).

MS *m/e* (%): 317 (M^+, 21), 316 (83); 315 (92); 272 (26); 245 (20); 244 (29); 204 (98); 191 (100); 176 (33).

7b (72 mg, 40%), m.p. 215—216 °C (from methanol).

IR(KBr): 2780, 2750 (Bohlmann bands), 1710 cm^{-1} (lactone CO).

MS *m/e* (%): 301 (M^+, 90), 300 (100); 228 (21); 190 (83); 175 (89).

Table XIII

Physical data of the O-acetyl derivatives **5g—i** *and* **6g—i**

Comp.	M.p., °C	Yield, %	Formula[a]	IR(KBr) cm^{-1}	^1H—NMR($CDCl_3$) δ(ppm), width at half height (Hz)
5g	122 235[b]	95[c]	$C_{20}H_{26}N_2O_4$	2780, 2320 1750	6.74, 6.67 (2 H, s, aromatic); 5.15 (1 H, m, 24, CH—$OCOCH_3$); 4.14 (6 H, s, OCH_3); 2.12 (3 H, s, $OCOCH_3$).
6g	148	70[c]		2300, 1740	6.63 (2 H, s, aromatic); 5.27 (1 H, m, CH—$OCOCH_3$); 3.86 (6 H, s, CH_3); 2.15 (3 H, s, $OCOCH_3$).
5h	102 245[b]	67[c]		2720, 2300 1730	6.68, 6.64 (2 H, s, aromatic); 4.74 (1 H, m, 24, CH—$OCOCH_3$); 4.61 (4 H, q, CH_2CH_3).
6h	104	70[c]	$C_{22}H_{31}N_2O_4Cl$[b]	2300, 1725	6.53 (2 H, s, aromatic); 5.20 (1 H, m, 7.15, CH—$OCOCH_3$); 3.99 (4 H, q, 6.5, CH_2CH_3); 2.06 (3 H, s, $OCOCH_3$); 1.34 (6 H, t, CH_2CH_3).
5i	129 254[b]	88[c]		2750, 2220 1718	6.60, 6.52 (2 H, s, aromatic); 5.85 (2 H, s, —OCH_2O—); 4.66 (1 H, m, 24, CH—$OCOCH_3$); 2.09 (3 H, s, $OCOCH_3$).
6i	146	30[d]	$C_{19}H_{22}N_2O_4$	2750, 2260 1725	6.54 (2 H, s, aromatic); 5.86 (2 H, s,—OCH_2O—); 4.25 (1 H, m, 6.0, CH—$OCOCH_3$); 2.13 (3 H, s, $OCOCH_3$).

[a] All compounds were analyzed for C, H and N. [b] Data of the hydrochlorides.
[c] The product was prepared by method(*A*) [d] The product was prepared by method(*B*)

Table XIV

Physical data of the O-acetyl derivatives **5j—l** *and* **6j—l**

Compd.	M.p., °C	Yield, %	Formula[a]	IR(KBr), cm^{-1}	MS, *m/e* (M^+, %)	^1H—NMR($CDCl_3$) δ(ppm), width at half height (Hz)
5j	125 239[b]	35[d]		2750 1730	391 (17)	6.62 (2 H, s, aromatic); 4.70 (1 H, m, 24, CH—$OCOCH_3$); 3.66 (3 H, s, CO_2CH_3); 2.10 (3 H, s, $OCOCH_3$).
6j	241[b]	14[d]	$C_{21}H_{30}NO_6Cl$[b]	1740	391 (65)	6.70 (2 H, s, aromatic); 5.40 (1 H, m, 6.0, CH—$OCOCH_3$); 4.00 (6 H, s, OCH_3); 3.84 (3 H, s, CO_2CH_3); 2.16 (3 H, s, $OCOCH_3$).
5k	104 222[c]	31[d]		2750 1730	419 (57)	6.67, 6.66 (2 H, s, aromatic); 4.70 (1 H, m, 18, CH—$OCOCH_3$); 4.06 (4 H, q, $CH_2—CH_3$); 3.60 (3 H, s, CO_2CH_3); 2.15 (3 H, s, $OCOCH_3$); 1.47 (6 H, t, $CH_2—CH_3$).
6k	208[b]	10[d]	$C_{23}H_{34}NO_6Cl$[b]	1750	419 (58)	6.58 (2 H, s, aromatic); 5.24 (1 H, m, 6.0, CH—$OCOCH_3$); 4.04 (4 H, q, $CH_3—CH_3$); 3.70 (3 H, s, CO_2CH_3); 2.18 (3 H, s, $OCOCH_3$); 1.47 (6 H, t, $CH_2—CH_3$).
5l	163 218[b]	81[c]		1725	375 (20)	6.61, 6.53 (2 H, s, aromatic); 5.87 (2 H, s, $—OCH_2O—$); 4.69 (1 H, m, 24.4, CH—$OCOCH_3$); 3.68 (3 H, s, CO_2CH_3); 2.10 (3 H, s, $OCOCH_3$).
6l	150	16[d]	$C_{20}H_{25}NO_6$	1722	375 (15)	6.53, 6.50 (2 H, s, aromatic); 5.82 (2 H, s, $—OCH_2O—$); 5.21 (1 H, m, 7.15, CH—$OCOCH_3$); 3.63 (3 H, s, CO_2CH_3); 2.08 (3 H, s, $OCOCH_3$).

[a] All compounds were analyzed for C, H and N
[b] Data of the hydrochlorides
[c] The product was prepared by method (*A*)
[d] The product was prepared by method (*B*)

REFERENCES

[1] Szabó, L., Honty, K., Tőke, L., Tóth, I., Szántay, Cs.: Chem. Ber. **105,** 3215 (1972)
[2] Tőke, L., Gombos, Zs., Blaskó, G., Honty, K., Szabó, L., Szántay, Cs.: J. Org. Chem. **38,** 2501 (1973)
[3] Whittaker, N.: J. Chem. Soc. *(C)* **1969,** 85
[4] Beke, D., Szántay, Cs.: Chem. Ber. **95,** 2132 (1962)
[5] Stork, G., Brizzolara, A., Landesman, H., Szmuckovicz, J., Terrel, R.: J. Am. Chem. Soc. **85,** 207 (1963)

[6] SZABÓ, L., TÓTH, I., TŐKE, L., TAMÁS, J., SZÁNTAY, Cs.: Ann. **1977,** 642
[7] BAITZ-GÁCS, E., KAJTÁR-PEREDY, M., RADICS, L. R., TÓTH, I., SZABÓ, L., SZÁNTAY, Cs. (To be published)
[8] GRIBBLE, G. W., NELSON, R. B., JOHNSON, J. L., LEVY, G. C.: J. Org. Chem. **40,** 3720 (1975)
[9] USKOKOVIC, M., BRUDERER, H., von PLANTA, C., WILLIAMS, T., BROSSI, A.: J. Am. Chem. Soc. **86,** 3364 (1964)
[10] TOURWÉ, D., van BINST, G., KAMETANI, T.: Org. Magn. Reson. **9,** 341 (1977)
[11] KAMETANI, T., FUKUMOTO, K., IHARA, M., UJIIE, A., KOIZUMI, H.: J. Org. Chem. **40,** 3280 (1975)
[12] KAMETANI, T., UJIIE, A., IHARA, M., FUKUMOTO, K., KOIZUMI, H.: Heterocycles, **3,** 371 (1975)
[13] HUGHES, D. W., HOLLAND, H. L., MACLEAN, D. B.: Can. J. Chem. **54,** 2252 (1976)
[14] van BINST, G., TOURWÉ, D., DE COCK, E.: Org. Magn. Reson. **8,** 618 (1976)
[15] COSSAIS, F.: Synthèse de Nouveaux Heterocycles de la Famille des Benzo[a]quinolizidines, Thesis, Orleans, 1975
[16] Bantwal R. Pai, Kuppuswamy Nayarajan, Hoslett Suguna and Saukaran Natarajan, Heterocycles, **6,** 1377 (1977)

Lajos SZABÓ
Katalin NÓGRÁDI } H-1521 Budapest, Gellért tér 4.

István TÓTH
Csaba SZÁNTAY
Lajos RADICS } H-1025 Budapest, Pusztaszeri út 59—67.

Sándor VIRÁG
Erzsébet KANYÓ } H-1054 Budapest, Tó u. 1—5.

Acta Chimica Academiae Scientiarum Hungaricae, Tomus 100 (1—4), pp. 37—52 (1979)

SYNTHESIS OF 1-ARYL-1,4-DIHYDRO-2-CARBAMOYL-3(2*H*)-ISOQUINOLINONES AND THEIR REACTION WITH AMINES

A NEW METHOD FOR THE PREPARATION OF 2-{[α-(*N*'-PHENYLUREIDO)] BENZYL}PHENYLACETAMIDES

E. ZÁRA-KACZIÁN, G. DEÁK, L. HAZAI, K. GÁLL-ISTÓK and J. HASKÓ-BREUER

(*Institute of Experimental Medicine, Hungarian Academy of Sciences, Budapest*)

Received May 11, 1978
Accepted for publication July 19, 1978

In the course of studies on the substitution of 1-aryl-1,4-dihydro-3(2*H*)-isoquinolinones, synthesized first by the authors, it was found that *N*-carbamoyl derivatives can be prepared with isocyanates in good yields. It has been observed that 2-carbamoyl-1-phenyl-1,4-dihydro-3(2*H*)-isoquinolinones having the diacylamine structure can react with amines in two ways, depending on the conditions (Scheme 2, Table V): with sterically non-hindered primary amines the open-ring urea derivatives *3* are exclusively produced in good yields, whereas with secondary amines the side chain is split off.

Studies on the substitution reactions of 1-aryl-1,4-dihydro-3(2*H*)-isoquinolinones, synthesized first by us [1] and having a significant biological activity [2], revealed that the *N*-acyl derivatives can be prepared with the well-known acylating agents (acid chlorides, acid anhydrides) in satisfactory yields (see Table I). The compounds are, in general, sensitive to bases and decompose with the formation of the starting isoquinolinone on the effect of sodium hydroxide, sodium hydride; in certain cases, chromatographic purification on alumina layers has the same effect. The acyl group is also split off with amines; for example, when the 2-benzoyl derivative (4) was made to react with propylamine, the product of transacylation, *N*-propylbenzamide, could also be isolated in addition to the starting isoquinolinone. The 2-acetyl-1-(4'-aminophenyl)-4,4-dimethyl derivative that seemed to be interesting from the pharmacological point of view was prepared by acetylation of 4,4-dimethyl-1-(4'-nitrophenyl)-1,4-dihydro-3(2*H*)-isoquinolinone followed by catalytic hydrogenation of the nitro group.

In the following, the 2-alkyl-(and aryl)-carbamoyl derivatives of 1-aryl-1,4-dihydro-3(2*H*)-isoquinolinones were to be prepared for the purpose of biological examination. The syntheses of the compounds were realized by the reaction of the starting compound and the appropriate isocyanate (Scheme 1). The data of the 1-aryl-2-carbamoyl derivatives prepared are given in Tables II and III.

Table I

2-Acyl-1,4-dihydro-3(2H)-isoquinolinones

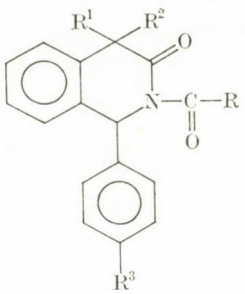

Compound	R^1	R^2	R^3	R	Method	Yield, %	M.p.[a] (recrystallization solvent)	Formula[d]
1	H	H	H	Me	*A*	66	123 °C (EtOH—Et_2O)	$C_{17}H_{15}NO_2$
2	Me	Me	H	Me	*A*	68	105 °C (L)[b]	$C_{19}H_{19}NO_2$
3	Me	Me	NO_2	Me	*A*	69	—[c]	
					B	98		$C_{18}H_{18}N_2O_4$
4	H	H	H	C_6H_5	*A*	35	171 °C	
					B	67		$C_{22}H_{17}NO_2$

[a] Uncorrected melting points, capillary tube method
[b] L : ligroin
[c] Oil ; its reduction gave a crystalline amino derivative
[d] All compounds were analyzed for C, H, N with results of at least 0.4% accuracy

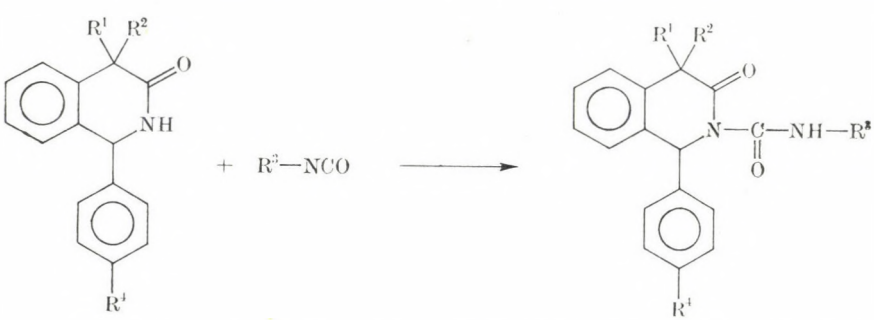

R^1=R^2=H or Me; R^3=Pr, Bu, hexyl, allyl, phenyl, *p*-NO_2-phenyl, *p*-OCH_3-phenyl, *p*-Cl-phenyl, cyclohexyl, α-naphthyl

Scheme 1

Kinetic measurements

Parallel to the preparative experiments, kinetic measurements were also made in order to get a picture of the rate ratios of the reactions taking place with the various isocyanates.

The measurements were carried out in chloroform free from water and alcohol, using carefully purified isocyanate compounds. The concentration of the isocyanate was determined on the basis of the intensity of the band characteristic of the isocyanate group in the IR spectrum at 2200—2300 cm^{-1}, since neither the solvent, nor the substrate and the end-product have absorption in

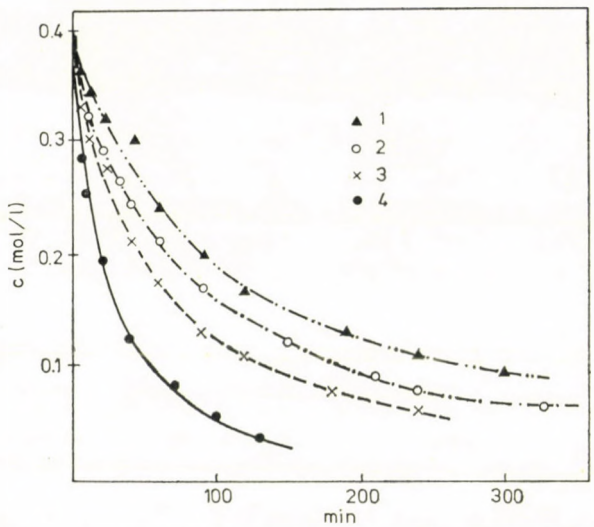

Fig. 1. Reaction of 1-phenyl-1,4-dihydro-3(2*H*)-isoquinolinone with equimolar amounts of aryl isocyanates in anhydrous chloroform at 61 °C. (1) *p*-methoxyphenyl isocyanate; (2) phenyl isocyanate; (3) *p*-chlorophenyl isocyanate; (4) *p*-nitrophenyl isocyanate

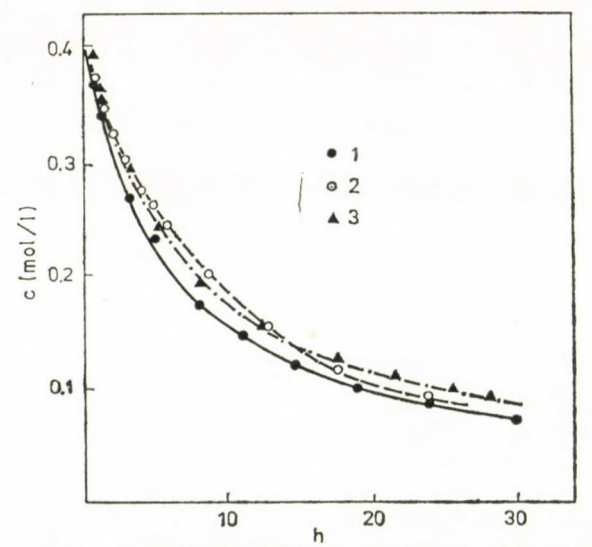

Fig. 2. Reaction of 1-phenyl-1,4-dihydro-3(2*H*)-isoquinolinone with equimolar amounts of alkyl isocyanates in anhydrous chloroform at 61 °C. (1) hexyl isocyanate; (2) cyclohexyl isocyanate; (3) propyl isocyanate

Table II

2-Carbamoyl-1,4-dihydro-3(2H)-isoqinolinones prepared from isocyanates and 1,4-dihydro-3(2H)-isoquinolinones

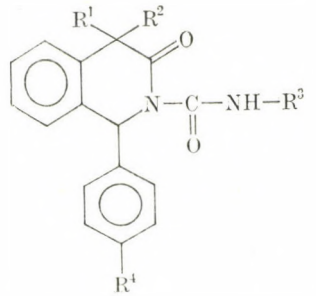

Compound	R^1	R^2	R^3	R^4	Solvent[a]	Yield, %	M.p.[b] (recrystallization solvent)[a]	IR[c] λ_{max} [cm^{-1}]	Method	Formula[f]
5	H	H	Pr	H	B	65	77 °C ($EtOH/H_2O$)	3300 (NH), 1695, 1665 (Amide I), 1530 (Amide II)	*A*	$C_{19}H_{20}N_2O_2$
6	H	H	Pr	NO_2	B	92	—[d]	3300 broad (NH), 1710, 1665, (Amide I), 1530 (Amide II)	*A*	$C_{19}H_{19}N_3O_4$
7	H	H	Bu	H	T	53	82 °C (EtOH)	3295 (NH), 1700, 1665 (Amide I) 1530 (Amide II)	*B*	$C_{20}H_{22}N_2O_2$
8	Me	Me	Bu	H	B	47	76 °C (P.e.)	3270 broad (NH), 1710, 1660 (Amide I), 1530 (Amide II)	*B*	$C_{22}H_{26}N_2O_2$
9	H	H	Bu	NO_2	B	63	—[e]		*B*	$C_{20}H_{21}N_3O_4$
10	Me	Me	Bu	NO_2	B	76	125 °C (EtOH)	3270 broad (NH), 1710, 1660 (Amide I), 1535 (Amide II), 1355 (symm. NO_2)	*B*	$C_{22}H_{25}N_3O_4$
11	H	H	Allyl	H	B	89	105 °C (EtOH)	3300 (NH), 1705, 1665 (Amide I), 1530 broad (Amide II)	*A*	$C_{19}H_{18}N_2O_2$
12	H	H	Allyl	NO_2	B	69	85 °C (MeOH)	3350—3450 broad, 3280 (NH) 1705, 1670 (Amide I), 1525 broad (Amide II), 1350 (symm. NO_2)	*A*	$C_{19}H_{17}N_3O_4$
13	H	H	C_6H_5	H	T	92	144 °C (MeOH)	3130, 3070 broad (NH), 1710, 1670 (Amide I), 1550 broad (Amide II)	*B*	$C_{22}H_{19}N_2O_2$

14	Me	Me	C_6H_5	H	T	68	137 °C (EtOH)	3220, 3185, 3060 broad (NH), 1710, 1670 (Amide I), 1550 (Amide II)	*B*	$C_{24}H_{22}N_2O_2$
15	H	H	C_6H_5	NO_2	T	56	176 °C (B, P.e.)	3000–3300 broad (NH), 1710, 1670 (Amide I), 1550 (Amide II), 1355 (symm. NO_2), 1525 (asymm. NO_2)	*B*	$C_{22}H_{17}N_3O_4$
16	Me	Me	C_6H_5	NO_2	T	40	134 °C (iPrOH)	3000–3300 broad (NH) 1710, 1655 (Amide I), 1550 (Amide II), 1355 (symm. NO_2), 1525 (asymm. NO_2)	*B*	$C_{24}H_{21}N_3O_4$
17	H	H	*p*-Cl–C_6H_4	H	T	69	126 °C (EtOH)	3300–3650 broad (NH) 1710, 1670 (Amide I), 1550 (Amide II)	*A*	$C_{22}H_{17}ClN_2O_2$
18	H	H	*p*-OMe–C_6H_4	H	T	69	158–160 °C (Ac)	3180, 3060 broad (NH), 1705, 1670 (Amide I), 1545 (Amide II), 1245 (C–O)	*A*	$C_{23}H_{20}N_2O_2$
19	H	H	*p*-NO_2–C_6H_4	H	T	71	163–165 °C (EtOH)	3060 (NH), 1715, 1670 (Amide I), 1555 (Amide II), 1340 (symm. NO_2)	*A*	$C_{22}H_{17}N_3O_4$
20	H	H	Hexyl	H	B	54	101 °C (MeOH)	3270 (NH), 1705, 1665 (Amide I), 1525 (Amide II)	*A*	$C_{22}H_{26}N_2O_2$
21	H	H	Cyclohexyl	H	B	48	57 °C (P. e.)	3380 (NH), 1705, 1665 (Amide I), 1520 (Amide II)	*A*	$C_{22}H_{24}N_2O_2$
22	H	H	α-Naphthyl	H	T	64	133 °C (EtOH)	3060 (NH), 1710, 1665 (Amide I), 1560 (Amide II), 1630 (C=C)	*B*	$C_{26}H_{20}N_2O_2$
23	Me	Me	α-Naphthyl	H	T	58	151 °C (EtOAc/P.e.)	3060 (NH) 1705, 1655 (Amide I), 1555 (Amide II)	*B*	$C_{28}H_{24}N_2O_2$
24	Me	Me	α-Naphthyl	NO_2	T	45	154 °C (EtOH)	3060 (NH), 1705, 1655 (Amide I), 1550 (Amide II), 1525 (symm. NO_2), 1355 (asymm. NO_2)	*B*	$C_{28}H_{23}N_3O_4$
25	H	H	α-Naphthyl	NO_2	T	41	160 °C (EtOH)	3060, 3250 (NH), 1720, 1670 (Amide I), 1530 (symm. NO_2), 1355 (assymm. NO_2), 1635 (C=C)	*B*	$C_{26}H_{19}N_3O_4$

[a] B, benzene; T, toluene; P.e., petroleum ether; Ac, acetone
[b] Uncorrected; capillary tube method
[c] The IR spectra were determined on a Perkin–Elmer 377 spectrometer (KBr pellets)
[d] Non-crystallizing foam, homogeneous in TLC
[e] Non-crystallizing oil, homogeneous in TLC
[f] See footnote d in Table I

Table III

1-Aminophenyl-2-carbamoyl-1,4-dihydro-3(2H)-isoquinolinones prepared by reduction of 2-carbamoyl-1-nitrophenyl-1,4-dihydro-3(2H)-isoquinolinones

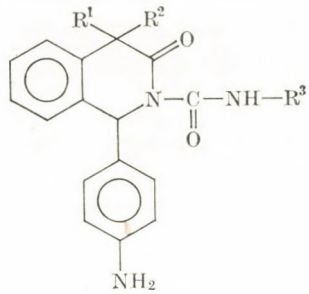

Compound	R^1	R^2	R^3	Yield, %	M.p.[a] (recrystallization solvent)	Formula[b]
26	H	H	Pr	49	91 °C (MeOH)	$C_{19}H_{21}N_3O_2$
27	H	H	Bu	50	98 °C (MeOH)	$C_{20}H_{23}N_3O_2$
28	Me	Me	Bu	60	122 °C (EtOH/H_2O)	$C_{22}H_{27}N_3O_2$
29	H	H	Allyl	49[c]	195 °C (EtOH)	$C_{19}H_{19}N_3O_2$
30	H	H	C_6H_5	55	182 °C (EtOH)	$C_{22}H_{19}N_3O_2$
31	Me	Me	C_6H_5	60	167 °C (EtOH)	$C_{24}H_{23}N_3O_2$
32	Me	Me	α-Naphthyl	36	180 °C (EtOAc)	$C_{28}H_{25}N_3O_2$
33	H	H	α-Naphthyl	55	152 °C (EtOH)	$C_{26}H_{21}N_3O_2$

[a] See footnote a in Table I; [b] See footnote d in Table I; [c] hydrochloride

Table IV

Half-life times of the reaction of isocyanates with 1-phenyl-1,4-dihydro-3(2H)-isoquinolinone in chloroform at 61 °C

Isocyanate	Half-life time, min
p-NO_2-phenyl-	18
p-Cl-phenyl-	47
Phenyl-	57
p-OMe-phenyl-	94
Cyclohexyl-	530
Hexyl-	375
Propyl-	490

this range. In the first step the log $I_0/I-c$ correlation was determined and this was used then as a calibration diagram. In Figs 1 and 2 the data obtained at the boiling point of chloroform with aryl and alkyl isocyanates, respectively, are given.

The half-life times of the the individual reactions are given in Table IV. It can be seen from the data that there is a significant difference in the rates of the reactions with aryl and alkyl isocyanates ; the half-life times lied along a straight line when plotted as a function of the Hammett σ constant, thus in the carbamoylation reactions with aromatic isocyanates the Hammett equation holds good.

Ring cleavage with amines

In the course of the experiments described above it was observed that on the effect of bases the carbamoyl group is split off from the nitrogen atom of the lactam ring, similarly to the acetyl group. When, however, one of the compounds prepared by us, the phenylcarbamoyl derivative **13** was allowed to react with propylamine, no detachment of the side chain was observed and the new compound *3* formed by cleavage of the lactam ring could be isolated in a satisfactory yield (Scheme 2).

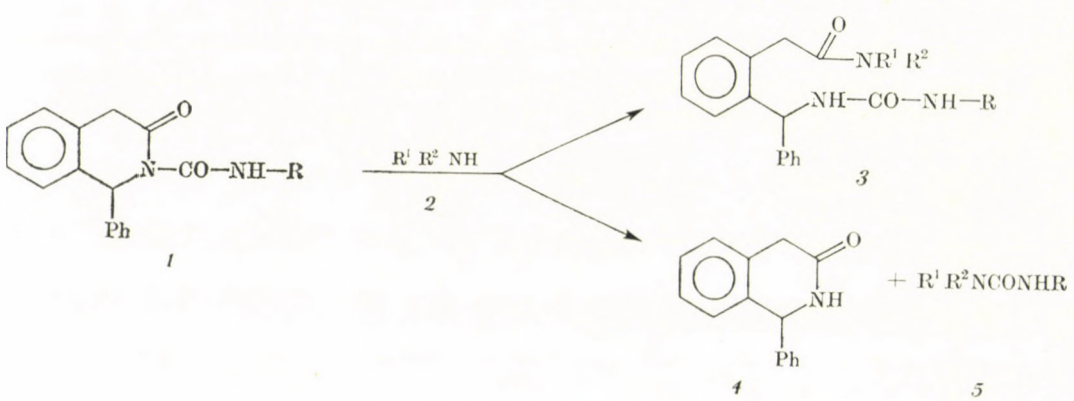

Scheme 2

It is known that cyclic triacylamines react either by cleavage of the ring or the acyl group is split off, depending on the structure of the compound ; the pertaining literature is well summarized in a recently published paper [3].

Since, according to the literature data, no such experiments have been effected on *N*-acyl lactams, it seemed to be of interest to establish whether in the carbamoyl derivatives prepared by us it is ring cleavage which takes place in every case, or detachment of the side chain can also occur, depending on the structure of the compound and the reagent (amine) and the reaction conditions.

Primarily the contingent role of the substituent at the nitrogen atom of the carbamoyl group (aryl or alkyl group) was to be elucidated, furthermore, possible differences in the reactions with primary and secondary amines were to be detected.

The carbamoyl derivative *1* (Scheme 2) was allowed to react with the amine *2* added in excess at the temperature given in Table V, usually until no

Table V

Reaction of 2-carbamoyl-1-phenyl-1,4-dihydro-3(2H)-isoquinolinones with amines (Scheme 2)

Starting *N*-Carbamoylisoquinolinone, *1*	Reagent amin *a2*		Reaction temp., °C	Products, % yield[a]		
R	R^1	R^2		*3*	*4*	*5*
Phenyl	H	H	25	78	—	—
Phenyl	Pr	H	50	85	—	—
Phenyl	$PhCH_2$	H	25	86	—	—
Phenyl	Me	Me	50	29	—[b]	46
Phenyl	Et	Et	100	—	92	98
Phenyl	Piperidine		100	—	—[b]	86
Phenyl	*t*-Bu	H	100	—	84	—
Phenyl[f]	Pr	H	50	—	75	—
p-Nitrophenyl	H	H	25	85	—	—
p-Nitrophenyl	Pr	H	50	55[c]	—	—
p-Nitrophenyl	$PhCH_2$	H	25	72	—	—
p-Chlorophenyl	H	H	60	48	—	—
p-Chlorophenyl	Pr	H	50	83	—	—
p-Chlorophenyl	$PhCH_2$	H	25	81	—	—
p-Methoxyphenyl	H	H	70	37[d]	—	—
p-Methoxyphenyl	Pr	H	50	65	—	—
p-Methoxyphenyl	$PhCH_2$	H	25	25[e]	—	—
Propyl	H	H	25	65	—	—
Propyl	Pr	H	50	33	—	—
Propyl	$PhCH_2$	H	100	28	45	—[b]
Propyl	Et	Et	100	—	67	46
Propyl	Piperidine		100	—	67	59

[a] Overall yield calculated for starting compound *1*
[b] Not isolated
[c] Crude product 77%
[d] Crude product 80%
[e] Crude product 74%
[f] 4,4-dimethyl derivative

unreacted starting material was found in the sample according to TLC. Product *3* separated from the solution and was filtered off. When detachment of the side chain also occurred as indicated by the TLC, the excess amine was evaporated in vacuum, the residue was separated by column chromatography and the individual fractions were purified by crystallization.

As shown by Table V, in the reactions effected with primary amines only the product of ring cleavage could be isolated, generally in satisfactory yields. In the reactions with 4'-nitro-, 4'-chloro- and 4'-metoxyphenylcarbamoyl derivatives the yield for the product of ring cleavage *3* was relatively lower owing to the significant loss during crystallization; products *4* and *5* could not be detected chromatographically in this case either. When the reagent was a secondary amine, there was hardly any (with dimethylamine) or no product of ring cleavage; the favoured process was the detachment of the side chain.

It is interesting to note that, while in the phenylcarbamoyl derivative **13** with benzylamine only ring cleavage took place, in the propylcarbamoyl derivative **5** the side chain was also split off. This was attributed first to the higher temperature of the reaction of the propylcarbamoyl derivative **5** at which the removal of the side chain can also take place. In order to check this assumption, the reaction of the phenylcarbamoyl derivative **13** with benzylamine was effected at 100 °C, too. It was observed that detachment of the side chain was an accompanying reaction at this temperature, thus the effect of temperature assumed seemed to be proved. The same result was obtained in the reaction of **13** with propylamine at 100 °C. It was striking, however, than in the course of the processing of the reaction mixture another substance could be isolated in pure state in addition to the corresponding isoquinolinone derivatives *3* and *4*, and this was found to be *N*-propyl-2-{[α-)*N*'-propylureido)]-benzyl}phenylacetamide (**48**). The formation of this substance can only be explained by a transamidation of the starting carbamoyl derivative or of the product of ring cleavage during the reaction. Since no change was observed in the *N*-phenylureido derivative **35** obtained in the reaction at 50 °C when heated in propylamine at 100 °C, it must be assumed that the transacylation takes place before the ring cleavage (Scheme 3).

The two-way reaction (ring cleavage and splitting off of the side chain) cannot be explained by the different basicities of the amines employed, since the difference is not significant. The fact, however, that ring cleavage practically cannot be achieved with secondary amines allows to conclude that steric hindrance must be considered. In the followings it was examined what kind of reaction takes place with tertiary butylamine being a primary amine but having a branched alkyl chain; the model compound was 1-phenyl-2-phenylcarbamoyl-1,4-dihydro-3(2*H*)-isoquinolinone (**13**). At the boiling point of tertiary butylamine no conversion could be detected after 5 h at 46 °C. The reaction was repeated under pressure at 100 °C; after refluxing for 7 h, the product of

Table VI

M.p. and IR spectral data of the 2-{[α-(N'-phenylureido)]benzyl}-phenylacetamides 3

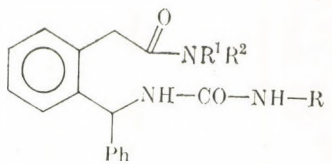

Compound	R	R^1	R^2	Formula[a]	M.p.[b] (recrystallization solvent)[c]	IR[d], cm^{-1}
34	Phenyl	H	H	$C_{22}H_{21}N_3O_2$	215—7 °C (MeOH)	3310 (NH), 3410, 3400, 3210 (NH, NH_2) 1660 (Amide I), 1615, 1548 (Amide II)
35	Phenyl	Pr	H	$C_{25}H_{27}N_3O_2$	202—4 °C	3290, 3330 (NH), 1645 (Amide I), 1555 (Amide II)
36	Phenyl	$PhCH_2$	H	$C_{29}H_{27}N_3O_2$	218—9 °C ($MeOH/H_2O$)	3290 broad (NH), 3350 (sh), 1652, 1642 (Amide I), 1555 (Amide II)
37	Phenyl	Me	Me	$C_{24}H_{25}N_3O_2$	217—8 °C (MeOH)	3325, 3285 (NH), 1695, 1625 (Amide I), 1555 (Amide II)
38	*p*-Nitrophenyl	H	H	$C_{22}H_{20}N_4O_4$	232 °C (n-BuOH)	3295, 3340, 3440 (NH), 1680, 1650, 1615 (Amide I), 1540, 1565 (Amide II) 1335 (symm. NO_2), 1515 (asymm. NO_2)
39	*p*-Nitrophenyl	Pr	H	$C_{25}H_{26}N_4O_4$	197 °C (MeOH)	3300, 3350, 3410 (NH), 1655, 1645 (Amide I), 1560 (Amide II), 1350 (symm. NO_2), 1510 (asymm. NO_2)
40	*p*-Nitrophenyl	$PhCH_2$	H	$C_{29}H_{26}N_4O_4$	206 °C (MeOH)	3275, 3340, 3410 (NH), 1660, 1640 (Amide I), 1555 broad (Amide II), 1350 (symm. NO_2), 1505/1510 (asymm. NO_2)
41	*p*-Chlorophenyl	H	H	$C_{22}H_{20}ClN_3O_2$	235 °C (n-BuOH)	3340, 3370 (NH), 1665, 1645 (Amide I), 1625, 1555 (Amide II)
42	*p*-Chlorophenyl	Pr	H	$C_{25}H_{26}ClN_3O_2$	240 °C (n-BuOH)	3290, 3350 (NH), 1645, 1655 (Amide I), 1555 broad (Amide II)

43	*p*-Chlorophenyl	$PhCH_2$	H	$C_{29}H_{26}ClN_3O_2$	221 °C (n-BuOH)	3370, 3300 (NH), 1640, 1655 (Amide I), 1555 broad (Amide II)
44	*p*-Methoxyphenyl	H	H	$C_{23}H_{23}N_3O_2$	219 °C (n-BuOH)	3330, 3195 (NH), 1685, 1665, 1640 (Amide I), 1560 broad (Amide II), 1240 (C—O)
45	*p*-Methoxyphenyl	Pr	H	$C_{26}H_{29}N_3O_3$	210 °C (MeOH)	3290 broad, 3345 (NH), 1645 (Amide I), 1560 (Amide II), 1245 (C—O)
46	*p*-Methoxyphenyl	$PhCH_2$	H	$C_{30}H_{29}N_3O_3$	235 °C (n-BuOH)	3280, 3320 (NH), 1645 (Amide I), 1555 (Amide II), 1240 (C—O)
47	Propyl	H	H	$C_{19}N_{23}N_3O_2$	194—5 °C (MeOH/P.e.)	3310, 3480, 3370, 3200, 3180 (NH), 1630, 1610 (Amide I), 1565 (Amide II)
48	Propyl	Pr	H	$C_{22}H_{29}N_3O_2$	184—5 °C ($MeOH—H_2O$	3285, 3325, 3355 (NH), 1655, 1645, 1625 (Amide I) 1565 (Amide II)
49	Propyl	$PhCH_2$	H	$C_{26}H_{29}N_3O_2$	175 °C (MeOH)	3270, 3310, 3350 (NH), 1645, 1630 (Amide I), 1565 (Amide II)

[a] See footnote d in Table I
[b] See footnote a in Table I
[c] See footnote a in Table II
[d] See footnote c in Table II

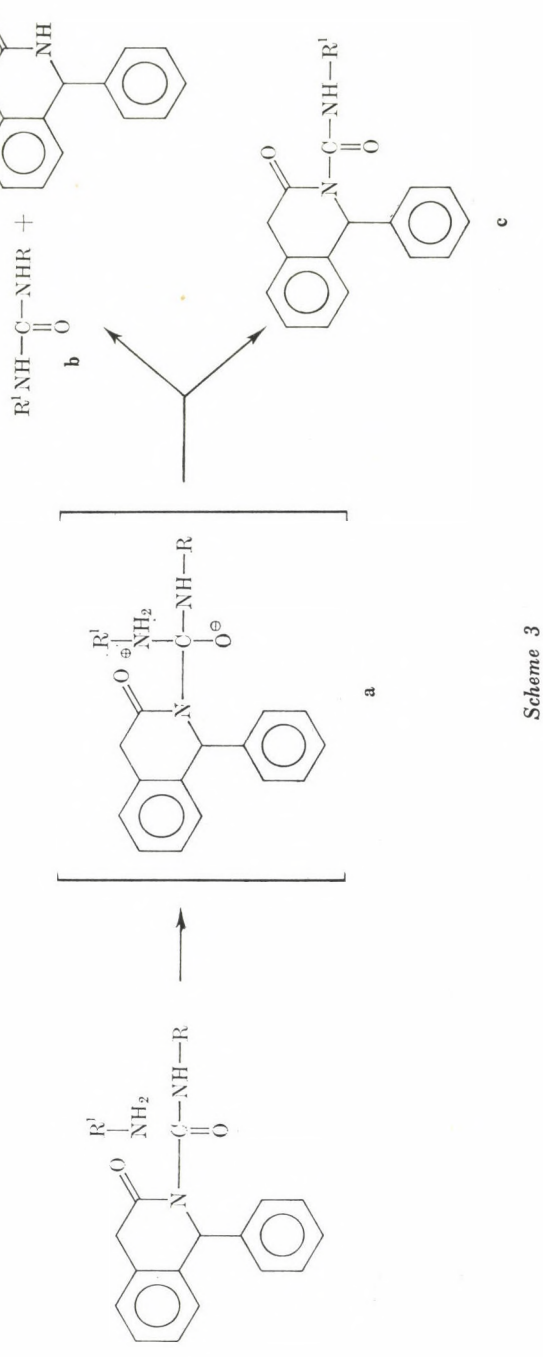

Scheme 3

the splitting, 1-phenyl-1,4-dihydro-3(2*H*)-isoquinolinone, was isolated in 84% yield, while no ring cleavage was observed. In order to elucidate the role of steric hindrance, further experiments were carried out with the 4,4-dimethyl derivative of 1-phenyl-2-phenylcarbamoyl-1,4-dihydro-3(2*H*)-isoquinolinone with propylamine at the boiling point of the amine. It was found that no product of ring cleavage was formed, only the splitting off of the side chain took place and the corresponding isoquinolinone derivative could be isolated in 75% yield.

On the basis of the experimental data, the dependence of the direction of the multidirection transamidation reaction on the structure of the reagent and the substrate can be explained as follows. The amine can exert a nucleophilic attack at the carbon atom of the carbonyl group in the lactam ring or the carbonyl group in the side chain. In the latter case (Scheme 3) either 1-phenyl-1,4-dihydro-3(2*H*)-isoquinolinone and the urea derivative **b** are formed, or, at elevated temperatures, a new carbamoylisoquinolinone derivative, **c**, is obtained, and the latter will react further with ring cleavage as shown in Scheme 2.

The various reaction paths have different activation energies, those involving the side chain are probably higher. Therefore, when the ring cleavage reaction is slow owing to steric hindrance due to the structure of the reagent or the substrate and thus a higher temperature is applied, the reaction in the side chain becomes favoured.

Ring cleavage reactions were also effected with hydroxylamine and hydrazine, and the corresponding hydrazides and hydroxamic acids were isolated in satisfactory yields. These compounds may serve as starting materials in the preparation of new heterocyclic compounds.

Experimental

Kinetic measurements

(a) *Construction of the calibration plot*

About 4 mmoles of the individual isocyanates were measured into 10-ml volumetric flasks and the contents were made up to the mark with chloroform free from water and alcohol. A dilution series was prepared from the stock solution (the maximum dilution was 40-fold), then the spectra of the individual samples were recorded in the 2000—2500 cm^{-1} range in KBr cells of 0.065 mm thickness using the solvent in a cell of identical thickness as a reference. The instrument used was a Perkin—Elmer 377 spectrophotometer. The log I_0/I value was determined for the band characteristic of isocyanate and plotted as a function of the concentration of isocyanate, then the calibration diagram was constructed and used in the measurements.

(b) *Measurements*

About 20 mmoles of 1-phenyl-1,4-dihydro-3(2*H*)-isoquinolinone and an equimolar amount of isocyanate were measured into a 50-ml volumetric flask, then it was made up to the mark with chloroform free from alcohol and water. Now the solution was transferred into a round-bottomed flask, equipped with a reflux condenser and protected against atmospheric moisture with a tube filled with $CaCl_2$, and heated to boil. The samples withdrawn at

given intervals were diluted as necessary and the IR spectra were recorded in the 2000—2500 cm^{-1} range as given under (a). The actual concentration of isocyanate was determined by means of the calibration diagram.

General methods for the acylation of 1-aryl-1,4-dihydro-3(2*H*)-isoquinolinones

Method A

2-Acetyl-1-phenyl-1,4-dihydro-3(2*H*)-isoquinolinone (1)

1-Phenyl-1,4-dihydro-3(2*H*)-isoquinolinone (11.15 g; 0.05 mole) was dissolved in acetic anhydride (100 ml); anhydrous sodium acetate (4.1 g; 0.05 mole) was added, and the mixture was refluxed for 1 h. The solvent was then evaporated in vacuum. The residue was an oily substance starting to solidify; it was converted into a powder by rubbing with petroleum ether (150 ml). The precipitate was filtered off, traces of the anhydride were washed with petroleum ether and water was used to remove traces of sodium acetate. After drying a pink powder was obtained, which was crystallized from a mixture of ethanol and ether to obtain a white crystalline substance (8.7 g; 66%), m.p. 123 °C.

Method B

2-Benzoyl-1-phenyl-1,4-dihydro-3(2*H*)-isoquinolinone (4)

1-Phenyl-1,4-dihydro-3(2*H*)-isoquinolinone (2.23 g; 0.01 mole) was dissolved in anhydrous pyridine (25 ml); the pale yellow, clear solution was mixed with benzoyl chloride (1.68 g; 0.011 mole) at room temperature, heated to 50 °C and stirred at this temperature for 24 h. The solution was then poured into ice-water (100 ml) whereupon an oily substance separated. The pH was adjusted to 6.0—6.5 with 20% hydrochloric acid, the oil which separated was dissolved in ether (100 ml) and the solution was extracted with further amounts of ether (2×20 ml). The reddish-yellow ethereal extract was clarified with carbon to obtain a pale yellow solution which was dried and the ether removed in vacuum. The yellowish residue was rubbed with a mixture of ether and petroleum ether (1 : 1), cooled and filtered to give a colourless product (2.2 g; 67%), m.p. 171 °C.

2-Acetyl-1-(4'-aminophenyl)-4,4-dimethyl-1,4-dihydro-3(2*H*)-isoquinolinone

2-Acetyl-4,4-dimethyl-1-(4'-nitrophenyl)-1,4-dihydro-3(2*H*)-isoquinolinone (4.6 g; 0.013 mole) was dissolved in 99.5% acetic acid (300 ml) and it was hydrogenated in the presence of 10% Pd/C catalyst (1 g) at atmospheric pressure until the calculated amount of hydrogen had been absorbed. The catalyst was filtered off, the filtrate evaporated in vacuum and the residue rubbed with water (100 ml). The resulting solid was filtered off and washed with water (6×50 ml). The crude product was recrystallized twice from 50% aqueous ethanol to give a colourless crystalline substance (3.1 g; 75%), m.p. 172 °C.

$C_{19}H_{20}N_2O_2$. Calcd. C 74.00; H 6.54; N 9.08. Found C 74.30; H 6.80; N 9.30%.

General methods for the synthesis of 2-carbamoyl-1,4-dihydro-3(2*H*)-isoquinolinones

Method A

1-Phenyl-2-propylcarbamoyl-1,4-dihydro-3(2*H*)-isoquinolinone (5)

1-Phenyl-1,4-dihydro-3(2*H*)-isoquinolinone (4.5 g; 0.02 mole) was dissolved, with stirring, in anhydrous benzene (50 ml); propyl isocyanate (1.9 g; 0.022 mole) was added and the mixture was refluxed for 16 h. The solution was concentrated to 20 ml in vacuum, then transferred onto a column prepared from silica gel (10 g) and eluted with benzene (200 ml). The eluate was evaporated in vacuum and the crude product was twice recrystallized from 40% aqueous ethanol (400 ml) to obtain a pure substance (4.0 g; 65%), m.p. 77 °C.

Method B

2-Butylcarbamoyl-1-phenyl-1,4-dihydro-3(2*H*)-isoquinolinone (7)

1-Phenyl-1,4-dihydro-3(2*H*)-isoquinolinone (4.5 g; 0.02 mole) was dissolved, with stirring, in anhydrous toluene (50 ml) butyl isocyanate (2.0 g; 0.02 mole) was added, and the

mixture was refluxed for 16 h. The solvent was evaporated in vacuum, the oily residue was rubbed with petroleum ether (50 ml), the solid filtered off and the product was recrystallized twice from ethanol (30 ml). A pure substance (3.4 g; 53%) was obtained, m.p. 82 °C.

General method for the preparation of 1-(4'-aminophenyl)-2-alkyl(aryl)carbamoyl-3(2*H*)-isoquinolinones

1-(4'-Aminophenyl)-2-propylcarbamoyl-3(2*H*)-isoquinolinone (26)

1-(4'-Nitrophenyl)-2-propylcarbamoyl-3(2*H*)-isoquinolinone (10.3 g; 0.03 mole) was dissolved in 99.5% acetic acid (300 ml) and hydrogenated in the presence of prehydrogenated Pd/C catalyst (2 g) at room temperature under atmospheric pressure until the calculated amount of hydrogen had been absorbed. The catalyst was then filtered off, the solution was evaporated, the residue was triturated with water (3×500 ml) and dissolved in chloroform (3×100 ml). The chloroform solution was clarified then evaporated in vacuum at room temperature and the residual oil (8.5 g) was dissolved in chloroform (10 ml). This solution was subjected to chromatographic separation on a column prepared with silica gel (30 g) in carbon tetrachloride; the eluting agent was chloroform (400 ml). The solvent was then evaporated and the residue recrystallized first from a mixture of ethanol (50 ml) and water (5 ml), then from 90% aqueous methanol (50 ml). A pure substance (4.6 g; 49%) was obtained, m.p. 91 °C.

2-Allylcarbamoyl-1-(4'-aminophenyl)-1,4-dihydro-3(2*H*)-isoquinolinone (29)

2-Allylcarbamoyl-1-(4'-nitrophenyl)-1,4-dihydro-3(2*H*)-isoquinolinone (4.0 g; 0.011 mole) was dissolved on 99.5% acetic acid (60 ml). Powdered iron (5 g) was added, and the solution was stirred at room temperature for 7 h. The precipitate was filtered off and washed with acetic acid (3×30 ml). The filtrate was diluted with water (600 ml) and extracted with chloroform (5×100 ml). The chloroform solution was dried over anhydrous sodium sulfate and the solvent evaporated. The residual brown oil (4 g) was dissolved in benzene (40 ml), transferred to a column prepared with silicagel (25 g) in carbon tetrachloride. Elution was effected with benzene (1000 ml), a mixture of benzene and chloroform (500 ml, 1 : 1), and finally with chloroform (1000 ml). The solvent was evaporated from each fraction, and the residual oils were converted into the hydrochlorides separately in alcohol solutions with ether containing hydrochloric acid. The salts were recrystallized from ethanol and the pure substances were combined to obtain a white powder (2.0 g; 49.0%), m.p. 195 °C.

General method for the synthesis of *N*-alkyl-2-{[α-(*N*'-aryl- or alkylureido)]benzyl}phenylacetamides

2-{[α-(*N*'-phenylureido)]benzyl}phenylacetamide (34)

1-Phenyl-2-phenylcarbamoyl-1,4-dihydro-3(2*H*)-isoquinolinone (1.71 g; 0.005 and ammoniacal methanol (60 ml) (22.5 g of NH_3 in 100 ml of methanol) were allowed to react in a bomb tube at room temperature for 5 days. The crystals which separated were filtered off and recrystallized from methanol (90 ml). The pure product (1.0 g; 56%) had m.p. 215—217 °C.

N-benzyl-2-{[α-(*N*'-propylureido)]benzyl}phenyl-acetamide (49)

1-Phenyl-2-propylcarbamoyl-1,4-dihydro-3(2*H*)-isoquinolinone (0.616 g; 0.002 mole) was dissolved in benzylamine (6.42 g; 6.54 ml; 0.06 mole) in a bomb tube and the reaction was allowed to proceed for 10 h at 100 °C. When the homogeneous solution was cooled, a crystalline substance separated; this was filtered off and washed with petroleum ether. Addition of petroleum ether (20 ml) to the filtrate caused the separation of additional amounts of the substance. The combined crude product was crystallized from a mixture of methanol and petroleum ether (25 ml). A pure substance (0.35 g; 28%) was obtained, m.p. 175 °C.

Reaction of 1-phenyl-2-phenylcarbamoyl-1,4-dihydro-3(2*H*)-isoquinolinone with hydroxylamine: preparation of 2-{[α-(*N*'-phenylureido)]benzyl}phenylacetohydroxamic acid

Metallic sodium (2.0 g; 0.08 mole) was added to anhydrous methanol (40 ml) with cooling, then a solution of powdered hydroxylamine hydrochloride (6.1 g; 0.088 mole) in hot water (2.1 ml) was added dropwise, with stirring. Stirring was continued for 20 min. The solution

was then cooled to 0 °C, the deposit of sodium chloride was filtered off, washed with anhydrous methanol (40 ml) and the methanolic filtrate and the washing liquid were combined; it contained 0.08 mole of hydroxylamine base. Now 1-phenyl-2-phenylcarbamoyl-1,4-dihydro-3(2*H*)-isoquinolinone (1 g; 0.03 mole) was dissolved in the solution and it was heated at 60 °C for 2 h. The pale yellow solution was then evaporated and the residue rubbed with ethanol (20 ml). It was filtered, the filtrate was evaporated again and the residue was dissolved in hot ethanol (12 ml). The precipitate obtained on cooling was filtered off, and the filtrate was evaporated to give the crude product (0,7 g; 65%). This was crystallized from 50% ethanol (10 ml) to obtain the pure product (0.45 g; 42%), m.p. 168 °C.

$C_{22}H_{21}N_3O_3$. Calcd. C 70.38; H 5.78; N 11;19. Found C 70.39; H 5.92; N 11.08%.

IR: 3300 s (νOH + νNH); 3230 m, broad (νNH); 1640 s, broad (Amide I); 1555/60 s broad (Amide II).

Reaction of 1-phenyl-2-phenylcarbamoyl-1,4-dihydro-3(2*H*)-isoquinolinone with hydrazine hydrate: preparation of 2-{[α-(*N*'-phenylureido)]benzyl}phenylacetohydrazide

1-Phenyl-2-phenylcarbamoyl-1,4-dihydro-3(2*H*)-isoquinolinone (0.68 g; 0.002 mole) and hydrazine hydrate (3 g; 0.06 mole) were heated in butanol (25 ml) at 50 °C for 2 h. On cooling the solution a solid deposited (0.6 g; 80%; m.p. 214 °C), which was recrystallized from butanol (30 ml) to give the pure product (0.4 g; 53%), m.p. 214 °C (d).

$C_{22}H_{22}N_4O_2$. Calcd. C 70.57; H 5.92; N 14.96. Found C 70.30; H 6.23; N 14.94%.

IR: 3290 s, 3330 m, 3360 m triplet (NH); 1660 vs, 1645 s, 1620 m (Amide I); 1550 s (Amide II).

Reaction of 1-phenyl-2-phenylcarbamoyl-1,4-dihydro-3(2*H*)-isoquinolinone with propylamine at an elevated temperature

1-Phenyl-2-phenylcarbamoyl-1,4-dihydro-3(2*H*)-isoquinolinone (2.72 g; 0.008 mole) was dissolved in propylamine (14.2 g; 0.024 mole) and the reaction was allowed to proceed in a bomb tube at 100 °C for 7 h. The cooled solution was evaporated in vacuum, and the residue was washed with petroleum ether (5×10 ml) and ether (2×10 ml). The crude product (1.65 g) contained mainly 1-phenyl-1,4-dihydro-3(2*H*)-isoquinolinone (68%) and a small amount (15%) of *N*-propyl-2-{[α-(*N*'-propylureido)]-benzyl}phenylacetamide (**48**), according to TLC analysis and IR spectroscopic measurements. The crude product was repeatedly recrystallized from ethyl acetate and finally from 40% aqueous methanol to yield a pure substance (**48**) (0.15 g; 5%), m.p. 181—182.5 °C. The combined mother liquor was evaporated in vacuum, the residue (0.9 g) was dissolved in benzene (10 ml), transferred onto a column prepared from Brockman II aluminium oxide and eluted with 1 : 1 benzene : chloroform (150 ml). The eluate was evaporated in vacuum and the product was washed with ether; pure 1-phenyl-1,4-dihydro-3(2*H*)-isoquinolinone was thus obtained in a yield of 40%, m.p. 164 °C.

*

We are indebted to Mrs. M. Horváth-Gál and Mr. L. Pongó for their assistance in the investigations and to Miss M. Fodor for the microanalyses.

REFERENCES

[1] Deák, Gy., Gáll-Istók, K., Hazai, L., Sterk, L.: Synthesis, **1975**, 393
[2] Deák, Gy., Dóda, M., György, L., Hazai, L., Sterk, L.: J. Med. Chem. **20**, 1384 (1977)
[3] Takács, K., Harsányi, K., Simay, A.: Acta Chim. Hung. Acad. Sci. **93**, 183 (1977)

Erzsébet Zára-Kaczián
Gyula Deák
László Hazai
Klára Gáll-Istók
Judit Haskó-Breuer

H-1450 Budapest, P.O. Box 67.

Acta Chimica Academiae Scientiarum Hungaricae, Tomus 100 (1—4), pp. 53—67 (1979)

АВТОМАТИИЗИРОВАННАЯ СИСТЕМА ПРОГРАММ ДЛЯ ИССЛЕДОВАНИЯ МЕХАИИЗМА ГОМОГЕННЫЙ ГАЗОВЫХ РЕАКЦИЙ

П. БЕНЕДЕК

(Vegyipari Számítástechnikai Fejlesztési Társulás, Budapest)

Поступила в редакцию 17 мая 1978 г.

Принята к печати 21 июня 1978 г.

Сделана попытка проанализировать рассуждения химика, проводимые им при изучении механизма гомогенных газовых реакций. Суть вопроса состоит в том, дает-ли анализ, проведенный химиком, возможность описать эти рассуждения в блочной схеме при изучении механизма реакций и, если да, то возможно-ли составить на этой базе такую программу, с помощью которой можно однозначно определить механизм гомогенных газовых реакций. Если и последнее возможно, то эту программу можно рассмотреть как запрограммированное мышление.

Первоначально предполагаем, что интуиция не играет основную роль в определении механизма, то есть не играет такую роль, без которой не возможно определить механизм.

Наш подход заключается в том, что берем одну публикацию, занимающуюся изучением гомогенных газовых реакций [1] и подвегаем её анализу. В данной статье рассматривается высокотемпературное окисление метана в изотермных — изохорных условиях. Выбор данной статьи объясняется и тем, что для автора эта реакция не является новой [2, 3].

Опытные наблюдения

Изучение механизма реакции начинается с опытом работы. Данные одного опыта Катоне и Джемса приведены на рис. 1. Из рисунка видно, что максимальная скорость окисления метана отмечается на интервале 20—30 сек., что хорошо видно и на рис 2. Увеличение скорости при изотермных условиях означает, что можно расчитывать на появление в механизме разветвлений. На рис. 3 сравнены четыре опыта в системе координат время — скорость. Во всех четырех опытах суммарное давление (обеспеченное добавлением азота) одинаково при различных соотношениях метана — кислорода. Видно, что увеличение соотношение метана — кислорода препятствует увеличению скорости реакции, то есть метан замораживает реакцию. В других, не приведен-

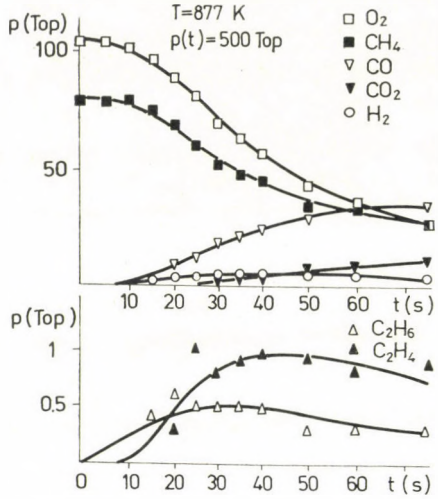

Рис. 1. Данные одного опыта Катоне и Ждемса

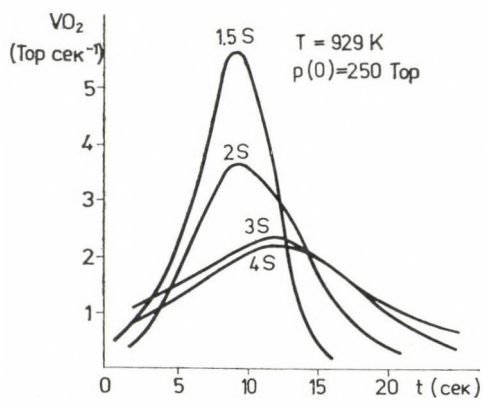

Рис. 2. Скорость увеличения при различных компонентах

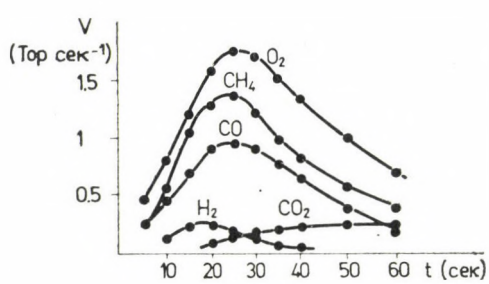

Рис. 3. Скорость реакции при различных соотношениях метана — кислорода

ных здесь, исследованиях авторов определено, что увеличение суммарного давления также уменьшает скорость реакции. Необходимо отметить, что вышеуказанные явления (уменьшение скорости реакций) происходит при температуре свыше 700°C. А при температуре ниже 650°C наблыдаются как раз противоположные явления. Первая часть статьи Катоне и Джемса заканчивается изложением опытных наблюдений.

Ход размышления кинетиков

Во второй части авторы пытаются на основе механизма реакции объяснить опытные наблюдения. Ход размышлений авторов показан на рис. 4, где в отдельных блоках приведены без изменения ссылки из сообщения авторов.

СТАРТ в этот раз означает получение вышерассмотренных опытных данных.

В первом блоке выражение «схема реакций» проблематично. Под «схемой реакций» авторы понимают раекции, перечисленные в таблице I. Эти реакции

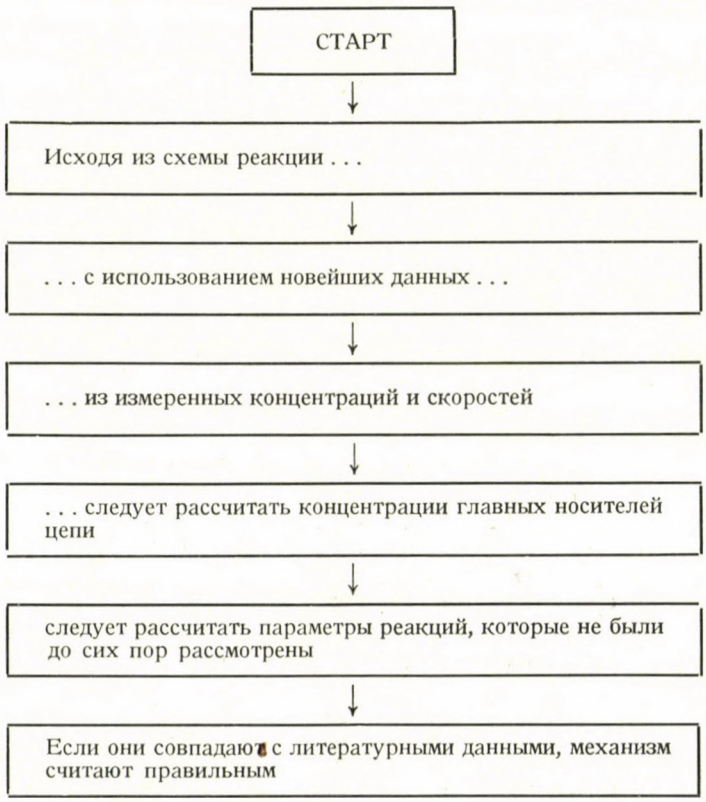

Рис. 4. Ход размышления кинетиков

Таблица I

№	Реакция	k_1 CH^3моль сек$^{-1}$	E_1 ккал моль$^{-1}$
1	$CH_4 + O_2 \rightarrow CH_3 + HO_2$		
2	$CH_4 + OH \rightarrow CH_3 + H_2O$	$3.31 \cdot 10^{13}$	3.77
3	$CH_4 + HO_2 \rightarrow CH_3 + H_2O_2$		
4	$CH_4 + H \rightarrow CH_3 + OH_2$	$6.9 \cdot 10^{13}$	11.8
5	$CH_4 + O \rightarrow CH_3 + OH$	$2.19 \cdot 10^{13}$	8.86
6	$CH_3 + O_2 \rightarrow CH_2O + OH$		
7	$CH_3 + H_2 \rightarrow CH_4 + H$	$1.5 \cdot 10^{13}$	15.5
8	$CH_2O + OH \rightarrow HCO + H_2O$		
9	$CH_2O + HO_2 \rightarrow HCO + H_2O_2$	10^{12}	10.7
10	$CH_2O + H \rightarrow HCO + H_2$	$2 \cdot 10^{13}$	3,3
11	$CH_2O + O \rightarrow HCO + OH$	10^{14}	3.3
12	$CH_2O + CH_3 \rightarrow HCO + CH_4$	$1.15 \cdot 10^{11}$	6.21
13	$CH_2 + O_2 \rightarrow HCO + HO_2$	$2.04 \cdot 10^{13}$	38.9
14	$H_2O_2 + M \rightarrow 2OH + M$	$1.2 \cdot 10^{17}$	45.5
14 bis	$H_2O_2 \rightarrow H_2O + {}^1/_2O_2$		
15	$H_2O_2 + OH \rightarrow H_2O + HO_2$	10^{13}	1.8
16	$H_2O_2 + H \rightarrow H_2O + OH$	$2.2 \cdot 10^{15}$	11.8
17	$H_2O_2 + H \rightarrow H_2 + HO_2$	$1.7 \cdot 10^{12}$	3.8
18	$H_2O_2 + CH_3 \rightarrow CH_4 + HO_2$		
19	$HCO + O_2 \rightarrow CO + HO_2$		
20	$HCO + M \rightarrow H + CO + M$		
21	$CO + OH \rightarrow CO_2 + H$	10^{12}	3.7
22	$CO + HO_2 \rightarrow CO_2 + OH$	10^{14}	23
23	$H_2 + OH \rightarrow H_2O + H$	$2.2 \cdot 10^{13}$	5.17
24	$H_2 + HO_2 \rightarrow H_2O_2 + H$	$7.3 \cdot 10^{11}$	18.7
25	$H_2 + O \rightarrow OH + H$	$1.8 \cdot 10^{10} \cdot I$	8.9
26	$H + O_2 \rightarrow OH + O$	$2.2 \cdot 10^{14}$	16.8
27	$H + O_2 \rightarrow M \rightarrow HO_2 + M$	$1.5 \cdot 10^{15}$(*)	−1
28	$H + H_2O \rightarrow H_2 + OH$	$9.3 \cdot 10^{13}$	20.36
29	$O + H_2O \rightarrow 2OH$	$6.8 \cdot 10^{13}$	18.35
30	$H + CO + M \rightarrow HCO + M$		
31	$HO_2 + HO_2 \rightarrow H_2O_2 + O_2$	$2 \cdot 10^{12}$	0
32	$H + HO_2 \rightarrow 2OH$	$2.5 \cdot 10^{14}$	1.9
33	$CH_3 + CH_3 \rightarrow C_2H_6$	$2.6 \cdot 10^{13}$	0
34	$C_2H_6 + OH \rightarrow C_2H_5 + H_2O$	$8.7 \cdot 10^{13}$	3.52
35	$C_2H_6 + HO_2 \rightarrow C_2H_5 + H_2O_2$	$1.5 \cdot 10^{13}$	16.6
36	$C_2H_6 + H \rightarrow C_2H_5 + H_2$	$1.32 \cdot 10^{14}$	9.7
37	$C_2H_6 + O \rightarrow C_2H_5 + OH$	$4 \cdot 10^{13}$	6.55
38	$C_2H_6 + CH_3 \rightarrow C_2H_5 + CH_4$	$5 \cdot 10^{14}$	21.5
39	$C_2H_5 + O_2 \rightarrow C_2H_4 + HO_2$	$3.17 \cdot 10^{12}$	5
40	$C_2H_5 + H_2 \rightarrow C_2H_6 + H$	$6.4 \cdot 10^{12}$	14.1
41	$C_2H_5 \rightarrow C_2H_4 + H$	$3.2 \cdot 10^{13}$	40.7
42	$C_2H_4 + OH \rightarrow C_2H_3 + H_2O$	$3 \cdot 10^{12}$	0
43	$C_2H_4 + H \rightarrow C_2H_5$	$8 \cdot 10^{12}$	1.9
44	$C_2H_4 + O \rightarrow CH_3 + HCO$	$2.26 \cdot 10^{13}$	2.7
45	$C_2H_3 + O_2 \rightarrow C_2H_2 + HO_2$	$1.6 \cdot 10^{13}$	10

* см^6 моль$^{-2}$ сек$^{-1}$

известны и литературы, и при точной работе в схему реакции необходимо включить все реакции, в которых происходят взаимодействия между метиловыми и гидроперекисными радикалами, метаном, кислородом. В этих реакциях образуются ещё не рассмотренные радикалы то есть необходимо уже рассмотреть все реакции, в которых реагируют уже образовавшиеся продукты. Продолжая эту работу, дойдем до реакций, в которых происходит образование стабильных продуктов окисления метана. «Схема реакций» составляется именно таким образом. Для этой работы очень полезным являются сборники [4, 5, 6, 7].

Во втором блоке приведено выражение «новейшие данные». Под этим необходимо понимать параметры реакций, включенные в схему, то есть преэкспоненциальные константы и энергию активации. Вместо «новейшей» праивльнее использовать выражение «наиболее подходящей».

Выбор идёт по двум направлениям:

а) Для одной и той же реакции возможно существование нескольких литературных данных. Среди них следует выбрать те, которые получены в опытах, проведенных в условиях, бликих в нашим условиям (температура, давление, концентрации и т. д.).

б) Параметры различных элементарных реакций, полученные из одного исследования предпочительнее по сравнению с параметрами, полученными из различных исследований. После выбора параметров данных можно заполнить две колоны таблицы I.

В третьем блоке идет речь о данных измерения концентраций и скорости. В действительности только данные концентрации определены путем аналитических измерений. Скорость означает производную непрерывной, проходящей через точки, соответствующие данному компоненту функции (рис. 5) Необходимо отметить, что эдесь речь идет не о скорости реакции а о скорости увеличения концентрации.

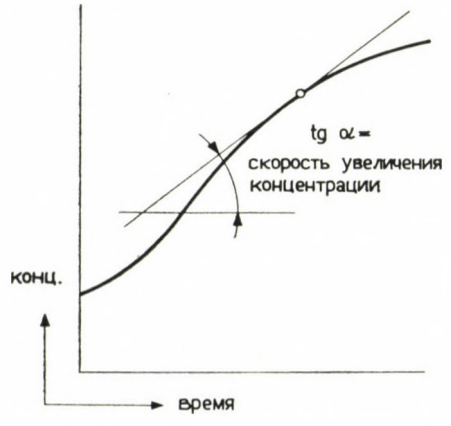

Рис. 5. Скорость увеличения концентрации

В четвертом блоке имеется команда о необходимости рассчитать концентрации важнейших цепных носителей. Основой решения команды служит то, что для каждого компонента можно написать дифференциальное уравнение:

$$\frac{dc_j}{dt} = \sum_{l=1}^{n_r} (R_{lj}^{+} - R_{lj}^{-}) \left(k_l e^{-\frac{E_l}{RT}}\right) \prod_{r=1}^{n_c} c_r^{\nu_{lr}} . \qquad \text{(а)}$$

Катоне и Джемс предлагают переход от дифференциальных уравнений к нелинейным алгебраическим уравнениям, так как для стабильных компонентов скорость, стоящая в левой части дифференциального уравнения уже известна, то есть

$$\left(\frac{dc_j}{dt}\right)_t \gtreqless 0 \qquad \text{(б)}$$

и только тогда равна 0, когда концентрация стабильных компонентов имеет экстремальное значение; для атомов и радикалов используем предложение квазистационарности концентрации (что иногда называют и принципом Боденштейна):

$$\left(\frac{d_{cj}}{d_t}\right)_t = 0 . \qquad \text{(в)}$$

Этим дифференциальная система уравнений (2) преобразуется в нелинейную алгебраическую систему уравнений, которая каким-то образом отдельно решима для каждого t, в которой имеются данные измерения. Так как расчеты не очень просты, Катоне и Джемс предлагают, чтобы расчитана была только концентрация носителей цепи. Главными носителями цепи являются:

$$CH_3, H, O, HO_2, OH, C_2H_5$$

(хотя в статье не дается описание и объяснение, почему именно вышеуказанные представляют собой главные носители цепи). Из этого следует, что необходимо решить нелинейную алгебраическую систему уравнений, представленную в таблице II, и для каждого опыта столько раз, сколько имеется в распоряжении серий данных измерения.

Результаты расчетов Катоне и Джемса для одного случая представлены на рис. 6. Проведя подобные расчеты для обработки данных всех опытов, назреет положение для объяснения кинетических явлений на основе механизма.

Кинетику набоходимо сейчас ответить на вопрос, какая реакция, вызывающая разветвление цепи отвечает за «ускорение» окисления, наблюдаемое при опыте.

Схема реакции дает возможности, указанные в таблице III.

Таблица II

$$\frac{d(CH_4)}{dt} = (CH_3)[k_7(H_2) + k_{38}(C_2H_6)] - (CH_4)[k_2(OH) + k_3(HO_2) + k_4(H) + k_5(O)]$$

$$\frac{d(H_2)}{dt} = (H)[k_4(CH_4) + k_{28}(H_2O) + k_{36}(C_2H_6)] - (H_2)[k_7(CH_3) + k_{23}(OH) + k_{24}(HO_2) + k_{25}(O) + k_4(C_2H_5)]$$

$$\frac{d(CO_2)}{dt} = (CO)[k_{21}(OH) + k_{22}(HO)]$$

$$\frac{d(C_2H_2)}{dt} = k_{33}(CH_3)^2 + k_{40}(C_2H_5)(H_2) - (C_2H_6)[k_{34}(OH) + k_{35}(HO_2) + k_{36}(H) + k_{37}(O) + k_{38}(CH_3)]$$

$$\frac{d(O)}{dt} = k_{26}(H(C_2) - (O)[k_5(CH_4) - d_{25}(H_2) + k_{29}(H_2O) + k_{37}(C_2H_6) + k_{44}(C_2H_4)]$$

$$\frac{d(C_2H_5)}{dt} = (C_2H_6)[k_{34}(OH) + k_{35}(HO) + k_{36}(H) + k_{37}(O) + k_{38}(CH_3)] + k_{43}(C_2H_4)(H) - (C_2H_5)[k_{39}(O_2) + k_{40}(H_2) + k_{41}]$$

Катоне и Джемс исследуют предложения других авторов [8, 9], которые в разложении гидроперекиси водорода:

$$H_2O_2 \xrightarrow{(M)} 2OH \qquad (14)$$

видят найважнейшую реакцию разветвления цепи. По нашему мнению авторы этим пунктом проводят с точки зрения ответа на вопрос излишний путь,

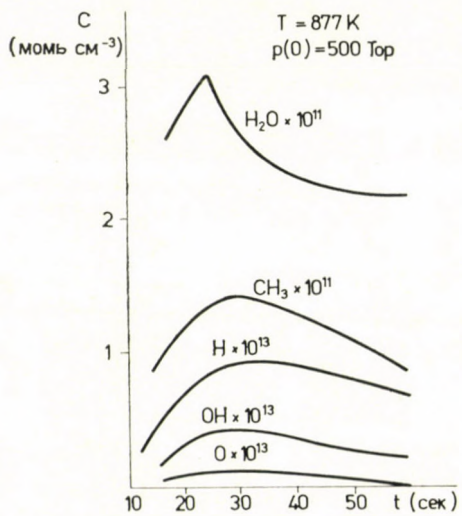

Рис. 6. Концентрации радикалов

Таблица III

№	Реакция
5	$CH_4 + O \rightarrow CH_3 + OH$
11	$CH_2O + O \rightarrow HCO + OH$
13	$CH_2O + O_2 \rightarrow HCO + HO_2$
14	$M + H_2O_2 \rightarrow 2OH + M$
25	$H_2 + O \rightarrow OH + H$
26	$H + O_2 \rightarrow OH + O$
29	$O + H_2O \rightarrow 2OH$
37	$C_2H_6 + O \rightarrow C_2H_5 + OH$
44	$C_2H_4 + O \rightarrow CH_3 + HCO$

Таблица IV

t(сек)	$V_3 \cdot 10^{10}$ ($CH_4 + HO_2^*$)	$V_0 \cdot 10^{10}$ ($CH_2O + HO_2^*$)	$V_{24} \cdot 10^{10}$ ($H_2 + HO_2^*$)	$V_{35} \cdot 10^{10}$ ($C_2H_6 + HO_2^*$)	$V_{31} \cdot 10^{10}$ ($HO_2 + HO_2^*$)
	a) 604 °C 500 тор				
15	1,46	0,81	0,09	0,17	15,3
20	1,31	0,78	0,18	0,21	14,5
25	1,33	0,86	0,3	0,27	18,6
30	0,97	0,65	0,3	0,24	12,2
35	0,85	0,57	0,32	0,23	11,6
40	0,75	0,46	0,33	0,22	11,1
	b) 659 °C 400 тор				
14	1,61	0,61	0,25	0,35	9,7
16	1,73	0,69	0,37	0,43	12,1
18	1,71	0,72	0,47	0,46	13,6
20	1,61	0,72	0,55	0,46	14,2
22	1,47	0,69	0,61	0,43	14
25	1,23	0,61	0,65	0,35	12,7
28	1,05	0,54	0,66	0,27	11,7
30	0,98	0,51	0,68	0,23	11,9
	c) 736 °C 200 тор				
10	0,8	0,23	0,24	0,16	2,35
12	1,1	0,32	0,5	0,25	5,65
14	1,25	0,32	0,91	0,3	10,4
16	1,06	0,17	1,18	0,25	16,6

однако последний важен с другой точки зрения, поэтому проследим его и дальше. Для решения вопроса, что ответственно ли разложение гидроперекиси водорода на два гидроксильных радикала из разтевление цепи, необходимо исследовать реакции, ведущие к образованию гидроперекиси водорода и доказать, что среди этих реакций наиважнейшие используют хотя бы одним радикал для образования молекулы гидроперекиси водорода. Для этой цели необходимо рассчитать скорость реакций, ведущих к образованию гидроперекиси водорода. Результаты расчета, взятые из статьи Катоне и Джемса, представлены в таблице IV. Из этого ясно, что при скорости нижеуказанной реакции

$$2HO_2 \rightarrow H_2O_2 + O_2 \tag{31}$$

другими с точки зрения образования перекиси водорода можно пренебречь.

В таблице V представлены скорости реакций, ведущих к разложению перекиси водорода. Из этого однозначно вытекает, что разложение перекиси водорода происходит с третьим компонентом согласно нижеследующей реакции:

$$H_2O_2 + M \rightarrow 2OH + M \tag{14}$$

Тогда следует, что в случае квазистационарной корцентрации перекиси водорода секвенция

$$2HO_2 \longrightarrow H_2O_2 \xrightarrow{(M)} 2OH$$

не содержит разветвления.

Таблица V

$t(s)$	$k_{14}(M)(s\ сек^{-1})$	$k_{15}(OH)(s\ сек^{-1})$	$\frac{(k_{16}+k_{17})}{(H)}\ (s\ сек^{-1})$
	604 °C 500 тор		
15	5,5	0,08	0,13
20	6	0,12	0,19
25	6,6	0,15	0,23
30	7,2	0,15	0,26
35	7,7	0,13	0,13
40	8,2	0,12	0,12
	736 °C 200 тор		
10	65,9	0,25	1,08
12	71,8	0,29	1,69
14	85,8	0,3	2,41
16	95,8	0,20	3,12

Таблица VI

t(сек)	1,5 S		2 S		3 S		4 S	
	$V_3 \cdot 10^{10}$	$V_{31} \cdot 10^{10}$	$V_3 \cdot 10^{10}$	$V_{31} \cdot 10^{10}$	$V_3 \cdot 10^{10}$	$V_{31} \cdot 10^{10}$	$V_3 \cdot 10^{10}$	$V_{31} \cdot 10^{10}$
6	2,21	9,82	2,15	5,66	2,97	3,45	2,96	1,87
8	2,70	26,41	2,1	5,24	2,66	3,06	2,16	1,07
10	1,8	26,26	1,58	4,33	2,14	2,24	1,7	0,72
12	0,86	16,33	1,32	4,44	1,66	1,57	1,37	0,52
14	0,59	42,7	1,03	3,69	1,36	1,25	1,17	0,42
16	0,51	22,45	0,78	2,68	1,19	1,1	1,11	0,42

Таблица VI показывает, что среди реакций, ведущих к образованию перекиси водорода скорость реакции

$$CH_4 + HO_2 \rightarrow CH_3 + H_2O_2 \qquad (3)$$

попадает в интервал скорости (31) при начальном увеличении соотношения метан/кислород.

В этом случае имеет место секвенция

$$HO_2 \rightarrow H_2O_2 \rightarrow 2OH,$$

которая хотя и содержит разветвление, но противоречит наблюдению (рис. 3), показывающему ингицирующее действие метана, ведь большая начальная концентрация метана увеличила бы скорость реакции

$$CH_4 + HO_2 \rightarrow CH_3 + H_2O_2 \qquad (3)$$

Следовательно реакция (3) не играет роли в ускорении реакции.

Следовательно, согласно вышеуказанному, предположенная роль перекиси водорода в разветвлении исключается. Поэтому Катоне и Джемс считают, что разветвление исходит из реакции

$$H + O_2 \rightarrow OH + O \qquad (26)$$

Реакция имеет относительно большую энергию активации (16, 8 ккал/моль). При низких температурах эту реакцию ингибирует реакция, обладающая отрицательной (—1 ккал/моль энергией активации

$$H + O_2 + M \rightarrow HO_2 + M \qquad (27)$$

которой благоприятствует и увеличению общего давления. Ингибирующее действие метана можно учесть реакцией, в которой израсходуется атом водорода.

$$CH_4 + H \rightarrow CH_3 + H_2 \qquad (4)$$

Естественно, что только три эти реакции нельзя рассматривать как адекватный механизм, в нем учавствуют и другие реакции. Если действительно разветвление цепи исходит из реакции

$$H + O_2 \rightarrow OH + O \tag{26}$$

то тогда при этом образуются весьма реакционноспсобные компоненты. На это указывает очень малая концентрация обоих компонентов, что показано н рис. 6. Оба компонента с большой скоростью реагируют с метаном согласно нижеследующим реакциям:

$$CH_4 + O \rightarrow CH_3 + OH \tag{5}$$

$$CH_4 + OH \rightarrow CH_3 + H_2O\,.$$

При учете квазистационарной концентрации гидроксильного радикала и атома кислорода, линейная комбинация последних трех реакций дает следующую общую реакцию:

$$3CH_4 + H + O_2 \rightarrow 3CH_3 + 2H_2O,$$

которая ясно показывает, что из одного атома водорода образуется три радикала метила. В этом состоит природа разветвления, ведущая к ускорению окисления метана.

В вышеуписанном разделе ознакомились с техникой исключения, с помощью которой можно сузить схему реакций, показанную в таблице I, т. е. получить адекватный механизм. Осталось ещё доказать механизм. Доказательство мехнизма основано на том, ещё не польностью использованы информации, содержащиеся в опытных данных. Мы имеем зависимости время — концентрации для семи компонентов, но из них использовали только четыре при расчетах зависимости время — концентрации для ведущих реакций. Скрытые в опытных данных ещё не использованные информации можно использовать для подтверждения механизма, произведя соответствующую обработку их.

Необходимо отметить, что ещё не занимались формальдегидом и формаловым радикалом. Можно выписать их из концентрации и, таким образом, определить константы нижеследующих двух реакций:

$$CH_3 + O_2 \rightarrow CH_2O + OH \tag{6}$$

$$CH_2O + OH \rightarrow HCO + H_2O\,. \tag{8}$$

Эти операции указаны в предпоследнем блоке схемы.

В последнем блоке — так как константы скорости реакции известны из литературы — можно сравнить расчитанные ранее данные и известные из

литературы, что в конечном итоге означает доказательство механизма (по крайней мере согласно Катоне и Джемсу).

Этим и мы завершили анализ мышления кинетика. Из анализа ясно, что его можно запрограммировать. Но более точная математическая обработка и наши опыты по вычислительной технике предлагают модификацию мышления.

Запрограммированное мышление

На рис. 7 представлена блочная схема запрограммированного мышления, используемого при изучении механизма гомогенных газовых реакций.

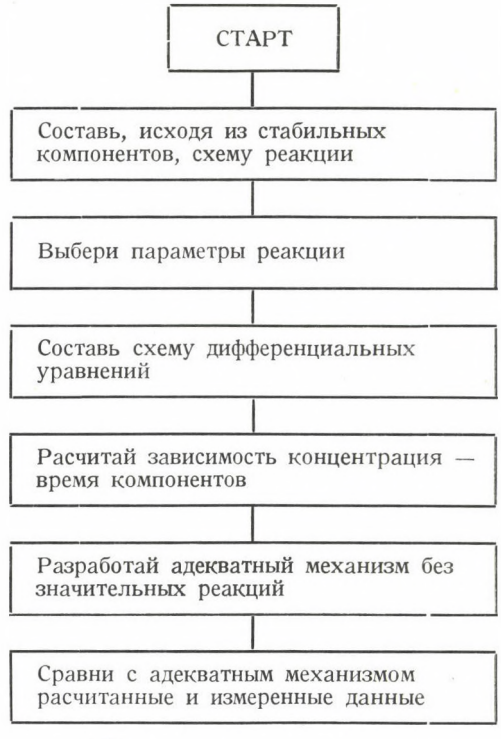

Рис. 7. Запрограммированное мышление

Старт в этом случае означает введение опытных данных в память ЭВМ.

Первый блок «составь схему реакций на основе стабильных соединений» означает, что, введя название стабильных исходных (метан, кислород) и остальных конечных соединений (CO_2, CO, вода, этилен, этан) в память машин, программа выбирает из реакций, хранящихся в памяти ЭВМ те, в которых всречаются этим компоненты.

Этот выбор легко подвергается алгоритмизации.

(Необходимо отметить, что описание, хранение, обратный поиск реакций в последнее время стало самостоятельной задачей. Как известно, уже есть журнал «Chemical Information and Computer Science», издаваемый Обществом Американских Химиков.)

Во втором блоке «выбирай параметры реакций» происходит выбор тех параметров, для которых интервал действительности согласуется с актуальным значением температуры.

Программа третьего блока «составь систему дифференциальных уравнений» проводит составление дифференциальных уравнений для концентраций всех компонентов заранее составленной схемы реакции. Так как в опытных работах могут быть и реакторы постоянного объема помимо реакторов постоянного давления, в дифференциальных уравнениях имеется и член, учитывающий изменения объема, целесообразно подготовить программу, составляющую систему дифференциальных уравнений и для этого. В исследовательских нет гарантий для соблюдения изотермических условий, поэтому программу разработали таким образом, чтобы она могла быть применима для политронных условий, при которых:

а) задано изменение температуры
б) задана адиабатика
в) заданы условия передачи тепла.

В случае «*б*» и «*в*» программа формулирует и дифференциальное уравнение температуры. Необходимые для этого полиномы энтальпии [10] являются исходными данными программы.

Принциипиально возможно хранение полиномов энтальпии в памяти, откуда они могут быть вызваны.

Данные, необходимые для расчетов полиномов энтальпии, находится в сборниках [11, 12].

Программа четвертого блока «расчитай зависимость концентрация компонентов — время» основывается на численном интегрировании системы дифференциальных уравнений. На этой фазе работы мышление кинетика и специалиста по вычислительной технике несколько отличаются.

Специалист по ЭВМ

а) не учитывает значения наблюдаемых концентраций и расчитанные значения скорости,

б) не предполагает квазистационарность концентрации ведущих компонентов, так как он

в) не ищет корни алгебраического уравнения, а решает систему дифференциальных уравнений. Последнее не простая задача, так как дифферен-

циальные уравнения гомогенных газовых реакций плохо кондицированные (то есть они жесткие) и могут быть решены специальным алгоритмом, который стал известным только несколько лет тому назад [13]. После решения системы дифференциальных уравнений данные концентрации — время вносятся в память ЭВМ, откуда они при надобности могут быть просто использованы.

Возможным методом дальнейшей обработки является выбор участвующих в схеме, но не играющих большую роль реакций; это описано в пятом блоке. В процессе этого происходит то же самое, что делал кинетик, когда выбрал те реакции, которые не играли значительную роль в процессе образования и перекиси водорода. Эту работу последовательно и систематически проводит программа пятого блока, то есть учитывает каждый компонент и каждую реакцию. Во всяком случае необходимо ответить на вопрос — когда можно пренебречь данной реакцией механизма. На этот вопрос можем дать весьма самовольный ответ: тогда, когда указанная реакция не играет в образовании и разложении каждого компонента роли большей, чем $\varepsilon\%$. Расчеты проведенные на основе этого ответа показывают, вес любой реакции в разложении или образовании компонентов изменяется и при том значительно с проведением общей реакции.

Однако, в конечном счете, выбором параметра ε схема реакции с помощью методов пятого блока может быть сужена до адекватного механизма.

До сих пор не использовали опытные данные. Сейчас наступла очередь сравнения данных концентрации, измеренных опытным путем и расчитанных с помощью методов шестого блока. Это можно провести с помощью известной техники математической статистики. Необходимо решить — отличаются ли сигнификационно две серии данных или нет. Если нет, то адекватный механизм можно считать обоснованным. Однако, если разница сигнификационна, возникает новый вопрос, а именно, что является причиной сигнификации? Имеет смысл рассмотреть два случая:

а) Механизм правилен (на основе химических закономерностей кажется правильным), но постоянные скорости реакций важных с точки зрения общей скорости по каким-то причинам не точны. В этом случае речь идет о новой задаче, об определении постоянной скорости. А она требует обратный подход, оптимализацию параметров, которую называют «обратной задачей». Новый метод решения задачи показан в работе [14].

б) Механизм содержит с точки зрения общей скорости значительные реакции, которые не описаны в литературе. Если непосредственное доказательство новой реакции не возможно то, что для механизма новых реакций необходимо определить кинетические параметры новых реакций. Таким образом, задаче сведена к обратной задаче.

По нашему мнению такой подход является источноком распространения (пропаганды) ошибок и является причиной неопределенности кинетических

параметров, приведенных в литературе. Этот факт подтверждает необходимость исследования методов, обеспечивающих непосредственное измерение элементарных реакций. Но последняя не является программируемой исследовательской работой.

Summary

On the basis of [1] the author analyses the generally accepted way of thinking on searching for mechanisms of homogeneous gas reactions. Combining the acquired experience with computer facilities an algorithm is proposed for the elucidation of mechanisms. Its main points are the following: programmed finding of every elementary reaction from the list of reactions using chemical evidences, automatic generation of the corresponding system of stiff differential equations, computation of reaction weights and elimination of reactions having small weight, comparison of the computed and measured data, study of parameter sensibilities for explaining significant differencies.

ЛИТЕРАТУРА

[1] Cathonnet, M., James, H.: J. Chim. phys. **72**, 247, 253 (1975)
[2] Benedek, P., László, A.: Magy. Kém. Folyóirat, **57**, 372 (1951)
[3] Benedek, P., László, A., Németh, A., Váczi, P.: Deuxieme Symposium Europeen sur la Combustion. Tome **1**, 154. Section Française du „Combustion Institute" 1975
[4] Кондратьев, В. Н.: Константы скорости газовых реакций. Наука, Москва 1970
[5] Веденеев, В. И., Кибкало: Константы скорости газовых мономолекулярных реакций. Наука, Москва 1970
[6] Benson, S. W., O'Neal, H. E.: Kinetic Data on Gas Phase Unimolecular Reactions. NSRDS—NBS 21., Washington 1970
[7] Bautch, D. L., *et al.*: Evaluated Kinetic Data for High Temperature Reactions, Vol. **1**. Butterworths, London 1972
[8] Hoare, D. E., Milne, G. S.: Trans. Faraday Soc., **63**. 101 (1967)
[9] Bhundell, R. V., *et al.*: Tenth International Symposium on Combustion,p. 455. The Combustion Institute, Pittsburgh 1965
[10] Antal, J., Benedek, P., Váczi, P.: Magy. Kém. Lapja, **28**, 497 (1973)
[11] Almássy, G., *et al.*: Bonyolult műveleti egységek matematikai szimulációja. Akadémiai Kiadó, Budapest 1973
[12] Stull, D. R., Prophet, H.: JANAF Thermochemical Tables. N.B.S, Washington 1971
[13] Gaer, C. W.: Communication of the ACM, **14**, 176 (1971)
[14] Vajda, S.: Диссертация. Veszprémi Vegyipari Egyetem 1975
[15] Cathonnet, M., James, H.: Deuxième Symposium Europeen sur la Combustion. Tome **I**, p. 78. Section Française du "Combustion Institute", 1975

Pál Benedek H-1393 Budapest P.O.B. 319

Acta Chimica Academiae Scientiarum Hungaricae, Tomus 100 (1—4), pp. 69—74 (1979)

SYNTHESIS AND STRUCTURE DETERMINATION OF GEOMETRIC ISOMERS OF 1-ARYL-2-ETHYL-1,2-DIPHENYLETHYLENES BY ^{1}H-NMR SPECTROSCOPY

P. SOHÁR,* G. ÁBRAHÁM, G. SCHNEIDER, T. HORVÁTH and E. FUGGERTH

(Institute for Drug Research, Budapest)

Received May 17, 1978

Accepted for publication June 22, 1978

The *Z* and *E* isomers of 1,2-diphenyl-1-arylethylene derivatives were separated and identified by ^{1}H-NMR spectroscopy.

Several triaryl-substituted ethylenes possess biological activity, some of the derivatives having antiestrogenic action ; *e.g.*, *Z*-1,2-diphenyl-1-[*p*-(β-dimethylamino)-ethoxyphenyl]-but-1-ene [1] (**1a**) has come into therapeutical use. This fact suggested the synthesis of derivatives **2**—**7**.

The Grignard reaction of α-ethyldesoxybenzoin derivatives with *p*-subtituted bromobenzenes in THF yielded mixtures containing the diastereomeric isomers of 1,2-diphenyl-1-(*p*-substituted-phenyl)-butan-1-ols [2] in different proportions, according to the Cram rule [3]. By eliminating water from the butanol derivatives obtained, geometric isomers of 2-ethyl-1,2-diphenyl-1-(*p*-substituted-phenyl)-ethylenes were prepared. The ratio of the geometric isomers depends on the diastereomeric structure of the butanol derivatives used as starting material [2].

The identification of geometric isomers is important as there is a considerable difference [4] in their pharmaceutical activity. In the case of tetrasubstituted ethylenes having different but similar substituents, this identification is generally a difficult task. Structure determinations based solely on the hardly differing spectroscopic data are often untrue [5]. The geometric isomers of the tetrasubstituted ethylenes mentioned above can, however, be identified from their ^{1}H-NMR spectra.

The geometric isomers of **1** have been known [6, 7] for a long time and their structures elucidated by X-ray diffraction [8, 9]; later their ^{1}H-NMR data [10, 11] confirmed [11] the same structures, using the chemical shift differences of the side chain protons ($-O-CH_2-CH_2-NMe_2$ group). As compounds **2**—**6** are devoid of any side chain, the key to structure determination in the case of **1**, threfore another route had to be found to solve this problem. At first the IR an ^{1}H-NMR spectra were studied.

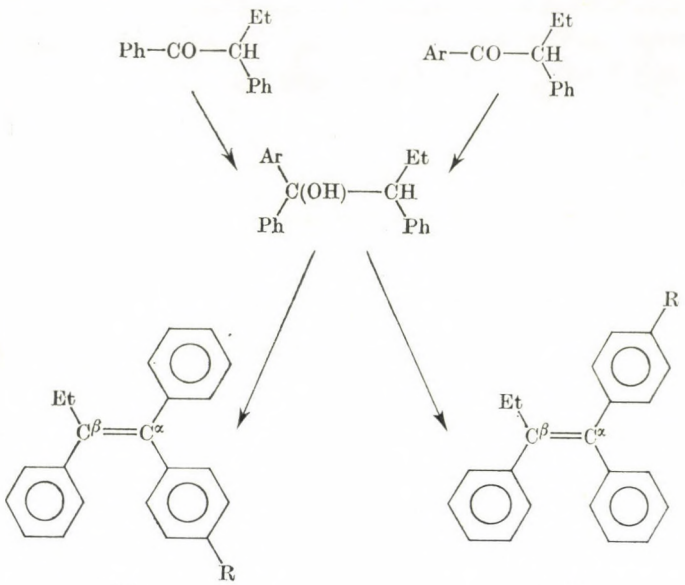

a (*Z*) **b** (*E*)

1: R = —O—$(CH_2)_2$—NMe_2 **4**: R = —OMe

2: R = —Br **5**: R = —OH

3: R = —F **6**: R = —C(OH)Me_2

7: R = —O—$(CH_2)_2$—Br

The geometric isomers of the mono- and symmetrically di- or tetrasubstituted ethylenes can easily be identified by their IR spectra [12], on the basis of the presence (*Z* isomer) or absence (*E* isomer) of the νC=C band. In the case of compounds **1**—**3** the IR spectra of the isomeric pairs are very similar. The νC=C bands of the *Z*—*E* isomeric pairs have almost the same intensity and frequency (they appear at 1595, 1590, and 1595 cm^{-1}, respectively), thus there is no possibility to distinguish between the structures in this way. The ^{1}H-NMR spectra of the compounds, however, will show expectedly characteristic differences.

For example, the aromatic protons of the *Z*-stilbene give a sharp singulet at 7,2 ppm, and there is a complicated multiplet at lower fields in the spectrum of the *E*-stilbene [13, 14]. Probably, the more extended conjugation in the *E* isomer causes an increase in the chemical shift of each ring proton and the shielding of the *ortho*- and *meta*- + *para*-protons show a geater difference because of polarization of the π-sextet and anisotropy of the double bond; therefore, the protons exhibit a multiplet ($\Delta\delta_{AB}$, $\Delta\delta_{AC} \neq 0$ for the $AA'BB'C$ spin system).

The *Z*-stilbene is non-planar because of the mutual steric hindrance of the *cis* vicinal aromatic rings, which are coplanar with each other and perpen-

Table I

^1H-NMR data for compounds **1—7** *in* $CDCl_3$ [$\delta_{TMS} = 0$ ppm]

Compound	M.p., °C	δCH_3 t^* (3H)	δCH_2 q^* (2H)	$\delta ArH^{\bullet}$ s (5H)	δArH° s (5H)	δArH_A m^+ (2H)	δArH_B m^+ (2H)	Chemical shift differences		
								$\Delta\delta ArH^{\bullet}$	$\Delta\delta ArH_A^{++}$	$\Delta\delta ArH_B^{++}$
1a$^{\times}$	98—100	0.90	2.43	7.20	7.05	6.46	6.68	~0.35	0.44	0.47
1b$^{\times}$	73—75	0.92	2.51	~7.95	7.10	6.90	7.15			
2a	89—92	0.92	2.48	~7.30	7.12	7.75	7.10	~0.40	0.38	0.36
2b	113—16	0.92	2.48	~6.90	7.08	7.13	7.46			
3a	77—79	0.92	2.48	7.30		6.69	6.85	~0.15	~0.29	~0.13
3b	70—73	0.92	2.48	7.15		~6.98				
4a$^{\blacksquare}$	125—27	1.00	2.54	7.35	7.20	6.61	6.85			
5a$^{\square}$	126—27	0.90	2.43	7.20	7.03	6.31	6.62			
6a$^{\blacktriangledown}$	129—31	0.90	2.40	7.07	6.90	6.64	6.89			
7a$^{\triangledown}$	107—09	0.90	2.45	7.25	7.10	6.55	6.79			

* A_2X_3 multiplet, $J_{AX} = 7$ Hz.

• phenyl group attached to the C_α atom.

○ phenyl group attached to the C_β atom.

+ estimated from the $AA'BB'$ ($AA'BB'X$ in the case of **3**) multiplet of the *para*-disubstituted phenyl ring by AB-approaching [14]. $J_{AB} = 9$ Hz, $J_{AX} \approx 8$ Hz (**3**), $J_{BX} \approx 6$ Hz (**3**).

× δNCH_2 (2H), t ($J = 7$ Hz, X_2 part of an A_2X_2 multiplet); 2.56 (**1a**) and 2.73 (**1b**) ppm; δNCH_3, s (6H): 2.25 (**1a**) and 2.32 (**1b**) ppm, δOCH_2 (2H), t (A_2 part of an A_2X_2 multiplet): 3.85 (**1a**) and 4.08 (**1b**) ppm.

■ δOCH_3, s (3H): 3.70 ppm.

□ δOH, broad s (1H): 5.05 ppm.

▼ δCH_3, s (6H): 1.40 ppm, δOH, s (1H): 1.67 ppm.

▽ δCH_2Br (2H), t ($J = 6$ Hz): 3.50 ppm, δCH_2O (2H), t ($J = 6$ Hz): 4.15 ppm.

++ *para*-disubstituted phenyl ring

dicular to the double bond. Owing to the mutual anisotropic effect of the rings and the weaker conjugation corresponding to the non-planar structure, the chemical shift decreases. It is corroborated by the similar shift of 1,1-diphenylethylene (7,21 ppm [15]) and the even greater shielding in tetraphenylethylene (7,03 ppm [16]). The shift differences of the ring protons decrease in consequence of both the more symmetrical electron distribution in the phenyl ring of *Z*-stilbene due to weaker conjugation and the stronger anisotropic effect at the *ortho*-protons, *i.e.* the $AA'BB'C$ spin-system approaching the A_5 limit (singulet).

In triphenylethylene the singulet of the phenyl group surrounded by the two other rings appears at 7,08 ppm [16] because of the additive anisotropic effect of the two outside rings, having higher chemical shift (7,29 ppm)*.

Consequently, as regards the protons of the three phenyl rings, in isomer **a** it is the *para*-disubstituted ring protons, whereas in isomers **b** it is the protons of the ring attached to the C_α atom which show lower chemical shift. The assignment of the separated isomeric pairs to the corresponding geometric isomers and their ^{1}H-NMR data are shown in the Table I.

The spectra of the isomeric pairs **1**—**3** are also visually different. In the spectra of the **b** isomers the signals of all the three aromatic ring protons overlap, whereas in the spectra of their **a** pairs the $AA'BB'$ multiplets of the *para*-disubstituted ring protons partly or wholly separate at lower chemical shifts. In this way the geometric structure can be easily determined even at glance. Using the compounds **1**—**3** as models, structures can be easily determined even if the spectrum of only one isomer is known. For example, the data of **4a**—**7a** can be found in the Table I. In these spectra the separation of the $AA'BB'$ multiplets at lower chemical shift directly support the structure *Z*.

Experimental

General methods. All m.p.'s are uncorrected. IR spectra were recorded with a Perkin—Elmer 457 type spectrometer and ^{1}H-NMR spectra at room temperature on a Varian A-60D spectrometer, in $CDCl_3$, using TMS as internal standard.

The ethylene derivatives **1**—**5** were prepared from the corresponding 1,1,2-triarylbutanols [2] by elimination of water.

General procedure. A solution of the butanol derivative (10 mmoles) in EtOH (40 ml) was refluxed with *conc.* HCl (1,0 ml) for 60 min. (In the case of **2a** and **2b**, for 5 h.) The solution was cooled, neutralized with 10*N* NaOH and evaporated. The residue was extracted with ether, dried ($MgSO_4$) and the solution evaporated and re-evaporated with benzene. From the syrup obtained the *Z* and *E* isomers were separated by crystallization or column chromatography.

Z-1,2-diphenyl-1-[*p*-(β-dimethylamino)-ethoxyphenyl]-but-1-ene (1a) [6, 7].

The syrup obtained was dissolved in hexane (20 ml). On cooling at —5 °C overnight, a crystalline product separated. This was recrystallized three times from heptane; m.p. 98—100 °C; *lit.* [6] m.p. 95—96 °C.

* In Ref. [16] the signal at 7,08 ppm has been assigned erroneously to the phenyl ring being geminal with the olefin hydrogen.

E-1,2-diphenyl-1-[p-(β-dimethylamino)-ethoxyphenyl]-but-1-ene (1b) [7].

The mother liquor of the previous first crystallization was evaporated. From the residue the hydrochloride was made and recrystallized twice from ethyl acetate. (*E*—HCl, m.p. 177—179 °C.) The base *E* was liberated from the salt and crystallized from 85% MeOH; m.p. 73—75 °C; *lit.* [7] m.p. 72—74 °C.

E-1,2-diphenyl-(p-bromophenyl)-but-1-ene (2b) [18].

The syrup was crystallized from isopropanol three times; m.p. 113—116 °C.

Z-1,2-diphenyl-1-(p-bromophenyl)-but-1-ene (2a) [18].

The mother liquor of the previous first crystallization was evaporated and the residue was recrystallized from methanol three times; m.p. 89—92 °C.

Z- and E-1,2-diphenyl-1-(p-fluorophenyl)-but-1-ene (3a and 3b) [18].

The isomers were separated by chromatography on a column of silica gel impregnated with 5% $AgNO_3$. Elution with hexane gave first the *Z* and then the *E* isomer; m.p. 77—79 °C (**3a**) and 70—73 °C (**3b**).

Z-1,2-diphenyl-1-(p-methoxyphenyl)-but-1-ene (4a).

The syrup was crystallized from EtOH then MeOH; m.p. 125—127 °C; *lit.* [17] m.p 117—118 °C and 88—89 °C.

Z-1,2-diphenyl-1-(p-hydroxyphenyl)-but-1-ene (5a).

The residue was crystallized from benzene. The mother liquor was evaporated. The residue was suspended in hexane and the crystals separated were recrystallized twice from isopropanol; m.p. 126—127 °C; *lit.* [17] m.p. 104—105 °C.

Z-1,2-diphenyl-1-[p-(α-hydroxyisopropyl)-phenyl]-but-1-ene (6a).

The Grignard reaction of **2a** with acetone afforded **6a** in the usual way; m.p. 129—131 °C (hexane).

Z-1,2-diphenyl-1-[p-(β-bromoethoxy)phenyl]-but-1-ene (7a).

The reaction of **5a** with 1,2-dibromoethane and sodium ethoxide in EtOH afforded **7a**; m.p. 107—109 °C (MeOH).

*

The authors are indebted to Mr. A. FÜRJES and Miss V. WINDBRECHTINGER for technical assistance.

REFERENCES

[1] HARPER, M. J. K., WALPOLE, A. L.: Nature **212,** 87 (1966)
[2] SOHÁR, P., SCHNEIDER, G., ÁBRAHÁM, G., HORVÁTH, T.: To be published.
[3] CRAM, D. J., WILSON, D. R.: J. Am. Chem. Soc. **85,** 1245 (1963)
[4] SKIDMORE, J., WALPOLE, A. L., WOODBURN, J.: Endocrin. **52,** 289 (1972)
[5] ERNST, S., HITE, G., CANTRELL, J. S., RICHARDSON, A., BENSON, H. D.: J. Pharm. Sci. **65,** 148 (1976)
[6] MICHAEL, M., KENNEDY, J., RICHARDSON, D. N.: Brit. Pat. 1,013,907 (1963)
[7] KENNEDY, J., HARPER, M. J. K., RICHARDSON, D. N., WALPOLE, A. L.: Brit. Pat. 1,064,629 (1966)
[8] KILBOURN, B. T., MAIS, R. H. B., OWSTON, P. G.: Chem. Commun. **1968,** 291
[9] KILBOURN, B. T., OWSTON, P. G.: J. Chem. Soc. *B*, **1970,** 1
[10] BEDFORD, G. R., RICHARDSON, D. N.: Nature **212,** 733 (1966)

[11] COLLINS, D. J., HOBBS, J. J., EMMENS, C. W.: J. Med. Chem. **14**, 952 (1971)
[12] HOLLY, S., SOHÁR, P.: Theoretical Introduction to Absorption Spectra in the Infrared Region. p. 57. (Eds. L. LÁNG and W. PRICHARD) Akadémiai Kiadó, Budapest, 1975
[13] Varian NMR Spectra Catalogue. pp. 305, 306. Varian Associates, 1962
[14] SOHÁR, P.: Nuclear Magnetic Resonance Spectroscopy. pp. 240 and 390. (In Hungarian). Akadémiai Kiadó, Budapest, 1976
[15] JEOL High Resolution NMR Spectra. No. 100—111. Sadtler Res. Lab., Heyden and Son, London, 1967
[16] Sadtler Nuclear Magnetic Resonance Spectra. Nos. 2355 and 6123. Sadtler Res. Lab., Philadelphia, 1965
[17] DOODS, E. C., GOLBERG, L., GRÜNFELD, E. I., LAWSON, W., SAFFER, C. M., ROBINSON, R.: Proc. Roy. Soc. *B* **132**, 83 (1944)
[18] HORVÁTH, T., ÁBRAHÁM, G., SCHNEIDER, G., TOLDY, L., FEHÉR, Ö., HERMANN, I.: Hung. Pat. 171, 269 (1976)

Pál SOHÁR
Gizella ÁBRAHÁM
Géza SCHNEIDER
Tibor HORVÁTH
Endre FUGGERTH
H-1325 Budapest P.O. Box 82.

Acta Chimica Academiae Scientiarum Hungaricae, Tomus 100 (1—4), pp. 75—80 (1979)

EXTRACTION OF EUROPIUM FROM A MOLTEN SALT PHASE

T. LENGYEL

(Institute of Isotopes, Hungarian Academy of Sciences, Budapest)

Received June 14, 1978

Accepted for publication July 14, 1978

The distribution of divalent europium between a molten salt phase and different organic ones has been studied. Some of the binary solvent mixtures reveal synergistic effects being favourable from the point of view of selective separation.

Introduction

In the reviews on rare earths the general judgement predominates that due to the rather similar chemical behaviour of these elements the separation thereof is a considerably difficult but at the same time an imposingly attractive task for the chemist.

This simplified and generalizing concept of similarity originates from the superficial review of the electronic configuration of the atoms which reveals that with increasing atomic number the additional electrons take place in the inner, well-shielded 4f level with no alteration of the $6s^2$ outer one.

Analogous statements are valid for the tervalent cations of the rare earths which all support that — the tripositive ions being the most probable species in aqueous solution — their separation can hardly be performed.

However, if a complex method of separation is aimed at, use can be made of the fact that oxidation states other than three are not at all exceptional ones and many of the lanthanide ions exist in dipositive and tetrapositive forms as well.

As far as fission-product rare earths are concerned, taking into account the cumulative fission yields and the corresponding half-lives, cerium, promethium, europium and, due to its analogous behaviour, yttrium are of technical interest.

Since the respective separation factors (under normal experimental conditions) are considerably low, the most promising procedures are based on the differences achieved by maintaining cerium in the tetravalent and europium in the divalent state [1, 2].

This means that — mainly under anhydrous conditions (*e.g.* in molten salt media) — Eu^{2+} has an outstanding stability and the complex species formed

behave much more similar to those of the analogous alkaline earth metals than to the corresponding rare earth ones. Accordingly, the dipositive Eu^{2+} ions resemble Sr^{2+} and some of the actinoid ions in their crystal radii [3].

Experimental

The molten salt phase which proved to be the most suitable one was the lithium nitrate—ammonium nitrate eutectic (mole ratio $\sim$ 1 : 3) with a properly low melting point of 367 K.

Keeping in mind that highly hygroscopic materials are concerned and the rating thereof becomes difficult as a powder, the molten mixture was dropped into well cooled carbon tetrachloride and the spheres formed predominantly of 2 mm diameter were stored in the solvent until direct use.

The following extractants: di-(ethylhexyl)-phosphoric acid (DEHP), tri-*n*-butyl phosphate (TBP), Amberlite LA-2 (LA-2), 4,4,4-trifluoro-1-(2-thienyl)-butane-1,3-dione = thenoyl-trifluoro-acetone (TTA), β-isopropyl-tropolone (IPT), 2,2'-bipyridyl (bipy), as well as the diluent of the organic phase (decaline) were of analytical purity.

$^{152}Eu-^{154}Eu$ mixture of high specific activity was produced by the conventional (n, γ) reaction and used as the nitrate salt as tracer. Due to the high activation cross section it was possible to keep the concentration of the central ion as low as 10^{-6} mole dm^{-3}. The determination of europium concentration of the samples was performed *via* measuring the relative activity on a well-type scintillation detector coupled to a single-channel analyzer (Nuclear Enterprises SR-3).

The distribution measurements were performed at 373 K in sealed glass ampoules placed into a shaken thermostat. After equilibration the system was quenched by rapid cooling. Aliquots of the liquid organic phase were taken for radiometric assay; the remaining solid phase was washed with acetone to remove organic contamination. Finally the salt phase was dissolved in water and aliquot part thereof was also taken for radiometric concentration determination.

Each experimental result represents the mean of five parallels. According to preliminary evaluation the deviation from the mean did not exceed $\pm 10\%$.

Results and discussion

The distribution ratio of europium between the organic and molten salt phase as a function of the concentration of the extractants used (which — according to previous measurements — proved to be promising ones [4]) — is shown in Fig. 1. Because the straight lines are very close to each other the experimental points are omitted.

It is unambiguous that the slope of each line in the lg—lg plot is two, indicating the extraction of the complexes formed with the dipositive ion and/or formation of adducts containing two molecules of the extractants. It is also obvious that the two organophosphorous compounds offer the best results from the point of view of extractive power; the other solvents may be advantageous as additives to the former ones if synergistic effects prevail.

According to the above-mentioned, different combinations of the solvents were prepared and beside these the effect of a representative σ-donor, 2,2'-bipyridyl was also investigated.

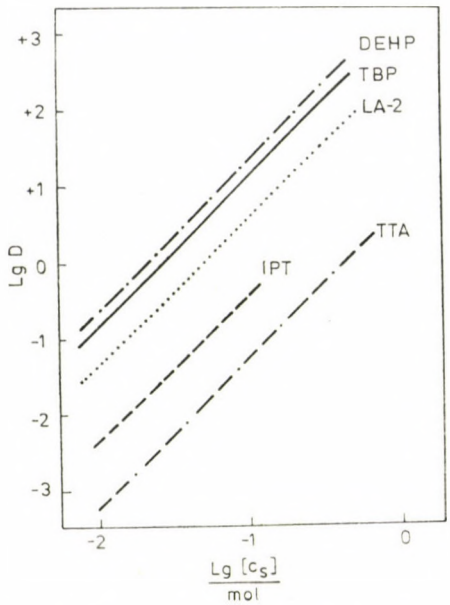

Fig. 1. Distribution ratio of europium as a function of solvent concentration (c_S)

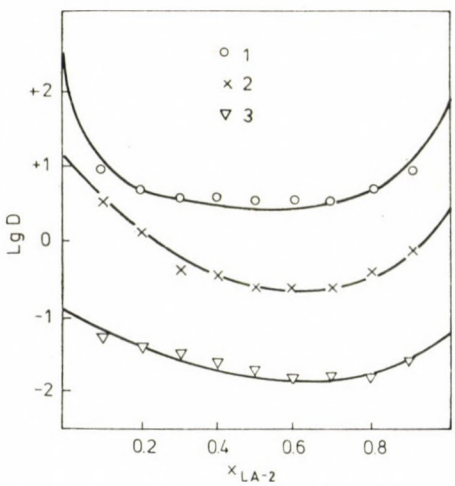

Fig. 2. Distribution ratio of europium as a function of the mole fraction of LA-2 in the system LA-2 — TBP; (1) lg T_{org} = —0.3; (2) lg T_{org} = —1.0; (3) lg T_{org} = —2.0

The results obtained are presented as the change of the distribution ratio as a function of the composition in the proper binary systems. Based on the experimental results the systems investigated can be divided into three groups.

The first one is represented by the systems LA-2 — TBP and LA-2 — DEHP (Figs 2 and 3) which demonstrate antagonistic interaction, *i.e.* mixtures

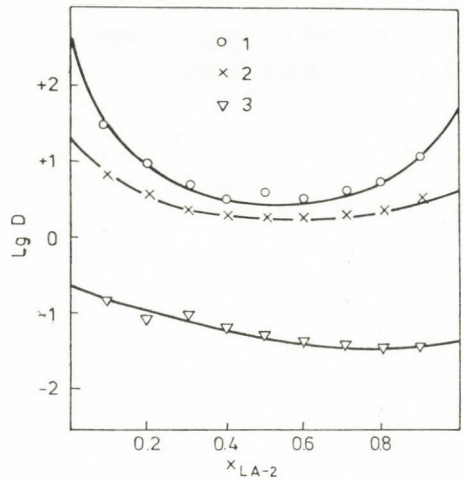

Fig. 3. Distribution ratio of europium as a function of the mole fraction of LA-2 in the system LA-2 — DEHP; (1) lg $T_{org} = -0.3$; (2) lg $T_{org} = -1.0$; (3) lg $T_{org} = -2.0$

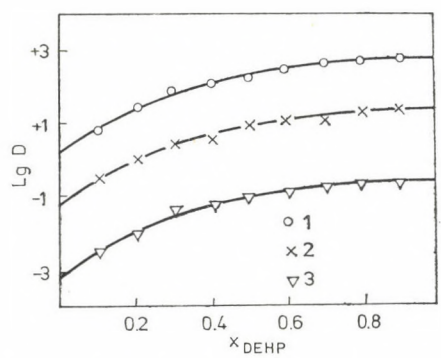

Fig. 4. Distribution ratio of europium as a function of the mole fraction of DEHP in the system DEHP — TTA; (1) lg $T_{org} = -0.3$; (2) lg $T_{org} = -1.0$; (3) lg $T_{org} = -2.0$

of these extractants behave inferior to the solvents alone and/or one might expect supposing simple additive action. The antagonistic behaviour is less pronounced at lower total concentration of the extractants.

The second group is constituted by the systems DEHP — TTA and TBP — TTA (Figs 4 and 5) which reveal a more or less additive action of the pure entities though at higher overall concentrations the TBP — TTA solvent pair suggests some tendency to synergism.

The third group is composed by the systems in which the synergistic effect is doubtless (Figs 6 and 7).

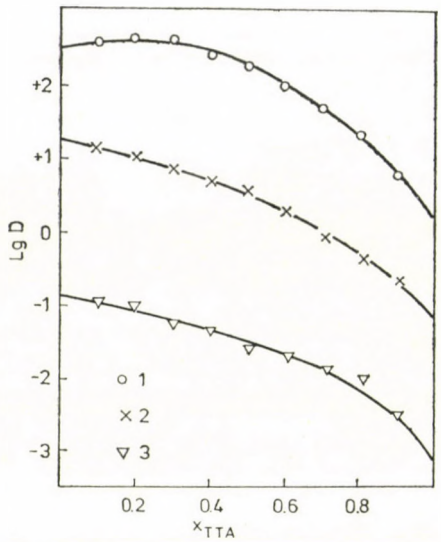

Fig. 5. Distribution ratio of europium as a function of the mole fraction of TTA in the system TTA — TBP; (1) lg $T_{org} = -0.3$; (2) lg $T_{org} = -1.0$; (3) lg $T_{org} = -2.0$

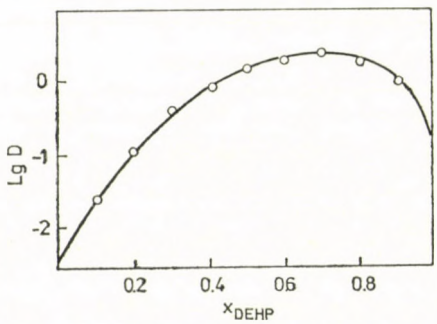

Fig. 6. Distribution ratio of europium as a function of the mole fraction of DEHP in the system DEHP — IPT; lg $T_{org} = -2.0$

Striking enough, the synergistic enhancement is considerably less than found in case of tervalent rare earths and in addition the absolute value of the distribution ratio is also rather low.

Due to the limited solubility of bipy and IPT in both of the systems studied (DEHP — IPT and bipy — TTA, respectively) only low overall concentration region could be studied and this proved to be disadvantageous from the point of view of extractive power. On the other hand, the appearance of synergism opens new vistas in enhancement of extractive separation and taking into consideration the advantages offered by the stability of the divalent form of europium, the isolation of individual fission-product rare earths can considerably be improved.

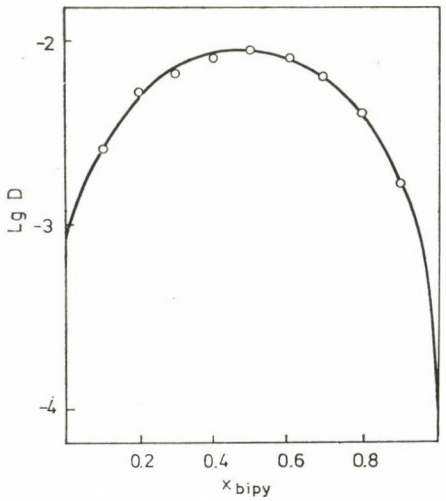

Fig. 7. Distribution ratio of europium as a function of the mole fraction of bipy in the system bipy — TTA; lg T_{org} = —2.0

Conclusion

According to the measurements performed europium exists predominantly as divalent ion in anhydrous media and — depending on the reagents used — can be extracted with proper efficiency from the molten salt phase into the organic one.

The binary solvent systems investigated reveal antagonistic, normal and synergistic behaviour. Use can be made from this attitude if the principle fission-product rare earths are to be separated.

REFERENCES

[1] Peppard, D. F., Mason, G. W., Maier, J. L., Driscoll, W. J.: J. Inorg. Nucl. Chem. **4,** 334 (1957)
[2] Peppard, D. F., Mason, G. W., Moline, S. W.: J. Inorg. Nucl. Chem. **5,** 141 (1957)
[3] Templeton, D. H., Dauben, C. H.: J. Am. Chem. Soc. **76,** 5237 (1954)
[4] Lengyel, T.: Radiochem. Radioanal. Lett. **20,** 143 (1974)
[5] Lengyel, T.: Radiochem. Radioanal. Lett. **25,** 197 (1976)
[6] Lengyel, T.: Radiochem. Radioanal. Lett. **30,** 109 (1977)

Tamás Lengyel H-1121 Budapest, XII. Konkoly Thege út

Acta Chimica Academiae Scientiarum Hungaricae, Tomus 100 (1—4), pp. 81—88 (1979)

THE MATHEMATICAL MODEL OF A PARTIAL OXIDATION FLAME REACTOR

A. LÁSZLÓ[1] and A. NÉMETH[2]

([1] University of Chemical Engineering, Veszprém, [2] University Computer Center, Budapest)

Received June 20, 1978

Accepted for publication June 27, 1978

Acetylene production by partial oxidation of hydrocarbons is an industrial example of chemical operations based on flame reactions. Flame reactor modelling studies of the present authors aim at the substitution of earlier empirical or semi-empirical models [1, 2] by a theoretically established model. This modelling attempt is facilitated on the one hand by the more detailed knowledge of the chemical reaction mechanism of combustion processes amassed in the literature in recent years and the availability of powerful computation methods on the other hand, which allow for the preparation and handling of flame reactor models based on the chemical reaction mechanism.

There are two decisive states during the technological characterization of the partial oxidation flame reactor. The first is the knowledge of processes taking place in the flame zone under steady state conditions. This process characterizes the normal operation of the reactor. The other is the knowledge of processes which might take place in the section just ahead of the flame zone when the undesirable flare up of the combustible fuel-air mixture disrupts the regular operation of the reactor. This is one of the non-steady-state conditions of the flame reactor.

The reaction mechanism satisfying technological purposes was presented in previous publications [3, 4]. It was shown that based on this mechanism a flame reactor model adequately describing the ignition temperature versus induction period relationship characterizing the non-steady-state condition of the flame reactor could be developed [5]. This paper deals with the modelling of processes taking place in the flame zone of the reactor under steady state conditions.

The Method of the Investigation

The model used to describe the ignition phenomenon proved inadequate for the description of steady state processes taking place in the flame zone. There was a significant difference between calculated and measured residence times. For conventional methane partial oxidation temperatures and feed gas compositions (900 K, 60% *v/v* CH_4 and 40% *v/v* O_2) calculated average residence time was 2 s, two orders of magnitude higher than the experimental value:

0.02 s. It became evident from the analysis of temperature versus time and composition versus time relationships computed from the model that an unduely long section of much too low temperature gradient did arise in front of the actual flame zone as a result of the structure of the model. This section of the flame is called the initial section. It became evident that factors decreasing the length of this initial section had to be considered in order to develop a model adequate for the description of the flame section.

It is known from studies dealing with flame processes that apart from the chemical reaction just starting, heat- and mass transport processes are the major factors which primarily influence the length of the flame. The investigation method finally adapted could account for the above effects yet the modifications required and carried out in the physical model did not prevent the use of the algorithm previously developed.

The Model and the Reaction Mechanism

Flame reaction takes place at constant pressure and, at least for a zeroth order approximation, without enthalpy loss. This process can be approximated by a tube reactor model in which there is a plug-flow of the adiabatic gas mixture. However, as mentioned above, the model had to be able to simulate both heat loss and heat uptake. The refined isobaric-polytropic flame reactor model satisfying these criteria consists of the differential equation system shown below: for the concentration changes of the species:

$$\frac{\mathrm{d}c_j}{\mathrm{d}t} = \sum_{l=1}^{n_r} (R_{lj}^{+} - R_{lj}^{-}) \left(k_l e^{-\frac{E_l}{RT}}\right) \prod_{r=1}^{n_r} c_r^{\nu_{lr}} - \frac{c_j \,\mathrm{d}\ln V}{\mathrm{d}t} \tag{1}$$

for the temperature changes:

$$\frac{\mathrm{d}T}{\mathrm{d}t} = \frac{\alpha(T_h - T) - \sum_{r=1}^{n_e} h_r \frac{\mathrm{d}c_r V}{\mathrm{d}t}}{\sum_{r=1}^{n_e} c_r V \frac{\mathrm{d}h_r}{\mathrm{d}T}} \tag{2}$$

for the volume changes:

$$\frac{\mathrm{d}\ln V}{\mathrm{d}t} = \frac{\sum_{j=1}^{n_e} \sum_{l=1}^{n_r} (R_{lj}^{+} - R_{lj}^{-}) \left(k_l c^{-\frac{E_l}{RT}}\right) \sum_{r=1}^{n_e} c_r^{\nu_{lr}}}{\sum_{j=1}^{n_e} c_j} + \frac{\mathrm{d}\ln T}{\mathrm{d}t}. \tag{3}$$

The source term of the conservation equations of the model is based on the mechanism of the complex chemical reaction. Therefore, this differential equation system is an insufficiently conditioned, so-called rigid differential equation system. The computer algorithm proposed by GIER [6] proved the fastest way

Table I

The reaction mechanism

		k cm³, mole, s	E kcal/mole
$CH_4 + M$	$CH_3 + H$	4.00×10^{17}	88
$CH_4 + H$	$CH_3 + H_2$	1.26×10^{14}	11.9
$CH_4 + O$	$CH_3 + OH$	2.00×10^{13}	9.2
$CH_4 + OH$	$CH_3 + H_2O$	3.00×10^{13}	6.0
$CH_3 + O_2$	$CH_2O + OH$	1.70×10^{12}	14
$CH_3 + O$	$H + CH_2O$	2.6×10^{14}	2.0
$CH_2O + OH$	$H_2O + CHO$	2.3×10^{13}	0
$OH + CHO$	$H_2O + CO$	$1.0+10^{13}$	0
$CH_2O + M$	$CO + H_2 + M$	2.1×10^{16}	33.4
$CHO + M$	$H + CO + M$	6.0×10^{13}	28.7
$OH + CO$	$H + CO_2$	4.0×10^{12}	7.9
$O_2 + CO$	$O + CO_2$	1.6×10^{13}	41.1
$O + CO$	$CO_2 + M$	4.0×10^{13}	0
$O + H_2$	$H + OH$	2.1×10^{14}	13.7
$H + O_2$	$OH + O$	5.5×10^{15}	16.6
$OH + H_2$	$H + H_2O$	5.2×10^{13}	6.5
$OH + OH$	$O + H_2O$	5.5×10^{13}	7.0
$H + H + M$	$H_2 + M$	7.1×10^{14}	0
$H + OH + M$	$H_2O + M$	1.0×10^{16}	0
$O_2 + H_2$	$OH + OH$	1.7×10^{13}	48
$O_2 + M$	$O + O + M$	2.9×10^{15}	117
$CH_3 + CH_3$	$H_2 + C_2H_4$	2.0×10^{16}	38
$CH_3 + CH_3$	$H + C_2H_5$	6.0×10^{13}	10
$CH_3 + CH_3$	C_2H_6	8.4×10^{12}	0
$C_2H_4 + M$	$H_2 + C_2H_2 + M$	1.0×10^{14}	50
$O + C_2H_4$	$CH_3 + CHO$	2.3×10^{13}	2.7
$O_2 + O + C_2H_4$	$H + H + CH_2O + CO_2$	2.5×10^{13}	5.0
$O_2 + O + C_2H_2$	$H + H + CO + CO_2$	1.2×10^{14}	20
C_2H_6	$CH_3 + CH_3$	8.5×10^{14}	80
$H + C_2H_6$	$H + H_2 + C_2H_4$	1.3×10^{14}	9.8
$CH_3 + C_2H_6$	$CH_4 + H + C_2H_4$	2.0×10^{11}	10.5
$CH_3 + H_2$	$CH_4 + H$	3.2×10^{12}	10
C_2H_5	$H + C_2H_4$	3.0×10^{14}	39
$OH + C_2H_6$	$H_2O + C_2H_5$	6.5×10^{13}	5.6
$O_2 + C_2H_5$	$OH + C_2H_4 + O$	2.3×10^{12}	5
$O + C_2H_6$	$CH_3 + H + CH_2O$	1.6×10^{14}	7.8

to solve it. The method of automatical generation and solution of this differential equation system has been published in part [7].

The reaction mechanism has been also refined making use of new published data. The reaction mechanism as used here is shown in detail in Table I.

Investigation with the Model

In order to study the effects of temperature changes on the processes taking place in the initial section two series of computations were made. In the first series the initial section was contacted with an external segment of space in which the temperature was 100 and 200 K above the temperature of the feed gas. Heat was transferred by conduction from this space segment into the system. In the second series the temperature of feed gas was changed. Results clearly proved in both cases that temperature profoundly effected the processes taking place in the initial section. To demonstrate this statement residence time values from the second series obtained at feed gas temperatures of 900 ; 1000 and 1100 K are summarized in Table II.

Table II

The effect of temperature upon the initial section

Temperature, K	900	1000	1100
Initial section, s	2.21	0.41	0.1

It is known that in the case of laminar flames mass transfer takes place *via* diffusion in the initial section. However, an important feature of the partial oxidation flame reactors studied here is the multi-orifice burner. These burners, in turn, are characterized by significant back-mixing (back flow) of the product gases from the flame zone *via* the openings of the holes. This phenomenon is caused by the special arrangement of the holes. Comparative simulations has shown that this transport can significantly outweigh diffusion. Therefore in the next stage of the analysis varying amounts of the product gases were admixed to the fresh feed gas mixture at the actual temperature of the feed gas. In the case of methane partial oxidation the main components of product gases are hydrogen, carbon monoxide, acetylene, ethylene and ethane. The average residence time values in the initial section determining the length of the flame calculated from the results of computations are summarized in Table III. According to the model most product components significantly decrease the length of the initial section. This is especially apparent

when the mixture of hydrogen and carbon monoxide is mixed back. This finding is very important because in partial oxidation under the conditions studied these two compounds account for some 50% of the product gas.

The above model calculations in which heat and mass transfer effects were studied separately show that the decisive factor determining the heat and mass transfer processes in the initial section of the partial oxidation flame reactor studied is the partial backmixing of the product gas into the fresh feed gas. In the case of a model truly describing the actual situation product gases are backmixed into the fresh feed gas at the temperature of the flame. Thus, there is both heat and mass transfer taking place during backmixing.

Table III

The effect of backmixing upon the initial section

Species subject to backmixing	—	C_2H_6	C_2H_4	C_2H_2	CO/H_2
Initial section, s	2.21	0.054	0.98	2.07	0.011

There is a direct water injection cooling section immediately behind the flame zone used to cool down the hot products gases. Obviously, processes taking place in the flame zone are influenced by heat losses flowing toward this section. Therefore, heat losses of the flame zone have also to be accounted for in the model.

Thus, it can be concluded that an isobaric-politropic model with product gas backmixing is an adequate model of the steady state operation of the flame reactor.

This model was used to simulate various steady state technological conditions of the flame reactor and to asses the effects of the changes of the various technological parameters. The following cases were calculated;

— partial backmixing of hot products gases
— complet backmixing of hot product gases (which, in fact, turns the tube reactor into a perfectly mixed tank reactor)
— the above cases but accounting for heat losses in the flame zone as well.

Computations resulted in the temperature and species concentration distributions along the flame zone. Such data series are presented in Figures 1 and 2 relating to a characteristic section of the flame zone.

In order to allow for easier visualization species accumulation and consumption values are plotted directly against temperature values instead of length or time coordinates.

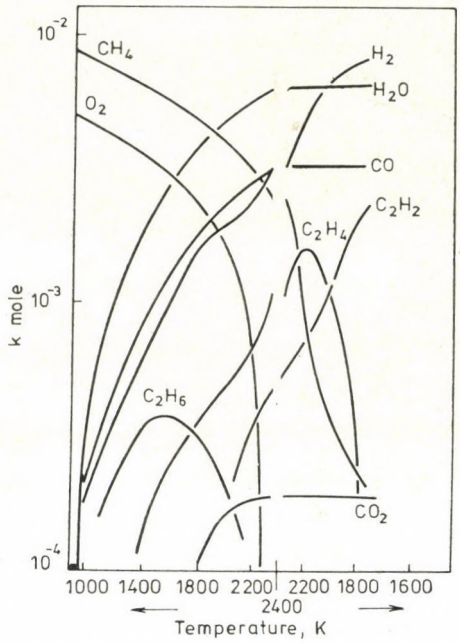

Fig. 1. **Distribution of the main components**

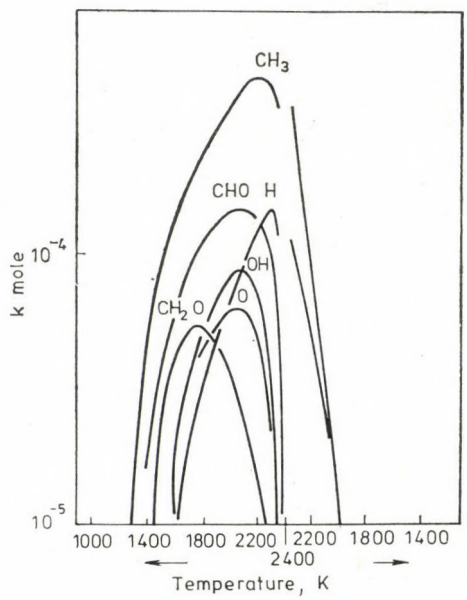

Fig. 2. **Distribution of the radicals**

The effects of backmixing of the hot product gases upon the composition of product gases in the case of 5% and complete backmixing are shown in Table IV.

Table IV

Composition of the product gas in the case of product gas backmixing

Component of the product gas	Composition of the product gas, mole fraction	
	5% backmixing	complete backmixing
CH_4	0.040	0.018
H_2O	0.350	0.526
CO	0.186	0.029
H_2	0.306	0.200
C_2H_4	0.089	0.006
C_2H_2	0.026	0.210
CO_2	0.010	0.010

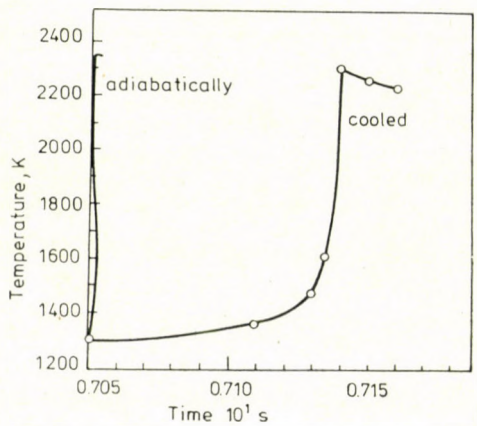

Fig. 3. Temperature profiles for adiabatic and cooled conditions

The temperature profile of the process is shown in Figure 3 in the case of the adiabatic flame reactor accounting also for the heat losses caused by the cooling section.

In summary it can be stated that

— the model is apparently adequate for the simulation of the steady state operation of the partial oxidation flame reactor
— spontaneous backmixing in the flame zone profoundly influences the process

— heat losses from the flame zone towards the cooling section decrease the temperature of the flame and increase the length of the flame zone to such an extent which cannot be neglected.

Symbols

c_j	concentration of species j
t	time
V	volume
p	pressure
T	temperature
T_H	temperature of the environment
R_{lj}^{+}	and R_{lj}^{-} the stochiometric coefficient of species j in reaction l, formation and consumption respectively
k_l	preexponential coefficient of reaction l
E	activation energy
R	gas constant
v	the order of reaction l for component j
n_r	number of reactions
n_c	number of components
h	partial molar enthalpy
α	heat transfer coefficient

REFERENCES

[1] NÉMETH, A., DOBAY, S.: Proceedings of the 2nd Conference on Applied Physical Chemistry, Vol. **2.** p. 539, Akadémiai Kiadó, Budapest, 1971
[2] STEPANOW, A. W., MACHORIN, K. E.: Chem. Techn. **24,** 135 (1972)
[3] BENEDEK, P., LÁSZLÓ, A., VÁCZI, P.: Deuxième Symposium Européen sur la Combustion, The Combustion Institute 1975. Vol. I. p. 154.
[4] BENEDEK, P., LÁSZLÓ, A., NÉMETH, A., VÁCZI, P.: Hungarian Journal of Industrial Chemistry **4,** 77 (1976)
[5] BENEDEK, P., LÁSZLÓ, A., NÉMETH, A., VÁCZI, P.: *ibid*, **5,** 133 (1977)
[6] GIER, C. W.: Communication of the ACM, **14,** 176, 185 (1971)
[7] BENEDEK, P., LÁSZLÓ, A., NÉMETH, A., VÁCZI, P.: Congres International "Contribution des calculateurs electroniques au development du génie chimique et de la chimie industrielle" Section *C* p. 120 (Paris 1978)

Antal LÁSZLÓ H-8201 Veszprém, Schönherz Z. u. 10. Pf. 28.
András NÉMETH H-1056 Budapest, V. Szerb u. 23.

Acta Chimica Academiae Scientiarum Hungaricae, Tomus 100 (1—4), pp. 89—99 (1979)

SYNTHESE UND UNTERSUCHUNG NEUER SPIROSTEROIDE, I

S. Sólyom, Z. Zubovics und L. Toldy

(Institut für Arzneimittelforschung, Budapest)

Eingegangen am 21. Juni, 1978

Zur Veröffentlichung angenommen am 26. Juli, 1978

Einige aus 17-Keto-steroiden hergestellte 17*S*-Spiro-oxirane wurden mit Methylamin umgesetzt. Aus den erhaltenen 17α-Methylaminomethyl-17β-hydroxysteroiden wurden Thioharnstoff-Derivate hergestellt und deren Ringschluss-Reaktionen unter oxydierenden und basischen Bedingungen untersucht. Es wurden 17-Spiro-steroide neuen Typs hergestellt: Spiroperhydro-1,2,4-oxathiazine, Spiro-(2'-imino-oxazolidine), sowie Spiro-(2'-thioxo-oxazolidine). Die Spiro-Verbindungen mit dem Perhydro-1,2,4-oxathiazin-Ring sind neue Vertreter dieses von uns zuerst hergestellten Ringsystems. Die chemischen und physikalischen Eigenschaften der Verbingunden wurden untersucht. Einige Verbindungen zeigten eine schwächere Antialdosteron-Wirkung als Spironolacton.

Verbindungen, die eine Aldosteron-blockierende Wirkung ausüben, bilden eine bedeutende Gruppe der Diuretika. Untersuchungen dieser Verbindungen erstreckten sich hauptsächlich auf Spirosteroide mit einer γ-Lacton-Gruppe am Kohlenstoffatom 17 [1]. Relativ wenig Interesse wurde für die Synthesen solcher Steroid-spiro-heterocyclen aufgebracht, die neben dem Sauerstoffatom auch ein anderes Heteroatom enthalten [2]. Wir hofften, auf diesem Gebiet Erfolg zu erzielen, und begannen eine vielfältige synthetische Arbeit.

Aus den Struktur-Wirkung Zusammenhängen [1b] der Aldosteron-blokkierenden Spirolacton-Steroide geht hervor, daß der Sauerstoff in 17β-Stellung — neben anderen Faktoren — für die Wirkung von Bedeutung zu sein scheint. Bei den angestrebten neuen Strukturen schienen daher die 17*S*-Spiro-oxirane geeignete Ausgangssubstanzen zu sein, bei denen das O-Atom β-orientiert ist, und die aus 17-Keto-steroiden stereospezifisch hergestellt werden können [3, 4]. Folgende, teilweise bekante Spiro-oxirane wurden nach der Methode von Hübner [3] synthetisiert: 3β-Hydroxy-5-androsten-17*S*-spiro-oxiran [5] (**1a**), 3-Methoxy-östra-2,5(10)-dien-17*S*-spiro-oxiran[3] (**1b**), 3-Methoxy-1,3,5(10),8-östratetraen-17*S*-spiro-oxiran (**1c**) und 13β-Äthyl-3-methoxy-gona-2,5(10)-dien-17*S*-spiro-oxiran (**1d**).

Steroid-17-spiro-oxirane kann man mit den meisten Nukleophilen leicht spalten (z. B. [6]). So wurden aus **1a**—**d** in flüssigem Methylamin in Gegenwart einer katalytischen Menge von *p*-Toluolsulfonsäure beim Erhitzen in einem geschlossenen Stahlgefäß die entsprechenden 17α-Methylaminomethyl-17β-hydroxysteroide **2a**—**d** hergestellt. Die 2-Aminoalkohol-Struktur dieser Verbindungen ermöglicht potentiell die Ausbildung verschiedener Heterocyclen. In dieser Arbeit wird über Ringschluß-Reaktionen der aus **2a**—**d** hergestellten **3a**—**d** Thioharnstoff-Derivate und über die so erhaltenen neuen Spiro-steroide berichtet.

	Steroid-Ringsystem
a	3β-Hydroxy-5-androsten
b	3-Methoxy-östra-2,5(10)-dien
c	3-Methoxy-1,3,5(10),8-östratetraen
d	13β-Äthyl-3-methoxy-gona-2,5(10)-dien
e	Androst-4-en-3-on
f	Östr-4-en-3-on
g	13β-Äthyl-gon-4-en-3-on

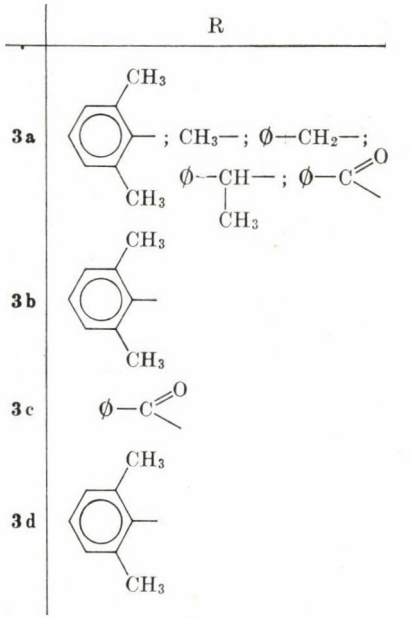

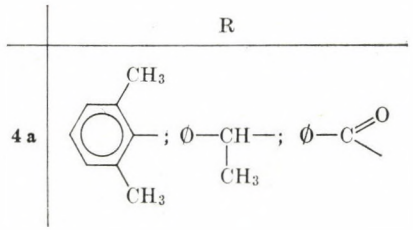

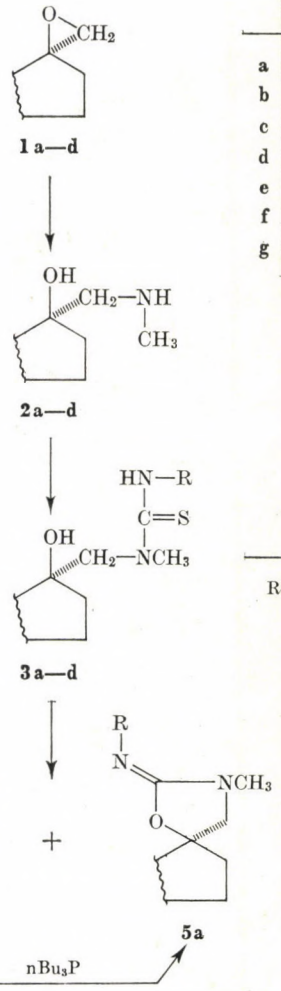

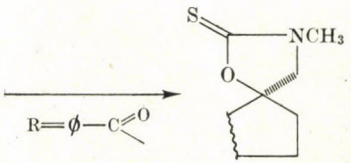

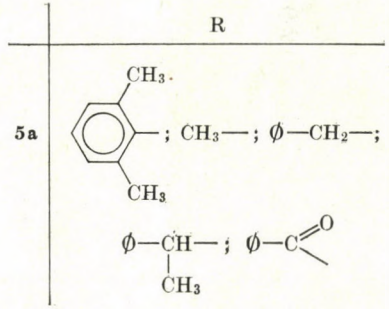

Die Verbindungen **2a—d** wurden mit Isothiocyanaten bzw. in einigen Fällen mit dem Methylester der entsprechenden Dithiocarbaminsäure in relativ guter Ausbeute zu den Thioharnstoffen **3a—d** umgesetzt [7]. Bei den Verbindungen **3a** wurde versucht, durch Säuren eine Ringschluß-Reaktion auszulösen [8], die Reaktion verlief aber nicht eindeutig. Verbindungen **3a** erlitten dabei eine Zersetzung, die nicht mehr weiter untersucht wurde.

In einer vorhergehenden Mitteilung berichteten wir über die dehydrierende Cyclisierung von *N*-(β-Hydroxyäthyl)-*N'*-benzoyl-thioharnstoff, die zu einer Verbindung mit einem neuen Hetero-Ringsystem, dem Perhydro-1,2,4-oxathiazin führte [9]. Es war naheliegend, diese dehydrierende Cyclisierung auch bei den Verbindungen **3a** auszuführen. Zu diesem Zweck wurden **3a** in Gegenwart von Pyridin mit Jod umgesetzt, wobei die Derivate **4a** und **5a** gebildet wurden. Bei der Substitution R = 2,6-Dimethylphenyl und Benzoyl entstand das Rohprodukt in guter Ausbeute und erwies sich als **4a**, das durch Schwefel-Eliminierung entstehende Imino-oxazolidin bildete sich durch Zersetzung beim Umkristallisieren. Während bei der Substitution R = α-Phenyläthyl die entsprechenden **4a** und **5a** in vergleichbaren Mengen im Rohprodukt der dehydrierenden Cyclisierung vorhanden waren, konnte bei R = Methyl und Benzyl nur **5a** isoliert werden.

Die Spiro-perhydro-1,2,4-oxathiazine **4a** setzen, ihrem Monothioperoxy-Bindungsystem entsprechend, aus Kaliumjodid Jod frei. Beim Erhitzen zersetzen sie sich und es entsteht unter anderem elementarer Schwefel. Im Massenspektrum von **4a** (R = 2,6-Dimethylphenyl und Benzoyl) erscheint das entsprechende Molekülion, aber seine Intensität verringert sich wegen Zersetzung schnell. Das durch Schwefel-Abspaltung entstehende Ion ist das Basis-Fragment und konnte jeweils als das entsprechende **5a** identifiziert werden.

Im IR-Spektrum der Verbindung **4a** (R = Benzoyl) fehlte jegliche Absorption im Bereich 1600—1800 cm^{-1}. Die Röntgen-Strukturanalyse der analogen Verbindung ohne Steroid-Ringsystem ließ eine starke Carbonylsauerstoff-Schwefel Wechselwirkung sowie eine verlängerte Carbonyl-Bindung [9] erkennen. Die fehlende ν C=O Bande im IR-Spektrum der analogen Spirosteroid-Verbindung ist dadurch erklärt. Dementsprechend kann **4a** (R = Benzoyl) mittels der folgenden Mesomerie beschrieben werden [10]:

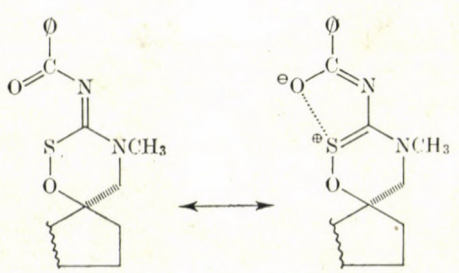

Bei dieser Verbindung wird der übrigens sich leicht zersetzende Perhydro-1,2,4-oxathiazin-Ring durch die Carbonylsauerstoff-Schwefel Wechselwirkung stabilisiert. Bei den Derivaten **4a** (R = 2,6-Dimethylphenyl und α-Phenyläthyl) besteht kein solcher stabilisierender Effekt. Wir nehmen an, daß die Stabilität und die Darstellbarkeit dieser Verbindungen einerseits vom größeren Raumbedarf des R-Substituenten und andererseits vom Steroid-Ringsystem abhängt. Aus 1-(β-Hydroxyäthyl)-3-(2',6'-dimethylphenyl)-thioharnstoff — der kein Steroid-Ringsystem enthält — konnte nähmlich keine entsprechende cyclische Oxathiazin-Verbindung hergestellt werden.

Bei der Umsetzung der Verbindungen **4a** mit 1,5—2 Äquivalenten Tributylphosphin konnten die schon früher als Zersetzungsprodukte isolierten Derivate **5a** glatt hergestellt werden.

Im weiteren wurde versucht **3a,c** (R = Benzoyl) in wäßrigem Alkohol mit Kaliumhydrogencarbonat zu hydrolisieren, um aus dem auf diese Weise potentiell herstellbaren **3a,c** (R = H) durch dehydrierende Cyclisierung **4a,c** zu gewinnen. Bei der Hydrolyse entstand aber nur **6a,c**. Die Struktur dieser Steroid-spiro-(2'-thiooxo-oxazolidin)-Derivate wurde, außer einer entsprechender Analyse, durch IR- und PMR-Spektren sowie durch eine unabhängige Synthese bewiesen.

Bei der Umsetzung von **2a** in Methylenchlorid mit Thiophosgen in Gegenwart von Triäthylamin wurde **6a** — wegen der ungeschützten Hydroxyl-Gruppe — nur in mäßiger Ausbeute erhalten. Die Ringschluß-Reaktionen von **2b, d** mit Thiophosgen wurden analog ausgeführt. Die Produkte erlitten aber wegen ihrer Enoläther-Struktur während der Reaktion eine partielle Hydrolyse (dünnschichtchromatographisch festgestellt). Die Hydrolyse wurde deshalb durch zugesetzte Mineralsäure vervollständigt und nur **6f, g** isoliert. Die Δ^4-3-Oxo-Struktur der letzteren Verbindungen war auch für die biologische Untersuchung wünschenswerter [1b].

Zwecks biologischer Untersuchungen wurden **5a** (R = 2,6-Dimethylphenyl), bzw. **6a** durch Oppenauer-Oxydation in **5e** (R = 2,6-Dimethylphenyl), bzw. **6e** überführt.

Die Aldosteron-blockierende Wirkung der hergestellten Verbindungen wurde nach Kagawa [11] getestet. Die Verbindungen **4a** (R = 2,6-Dimethylphenyl) und **5a** (R = 2,6-Dimethylphenyl, Benzyl, Methyl, Benzoyl) zeigten eine signifikante, jedoch schwächere Wirkung als das Spironolacton (7α-Acetylthio-17α-carboxyäthyl-17β-hydroxy-androst-4-en-3-on-lacton) [1]. Diese Beobachtung diente als Ausgangspunkt für weitere Untersuchungen.

Experimenteller Teil

Schmelz- und Zersetzungspunkte wurden auf einem Küstner-Heizmikroskop bestimmt und sind unkorrigiert. Optische Drehwerte, soweit nicht anders angegeben, wurden in Chloroform mit einem LEP-OPTON-Gerät gemessen. Die IR-Spektren wurden mit einem Perkin—Elmer 457, PMR-Spektren mit einem Varian A-60D-Gerät registriert.

A. Steroid-spiro-oxirane (1c, d)

3-Methoxy-1,3,5(10),8-östratetraen-17S-spirooxiran (1c)

Aus 15,3 g 3-Methoxy-1,3,5(10),8-östratetraen-17-on wurden nach Lit. [3] 11,0 g (68%) farblose Kristalle (aus Methanol) erhalten. Schmp. 108—110 °C; $[\alpha]_D^{20} = -60{,}9°$ ($c = 1$). $C_{20}H_{24}O_2$ (296,39). Ber. C 81,04; H 8,16. Gef. C 81,05; H 8.10%.

13β-Äthyl-3-methoxy-gona-2,5(10)-dien-17S-spiro-oxiran (1d)

1d wurde aus 6,0 g (20 mmol) 13β-Äthyl-3-methoxy-gona-2,5(10)-dien-17-on [12] analog **1c** hergestellt. Das Rohprodukt wurde mit 20 ml Äthanol aufgekocht und warm filtriert, wobei 5,44 g Substanz (Schmp. 183 °C) zurückblieb. Eine kleine Probe wurde für die Analyse aus der 30-fachen Menge Essigester umkristallisiert, Schmp. 187—189 °C; $[\alpha]_D^{20} = +106°$ ($c = 0{,}5$).

$C_{21}H_{30}O_2$ (314,45). Ber. C 80,20; H 9,61; Gef. C 80,45; H 9,89%.

B. 17α-Methylaminomethyl-17β-hydroxy-steroide (2a-d)

3β,17β-Dihydroxy-17α-methylaminomethyl-5-androsten (2a)

14,0 g (0,046 mol) **1a** und 1,40 g *p*-Toluolsulfonsäure wurden mit 50 ml flüssigem Methylamin vermischt und in einem Stahlgefäß 16 h auf 130 °C (Ölbadtemperatur) erwärmt. Nach Abkühlen und Öffnen wurde das überflüssige Methylamin abgedampft und der Rückstand auf der Glasfritte mit Wasser neutral gewaschen. Das trockene Rohprodukt (14,8 g) wurde in 600 ml warmen Essigester gelöst, filtriert und die Lösung auf etwa 200 ml Volumen eingeengt. Nach Zugabe von 200 ml *n*-Hexan kristallisierten beim Stehenlassen 11,56 g (75%) farblose Kristalle. Schmp. 197—199 °C; $[\alpha]_D^{20} = -85°$ ($c = 0{,}5$).

$C_{21}H_{35}NO_2$ (333,50). Ber. C 75,62; H 10,58; N 4,20. Gef. C 75,58; H 10,26; N 4,10%.

3-Methoxy-17α-methylaminomethyl-17β-hydroxy-2,5(10)-östradien (2b)

Aus 13,0 g (43 mmol) **1b** wurde analog zu **2a** 13,65 g Rohprodukt hergestellt und aus Methanol umkristallisiert. Ausbeute: 10,1 g (71%). Schmp. 136—137 °C; $[\alpha]_D^{20} = +87{,}3°$ ($c = 0{,}5$).

$C_{21}H_{33}NO_2$ (331,48). Ber. C 76,08; H 10,03; N 4,22. Gef. C 75,90; H 9,96; N 4,19%.

3-Methoxy-17α-methylaminomethyl-17β-hydroxy-1,3,5(10),8-östratetraen (2c)

Das aus 11,05 g (37 mmol) **1c** analog zu **2a** erhaltene Rohprodukt (9,46 g) wurde aus 180 ml Methanol umkristallisiert. Ausbeute: 6,16 g (51%). Schmp. 139 °C; $[\alpha]_D^{20} = -49{,}5°$ ($c = 1$).

$C_{21}H_{29}NO_2$ (327,45). Ber. C 77,02; H 8,92; N 4,28. Gef. C 76,79; H 8,79; N 4,34%.

13β-Äthyl-3-methoxy-17α-methylaminomethyl-17β-hydroxy-gona-2,5(10)-dien (2d)

Das aus 30,0 g (95 mmol) **1d** analog zu **2a** erhaltene Rohprodukt (32,6 g) wurde in zweifachem Volumen Äthanol einige Minuten zum Sieden erhitzt und warm filtriert. Ausbeute: 25,48 g (77%). Schmp. 188—189 °C; $[\alpha]_D^{20} = +66{,}9°$ ($c = 0{,}5$).

$C_{22}H_{35}NO_2$ (345,51). Ber. C 76,47; H 10,21; N 4,05. Gef. C 76,66; H 10,02; N 4,09%.

C. 17α-[*N*-Methyl-*N*-(R-thiocarbamoyl)]-aminomethylsteroide (3a-d)

Allgemeine Vorschrift:

2a—d wurden in Äthanol mit einem in 5—30% molaren Überschuß angewandten Isothiocyanat oder dem Methylester der entsprechenden Dithiocarbaminsäure 2—6 h zum Sieden erhitzt. Die Umsetzung wurde dünnschichtchromatographisch verfolgt. Die Produkte wurden durch Einengen und Absaugen isoliert.

17α-[*N*-Methyl-*N*-(2',6'-dimethylphenyl-thiocarbamoyl)]-aminomethyl-3β, 17β-dihydroxy-5-androsten (3a; R = 2,6-Dimethylphenyl)

Schmp. 217—220 °C (aus Äthanol). Ausbeute: 88%; $[\alpha]_D^{20} = -199°$ ($c = 0{,}5$).

$C_{30}H_{44}N_2O_2S$ (496,73). Ber. C 72,53; H 8,93; N 5,64; S 6,45. Gef. C 72,55; H 8,93; N 5,46; S 6,30%.

17α-[*N*-Methyl-*N*-(methylthiocarbamoyl)]-aminomethyl-3β,17β-dihydroxy-5-androsten (3a; R = Methyl)

Schmp. 227—230 °C (aus Acetonitril). Ausbeute: 84%; $[\alpha]_D^{20} = -75{,}9°$ ($c = 1$, Pyridin).

$C_{23}H_{38}N_2O_2S$ (406,64). Ber. C 67,94; H 9,42; N 6,89; S 7,89. Gef. C 67,87; H 9,14; N 6,94; S 8,03%.

17α-[*N*-Methyl-*N*-(benzylthiocarbamoyl)]-aminomethyl-3β,17β-dihidroxy-5-androsten (3a; R = Benzyl)

Schmp. 131 °C (aus Acetonitril). Ausbeute: 75%; $[\alpha]_D^{20} = -148{,}3$ °($c = 1$).

$C_{29}H_{42}N_2O_2S$ (482,73). Ber. C 72,16; H 8,77; N 5,80; S 6,64. Gef. C 72,19; H 8,92; N 5,52; S 6,47%.

17α-[N-Methyl-N-(α-phenyläthyl-thiocarbamoyl)]-aminomethyl-3β, 17β-dihydroxy-5-androsten (3a; R = α-Phenyläthyl)

Schmp. 184—185 °C (aus Essigester). Ausbeute: 67%; $[\alpha]_D^{20} = -160{,}4°$ ($c = 1$).
$C_{30}H_{44}N_2O_2S$ (496,76). Ber. C 72,54; H 8,93; N 5,64; S 6,45. Gef. C 72,81; H 8,85; N 5,51; S 6,54%.

3-Methoxy-17β-hydroxy-17α-[*N*-methyl-*N*-(2',6'-dimethylphenyl-thiocarbamoyl)]-aminomethyl-östra-2,5(10)-dien (3b; R = 2,6-Dimethylphenyl)

Schmp. 201—204 °C (aus Acetonitril). Ausbeute: 81%; $[\alpha]_D^{20} = -85{,}4°$ ($c = 1$).
$C_{30}H_{42}N_2O_2S$ (494,76). Ber. C 72,83; H 8,56; N 5,66; S 6,48. Gef. C 73,20; H 8,79; N 5,76; S 6,26%.

13β-Äthyl-3-methoxy-17β-hydroxy-17α-[*N*-methyl-*N*-(2',6'-dimethylphenyl-thiocarbamoyl)]-aminomethyl-gona-2,5(10)-dien (3d; R = 2,6-Dimethylphenyl)

Schmp. 193—196 °C (aus Acetonitril). Ausbeute: 88%; $[\alpha]_D^{20} = -88{,}6°$ ($c = 1$).
$C_{31}H_{44}N_2O_2S$ (508,77). Ber. C 73,19; H 8,72; N 5,51; S 6,30. Gef. C 73,51; H 8,95; N 5,41; S 6,24%.

D. Spiro-perhydro-1,2,4-oxathiazine und Spiro-iminooxazolidine (4a und 5a)

3β-Hydroxy-5-androsten-17*S*-spiro-6'-[3'-(2,6-dimethylphenylimino)-4'-methyl-perhydro-1,2,4-oxathiazin] (4a; R = 2,6-Dimethylphenyl)

12,0 g (24,2 mmol) **3a** (R = 2,6-Dimethylphenyl) wurden in 65 ml trockenem Pyridin und 65 ml Äther gelöst. Der auf 5 °C gekühlten und gerührten Lösung wurde während 30 Minuten eine Lösung von 6,17 g (0,0485 g Atom) Jod in 85 ml Äthanol tropfenweise zugesetzt.

Am Anfang verschwindet die braune Farbe des Jodes merklich, später wird die Lösung allmählich rotbraun. Der Ansatz wurde 3,5 h bei Raumtemp. gerührt und danach in 700 ml 0,5 *N* eiskalte Natriumhydroxyd-Lösung gegossen. Die ausgeschiedene Substanz wurde abgesaugt und mit Wasser neutral gewaschen. Ausbeute: 11,85 g (98%); Schmp. 191—192 °C. 6,0 g Substanz wurden in 700 ml Essigester warm gelöst, die filtrierte Lösung wurde auf etwa 100 ml eingeengt. Beim Stehenlassen kristallisierten 4,37 g weiße Kristalle. Schmp. 193 °C; $[\alpha]_D^{20} = -45{,}7°$ ($c = 0{,}5$).

$C_{30}H_{42}N_2O_2S$ (494,72). Ber. C 72,83; H 8,56; N 5,66; S 6,48. Gef. C 72,38; H 8,55; N 5,49; S 6,52%.

MS: $M^{+\cdot} = 494$ (die Intensität nimmt schnell ab); $(M-S)^{+\cdot} = 462$ (100%); Schwefel; R—NCS ($M^{+\cdot} = 163$).

In der Mutterlauge der Kristallisation konnte dünnschichtchromatographisch (Kieselgel, Benzol-Methanol-Aceton = 8 : 1 : 1) nur eine geringe Menge an **4a** (R = 2,6-Dimethylphenyl) (R_f: 0,6), dafür aber ein zweiter Fleck mit niedrigerem R_f-Wert (0,35) nachgewiesen werden. Die Mutterlauge wurde eingedampft und der Rückstand zur Vervollständigung der Zersetzung in Dioxan gelöst und 4 h zum Sieden erhitzt. Nach dem Eindampfen wurde der kristalline Rückstand mit Petroläther angerieben, gewaschen und aus Methanol zweimal umkristallisiert. Es wurden 0,48 g (Schmp. 256 °C) einer nicht ganz analysenreinen, mit **5a** (R = 2,6-Dimethylphenyl) identischen Substanz erhalten.

3β-Hydroxy-5-androsten-17*S*-spiro-5'-[2'-(2,6-dimethylphenylimino)-3'-methyl-oxazolidin] (5a; R = 2,6-Dimethylphenyl)

Einer gerührten Lösung von 2.47 g (5 mmol) **4a** (R = 2,6-Dimethylphenyl) in 80 ml trockenem Methylenchlorid wurde bei Raumtemp. während 40 Minuten eine Lösung von 0,72 ml (5 mmol) Tributylphosphin in 10 ml Methylenchlorid zugetropft. Nach 24 h wurde der Ansatz erneut mit 0,72 ml Tributylphosphin versetzt und anschließend 4 h zum Sieden erhitzt. Nach dem Eindampfen blieb ein Öl zurück, das mit 20 ml Petroläther geschüttelt wurde. Allmählich schieden sich Kristalle aus. Nach Dekantieren wurde der Kristallbrei nochmals mit reinem Petroläther durchgeschüttelt und die kristalline Substanz abgesaugt: 2,23 g (96%); Schmp. 256—260 °C. Das Produkt wurde aus 130 ml Methanol umkristallisiert: 1,64 g, Schmp. 260 °C; $[\alpha]_D^{20} = +26{,}4°$ ($c = 1$).

$C_{30}H_{42}N_2O_2$ (462,66). Ber. C 77,87; H 9,15; N 6,05. Gef. C 77,54; H 9,04; N 5,79%.
MS: $M^{+\cdot} = 462$ (100%); *m/e*: 147 (29%); 44 (23%); 300 (8,6%).

3-Acetat (bereitet in Benzol mit Essigsäureanhydrid-Pyridon): Schmp. 261 °C.

Androst-4-en-3-on-17*S*-spiro-5'-[2'-(2,6-dimethylphenylimino)-3'-methyl-oxazolidin] (5e; R = 2,6-Dimethylphenyl)

Eine Lösung von 1,40 g (3 mmol) **5a** (R = 2,6-Dimethylphenyl) und 2,04 g (12 mmol) Aluminiumisopropylat in 12,3 ml (0,12 mol) Cyclohexanon und 40 ml trockenem Toluol wurde 2 h gekocht. Nach dem Abkühlen wurde die Lösung mit 3×30 ml einer wäßrigen 5 proz. Kochsalz- und 5 proz. Seignette-Salz-Lösung durchgeschüttelt. (Die entstandene Emulsion wurde durch Filtrieren zerstört und die wäßrige Phase wurde jeweils mit Benzol extrahiert.) Die vereinigte organische Phase wurde getrocknet und eingedampft. Der ölige Rückstand kristallisierte nach Anreiben mit Diisopropyläther. Das Rohprodukt (0,56 g) wurde aus 10 ml Essigester umkristallisiert: 0,45 g, Schmp. 210—211 °C; $[\alpha]_D^{20} = +158°$ ($c = 0{,}5$).

$C_{30}H_{40}N_2O_2$ (460,64). Ber. C 78,22; H 8,75; N 6,08. Gef. C 78,46; H 8,98; N 6,44%.

3β-Hydroxy-5-androsten-17*S*-spiro-6'-[3'-(α-phenyläthylimino)-4'-methyl-perhydro-1,2,4-oxathiazin] (4a; R = α-Phenyläthyl) **und 3β-Hydroxy-5-androsten-17*S*-spiro-5'-[2'-(α-phenyläthylimino)-3'-methyl-oxazolidin) (5a**; R = α-Phenyläthyl)

2,20 g (4,5 mmol) **3a** (R = α-Phenyläthyl) wurde auf die unter D (**4a**) beschriebene Weise umgesetzt. Der Unterschied war, daß der Ansatz in eine eiskalte wäßrige 0,1 *N* Natriumhydroxid-Lösung gegossen wurde. Das abgesaugte Rohprodukt (2,14 g) wurde in 40 ml Isopropanol gelöst, und nach Zugabe von 50 ml Äther konnte eine ausgefallene Substanz durch Absaugen isoliert werden. Diese Substanz ergab nach Umkristallisieren aus Isopropanol 0,08 g **5a**-Hydrojodid (R = α-Phenyläthyl), Schmp. 191—194 °C.

$C_{30}H_{43}IN_2O_2$ (590,58). Ber. C 61,01; H 7,34; N 4,74. Gef. C 61,15; H 7,85; N 4,65%.

Der Rückstand, der beim Eindampfen der vorstehend beschriebenen Isopropanol-Äther-Lösung erhalten wurde, wurde mit Äther verrieben und gewaschen. Das Rohprodukt (0,50 g) wurde aus Methanol umkristallisiert, wobei 0,24 g (11%) **4a** (R = α-Phenyläthyl) als farblose Kristalle erhalten wurden. Schmp. 192—195 °C; $[\alpha]_D^{20} = +7{,}4°$ ($c = 0{,}5$).

$C_{30}H_{42}N_2O_2S$ (494,73). Ber. C 72,83; H 8,56; N 5,66; S 6,48. Gef. C 72,23; H 9,11; N 5,60; S 5,97%.

Die letzte Mutterlauge (Behandlung mit Äther) wurde ebenfalls eingedampf und der Rückstand mit Hexan gewaschen. Nach zweimaligem Umkristallisieren des Rohprodukts aus Acetonitril wurden 0,23 g (11%) **5a** (R = α-Phenyläthyl) als farblose Kristalle erhalten. Schmp. 163 °C.

$C_{30}H_{42}N_2O_2$ (462,67). Ber. C 77,88; H 9,15; N 6,05. Gef. C 77,96; H 9,45; N 6,20%.

3β-Hydroxy-5-androsten-17*S*-spiro-5'-(2'-methylimino-3'-methyl-oxazolidin) (5a; R=Methyl)

Bei der Umsetzung von 2,43 g (5,98 mmol) **3a** auf die unter D (**4a**) beschriebene Weise wurden 2,23 g Rohprodukt erhalten, das aus Essigester umkristallisiert 1,67 g (75%) farblose Kristalle ergab. Schmp. 240—242 °C; $[\alpha]_D^{20} = -59{,}5°$ ($c = 1$).

$C_{23}H_{36}N_2O_2$ (372,51). Ber. C 74,15; H 9,74; N 7,52. Gef. C 74,06; H 9,83; N 7,42%.

3β-Hydroxy-5-androsten-17*S*-spiro-5'-(2'-benzylimino-3'-methyl-oxazolidin) (5a; R = Benzyl)

7,0 g (14,6 mmol) **3a** (R = Benzyl) wurden wie unter D (**4a**) beschrieben umgesetzt, nur mit dem Unterschied, daß das Isolieren, nachdem der Ansatz in Lauge gegossen wurde, durch Extrahieren mit 5 × 300 ml Äther erfolgte. Der Äther-Extrakt wurde neutral gewaschen, getrocknet und eingedampft. Man erhielt 5,14 g (78%) Rohprodukt, das aus Acetonitril umkristallisiert wurde: 3,9 g (60%), Schmp. 170—173 °C; $[\alpha]_D^{20} = -24{,}7°$ ($c = 0{,}5$).

$C_{29}H_{40}N_2O_2$ (448,66). Ber. C 77,63; H 8,49; N 6,24; Gef. C 77,55; H 9,05; N 6,37%

3β-Hydroxy-5-androsten-17*S*-spiro-6'-(3'-benzoylimino-4'-methyl-perhydro-1,2,4-oxathiazin) (4a; R = Benzoyl)

a) Zu einer gerührten Lösung von 2,14 g (22 mmol) Kaliumrhodanid in 20 ml trockenem Aceton wurde bei Zimmertemp. 2,50 ml (21,8 mmol) Benzoylchlorid tropfenweise zugegeben. Anschließend wurde der Ansatz 40 Minuten zum Sieden erhitzt, dann abgekühlt und eine Suspension von 6,66 g (20 mmol) **2a** in 150 ml Chloroform zugegeben. Die erhaltene gerührte Suspension wurde 4 h zum Sieden erwärmt. Nach Einengen wurde der Kristallbrei ins Wasser gegossen, abgesaugt und gründlich mit Wasser gewaschen. Das so erhaltene **3a** (R = Benzoyl) erwies sich (Schmp. 128—132 °C) dünnschichtchromatographisch als einheitlich, konnte aber durch Umkristallisieren nicht weiter gereinigt werden. Es wurde deshalb in Form des Rohprodukts weiter benutzt. (Befriedigende Analysenwerte wurden nur für N und S erhalten.)

b) 1,0 g (2,02 mmol) des vorstehend beschriebenen **3a** (R = Benzoyl) wurde in 5 ml trockenem Pyridin und 5 ml Äther gelöst. Unter Rühren und Kühlen auf 5 °C wurde eine Lösung von 0,54 g g (2,12 mmol) Jod in 10 ml Äthanol zugetropft (etwa 30 Minuten). Anschließend wurde der Ansatz 2,5 h weitergerührt, dann unter 30 °C im Vakuum auf etwa das halbe Volumen eingeengt und in eine eiskalte 10 proz. wäßrige Kaliumcarbonat-Lösung gegossen. Die ausgeschiedenen Kristalle wurden abgesaugt, mit Wasser gewaschen und über Phosphorpentoxid getrocknet. Das Rohprodukt (0,94 g) wurde in 150 ml Methanol warm gelöst, die Lösung filtriert und auf etwa das halbe Volumen eingeengt. Beim Stehenlassen kristallisierten 0,40 g farblose Kristalle. Schmp. 199—202 °C; $[\alpha]_D^{20} = -53{,}7°$ ($c = 0{,}5$).

$C_{29}H_{38}N_2O_3S$ (494,67). Ber. C 70,40; H 7,74; N 5,66; S 6,48. Gef. C 69,27; H 7,92; N 5,46; S 6,49.

MS: $M^{+\cdot} = 494$ (die Intensität nimmt schnell ab); $(M-S)^{+\cdot} = 462$; Schwefel; *m/e*: 113.

Der Eindampfrückstand der Mutterlauge wurde in Dioxan gelöst, 4 h zum Sieden erhitzt, anschließend eingedampft, mit Petroläther verrieben und auf der Glasfritte gewaschen. Man kristallisierte die erhaltene Substanz (0,28 g) aus Methanol um und erhielt 0,14 g farblose Kristalle, die sich nach IR-, PMR-Spektrum und Mischschmelzpunkt-Bestimmung als **5a** (*R* = Benzoyl) erwiesen (siehe weiter). Die Kristalle zeigen Polymorphie und folgende Schmelzpunkte konnten bei der Schmelzpunkt-Bestimmung erhalten werden: 120—122 °C, 178—183 °C, 210—212 °C.

3β-Hydroxy-5-androsten-17*S*-spiro-5'-(2'-benzoylimino-3'-methyl-oxazolidin) (**5a**; R = Benzoyl)

Zu einer gerührten Lösung von 1,44 g (2,92 mmol) **4a** (R = Benzoyl) in 20 ml trockenem Methylenchlorid wurde unter Stickstoff während 30 Minuten eine Lösung von 0,42 ml (2,92 mmol) Tributylphosphin in 6 ml Methylenchlorid tropfenweise zugegeben. Nach 16 h wurde die Lösung nochmals mit 0,42 ml Tributylphosphin versetzt und nach weiteren 2 h eingedampft. Der kristalline Rückstand wurde mit Petroläther gewaschen. Das so erhaltene fast reine Rohprodukt (1,36 g — 100%; Schmp. 208—213 °C) ergab nach Umkristallisieren aus 14 ml Methanol 0,86 g farblose Kristalle, die bei 120—122 °C schmolzen. Bei weiterem Aufheizen erstarrte die Schmelze zwischen 140—155 °C, und die entstandenen Kristalle schmolzen endgültig bei 212—213 °C. $[\alpha]_D^{20} = +37{,}4°$ ($c = 0{,}5$).

$C_{29}H_{38}N_2O_3$ (462, 61). Ber. C 75,28; H 8,28; N 6,05. Gef. C 74,94; H 8,21; N 5,87%.

MS: $M^{+\cdot} = 462$ (100%); *m/e*: 113 (81%); 105 (56%); 385 (16%); 77 (16%); 300 (14%); 314 (14%); 44 (12,4%).

E. Spiro-thiooxo-oxazolidine (6a, c, e, f, g)

3β-Hydroxy-5-androsten-17*S*-spiro-5'-(2'-thiooxo-3'-methyl-oxazolidin) (6a)

a) Ein Gemisch aus 5,0 g (10 mmol) **3a** (R = Benzoyl) (siehe **4a**; **R** = Benzoyl, *a* 3,5 g Kaliumhydrogencarbonat, 30 ml Wasser und 160 ml Äthanol wurde 2,5 h zum Sieden erhitzt. Die entstandene Lösung wurde nachher eingeengt und ins Wasser gegossen. Das ausgefallene Produkt wurde abgesaugt und mit Wasser gewaschen. Das trockene Rohprodukt wurde zweimal aus Methanol umkristallisiert und ergab 2,31 g (60%) weisse Kristalle. Schmp. 246—247 °C; $[\alpha]_D^{20} = -84°$ ($c = 0{,}5$).

$C_{22}H_{33}NO_2S$ (375,55). Ber. C 70,35; H 8,85; N 3,73; S 8,54. Gef. C 69,93; H 9,01; N 3,72; S 8,70%.

IR (KBr): νOH: 3600—3100, Thiourethan-Banden: 1520, 1330, 1300, 1190 cm^{-2}.

PMR ($CDCl_3$): δCH_3 (18,19): 1,00 ppm, s (6H); δNCH_3: 3,15 ppm, s (3H); δCH_2 (Spiro-Ring): 3,40 und 3,85 ppm, m (2H, AB-Spektrum, $J_{AB} = 11$ Hz); δOH: 3,45 ppm, s (1H); δH-6: 5,35 ppm, m (1H).

3-Acetat (hergestellt in Pyridin mit Essigsäureanhydrid): Schmp. 190 °C.

b) Zu einer Lösung von 3,33 g (10 mmol) **2a** und 6 ml (43 mmol) Triäthylamin in 100 ml Tetrahydrofuran wurden 2,50 g (22 mmol) Thiophosgen mit 5 ml Tetrahydrofuran verdünnt zugetropft. Die erhaltene braune Lösung wurde 3 h bei Raumtemp. gerührt und anschließend eingedampft. Der Rückstand wurde in 5 proz. Natriumhydrogencarbonat-Lösung aufgenommen. Das Produkt wurde mit Chloroform extrahiert, und die organische Phase neutral gewaschen. Nach dem Eindampfen erhielt man ein Gemisch, das dünnschichtchromatographisch mehrere Produkte aufwies. Nach dreimaligem Umkristallisieren aus Methanol erhilt man 1,02 g (27%) einer reinen Substanz (Schmp. 246 °C), die mit der voranstehenden Substanz **6a** identisch war.

Androst-4-en-3-on-17*S*-spiro-5'-(2'-thiooxo-3'-methyl-oxazolidin) (6e)

Eine Lösung aus 1,88 g (5 mmol) **6a**, 15,5 ml (0,15 mol) Cyclohexanon, 4,1 g (20 mmol) Aluminiumisopropylat und 50 ml trockenem Toluol wurde 4,5 h gerührt und zum Sieden erhitzt. Die Lösung wurde anschließend gekühlt und mit 2×25 ml einer 5 proz. Salzsäure-Lösung durchgeschüttelt. Die organische Phase wurde nacheinander mit 25 ml Wasser, 25 ml 10 proz. Natriumhydrogencarbonat-Lösung und erneut mit Wasser gewaschen, getrocknet und eingedampft. Der Rückstand wurde mit Diisopropyläther gewaschen und das Rohprodukt (1,11 g) aus 90 ml Methanol umkristallisiert. Ausbeute: 0,81 g (44%); Schmp. 282—285 °C; $[\alpha]_D^{20} = +91{,}2°$. ($c = 1$). UV λ_{max}^{EtOH}: 243 mμ (ε: 31700).

$C_{22}H_{31}NO_2S$ (373,54). Ber. C 70,73; H 8,36; N 3,75; S 8,58. Gef. C 70,75; H 8,46; N 3,64; S 8,55%.

3-Methoxy-1,3,5(10)8-östratetraen-17*S*-spiro-5'-(2'-thioxo-3'-methyl-oxazolidin) (6c)

Aus 3,27 g (10 mmol) **2c** wurde zuerst **3c** (R = Benzoyl) hergestellt (nach der unter **4a**; R = Benzoyl, *a*) beschriebenen Methode,) und dann das erhaltene Rohprodukt analog zu **6a** umgesetzt. Das Produkt wurde aus Äthanol umkristallisiert: 1,40 g (38% auf **2c** berechnet). Schmp. 207—210 °C; $[\alpha]_D^{20} = -59{,}9°$ ($c = 1$).

$C_{22}H_{27}NO_2S$ (369,51). Ber. C 71,50; H 7,36; N 3,79; S 8,67. Gef. C 71,17; H 7,58; N 3,80; S 8,50%.

IR (KBr): Methoxy-Banden: 2835, 2800, 1250, 1035 cm^{-1}; Thiourethan: 1520, 1330, 1320, 1300, 1190 cm^{-1}; aromatische Banden: 1610, 1565, 1490, 865, 795 cm^{-1}.

PMR ($CDCl_3$): δCH_3 (18): 1,00 ppm, s (3H); δNCH_3: 3,20 ppm, s (3H); δOCH_3: 3,80 ppm, s (3H); δCH_2 (Spiro-Ring): 3,45 und 3,85 ppm, m (2H, AB-Spektrum, $J_{AB} = 11$ Hz).

Östr-4-en-3-on-17*S*-spiro-5'-(2'-thiooxo-3'-methyl-oxazolidin) (6f)

Zu einer gerührten und auf 5 °C gekühlten Lösung von 1,72 g (5,2 mmol) **2b** und 2,10 ml (15 mmol) Triäthylamin in 30 ml trockenem Methylenchlorid wurde eine Lösung von 0,67 g (5,8 mmol) Thiophosgen in 5 ml Methylenchlorid zugetropft. Danach wurde die Lösung 1 h bei 5 °C und anschließend 2 h bei Raumtemp. gerührt und anschließend mit Wasser neutral gewaschen. Nach Trocknen und Eindampfen blieb ein öliger Rückstand zurück, der in Methanol gelöst und nach Zugabe einer Mischung von 0,80 ml konz. Salzsäure und 1,7 ml Wasser 1,5 h bei 60 °C gerührt wurde. Die Lösung wurde eingedampft und die ausgeschiedenen Kristalle mit Wasser gewaschen. Das Rohprodukt (1,59 g) wurde in Äthanol gelöst, mit Aktivkohle geklärt und umkristallisiert. Ausbeute: 1,27 g (67%). Schmp. 217—219 °C; $[\alpha]_D^{20} = +42{,}5°$ ($c = 0{,}5$).

$C_{21}H_{29}NO_2S$ (359,51). Ber. C 70,15; H 8,13; N 3,89; S 8,92. Gef. C 70,08; H 8,13; N 3,71; S 8,96%.

13β-Äthyl-gon-4-en-3-on-17*S*-spiro-5'-(2'-thiooxo-3'-methyl-oxazolidin) (6g)

6g wurde aus 3,21 g (9,3 mmol) **2d** analog **6f** hergestellt. Das Produkt wurde aus Methanol umkristallisiert. Die Ausbeute betrug 1,83 g (53%). Schmp. 193 °C; $[\alpha]_D^{20} = +38{,}9°$ ($c = 0{,}5$).

$C_{22}H_{31}NO_2S$ (373,54). Ber. C 70,73; H 8,36; N 3,75; S 8,58. Gef. C 70,56; H 8,47; N 3,61; S 8,90%.

*

Für die bei der Auswertung der IR- und PMR-Spektren geleistete Hilfe sei Dr. P. SOHÁR und dr. G. TÓTH, für die Aufnahme und Deutung der Massenspektren Gy. HORVÁTH und Gy. JERKOVICH an dieser Stelle gedankt.

LITERATUR UND BEMERKUNGEN

[1] *a)* DE STEVENS, G.: Medicinal Chemistry, Vol. **1.** Diuretics, Chemistry and Pharmacology, S. 123—126. (Academic Press, New York and London, 1963)
b) FUNDER, J. W., FELDMAN, D., HIGHLAND, E., EDELMAN, J. S.: Biochem. Pharm. **23,** 1493 (1974)

[2] SHARMA, R. K., DOORENBOS, N. J., BHACCA, N. S.: J. Pharm. Sci., **60,** 1677 (1971) und Literatur darin
Ferner z. B.: Niederländisches Patent 6,509,280 (25. Jan. 1966; C. A. **64,** 17689c); Japanisches Patent 71 19 956 (29. Jun. 1968; C. A. **75,** 98731k)

[3] HÜBNER, M., NOACK, I.: J. f. prakt. Chem. **314,** 667 (1972)

[4] IUPAC-Nomenklatur: HOPPE—SEYLERS Z. Physiol. Chem. **351,** 687 (1970)

[5] KIRK, D. N., WILSON, M. A.: J. Chem. Soc. *(C)*, **1971,** 414

[6] PONSOLD, K., HÜBNER, M., KASCH, H., NOACK, I.: Z. Chem. **11,** 106 (1972)

[7] **3a** und **3c** (R = Benzoyl) entstanden als dünnschichtchromatographisch einheitliche Rohprodukte, konnten aber durch Umkristallisieren nicht weiter gereinigt werden.

[8] Zur sauren Ringschluß-Reaktion von β-Hydroxyäthyl-thioharnstoffen siehe z. B.: GRIFFIN, T. S., WOODS, T. S., KLAYMAN, D. L.: "Thioureas in the Synthesis of Heterocycles" in Advances in Heterocyclic Chemistry **18,** S. 113 (Academic Press, New York and London, 1975)

[9] SÓLYOM, S., SOHÁR, P., TOLDY, L., KÁLMÁN, A., PÁRKÁNYI, L.: Tetrahedron Letters, **1977,** 4245

[10] Bemerkenswert ist die Alkalistabilität dieser Verbindung. In THF-wäßrigem Kaliumhydroxid (48 h bei 50 °C) konnte keine Hydrolyse erzielt werden. Wir isolierten die Verbindung unverändert in guter Ausbeute. Eine mögliche Erklärung dafür könnte das delokalisierte Bindungssystem sein.
[11] KAGAWA, C. M. und Mitarb.: J. Pharmacol. Exp. Ther. **126,** 123 (1959)
[12] RUFER, C. und Mitarb.: J. Liebigs Ann. d. Chemie **702,** 141 (1967)

Sándor SÓLYOM
Zoltán ZUBOVICS
Lajos TOLDY
H-1045 Budapest, Szabadságharcosok u. 47—49.

Acta Chimica Academiae Scientiarum Hungaricae, Tomus 100 (1—4), pp. 101—109 (1979)

EINBAU VON α-AMINOOXYSÄUREN IN BIOLOGISCH AKTIVE PEPTIDE*

L. KISFALUDY, M. LŐW, I. SCHŐN und O. NYÉKI

(Chemische Fabrik Gedeon Richter AG, Budapest)

Eingegangen am 23. Juni, 1978

Zur Veröffentlichung angenommen am 17. August, 1978

Es wurde festgestellt, daß der Einbau von α-Aminooxysäuren in biologisch aktive Peptide eine wesentliche Wirkungsänderung herbeiführen kann, je nachdem, wo die Substitution durchgeführt wurde. Beim Pentagastrin Molekül konnte bei *N*-terminale Substitution eine auch in praktischer Hinsicht wertvolle, qualitative Wirkungsänderung beobachtet werden: die Wirkung nimmt zu und ist auch bei jejunaler Verabreichung ausgeprägt. Auch bei der *N*-terminalen Substitution des Angiotensin-II gelangten wir zu wertvollen Analogen mit antagonistischer Wirkung. Die *C*-terminale Substitution führte dagegen bei beiden Molekülen zu inaktiven Verbindungen. Beim ACTH-Molekül sind die durch verschiedene Substitutionen hervorgerufenen Wirkungsänderungen nicht so eindeutig. Die Änderung ist in hohem Maße von der Länge der peptidkette abhängig.

Der Einbau einer nicht-proteinogenen Aminosäure in biologisch aktive Peptide zwecks günstigerer Wirkung, Untersuchung des Zusammenhangs zwischen Struktur und Aktivität usw. macht gegenwärtig einen wesentlichen Teil der peptidchemischen Forschung aus. Häufig wird dabei auch das Ziel verfolgt, die praktische (klinische) Verwendung der Peptide durch Verlängern ihrer kurzen biologischen Halbwertszeit zu ermöglichen. Da die *chemischen* Eigenschaften des Moleküls sowohl im Transportmechanismus als auch bei der Bindung an der Rezeptor und beider Ausübung der Wirkung eine entscheidende Rolle spielen, muß man eine klare Vorstellung über den chemischen Charakter der einzubauenden Aminosäure haben. Die chemischen Eigenschaften eines biologische aktiven Peptids bestimmen jedoch auch dessen *Konformation*, die in den obengenannten Vorgängen ebenfalls eine wesentliche Rolle spielt.

Die Ergebnisse des systematischen chemischen, physikochemischen und biologischen Untersuchung [1] der α-Aminooxysäuren können kurz folgendermaßen zusammengefaßt werden.

1. Die Basizität der primären Aminogruppe der α-Aminooxysäuren (α-AOA) ist um etwa 4 pK-Werte geringer als die der strukturell analogen Aminosäuren. Dennoch sind α-AOA — nach IR-spektroskopischen Untersuchungen [2] — in der festen Phase ausschließlich in Form von Zwitterionen zugegen und ihre Bereitschaft zur Assoziation ist sogar höher als die der Amino-

* Teilweise vorgetragen am ersten »Rundtischgespräch in Memoriam Max Bergmann«, München, Dezember 1977.

säuren. Die Ursache für diesen Befund ist vermutlich, daß die sterisch leichter zugängliche Aminogruppe das Entstehen der durch Dipol-Dipol-Wechselwirkung zustandekommenden Molekülketten fördert. Die präparative Folge der geringeren Basizität der Aminogruppe ist ihre langsamere Acylierbarkeit; dies konnte eindeutig durch kinetische Untersuchungen bestätigt werden [3]. Ein weiterer interessanter Zug der primären Aminogruppe ist ihre hohe Reaktionsbereitschaft mit Carbonylverbindungen. Mit Aceton oder acetonhaltigen Lösungsmitteln entstehen z.B. sofort die entspechenden Isopropyliden-Derivate. Eine in präparativer Hinsicht ebenfalls wichtige Eigenschaft der N—O-Bindung ist ihre quantitative Spaltung unter den Bedingungen der katalytischen Hydrierung. Säuren gegenüber ist diese Bindung weniger empfindlich, sie wird z.B. durch flüssigen Fluorwasserstoff nicht gespaltet.

2. Für die Untersuchung der Eigenschaften der Carboxylgruppe der α-AOA wurde der Stickstoff geschützt. Die Carbonylgruppe der Boc-α-AOA ist etwas polarisierter als die der entsprechenden Aminosäuren. Dies weist auf eine höhere Acylierungsfähigkeit hin, die auch durch kinetische Untersuchungen bestätigt wurde [3].

3. Der erste Schritt der biologischen Untersuchungen bestand in der Prüfung der Enzymresistenz. Aus dem *in vitro*-Verhalten von *N*- und *C*-terminal α-AOA enthaltenden Modell-Tripeptiden gegenüber üblichen proteolytischen Enzymen gefolgert werden, daß die Enzymresistenz der α-AOA der von D-Aminosäuren entspricht [4]. Daten über die Wirkung von *spezifischen Enzymen* wurden bei der Metabolismus-Untersuchung der Verbindung OHA-5 (*N*-Aminooxyacetyl-*N*'-isonicotinoylhydrazid) erhalten [5]. Danach geht in der Leber vermutlich die Umsetzung H_2NO- → HO- → H_2N- vor sich, d.h. entsteht eine α-Aminosäure aus einer α-AOA.

In Kenntnis des Gesagten können bestimmte *prädiktive* Folgerungen gezogen werden, wenn eine Aminosäure eines biologisch aktiven Peptids gegen eine α-AOA ausgetauscht wird:

a) es ist sicher daß das Verlängern der Peptidbackbone um ein Sauerstoffatom eine derartige Konformationsänderung verursacht, die durch das aktive Zentrum und/oder die Bindestelle des Moleküls »empfunden« wird. Die Frage ist in welchem Ausmaß?

b) bei denjenigen Peptiden, bei denen die *N-terminale* Aminogruppe eine Rolle bei der Bingung an den Rezeptor oder bei der Gestaltung der sog. »aktiven« Konformation spielt, muß wegen der geringeren Basizität der Aminogruppe der α-AOA mit einer verminderten Wirkung gerechnet werden. Dies wird nur zum Teil durch sterisch leichtere Zugänglichkeit kompensiert. Es kann sogar nicht ausgeschlossen werden, da die α-AOA enthaltenden Peptide im Verlaufe ihrer Stoffwechselprozesse mit aktiven Carbonylverbindungen in Reaktion treten und dadurch sozusagen eine »geschützte« From annehmen.

c) beim Einbau in die *C-terminale* Lage ist wiederum entscheidend, welche Rolle diese Stelle ursprünglich im Ausüben der biologischen Wirkung spielt.

d) im allgemeinen kann eine Verlängerung der biologischen Halbwertszeit infolge der hohen Enzymresistenz der α-AOA erwartet werden.

Auf Grund der obigen Überlegungen führten wir *N*- und *C*-terminale Substitutionen bei Pentagastrin, Angiotensin-II und ACTH durch.

Charakteristisch für das *Gastrin-Moleküls* ist die besonders hohe Konzentrierung der biologischen Wirkung im *C*-terminalen Tetrapeptid-Teil [6]. Die Herstellung zahlreicher Analogen [7] ermöglichte die Wahl von Peptavlon^R (Boc-β-Ala-Trp-Met-Asp-Phe-NH_2) sowie die Klärung vieler Zusammenhänge zwischen Struktur und Aktivität. Unter den neueren Untersuchungen sind zwei — gewissermaßen einander widersprechende — Feststellungen erwähnungswert. Nach HIGAKI [8] erfolgt aus der zweifachen Substitution des Pentapeptids ein inaktives Produkt; nach LIN [9] enthält das Pentapeptid-Molekül keinen absolut essentiellen Teil.

Wir stellten nahezu 40 Pentagastrin-Analoge her [10], darunter sollen hier jedoch nur jene behandelt werden, die eine Antwort auf unsere grundlegende Frage geben. Auch hinsichtlich ihrer Synthese soll nur soviel gesagt werden, daß wir nach der stepwise-Methode unter Anwendung von Aktivester-

Tabelle I

*Sekretorische Aktivität von α-Aminooxysäuren enthaltenden Pentagastrin-Analogen**

Analoge*** D:	Intravenös 0,2 μg/100 g	Intrajejunal 20 μg/100 g
1. Boc-OGly-Trp-Met-Asp-Phe-NH_2	142	51**
2. Boc-L-OAla-Trp-Met-Asp-Phe-NH_2	66	59
3. Boc-OGly-Trp-Leu-Asp-Phe-NH_2	124	0
4. Boc-D-OAla-Trp-Leu-Asp-Phe-NH_2	140	35
5. Boc-D-OAla-Trp-Met-Asp-L-Phg-NH_2	180	7
6. Boc-OGly-Trp-Met-Asp-L-Phg-NH_2	10	50
7. Boc-D-OAla-Trp-Leu-Asp-L-Chg-NH_2	50	—
8. Boc-D-OAla-Trp-Leu-Asp-L-Phg(4Cl)-NH_2	50	—
9. Boc-OGly-Trp-Met-Asp-D-OPhe-NH_2	0	0
10. Boc-D-OAla-Trp-Met-Asp-D-OPhe-NH_2	0	0
11. Boc-L-OAla-Trp-Met-Asp-Phe-OGly-OH	56	0

* Kontrolle: 0,2 μg/100 g Körpergewicht Peptavlon *i.v.* = 100;
** Dosis: 10 μg/100 g; Phg = Phenylglycin; Chg = Cyklohexylglycin
*** OGly, OAla, OPhe, OSer, OLys hießen anstatt der α-Aminosäuren Gly, Ala, Phe, usw., die entsprechenden α-Aminooxysäuren wie z. B. OGly = Aminooxy-essigsäure.

Kupplung arbeiteten. Die biologischen Prüfungen wurden in der I. Internen Klinik der Medizinischen Universität Szeged (Direktor: Prof. VARRÓ) durchgeführt. Die Ergebnisse sind in Tab. I zusammengefaßt.

Aus den Versuchsergebnissen können folgende Schlüsse gezogen werden:

a) die *N*-terminale α-AOA enthaltenden Analogen (1., 3., 4., 5.) steigern bei intravenöser Verabreichung die sekretorische Aktivität und nähern sich in der Aktivität dem Gesamthormon an. Die dosisabhängige Wirkung der aktivsten Verbindungen ist in folgender Abbildung dargestellt:

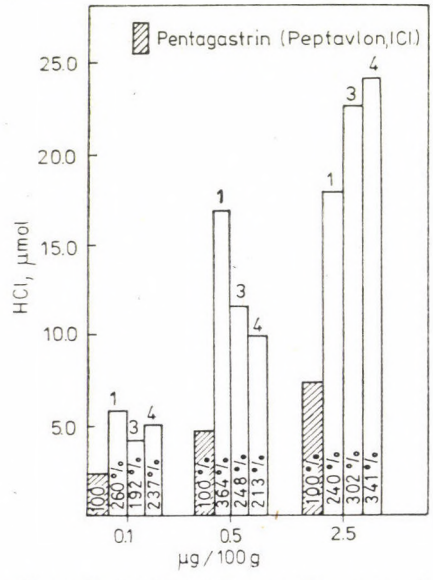

Abb. 1. Dosisabhängige sekretorische Aktivität von Pentagastrin Analogen verglichen mit Peptavlon

b) die Bedeutung der auch bei jejunaler Verabreichung aktiven Verbindungen (1., 2., 4., 6.) besteht darin, daß auch eine perorale Wirksamkeit nicht ausgeschlossen ist. Diese sind unseres Wissens nach die ersten Pentagastrin-Analogen, die auch jejunal wirksam sind. Da der Unterschied zwischen Peptavlon und dem Analogen 1. allein darin besteht, daß sich im letzteren anstelle der CH_2-Gruppe ein Sauerstoffatom befindet, Peptavlon aber selbst in hohen Dosen nicht im aktiven Zustand aus dem Jejunum resorbiert wird [11], stehen wir einem beachtenswerten Befund gegenüber. Es kann angenommen werden, daß der Boc-β-Ala-Teil proteolitischen Enzymen gegenüber ebenso resistent ist wie der Boc-OGly-Teil. Dadurch kann also die höhere und spezifische Wirksamkeit nicht erklärt werden. Es ist dagegen vorstellbar, daß die jejunale Schleimhaut irgendein spezifisches Enzym enthält, das imstande ist, ersteres zu spalten, letzteres dagegen — gerade wegen des Uterschieds $CH_2 \rightarrow O$ — nicht spalten kann. Ein Beispiel dafür ist die Untersuchung mit markiertem

Boc-Gly-Trp-Met-Asp-Phe-NH_2, wobei Boc-Gly-OH im Urin nachgewiesen werden konnte [12].

c) die Analogen 5—8 besitzen — trotz der Phe-Substitution — eine bedeutende sekretionssteigernde Wirkung, einzelne sind auch bei jejunaler Administration wirksam.

d) die Analogen 9. und 10. üben weder eine agonistische noch eine antagonistische Wirkung aus. Dieser Befund weist darauf hin, daß die Bindung weniger durch den Charakter der Seitenketten, sondern eher infolge der durch die genaue Struktur der Peptidbackbone bestimmten Konformation beeinflußt wird.

e) endlich erfolgt aus der Verlängerung der Peptidkette mit einer α-AOA (Analog 11.) eine Verminderung der sekretorischen Wirkung um nur etwa 30—70%, doch konnte keine jejunale Wirksamkeit beobachtet werden.

Die Untersuchung obiger Analogen ist ein gutes Beispiel dafür, wie vorsichtig man bei Verallgemeinerungen vorgehen muß: auch zweifach substituierte Analogen (5., 7., 8.) wiesen eine bedeutende sekretorische Wirkung auf, während der Einbau eines einzigen Sauerstoffatoms in die Peptidkette zu völliger Inaktivierung führte (9., 10).

Unsere Zielsetzung bei der Synthese von *Angiotensin-II*-Analogen war, auch bei subkutaner Administration wirksame Antagonisten herzustellen. Der erste kompetitive Inhibitor des Angiotensin-II wurde 1970 beschrieben [13], und seitdem werden auch weitverbreitet Forschungen zur Herstellung solche Analogen durchgeführt, die für die Diagnostizierung und eventuelle therapeutische Behandlung reninabhängiger Hypertensionen geeignet wären [14]. Bereits beim Beginn der Untersuchungen stellte sich heraus, daß der Austausch des endständigen Phe gegen eine Aminosäure mit aliphatischer Seitenkette zur praktischen Behebung der agonistischen Wirkung führt, wobei aber die Bindungsfähigkeit des Moleküls zum Rezeptor bleibt, so daß diese Analogen eine wesentliche antagonistische Wirkung ausüben [15]. Die Wirkung kann noch gesteigert werden, wenn z.B. in Stellung 1 eine stärker basische Aminosäure (z.B. Sar) eingebaut wird. So kam es zur Einführung von *Saralasin*^{R}, dem [Sar^1, Ala^8]-Angiotensin-II-Analogen [16], das zwar gegenwärtig nicht mehr der beste, jedoch der zur Zeit als Standard verwendete kompetitive Inhibitor ist. Im Vordergrund der gegenwärtigen Untersuchungen steht die Herstellung von Antagonisten ohne Nebenwirkungen und mit längeren biologischen Halbwertszeiten [17].

Bei den Versuchen wurden selbstverständlich die bisherigen Erfahrungen verwendet und in Stellung 8 von vornherein Aminosäuren mit aliphatischer Seitenkette eingebaut. Auf Einzelheiten der Synthese soll auch hier nicht eingegangen, sondern nur bemerkt werden, daß unser Verfahren, nämlich die Pentafluorphenylester-Technik [18], es ermöglichte, z.B. das geschützte Heptapeptid Boc-Arg(Tos)-Val-Tyr(Bzl)-Ile-His(Dnp)-Pro-Ile-ONB mit einer

Ausbeute von 80% herzustellen, was einer Ausbeute von 96% pro Schritt (Kupplung + Entfernung der Schutzgruppe) entspricht.

Die Ergebnisse sind kurz in Tab. II zusammengefaßt.*

Tabelle II

*Wirkung von α-Aminooxysäuren enthaltenden Angiotensin-II-Analogen auf den Blutdruck bei Hypertensin-Infusion**

Analoge D:	Blutdrucksenkung (mm Hg) 10 μg/kg	20 μg/kg
1. [OGly^1,Leu^8]-Angiotensin-II	−33±3,6	−42±4,2
2. [D-OAla^1,Leu^8]-Angiotensin-II	−30±3,4	−38±3,8
3. [OGly^1,Ile^8]-Angiotensin-II	−28±2,0	−40±5,7
4. [L-OAla^1,Ile^8]-Angiotensin-II	−14±4,3	−21±3,4
5. [OGly^1,L-OAla^8]-Angiotensin-II	inaktiv	
6. [Sar^1,L-OAla^8]-Angiotensin-II	inaktiv	
7. Saralasin	−41±2,5	—

* Die Versuche wurden an narkotisierten Katern bei *i.v.* Verabreichung durchgeführt.

Die Analogen 1—3 senken den experimentell hervorgerufenen hohen Blutdruck auch bei subkutaner Verabreichung selbst nach 60 Minuten signifikant (10—16 mm Hg).

Aus der in der Tabelle ersichtlichen Wirkung der Analogen können im wesentlichen dieselben Schlüsse, wie aus der Wirkung der Pentagastrin-Analogen gezogen werden:

a) die *N*-terminal α-AOA enthaltenden Analogen (1—3.) verringern die Bindung an der Rezeptor nicht, da sie eine wesentliche blutdrucksenkende Wirkung ausüben. Dies bedeutet zugleich, daß eine erhöhte Basizität der *N*-terminalen Gruppe nicht unbedingt nötig ist, um eine gute Bindung an den Rezeptor zu erreichen.

b) der Austausch des in der antagonistischen Wirkung eine so entscheidende Rolle spielenden *C*-terminalen Ala gegen OAla (5., 6.) führt auch hier praktisch zur Aufhebung der Wirksamkeit. Diese Analogen besitzen weder eine agonistische noch eine antagonistische Wirkung: ein weiteres Beispiel für die grundlegende, bestimmende Bedeutung der Peptidbackbone.

Hinsichtlich des *ACTH-Moleküls* scheint es, daß unsere Kentnisse in Bezug auf »active site«, »binding site«, »recognition site« hinreichend sind. Einige neuere Beobachtungen stellen jedoch diese Kenntnisse in ein neues Licht. Bisher wurde z.B. das unter die »sychnologischen« Hormone eingereichte

* Die biologischen Versuche der Angiotensin-II sowie der ACTH-Analogen wurden in unserer pharmakologischen Abteilung (Leiter: Dr. SZPORNY) durchgeführt.

ACTH als ein völlig flexibiles Molekül angesehen. Nach unseren Untersuchungen [19] müssen wir jedoch auch unter physiologischen Bedingungen mit einer bestimmten Geordnetheit des Moleküls rechnen. Diese Geordnetheit spielt vermutlich im ganzen biologischen Leben des ACTH-Moleküls eine äußerst wichtige Rolle. Auch hat sich herausgestellt, daß *nicht alle* Substitutionen des in aktiven Zentrum befindlichen Trp zu einer drastischen Abnahme der biologischen Wirkung führen, da z.B. das Analoge mit *t*-butyliertem Trp eine wesentliche, 40—60%-ige Aktivität besitzt [20].

Auch am ACTH-Molekül führten wir verschiedene *N*- und *C*-terminale Substitutionen durch, deren Wirkung auf die biologische Aktivität in Tab. III gezeigt wird.

Tabelle III

Biologische Aktivität verschiedener α-Aminooxysäuren enthaltender ACTH-Analogen

Analoge	*Einheiten** mg Peptid	Relative Wirkung (%)
1. α_h-ACTH-(1—32)	190	
2. [D-OSer[1]]-α_h-ACTH-(1—32)	153	80 2/1
3. α-ACTH-(1—19)-NH_2	140	
4. [D-OSer[1]]-α-ACTH-(1—19)-NH_2	97	70 4/3
5. α-ACTH-(1—18)-NH_2	142	
6. [D-OSer[1]]-α-ACTH-(1—18)NH_2	73	52 6/5
7. [D-OSer[1],Lys[17,18]]-α-ACTH-(1—18)-NH_2	66	
8. [D-OSer[1],Lys[17],D-OLys[18]]-α-ACTH-(1—18)-NH_2	27	41 8/7
9. [D-OSer[1],Lys[17],OLys[18]]-α-ACTH-(1—18)-NH_2	13	20 9/7
10. [D-OSer[1],Lys[17,18]]-α-ACTH-(1—19)-NH_2	85	
11. [D-OSer[1],Lys[17,18],OGly[19]]-α-ACTH-(1—19)-NH_2	123	144 11/10
12. [D-OSer[1],Lys[17,18],D-OAla[19]]-α-ACTH-(1—19)-NH_2	47	55 12/10
13. [D-OSer[1],Lys,[17,18],D-OLys[19]]-α-ACTH-(1—19)-NH_2	81	95 13/10
14. [D-OSer[1],Lys[17,18],OGly[19]]-α-ACTH-(1—19)-OBzl	106	125 14/10

* bestimmt nach USP XIX

Die *N*-terminal mit D-OSer substituierten Analogen (2., 4., 6.) besitzen eine um 20—50% verringerte *in vivo*-Aktivität. Mit anderen α-AOA *N*-terminal substituierte Analogen sind in der Tabelle nicht angeführt. Bei diesen war die Wirkungsabnahme noch ausgeprägter, so daß bei der weiteren Arbeit die D-OSer Substitution beibehalten wurde. Die Folgen der Substitution des *C*-terminalen Teils (8., 9., 11.—14.) sind stark von der Länge der Peptidkette abhängig. Während beim Segment 1—18 die Aktivität um 60—80% abnimmt (8., 9.) führt dieselbe Substitution beim Segment 1—19 kaum zu einer Änderung (13.). Es ist hervorzuheben, daß die Substitution mit OGly[19] (11.) eine signifi-

kante Erhöhung der Aktivität ergibt. Die Wirkungserhöhung erscheint noch ausgeprägter, wenn diese Verbindung als das Hydroxamsäure-Derivat des Segment 1—18 betrachtet wird (11./7. = 187%). Die Verbindung 14., am *C*-terminal anstelle von Säureamid mit Benzylester substituiert ist, hat eine stark protrahierte Wirkung. Der Corticosterol-Spiegel im Blut beträgt noch nach 2 bzw. 3 Stunden 88 bzw. 75% des nach einer Stunde erreichten Wirkungsmaximums.

Nach den obigen Angaben führt also die Substitution des ACTH-Moleküls am *N*-terminalen Teil mit α-AOA — wider Erwartenen — zu einer Aktivitätsabnahme. Dieser Befund bestätigt die frühere Beobachtung, daß dieser Teil eine wirkungspotenzierende Rolle spielt. Der *C*-terminale Teil, welcher in der Bindung die primäre Rolle spielt, reagiert empfindlicher auf die Substitution. Wesentliche Unterschiede konnten bei den Segmenten 1—18 und 1—19 beobachtet werden. Beim ersteren verursachte der Austausch der letzten Aminosäure eine wesentliche Abnahme der Aktivität, während beim letzteren einige Analogen eine erhöhte bzw. protrahierte Wirkung im Vergleich zum Muttermolekül aufweisen.

Zusammenfassend kann folgendes gesagt werden: der Einbau von α-AOA in biologisch aktive Peptide kann eine wesentliche Wirkungsänderung herbeiführen, je nachdem, wo die Substitution durchgeführt wird. Beim Pentagastrin Molekül konnte bei *N*-terminale Substitution eine auch in praktischer Hinsicht wertvolle, qualitative Wirkungsänderung beobachtet werden. Die Wirkung nimmt zu und ist auch bei jejunaler Verabreichung deutlich vorhanden. Auch bei der *N*-terminalen Substitution des Angiotensin-II gelangten wir zu wertvollen Analogen mit antagonistischer Wirkung. Die *C*-terminale Substitution führte dagegen bei beiden Molekülen zu inaktiven Verbindungen, woraus die Wichtigkeit der durch die Backbone des Peptids bestimmten Konformation im aktiven Zentrum ersichtlich wird. Die Substitution des ACTH-Molekül mit D-OSer[1] hat eine andere Wirkung als z.B. die mit D-Ser[1] zur Folge. Die Auswirkungen von Änderungen im *C*-terminalen Teil sind in hohem Maße von der Länge der Peptidkette abhängig. Eine signifikante Wirkungssteigerung und eine protrahierte Wirkung konnte bei der OGly[19]-Verbindung beobachtet werden.

*

Wir danken Herr Dr. J. NÁFRÁDI für die biologischen Prüfungen der Pentagastrin-Analogen sowie Herrn Dr. E. KÁRPÁTI und Dr. Gy. HAJÓS für die Teste der Angiotensin-II- bzw. ACTH-Analogen.

LITERATUR

[1] KISFALUDY, L., DANCSI, L., PATTHY, Á., FEKETE, GY., SZABÓ, I.: Experientia, **27**, 1055 (1971); KISFALUDY, L., LŐW, M., DANCSI, L., PATTHY, Á., NYÉKI, O., SÁRKÖZI, M.: in Peptides 1972 (H. HANSON, H. D. JAKUBKE eds.) North Holland Publ., Amsterdam, pp 409 (1973); KISFALUDY, L., DANCSI, L., PATTHY, Á., KLUMPP, E.: Hung. Pat. 165 117, 166 480, 166 481 (1971)

[2] SOHÁR, P., DANCSI, L., KISFALUDY, L.: Acta Chim. Acad. Sci. Hung., **83,** 391 (1974)
[3] KISFALUDY, L., SCHÖN, I., GÖRÖG, S.: Acta Chim. Acad. Sci. Hung., **95,** 315 (1977)
[4] KISFALUDY, L., LŐW, M., DÉVÉNYI, T.: Acta Biophys. Biochim. Acad. Sci. Hung., **6,** 393 (1971)
[5] Nicht veröffentliche Daten
[6] TRACY, H. J., GREGORY, R. A.: Nature, **204,** 933 (1964)
[7] MORLEY, J. S.: Proc. Roy. Soc., **170** B, 97 (1968)
[8] HIGAKI, K., DANNO, T., MIYOSHI, M.: Parmacometrics, **8,** 147 (1974)
[9] LIN, T.-M., SPRAY, G. F., SOUTHARD, G. L.: Gastroenterology, **72,** 566 (1977)
[10] KISFALUDY, L., SCHÖN, I., NÁFRÁDI, J., VARGA, L., VARRÓ, V.: Hoppe Seyler's Z. Physiol. Chem., **359,** 887, 897 (1978)
[11] VARRÓ, V., NÁFRÁDI, J.: Acta Hepato-Gastroenter., **21,** 441 (1974)
[12] VARGA, L., NÁFRÁDI, J., CSERNAY, L., BALÁSPIRI, L., PENKE, B., VARRÓ, V.: Orvostudomány, **24,** 13 (1973)
[13] MARSHALL, G. R., VINE, W., NEEDLEMAN, P.: Proc. Natl. Acad. Sci. USA, **67,** 1624 (1970); KHAIRALLAH, P. A., TOTH, A., BUMPUS, F. M.: J. Med. Chem., **13,** 181 (1970)
[14] GANTEN, D., GROSS, F.: Med. Klin., **71,** 2043 (1976)
[15] KHOSLA, M. C., SMEBY, R. R., BUMPUS, F. M.: Handbook Exp. Pharm., **37,** 126 (1974)
[16] PALS, D. T., MASUCCI, F. D., DENNING, G. S., SIPOS, F., FESSLER, D. C.: Circ. Res., **29,** 673 (1971)
[17] KHOSLA, M. C., HALL, M. M., MUNOZ-RAMIREZ, H., KHAIRALLAH, P. A., BUMPUS, F. J., SEELY, J. H., THOMAS, A. M.: J. Med. Chem., **20,** 253 (1977)
[18] KISFALUDY, L., SCHÖN, I., SZIRTES, T., NYÉKI, O., LŐW, M.: Tetrahedron Letters, **1974,** 1785
[19] LŐW, M., KISFALUDY, L., FERMANDJIAN, S.: Acta Biochim. Biophys. Acad. Sci. Hung., **10,** 229 (1975); GREFF, D., TOMA, F., FERMANDJIAN, S., LŐW, M., KISFALUDY, L.: Biochim. Biophys. Acta, **439,** 219 (1976); TOMA, F., GREFF, D., FERMANDJIAN, S., LŐW, M., KISFALUDY, L.: in Peptides 1976 (LOFFET, A. ed.) Éditions de l'Université de Bruxelles pp 625 (1976); TOMA, F., FERMANDJIAN, S., LŐW, M., KISFALUDY, L.: Biochim. Biophys. Acta, **534,** 112 (1978)
[20] LŐW, M., KISFALUDY, L., SÁRKÖZI, M.: Hoppe Seyler's Z. Physiol. Chem. **360,** 1 (1979)

Lajos KISFALUDY
Miklós LŐW
István SCHŐN
Olga NYÉKI

Chemische Fabrik Gedeon Richter AG, H-1475 Pf. 27, Budapest

Acta Chimica Academiae Scientiarum Hungaricae, Tomus 100 (1—4), pp. 111—119 (1979)

KINETICS OF HYDROGEN ATOM ABSTRACTION FROM *n*-BUTYRALDEHYDE BY *n*-PROPYL RADICALS

S. FÖRGETEG, T. BÉRCES,* F. MÁRTA and S. DÓBÉ

(Central Research Institute for Chemistry of the Hungarian Academy of Sciences, Budapest)

Received June 26, 1978

Accepted for publication July 20, 1978

Hydrogen atom abstraction by *n*-propyl radicals from various positions of *n*-butyraldehyde was studied in the temperature range of 253—529 K. The *n*-propyl radicals were produced by photolysis of *n*-C_3H_7CHO at 313 nm. With an estimated rate constant of $10^{9.8}$ for n-propyl recombination, the expressions $\log k_{1a} = (7.8 \pm \pm 0.2) - (6300 \pm 300)/2.303\,RT$, $\log k_{1b} = (7.1 \pm 0.2) - (8100 \pm 300)/2.303\,RT$ and $\log k_{1c} = 7.1 - 9000/2.303RT$ (assuming $A_{1c} = A_{1b}$) were obtained (mol, dm^3, s units) for hydrogen abstraction from the formyl group, the α- and β-carbon atom of the alkyl chain, respectively.

I. Introduction

Comparatively few systematic investigations dealing with hydrogen atom abstractions from various positions of a given molecule have been carried out in spite of the important kinetic and mechanistic consequences that the simultaneous occurrence of such reactions may have in the chain decomposition of organic molecules. The occurrence of a second or even third competitive hydrogen abstraction reaction may change or leave unchanged the product distribution (depending on the fate of the radical formed), furthermore, may influence the chain length and by this means the kinetics of the reaction (depending on the reactivities of the alternative radical species). In a previous study [1,2] concerned with the reactions between $\dot{C}H_3$ and CH_3CHO, we have shown that the kinetics and mechanism of acetaldehyde decomposition changes considerably with temperature due to the varying contribution of hydrogen atom abstractions from the alternative carbon atoms of the molecule. As a continuation of the acetaldehyde studies, in this paper we present kinetic results on hydrogen abstraction by *n*-propyl radicals from the *n*-butyraldehyde molecule which possesses four different types of hydrogen atoms.

II. Experimental

A detailed description of materials, apparatus, experimental technique as well as identification and analysis of the reaction products has been given in a previous publication [3].

The *n*-butyraldehyde (FLUKA), purified by precipitation and repeated vacuum distillation, contained 0.5% *iso*-butyraldehyde and traces of C_3H_8 and C_2H_4.

Experiments were carried out in an all-glass apparatus equipped with greaseless Teflon valves. Butyraldehyde was introduced into the reaction vessel by expansion ; pressure measurements were made with a spiral manometer used as a null-instrument.

The *n*-propyl radicals were produced by photolysis of *n*-C_3H_7CHO at 313 nm in a cylindrical quartz cell equipped with planparallel ULTRASIL windows (36 mm i.d. and 25 mm optical depth). Since investigations were carried out in a broad temperature range extending from 353 to 529 K, different equipments had to be used to provide a constant temperature. Experiments at 253—363 K were carried out in a reaction vessel surrounded by a thermostating jacket, which was connected to a thermostat, and an electric oven was used at the two highest temperatures.

Irradiation was carried out by means of an OSRAM super pressure mercury arc. The parallel light beam filled the whole cross-section of the reaction vessel. A band in the 313 nm region was isolated using a filter combination [3].

Products were separated into two parts. The gases not condensable at liquid air temperature were introduced into the gas chromatograph by means of a sampling valve, while the condensable ones were dissolved in isooctane and injected as a solution. The products were separated on various columns [3] and were measured against internal standards.

Conversion in the experiments described below was kept between 2 and 7%.

III. Results and Discussion

The *n*-propyl radicals may abstract four different types of hydrogen atoms from the *n*-butyraldehyde molecule :

$$\dot{C}_3H_7 + C_3H_7CHO \rightarrow C_3H_8 + C_3H_7\dot{C}O \qquad (1a)$$

$$\dot{C}_3H_7 + C_3H_7CHO \rightarrow C_3H_8 + CH_3CH_2\dot{C}HCHO \qquad (1b)$$

$$\dot{C}_3H_7 + C_3H_7CHO \rightarrow C_3H_8 + CH_3\dot{C}HCH_2CHO \qquad (1c)$$

$$\dot{C}_3H_7 + C_3H_7CHO \rightarrow C_3H_8 + \dot{C}H_2CH_2CH_2CHO \qquad (1d)$$

In order to be able to determine the rate constants for these abstraction reactions, the rates of formation of characteristic reaction products have to be known and a reference reaction suitable to monitor the $\dot{C}_3H_7$ radical concentration has to be found. The concentration of *n*-propyl radicals will be obtained from the rate of recombination

$$\dot{C}_3H_7 + \dot{C}_3H_7 \rightarrow C_6H_{14}. \qquad (2)$$

Although direct determinations of the kinetic parameters for reaction (2) have not been published, a good estimate of $\log(k_2/\mathrm{dm^3\ mol^{-1}s^{-1}}) = \log A_2 = 9.8$ can be given on the basis of the rate constant obtained for ethyl recombination [4] and reported for ethyl [5] and isopropyl [5] self-combination.

Rate measurements were carried out at six temperatures at 2.3×10^{-10} mol-photon $\mathrm{cm^{-2}\ s^{-1}}$ incident light intensity. The initial aldehyde concentrations were 10, 40 and 100 Torr at 253 K, 273 K and higher temperatures, respectively ; lower initial pressures at 273 and 253 K were due to the limited vapour pressure at these temperatures. Measured rates of formation for the hydrocarbon products are given in Table I.

The major features of product formation in the photolysis of *n*-butyraldehyde have been outlined in a previous publication [3] and a more detailed discussion of the mechanism will be given [6]. In the following we examine how the rates of reactions (1a)—(1d) can be obtained from measured rates of formation of reaction products. In most cases the fate of the free radical formed in the hydrogen abstraction reaction has to be considered. Since experimental results are available at low temperatures (298 K and below) where radical-radical reactions predominate, as well as at higher temperatures (363 K and above) where reactions first order with respect to radical concentrations prevail, a separate discussion of the "low temperature" (253—298 K) and "higher temperature" (363—529 K) results is desirable.

The most important reaction between the *n*-propyl radical and *n*-butyraldehyde is the abstraction of the formyl hydrogen atom due to the low strength

Table I

Rates of product formation (10^{-9} *mol* dm^{-3} s^{-1}); $I_0 = 2.3 \times 10^{-10}$ *mol-photon* cm^{-2} s^{-1}

Number of experiments	3	5	13	7	3	3
T/K	253	273	298	363	426	529
$10^3[C_3H_7CHO]_0$	0.54	2.13	5.32	5.34	3.76	3.04
H_2	0.021	0.099	0.214	0.412	1.97	4.31
CH_4	0.0025	0.0037	0.0094	0.051	0.061	1.18
C_2H_6	0.0014	0.0004	0.0028	0.0119	0.0207	0.144
C_3H_6	0.032	0.097	0.36	0.28	0.17	1.09
C_3H_8	0.238	1.43	6.84	20.8	32.0	90.8
n-C_4H_{10}	0.0006	0.003	0.012	0.008	<0.001	
n-C_6H_{14}	0.16	0.50	1.81	1.14	0.26	0.14
$C_3H_7CH(C_2H_5)CHO$	0.0001	0.0023	0.039	0.41	0.78	0.68
C_2H_4	0.216	1.11	3.10	3.24	1.96	1.89
CH_3CHO	0.201	1.07	3.21	3.20	2.05	1.86

of the formyl C—H bond. The rate of reaction (1a) can best be given by the rate of propane formation after appropriate corrections for the C_3H_8 originating from other sources.

At higher temperatures the reaction chains are considerable and the rate of C_3H_8 formation in disproportionation reactions of $\dot{C}_3H_7$ radicals may be neglected compared to that in hydrogen abstractions (see *e.g.* the high C_3H_8/C_3H_6 ratios at higher temperatures). Thus, at 363, 426 and 529 K the rate of reaction (1a) will be given by

$$R_{1a} = R_{C_3H_8} - R_{1b} - R_{1c} = k_{1a}[\dot{C}_3H_7][C_3H_7CHO], \qquad (3)$$

where R_{1b} and R_{1c} may be obtained according to Eqs (13) and (19), respectively. Expressing the propyl radical concentration with the rate of *n*-hexane formation, it follows that

$$\frac{R_{C_3H_8} - R_{1b} - R_{1c}}{R_{C_6H_{14}}^{1/2}} = \frac{k_{1a}}{k_2^{1/2}} [C_3H_7CHO]. \tag{4}$$

At low temperatures, C_3H_8 formation in disproportionation reactions

$$\dot{C}_3H_7 + \dot{C}_3H_7 \rightarrow C_3H_8 + C_3H_6 \tag{5}$$

$$\dot{C}_3H_7 + \dot{C}HO \rightarrow C_3H_8 + CO \tag{6}$$

may not be neglected. The contribution to C_3H_8 from reaction (5) can be taken into account simply by the propylene formed, since reaction (5) is the only major source of C_3H_6 at low temperatures. However, contribution from reaction (6) has to be obtained in an indirect way. Considering reactions (6), (2) and (7),

$$\dot{C}HO + \dot{C}HO \rightarrow H_2 + 2CO, \tag{7}$$

the rate of propane formation in reaction (6) can be calculated from $\frac{k_6}{k_2^{1/2} k_7^{1/2}} \times$ $\times R_{C_6H_{14}}^{1/2} R_{H_2}^{1/2}$ with the known value of $\frac{k_6}{k_2^{1/2} k_7^{1/2}} = 3.8 \pm 0.5$ [6]. Thus, at 253, 273 and 298 K the rate of reaction (1a) will be given by

$$R_{1a} = R_{C_3H_8} - R_{C_3H_7CH(C_2H_5)CHO} - R_{C_3H_6} - \frac{k_6}{k_2^{1/2} k_7^{1/2}} R_{C_6H_{14}}^{1/2} R_{H_2}^{1/2} = \tag{8}$$

$$= k_{1a}[\dot{C}_3H_7][C_3H_7CHO],$$

where $R_{C_3H_7CH(C_2H_5)CHO}$ replaces R_{1b} (see below). Hence

$$\frac{R_{C_3H_8} - R_{C_3H_7CH(C_2H_5)CHO} - R_{C_3H_6} - \frac{k_6}{k_2^{1/2} k_7^{1/2}} R_{C_6H_{14}}^{1/2} R_{H_2}^{1/2}}{R_{C_6H_{14}}^{1/2}} = \frac{k_{1a}}{k_2^{1/2}} [C_3H_7CHO]. \tag{9}$$

Equation (9) has been verified at 298 K where the initial aldehyde pressure was varied from 10 to 100 Torr. The $k_{1a}/k_2^{1/2}$ ratio calculated according to Eq. (9) was found to be independent of the *n*-butyraldehyde concentration.

An Arrhenius plot of the rate constant ratios $k_{1a}/k_2^{1/2}$ calculated in the "low" and "higher" temperature ranges from Eqs (9) and (4), respectively, is shown in Fig. 1. From the straight line, determined by the least square method, $\log (k_{1a}/k_2^{1/2}) = (2.9 \pm 0.2) - (6300 \pm 300)/2.303\, RT$. Hence, with the assumed rate constant for *n*-propyl recombination, one obtains

$$\log (k_{1a}/\mathrm{dm^3\ mol^{-1}\ s^{-1}}) = (7.8 \pm 0.2) - (6300 \pm 300)/2.303\, RT \tag{10}$$

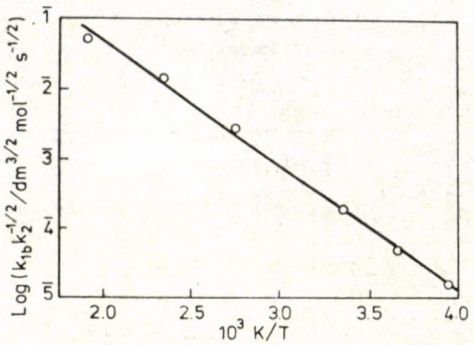

Fig. 1. Arrhenius plot of the rate constant ratio $k_{1a}/k_2^{1/2}$

in good agreement with the results of KERR and TROTMAN-DICKENSON [7].

Hydrogen atom abstraction from the α-carbon atom of the alkyl chain yields $CH_3CH_2\dot{C}HCHO$ radicals. Abstraction reaction (1b) can be studied by considering the fate of the $CH_3CH_2\dot{C}HCHO$ radicals. These radicals may either combine with n-$\dot{C}_3H_7$, the most abundant radical present in the system, to yield $C_3H_7CH(C_2H_5)CHO$

$$CH_3CH_2\dot{C}HCHO + \dot{C}_3H_7 \rightarrow C_3H_7CH(C_2H_5)CHO \qquad (11)$$

or decompose by $\dot{C}H_3$ elimination

$$CH_3CH_2\dot{C}HCHO \rightarrow \dot{C}H_3 + CH_2 : CHCHO \qquad (12)$$

No other product of reactions of $CH_3CH_2\dot{C}HCHO$ could be detected. $C_3H_7CH(C_2H_5)CHO$ is formed in the whole temperature range, while decomposition occurs only at higher temperatures. The latter manifests itself in a considerable increase of the rate of formation of methane at 363 K and above. (In the low temperature range, the $\dot{C}H_3$ radicals are formed in a primary reaction and the slow increase of CH_4 formation arises from the change of the aldehyde concentration.)

At the higher temperatures, the rate of reaction (1b) can be given by the sum of the rate of formation of $C_3H_7CH(C_2H_5)CHO$ and that of $\dot{C}H_3$ production in decomposition reaction (12). The only other source of $\dot{C}H_3$ radicals in the photolysis of n-butyraldehyde is the primary decomposition of the aldehyde into $\dot{C}H_3$ and $\dot{C}H_2CH_2CHO$ [6], however, in the higher temperature range, the rate of $\dot{C}H_3$ formation in the primary decomposition is small compared with that in reaction (12). (On the basis of the low temperature results, the rate of $\dot{C}H_3$ formation in the primary process can be estimated to be 0.01×10^{-9} mol dm^{-3} s^{-1} at 100 Torr aldehyde pressure.) Thus, the rates of formation of CH_4 (H-abstraction by $\dot{C}H_3$) and n-C_4H_{10} ($\dot{C}H_3 + \dot{C}_3H_7$ combination) may be

taken — to a first approximation — as a measure of $CH_3\dot{C}HCHO$ decomposition. Consequently, at 363, 426 and 529 K, the rate of reaction (1b) will be given by

$$R_{1b} = R_{C_3H_7CH(C_2H_5)CHO} + R_{CH_4} + R_{C_4H_{10}} = k_{1b}[\dot{C}_3H_7][C_3H_7CHO]. \quad (13)$$

Hence

$$\frac{R_{C_3H_7CH(C_2H_5)CHO} + R_{CH_4} + R_{C_4H_{10}}}{R_{C_6H_{14}}^{1/2}} = \frac{k_{1b}}{k_2^{1/2}}[C_3H_7CHO]. \quad (14)$$

At low temperatures, $CH_3\dot{C}HCHO$ radical decomposition is slow; practically all CH_4 and C_4H_{10} can be accounted for by reactions of primary $\dot{C}H_3$ radicals. Thus, the rate of reaction (1b) can be given at 253, 273 and 298 K simply by

$$R_{1b} = R_{C_3H_7CH(C_2H_5)CHO} = k_{1b}[\dot{C}_3H_7][C_3H_7CHO] \quad (15)$$

and

$$\frac{R_{C_3H_7CH(C_2H_5)CHO}}{R_{C_6H_{14}}^{1/2}} = \frac{k_{1b}}{k_2^{1/2}}[C_3H_7CHO] \quad (16)$$

As required by Eq. (16), the ratio $R_{C_3H_7CH(C_2H_5)CHO}/R_{C_6H_{14}}^{1/2}[C_3H_7CHO]$ was shown to be constant and independent of the aldehyde concentration between 10 and 100 Torr at 298 K.

An Arrhenius plot of the rate constant ratio $k_{1b}/k_2^{1/2}$, calculated in the low and higher temperature ranges from Eqs (16) and (14), respectively, is shown in Fig. 2. The straight line, drawn by the least squares method, yields $\log(k_{1b}/k_2^{1/2}) = (2.2 \pm 0.2) - (8100 \pm 300)/2.303\,RT$. Hence, with the assumed value for the recombination rate constant, one obtains

$$\log(k_{1b}/\mathrm{dm^3\,mol^{-1}\,s^{-1}}) = (7.1 \pm 0.2) - (8100 \pm 300)/2.303\,RT. \quad (17)$$

Hydrogen atom abstraction by n-$\dot{C}_3H_7$ from the carbon atom in β-position to the carbonyl group results in the formation of C_3H_8 and $CH_3\dot{C}HCH_2CHO$. A thorough search for the products of reaction of the $CH_3\dot{C}HCH_2CHO$ radicals has been carried out. Its combination with $\dot{C}_3H_7$ does not occur to a notable extent since the expected aldehyde, $C_3H_7CH(CH_3)CH_2CHO$, could not be detected. This indicates that at low temperatures, where the conditions for radical-radical reactions are favourable, reaction (1c) is of little importance. However, one can detect β-hydrogen abstraction at the highest temperatures by the extra propylene formed in the decomposition reaction

$$CH_3\dot{C}HCH_2CHO \rightarrow C_3H_6 + \dot{C}HO. \quad (18)$$

At low temperatures, propylene is formed *via* disproportionation reactions of the n-propyl radical. In the temperature range of 253—298 K, the C_3H_6/

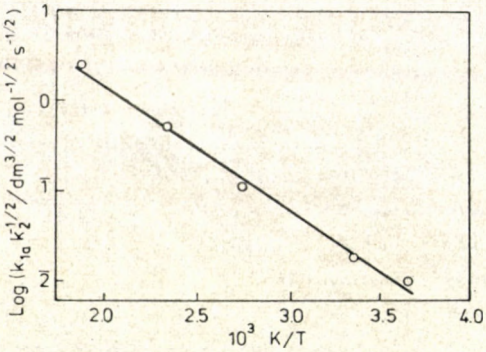

Fig. 2. Arrhenius plot of the rate constant ratio $k_{1b}/k_2^{1/2}$

C_6H_{14} ratio was found to be 0.19 ± 0.02, independently of the temperature and other experimental conditions. This value is close to the disproportionation/combination ratio reported for *n*-propyl radicals [8], indicating reaction (5) to be the major source of propylene at low temperatures with minor contributions from other disproportionation reactions of $\dot{C}_3H_7$. However, at 426 and 529 K an additional source of C_3H_6 through reactions (1c) and (18) is evident; the rate of formation of C_3H_6 through this channel can be given by

$$R_{1c} = R_{C_3H_6} - \frac{k_5}{k_2} R_{C_6H_{14}} = k_{1c}[\dot{C}_3H_7][C_3H_7CHO] \tag{19}$$

Expressing the *n*-$\dot{C}_3H_7$ concentration with the rate of recombination, one obtains

$$\frac{R_{C_3H_6} - \frac{k_5}{k_2} R_{C_6H_{14}}}{R_{C_6H_{14}}^{1/2}} = \frac{k_{1c}}{k_2^{1/2}} [C_3H_7CHO] \tag{20}$$

The rate constant ratios $k_{1c}/k_2^{1/2}$ calculated according to Eq. (20) were 0.002 and 0.030 dm$^{1/2}$ mol$^{-1/2}$ s$^{-1/2}$ at 426 and 529 K, respectively. Hence log (A_{1c}/dm^3 mol^{-1} s^{-1}) = 8.1 and E_{1c} = 11.8 kcal mol^{-1}. However, the value of $k_{1c}/k_2^{1/2}$ obtained at 426 K is not very accurate since most of the C_3H_6 formed at this temperature comes from disproportionation and not from decomposition (18). An alternative derivation of k_{1c} can be based on the accurate $k_{1c}/k_2^{1/2}$ value at 529 K and an assumption of $A_{1c} = A_{1b}$ In this way one obtains

$$\log (k_{1c}/\text{dm}^3\,\text{mol}^{-1}\,\text{s}^{-1}) = 7.1 - 9000/2.303\,RT \tag{21}$$

in reasonable agreement with the data of KERR and TROTMAN-DICKENSON [7] (recalculated on the basis of the recombination rate coefficient used in this work).

Hydrogen atom abstraction by $\dot{C}_3H_7$ from the γ-position yields C_3H_8 and $\dot{C}H_2CH_2CH_2CHO$ radical. If reaction (1d) occurred to an appreciable extent,

one would expect n-$C_6H_{13}CHO$ and excess C_2H_4 (compared to the CH_3CHO) to be formed in combination and decomposition reactions, respectively, of the $\dot{C}H_2CH_2CH_2CHO$ radicals. (Note that C_2H_4 and CH_3CHO are formed with equal rates in the NORRISH type II primary reaction of n-butyraldehyde.) The formation of these products did not exceed the limits of detection, indicating that reaction (1d) was slow in the whole temperature range studied.

The experimental study of hydrogen atom abstraction by n-propyl radicals from the formyl group and from various positions of the alkyl group of the aldehyde shows the sequence of reactivities $k_{1a} > k_{1b} > k_{1c} > k_{1d}$.

We have calculated Arrhenius parameters and rate constants for reactions (1a)—(1c) by the BEBO method [9, 10]. The input data used in the calculations are given in Table II. These were taken from compilations or were estimated using known bond properties of analogous compounds. It has been assumed that $DH^0_{298}(H-CH(C_2H_5)CHO) = DH^0_{298}(H-CH(CH_3)CH_2CHO)$, since the stabilization energies of $O = C-\dot{C}$ type radicals are belived to be low [11]. In order to obtain Arrhenius activation energies from the potential energy of activation and to derive the preexponential factors, force constants and vibra-

Table II

Input data used in the BEBO calculations (units: DH^0_{298}, zpe and V° in kcal mol^{-1}; β in Å^{-1} F° in mdyne Å^{-1}; ω in cm^{-1}; p unitless)

	C_3H_7—H	$C_3H_7C(O)$—H	H—$CH(C_2H_5)CHO$ and H—$CH(CH_3)CH_2CHO$	$C_3H_7C(O)$—C_3H_7	C_3H_7—$CH(C_2H_5)CHO$ and C_3H_7—$CH(CH_3)CH_2CHO$
DH°_{298}	97.7	86.0	94.7	80.1	80.4
ω	2396	2800	2930	950	920
zpe	4.2	4.0	4.2	1.4	1.3
V°	101.9	90.0	98.9	81.5	81.7
p	1.082	1.084	1.082		
β	1.819	1.855	1.842	1.760	1.623
R°	1.080	1.114	1.090	1.525	1.540
F°	4.69	4.30	4.63		

tional frequencies were evaluated for the transition complexes using a five-mass-point approach and standard BEBO procedure. Tunneling corrections were not applied.

In Table III, the results of calculations are given and are compared with the experimental data. In the case of formyl hydrogen abstraction (reaction (1a)) and β-hydrogen atom abstraction (reaction (1c)), the agreement between calculated and experimental data is excellent. However, the calculated rate constant for reaction (1b) is considerably smaller than the experimental one.

Table III

Comparison of calculated kinetic properties with experimental data at 400 K (units: E in kcal mol^{-1}, A in dm^3 mol^{-1} s^{-1})

	E_{1a}	$\log A_{1a}$	$\log k_{1a}$	E_{1b}	$\log A_{1b}$	$\log k_{1b}$	E_{1c}	$\log A_{1c}$	$\log k_{1c}$
Calculated	6.1	7.6	4.3	11.0	7.9	1.9	10.7	7.9	2.1
Experimental	6.3	7.8	4.4	8.1	7.1	2.7	9.0	7.1	2.2

It seems that the observed "high" rate of α-hydrogen atom abstraction cannot be explained properly on the basis of the accepted high bond strength and the corresponding low resonance energies of O = C—Ċ type free radicals [11]. Nevertheless, it is to be mentioned that opinions regarding these stabilization energies are not unanimous (see *e.g.* [12]). If the stabilization energies of O = C—Ċ type free radicals were considerably smaller than those of the allyl radicals, some other hitherto undiscovered reason would have to be assumed to explain the higher rate of hydrogen abstraction from the α than from the β position.

REFERENCES

[1] Bárdi, I., Bérces, T., Szilágyi, I.: Int. J. Chem. Kinet., **8,** 285 (1976)
[2] Bérces, T., Márta, F.: Int. J. Chem. Kinet., **8,** 295 (1976)
[3] Förgeteg, S., Bérces, T., Dóbé, S.: Acta Chim. Acad. Sci. Hung., **96,** 321 (1978)
[4] Golden, D. M., Choo, K. Y., Perona, M. J., Piskiewicz, L. W.: Int. J. Chem. Kinet., **8,** 381 (1976)
[5] Parkes, D. A., Quinn, C. P.: J.C.S. Faraday Trans. I, **72,** 1952 (1976)
[6] Förgeteg, S., Bérces, T., Dóbé, S.: Int. J. Chem. Kinet., **11,** 219 (1979)
[7] Kerr, J. A., Trotman-Dickenson, A. F.: Trans. Faraday Soc., **55,** 572 (1959)
[8] Terry, J. O., Futrell, J. H.: Canad. J. Chem., **45,** 2327 (1967)
[9] Johnston, H. S., Parr, C.: J. Amer. Chem. Soc., **85,** 2544 (1963)
[10] Johnston, H. S.: "Gas Phase Reaction Rate Theory". The Ronald Press Co., New York, 1966
[11] Solly, R. K., Golden, D. M., Benson, S. W.: Int. J. Chem. Kinet., **2,** 11, 381, 393 (1970); King, K. D., Golden, D. M., Benson, S. W.: J. Amer. Chem. Soc., **92,** 5541 (1970)
[12] Cocks, A. T., Egger, K. W.: J. C. S. Perkin Trans. II, **1973,** 197, 199

Sándor Förgeteg
Tibor Bérces
Ferenc Márta
Sándor Dóbé

H-1025 Budapest, Pusztaszeri út 59—67.

Acta Chimica Academiae Scientiarum Hungaricae, Tomus 100 (1—4), pp. 121—134 (1979)

STUDY OF THE POLYMERIZATION OF UNSATURATED *cardo*-DIAMIDES BY THE SEMIDYNAMIC DSC METHOD

T. SZÉKELY[1], V. V. KORSHAK[2], S. V. VINOGRADOVA[2], M. LENGYEL[1], Ya. S. VIGODSKII[2] and G. S. GURBICH[2]

([1] *Research Laboratory for Inorganic Chemistry, Hungarian Academy of Sciences, Budapest,*

[2] *Institute for Elemento-Organic Compounds, USSR Academy of Sciences, Moscow*)

Received June 26, 1978

Accepted for publication September 22, 1978

Four *cardo*-diamine bisacryl- and bismethacrylamides have been synthesized and some important physical properties of the new compounds measured. The unsaturated monomers have been thermally polymerized and the solubility of the polymers determined. The polymerization of two compounds, the 9,9-bis(4'-acrylylaminophenyl) phthalide and the 9,9-bis(4'-acrylylaminophenyl)fluorene has been extensively studied by means of a Perkin—Elmer DSC-2 calorimeter. The thermomechanical behaviour of the two samples has also been investigated. The experiments revealed correlation between the physical properties of the monomer (crystallinity, melting or softening), the polymerization process and the properties of the polymer formed.

Introduction

It is well known that the reactivity of monomers capable of thermal polymerization, containing unsaturated bonds strongly depends on the physical properties of the solid of molten phase, and the chemical process itself, thus the formation of the macromolecule is strictly related to the melting or softening of the monomer. It is also known that the solid-phase polymerization is significantly influenced by the crystal structure, as well. The majority of authors, however, use the physical change as interpretation of the kinetic properties of the polymerization process, but there are very few direct measurements to prove the correlation of the two processes.

The aim of this work is to study the thermal polymerization of two unsaturated monomers, very different in their physical properties, namely 9,9-bis(4'-acrylylaminophenyl)fluorene (aniline fluorene-bisacrylamide, henceforth **I**) and 9,9-bis(4'-acrylylaminophenyl) phthalide (aniline-phthaleinbisacrylamide, henceforth **II**) by the DSC method.

Both monomers are characteristic representatives of the so-called "*cardo*"-polymer [1] family. They can be characterized by complicated cyclic or polycyclic groups in the polymer chain. The difference relative to a simple side-chain substitution is that the cyclic group is at the same time part of the main chain too. Such polymers generally have high thermostability, but their solu-

bility in organic solvents is increased as compared to chains not containing *cardo*-groups. Both properties are very important in plastics applications. Besides, the *cardo*-group also influences significantly the polymer-physical properties of the system, as for example the glassy transformation, softening, extent of crystallinity, *etc.* The unsaturated amides of the *cardo*-diamines seemed to be advantageous, because the differences in the physical properties already exist in the monomers, namely **I** crystallizes well, whereas **II** only to a very small extent. At the same time, the polymers are the first representatives of cross-linked *cardo*-polymers. The two compounds studied are typical examples of a group consisting of eight related compounds. The compounds synthesized are the following:

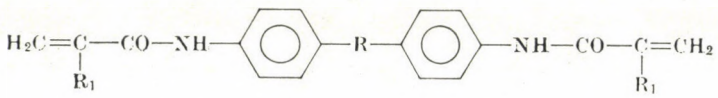

where

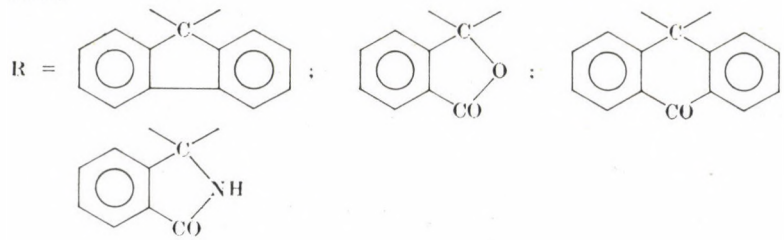

$R_1 =$ H; CH_3

Experimental

Preparation of the compounds

The bisacrylamides of the *cardo*-diamines were prepared by low temperature (between 273 and 243 K, in general from 253 to 243 K) in a polar aprotic solvent, by the condensation of the corresponding diamines and acrylic acid chloride. The acrylic acid chloride was added dropwise to the cooled solution of the diamine, then kept at the given temperature for 30 min, and for further 30—60 min at room temperature. The condensation of the acid chloride and diamine is preferably carried out at a mole ratio of 2 : 1, and a diamine concentration of 0.5—2 mol/l. *N*,*N*-dimethylacetamide or *N*-methylpyrrolidone can be used as solvent. The unsaturated derivatives formed in the solution were precipitated and washed with water, then dried in vacuum at 313—323 K. Under these conditions bisamides of high purity were obtained in a yield of about 100%. The bisamides of *cardo*-diamines are white powders, soluble in organic solvents.

Some data for **I** and **II** and the related compounds synthesized are listed in Table I. Figure I shows the thermomechanical curves of **I** and **II**. Apparently, the fact, that the *cardo*-group is symmetric or asymmetric seems to be the essential factor influencing the crystallization and solubility of the monomer molecule. Thus, *e.g.* the anthrone and fluorene derivatives crystallize well [2, 3] whereas the phthalides only to a very small extent [4, 5].

We also carried out thermal treatment with greater amounts of monomers under normal laboratory conditions. From these measurements it became apparent that monomers con-

taining symmetrical *cardo*-groups, *e.g.* **I** soften only above 520 K, and their polymerization ability is less pronounced. Consequently, by their thermal treatment linear and slightly branched oligomers and polymers are formed which completely dissolve upon extraction with hot DMFA for 10 hrs.

Asymmetric monomers, however, (*e.g.* **II**) polymerize in bulk easily, already at 420—470 K with melting or softening. Upon continuing the thermal treatment at about 470 K in air,

Table I

Characteristics of acryl- and methacrylamides of cardo-diamines

No.	Bisamide	Yield %	Solubility				Elemental analysis			Structure
			DMFA	Acetone	Cyclohexanone	Chloroform	Found		Calcd.	
1	Anilinefluorene-bisacrylamide	93	S	S	S	I	C 81.94 H 5.39 N 6.20	81.76 5.48 6.21	81.60 5.45 6.10	crystalline
2	Anilinephthalein-bisacrylamide	94	S	S	S	I	C 73.42 H 4.81 N 6.52	73.20 4.87 6.57	73.58 4.71 6.60	mostly amorphous
3	Anilineanthrone-bisacrylamide	95	S	S	S	S	C 79.24 H 5.15 N 5.48	79.38 5.15 5.60	79.34 4.96 5.78	crystalline
4	Anilinephthalein-imidebisacrylamide	95	S	S	S	I	N 9.76	9.49	9.93	amorphous
5	Anilinefluorene-bismethacrylamide	93	S	S	S	I	C 81.98 H 5.78 N 5.90	81.96 5.83 5.90	81.82 5.78 5.78	crystalline
6	Anilinephthalein-bismethacrylamide	95	S	S	S	I	C 74.36 H 5.38 N 6.22	74.49 5.39 6.35	74.33 5.31 6.20	amorphous
7	Anilineanthrone-bismethacrylamide	95	S	S	S	S	N 5.52	5.40	5.46	amorphous
8	Anilinephthalein-imide-bismethacrylamide	90	S	S	S	I	—		—	—

S — Soluble
I — Insoluble

complete cross-linking is achieved and the polymer does not change up to the beginning of thermal decomposition (see Table II).

In order to follow the process itself, the above polymerization was repeated with mg samples, whose behaviour reflects the chemical process rather than the physical properties of a large sample. Measurements were carried out in a Perkin—Elmer DSC-2 instrument under standard conditions.

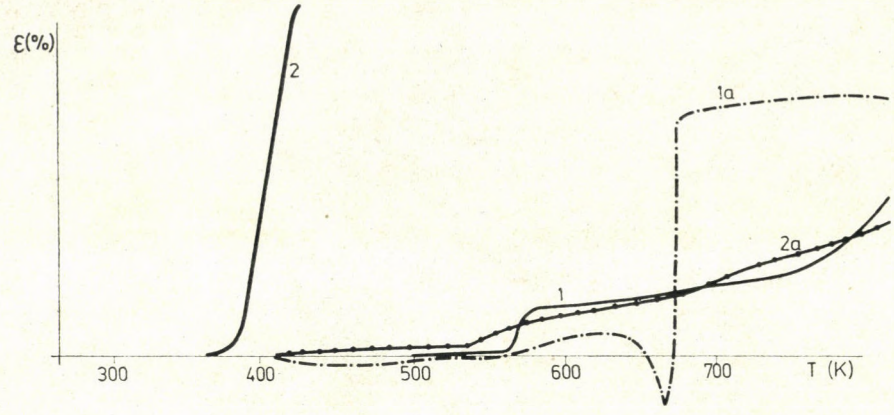

Fig. 1. Thermomechanical curves of **I** and **II** *(1)* thermomechanical curve of **I** without thermal treatment, *(2)* thermomechanical curve of **II** without thermal treatment, *(1a)* thermal treatment at 473 K for 5 hrs **I** *(2a)* thermal treatment at 473 K for 5 hrs **II**; Heating rate 150 deg/hr, Pressure on sample 0.8 kp/cm²

Table II

Insoluble fraction of polymers produced on the basis of cardo bisacryl- and bismethacrylamides produced by thermal polymerization in air at **473** *K for* **5** *hrs**

No.	Bisamide	Quantity of insoluble fraction	
		Extraction with DMFA	Extraction with acetone
1	Anilinefluorenebisacrylamide	0	62
2	Anilinephthaleinbisacrylamide	63	85
3	Anilineanthronebisacrylamide	0	15
4	Anilinephthaleinimidebisacrylamide	68	96
5	Anilinefluorenebismethacrylamide	0	0
6	Anilinephthaleinbismethacrylamide	66	81
7	Anilineanthronebismethacrylamide	0	0
8	Anilinephthaleinimidebismethacryl-amide	0	18

* The insoluble fraction has been determined by extracting the polymers with DMFA and acetone for 10 hrs in a Soxhlet apparatus.

Results and Discussion

As it has been shown the melting of crystalline and the softening of glassy samples occur simultaneously with polymerization, *i.e.* the exothermic and endotermic processes overlap. Besides, melting, crystallization and polymerization cause changes also in the specific heat. DSC measures the resultant of all these as a change in the enthalpy. The DSC method has already been successfully applied for measuring the polymerization of crystalline monomers [6]. [6]. Dynamic measurements with a simple non-isothermal linear program are not very informative in such cases : the mechanism of the process can be better investigated by combining isothermal and non-isothermal sections, *i.e.* by carrying out so-called "semidynamic" measurements.

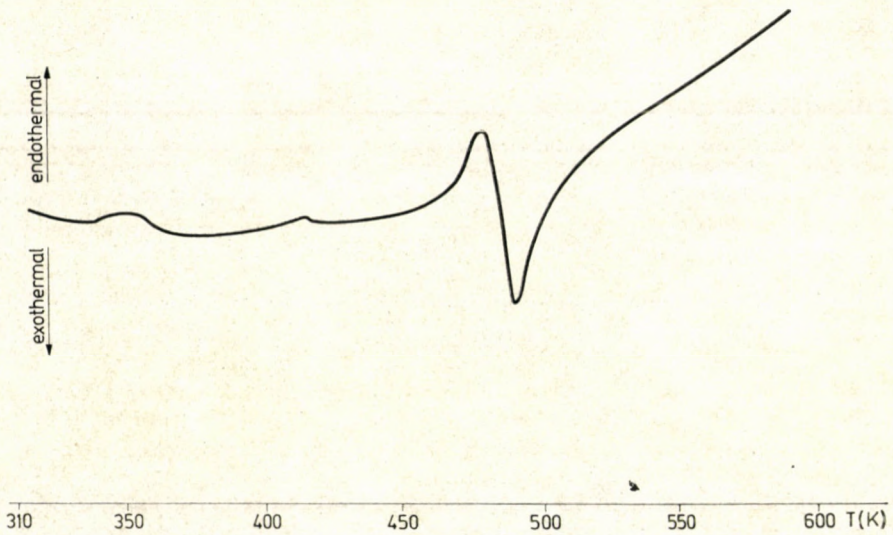

Fig. 2. DSC curve of **II** in an open crucible. Weight of sample 3.591 mg

The asymmetric compound (**II**) will be discussed first. The results are shown in Figs 2—10. Figure 2 shows the behaviour of **II**, when heated at a constant rate of 5 deg/min. The process begins with a characteristic endothermic peak, which later turns sharply into an exothermic one. **II** being mainly X-ray-amorphous, the endothermic peak corresponds to softening or partial melting while the exotermic one to polymerization and partly to recrystallization. At the end of the thermal treatment the system consists of stable and thermally inactive polymer, as is seen in Fig. 3. This curve shows the repeated heating of the sample after polymerization. The curve is smooth, neither peaks, nor steps pointing to a glass-transformation are present, and the increasing

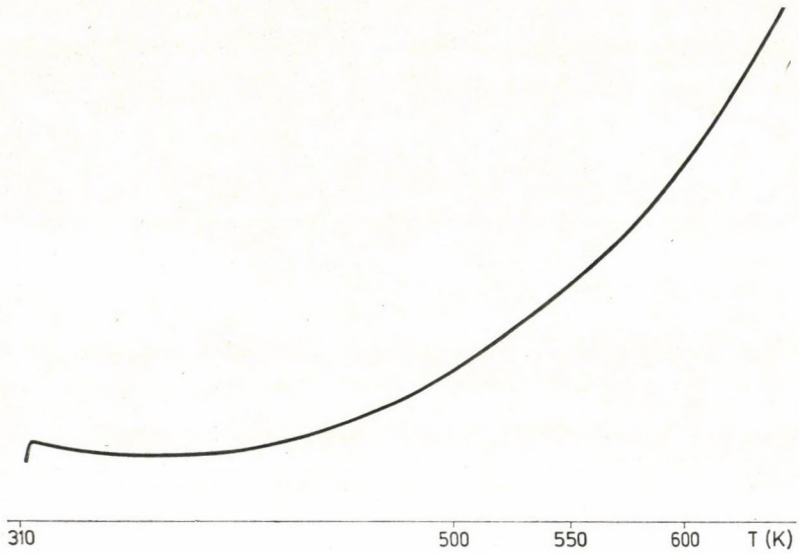

Fig. 3. DSC curve of former sample (Fig. 2) with repeated heating

section after the polymerization peak in Fig. 2 is the characteristic specific heat function.

In Fig. 4 the result of a similar dynamic experiment in a tightly closed crucible is shown. Apparently, the results are identical with those in Fig. 2 which prove that during and after melting, crystallization and polymeriza-

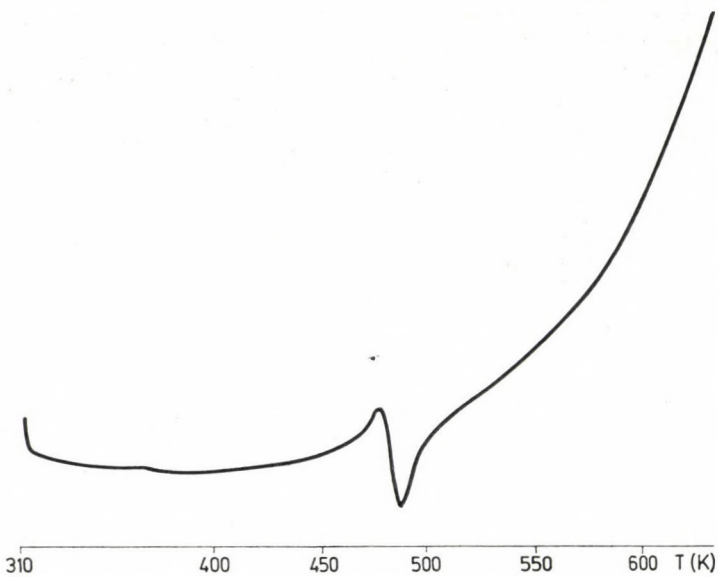

Fig. 4. DSC curve of **II** in a closed crucible. Weight of sample 2.361 mg

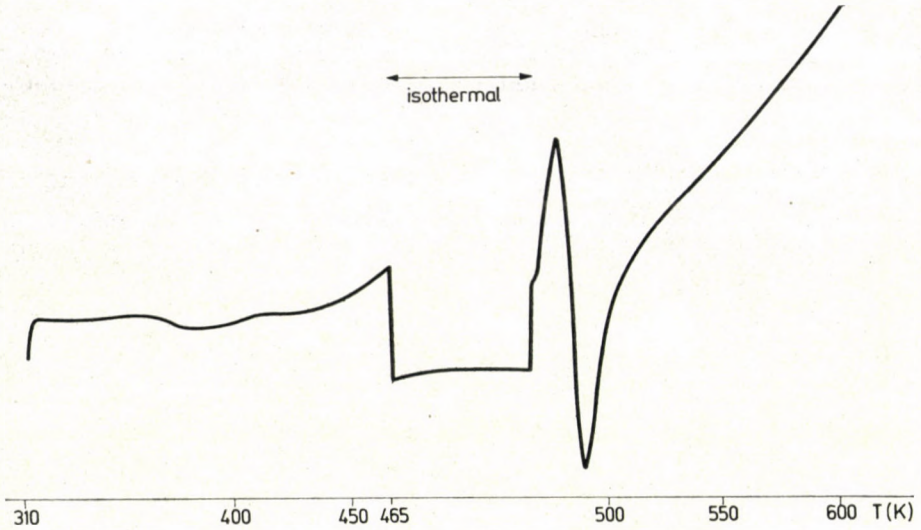

Fig. 5. Semidynamic curve of **II** with isothermal treatment at 465 K. Wegiht of sample 6.042 mg

tion, no evaporation or other mass transfer occurs, *i.e.* the curves are correctly interpreted. In subsequent experiments, the heating was stopped at different temperatures of the endothermic section, that is a semidynamic heat treatment was performed. The isothermal temperatures were 465 K (Fig. 5), 476 K (Fig. 6) and 479 K (Fig. 7). These temperatures were maintained until no more changes occurred on the DSC curve. Thereafter, the heating was continued. If the melting of the sample occurs in a wider temperature range, then at the iso-

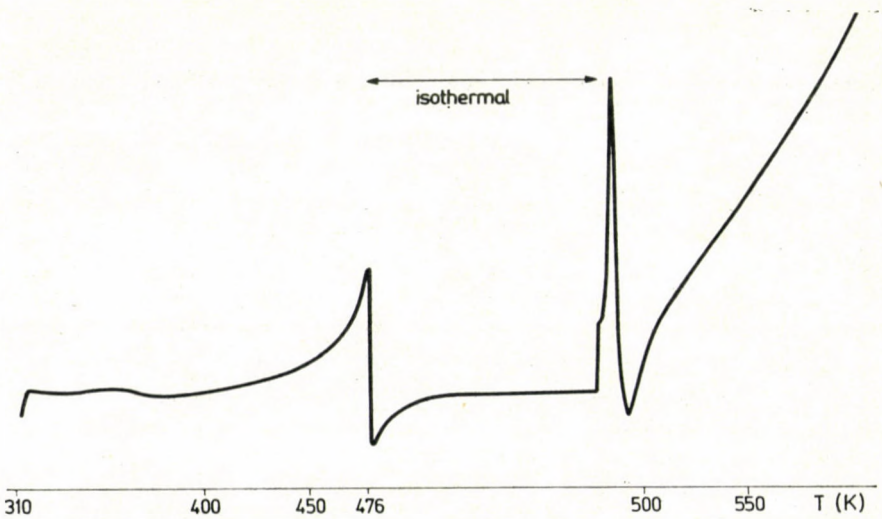

Fig. 6. Semidynamic curve of **II** with isothermal treatment at 476 K. Weight of sample 5.255 mg

thermal temperature only part of the material melts : upon increasing the temperature further the remaining material also melts, giving another endothermic peak. However, when interrupting the melting of **II**, instead of a simple step, a large, exothermic jump is obtained, which slowly approaches a constant value with a concave curve section.

A similar curve was obtained by the semidynamic tratment of polypropylene, as well [7]. Upon continuing the melting, at first a small specific heat step is observed, then an endothermic deflection is apparent, followed by an exothermic peak. This latter occurs in all three cases at about the same temperature.

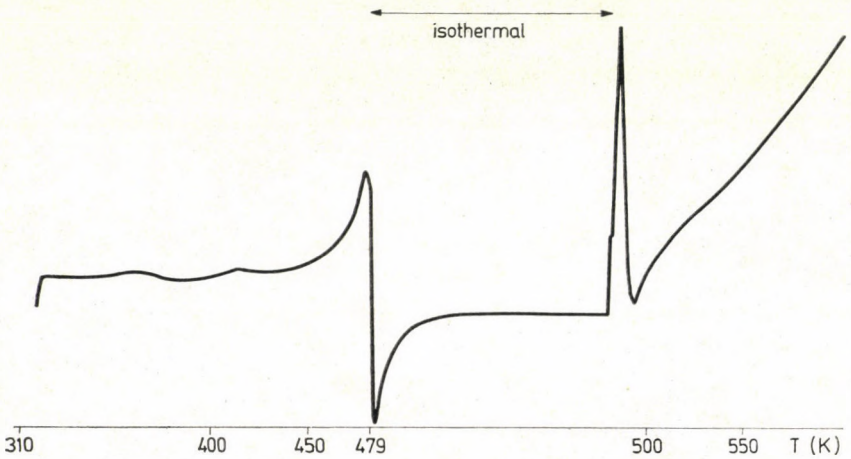

Fig. 7. Semidynamic DSC curve of **II** with isothermal treatment at 479 K. Weight of sample 6.015 mg

The concave section of the curve and the exothermic peak connected with it show that the latter is the greater, the higher is the temperature of the isothermal section, that is, the nearer it is to the temperature of the exothermic peak. Consequently, the polymerization already begins during the apparently endothermic process, and is to be observed until the molten monomer is "consumed". Further polymerization occurs only when the remaining monomer also melts. This latter is presumably the crystalline part embedded into the glassy phase, which naturally melts at a higher temperature. The melting and subsequent polymerization can be completely stopped by the insertion of an isothermal section. For proving this, we stopped the melting by including an isothermal section but before continuing the thermal program, cooled the sample to room temperature and heated it up again. We observed (see Fig. 8) that, up to the highest isothermal temperature reached by the first heating, no effect was apparent. However, the endothermic peak (*i.e.* the continuation of melting) appeared at the same place and in the same way as if the sample had

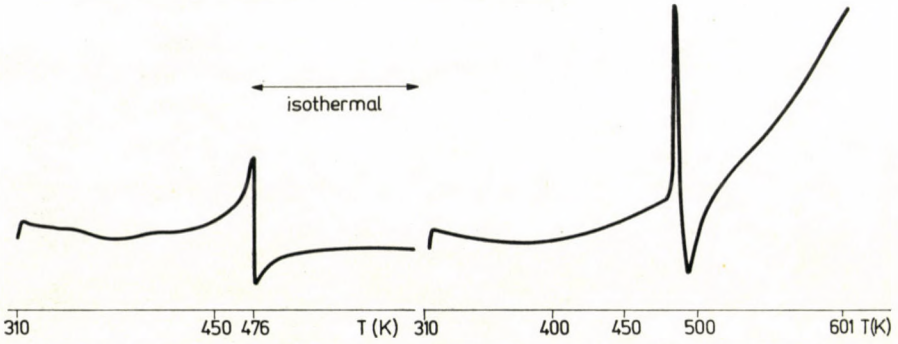

Fig. 8. Semidynamic and dynamic DSC curve of **II** with isothermal heat treatment at 476 K. Weight of sample 5.490 mg

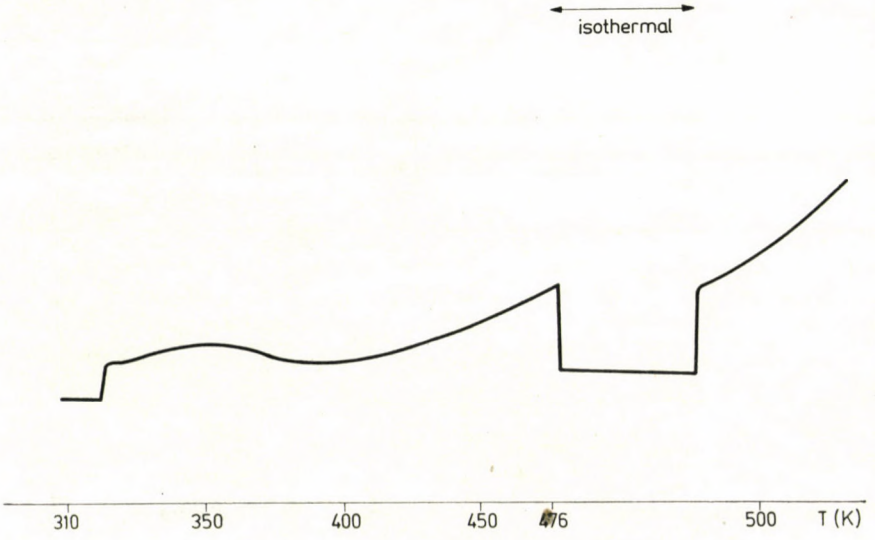

Fig. 9. Semidynamic DSC curve, repeated on the sample of Fig. 6, with isothermal heat treatment at 476 K. Weight of sample 5.255 mg

not been cooled down and the actual starting temperature of the endothermic peak had not been reached upon repeated heating. This means that the system in the non-isothermal process passes through both the endothermic and exothermic phase through quasi-equilibrium states.

Clearly, the partial melting occurs mainly in the amorphous phase and this and the accompanying polymerization have crystallizing effect on the remaining monomer, for after isothermal conditioning, both peaks, but mainly the endothermic one, become sharper, thus more similar to the melting curve of the crystalline material of high purity. Naturally, during the first heating and isothermal period, more and more material is polymerized due to the increasing temperature of the isothermal section, thus the following exothermic

peak decreases. This proves that polymerization starts simultaneously with melting.

In order to demonstrate that without prior heating only the constant base line can be reached, but no exothermic overshoot is to be expected on the basis of either the specific heat function or of other properties of the polymer, one sample was cooled down after polymerization and then repeatedly heated up semidynamically. It is seen in Fig. 9 that in this case identical jumps appear

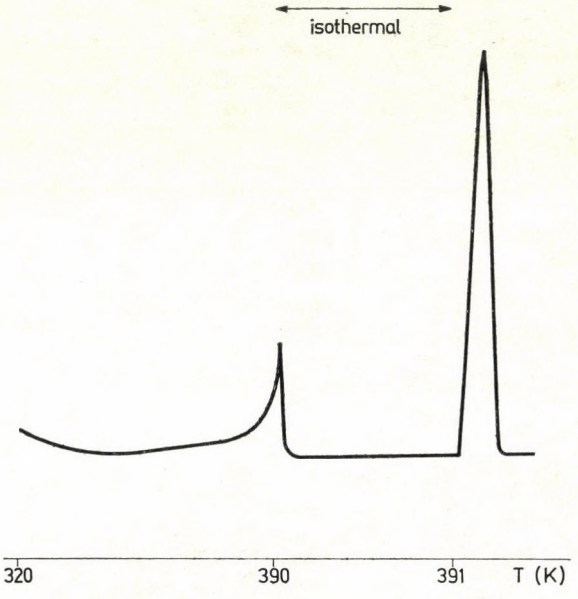

Fig. 10. Semidynamic melting curve of tetraphenylsilane. Heating rate 5 deg/min

at the beginning and end of the isothermal section with a linear base line between them.

In order to prove that the stopping of the melting can not cause an overshoot either if the endothermic process is not accompanied by an exothermic one, polyethylene and tetraphenylsilane have been studied in the same semidynamic way. According to Figs 10 and 11 a smooth change in the base lines occurs and the ceased melting begins again with the heating, but no overshoot beyond the base line of the isothermal section is to be seen.

Thus, it has been proved reliably — and in this case also quantitatively — that endothermic and exothermic processes take place simultaneously.

In Fig. 12 the behaviour of **I** is illustrated in a linear heat program, whereas Fig. 13 shows the same in a closed crucible. Both differ significantly from the behaviour of **II** not only in the temperature of the exothermic peak, but

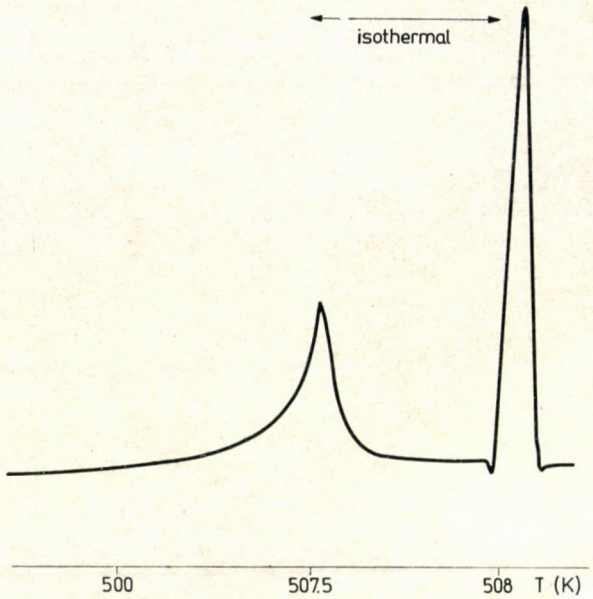

Fig. 11. Semidynamic melting curve of polyethylene (Hostalen GE). Heating rate 5 deg/min

also in that here apparently no melting occurs, though the material is — according to X-ray diffraction measurement — crystalline. Although theoretically unlikely, it cannot be fully excluded that the two events with positive and negative heat effects overlap in time and temperature to such an extent that we observe only the difference, which is exothermic. If we do not assume solid

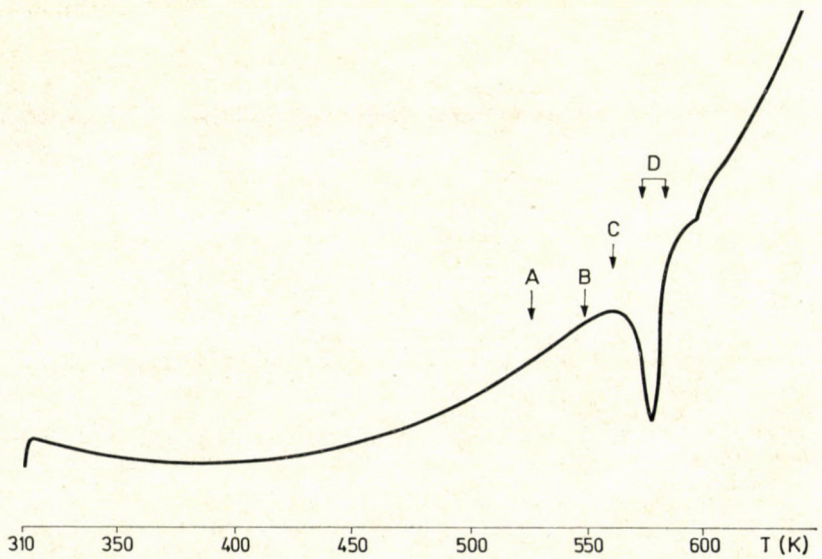

Fig. 12. DSC curve of **I** in an open crucible. Weight of sample 4.723 mg

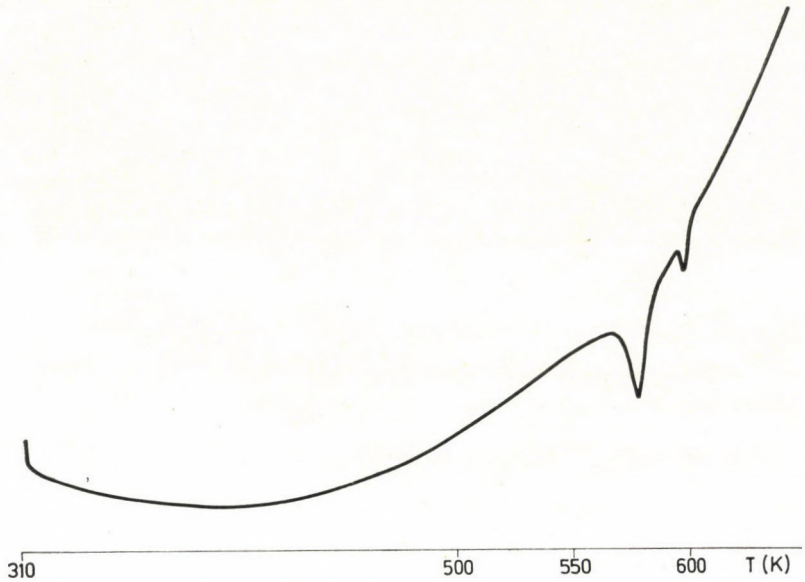

Fig. 13. DSC curve of **I** in a closed crucible. Weight of sample 3.888 mg

phase thermal polymerization without melting, this total overlap is impossible, and the former assumption is very unlikely. The dynamic measurements revealed a very flat, extended endothermic deflection. The above view is supported by thermomechanical (see Fig. 1) and thermooptical (microscopic) investigations as well.

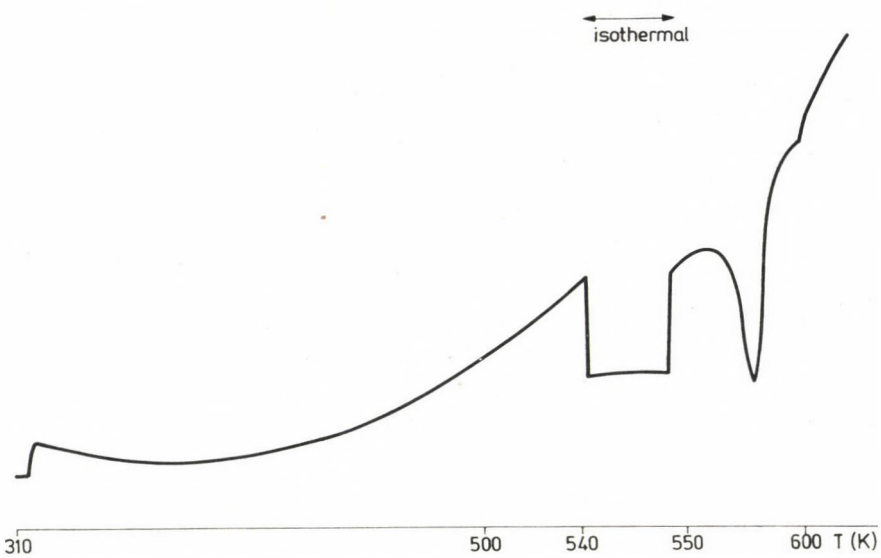

Fig. 14. Semidynamic DSC curve of **I** with isothermal heat treatment at 540 K. Weight of sample 5.739 mg

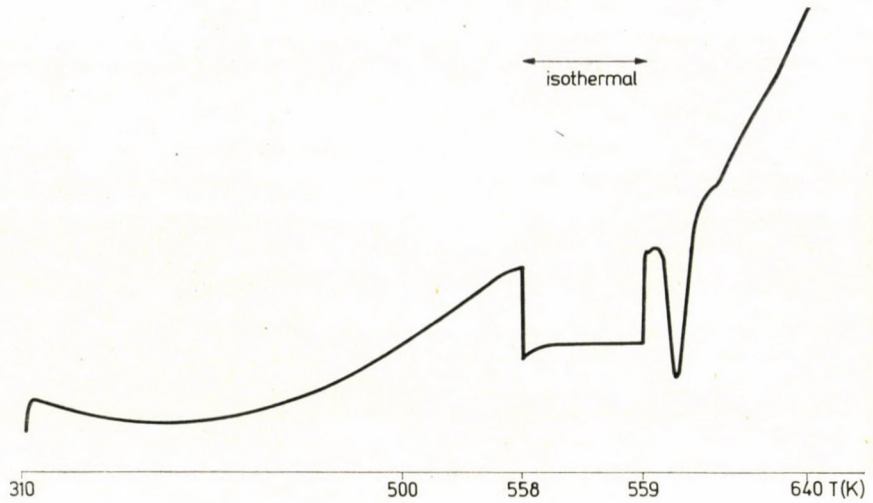

Fig. 15. Semidynamic DSC curve of **I** with isothermal heat treatment at 558 K. Weight of sample 5.850 mg

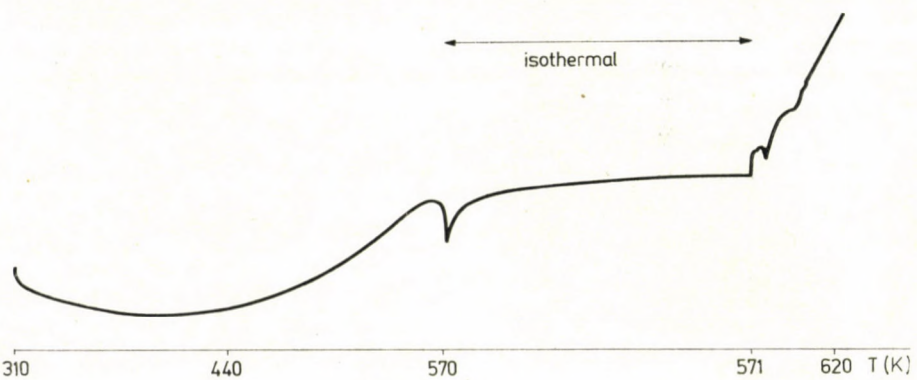

Fig. 16. Semidynamic DSC curve of **I** with isothermal heat treatment at 705 K. Weight of sample 4.462 mg

At point *A* a definite softening is to be observed. At point *B* inspection through a microscope with a heated sample holder shows incipient melting, ending at *C*. Interval *D* marks — according to the thermomechanical curve — the intensive mechanical change connected with polymerization. Figures 14, 15 and 16 show the results of semidynamic measurements with isothermal sections at 540, 558 and 570 K, respectively. Results are qualitatively similar to those for **II**, with quantitative differences, but clearly, the above argumentation is also valid for **I**. The reason of the difference is that, though **I** is crystalline, due to the large, symmetrical and nonpolar *cardo*-group, there are but weak intermolecular forces, corresponding to a small crystal energy. With **II**, the interaction of the polar *cardo*-groups hinders the regular arrangement of

the molecules, but stabilizes a glassy state that readily leads to the formation of cross-linked polymers.

After the isothermal section, an endothermic deflection appears, which is more pronounced than in the simple dynamic measurements. In this case there exists an early period of melting (see Fig. 12) without exothermic overshoot, *i.e.* with **I**, the liquid state precedes polymerization more markedly than with the glassy and softening **II**.

The above studies will be continued by quantitative calorimetric measurements, which are rendered difficult by the strong influence of the specific heat functions on the base line. The investigations will be extended also to other representatives of this group of compounds.

*

The authors are indebted to Dr. G. BODOR for the X-ray diffraction investigation of the two model substances, and to F. CSER for the thermooptical investigation of the polymerization of the two monomers.

REFERENCES

[1] VIGODSKII, YA. S., VINOGRADOVA, S. V.: Pecularities of the Synthesis and Properties of "*Cardo*-Polymers". "Chemistry and Technology of High Molecular Compounds", VINITI, **7**, 14 (1975)
[2] MEYERSON, S. I., LIPATOV, S. M.: Koll. Zh., **18**, 447 (1956)
[3] SHISHKIN, N. I.: Zh. T. F., **25**, 196 (1955)
[4] VINOGRADOVA, S. V., VIGODSKII, YA. S.: Usp. Khim., **42**, 1225 (1973)
[5] KORSHAK, V. V., VINOGRADOVA, I. V., VIGODSKII, YA. S.: J. Macromol. Sci., Rev. Macromol. Chem., **c11**, 45 (1974)
[6] SZÉKELY, T., LENGYEL, M., PAPKOV, V. S., ZAKHERNYUK, A. E., ZHDANOV, A. A. ANDRIANOV, K. A.: Acta Chim. Acad. Sci. Hung. **89**, 307 (1976)
[7] LENGYEL, M., MÁTHÉ, K., BODOR, G.: Acta Chim. Acad. Sci. Hung. **94**, 309 (1977)

Tamás SZÉKELY
Mária LENGYEL
H-1112 Budapest, Budaörsi út 45.

Vasilii Vladimirovich KORSHAK
Svetlana Vasilevna VINOGRADOVA
Ya. S. VIGODSKII
G. S. GURBICH
Москва, Улица Вавилова, 32

Acta Chimica Academiae Scientiarum Hungaricae, Tomus 100 (1—4), pp. 135—143 (1979)

SPONTANEOUS PROCESSES ON METAL SURFACE INDUCED BY ITS OWN METAL IONS, III

L. KISS*, J. FARKAS and I. MÁTRAI

*(Departement of Physical Chemistry and Radiology
L. Eötvös University, Budapest)*

Received June 27, 1978

Accepted for publication August 15, 1978

A method has been developed which allows us to determine the rate constants of the single steps of processes spontaneously proceeding in the system $M-M^{z_1+}-M^{z_2+}$ by measurement with a rotating ring-disc electrode. The applicability of the method is demonstrated by results obtained for the system $Cu-Cu^{+}-Cu^{2+}$ in HCl and $HClO_4$ solutions.

In an earlier communication [1] the kinetics of processes proceeding spontaneously in the system $M-M^{z_1+}-M^{z_2+}$ has been discussed. Relationships have been established in a few characteristic marginal cases for the dependence of the rate of the spontaneous processes, and of the steady state potential of metal M on the concentration of ions M^{z_2+}, and M^{z_1+} in the solution as well as on the hydrodynamical conditions of the electrolyte solution. On the basis of the relationships obtained, processes proceeding spontaneously in the system $Cu-Cu^{+}-Cu^{2+}$ in aqueous HCl and $HClO_4$ solutions could be well interpreted [2].

In the system investigated [1] the following processes may proceed:

$$M \underset{k_{k_1}}{\overset{k_{a_1}}{\rightleftharpoons}} M^{z_1+} + z_1 e \qquad \text{(I)}$$

$$M^{z_1+} \underset{k_{k_2}}{\overset{k_{a_2}}{\rightleftharpoons}} M^{z_2+} + n_2 e \qquad \text{(II)}$$

where k_{a_i} and k_{k_i} $(i = 1, 2)$ are the rate constants depending exponentially on the electrode potential.

It is to be shown in the present communication that on the basis of the investigation of the spontaneous processes using rotating ring-disc electrode informations may be obtained on the kinetic parameters of the electrode reactions (I) and (II) besides the marginal cases discussed earlier [1] also in those cases when the rate constants are of the same order of magnitude.

In the system $M-M^{z_1+}-M^{z_2+}$ the spontaneous reactions proceed under the following conditions:

1. If the concentration (c_2) of the metal ion of charge z_2 is increased as compared to the equilibrium concentration $\bar{c}_2$ ($c_2 \gg \bar{c}_2$). In this case, reaction (I) proceeds mainly in the forward direction, while reaction (II) in the backwards direction. Thus, metal M is dissolved and M^{z_2+} is reduced to M^{z_1+}.

2. If the concentration (c_1) of the metal ion with charge z_1 is substantially increased as compared to the equilibrium value $\bar{c}_1$ ($c_1 \gg \bar{c}_1$). In this case, reaction (I) proceeds mainly in the backwards direction, while (II) in the forward direction, *i.e.* the ion M^{z_1+} disproportionates, and metal M and ion M^{z_2+} are formed.

M^{z_1+} ions formed under condition 1 at the disc electrode made from metal M can be oxidized to M^{z_2+} ions at the indifferent ring electrode. Under the conditions given above, when no M^{z_1+} ions are present in the solution, ($c_1 \simeq 0$), and no current passes through the electrode, *i.e.* $j = 0$, the limiting current of oxidation, I_{R_1} is the following according to relationships given earlier [3]:

$$I_{R_1} = r_1^2 \pi n_2 X_1 N \frac{z_2 X_2 c_2}{\left(z_1 X_1 + \frac{\frac{z_2}{n_2} k_{a_2}}{1 + \frac{k_{k_2}}{n_2 X_2}} \right) \left(1 + \frac{n_2 X_2}{k_{k2}} \right)}, \tag{1}$$

where r_1 is the radius of the disc electrode, c_2 the concentration of the ions M^{z_2+} in the solution, N the geometric factor of the rotating ring-disc electrode, and X_1 and X_2 are the diffusion rate constants of ions M^{z_1+} and M^{z_2+}, respectively.

$$X_i = 0.62\ F D_i^{2/3} \nu^{-1/6} \left(\frac{2\pi}{60} \right)^{1/2} f^{1/2} = X_i' \cdot f^{1/2}, \tag{2}$$

where F is the Faraday constant, D the diffusion coefficient, ν the kinematic viscosity of the solution, f the revolution per minute of the electrode.

On rearranging relationship (1), the following expression is obtained:

$$A_1 = \frac{z_1}{k_{k_2}} + B_1 f^{-1/2}, \tag{3}$$

where:

$$A_1 = \frac{z_2 r_1^2 \pi N c_2}{I_{R_1}} \tag{4}$$

$$B_1 = \left(\frac{z_1 X_1}{n_2 X_2} + \frac{z_2 k_{a_2}}{n_2 k_{k_2}} \right) \frac{1}{X_1'} \tag{5}$$

Each component in term A_1 is either known or measured. To determine the I_{R_1} and c_2 values belonging together, at constant electrode potential I_{R_1} and the potential on the disc electrode at different r.p.m. and at different concentration of c_2 are to be measured. Using the I_{R_1} and c_2 values obtained in this way, the values of A_1 are calculated. Plotting the A_1 values at constant electrode potential (ε) as a function of the reciprocal value of the square root of r.p.m. ($f^{-1/2}$) a straight line is obtained (k_{k_2} and k_{a_2} are exponential functions of the electrode potential [1]). From the intercept of the straight line the reciprocal of k_{k_2} can be calculated. On the basis of intercept belonging to various potentials the function ε-lg k_{k_2} can be plotted, which must give a straight line, with a slope value of $\frac{2.303\,RT}{(1-\alpha_2)\,n_2F}$, where α_2 is the transfer coefficient of the anodic step of the electrode process (II).

The slope of Eq. (3) gives B_1, from the dependence of which on the electrode potential conclusions may be drawn on the value of k_{a_2}/k_{k_2}, since $X_1/X_2 \simeq 1$ (if the diffusion coefficients of ions M^{z_1+} and M^{z_2+} are approximately equal).

a) As can be seen from relationship (5), if B_1 is independent of the electrode potential then

$$k_{a_2}/k_{k_2} \ll 1 \tag{6}$$

and the value of X_2 can be calculated from B_1. According to (6), in this case $k_{k_2} \gg k_{a_2}$. If $k_{k_2} \gg 1$, the straight line given by Eq. (3) starts from the origo, and straight lines belonging to various potentials coincide.

b) On the other hand, if

$$k_{a_2}/k_{k_2} \gg 1 \tag{7}$$

B_1 changes with the electrode potential.

As k_{a_2} and k_{k_2} depend exponentially on the electrode potential ε, the relationship ε-lg B_1 must give in this case a straight line, with slope value of $\frac{2.303\,RT}{n_2F}$.

c) If in B_1 the two terms in bracket are of identical order of magnitude, then the values of k_{a_2} and k_{k_2} will also be approximately the same.

On the basis of the aforesaid, the k_{a_2} and k_{k_2} rate constants and the transfer coefficient of reaction (II) can be determined.

From relationship (1) and from Eq. (2) in communication [3] [taking into consideration in the use of this latter equation that the process is spontaneous ($j = 0$), and $c_1 \simeq 0$] the following relationship is obtained by appropriate rearrangement:

$$A_2 = \frac{z_1}{k_{a_1}} + B_2 f^{-1/2}, \tag{8}$$

where :

$$A_2 = \frac{z_2 r_1^2 \pi N}{I_{R_1}} \tag{9}$$

$$B_2 = \frac{z_2}{n_2} \frac{k_{k_1}}{k_{a_1}} \cdot \frac{1}{X_1'}, \tag{10}$$

where the interpretation of X_1 is given by Eq. (2).

As can be seen from relationships (8)—(10), on the basis of the train of thought used in the discussion of expression (3) k_{a_1} and k_{k_1} and their potential dependence can be determined.

In the second case mentioned in the introduction, when the ion M^{z_1+} is present in high concentration in the solution as compared to equilibrium concentration, it will disproportionate and metal M and the ion M^{z_2+} are formed. Under appropriate conditions, the rotating ring disc electrode makes possible also in this case to determine a few kinetic parameters of the process. Thus, if the disc electrode is prepared from metal M and the ring electrode from a conductor (*e.g.* carbon paste) at which the reduction of the ion M^{z_1+} proceeds at a high overvoltage, the M^{z_2+} ions, formed by disproportioning at the disc, can be reduced to M^{z_1+} ions at the ring electrode. If $c_2 \simeq 0$, and the process is spontaneous ($j = 0$), according to the relationship given in our earlier communication [3], the limiting current $-I_{R_2}$ of the reduction is :

$$-I_{R_2} = r_1^2 \pi n_2 X_2 N \frac{k_{a_2}}{k_{k_2} + n_2 X_2} \cdot \frac{z_1 X_1 c_1}{z_1 X_1 + \dfrac{\dfrac{z_2}{n_2} k_{a_2}}{1 + \dfrac{k_{k_2}}{n_2 X_2}}}. \tag{11}$$

By a suitable rearrangement of Eq. (11) the following expression is obtained :

$$A_3 = \frac{n_2}{k_{a_2}} + B_3 f^{-1/2}, \tag{12}$$

where :

$$A_3 = \frac{n_2 r_1^2 \pi N c_1}{-I_{R_2}} \tag{13}$$

$$B_3 = \left(\frac{z_2 X_2}{z_1 X_1} + \frac{k_{k_2}}{k_{a_2}} \cdot \right) \frac{1}{X_2'}. \tag{14}$$

Relationship (12) can be discussed in a similar way as Eq. (3), that is to say, knowing I_{R_2} and c_1 values belonging together at constant electrode po-

tential, as a function of the rotation speed of the electrode, k_{k_2} and k_{a_2} can be determined at various potentials, as well as the value of α_2.

It should be mentioned that in disproportionation expression analogous to Eq. (8) involves values of k_{a_1}, k_{a_2}, k_{k_1} as well as k_{k_2}. Therefore, on the basis of parameters measurable at spontaneous disproportionation k_{a_1} and k_{k_1} can not be determined with the method described above.

With the method described investigations have been carried out in the system $Cu—Cu^+—Cu^{2+}$. The kinetics of processes proceeding spontaneously have been studied in 1.0 mol/dm³ HCl and in 3.0 mol/dm³ $HClO_4$ solutions,

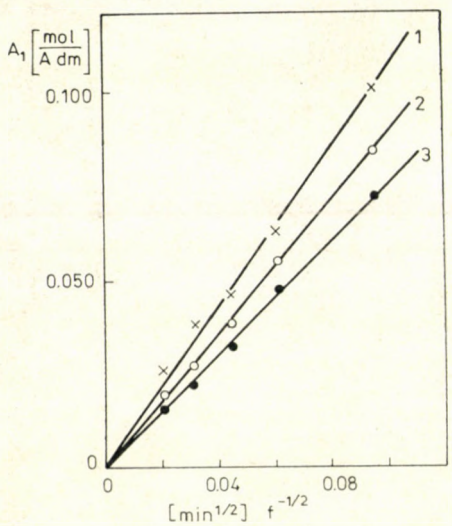

Fig. 1. Plot of A_1 against $f^{-1/2}$ in 1.0 mol/dm³ of HCl solution at different temperatures (1): 10 °C; (2): 20 °C; (3): 30 °C

in which the concentration of copper (II) ions ($c_{Cu^{2+}}$) was much higher than the equilibrium concentration $\bar{c}_{Cu^{2+}}$, that is to say, $c_2 \gg \bar{c}_2$ and $c_{Cu^+} \simeq 0$.

Equipment and methods used in the experiments, and the quality of the substances were the same as those described in an earlier work [4]. Measurements were carried out in oxygen-free nitrogen atmosphere. Electrode potentials values referred to the normal calomel electrode.

Figures 1 and 2 show the straight lines $A_1 - f^{-1/2}$ (Fig. 1) and $A_2 - f^{-1/2}$ (Fig. 2) plotted on the basis of experimental results obtained in 1.0 mol/dm³ HCl solution [See Eqs (3) and (8)]. The three straight lines shown in Fig. 1 belong to different temperatures and all three start from the origo. On the other hand, points belonging to constant temperature but different electrode potentials give the same straight line, that is why B_1 is not dependent on the electrode potential. The fact that the straight lines intersect the ordinate axis at the origo means according to the aforesaid that $k_{k_2} \gg 1$, while the indepen-

dence of B_1 from the electrode potential indicates that $k_{a_2}/k_{k_2} \ll 1$, that is to say $k_{a_2} \ll k_{k_2}$. This result is in accordance with the well known experience that in hydrochloric acid solution the anodic dissolution of copper at not too positive potentials proceeds by formation of only coprous ions [5].

Data shown in Fig. 2 belong to three different electrode potentials at 20 °C. It will be noted that the plotting of A_2 values as a function of $f^{-1/2}$ gives a straight line, in accordance with relationship (8). The intercept proportional to k_{a_1}, and B_2 obtained from the slope of the line proportional to k_{k_1}/k_{a_1}. As it is expected the slope of the curves decreases when the potential becomes more positive.

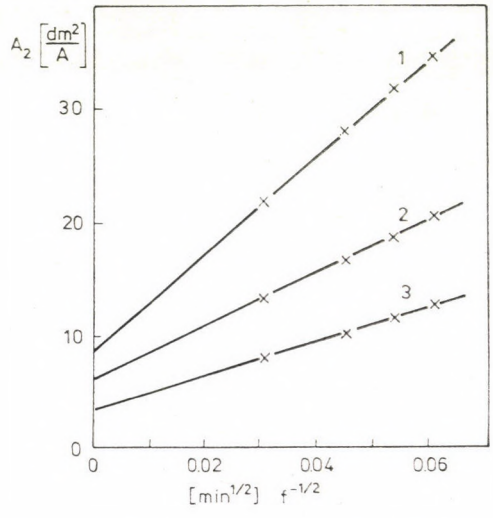

Fig. 2. Plot of A_2 against $f^{-1/2}$ in 1.0 mol/dm³ of HCl solution at different potentials. (1): —270 mV; (2): —260 mV; (3): —250 mV

Figures 3 and 4 shows at different electrode potentials the relationship $A_1 - f^{-1/2}$, plotted on the basis of data measured in 3.0 mol/dm³ $HClO_4$ solution at 10 °C (Fig. 3) and at 60 °C (Fig. 4). Experimental points belonging to the same potential yield a straight line again. The approximate value (order of magnitude) of k_{k_2} can be established on the basis of the intercept of the straight lines. It can be seen from Figs 3 and 4 that an increase in temperature by 50 °C increases k_{k_2} by about two orders of magnitude.

As B_1 is changing with the electrode potential, $k_{a_2}/k_{k_2} \gg 1$, *i.e.* $k_{a_2} \gg k_{k_2}$. On the basis of B_1 values obtained at 10 and 60 °C, k_{a_2} increases by about an order of magnitude when temperature is increased by 50 °C.

Figures 5 and 6 show at different electrode potentials the relationship $A_2 - f^{-1/2}$, in 3.0 mol/dm³ $HClO_4$ solution at 10 °C (Fig. 5) and at 60 °C (Fig. 6). In accordance with Eq. (8) points belonging to the same potential give

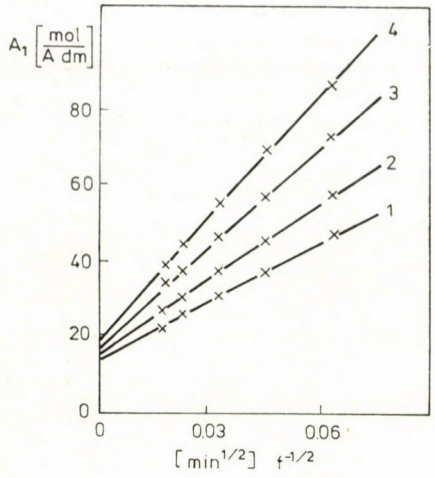

Fig. 3. Plot of A_1 against $f^{-1/2}$ in 3.0 mol/dm³ of $HClO_4$ solution at 10 °C. (1): —35 mV; (2): —30 mV; (3): —25 mV; (4): —20 mV

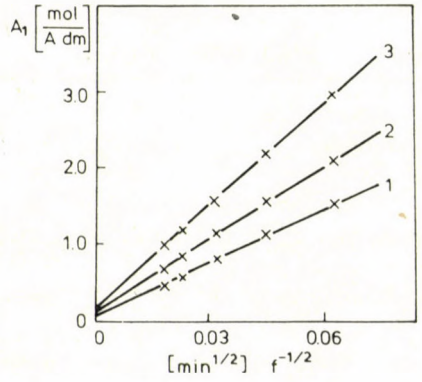

Fig. 4. Plot of A_1 against $f^{-1/2}$ in 3.0 mol/dm³ of $HClO_4$ solution at 60 °C. (1): —40 mV; (2): —30 mV; (3): —20 mV

a straight line. The values of the anodic (k_{a_1}) and cathodic rate constants (k_{k_1}) estimated on the basis of data of Figures indicate that by increasing the temperature by 50 °C the k_{a_1} increases by about of two orders of magnitude, while k_{k_1} grows only by about one orders of magnitude. These experimental results prove the experience according to which the equilibrium of the system Cu—Cu(I)—Cu(II) in $HClO_4$ solution is shifting to the direction of Cu(I) formation, when increasing the temperature.

It can be established on the basis of the above-said that the rate constants of the single steps of processes spontaneously proceeding in the system M—M^{z_1+}—M^{z_2+} can be determined by measurements with rotating ring-disc electrode.

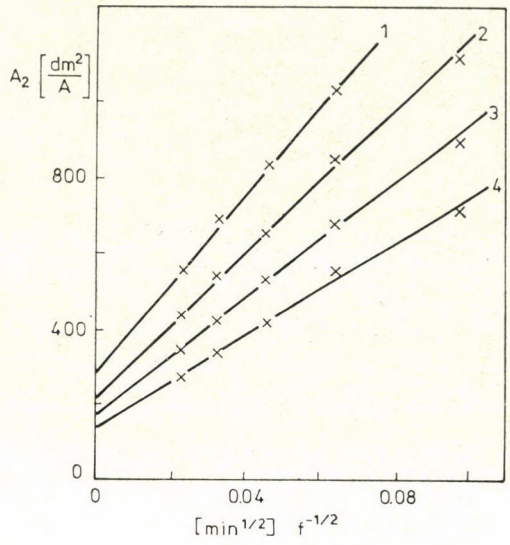

Fig. 5. Plot of A_2 against $f^{-1/2}$ in 3.0 mol/dm³ of $HClO_4$ solution at 10 °C. (1): —35 mV; (2): —30 mV; (3): —25 mV; (4): —20 mV

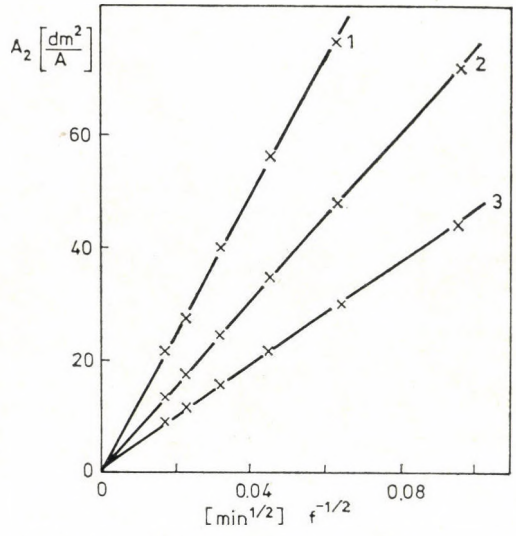

Fig. 6. Plot of A_2 against $f^{-1/2}$ in 3.0 mol/dm³ of $HClO_4$ solution at 60 °C. (1): —40 mV; (2): —30 mV; (3): —20 mV

REFERENCES

[1] KISS, L., FARKAS, J.: Magy. Kém. Folyóirat, **83,** 337 (1977); Acta Chim. Acad. Sci. Hung., **96,** 127 (1977)
[2] KISS, L., FARKAS, J., KOVÁCS, P., KOZÁRI, L.: Magy. Kém. Folyóirat, **84,** 97 (1978)
[3] KISS, L.: Kémiai Közl., **44,** 91 (1975); **45,** 425 (1976)
[4] KISS, L., FARKAS, J., KÖRÖSI, A., MANDL, J.: Acta Chim. Acad. Sci. Hung. **79,** 43 (1973)
[5] KISS, L., FARKAS, J., KÖRÖSI, A.: Magy. Kém. Folyóirat, **77,** 35 (1971)

László KISS
József FARKAS
István MÁTRAI
H-1088 Budapest, Puskin u. 11—13.

Acta Chimica Academiae Scientiarum Hungaricae, Tomus 100 (1—4), pp. 145—162 (1979)

A NEW METHOD FOR THE DIFFERENTIATION OF THE S_N AND $S_{RN}1$ MECHANISMS

THE *CINE* SUBSTITUTION REACTION OF 2-HALO-*N*,*N*-DIMETHYL-2,2-DIPHENYL-ACETAMIDES WITH SODIUM METHOXIDE IN METHANOL. THE NON-OPERATION OF THE $S_{RN}1$ MECHANISM

GY. SIMIG,[1] K. LEMPERT,[1] G. TÓTH[2] and J. TAMÁS[3]

([1]Research Group for Alkaloid Chemistry of the Hungarian Academy of Sciences, Budapest,

[2] NMR Laboratory of the Semmelweis Medical University, Budapest,[+]

[3] Central Research Institute for Chemistry of the Hungarian Academy of Sciences, Budapest)

Received June 29, 1978

Accepted for publication September 7, 1978

Reaction of the haloamides **1a** and **1b** with sodium methoxide in methanol furnishes, in addition to the normal product **2a**, two *cine* products **3a** and **3b**. The ratio **3b**/**3a** does not depend on the nature of the halogen present in the starting haloamides, which indicates that formation of **3a** and **3b** is likely to take place either by the $S_{RN}1$ or the S_N1/S_N1' mechanisms (Charts 2 and 3). Independently generated radical **12** (one of the key intermediates of the conceivable $S_{RN}1$ pathway) does not furnish even traces of **2a**, **3a** and **3b** with methoxide in methanol, which rules out the $S_{RN}1$ mechanism for the reaction in question. The products **2c**, **3c** and **4**, obtained from the haloamide **1c** with methoxide in methanol, too, may be rationalized on the basis of the operation of the S_N1/S_N1' mechanism.

Reaction of the radicals **12** with pure methanol and methanolic hydrogen chloride has also been studied; mechanisms for the formation of the products obtained from **12** under the various conditions are advanced.

Reaction of the 2-halo-*N*,*N*-dimethyl-2,2-diphenylacetamides **1a** and **1b** with excess sodium methoxide in methanol at room temperature was recently found to yield, in addition to the normal product **2a** (32—38%), unseparable mixtures of the two *cine* substitution products **3a** and **3b*** (total yield 43—53%)**, while in the absence of sodium methoxide the normal product **2a** was formed exclusively [1, 2]***. The related di(*p*-chloro) derivative **1c**, when refluxed with excess methanolic sodium methoxide, similarly gave mixtures of the normal (**2c**; 50—58%), the *cine mono*substitution (**3c**; 12—15%) and the anomalous *di*substitution product **4** (3—11%) [1]. In 2,2-dimethoxypropane (DMP) the bromoamide **1b** with excess sodium meth-

[+] Present address: Faculty of Chemical Engineering, Technical University, Budapest.

* For the proof of structure of compounds **3a** and **3b**, see below.

** Small amounts of the normal hydrolysis product **2b** were also isolated.

*** Similarly, hydrolysis of compound **1a** under neutral conditions ($DMSO/H_2O$) furnishes the normal hydrolysis product **2b** exclusively [3].

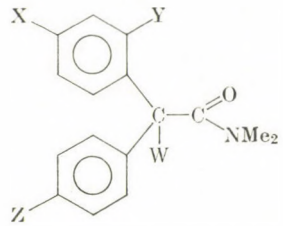

	X	Y	Z	W		X	Y	Z	W
1a	H	H	H	Cl	**3c**	Cl	MeO	Cl	H
1b	H	H	H	Br	**4**	MeO	H	Cl	MeO
1c	Cl	H	Cl	Br	**5**	H	H	H	H
2a	H	H	H	MeO	**6**	H	H	H	Ph–NH–NH–
2b	H	H	H	OH	**7**	H	H	H	Ph–N=N–
2c	Cl	H	Cl	MeO	**8***	Ph	H	H	H
3a	MeO	H	H	H	**9**	H	H	H	Ph
3b	H	MeO	H	H	**10**	H	H	H	$-CH_2OH$

* The isomeric *o*-biphenylyl structure (*x* and *y* reversed) is not ruled out with complete certainty.

oxide furnished mixtures consisting mainly of the reduced (**5**) and the dimeric product (**14**) [1]. The formation of the dimeric product by itself suggested the operation of the radical-anion — radical mechanism [4] (Chart 1) which was substantiated with the aid of crossing experiments [2].

In order to get some insight into the mechanism of the reaction of the haloamides **1a** and **1b** with sodium methoxide in methanol, the influence of the nature of the halogen atom of the starting compound on the product composition was studied. Analysis of the product mixtures with the aid of the PMR technique has shown that while the ratio **2a**/(**3a** + **3b**) of the amount of the normal product to the sum of the amounts of the two *cine* products strongly depends on the nature of the halogen present in the starting compound, the ratio of the two *cine* products does not, the *cine* product mixtures being made up in all cases of 91—92% of the *p*- (**3a**) and 9—8% of the *o*-product (**3b**), independently of the nature of the halogen. This observation appeares to indicate* the existence of a *common, halogen-free intermediate* on the pathway leading to the two *cine* products. The same intermediate may, of course, be also one of the precursors of the normal product, but at least one additional pathway, *not* involving a halogen-free intermediate, must exist for the formation of this compound.

* A more definite statement must be postponed until the effect of various other leaving groups on the ratio of the two *cine* products has been studied.

Initiation

(1) 

1b **11**

Propagation

(2) **11** $\xrightarrow{-Br^{\ominus}}$ 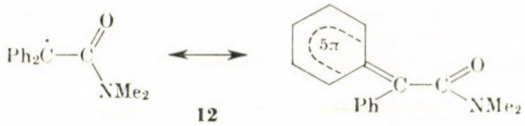

12

(3a) **12** + $MeO^{\ominus}$ → 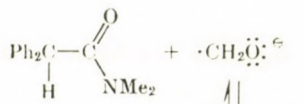 + $\cdot CH_2O^{\ominus}$

5*

$-H^{\oplus}$ ⇅ $+H^{\oplus}$

(3b) **12** + MeOH → **5*** + $\cdot CH_2OH$

(4) **1b** + $\cdot CH_2O^{\ominus}$ → **11** + HCHO

Termination

(5) 2 **12** → 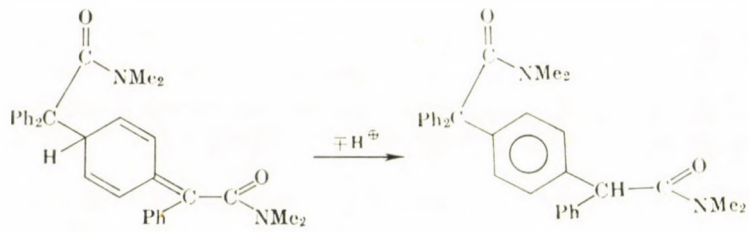

13 **14**

(6) **12** + MeO· → **5*** + HCHO

Chart 1. The radical-anion—radical mechanism of formation of compounds **5** and **14**

* Compound **5** is not necessarily directly formed; its formation may as well involve the intermediacy and subsequent rearrangement of compound **15,** cf. Ref. [5].

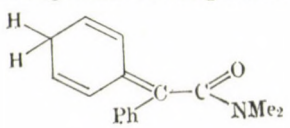

15

Initiation

(1) 

1a, 1b **11A**

Propagation

(2) **11A** $\xrightarrow{-Hlg^{\ominus}}$ 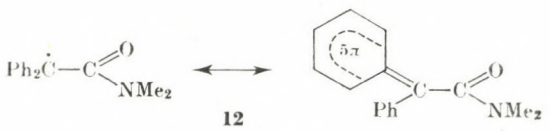

12

(3) **12** + $MeO^{\ominus}$ $\rightleftharpoons$ 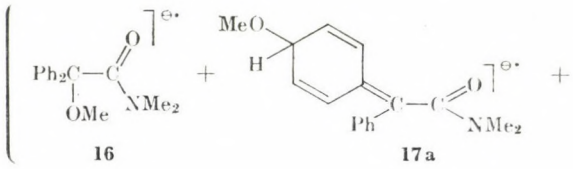

16 **17a**

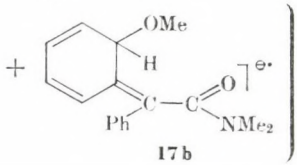

17b

(4) **1a, 1b** + **16** $\longrightarrow$ 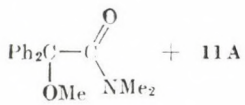 + **11A**

2a

(5a) **1a, 1b** + **17a** $\longrightarrow$ 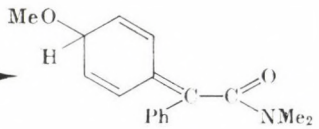 + **11A**

18a

(5b) **1a, 1b** + **17b** $\longrightarrow$ 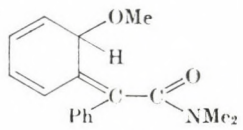 + **11A**

18b

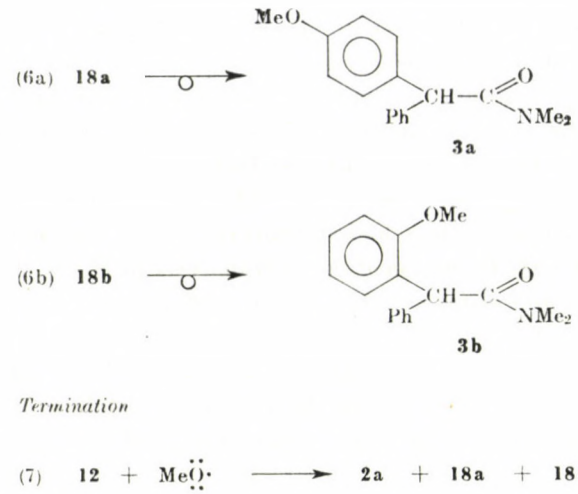

Chart 2. The conceivable $S_{RN}1$ mechanism of formation of compounds **2a, 3a** and **3b**

These considerations immediately lead to the question whether the formation of the *cine* products **3a** and **3b** involves some sort of classical nucleophilic substitution, *e.g.* the intermediacy of the mesomeric cation **19** (see Chart 3), or, similarly to the formation in DMP of the reduced product **5** and the dimer **14**, the $S_{RN}1$ mechanism with the radical **12** as the intermediate (Chart 2)*. In order to clarify this point, the radicals **12** were independently generated by refluxing methanolic solutions of the azo compound **7** and sodium methoxide**; compounds **5**, **8** and **14**** were obtained (see Table I) but none of compounds **2a**, **2b**, **3a** and **3b**. This observation, by itself does *not* rule out the $S_{RN}1$ mechanism for the formation of the latter products from the haloamides and sodium methoxide in methanol, because the failure of formation of the methoxy derivatives from the radicals **12** could be the result of the reversibility of step (3) of Chart 2 [which has to be assumed if step (2) is considered real], coupled with the absence of the electron acceptors **1a** and **1b** under the

* Most $S_{RN}1$ reactions are thought to take place by the chain mechanism [4] (depicted for the special case under discussion in Chart 2) but a non-chain sequence which, in the present case, would consist of steps (1), (2), (7), (6a) and (6b), would equally well be conceivable and has been proven in one case [6]. Furthermore, depending on whether step (2) takes place within the solvent cage in which the anion radical **11A** had been originally formed or after its escape from this cage, step (7) may be either a cage or a non-cage process.

** The conditions of the two reactions are not strictly identical: the haloamides **1a** and **1b** were allowed to react with methanolic sodium methoxide at room temperature, whereas the radicals **12** were generated at the boiling point of the solvent methanol. However, the same products were obtained from the haloamides and methoxide at the boiling point of the solvent methanol.

*** Since **5** and **14** are the products of the haloamides **1a** and **1b** with sodium methoxide in DMP [1], this may be regarded as an additional proof for the operation of the $S_{RN}1$ mechanism in DMP.

conditions of the thermolyses. However no significant change in the product composition was observed when thermolysis of compound **7** was carried out under otherwise identical conditions but in the presence of nitrobenzene which is known [4b, 7] to be a potent electron acceptor and which, therefore, should be able to replace the haloamides **1a** and **1b** in steps (4), (5a) and (5b) of Chart 2 ; in particular, no methoxy derivatives **2a**, **3a** and **3b** were obtained even in the presence of nitrobenzene, which definitely *rules out the chain version of the* $S_{RN}1$ *mechanism for the formation of the methanolysis products*, **2a**, **3a** *and* **3b** *from the haloamides* **1** *and sodium methoxide in methanol.*

Moreover, the non-chain — non-cage version of the $S_{RN}1$ mechanism is ruled out by the fact that no methoxy compounds **2a**, **3a** and **3b** were formed in the thermolysis experiments carried out in the presence of sodium methoxide which, as will be discussed below (p. 154), demonstrates that step (7) of the non-chain — non-cage sequence, and therefore the entire sequence as well, must at least be inefficient*. Furthermore compound **6**, when refluxed with sodium methoxide in methanol, furnishes mixtures of the reduced product **5** and the corresponding methyl ester (the formation of the latter by $B_{AC}2$ type methanolysis being obviously independent of the reduction process), again without formation even of traces of the methoxy compounds **2a**, **3a** and **3b**. If reaction **6** → **5** could be shown to be analogous to reaction **1b** → **5** (with PhNHNH- replacing Br- in Chart 1), this observation would provide evidence for the inefficiency of both the cage and the non-cage versions of step (7) of Chart 2 and rule out the $S_{RN}1$ mechanism for the formation of compounds **2a**, **3a** and **3b** with complete certainty. However, probably as a result of its known instability towards methanolic sodium methoxide (demonstrated furthermore in a separate experiment), phenylhydrazine could not de detected as a by-product of reaction **6** → **5**. The analogy of the mechanisms of the two reactions **6** → **5** and **1b** → **5** is therefore not yet established. Experiments towards this goal are in progress. In any case, *some sort of the classical nucleophilic substitution, e.g. the mechanism depicted in Chart 3, is left with a high degree of probability as the only mechanistic possibility for the reaction of the haloamides* **1a** *and* **1b** with methoxide in methanol.

If the cation **19** is assumed to be the intermediate leading to the formation of compounds **3a**, **3b** and of a part of compound **2b** (*i.e.* the combined S_N1' and S_N1 mechanisms are assumed to operate), the solvent dependence of the reaction of the haloamides **1** and sodium methoxide may easily be rationalized by noting that formation of the cation **19** is possible in the ionizing solvent methanol, but is not in the non-ionizing solvent DMP.

Since the reaction of the haloamides **1a** and **1b** with sodium methoxide in methanol does not take place by the $S_{RN}1$ mechanism, this appears even less

* The same has already been shown to be the case in solvent DMP [2].

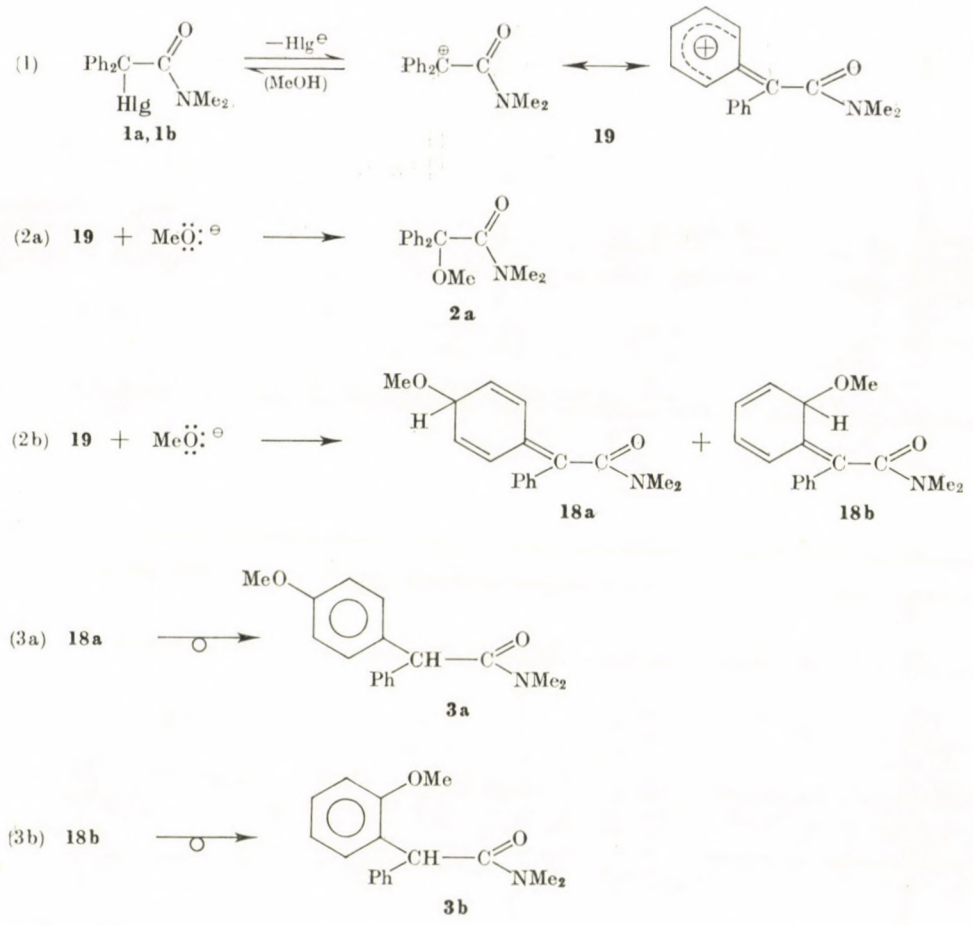

Chart 3. The S_N1/S_N1' mechanism of formation of compounds **2a, 3a** and **3b**

likely to be the case for their reaction with methanol alone, since the ability of the latter to act as an electron donor is much less pronounced ; *i.e.* the cation **19** should be the intermediate of the reaction of the haloamides with pure methanol as well. As a corollary, it must be assumed that while with methanol **19** reacts only in the α-position (furnishing thereby **2a** as the sole product), it exhibits ambident reactivity towards methoxide to yield mixtures of compounds **2a**, **3a** and **3b**. The reason for the different behaviour of **19** towards the two nucleophiles is not clear ; it may perhaps be a consequence of the differences in the hardness and softness of the latter ; or possibly of the reversibility of step (2b) of Chart 3 and of the analogous reaction of **19** with methanol, coupled with the need for the presence of a basic catalyst for steps (3a) and (3b) of

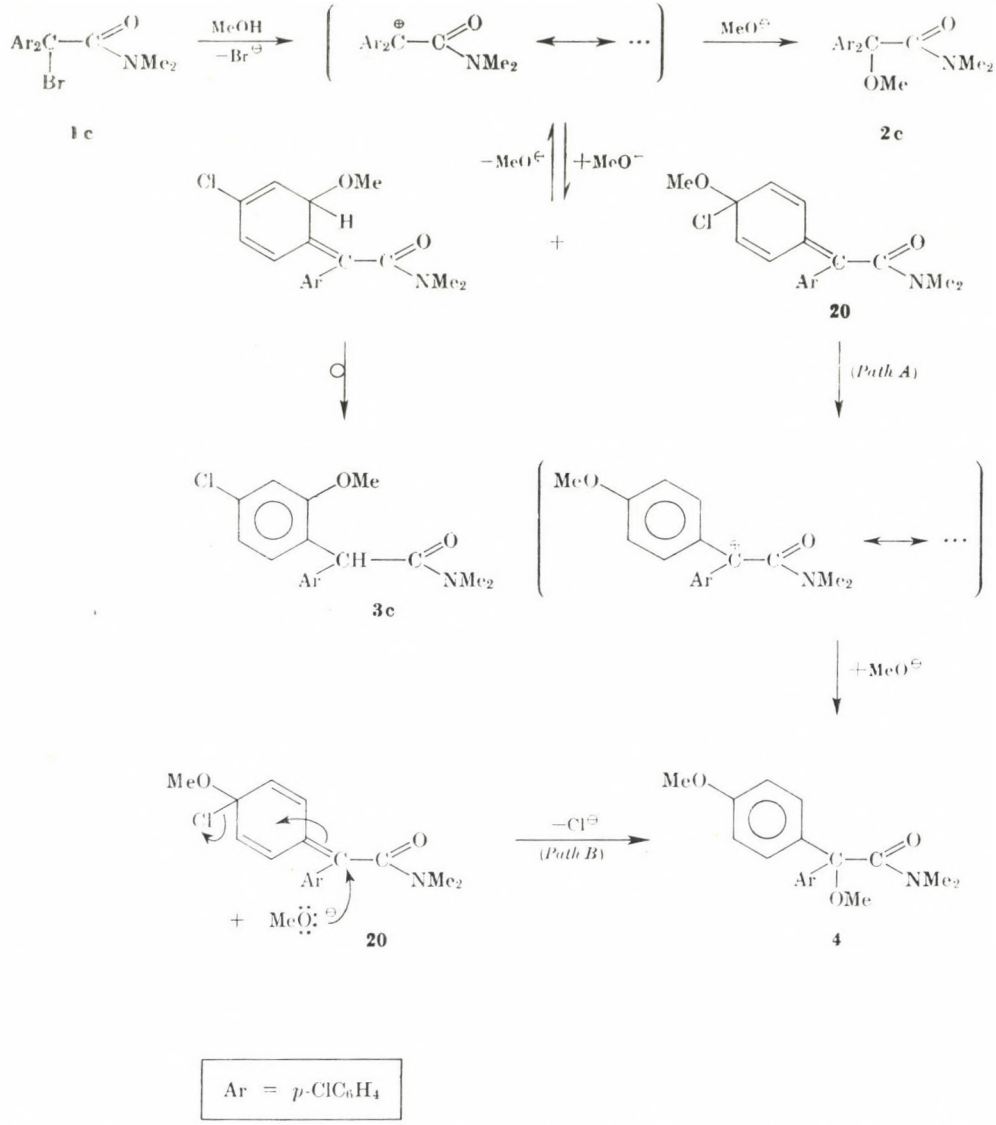

Chart 4. Mechanism of the reaction of compound **1c** with sodium methoxide in methanol

Chart 3, as well as for the analogous rearrangements of the *O*-protonated forms of compounds **18a** and **18b**, to occur.

The formation of compounds **2c** and **3c** on treatment of the di(*p*-chloro) derivative **1c** with sodium methoxide in methanol may be explained (see Chart 4) on the same lines as the formation of compounds **2a** and **3b** on similar treatment of compounds **1a** or **1b**. The formation of compound **4** from **1c** obviously

involves the intermediate **20***, related to the intermediate **18a** of Chart 3; loss of chloride and addition of methoxide, either in a stepwise (Path A) or in a concerted manner (Path B) then leads to **4**.

Thermolysis of compound 7 in methanol. The effect of added sodium methoxide and hydrogen chloride

In order to study the effect of the acidity and basicity of the medium on the reaction of the radical **12** with methanol, the azo compound **7** was furthermore thermolyzed both in pure methanol and in methanolic hydrogen chloride solution.

The results are shown in Table I.

Table I

Thermolyses of compound 7 in methanol

Added substances	Products and yields, %							
	2a	**2b**	**3a+3b**	**5**	**8**	**9**	**10**	**14**
NaOMe	—	—	—	74	2		—	1.4
NaOMe + $PhNO_2$	—	—	—	74	1	<1	—	traces
—				24—27	traces	2	12—16	
HCl	4—9	31—26	—	22			2—0	14—17

In the thermolyses carried out in pure methanol the only possibility for the formation of compound **5** is hydrogen abstraction by the radicals **12** from the solvent (Equation I); the resulting hydroxymethyl radical should then lead by recombination with another radical **12** to compound **10** (Equation II), the second main product isolated under these conditions.

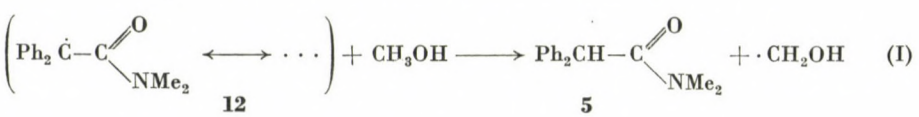

(I)

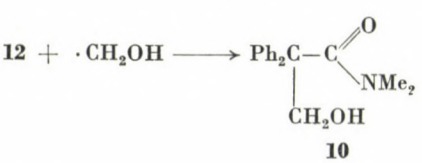

(II)

(III)

* In a separate experiment the formation of **4** has been shown not to involve **2c** as an intermediate; *i.e.* both the S_N and the $S_{RN}1$ reactions at aromatic carbon are ruled out as the mechanism of formation of **4**.

$$\cdot CH_2\ddot{O}:^{\ominus} + CH_3OH \rightleftharpoons \cdot CH_2OH + CH_3\ddot{O}:^{\ominus} \qquad \text{(IV)}$$

$$\mathbf{12} + CH_3\ddot{O}:^{\ominus} \longrightarrow \left(Ph_2\ddot{C}^{\ominus}-C(=O)-NMe_2 \longleftrightarrow \cdots \right) + CH_3\ddot{O}\cdot \qquad \text{(V)}$$

$$\mathbf{21} \xrightarrow{+\,H^{\oplus}} \mathbf{5}$$

In the thermolyses carried out in the presence of sodium methoxide Equation I is not a likely pathway for the formation of compound **5**, since under these conditions compound **10** was not formed as a by-product. Instead, two other possibilites have to be envisaged for the formation of **5** in the presence of methoxide: hydrogen abstraction from methoxide by the radicals **12** (Equation III) and one-electron reduction of the radicals by methoxide followed by protonation of the resulting anions **21** (Equation V). The formaldehyde radical--anions generated according to Equation III are known [7] to react reversibly with methanol according to Equation IV; although the equilibrium is shifted to the left, hydroxymethyl radicals would be present in the reaction mixture and again should lead to the formation of compound **10**. This leaves Equation V as the only possibility for the formation of compound **5** in the presence of methoxide*,**.

Process V is an abundant source of methoxy radicals which, in principle, could react with unchanged radicals **12** to furnish either of the methoxy compounds **2a**, **3a** and **3b**. That none of these products could be detected in the thermolysis mixtures proves that the non-cage version of step (7) of Chart 2 must be rather inefficient.

Compounds **8** and **9** are clearly the isomeric recombination products of two unlike radicals **12** and Ph·, while **14** is formed by recombination of two like radicals **12** or, in the thermolyses carried out in the presence of hydrogen chloride, possibly by recombination of two protonated radicals **12**, *i.e.* two radical--cations **22**, or of a radical **12** and a radical-cation **22**, followed by prototropy and loss of the appropriate number of protons. Since the prototropy step may be assumed to require the presence of an acid or base catalyst, it is not surprising that no dimer **14** was obtained in the thermolysis carried out in pure methanol.

In the thermolysis experiments carried out in the presence of hydrogen chloride the yields of compound **10** were much too low to permit the assumption

* The mechanism of formation of compound **5** in the thermolyses carried out in the presence of hydrogen chloride will be discussed below.

** Although the same radicals **12** are the intermediates of the reaction of **1b** with methoxide in DMP (see Chart 1), considerable less (40%) of **5** and more (30%) of the dimer **14** are obtained under comparable conditions in the latter reaction [2] than in the thermolysis. This may indicate that process V is less efficient in DMP than in MeOH.

that the entire amount of compound **5** is formed by the hydrogen abstraction mechanism (Equation I). A considerable amount of compound **5** is probably formed *via* disproportionation of the radical cations **22*** as shown in Equations VI and VII. The disproportionation mechanism explains at the same time also the formation of compound **2a** (Equations VI and VIII) which, as shown by a separate experiment, is partly hydrolized to **2b** under the conditions of its formation in the course of the thermolysis experiment. (The water, necessary for the hydrolysis to occur, apparently comes from the metathesis MeOH + + HCl → H_2O + MeCl.) This hypothesis for the formation of compound **2b** is

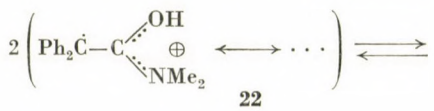

22

23 **24** (VI)

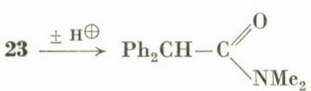

5 (VII)

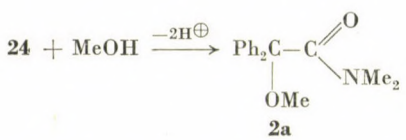

2a (VIII)

substantiated by the observation that the total amounts of the compounds **2a** and **2b** obtained in the two thermolysis experiments, carried out in the presence of hydrogen chloride, are identical.

Proofs of structure of some reaction products

The structure assignments of the methanolysis and thermolysis products are based on their IR, PMR and mass spectra and, when possible, were substantiated by comparison with authentic samples.

The structures of the components of the unseparable mixture of compounds **3a** and **3b** were proven by subjecting the mixture to acid hydrolysis to obtain mixtures of compounds **25**** (from **3a**) and **26** (from **3b**) which were

* Disproportionations of radical cations are rather common see *e.g.* Ref. [8].

** In the preliminary communication [1] the formula of this product was erroneously depicted as the corresponding dimethylamide.

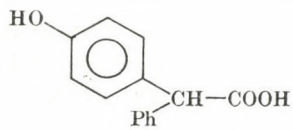

25

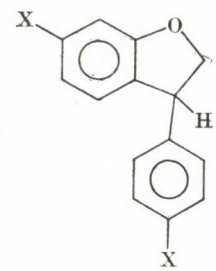

26: X = H

27: X = Cl

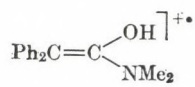

28

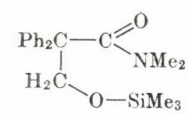

29

separated by chromatography and proved identical with authentic samples [9]. Hydrolysis of compound **3c** similarly furnished **27** which also proved identical with an authentic sample [10].

The MS of compound **10** does not exhibit a molecular ion peak; the peak of highest mass number (*m/z* 239) corresponds to a fragment formed by loss of CH_2O from $M^{+\cdot}$. Considering the further fragmentation modes of the *m/z* 239 fragment, it appears to be an isomer of the molecular ion of compound **5**. It is probably formed by McLafferty rearrangement and loss of formaldehyde from the molecular ion of **10** and appears to possess structure **28**. Trimethylsilylation of **10** by BSA (see *e.g.* [11]); furnished the *O*-trimethylsilyl derivative **29** whose MS exhibits an abundant molecular peak and whose structure follows from its MS which clearly demonstrates the frequent loss of $CONMe_2$ from the molecular ion. Proof of the structure of the trimethylsilyl derivative at the same time substantiates the structure of the parent compound **10**, derived from the IR and PMR spectra of the latter. Another abundant fragmentation mode of the molecular ion of **29** consists in the loss of formaldehyde with a McLafferty rearrangement involving migration of the trimethylsilyl group.

Experimental

IR spectra were run on a Spektromom 2000 spectrometer (Hungarian Optical Works, Budapest); mass spectra obtained at 70 eV with an AEI MS-902, equipped with a direct inlet system; the PMR spectra were recorded at 60 MHz with a Perkin—Elmer R-12 spectrometer, using TMS as internal reference. The quantitative analyses of the product mixtures obtained from the haloamides **1a** and **1b** with sodium methoxide in methanol were carried out with a JEOL PS-100 at 100 MHz, using TMS as internal reference.

Reactions of the haloamides 1a and 1b with sodium methoxide in methanol

(a) Compound **1a** [3] (1.0 g; 3.65 mmoles) was added to a solution of metallic sodium (0.34 g; 14.6 mmoles) in anhydrous methanol (10 ml) and the mixture kept, with occasional stirring, for 7 days* at room temperature. After acidification with *conc.* hydrochloric acid, the mixture was poured into water (40 ml) and extracted with three portions of dichloromethane (30 ml, each). The combined organic solutions were worked up by chromatography on a column of silica (Kieselgel 60, Merck, Korngrösse 0.063—0.200 mm; solvent: benzene with gradually added acetone to end up with a benzene-acetone 97 : 3 mixture) to yield** 32—34% of compound **2a** m.p. and *lit.* [2] m.p. 127 °C, 1—4% of compound **2b**, m.p. and *lit.* [3] m.p. 131—132 °C, and 51—53% of mixtures of the *cine* products **3a** and **3b**.

2a, IR(KBr): 1640, 760, 740, 700/690 cm^{-1}. NMR($CDCl_3$): δ 2.95 bs, 6H, NMe_2; 3.3 s, 3H, OMe; 7.05—7.45 m, 10H, Ph protons.

3a + **3b**, $C_{17}H_{19}NO_2$ (269.33). Calcd. C 75.81; H 7.11; N 5.20. Found C 76.08; H 7.28; N 5.36%. IR(KBr): 1640, 800, 740, 695 cm^{-1}. NMR($CDCl_3$): δ 3.00 s, 6H, NMe_2; 3.75 s with sh at 3.78, 3H, OMe; 5.17 s, 1H, $\rangle$C—H; 6.8—7.4 m, 9H, ArH's.

(b) By allowing compound **1b** [2] (1.0 g; 3.14 mmoles) to react with freshly prepared anhydrous methanolic (10 ml) sodium methoxide (12.6 mmoles) for 5 days* at room temperature and work-up of the resulting mixture as described above, 33—38% of compound **2a**, 0.5—3% of compound **2b** and 43—48% of mixtures of compounds **3a** and **3b** were obtained.

Proof of structure of compounds 3a and 3b

(*a*) The mixture of compounds **3a** and **3b**, obtained from compound **1a** (455 mg; 1.7 mmoles) as described above, was refluxed for 8 h with a mixture of acetic acid and *conc.* hydrobromic acid (5.7 ml, each) and evaporated to dryness in vacuum. The residue was taken up in water, the mixture extracted with ether, and the ethereal solution worked up by chromatography on a column of silica (specification as above; solvent: benzene with gradually added methanol to end up with a benzene-methanol 7 : 3 mixture) to obtain 202 mg (52%) of compound **25**, m.p. (from toluene) and *lit.* [8b] m.p. 173 °C, from **3a**, and 22.5 mg (6%) of compound **26**, m.p. and *lit.* [8a] 113—114 °C, from **3b**.

25, IR(KBr): 3500—2800, 1720, 820, 700 cm^{-1}, identical with the spectrum of an authentic sample [8b].

26, IR(KBr): 1810, 760, 730, 700 with sh at 710 cm^{-1}, identical with the spectrum of an authentic sample [8a].

(*b*) The mixture of compounds **3a** and **3b**, obtained from compound **1b** (240 mg; 0.9 mmole) was treated with a mixture of acetic acid and *conc.* hydrobromic acid (3 ml, each) and worked up as described above to obtain 115 mg (56%) of compound **25**, m.p. 113—114 °C (from toluene), and 9.3 mg (5%) of compound **26**, m.p. 173 °C.

Determination of the ratio of the products 2a, 2b, 3a and 3b

Mixtures of the haloamides **1a** or **1b** (0.5 g), sodium methoxide and anhydrous methanol (molar ratio 1 : 4 : 100) were stirred for 7 and 5 days, respectively, at room temperature, acidified with *conc.* hydrochloric acid and poured into water (20 ml). The resulting mixtures were extracted with three portions of chloroform (30 ml, each), the chloroform solutions dried ($MgSO_4$) and evaporated to dryness. The residues were dissolved in tetrachloromethane and the proportion of the normal (**2a**) and the sum of the two *cine* products (**3a** + **3b**) was calculated by the formula

$$\% \text{ of methoxy compound} = 200\ [MeO]\ \Sigma\ [Me_2N]$$

where [MeO] and Σ[Me_2N] are the intensities of the appropriate methoxy signal (or signals) and of the total Me_2N signal, respectively, in the PMR spectrum of the mixtures. The chemical shift difference of the methoxy signals of the two *cine* products was so small that the signal

* Recent observations indicate that much shorter reaction times would have been sufficient.

** Results of three identical runs.

areas could not be accurately integrated separately. The ratio **3b** : **3a** was therefore determined by comparing the peak-heights of the methoxy signals. (This was permissible since the half-widths of the two methoxy signals were identical.) In case the total amount of the methoxy compounds **2a**, **3a** and **3b** was found to be considerable lower than 100%, the difference was attributed to the presence of the hydrolysis product **2b**.

The assignment of the individual signals to the three methoxy isomers was carried out on the basis of a comparison with the PMR spectra of authentic samples of compounds **2a** and **2b**, and on the basis of the hydrolysis experiments described above, according to which the proportion of the *p*-isomer **3a** in the mixtures was much higher than that of the *o*-isomer **3b**. The result of this assignment is in agreement with the expected downfield shift (0.42 ppm) (caused by the *o*-methoxy group) of the $\rangle C-H$ signal of **3b** relative to the corresponding signal of **3a**.

PMR spectra (CCl_4):

2a : δ 2.88 s, 3H and 2.98 s, 3H, NMe_2; 3.30 s, 3H, OMe; 7.0—7.3 m, 6H, and 7.53—7.45 m, 4H, ArH's;

2b : δ 2.85 bs, 6H, NMe_2; 5.57 s, 1H, OH; 7.25 s, 10H, ArH's;

3a : δ 3.75 s, OMe; 5.01 s, $\rangle C-H$;

3b : δ 3.81 s, OMe; 5.43 s, $\rangle C-H$;

3a + **3b** : δ 2.97 s, and 2.99 s, NMe_2; 6.71 d and 7.04 d (AA'BB') and 7.1—7.2 m, intensity ratio 2 : 2 : 5, ArH's.

Product analyses gave the results shown in Table II.

Table II

Starting compound	Relative amounts of products			Product ratio
	2a	**2b**	**3a + 3b**	**3b : 3b**
	41%	~0	59%	8 : 92
1a	41.5%	<1%	57.2%	9 : 91
	47.5%	~0	53.5%	8 : 92
	42.3%	<1%	56.7%	8 : 92
	65%	~0	35%	8 : 92
1b	50%	~0	50%	8 : 92
	65%	~0	35.5%	8 : 92
	74%	3%	23%	8 :92

2-Bromo-2,2-di(*p*-chlorophenyl)-*N*,*N*-dimethylacetamide (1c)

Di(*p*-chlorophenyl)acetic acid (20 g; 71 mmoles) was refluxed for 1 h with thionyl chloride (80 ml) and the excess reagent distilled off. Bromine (5 ml; 90 mmoles) was added to the resulting oil, the flask was equipped with an efficient reflux condenser and the mixture heated for 4 h at 130 °C. The oily product was dissolved in dry dichloromethane (100 ml); an ethereal dimethyl amine solution was added by drops with ice-water cooling until the mixture was permanently alkaline. The solution was washed with water, 5% aqueous $NaHCO_3$ solution and water, dried ($MgSO_4$) and evaporated to dryness. When triturated with ether, the residue turned into 11.2 g (41%) of the crystalline title compound, m.p. 118—119 °C (from gasoline).

$C_{26}H_{14}BrCl_2NO$ (387.10). Calcd. total halogen, expressed as Cl 27.48; N 3.62. Found: total halogen, expressed as Cl 27.43; N 3.45%.

IR(KBr): 1650 cm^{-1}.

Reaction of the haloamide 1c with sodium methoxide in methanol

Mixtures of compound **1c**, sodium methoxide and methanol were refluxed for several hours (for the composition of the starting mixtures and the reaction times, see Table III) and evaporated to dryness. When triturated with water, the oily residues turned into mixtures of crystalline products which were worked up by column chromatography as described for the analogous reaction of compound **1a**. The inhomogeneous fractions were worked up by preparative TLC (Kieselgel $PF_{254+366}$; solvent: benzene-acetone, 9 : 1) to obtain the following products in the yields shown in Table III.

Compound **2c**, m.p. 136—137 °C, identical with an authentic sample (see below); compound **3c**, m.p. 183—184 °C (from $CHCl_3$ — light petroleum; or methanol); $C_{17}H_{17}Cl_2NO_2$ (338.23). Calcd. Cl 20.94; N 4.14. Found Cl 20.78; N 3.96%;
IR(KBr): 1630, 890, 850, 790 cm^{-1};

PMR($CDCl_3$): δ 2.97 s, 6H, NMe_2; 3.77 s, 3H, OMe; 5.45 s, 1H, $\rangle$CH; 6.7—7.25 m, 7H, ArH's;

MS (150 °C); *m/z* (relative intensity): 339 (4.7%, i); 337 (7.1%, $M^{+\cdot}$); 267 (32%, i); 265 (47%, M — $CONMe_2$); 217 (1.5%, i); 215 (3.8%, 265 — [^{35}Cl + Me]); 165 (7.1%), 152 (7.1%); 127 (19%, i); 125 (61%, $C_6H_2ClO^+$); 72 (100%, $CONMe_2$);

Table III

Reaction of **1c** *with methoxide/methanol*

Reagents					Reaction time	Products and yields					
1c		sodium		MeOH		2c		3c		4c	
g	mmoles	g	mmoles	ml		g	%	g	%	g	%
2.0	5.2	0.40	17.4	20	1 h	0.90	51	0.22	12	0.12	7
5.0	12.9	1.19	51.6	50	4 h	2.17	50	0.66	15	0.46	11
5.0	12.9	1.19	51.6	50	4 h	2.54	58	0.64	15	0.14	3

compound **4**, m.p. 101—102 °C (from aqueous EtOH);
$C_{18}H_{20}ClNO_3$ (331.81). Calcd. C 64.76; H 6.04; N 4.19. Found C 64.46; H 5.84; N 3.92%;
IR(KBr): 1645, 815, sh at 830 cm^{-1};
PMR($CDCl_3$): δ 2.95 bs, 6H, NMe_2; 3.28 s, 3H, aliphatic MeO; 3.72 s, 3H, aromatic MeO; 6.75 d, J = 10 Hz, 2H, high field d of $MeOC_6H_4$ group; 7.1—7.5 m, 6H, other ArH's;
MS (150 °C); *m/z* (relative intensity): 263 (36%, i); 261 (100%, M — $CONMe_2$); 141 (8%, i); 139 (27%, ClC_6H_4CO); 135 (29%, $MeOC_6H_4CO$); 113 (2.8%, i); 111 (8.4%, ClC_6H_4); 72 (11%, $CONMe_2$).

Proof of structure of compound 3c

A mixture of compound **3c** (0.27 g; 0.8 mmole), acetic acid and conc. hydrobromic acid (3 ml, each) was refluxed for 6 h, evaporated to dryness in vacuum and the residue worked up by chromatography on a column of silica (specification as above; solvent: benzene-cyclohexane 1 : 4 with gradually increased proportions of benzene, to end up with a 1 : 1 solvent mixture) to obtain 0.12 g (54%) of compound **27**, m.p. 121—122 °C (from EtOH), *lit.* [10] m.p. 119—121 °C, identical (mixed m.p., IR) with an authentic sample obtained according to Ref. [10].

IR(KBr): 1810, 845, 790 with sh at 800 cm^{-1}.

Methanolysis of the haloamides 1a-c in methanol

(a) Methanolysis of compound **1b** to give compound **2a** has been described in Ref. [2]. Methanolysis of compound **1a** was carried out similarly and furnished product **2a** in practically the same yield.

(b) Compound **1c** (0.4 g; 1 mmole) was refluxed for 2 h with anhydrous methanol (4 ml) to obtain 0.26 g (73%) of compound **2c** in crystalline form, m.p. 136—137 °C (from MeOH).

$C_{17}H_{17}Cl_2NO_2$ (338.23). Calcd. C 60.36; H 5.07; N 4.14. Found C 60.12; H 5.19; N 3.87%.

IR(KBr): 1640, 800 cm^{-1}.

PMR($CDCl_3$): δ 2.9 bs + 3.0 bs, total 6H, NMe_2; 3.3 s, 3H, OMe; 7.20 + 7.42, AA'BB', J = 9 Hz, 8H, ArH's.

MS (150 °C); *m/z* (relative intensity): 267 (69%, i); 265 (100%, M — $CONMe_2$); 141 (15%, i); 139 (45%, ClC_6H_4CO); 113 (5.4%, i); 111 (17%, ClC_6H_4); 72 (11%, $CONMe_2$).

N,N-Dimethyl-2,2-diphenyl-2-(2-phenylhydrazino)-acetamide (6)

A mixture of compound **1a** (26.7 g; 98 mmoles), phenylhydrazine (19.2 ml; 196 mmoles) and dry ether (270 ml) was stirred at room temperature for a total of 24 h, the stirring being interrupted overnight twice. The crystalline product was collected, and the filtrate evaporated to dryness in vacuum to obtain an oily product which was triturated with ethanol (100 ml). The ethanolic mixture was kept in a refrigerator to obtain a second crop of crystals. The combined crystalline product was taken up in 5% aqueous $NaHCO_3$ solution (200 ml), the mixture heated to its b.p. and rapidly cooled to room temperature. The resulting product was recrystallized from ethanol to yield 7.7 g (23%)* of the title compound, m.p. 145—146 °C (dec.).

$C_{22}H_{23}N_3O$ (345.42). Calcd. C 76.49; H 6.71; N 12.17%. Found: C 76.29; H 6.58; N 12.25%.

NMR($CDCl_3$): δ 2.4 bs and 3.1 bs, 3H each, NMe_2; 4.9 bs and 6.35 bs, exchangeable, NH's; 6.45—7.7 m, 15H, Ph's.

MS (150 °C); *m/z* (relative intensity): 345 (2%, $M^{+\cdot}$); 273 (12.4%, M — $CONMe_2$); 239 (100%, M — PhNHNH + H); 167 (9.6%, Ph_2CH); 166 (6.4%); 165 (9.6%, $C_{13}H_9^+$); 91 (30%); 77 (9.2%); 72 (10.8%, $CONMe_2$).

N,N-Dimethyl-2,2-diphenyl-2-phenylazoacetamide (7)

A solution of compound **6** (5.0 g; 14.5 mmoles) in dichloromethane (50 ml) was covered with 10% aqueous Na_2CO_3 solution (50 ml). Iodine (3.7 g; 14.5 mmoles) was added in portions within about 0.5 h to the vigorously stirred solution. After addition of the last portion, the iodine colour of the reaction mixture remained persistent. The mixture was decolorized by adding a few of drops of aqueous $NaHSO_3$ solution, the dichloromethane layer separated, washed with three portions of water (50 ml each) and evaporated to dryness in vacuum at room temperature to obtain 4.75 g (95%) of the practically pure title compound m.p. 131—132 °C (dec.) which did not change after recrystallization from ethanol.

$C_{22}H_{21}N_3O$ (343.41). Calcd. N 12.24. Found: N 12.00%.

IR(KBr): *no* NH bands.

PMR($CDCl_3$): δ 2.25 bs and 3.0 bs, 6H, NMe_2; 7.2—7.6 m, 13H, and 7.75—8.0 m, 2H, Ph's.

Since recrystallization from ethanol caused considerable losses, the crude product, which proved homogeneous according to TLC, IR and PMR, was used without further purification.

Thermolyses of the azo compound 7 in methanol

(*a*) Compound **7** (2.0 g; 5.8 mmoles) was added to an anhydrous methanolic (15 ml) solution of sodium (0.54 g; 23.3 mmoles) and the mixture was refluxed for 5 h during which time the starting suspension turned into a clear solution. The mixture was acidified with *conc.* hydrochloric acid, evaporated to dryness, the residue triturated with water (40 ml) and extracted with dichloromethane (three portions, 30 ml each). The dichloromethane solution was dried ($MgSO_4$), evaporated to dryness and the residue worked up by chromatography on

* One of the co-products of this reaction was compound **5**. Structure elucidation of the other coproducts is in progress.

a column of silica (specification, see above; solvent: benzene with gradually added acetone to end with benzene-acetone, 7 : 3); the non-homogeneous fractions were subsequently worked up by preparative TLC. The following products were isolated: 1.03 g (74%) of compound **5**, identical (IR spectrum [2], m.p. and mixed m.p.) with an authentic sample obtained according to Ref. [12]; 23 mg (1.4%) of compound **14**, identical (TLC, IR spectrum) with an authentic sample [2]; and 37 mg (2%) of compound **8**, m.p. 136—137 °C (crude product).

IR(KBr): 1635, 1490, 1400, 1130, 760, 740, 700 cm^{-1}.

PMR(CCl_4): δ 3.08 s, and 3.09 s, total 6H, NMe_2; 5.12 s, 1H, $\rangle C-H$; 7.05—7.38 m, 10H, and 7.38—7.55 m, 4H, ArH's.

MS (150 °C); *m/z* (relative itensity): 315 (13%, $M^{+\cdot}$); 243 (100%, M $\pm$ $CONMe_2$); 241 (5%, 243 — H_2); 239 (3.2%); 228 (3.5%, 243 $\pm$ Me); 165 (8%, 243 8); 115 (2.2%); 91 (3.5%); 72 (32%, $CONMe_2{}^{+}$).

Not even traces of compounds **2a**, **3a**, **3b** and **10** could be detected by TLC in the product.

(*b*) When the above reaction was carried out in the presence of an equimolar amount of nitrobenzene (based on the amount of compound **7**), the following products were obtained: 1.03 g (74%) of compound **5**, 15 mg (≈1%) of compound **8**, 12 mg (<1%) of compound **9**, identical (TLC, IR) with an authentic sample [2], and traces of compound **14**.

(*c*) Compound **7** (2.0 g; 5.8 mmoles) was refluxed for 7 h with anhydrous methanol (a clear solution formed after about 2 h) and evaporated to dryness. The residue was taken up in benzene (5 ml), the insoluble material (55 mg) filtered off and the filtrate worked up by column chromatography followed, if necessary, by preparative TLC as described under *(a)* to obtain the following products: 0.37 g (26.6%) of compound **5**, identical (IR spectrum, m.p. and mixed m.p.) with an authentic sample obtained according to Ref. [12]; 0.26 g (16.5%) of compound **10**, m.p. 161—162 °C (from gasoline); 0.04 g (2%) of compound **9**, identical (TLC, IR) with an authentic sample [?], and traces of compound **8**.

Compound **10**, $C_{17}H_{19}NO_2$ (269.33). Calcd. N 5.20. Found: N 5.07%.

IR(KBr): 3400, 1600, 1490, 1370, 1050, 1000, 750, 690 cm^{-1}.

PMR($CDCl_3$): δ 2.4 bs and 3.0 bs, total 6H, NMe_2; 4.15 s, 2H, CH_2; 7.35 s, 10H, Ph's.

MS (150 °C); *m/z* (relative intensity): 239 (100%, M—CH_2O); 210 (4.2%); 194 (6.3%); 167 (16%, 239—$CONMe_2$); 166 (13%); 165 (21%); 105 (11%); 91 (50%); 72 (26%, $CONMe_2{}^{+}$).

MS, after trimethylsilylation (120 °C): 341 (63%, $M^{+\cdot}$); 326 (32%, M —Me); 311 (100%, M $\pm$ 30); 296 (16%, 311 $\pm$ 15); 269 (16%, M — 72); 251 (33%); 238 (3.6%, M — Me_3SiOCH_2); 220 (10%, 311 $\pm$ 91); 210 (14%); 207 (34%); 194 (6.6%); 179 (14%, Ph_2C_2H); 178 (17%); 177 (14%); 167 (8.4%, Ph_2CH); 166 (7.9%); 165 (22%); 148 (10%, 296^{2+}); 140.5 (4.5%, 281^{2+}); 103 (26%, $Me_3SiOCH_2{}^{+}$); 73 (140%, Me_3Si); 72 (31%, $CONMe_2{}^{+}$).

In another, otherwise identical experiment the reaction mixture was refluxed for only 4 h. The following compounds were obtained: 40 mg of the benzene-insoluble substance of unknown structure, 0.34 g (24.5%) of compound **5** and 0.18 g (11.5%) of compound **10**.

In both runs several further minor products of unknown structures, with R_f values lower than that of the dimer **14**, were also obtained.

(*d*) Compound **7** (2.0 g; 5.8 mmoles) was refluxed (1) for 5, (2) for 3 h with methanol (20 ml) previously saturated at room temperature with dry HCl (two runs). The resulting mixtures were worked up as described under (*c*) to obtain the following products:

(1): 0.06 g (4%) of compound **2a**, identical (TLC, IR) with an authentic sample [3]; 0.46 g (31%) of compound **2b**, m.p. and *lit.* [3] m.p. 131—132 °C, identical (TLC, IR) with an authentic sample [3]; 0.31 g (22%) of compound **5** contaminated, according to its PMR spectrum, with traces of a substance of unknown structure; 0.04 g (≈2%) of compound **10**; and 0.19 g (14%) of compound **14**, identical (IR, PMR) with an authentic sample [2].

(2): 0.14 g (9%) of compound **2a**; 0.39 g (26%) of compound **2b**; 0.31 g (22%) of compound **5** contaminated, according to its PMR spectrum with traces of a substance of unknown structure; and 0.23 g (17%) of compound **14**.

Hydrolysis of compound 2a by refluxing in methanolic hydrogen chloride

Compound **2a** was refluxed with anhydrous methanol which had been saturated with dry HCl at room temperature; the reaction was followed by TLC. A considerable portion of **2a** was gradually converted into **2b**.

Reaction of compound 6 with sodium methoxide/methanol

A mixture of compound **6** (0.5 g; 1.45 mmoles), sodium methoxide (0.94 g; 5.8 mmoles) and anhydrous methanol (5 ml) was refluxed for 8 h. The mixture was allowed to cool, acidified with *conc.* hydrochloric acid and poured into water (30 ml) to obtain a crystalline product (0.28 g) which, according to its IR spectrum, proved to be a mixture of compound **5** and the corresponding methyl ester. The crude product was stirred for 1 h with a mixture of 1*N* NaOH (6 ml) and ethanol (3 ml) at room temperature ot obtain 0.12 g (35 %) of compound **5**, m.p. 135—136 °C, identical (IR, mixed m.p.) with an authentic sample, as the insoluble product. The filtrate was acidified with *conc.* hydrochloric acid to obtain 0.10 g (33%) of 2,2-diphenylacetic acid, m.p. 144—145 °C, identical with an authentic sample.

Phenylhydrazine could not be detected (in the form of its *N*-benzylidene derivative) in the filtrate of the original crude mixture of the amide **5** and the corresponding methyl ester, nor in a mixture of phenylhydrazine (1.45 mmoles), sodium methoxide (5.8 mmoles) and anhydrous methanol (8 ml) after being refluxed for 8 h.

*

The authors are indebted to Mrs. I. BALOGH-BATTA and staff for the microanalyses, to Dr. P. KOLONITS and staff for part the PMR spectra and Dr. K. KISS-ERŐS and staff for the IR spectra.

REFERENCES

[1] SIMIG, GY., LEMPERT, K., TAMÁS, J., SZEPESY, P.: Tetrahedron Letters **1977,** 1151
[2] SIMIG, GY., LEMPERT, K., VÁLI, ZS., TÓTH, G., TAMÁS, J.: Tetrahedron **34,** 2371 (1978)
[3] SIMIG, GY., LEMPERT, K.: Tetrahedron **31,** 983, (1975)
[4] a. BUNNETT, J.: J. Chem. Educ. **51,** 312 (1974)
b. KORBNUM, N.: Angew. Chem. **87,** 797 (1975)
c. ZOLTEVICZ, J. A., in "Topics in Current Chem.", Vol. **59** (Ed. F. L. Boschke), p. 53, Springer Verlag, Berlin, Heidelberg, New York, 1975
d. RUSSEL, G. A., NORRIS, R. K. in "Organic Reactive Intermediates" (Ed. S. P. McManus), p. 437. Academic Press, New York, London, 1973
[5] SIMIG, GY., LEMPERT, K., TAMÁS, J., MIKLÓS, P.: Tetrahedron Letters **1975,** 93
[6] KORNBLUM, N., EARL, G. W., HOLY, N. L., MANTHEY, J. W., MUSSER, M. T., SNOW, D. H., SWIGER, R. T.: J. Am. Chem. Soc. **90,** 6221 (1968)
[7] BUNNETT, J. F., WAMSER, C. C.: J. Am. Chem. Soc., **89,** 6712 (1967)
[8] MICHAELIS, L., SCHUBERT, M. P.: Chem. Revs. **22,** 437 (1938); ANSCHÜTZ, L., BROEKER, K., OTHNEISER, A.: Ber. **77,** 443 (1944); RUSSEL, G. A. *et al.:* J. Am. Chem. Soc. **84,** 4155 (1962)
[9] BISTRZYCKI, A., FLATAU, J.: *a)* Ber. **28,** 989 (1895); b) Ber. **30,** 124 (1897)
[10] REIF, V. D., SINSHEIMER, J. E., WARD, J. C., SCHTEINGAST, D. E.: J. Pharm. Sci. **1974,** 1734
[11] DRAFFAN, G. H., STILLWELL, R. N., MCCLOSKEY, J. A.: Org. Mass Spectrom. **1,** 669 (1968)
[12] GOKHALE, V. G., PHALNIKAR, N. L., BHIDE, B. V.: J. Univ. Bombay, **16,** 32 (1948); Chem. Abstr., **43,** 1144d (1949)

Dr. Gyula SIMIG
Dr. Károly LEMPERT
Dr. Gábor TÓTH
H-1111 Budapest, Gellért tér 4.

Dr. József TAMÁS
H-1025 Budapest, Pusztaszeri út 59—67.

Acta Chimica Academiae Scientiarum Hungaricae, Tomuë 100 (1—4), pp. 163—177 (1979)

PHOTOCATALYTIC METHODS, I

IRON(III)-CATALYZED PHOTO-OXIDATION OF ERIOGLAUCIN-A

A. PÉTER and L. J. CSÁNYI*

(Reaction Kinetics Research Group of the Hungarian Academy of Sciences, Department of Inorganic and Analytical Chemistry, József Attila University, Szeged)

Received June 30, 1978

Accepted for publication July 17, 1978

It was found that the fairly photo-resistent dye, Erioglaucin-A undergoes a considerable decolourisation when irradiated by photons of $\lambda < 360$ nm in the presence of iron(III). It was disclosed that the fading is caused by OH radicals formed during the excitation of hydrolized iron(III) species [especially $Fe(OH)^{2+}$. aq]. The fading has a maximum at pH 2.7 and increases with the increase of iron(III) and dye concentrations. The decolourisation occur both in the presence and in the absence of dissolved oxygen. When oxygen was removed *ca.* 12 moles of OH radicals were consumed per dye molecule and equivalent of ferrous iron was formed. In the presence of oxygen, however, about 8.5 times more dye was decolourised on the expense of O_2 without any formation of ferrous iron.

The fading of the dye is inhibited by halide (but chloride is ineffective) and pseudo-halide, copper(II), nitrite and arsenite ions.

A method based on photocatalytic effect of iron(III) is recommended for the selective estimation of iron on micro scale in the presence of other transition metals.

An increasing number of authors are nowadays paying more and more attention to the utilization of photochemical reactions in chemical analysis. Reviews have already appeared on the results to date [1—3]. Of the procedures based on photochemical reactions, the photocatalytic method appears to offer the greatest promise.

Photocatalysis has so far been employed in two ways in chemical analysis. It was observed by ALMÁSSY and KOVÁCS [4] that certain reactions which take place slowly in the dark can be accelerated if the reaction mixture is illuminated in the presence of a photon-transmitting substance. For example, solutions containing chromate can be titrated with a methyl orange reagent solution if iron(III) oxalate, as sensitizer, is added to the chromate to be determined, and the mixture is illuminated with a tungsten lamp. This method has also been used for the indirect determination of iron(II) and hydrogen peroxide *via* chromate [5].

Another possibility for the application of photocatalysis was pointed out by HARLAMOV *et al.* [6], who drew conclusions on the quantity of the catalyst from the extent of photo-oxidation of methyl orange catalyzed by iron(III). The photo-oxidation was followed by measurement of the concentra-

tion of the dye *via* the absorption band at 510 nm, and was found to occur to the greatest extent at pH 1.9—2.1; the alkaline form of the dye (at around pH 4) was considered photoresistent.

We have carried out work with the aim of acquiring a more thorough understanding of the nature of the photocatalysis and the optimum experimental conditions for determination of iron(III), and in the present paper an account is given of the catalyzed photo-oxidation of Erioglaucin-A. The reason why this dye was chosen was that, in the absence of a photocatalyst, it is more photoresistent than methyl orange. In addition, Erioglaucin-A has a higher molar absorptivity than methyl orange, and accordingly it appeared possible by this means to attain a higher sensitivity in the determination of iron(III).

Experimental

Chemicals used. The compounds employed in the measurements were of *p.a.* purity. Triply-distilled water was used to prepare the solutions. Water distilled in the usual manner was first redistilled from alkaline permanganate, then boiled with 2—4 g potassium peroxydisulphate for 15—30 min and again redistilled.

Irradiation apparatus. In the apparatus used for irradiation (Fig. 1), the Osram HBO 500 high-pressure mercury vapour lamp (1) was surrounded by a double-walled metal jacket (2). The quartz lens (3) was incorporated into the outer jacket. Behind this were the colour filters (4) and the metal screens serving to reduce the light intensity (5). Irradiation was performed in a normal 1-cm quartz cell (6) placed into a thermostatable cell-holder. A carefully thermostated VTH8 thermo-column (7) served to check the photo-emission of the lamp. The photo-emission was regulated by means of a voltage supply unit.

Measurements. Solutions of the appropriate composition were pre-thermostated at 25° for 20—30 min, and in the meantime were saturated with pure O_2 gas that had been bubbled through a water-filled washing system. Following this, solution was transferred to the cell and irradiated for a suitable period, in general for 10 min. After irradiation, the change in light absorption compared to the initial solution was determined.

The pH values of the solutions were measured by means of a Radiometer PHM 52 pH-meter with a combined glass/calomel electrode. Spectrophotometric measurements were made on Beckman DBG and B instruments. In the recording of the difference spectra, solution of appropriate composition and pH so that they had a concentration corresponding to that of the irradiated sample, and the spectrum of the irradiated solution was then recorded against this solution.

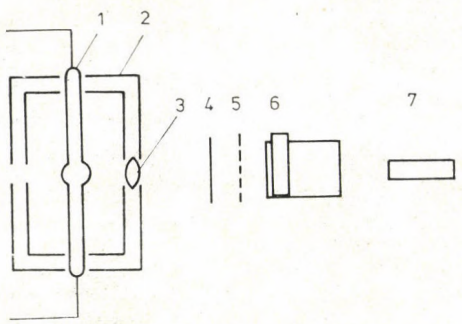

Fig. 1. Outline of apparatus used for the irradiation

Results

Erioglaucin-A (*N,N*-diethyl-di-*p*-sulphobenzyl-*p*-amino-*o*-sulphofuchsonimonium sulphate) is a dye generally available commercially in reduced form. Its pure aqueous solution is completely resistant to irradiation for 10 min. with UV light if O_2 was expelled with pure nitrogen. In the presence of oxygen a bleaching of *cca.* 2% of the initial dye concentration was observed at otherwise similar experimental conditions.

In the spectrum of the reduced form (Fig. 2), maxima are found at 634, 410, 305 and 260 nm, the heights of these varying with the pH in the pH interval of 1—5 (Fig. 3). Isobestic points occur at 500, 320, 280 and 240 nm. Our measurements gave a value of $(1.40 \pm 0.1) \cdot 10^{-3}$ mol · dm^{-3} for the acid dissociation constant, while for the molar absorptivities: $\varepsilon_{RH_2^+}^{634} + = 0.00$, $\varepsilon_{RH}^{634} = 79{,}000$, $\varepsilon_{RH_2^+}^{410} + = 21{,}000$ and $\varepsilon_{RH}^{410} = 8{,}500$ dm^3 · mol^{-1} · cm^{-1}.

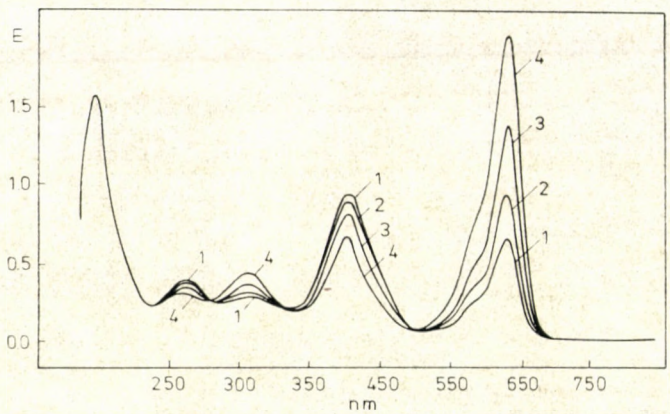

Fig. 2. Spectrum of Erioglaucin-A and its variation with the pH of the solution. (1): 4×10^{-5} *M* Erioglaucin-A, pH = 2.0; (2): 4×10^{-5} *M* Erioglaucin-A, pH = 2.2; (3): 4×10^{-5} *M* Erioglaucin-A, pH = 2.5; (4): 4×10^{-5} *M* Erioglaucin-A, pH = 2.8

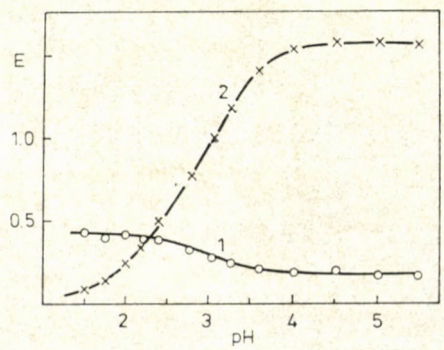

Fig. 3. Variation of absorbance of Erioglaucin-A with the pH of the solution. Dye concentration: 2×10^{-5} *M*. (1): absorbance measured at 410 nm; (2): absorbance measured at 634 nm

If the Erioglaucin-A solution is irradiated at its 410 nm band a weak fluorescence with a maximum at 480 nm is obtained both in the presence and in the absence of dissolved oxygen. The fluorescence is not influenced by the addition of iron(III) ions.

There is some optical interaction between the dye and iron(III): the peak at 634 nm is somewhat reduced, while peaks at 410 and 260 nm are increased on the effect of iron(III) at pH = 2.7. The spectrum is influenced by iron(II), too, but at 634 and 310 nm an increase while at 410 and 260 nm a decrease is caused by adding iron(II) ions at pH = 2.7.

In our experience, only light with a wavelength shorter than 360 nm causes fading in the presence of the iron(III) ion; photons with lower energies are completely ineffective.

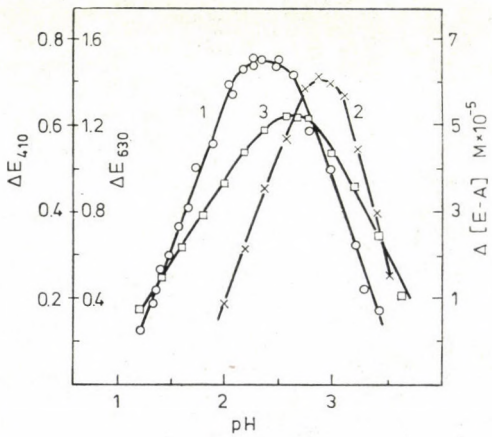

Fig. 4. pH-dependence of iron(III)-catalyzed photo-oxidation of Erioglaucin-A. 8×10^{-5} *M* Erioglaucin-A, 8.14×10^{-5} *M* $Fe(ClO_4)_3$. (1): absorbance change measured at 410 nm; (2): absorbance change measured at 634 nm; (3): molar concentration change calculated with the aid of the apparent molar absorptivity

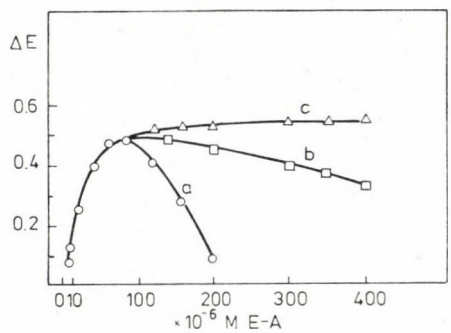

Fig. 5. Dependence of photo-oxidation of Erioglaucin-A on the dye concentration. 4.07×10^{-5} *M* $Fe(ClO_4)_3$, pH = 2.5; Values measured at layer thicknesses of 1 cm (a), 2 mm (b) and 1 mm (c), converted to 1 cm

In the presence of iron(III) ion, the photo-oxidation of Erioglaucin-A is strongly dependent on the pH. It is worth to note, however, that no change in pH can be observed during the photo-oxidation of the dye. If the absorbance is measured at 410 nm, the maximum in the ΔE *vs.* pH curve is to be found at pH 2.4, while if the change is measured at 634 nm, the decolourization maximum is obtained at pH 2.94 (Fig. 4).

If the dye concentration is varied at constant pH and iron(III) concentration, the absorbance change to be seen in Fig. 5 is obtained. Up to a dye concentration of 10^{-4} *M*, the decolourization increases almost linearly, whereas at higher dye concentrations saturation or a slight decrease of the decolourization ensue. On standing for a fairly long period, a dye solution with high concentration exhibits a slight turbidity.

On variation of the concentration of the photocatalyst, the extent of decolourization of the dye also varies. In the case of lower irradiating light intensity (3.8×10^{14} photon $\cdot$ s^{-1}), the absorbance decrease is directly proportional to the iron(III) concentration, while with a higher photon current (1.3×10^{15} photon $\cdot$ s^{-1}) a saturation curve is observed even at low catalyst concentration, and only a short section of this curve displays a linear correlation (Fig. 6, curves *a* and *b*). In the latter case, the ascending branch varies linearly with the iron(III) concentration over a larger section if oxygen is passed through the solution during irradiation.

In the course of the photo-oxidation of Erioglaucin-A, the iron(III) content of the solution does not change to a detectable extent. If the irradiation s carried out on an oxygen-free dye solution, a decolourization is observed unchangingly, but in the meantime the iron(III) also undergoes reduction.

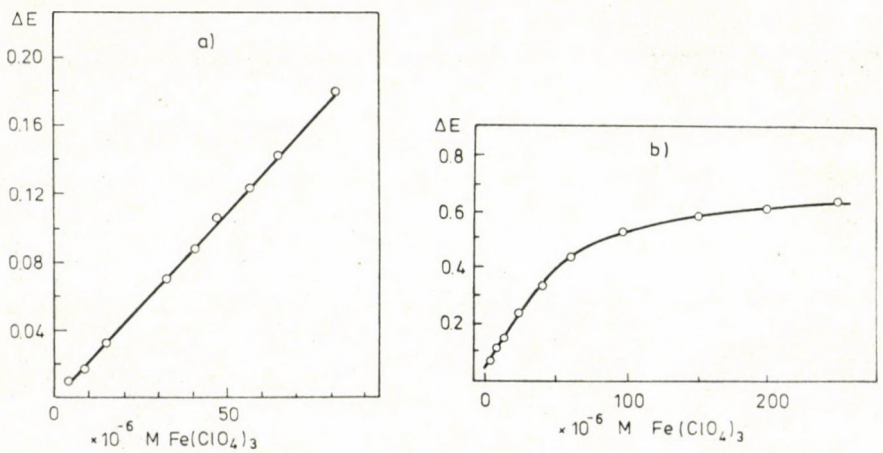

Fig. 6. Dependence of photo-oxidation of Erioglaucin-A on iron(III) concentration; *a:* $4.0 \times \times 10^{-5}$ *M* Erioglaucin-A, pH = 2.5, 3.8×10^{14} photon/s; *b:* 4.0×10^{-5} *M* Erioglaucin-A, pH = = 2.5, 1.3×10^{15} photon/s

In this case, it is found that on average 12 moles of iron(II) are formed on the decolourization of 1 mole of dye. During the photo-oxidation of dye solution saturated with oxygen, the fading is accompanied by the reduction of 3.0—3.5 moles of oxygen.

The iron(III)-catalyzed photo-oxidation of Erioglaucin-A is practically unaffected by certain oxidants, such as chlorate, bromate or nitrate (Table I). If the irradiation is performed with the exclusion of oxygen, the decolourization of the dye is completely suppressed in the presence of chlorate and bromate.

Table I

Effects of various ions on iron(III)-catalyzed photo-oxidation of Erioglaucin-A. Experimental conditions: pH = 2.50, 8.0×10^{-5} M Erioglaucin-A, 8.14×10^{-5} M $Fe(ClO_4)_3$, 1.3×10^{15} photon. s^{-1}, irradiation time 10 min.

Conc. $M\times10^5$	ΔE^{410}							
	ClO_3^-	BrO_3^-	NO_3^-	NO_2^-	CrO_4^{2-}	MoO_4^{2-}	AsO_4^{3-}	Cu^{2+}
0.0	0.75	0.75	0.75	0.75	0.75	0.75	0.75	0.74
2.0	—	—	—	—	—	—	0.73	0.72
4.0	0.82	0.69	—	0.62	0.73	0.54	—	0.74
8.0	0.72	0.69	0.74	0.50	0.59	0.58	—	—
20.0	0.77	0.72	—	—	0.54	0.23	0.68	0.73
30.0	0.80	0.67	—	—	0.48	0.11	—	—
40.0	0.75	0.71	—	0.46	0.34	0.05	0.58	—
80.0	—	—	0.75	0.35	—	—	—	—
200.0	—	—	—	0.19	—	—	—	—
400.0	0.68	0.72	0.75	0.08	0.05	—	0.10	0.67
800.0	—	—	0.77	0.05	—	—	—	—

In the case of the nitrate ion, decolourization of the dye can also be observed in the absence of iron(III); the extent of this is proportional to the concentration of the nitrate ion. In contrast with the former ions, nitrite ion definitely decreases the photo-oxidation. In the absence of iron(III), low concentrations of nitrite ion similarly promote photo-oxidation to a slight extent, but a larger quantity ($> 10^{-3}$ M) decidedly inhibits decolourization of the dye. If alkali metal chromates are added, the extent of photo-oxidation decrease in proportion to the increase of the chromate concentration. Molybdate displays a similar, but somewhat stronger inhibitory effect than that of chromate. Arsenite ion inhibits the photo-oxidation strongly, but copper(II) ion to a much lower extent.

The photo-oxidation is affected in different ways in the presence of halide and pseudohalide ions. An appreciable decrease can be observed in the presence

of fluoride, bromide, iodide or thiocyanate ions. On addition of azide ion, the photo-oxidation decreases slightly, while chloride ion, even in high amounts, does not influence the decolourization of the dye (Table II).

Table II

Photo-oxidation of Erioglaucin-A in presence of halide and pseudohalide ions. Conditions: 8.0×10^{-5} *M Erioglaucin-A,* 8.14×10^{-5} *M* $Fe(ClO_4)_3$, $pH = 2.5$, *irradiation time* **10** *min,* 1.3×10^{15} *photon.* s^{-1}

Conc. of anion $M\times10^{-5}$	ΔE^{410}					
	F^-	Cl^-	Br^-	I^-	SCN^-	N_3^-
0.0	0.75	0.75	0.75	0.75	0.75	0.75
4.0	0.62	0.74	0.56	0.50	0.54	0.72
8.0	0.39	0.72	0.47	0.37	0.42	0.71
12.0	—	0.73	0.41	0.30	0.36	0.69
20.0	0.23	0.73	0.30	0.20	0.26	0.66
40.0	0.10	0.72	0.16	0.10	0.14	0.60
80.0	0.04	0.71	0.09	0.05	0.08	0.41

In the presence of hydrogen peroxide, even when oxygen is excluded, catalyzed photo-oxidation of the dye is to be observed. In the presence of this reagent, however, a reaction occurs in the dark too, which makes evaluation uncertain.

It should be mentioned that the photo-oxidation of Erioglaucin-A was also carried out in the presence of methylene blue and fluorescein, in aqueous solution and in a 4 : 1 benzene — methanol solvent mixture. In the absence of the iron(III) catalyst, these additives did not give rise to a perceptible measure of decolourization in an oxygen-saturated dye solution of pH 2.5. In the presence of the iron(III) catalyst, the added dyes did not influence the photo-oxidation of Erioglaucin-A.

Attempts were made to establish the products of photo-oxidation, by separating them on thin-layer plates of silica gel (Merck Silica gel G) pretreated in various ways, with running mixtures of benzene and methanol in various proportions. Some of the oxidation products migrated together with the solvent front, while others scarcely moved away from the start-line.

The difference spectra recorded in the visible and UV ranges did not offer convincing evidences for identifying the products of photo-oxidation. Cyclic voltammetric curves recorded at a carbon paste electrode were similar to those obtained by GALUS and ADAMS [7] during the electro-oxidation of crystal violet and malachite green.

Discussion

According to GOLLNICK [8], two main mechanism types may be assumed for the interpretation of photochemical oxidations. Radicals and excited molecules take part in photo-oxidations of type I, and only excited molecules in those of type II. In photo-oxidations of this latter type, if the substrate (acceptor) molecule is activated, we speak of acceptor activation, while if it is the oxygen molecule that is excited, we speak of an oxygen-activation mechanism. Naturally, in both cases the acceptor or the oxygen molecule may be excited directly, but the excitation may be brought about indirectly, by the mediation of some photon-transmitting sensitizer.

Under the excitation conditions we employed ($\lambda > 250$ nm), direct oxygen activation can not be reckoned with. In principle, oxygen could be activated as a result of Erioglaucin-A acting as an energy-transmitter, for this dye shows luminescence when excited at its 410 nm band. However, only 2% photo-oxidation was observed. Further, the extent of the photo-oxidation of Erioglaucin-A did not change even when the photo-oxidation was carried out under aqueous and non-aqueous conditions in the presence of fluorescein or methylene blue. These two dyes are known to be effective sensitizers for the production of singlet oxygen, particularly in non-aqueous medium (*e.g.* in a benzene — methanol solvent mixture), in which the life-time of singlet oxygen is much longer then in water [9, 10]. Since not even these sensitizers brought about a change in the photo-oxidation of Erioglaucin-A, we feel that it may be stated that singlet oxygen does not participate or has only a subordinate role in the photo-oxidation. This conclusion is supported by the observation that in every case Erioglaucin-A underwent destructive oxidation, the formation of endoperoxide or carbonyl was not detectable; these compounds frequently accompany the reactions of aromatic hydrocarbon derivatives with singlet oxygen.

It was found that the iron(III)-catalyzed photo-oxidations of the various dyes exhibit optima at different pH values in each case (Table III). On this basis it appears obvious to conclude that acceptor activation occurs in these cases. However, it was also observed that for certain dyes the maximum in the decolourization *vs.* pH function depends on the wavelength at which the variation in the absorption of the dye is measured. Figure 4 shows that in the case of Erioglaucin-A the maximum is at pH 2.4 if the measurement is made at 410 nm, but at pH 2.94 if it is made at 634 nm. Similar phenomena are found for methyl orange and thymol blue too (Table III). From this observation, the general conclusion may be drawn that for every dye with acid — base properties, the acid exponent of which is in or near to the pH range under examination, the maximum in the ΔE_λ *vs.* pH curve lies at different positions if the ratio of the molar absorptivity of the protonated and non-protonated dye forms changes appreciably with the variation of the pH (see Fig. 3 in the

case of Erioglaucin-A). However, if the decolourization measured at an optional wavelength is converted to a molar concentration change with the aid of the apparent molar absorptivity value corresponding to the actual pH, then the maximum in the decolourization is found uniformly at pH 2.7 for the iron(III)-catalyzed photo-oxidations of the different dyes (Fig. 4 and Table III). Accordingly, therefore, the acceptor activation mechanism can not be assumed either to explain the iron(III)-catalyzed photo-oxidations of Erioglaucin-A.

Table III

pH optimum for iron(III)-catalyzed photo-oxidation of various dyes

Dye	pK_{acid}	λ, nm	position of pH optimum		Reference
			A	B	
Erioglaucin-A	2.85	RH_2^+ : 410	2.40	2.70	Present work
		RH : 634	2.94	2.70	
Methyl orange	3.90	RH_2^+ : 510	1.9—2.1	2.70	[6]
		RH : 520	2.40	2.70	
Safranine-T		RH_2^+ : 577	2.70	2.70	Unpublished results
		RH : 520	2.70	2.70	
Thymol blue	1.6	RH_2^+ : 552	1.50	2.70	Present work
		RH : 435	2.90	2.70	

A : ΔE_λ *vs.* pH curve
B : Δ[dye] *vs.* pH curve

On the above basis, it is probable that the catalyst ions play the determining role in the non dye-specific photo-oxidations of the various dyes in the presence of iron(III). In the pH range in question, the iron(III) is present in the form of mononuclear or polynuclear aqua and hydroxo complexes. The data of many authors, but particularly HEDSTRÖM [11] and BIEDERMANN [12], indicate that in the absence of complex-forming ions it is necessary to take the following equilibria into consideration to characterize iron(III) solutions :

$$Fe^{3+} \cdot aq + H_2O \rightleftarrows Fe(OH)^{2+} \cdot aq + H_3O^+ \quad (1)$$

$$Fe(OH)^{2+} \cdot aq + H_2O \rightleftarrows Fe(OH)_2^+ \cdot aq + H_3O^+ \quad (2)$$

$$2\,Fe^{3+} \cdot aq + 2\,H_2O \rightleftarrows Fe_2(OH)_2^{4+} \cdot aq + 2\,H_3O^+ \quad (3)$$

$$3\,Fe^{3+} \cdot aq + 8\,H_2O \rightleftarrows Fe_3(OH)_4^{5+} \cdot aq + 4\,H_3O^+ \quad (4)$$

When the data of the above authors ($K_1 = 8.91 \times 10^{-4}$; $K_2 = 5.49 \times 10^{-4}$; $K_3 = 1.22 \times 10^{-3}$; $K_4 = 1.7 \times 10^{-6}$) were utilized, the equilibrium distribution

illustrated in Fig. 7 was calculated under the experimental conditions we employed. Accordingly, in 8×10^{-5} *M* iron(III) perchlorate solution at pH $\sim$ 3.2, the concentrations of the 1 : 1 and 2 : 2 complexes exhibit maxima; at a lower pH the aqua ion predominates, and at a higher pH the dihydroxo complex. There is a considerable difference between the calculated pH value of 3.2 and the experimentally-found value of 2.7. In spite of this, we feel that our observations can be interpreted with equilibria (1)—(4), and that the species $Fe(OH)^{2+} \cdot aq$ plays an essential role in the photo-oxidation. On the basis of the quantum yield data to be found in the literature [13], the following photo-activity sequence can be established:

$$FeHO_2^{2-} > FeN_3^{2-} > Fe(OH)^{2+} > FeCl^{2+} > Fe^{3+} \cdot aq > FeSCN^{2+}$$

The differences in the experimental conditions do not permit a more quantitative comparison.

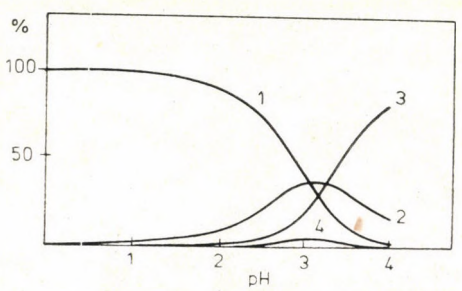

Fig. 7. Distribution of iron(III) species occurring in 8.14×10^{-5} *M* $Fe(ClO_4)_3$ solution, calculated on the basis of the data of HEDSTRÖM [11] and BIEDERMANN [12]. 1. Fe^{3+}. aq; 2. $Fe(OH)^{2+}$. aq; 3. $Fe(OH)_2^+$. aq; 4. $Fe_2(OH)_2^{4+}$. aq

For better orientation the quantum yields of photo-reduction of iron(III) species were determined at different pH values under excitation conditions we used:

$$\varphi_{pH=1.0} = 0.02, \quad \varphi_{pH=2.7} = 0.13, \quad \varphi_{pH=3.7} = 0.05$$

These data convincingly demonstrate that the photo-activity of the $Fe(OH)^{2+}$ ion is higher than those of the aqua and the more completely hydrolyzed (possibly dinuclear and polynuclear) iron(III) species, and hence primarily the former must be taken into account in an interpretation of the photo-oxidation. In agreement with this conclusion is the finding that only the light components with wavelengths less than 360 nm are effective, as the absorption by the hydrolyzed iron(III) species can be observed in the same range.

The initial steps in the photo-oxidation are as follows:

$$Fe^{3+}X^- \xrightarrow{h\nu} Fe^{2+}X \qquad (5)$$

$$Fe^{2+}X \rightarrow Fe^{3+}X^- \qquad (-5)$$

$$Fe^{2+}X \rightarrow Fe^{2+} + X \qquad (6)$$

$$Fe^{2+} + X \rightarrow Fe^{2+}X\,. \qquad (-6)$$

The quantum yield is governed by the extents of the back-reactions (−5) and (−6) and by the probability of the photolysis products (Fe^{2+}, X) escaping from the solvent cage.

The decolourization of the dye is conceived to occur in the following manner. Radical X formed in reaction (6) (OH in perchloric acid solution) splits an H atom off the dye molecule (RH) and a dye radical $\dot{R}$ is formed:

$$RH + X \rightarrow \dot{R} + HX\,. \qquad (7)$$

The dye radical reacts very rapidly with the oxygen present to give a dye peroxide radical $\dot{R}O_2$:

$$\dot{R} + O_2 \rightarrow \dot{R}O_2 \qquad (8)$$

the further transformation of which yields inactive products. Since the formation of iron(II) ions can not be observed in the course of the photolysis if sufficient oxygen is present, it must be assumed that the dye peroxide radical oxidizes iron(II) to iron(III):

$$\dot{R}O_2 + Fe^{2+} + H_3O^+ \rightarrow ROOH + Fe^{3+} + H_2O\,. \qquad (9)$$

A role may also be played in the reconversion to iron(III) by the hydroperoxide.

Reactions (5)—(9) agree well with experience.

If the extents of iron(III)-catalyzed fading of the dye both in the presence and in the absence of oxygen are compared, it appears that oxygen has a decisive role in the multiplicative stabilization of primary oxidation product of Erioglaucin-A (see Table IV).

Table IV

Effects of experimental conditions and intensity of irradiating light on photo-oxidation of Erioglaucin-A

Photon current/ photon.s^{-1}	Irradation time/min.	$Fe(ClO_4)_3$, M	pH	Erioglaucin-A, M	$(\Delta E^{410})_{O_2}$	$(\Delta E^{410})_{O_2=0}$	$\frac{(\Delta E)_{O_2}}{(\Delta E)_{O_2=0}}$
1.5×10^{15}	10	8.14×10^{-5}	2.50	8.0×10^{-5}	0.85	0.10	8.5
3.8×10^{14}	10	4.07×10^{-5}	2.50	4.0×10^{-5}	0.12	0.02	8.0

The decolourization of Erioglaucin-A can similarly be observed in the absence of oxygen. In this case the fading of 1 mole of dye is accompanied by the formation of 11—13 moles of iron(II). In the presence of sufficient oxygen,

however, iron(II) can not be detected, but the oxygen is consumed: 3.0—3.5 moles of oxygen are reduced during the decolourization. The oxygen consumption practically agrees with the amount of iron(II) formed in the absence of oxygen, and it may therefore be stated that the dye is oxidized at the expense of the oxygen present by the mediation of the photochemically-excited iron(III) ion ; that is, the iron(III) in fact plays the role of a photocatalyst.

The paper-chromatographic examinations showed that during the photo-oxidation of Erioglaucin-A fragments with low relative molecular masses are formed, which migrate together with the solvent front ; however, polymeric species with high relative molecular masses are also formed, which scarcely migrate at all. The paper-chromatographic findings are in agreement with the results of the voltammetric studies by GALUS and ADAMS [7], who found that, on anodic oxidation of dyes of triphenylmethane type analogous to Erioglaucin-A (crystal violet, malachite green), the dye loses the central (methyl)carbon-phenyl unit, and the substituted phenyl radicals then released combine to yield benzidine derivatives. Destructive oxidation similarly occurs with strong oxidants [*e.g.* the cerium(IV) ion] [7].

The stoichiometry of the photo-oxidation varies with the intensity of the exciting light. The dye decolourization observed at a decreased reduced light intensity is directly proportional to the quantity of catalyst in the higher concentration range, while at higher intensity a curve tending to saturation is obtained even at a lower catalyst concentration (Fig. 6). The cause of this latter is presumably that at high intensities the solution may become poor as regards oxygen, for the rate of consumption of oxygen may then approximate to its rate of dissolution.

The decolourization varies in accordance with a saturation curve with the increase of the concentration of the dye. This behaviour does not require any special explanation. However, it is necessary to justify the finding that a saturation curve is obtained only if the decolourization is determined at a low layer thickness. If the layer thickness is greater, the weakening of the light due to scattering from the polymeric species formed in the more concentrated dye solution and precipitated from water may compensate the apparent absorbance decrease accompanying the higher extent of oxidation as the dye concentration is increased, and as a result of this a maximum curve is produced.

It emerges from the data of Table I that from the aspect of the photo-oxidation, the oxygen molecule can practically not be replaced by other oxidants. Although hydrogen peroxide is capable of taking over the role of the oxygen, the system becomes too complicated, for decolourization of the dye can also be brought about by the radicals formed in the reactions between hydrogen peroxide and iron(II) or iron(III) in the dark, and hence evaluation of the photo-oxidation presents great difficulty. In addition, the reproducibility is poor.

In our experience, chlorate and bromate do not induce photo-oxidation in the absence of oxygen, and similarly the nitrate ion is not a satisfactory oxidant either. It is particularly surprising that chromate and nitrite ions, which react very rapidly with iron(II), are not only unable to take over the role of the oxidant, but exert inhibitory effects even in the presence of oxygen. This question will be returned to later.

The effects of the halide and pseudohalide ions can be explained partly by the stability and photochemical activity of the complex formed with the catalyst, and partly by the redox reactions between the radicals and these ions. The stability constants of the $Fe^{3+}X^-$ ion-pair complexes [15] are as follows:

$$Fe^{3+}F^- : 10^5—10^6;\ Fe^{3+}N_3^- : 10^5—10^6;\ Fe^{3+}SCN^- : 10^2—10^3;\ Fe^{3+}Cl^- : 20;$$

$$Fe^{3+}Br^- : 10;\ Fe^{3+}I^- : 80$$

Very little is known of the photo-activities of the complex ions formed between iron(III) and fluoride, but on the basis of the high electronegativity of fluorine it is probable that these are lower than that of $Fe(OH)^{2+}$, and it can be ascribed to this that the photo-oxidation virtually ceases in the event of a fluoride ion excess.

A strong complex is formed with azide ion. Further, the quantum yield of the FeN_3^{2+} ion is higher than that of $Fe(OH)^{2+}$, and accordingly an increasing extent of photo-oxidation would be expected with an increase of the azide concentration. Instead of this, the photo-oxidation decreases, presumably because a fast redox reaction takes place between OH and N_3^-, and also because the reaction between the dye and the N_3 radical is not fast enough.

The reasons why the chloride ion is ineffective, even in a higher excess, are the low stability of the chloro complexes and the fact that the photo-activity of the species $FeCl^{2+}$ is nearly the same as that of $Fe(OH)^{2+}$. The iodide, thiocyanate and bromide ions exert strong inhibitory effects in the sequence $I^- > SCN^- > Br^-$. A quantum yield datum is known only for the thiocyanate, according to which $FeSCN^{2+}$ has about half the photo-activity of $Fe(OH)^{2+}$ [13]. These ions react at high rate with the OH radical, and thereby inhibit the chain-oxidation of the dye. The sequence of the rate constants of their reactions with the OH radical coincides with the inhibition sequence observed in the photo-oxidation.

In higher quantities, the chromate and molybdate ions inhibit the photo-oxidation of Erioglaucin-A. The reason why these ions decrease or inhibit the oxidation is that they form photo-inactive complexes with the catalyst. The stability constants of the ion-pair complexes $FeQO_4^+$ are 7.2×10^7 for molybdate and $1.2—4.2 \times 10^6$ for chromate [15]. In a medium containing sulphate ion the extent of the photo-oxidation is lower, in accordance with the fact that the stability of the sulphato complex is lower too: $K \approx 10^2$ [15].

The inhibitory effect of the arsenite ion is connected with its ready reaction with the OH radical:

$$As(III) + OH \rightarrow As(IV) + OH^- \qquad (11)$$

The As(IV) radical ion formed may oxidize iron(II), but it may also reduce oxygen. The ratio of the reaction rates $k_{As(IV)+O_2} : k_{As(IV)+Fe(II)} = 40$ [14], and therefore the predominant reaction will be

$$As(IV) + O_2 + H^+ \rightarrow As(V) + HO_2. \qquad (12)$$

By reducing iron(III), HO_2 formed decreases the rate of initiation of the photo-oxidation.

Insufficient information is available for an interpretation of the weak inhibitory effect of copper(II) ion.

The decrease in the decolourization observed in the presence of nitrite ion may be related to the fact that nitrite reacts very rapidly with the OH radical.

It has been mentioned that nitrate ion (in a concentration of 10^{-3} M) and nitrite ion (at even lower concentrations: $10^{-5}\ M < [NO_2^-] < 10^{-3}\ M$) are also able to induce the photo-oxidation of Erioglaucin-A in the absence of iron(III). The cause of this in all probability is that UV photolysis of the nitrate and nitrite ions gives rise to low yields of OH radical.

Analytical conclusions

In the absence of a photocatalyst, Erioglaucin-A is satisfactorily photoresistant. Accordingly, its light absorption does not change during a fairly brief irradiation of moderate intensity. However, it is rapidly decolourized in the course of irradiation in the presence of the photocatalyst iron(III). The decolourization depends on the concentration of the dye, on the oxygen content of the solution, on the pH, and above all on the concentration of iron(III). At lower intensities of the irradiating light, a linear calibration curve is obtained in the concentration interval of 0.2—5.0 μg iron/cm^3; at higher intensities, linearity is observed in the range of 0.1—1.0 μg iron/cm^3. It is convenient to use the dye in a concentration of 5×10^{-5} M, for in this case association of the dye has still not attained a perceptible extent. Decolourization of the dye shows an optimum at pH 2.7.

Procedure: An appropriate aliquot of the sample to be analyzed, in which 2—25 μg iron is present, is measured into a beaker, a few drops of concentrated perchloric acid is added, and the material is evaporated almost to dryness. If necessary, in the interest of making the conversion to perchlorate total, further perchloric acid is added and the process is repeated. The almost dry

residue is dissolved in a small volume of water and 5 cm^3 10^{-3} M Erioglaucin-A dye solution is added. Then, with a sodium hydrogen carbonate or a dilute perchloric acid solution the pH is adjusted to 2.7 on a glass electrode, and the volume is made up to 25 cm^3. Some of this solution is transferred into a quartz cell, maintained at constant temperature, and irradiated for 10 min with a light source of sufficiently constant intensity. After this irradiation, the decrease in the light absorption at 634 or 410 nm is determined compared to the initial solution. The resulting absorbance difference is evaluated by means of a calibration curve taken in the described manner. The accuracy of the iron determination depends above all on how successful it proves to maintain the emission of the light source at a constant value. In a favourable case the reproducibility can be kept within $\pm 2\%$, but even if a simpler set-up is employed an accuracy of $\pm 5\%$ can be achieved.

The method described is not disturbed at all by transition metal ions in their lower oxidation states and it is therefore well applicable for the determination of the very low iron contents of certain metals such as cobalt and nickel, as well as alloys.

REFERENCES

[1] Nemodruk, A. A., Bezrogova, E. V.: Fotokhimicheskiye reaktsii v analiticheskoy khimii. Izd.: Khimiya, Moscow, 1972
[2] Péter, A., Csányi, L. J.: Acta Phys. et Chem. Szeged. **21,** 37 (1975)
[3] Fitzgerald, J. M.: Analytical photochemistry and photochemical analysis. M. Dekker, Inc., New York, 1971
[4] Almássy, Gy., Kovács, E.: Magyar Kém. Folyóirat **60,** 182 (1954)
[5] Almássy, Gy., Dezső, I.: Magyar Kém. Folyóirat **61,** 300 (1955)
[6] Harlamov, I. P., Dodyin, E. I., Mantsevich, A. D.: Zh. Anal. Khim. **22,** 371 (1967)
[7] Galus, Z., Adams, R. N.,: J. Amer. Chem. Soc. **86,** 1666 (1964)
[8] Gollnick, K.: Adv. in Photochem. **6,** 1 (1968)
[9] Kearns, D. R., Khan, A. V.: J. Amer. Chem. Soc. **89,** 5455 (1967)
[10] Ogryzlo, E. A.: Adv. Chem. Ser. **77,** 133 (1968)
[11] Hedström, B. O. A.: Arkiv för Kemi **6,** 1 (1953)
[12] Biedermann, G.: Kungl. Tekn. Högsk. Handl. Nr. 196 (1962)
[13] Balzani, V., Carassiti, V.: Photochemistry of coordination compounds. Academic Press, London and New York 1970
[14] Woods, R., Kolthoff, I. M., Meehan, E. J.: J. Amer. Chem. Soc. **85,** 3334 (1963)
[15] Sillén, L. G., Martell, A. E.: Stability Constants, Spec. Publ. Nos. 17 (1964) and 25 (1971). The Chemical Society, London.

Antal Péter
László J. Csányi } H-6720 Szeged, Dóm tér 7.

Acta Chimica Academiae Scientiarum Hungaricae, Tomus 100 (1—4), pp. 179—182 (1979)

CONVERSION OF A 2'-HYDROXYISOFLAVONE TO AN 11*H*-BENZOFURO[2,3-*b*][1]-BENZOPYRAN-11-ONE*

S. ANTUS and M. NÓGRÁDI

(Research Group for Alkaloid Chemistry of the Hungarian Academy of Sciences, Budapest)

Received June 30, 1978

Accepted for publication July 14, 1978

Oxidation of a 2'-hydroxyisoflavone with silver carbonate in quinoline gave the corresponding 11*H*-benzofuro[2,3-*b*][1]benzopyran-11-one.

A planned synthesis of the diastereomeric natural pterocarpan glucosides sophorajaponicin [(6a*S*, 11a*S*)-] [2] and trifolrhizin [(6a*R*, 11a*R*)-3-hydroxy-8,9-methylenedioxypterocarpan-3-*O*-β-D-glycopyranoside] [3] required the preparation of the isoflavone glucoside **1**. For this purpose the 2',7-dihydroxyisoflavone **2** [4] was coupled with acetobromoglucose in quinoline in the presence of silver carbonate. This gave a mixture from which by fractional crystallization instead of the expected isoflavone tetraacetylglycoside **3** a compound of m.p. 256—258 °C was isolated to which the pentacyclic structure **7** was assigned. This was based on the following arguments:

The product did not change on acetylation.

In the ^{1}H-NMR spectrum signals of the tetraacetylglucosyl moiety and of five aromatic protons could be recognized but the characteristic signal of the C-2 proton in isoflavones expected around $\delta = 8$ ppm was missing.

Hydrolysis of **7** yielded the corresponding aglycon (**9**) which gave in the mass spectrum a molecular ion at *m/e* 306.

Structure **7** explained the downfield shift by 0.9 ppm of the signal of 6'-H compared with that in **6** caused by the deshielding effect of the nearby carbonyl group. The shift of the carbonyl absorption from 1645 cm^{-1} (in **6**) to 1665 cm^{-1} in **7** was also characteristic.

A similar oxidative cyclization of a 2'-hydroxyisoflavone using $K_3Fe(CN)_6$ as oxidant was reported by FALSHAW *et al.* [5].

The required glucoside could later conveniently be prepared by the following sequence: thallium(III) nitrate oxidation of the chalcone acetate **11** in methanol–trimethyl orthoformate [1], followed by saponification and ring

* Part IX of the series: "Oxidative rearrangement of chalcones by thallium(III)-nitrate"; (for Part VIII, see Ref. [1]) and Part XV of the series "Synthesis of isoflavone glycosides" (for Part XIV, see Ref. [1]).

closure by sodium methoxide [7] furnished the benzylisoflavone glucoside **4**. Debenzylation of the corresponding acetate (**5**) and saponification of the product (**3**) gave **1** characterized as the pentaacetate **6**.

Conversion of **1** into the desired pterocarpan glucosides is in progress.

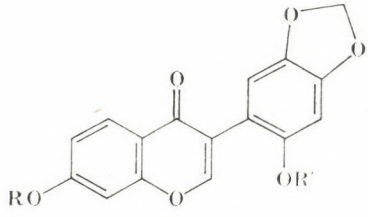

1: R = Gluc, R' = H
2: R = R' = H
3: R = Ac_4Gluc, R' = H
4: R = Gluc, R' = CH_2Ph
5: R = Ac_4Gluc, R' = CH_2Ph
6: R = Ac_4Gluc, R' = $COCH_3$

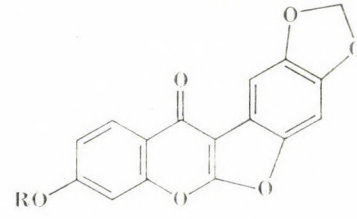

7: R = Ac_4Gluc
8: R = Gluc
9: R = H

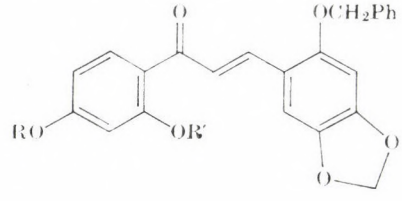

10: R = Gluc, R' = H
11: R = Ac_4Gluc, R' = CH_3CO

Gluc = β-D-glucopyranosyl; Ac_4Gluc = tetra-*O*-acetyl-β-D-glucopyranosyl

Experimental

M.p.'s were taken on a Kofler hot stage and are uncorrected. ^1H-NMR spectra were obtained on a Varian XL 100 instrument with tetramethylsilane as internal standard.

3-Hydroxy-8,9-methylenedioxy-11*H*-benzofuro[2,3-b][1]benzopyran-11-one-3-*O*-tetra-*O*-acetyl-β-*D*-glucopyranoside (7)

To a stirred solution of the isoflavone **2** (0.596 g; 2 mmol) [4] in dry quinoline (5.0 ml) silver carbonate (0.90 g; 3.3 mmol) was added. After stirring for 30 min α-acetobromoglucose (1.24 g; 3.0 mmol) was added and stirring continued for 4 h. After dilution with CH_2Cl_2 (30 ml) quinoline was removed by extraction with 5% H_2SO_4 and the solution was evaporated. Repeated recrystallization from acetone afforded **7** as colorless prisms (0.15 g; 12%), m.p. 256—258 °C.

$^1H-NMR(CDCl_3)$: δ = 2.02, 2.04, 2.06 and 2.10 (s, 12H, 4×OAc), 4.00 (mc, 1H), 4.25 (mc, 2H) and 5.1—5.3 (m, 4H) (sugar protons), 6.02 (s, 2H, OCH_2O), 7.00 (s, 1H, 3'-H), 7.20 (q, J_o = 8.5, J_m = 2.5 Hz, 1H, 6-H), 7.16 (d, J_m = 2.5 Hz, 8-H), 7.63 (s, 1H, 6'-H), and 8.28 (d, J_o = 8.5 Hz, 5-H).

$C_{30}H_{26}O_{15}$ (626.5). Calcd. C 57.51; H 4.18. Found C 57.23; H 4.09%.

3-Hydroxy-8,9-methylenedioxy-11*H*-benzofuro[2,3-b][1]benzopyran-11-one-3-*O*-β-*D*-glucopyranoside (8)

Saponification of **7** with 0.1 *N* sodium methoxide gave **8**, m.p. 288—290 °C (from AcOH).

$C_{22}H_{18}O_{11}$ (458.4). Calcd. C 57.65; H 3.96. Found C 57.74; H 4.36%.

3-Hydroxy-8,9-methylenedioxy-11*H*-benzofuro[2,3-b][1]benzopyran-11-one (9)

7 (72 mg) was boiled in ethanol (2.0 ml) containing hydrochloric acid (10%, 0.2 ml) for 5 h. On partial evaporation **9** (25 mg; 70%) precipitated. Colourless needles (from AcOH), no melting or sublimation up to 360 °C.

$C_{16}H_8O_6$ (306.3). Calcd. C 62.74; H 5.92. Found C 62.88; H 5.64%.

2-Benzyloxy-2',4'-dihydroxy-4,5-methylenedioxychalcone-4'-*O*-β-*D*-glucopyranoside (10)

To a hot solution of 2,4-dihydroxyacetophenone-4-*O*-tetra-*O*-acetyl-β-*D*-glucopyranoside (24.1 g; 0.05 mol) [6], and 2-benzyloxy-4,5-methylendioxybenzaldehyde (12.8 g; 0.05 mol) [4] in ethanol (250 ml) aqueous potassium hydroxide (25%, 50 ml) was added in portions and boiling continued for 1 h. On acidification with acetic acid a precipitate formed which was separated and then boiled with methanol (200 ml) for 40 min. The residue (6.2 g; 21%) was sufficiently pure for acetylation. A sample was purified for analysis by recrystallization from dimethylformamide—ethanol, orange needles, m.p. 238—242 °C.

$C_{29}H_{28}O_{11}$ (552.5). Calcd. C 63.04; H 5.11. Found C 62.83; H 5.24%.

Pentaacetate (11): Yellow needles, m.p. 214—216 °C (from $CHCl_3$—EtOH).

$C_{39}H_{38}O_{16}$ (762.7). Calcd. C 61.42; H 5.02. Found C 61.08; H 5.04%.

2'-Benzyloxy-7-hydroxy-4',5'-methylenedioxyisoflavone-7-*O*-β-*D*-glucopyranoside (4)

11 (7.6 g; 0.010 mol) was suspended in a mixture of $CHCl_3$ (100 ml) and CH_2Cl_2 (50 ml). This was added dropwise to a solution of $Tl(NO_3)_3 \cdot 3H_2O$ (7.05 g; 0.016 mol) in trimethyl orthoformate (50 ml) and MeOH (50 ml). After 135 min, 1*N* NaOMe (34 ml) was added followed by evaporation. The residue was distributed between water and CH_2Cl_2, the latter evaporated and the residue dissolved in warm methanol (100 ml). Precipitated Tl_2O_3 was filtered off, and 1*N* NaOMe (5 ml) was added to the solution which was then boiled for 20 min. The solution, acidified with acetic acid, was evaporated to a small volume.

The precipitated product was separated (3.7 g; 67%). **4** could be reprecipitated from hot ethanol, but remained amorphous.

$C_{29}H_{26}O_{11} \cdot 2H_2O$ (586.7). Calcd. C 59.38; H 5.15. Found C 59.77; H 5.43%.

Tetraacetate (5): Colourless crystals, m.p. 156—158 °C (from EtOH).

$C_{37}H_{34}O_{15}$ (718.7). Calcd. C 61.84; H 4.77. Found C 61.49; H 4.75%.

2',7-Dihydroxy-4',5'-methylenedioxyisoflavone-7-*O*-tetra-*O*-acetyl-β-*D*-glucopyranoside (3)

Debenzylation of **5** (3.1 g) by catalytic hydrogenation in acetone gave after elution of the precipitated product with CH_2Cl_2 and evaporation **6** (2.6 g; 96%), m.p. 212—214 °C, unchanged on recrystallization from EtOH.

$C_{30}H_{28}O_{15}$ (628.5). Calcd. C 57.33; H 4.49. Found C 57.65; H 4.78%.

Pentaacetate (6) Colourless: needles, m.p. 174—176 °C (from MeOH).

^1H—NMR($CDCl_3$): δ = 2.04, 2.06—2.08 (15H, 5×OAc), 3.96 (mc, 1H), 4.24 (mc, 2H), 5.1—5.4 (m, 4H) (sugar protons), 6.01 (s, 2H, OCH_2O), 6.70 and 6.78 (s, 1—1H, 3',6'-H), 6.96—7.12 (m, 2H, 6,8-H), 7.92 (s, 1H, 2-H), 8.22 (d, J_0 = 9 Hz, 5-H).

$C_{32}H_{30}O_{16}$ (670.6) Calcd. C 57.32; H 4.51. Found C 57.51; H 4.40%.

2',7-Dihydroxy-4',5'-methylenedioxyisoflavone-7-*O*-β-*D*-glucopyranoside (1)

Saponification of **3** afforded **1** as pale yellow needles, m.p. 221—223 °C (from dimethylformamide—ethanol).

$[\alpha]_D$ −27.4° (c = 2.3, dimethylformamide).
$C_{22}H_{20}O_{11}$ (460.4). Calcd. C 57.39; H 4.38. Found C 57.23; H 4.89%.

*

We are indebted to Drs. E. GÁCS-BAITZ and L. RADICS for NMR spectra and to Mr. Z. NAGY for technical assistance.

REFERENCES

[1] ANTUS, S., NÓGRÁDI, M.: Chem. Ber. **112,** 480 (1979)
[2] SHIBATA, S., NISHIKAWA, Y.: Chem. Pharm. Bull. **11,** 167 (1963)
[3] BREDENBERG, J. B., HIETALA, P. K.: Acta Chem. Scand. **15,** 696 (1961)
[4] FARKAS, L., GOTTSEGEN, Á., NÓGRÁDI, M.: J. Chem. Soc. Perkin 1, **1974,** 305
[5] FALSHAW, C. P., OLLIS, W. D., MOORE, J. A., MAGNUS, K.: Tetrahedron Suppl. **1966,** 333
[6] REICHEL, L., STEUDEL, J.: Ann. **553,** 83 (1942)
[7] ANTUS, S., BOROSS, F., NÓGRÁDI, M.: Ann. **1978,** 107.

Sándor ANTUS
Mihály NÓGRÁDI
H-1521 Budapest, Gellért tér 4.

Acta Chimica Academiae Scientiarum Hungaricae, Tomus 100 (1—4), pp. 183—202 (1979)

STUDY OF THE RATE OF CORROSION OF METALS BY A FARADAIC DISTORTION METHOD, I

J. DÉVAY and L. MÉSZÁROS

(Research Group of Electrochemistry of the Hungarian Academy of Sciences, Veszprém)

Received June 30, 1978

Accepted for publication August 8, 1978

A method based on faradaic distortion is presented for the study of the kinetics of corrosion processes for the case when the current-voltage characteristics of both the anodic and the cathodic reactions can be expressed by Tafel's equation. The harmonic components of the current flowing through the electrode under the effect of a sinusoidal alternating voltage superimposed on the polarizing direct voltage are examined as functions of the time-average value of the polarizing direct voltage and the amplitude of the alternating voltage. The corrosion current and the Tafel slopes of the anodic and cathodic reactions can be determined by measuring the first, second and third harmonic components of the faradaic current at one potential in each of the anodic and cathodic Tafel ranges. The evaluation of the corrosion current and of the Tafel's slopes from the harmonic component of the current measured at the corrosion potential is also presented. Simple relationships are obtained if the amplitude of the alternating voltage is small.

Introduction

The current-voltage characteristics of electrode-solution interface *i.e.* the polarization curve is generally nonlinear mainly as a consequence of the nonlinearity of the faradaic impedance. (The nonlinearity i.e. the potential dependence of the capacity of the double-layer is an additional cause of the above effect.) It follows from the above fact that current rectification is observed when the electrode is polarized by a nondistorted sinusoidal alternating voltage and the current is distorted as compared to the applied voltage *i.e.* the current contains higher harmonic components in addition to the one having the same frequency as the polarizing voltage. The latter phenomenon is termed faradaic distortion while the former is the faradaic rectification. Consider as an example of this phenomenon a currentvoltage characteristics given by an expression of second order

$$I = AU + BU^2 \tag{1}$$

substituting voltage U by $U_0 \sin \omega t$ (where U_0 is the amplitude and ω the angular frequency of the alternating voltage) current I will be given by the following formula :

$$I = AU_0 \sin \omega t + BU_0^2 \sin^2 \omega t = \frac{BU_0^2}{2} + AU_0 \sin \omega t + \frac{BU_0^2}{2} \cos 2\omega t. \tag{2}$$

Thus, in addition to the component having frequency ω the current is composed of a d.c. component $\frac{BU_0^2}{2}$ and a second harmonic component having frequency 2ω and amplitude $\frac{BU_0^2}{2}$. Both rectification and distortion originate from term BU^2 containing the second power of U and causing the nonlinearity. When the current-voltage characteristics is described by an expression containing higher powers of U (*e.g.* by a transcendent integer function defined by a power series) the current also contains higher harmonic components of frequency $k\omega$ ($k = 1, 2, 3 \ldots$). The parameters of the current-voltage characteristics (A and B in the above example) appear in the amplitudes of both the rectified current and the harmonic components consequently these parameters can be evaluated if the amplitudes are known.

The above considerations also apply to the case of the polarization by alternating current of an electrode having a nonlinear current-voltage characteristics. In this case the potential of the electrode exhibits faradaic distortion and faradaic rectification.

A similar approach is valid for the case when an alternating voltage or alternating current is superimposed on the direct voltage or direct current, respectively, polarizing the electrode. In this case the d.c. polarization curve observed in the absence of a.c. current is modified by the faradaic rectification component, and the harmonic components of the current or those of the potential can be studied as a function of the polarizing direct voltage or direct current, respectively. Thus valuable information is obtained on the kinetics of the electrode reaction.

Faradaic rectification has been studied first by Doss and Agarwal [1, 2] in the audio-frequency range. These authors applied the above method for the study of the kinetics of redox processes near the reversible potential. Barker [3, 4, 5] employed radio-frequency signals for the investigation of rapid electrode processes. Later several authors studied the details of the method. Delahay *et al.* [6] studied the rectification and distortion effects caused by the nonlinear current-voltage characteristics of redox processes in the case of simultaneous diffusion and charge transfer polarizations in the vicinity of the reversible potential.

Van Cakenberghe [7] has suggested the use of the second harmonic component generated by faradaic distortion for the determination of the transfer coefficient. This method has been developed further by Bauer and Elving [8]. Several authors have derived expressions for diffusion and charge transfer polarization [9, 10, 11]. The potential dependence of the second harmonic current component was mainly studied from a polarographic point of view aiming at kinetic investigations [12 through 19] or at analytical determinations [11, 20, 21].

An extremely lucid summary of the effect related to faradaic impedance, faradaic rectification and distortion has been presented by DEVANATHAN [22] for the case of redox reactions in the vicinity of the reversible potential. DEVANATHAN *et al.* [23] determined the kinetic parameters of some redox reactions by the measurement of faradaic distortion at radio-frequency signals (100 kHz to 1 MHz).

RANGARAJAN [24, 25, 26] has developed an operator method for the mathematical evaluation of the non-linear response of the faradaic impedance. This method is applicable in the case of any current or voltage perturbations.

In recent years some attempts have been presented regarding the use of faradaic rectification and distortion in the study of corrosion processes. SANTHYARAYANA [27, 28] determined the rate of corrosion by faradaic rectification measurement at the electrode polarized by sinusoidal alternating voltage in the vicinity of the corrosion potential. This method can only be applied if the Tafel slope of at least one of the partial processes is known. SANTHYARAYANA and SRINIVASAN [29] have derived a relation for the determination of the corrosion current from the potential shift caused by faradaic rectification for such cases when the corrosion potential does not considerably differ from the reversible potential of the metal electrode. The Tafel slopes of the partial electrode processes must be known also in this case. Experimental evidence of the above mentioned relationship has also been presented [30]. PRABHAKARA RAO and MISRA [31] have studied the potential dependence of the first and second harmonic a.c. and that of the intermodulation current components generated by a small amplitude alternating voltage superimposed on the direct voltage. These authors confined their study to the vicinity of the corrosion potential assuming that the polarization curve could be considered linear with respect to d.c. in this potential range and they substituted the exponential expressions relating to the a.c. component with fourth order Taylor polynomials. This method permits the determination of the corrosion current and that of the Tafel slopes as well.

In our previous work we have considered the effect of alternating current on electrode reactions and corrosion processes having various current-voltage characteristics [32 through 40]. It has been shown that the polarization curve of the electrode and consequently the rate of corrosion were altered by a.c. to an extent depending on the amplitude and the frequency of the latter. The effect of the double-layer capacity has also been considered.

In this communication a new a.c. method will be presented for the determination of the electrochemical rate of corrosion of metals. The potential dependence of the harmonic components of the current is examined in the case of the polarization of the electrode by an alternating voltage superimposed on the direct voltage which permits the evaluation of the kinetic parameters (corrosion current, Tafel slopes) of the corrosion process. It was assumed that both

the cathodic and the anodic reactions of the corrosion process can be represented by a Tafel-type current-voltage characteristics and the reversible potential of the two partial processes sufficiently differ from the corrosion potential.

Harmonic components of the faradaic current

In the present case the polarization curve of the electrode is expressed by the following equation:

$$\mathbf{j} = \mathbf{j}_K \left(e^{\frac{\Delta E}{\beta_a}} - e^{-\frac{\Delta E}{\beta_c}} \right), \tag{3}$$

where $\mathbf{j}$ is the current density, $\mathbf{j}_k$ the corrosion current density, $\Delta E = E - E_k$ is the polarization *i.e.* the difference of the actual potential and the corrosion potential while β_a and β_c are parameters proportional to Tafel slopes b_a and b_c of the anodic and cathodic processes, respectively:

$$\beta_a = \frac{b_a}{\ln 10} \quad \text{and} \quad \beta_c = \frac{b_c}{\ln 10}.$$

If the electrode is polarized by a sinusoidal voltage having angular frequency ω and amplitude U_0 superimposed on the direct voltage $\overline{\Delta E}$

$$\Delta E = \overline{\Delta E} + U_0 \sin \omega t \tag{4}$$

the current density can be calculated by the following equation

$$\mathbf{j} = \mathbf{j}_K \left(e^{\frac{\overline{\Delta E} + U_0 \sin \omega t}{\beta_a}} - e^{-\frac{\overline{\Delta E} + U_0 \sin \omega t}{\beta_c}} \right) + C \frac{d(\Delta E)}{dt}. \tag{5}$$

The first term of equation (5) is faradaic current density $\mathbf{j}$ while the second term represents the capacitive current density, C being the double layer capacity referred to the unit area of the electrode. The capacity of the double layer is assumed to be independent of the frequency [41] and of the potential in the potential range used in the investigation. The resistance of the solution between the working electrode and the reference electrode is disregarded in the theoretical derivation. The effect of the nonlinearity of the double layer capacity and the influence of the solution resistance will be considered in a future publication. Note that amplitude U_0 of the alternating voltage is not limited except in so far as it is assumed that in the potential range $\Delta E = \overline{\Delta E} + U_0 \sin \omega t$ only one cathodic reaction (*e.g.* H_2 evolution) takes place in addition to the anodic reaction consisting of metal dissolution.

We examine the faradaic current density

$$\mathbf{j}_F = \mathbf{j}_K \left(e^{\frac{\overline{\Delta E} + U_0 \sin \omega t}{\beta_a}} - e^{-\frac{\overline{\Delta E} + U_0 \sin \omega t}{\beta_c}} \right), \tag{6}$$

the capacitive current density

$$C \frac{\mathrm{d}(\Delta E)}{\mathrm{d}t} = \omega C U_0 \cos \omega t \tag{7}$$

will be considered later.

The exponential terms of equation (6) can be written in the form of products and thus the factors depending on the time average value of $\overline{\Delta E}$ are separated and the following relation is obtained

$$\mathbf{j}_F = \mathbf{j}_K \left(e^{\frac{\overline{\Delta E}}{\beta_a}} \cdot e^{\frac{U_0 \sin \omega t}{\beta_a}} - e^{-\frac{\overline{\Delta E}}{\beta_c}} \cdot e^{-\frac{U_0 \sin \omega t}{\beta_c}} \right). \tag{8}$$

The faradaic current density has a distorted sinusoidal form because of the non-linear (exponential) characteristics of the anodic and cathodic charge transfer reactions and thus in addition to the fundamental harmonic having frequency ω, higher harmonics of frequency $k\omega$ ($k = 1, 2, 3 \ldots$) are also present in the current. The harmonic components of the current density can be obtained by developing the exponential terms

$$e^{\frac{U_0 \sin \omega t}{\beta_a}} \quad \text{and} \quad e^{-\frac{U_0 \sin \omega t}{\beta_c}}$$

in Fourier series [37]

$$\begin{aligned} \mathbf{j}_F = \mathbf{j}_k \Bigg\{ & \left[I_0 \left(\frac{U_0}{\beta_a} \right) + 2 \sum_{k=0}^{\infty} (-1)^k I_{2k+1} \left(\frac{U_0}{\beta_a} \right) \sin (2k+1)\, \omega t + \right. \\ & \left. + 2 \sum_{k=1}^{\infty} (-1)^k I_{2k} \left(\frac{U_0}{\beta_a} \right) \cos 2k\, \omega t \right] e^{\frac{\overline{\Delta E}}{\beta_a}} - \\ & - \left[I_0 \left(\frac{U_0}{\beta_c} \right) - 2 \sum_{k=0}^{\infty} (-1)^k I_{2k+1} \left(\frac{U_0}{\beta_c} \right) \sin (2k+1)\, \omega t + \right. \\ & \left. + 2 \sum_{k=1}^{\infty} (-1)^k I_{2k} \left(\frac{U_0}{\beta_c} \right) \cos 2k\, \omega t \right] e^{-\frac{\overline{\Delta E}}{\beta_c}} \Bigg\}, \end{aligned} \tag{9}$$

where I_n ($n = 0, 1, 2 \ldots$) are modified Bessel functions of the first kind. However, it is sufficient to substitute the faradaic current density by a third order Fourier polynomial as the measurement of harmonic components higher

than the third one is burdened with difficulty and inaccuracy. The amplitudes of the higher harmonic components are so small as to be commensurable with the noise level of the measuring system. Thus, by rearranging the terms having identical frequencies one obtains

$$\begin{aligned}\mathbf{j}_F = \mathbf{j}_k &\left\{ I_0 \left(\frac{U_0}{\beta_a}\right) e^{\frac{\overline{\Delta E}}{\beta_a}} - I_0 \left(\frac{U_0}{\beta_c}\right) e^{-\frac{\overline{\Delta E}}{\beta_c}} \right\} + \\ &+ 2\mathbf{j}_k \left\{ I_1 \left(\frac{U_0}{\beta_a}\right) e^{\frac{\overline{\Delta E}}{\beta_a}} + I_1 \left(\frac{U_0}{\beta_c}\right) e^{-\frac{\overline{\Delta E}}{\beta_c}} \right\} \sin \omega t - \\ &- 2\mathbf{j}_k \left\{ I_2 \left(\frac{U_0}{\beta_a}\right) e^{\frac{\overline{\Delta E}}{\beta_a}} - I_2 \left(\frac{U_0}{\beta_c}\right) e^{-\frac{\overline{\Delta E}}{\beta_c}} \right\} \cos \omega t - \\ &- 2\mathbf{j}_k \left\{ I_3 \left(\frac{U_0}{\beta_a}\right) e^{\frac{\overline{\Delta E}}{\beta_a}} + I_3 \left(\frac{U_0}{\beta_c}\right) e^{-\frac{\overline{\Delta E}}{\beta_c}} \right\} \sin 3\omega t.\end{aligned} \tag{10}$$

The first term of equation (10) is the time average of the current density, $\bar{\mathbf{j}}$ (d.c. component) while the second, third and fourth terms are the first, second and third harmonic components, respectively. The latter terms can be measured by a frequency selective measuring receiver. Thus the d.c. component is given by the following formula

$$\bar{\mathbf{j}} = \mathbf{j}_k \left\{ I_0 \left(\frac{U_0}{\beta_a}\right) e^{\frac{\overline{\Delta E}}{\beta_a}} - I_0 \left(\frac{U_0}{\beta_c}\right) e^{-\frac{\overline{\Delta E}}{\beta_c}} \right\}, \tag{11}$$

while the faradaic rectificaion term is

$$\begin{aligned}\overline{\Delta \mathbf{j}} &= \mathbf{j}_k \left\{ I_0 \left(\frac{U_0}{\beta_a}\right) e^{\frac{\overline{\Delta E}}{\beta_a}} - I_0 \left(\frac{U_0}{\beta_c}\right) e^{-\frac{\overline{\Delta E}}{\beta_c}} \right\} - \mathbf{j}_k \left\{ e^{\frac{\overline{\Delta E}}{\beta_a}} - e^{-\frac{\overline{\Delta E}}{\beta_c}} \right\} = \\ &= \mathbf{j}_k \left\{ \left(I_0 \left(\frac{U_0}{\beta_a}\right) - 1 \right) e^{\frac{\overline{\Delta E}}{\beta_a}} - \left(I_0 \left(\frac{U_0}{\beta_c}\right) - 1 \right) e^{-\frac{\overline{\Delta E}}{\beta_c}} \right\},\end{aligned} \tag{12}$$

and the amplitudes of the harmonic components relating from faradaic distortion are

$$\hat{\mathbf{j}}_1 = 2\mathbf{j}_k \left\{ I_1 \left(\frac{U_0}{\beta_a}\right) e^{\frac{\overline{\Delta E}}{\beta_a}} + I_1 \left(\frac{U_0}{\beta_c}\right) e^{-\frac{\overline{\Delta E}}{\beta_c}} \right\}, \tag{13}$$

$$\hat{\mathbf{j}}_2 = 2\mathbf{j}_k \left| I_2 \left(\frac{U_0}{\beta_a}\right) e^{\frac{\overline{\Delta E}}{\beta_a}} - I_2 \left(\frac{U_0}{\beta_c}\right) e^{-\frac{\overline{\Delta E}}{\beta_c}} \right|, \tag{14}$$

$$\hat{\mathbf{j}}_3 = 2\mathbf{j}_k \left\{ I_3 \left(\frac{U_0}{\beta_a}\right) e^{\frac{\overline{\Delta E}}{\beta_a}} + I_3 \left(\frac{U_0}{\beta_c}\right) e^{-\frac{\overline{\Delta E}}{\beta_c}} \right\}. \tag{15}$$

Note that the signs in equation (10) were neglected in expression (14) and (15), similarly the phase reversal of the second harmonic is not indicated either because the amplitudes are defined as positive quantities. Thus the faradaic rectification component and the amplitudes of the first, second and third harmonic components generated by faradaic distortion are related to the polarizing direct voltage and the amplitude of the alternating voltage by equations (12) through (15).

The above relationship do not contain any restriction regarding the amplitude of the alternating voltage. However, much simpler expressions can be obtained if the amplitude of the alternating voltage is reduced to an extent permitting the substitution of the Bessel functions by the first or first and second terms of their Taylor polynomials.

The approximate value of the Bessel function used in the above equation are the following

$$I_0(x) \cong 1 + \left(\frac{x}{2}\right)^2, \tag{16}$$

$$I_1(x) \cong \frac{x}{2}, \tag{17}$$

$$I_2(x) \cong \frac{1}{2}\left(\frac{x}{2}\right)^2, \tag{18}$$

$$I_3(x) \cong \frac{1}{6}\left(\frac{x}{2}\right)^3. \tag{19}$$

The error caused by the above approximation when $x = \dfrac{U_0}{\beta} = 1$ amounts to 10 per cent approximately and it can be reduced further by decreasing amplitude U_0. The error becomes negligible as compared to the inaccuracies of the measuring method when the amplitude is 5 to 10 mV. Equations (12) through (15) are simplified to the following formulas by substituting the approximate values of the Bessel functions :

$$\overline{\Delta \mathbf{j}} = \mathbf{j}_k \left(\frac{1}{\beta_a^2} e^{\frac{\overline{\Delta E}}{\beta_a}} - \frac{1}{\beta_c^2} e^{\frac{\overline{\Delta E}}{\beta_c}}\right) \frac{U_0^2}{4}, \tag{20}$$

$$\hat{\mathbf{j}}_1 = \mathbf{j}_k \left(\frac{1}{\beta_a} e^{\frac{\overline{\Delta E}}{\beta_a}} + \frac{1}{\beta_c} e^{\frac{\overline{\Delta E}}{\beta_c}}\right) U_0, \tag{21}$$

$$\hat{\mathbf{j}}_2 = \mathbf{j}_k \left| \frac{1}{\beta_a^2} e^{\frac{\overline{\Delta E}}{\beta_a}} - \frac{1}{\beta_c^2} e^{-\frac{\overline{\Delta E}}{\beta_c}} \right| \frac{U_0^2}{4}, \tag{22}$$

$$\hat{\mathbf{j}}_3 = \mathbf{j}_k \left(\frac{1}{\beta_a^3} e^{\frac{\overline{\Delta E}}{\beta_a}} + \frac{1}{\beta_c^3} e^{-\frac{\overline{\Delta E}}{\beta_c}}\right) \frac{U_0^3}{24}. \tag{23}$$

Faradaic rectification current component $\overline{\Delta \mathbf{j}}$ is represented in Fig. 1 as a function of the time average value of polarizing voltage $\overline{\Delta E}$, while the potential dependence of the amplitude of the fundamental harmonic component and that of the higher harmonic components generated by faradaic distortion are shown in Figs 2 through 4, respectively. The curves shown in the figures were calculated according to equations (20) through (23) with the following parameters: $U_0 = 0.010$ V, $\beta_a = \beta_c = 0.050$ V and $\beta_a = 0.025$ V and $\beta_c = 0.050$ V, respectively. The difference between the data calculated with exact formulas (12) through (15) and approximate equations (20) through (23), respectively, are shown in Figs 5 through 8 as functions of amplitude U_0 of the alternating voltage for the case when $\Delta E = 0$ *i.e.* at the corrosion potential while Figs 9 through 12 represent the same relationship for the case of polarization $\Delta E = 0.100$ V. The parameters used in this calculation were the following $\beta_a = 0.025$ and $\beta_c = 0.050$ V.

Determination of the corrosion current and of the Tafel slopes

The kinetic parameters of the corrosion process ($\mathbf{j}_k$, β_a, β_c) can be evaluated from data obtained in measurements made with an electrode either polarized in the range of the validity of Tafel's equation or maintained at the corrosion potential using either exact equations (13) through (15) or approximate formulas (21) through (23).

The harmonic components of the faradaic current are given by the following formulas deduced from equations (13) through (15) for the case of measurements with an anodically polarized electrode at a sufficiently large polarization $\left(\frac{\overline{\Delta E_a}}{\beta_a} > 1\right)$ in the range of the validity of Tafel's equation.

$$\hat{\mathbf{j}}_{1a} = 2\mathbf{j}_k I_1\left(\frac{U_0}{\beta_a}\right) \mathrm{e}^{\frac{\overline{\Delta E_a}}{\beta_a}}, \tag{24}$$

$$\hat{\mathbf{j}}_{2a} = 2\mathbf{j}_k I_2\left(\frac{U_0}{\beta_a}\right) \mathrm{e}^{\frac{\overline{\Delta E_a}}{\beta_a}}, \tag{25}$$

$$\hat{\mathbf{j}}_{3a} = 2\mathbf{j}_k I_3\left(\frac{U_0}{\beta_a}\right) \mathrm{e}^{\frac{\overline{\Delta E_a}}{\beta_a}}. \tag{26}$$

The quotients of the amplitudes of the harmonic components measured at the same potential $\overline{\Delta E_a}$ namely

$$\frac{\hat{\mathbf{j}}_{1a}}{\hat{\mathbf{j}}_{2a}} = \frac{I_1\left(\frac{U_0}{\beta_a}\right)}{I_2\left(\frac{U_0}{\beta_a}\right)}, \tag{27}$$

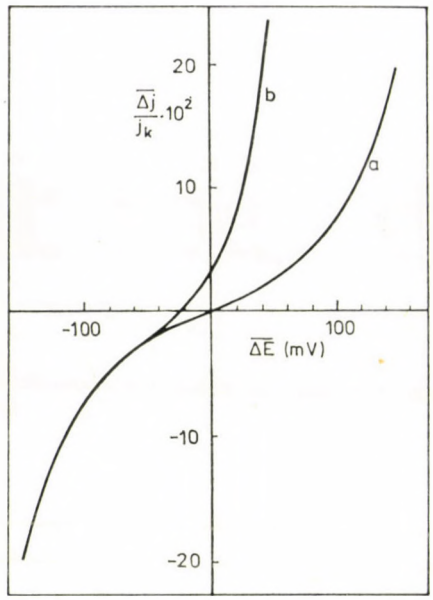

Fig. 1. Faradaic rectification component plotted as a function of polarization $\overline{\Delta E}$; $U_0 = 10$ mV; *a:* $\beta_a = \beta_c = 50$ mV; *b:* $\beta_a = 25$ mV, $\beta_c = 50$ mV

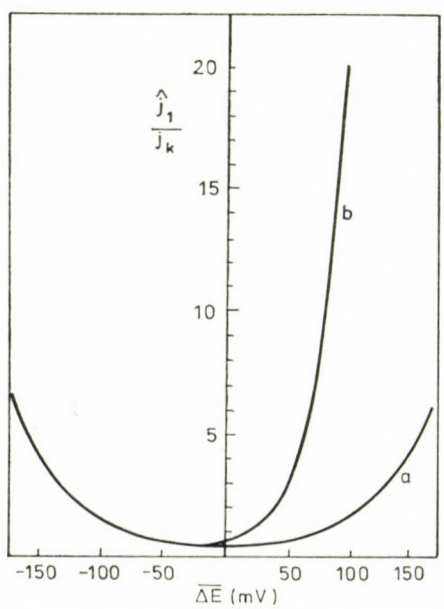

Fig. 2. Amplitude of the fundamental harmonic component plotted as a function of polarization. $U_0 = 10$ mV; *a:* $\beta_a = \beta_c = 50$ mV; *b:* $\beta_a = 25$ mV, $\beta_c = 50$ mV

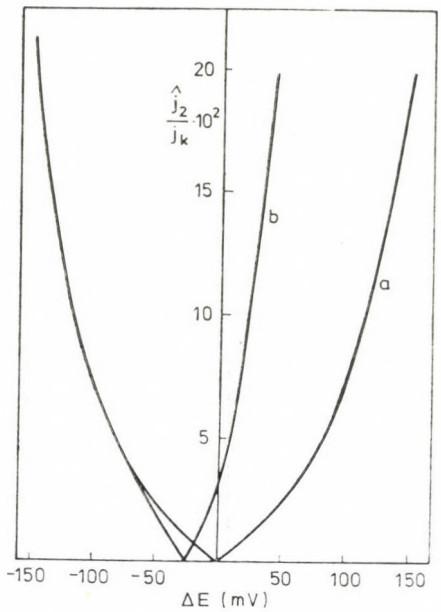

Fig. 3. Amplitude of the second harmonic current plotted as a function of polarization. $U_0 = 10$ mV. *a:* $\beta_a = \beta_c = 50$ mV; *b:* $\beta_a = 25$ mV; $\beta_c = 50$ mV

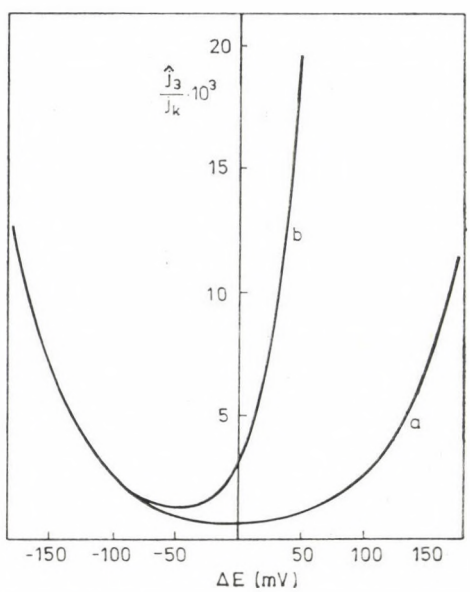

Fig. 4. Amplitude of the third harmonic component plotted as a function of polarization. $U_0 = 10$ mV. *a:* $\beta_a = \beta_c = 50$ mV; *b:* $\beta_a = 25$ mV, $\beta_c = 50$ mV

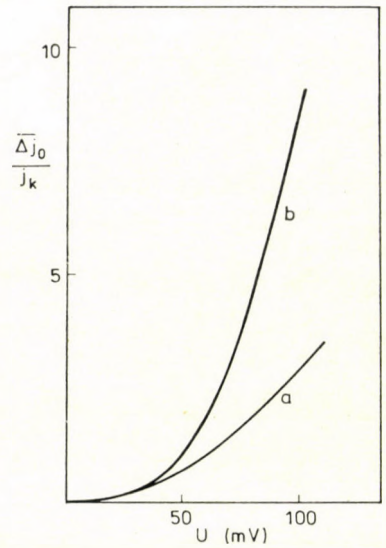

Fig. 5. Faradaic rectification component plotted as a function of amplitude U_0 of the alternating voltage at the corrosion potential $\overline{\Delta E} = 0$; $\beta_a = 25$ mV, $\beta_c = 50$ mV. *a:* calculated with approximate formula (20); *b:* calculated with exact formula (12)

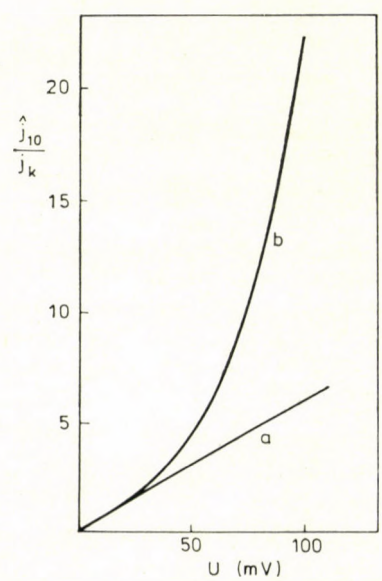

Fig. 6. Amplitude of the fundamental harmonic component plotted as a function of amplitude U_0 of the alternating voltage at the corrosion potential $\overline{\Delta E} = 0$, $\beta_a = 25$ mV, $\beta_c = 50$ mV. *a:* calculated with approximate formula (21), *b:* calculated with exact formula (13)

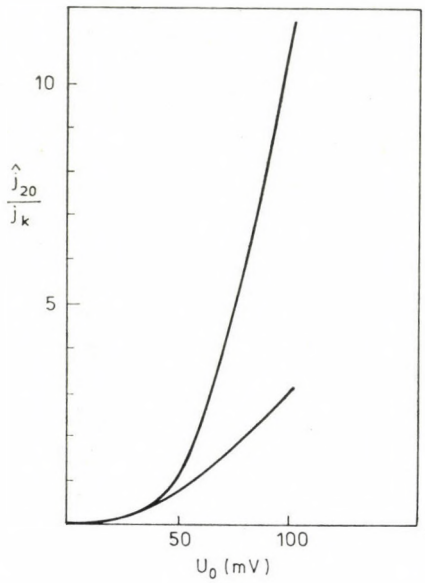

Fig. 7. Amplitude of the second harmonic component plotted as a function of amplitude U_0 of the alternating voltage at the corrosion potential $\overline{\Delta E} = 0$; $\beta_a = 25$ mV, $\beta_c = 50$ mV; *a:* calculated with approximate formula (22); *b:* calculated with exact formula (14)

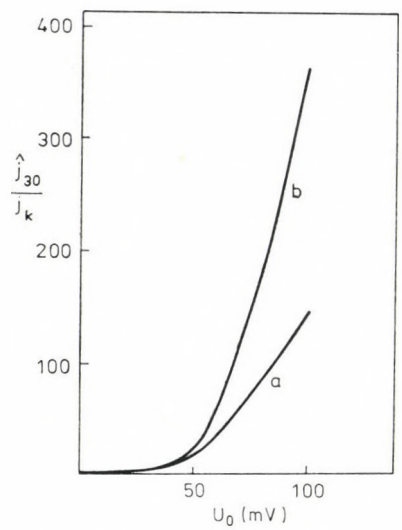

Fig. 8. Amplitude of the third harmonic component plotted as a function of amplitude U_0 of the alternating voltage at the corrosion potential $\overline{\Delta E} = 0$; $\beta_a = 25$ mV, $\beta_c = 50$ mV. *a:* calculated with approximate formula (23); *b:* calculated with exact formula (15)

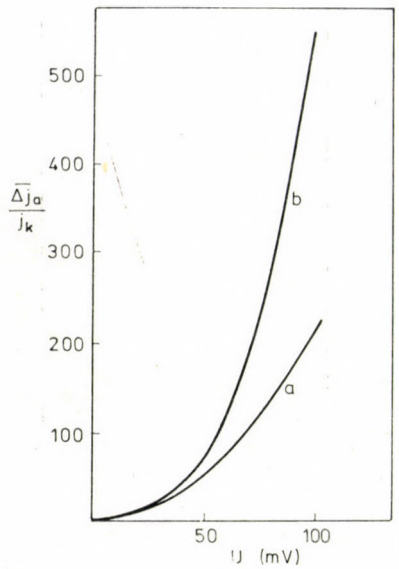

Fig. 9. Faradaic rectification component plotted as a function of amplitude U_0 of the alternating voltage at anodic polarization $\overline{\Delta E} = 100$ mV. $\beta_a = 20$ mV. $\beta_c = 50$ mV. *a:* calculated with approximate formula (20); *b:* calculated with exact formula (19)

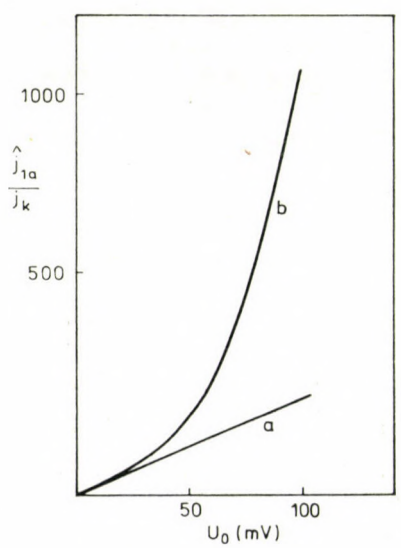

Fig. 10. Amplitude of the fundamental harmonic component plotted as a function of amplitude U_0 of the alternating voltage at anodic polarization $\overline{\Delta E} = 100$ mV. $\beta_a = 25$ mV, $\beta_c = 50$ mV; *a:* calculated with approximate formula (21); *b:* calculated with exact formula (13)

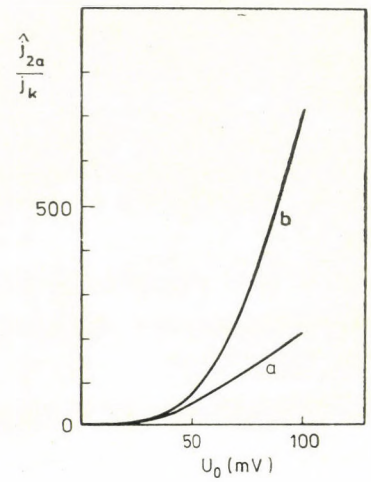

Fig. 11. Amplitude of the second harmonic component plotted as a function of amplitude U_0 of the alternating voltage at anodic polarization $\overline{\Delta E} = 100$ mV. $\beta_a = 25$ mV, $\beta_c = 50$ mV. *a:* calculated with approximative formula (22); *b:* calculated with exact formula (14)

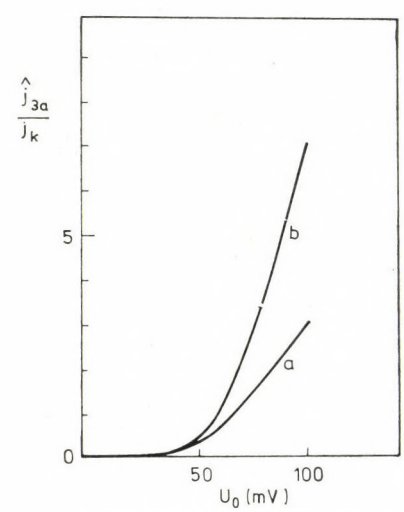

Fig. 12. Amplitude of the third harmonic component plotted as a function of amplitude U_0 of the alternating voltage at anodic polarization $\overline{\Delta E} = 100$ mV. $\beta_a = 25$ mV, $\beta_c = 50$ mV. *a:* calculated with approximative formula (23); *b:* calculated with exact formula (15)

and

$$\frac{\hat{\mathbf{j}}_{2a}}{\hat{\mathbf{j}}_{3a}} = \frac{I_2\left(\frac{U_0}{\beta_a}\right)}{I_3\left(\frac{U_0}{\beta_a}\right)} \tag{28}$$

respectively, permit the evaluation of β_a by successive approximation using mathematical tables.

β_a can be obtained also by a simpler method without resorting to successive approximations if one employs recursion formulas [42] valid for modified Bessel functions of the first kind.

$$\frac{2n}{x} I_n(x) = I_{n-1}(x) - I_{n+1}(x). \tag{29}$$

Equation (29) yields for $n = 2$

$$\frac{4}{x} I_2(x) = I_1(x) - I_3(x), \tag{30}$$

whence one obtains by substitution of $x = \frac{U_0}{\beta_a}$ and rearrangement

$$\beta_a = \frac{U_0}{4}\left[\frac{I_1\left(\frac{U_0}{\beta_a}\right)}{I_2\left(\frac{U_0}{\beta_a}\right)} - \frac{I_3\left(\frac{U_0}{\beta_a}\right)}{I_2\left(\frac{U_0}{\beta_a}\right)}\right]. \tag{31}$$

Substitution of equations (27) and (28) in equation (31) gives

$$\beta_a = \frac{U_0}{4}\,\frac{\hat{\mathbf{j}}_{1a} - \hat{\mathbf{j}}_{3a}}{\hat{\mathbf{j}}_{2a}}. \tag{32}$$

Thus parameter β_a can be determined from measurement data of the amplitudes of the first, second and third harmonic current component, respectively, at one potential $\overline{\Delta E_a}$ in the range of validity of Tafel's equation.

When

$$\hat{\mathbf{j}}_{3a} \ll \hat{\mathbf{j}}_{1a},$$

equation (32) can be simplified to yield

$$\beta_a \simeq \frac{U_0}{4}\,\frac{\hat{\mathbf{j}}_{1a}}{\hat{\mathbf{j}}_{2a}}. \tag{33}$$

Parameter β_c relating to the cathodic reaction $\left(-\frac{\overline{\Delta E_c}}{\beta_c} > 1\right)$ can be obtained by a similar procedure.

Namely

$$\hat{\mathbf{j}}_{1c} = 2\mathbf{j}_k I_1\left(\frac{U_0}{\beta_c}\right) \mathrm{e}^{-\frac{\overline{\Delta E_c}}{\beta_c}}, \tag{34}$$

$$\hat{\mathbf{j}}_{2c} = 2\mathbf{j}_k I_2\left(\frac{U_0}{\beta_c}\right) \mathrm{e}^{-\frac{\overline{\Delta E_c}}{\beta_c}}, \tag{35}$$

$$\hat{\mathbf{j}}_{3c} = 2\mathbf{j}_k I_3\left(\frac{U_0}{\beta_c}\right) \mathrm{e}^{-\frac{\overline{\Delta E_c}}{\beta_c}}, \tag{36}$$

thus

$$\frac{\hat{\mathbf{j}}_{1c}}{\hat{\mathbf{j}}_{2c}} = \frac{I_1\left(\frac{U_0}{\beta_c}\right)}{I_2\left(\frac{U_0}{\beta_c}\right)}, \tag{37}$$

and

$$\frac{\hat{\mathbf{j}}_{2c}}{\hat{\mathbf{j}}_{3c}} = \frac{I_2\left(\frac{U_0}{\beta_c}\right)}{I_3\left(\frac{U_0}{\beta_c}\right)}. \tag{38}$$

Parameter β_c is given by the following expressions from equations (37) and (38) using recursion formula (29).

$$\beta_c = \frac{U_0}{4} \frac{\hat{\mathbf{j}}_{1c} - \hat{\mathbf{j}}_{3c}}{\hat{\mathbf{j}}_{2c}}, \tag{39}$$

or

$$\beta_c \cong \frac{U_0}{4} \frac{\hat{\mathbf{j}}_{1c}}{\hat{\mathbf{j}}_{2c}}, \tag{40}$$

where $\hat{\mathbf{j}}_{1c}$, $\hat{\mathbf{j}}_{2c}$ and $\hat{\mathbf{j}}_{3c}$ are the amplitudes of the harmonic components measured at potential $\overline{\Delta E_c}$ corresponding to a cathodic polarization in the range of the validity of Tafel's equatiom.

The corrosion current density can be calculated using anyone among equations (24) through (26) and equations (34) through (36) knowing β_a or β_c and polarization $\overline{\Delta E_a}$ and $\overline{\Delta E_c}$ employed during the measurement of $\hat{\mathbf{j}}_{1a}$, $\hat{\mathbf{j}}_{2a}$ and $\hat{\mathbf{j}}_{3a}$ as well as $\hat{\mathbf{j}}_{1c}$, $\hat{\mathbf{j}}_{2c}$ and $\hat{\mathbf{j}}_{3c}$, respectively.

$$\mathbf{j}_k = \frac{\hat{\mathbf{j}}_{1a}}{2I_1\left(\frac{U_0}{\beta_a}\right)} \mathrm{e}^{-\frac{\overline{\Delta E_a}}{\beta_a}} = \frac{\hat{\mathbf{j}}_{2a}}{2I_2\left(\frac{U_0}{\beta_a}\right)} \mathrm{e}^{-\frac{\overline{\Delta E_a}}{\beta_a}} = \frac{\hat{\mathbf{j}}_{3a}}{2I_3\left(\frac{U_0}{\beta_a}\right)} \mathrm{e}^{-\frac{\overline{\Delta E_a}}{\beta_a}} =$$

$$= \frac{\hat{\mathbf{j}}_{1c}}{2I_1\left(\frac{U_0}{\beta_c}\right)} \mathrm{e}^{\frac{\overline{\Delta E_c}}{\beta_c}} = \frac{\hat{\mathbf{j}}_{2c}}{2I_c\left(\frac{U_0}{\beta_c}\right)} \mathrm{e}^{\frac{\overline{\Delta E_c}}{\beta_c}} = \frac{\hat{\mathbf{j}}_{3c}}{2I_3\left(\frac{U_0}{\beta_c}\right)} \mathrm{e}^{\frac{\overline{\Delta E_c}}{\beta_c}}. \tag{41}$$

The above formulas can be used also when a small amplitude alternating voltage ($U_0 \leq 10$ mV) is superimposed on the polarizing direct voltage, however, simpler expressions can be obtained if one takes into account the approximate formulas (17) through (19) derived by developing Bessel's functions in Taylor series. Parameters β_a and β_c can be calculated using the following formulas

$$\beta_a = \frac{U_0}{4} \frac{\hat{\mathbf{j}}_{1a}}{\hat{\mathbf{j}}_{2a}} = \frac{U_0}{6} \frac{\hat{\mathbf{j}}_{2a}}{\hat{\mathbf{j}}_{3a}}, \tag{42}$$

and

$$\beta_c = \frac{U_0}{4} \frac{\hat{\mathbf{j}}_{1c}}{\hat{\mathbf{j}}_{2c}} = \frac{U_0}{6} \frac{\hat{\mathbf{j}}_{2c}}{\hat{\mathbf{j}}_{3c}}, \tag{43}$$

respectively. Equations (42) and (43) were obtained by substituting equations (17) through (19) in equations (27), (28) and (37), (38), respectively. Equations (41) relating to the corrosion current density can also be rewritten in the simpler form

$$\mathbf{j}_k = \hat{\mathbf{j}}_{1a} \frac{\beta_a}{U_0} e^{-\frac{\overline{\Delta E_a}}{\beta_a}} = \hat{\mathbf{j}}_{2a} \frac{4\beta_a^2}{U_0^2} e^{-\frac{\overline{\Delta E_a}}{\beta_a}} = \hat{\mathbf{j}}_{3a} \frac{24\beta_a^3}{U_0^3} e^{-\frac{\overline{\Delta E_a}}{\beta_a}} =$$

$$= \hat{\mathbf{j}}_{1c} \frac{\beta_c}{U_0} e^{\frac{\overline{\Delta E_c}}{\beta_c}} = \hat{\mathbf{j}}_{2c} \frac{4\beta_c^2}{U_0^2} e^{\frac{\overline{\Delta E_c}}{\beta_c}} = \hat{\mathbf{j}}_{3c} \frac{24\beta_c^3}{U_0^3} e^{\frac{\overline{\Delta E_c}}{\beta_c}}. \tag{44}$$

We note that parameters β_a and β_c as well as corrosion current $\mathbf{j}_k$ can also be evaluated by the well-known Tafel's extrapolation method *i.e.* by plotting the logarithm of the harmonic components of the faradaic current as a function of polarization $\overline{\Delta E}$ according to equations (13) through (15) or according to equations (21) through (23) when $U_0 \leq 10$ mV. However, the advantage of our method as compared to Tafel's extrapolation technique consists in the fact that it is sufficient to measure the amplitude of the harmonic components at one potential either ΔE_a in the anodic Tafel range or ΔE_c in the cathodic Tafel range and it is not necessary to plot the complete polarization curve.

Parameters β_a and β_c as well as corrosion current density $\mathbf{j}_k$ can also be evaluated from the data of harmonic components $\hat{\mathbf{j}}_{10}$, $\hat{\mathbf{j}}_{20}$ and $\hat{\mathbf{j}}_{30}$ measured at the corrosion potential ($\overline{\Delta E} = 0$). In fact, substituting $\overline{\Delta E} = 0$ in equations (13) through (15) one obtains

$$\hat{\mathbf{j}}_{10} = 2\mathbf{j}_k \left\{ I_1\left(\frac{U_0}{\beta_a}\right) + I_1\left(\frac{U_0}{\beta_c}\right) \right\}, \tag{45}$$

$$\hat{\mathbf{j}}_{20} = 2\mathbf{j}_k \left| I_2\left(\frac{U_0}{\beta_a}\right) - I_2\left(\frac{U_0}{\beta_c}\right) \right|, \tag{46}$$

$$\hat{\mathbf{j}}_{30} = 2\mathbf{j}_k \left\{ I_3\left(\frac{U_0}{\beta_a}\right) + I_3\left(\frac{U_0}{\beta_c}\right) \right\}, \tag{47}$$

and corrosion current density $\mathbf{j}_k$ can be evaluated if β_a and β_c are *a priori* known.

It is noteworthy that equation (46) is not applicable if $\beta_a = \beta_c$ as in this case $\hat{\mathbf{j}}_{20} = 0$. Faradaic rectification component $\overline{\Delta\mathbf{j}_0}$ can also be employed for the evaluation of the corrosion current density if $\beta_a \neq \beta_c$ as equation (12) can be rewritten in the following form for the case when $\overline{\Delta E} = 0$.

$$\overline{\Delta\mathbf{j}_0} = \mathbf{j}_k \left\{ I_0\left(\frac{U_0}{\beta_a}\right) - I_0\left(\frac{U_0}{\beta_c}\right) \right\}. \tag{48}$$

It is not essential to know parameters β_a and β_c *a priori* for the evaluation of the corrosion current density if three data among $\hat{\mathbf{j}}_{10}$, $\hat{\mathbf{j}}_{20}$, $\hat{\mathbf{j}}_{30}$ and $\Delta\mathbf{j}_0$ are simultaneously measured at corrosion potential $\overline{\Delta E} = 0$ as any three formulas among expressions (45) through (48) form an independent linear equation system for the evaluation of β_a, β_c and $\mathbf{j}_k$. The equation system can be solved by a suitable computer program.

A much simpler set of equations is obtained when a small amplitude alternating voltage ($U_0 \leq 10$ mV) is employed in the measurements. In this case equation (20) through (23) yield the following expressions by substituting $\overline{\Delta E} = 0$.

$$\overline{\Delta\mathbf{j}_0} = \mathbf{j}_k \left(\frac{1}{\beta_a^2} - \frac{1}{\beta_c^2}\right) \frac{U_0^2}{4}, \tag{49}$$

$$\hat{\mathbf{j}}_{10} = \mathbf{j}_k \left(\frac{1}{\beta_a} + \frac{1}{\beta_c}\right) U_0, \tag{50}$$

$$\hat{\mathbf{j}}_{20} = \mathbf{j}_k \left|\frac{1}{\beta_a^2} - \frac{1}{\beta_c^2}\right| \frac{U_0^2}{4}, \tag{51}$$

$$\hat{\mathbf{j}}_{30} = \mathbf{j}_k \left(\frac{1}{\beta_a^3} + \frac{1}{\beta_c^3}\right) \frac{U_0^3}{24}. \tag{52}$$

Solving set of equations (50) through (52) the corrosion current density can be evaluated according to the following formula

$$\mathbf{j}_k = \frac{\hat{\mathbf{j}}_{10}^2}{\sqrt{48}\sqrt{2\hat{\mathbf{j}}_{10}\hat{\mathbf{j}}_{30} - \hat{\mathbf{j}}_{20}^2}}. \tag{53}$$

Comparing equations (49) and (51) we observe that

$$\hat{\mathbf{j}}_{20}^2 = (\overline{\Delta\mathbf{j}_0})^2, \tag{54}$$

thus the second harmonic amplitude in equation (53) can be substituted by faradaic rectification $\overline{\Delta\mathbf{j}_0}$ whence

$$\mathbf{j}_k = \frac{\hat{\mathbf{j}}_{10}^2}{\sqrt{48}\sqrt{2\hat{\mathbf{j}}_{10}\hat{\mathbf{j}}_{30} - (\overline{\Delta\mathbf{j}_0})^2}} \tag{55}$$

β_a and β_c can be expressed from equations (49) and (50) or (50) and (51) if corrosion current density $\mathbf{j}_k$ is known.

Thus from equations (49) and (50)

$$\frac{1}{\beta_a} = \frac{1}{2U_0}\left(\frac{\hat{\mathbf{j}}_{10}}{\mathbf{j}_k} + 4\frac{\overline{\Delta\mathbf{j}_0}}{\hat{\mathbf{j}}_{10}}\right), \tag{56}$$

$$\frac{1}{\beta_c} = \frac{1}{2U_0}\left(\frac{\hat{\mathbf{j}}_{10}}{\mathbf{j}_k} - 4\frac{\overline{\Delta\mathbf{j}_0}}{\hat{\mathbf{j}}_{10}}\right); \tag{57}$$

while from equations (50) and (51), if $\beta_a < \beta_c$:

$$\frac{1}{\beta_a} = \frac{1}{2U_0}\left(\frac{\hat{\mathbf{j}}_{10}}{\mathbf{j}_k} + 4\frac{\hat{\mathbf{j}}_{20}}{\hat{\mathbf{j}}_{10}}\right), \tag{58}$$

$$\frac{1}{\beta_c} = \frac{1}{2U_0}\left(\frac{\hat{\mathbf{j}}_{10}}{\mathbf{j}_k} - 4\frac{\hat{\mathbf{j}}_{20}}{\hat{\mathbf{j}}_{10}}\right); \tag{59}$$

or if $\beta_a > \beta_c$

$$\frac{1}{\beta_a} = \frac{1}{2U_0}\left(\frac{\hat{\mathbf{j}}_{10}}{\mathbf{j}_k} - 4\frac{\hat{\mathbf{j}}_{20}}{\hat{\mathbf{j}}_{10}}\right), \tag{60}$$

$$\frac{1}{\beta_c} = \frac{1}{2U_0}\left(\frac{\hat{\mathbf{j}}_{10}}{\mathbf{j}_k} + 4\frac{\hat{\mathbf{j}}_{20}}{\hat{\mathbf{j}}_{10}}\right). \tag{61}$$

The sign of $\overline{\Delta\mathbf{j}_0}$ permits to decide whether equations (58) and (59) or equation (60) and (61) have to be used as $\overline{\Delta\mathbf{j}_0} > 0$ in the case of $\beta_a < \beta_c$, while $\overline{\Delta\mathbf{j}_0} < 0$ in the case of $\beta_a > \beta_c$ according to equation (49); $\beta_a = \beta_c$ if $\overline{\Delta\mathbf{j}_0} = 0$ (and in this case $\hat{\mathbf{j}}_{20} = 0$).

Thus the above method permits the determination of the corrosion current density and parameters β_a and β_c proportional to the Tafel's slope from measurements made at the corrosion potential only. The advantage of this method as compared to the well-known "linear polarization" technique and its various modifications [43] consists in the fact that d.c. polarization is not involved and thus any shift in the corrosion potential caused by polarization can be avoided or at least decreased. It is well-known that change in the corrosion potential can considerably alter the slope of the polarization curve and thus the corrosion current density evaluated from the latter.

The relations derived in this paper refer to the faradaic current components only. The effect of the double layer capacity connected parallelly to the faradaic impedance and the possibility of the elimination of the capacitive current will be dealt with in a subsequent paper as well as the effect of the ohmic drop on the solution resistance between the working electrode and the reference electrode. The experimental verification of the above theoretical relations will also be presented in the next future.

REFERENCES

[1] Doss, K. S., Agarwal, H. P.: Proc. Indian Acad. Sci. **34** A, 263 (1951)
[2] Doss, K. S., Agarwal, H. P.: Proc. Indian Acad Sci. **35** A, 45 (1952)
[3] Barker, G., in Charlot, G. Ed., Modern Electroanalytical Methods, Elsevier, Amsterdam, 1958. p. 122
[4] Barker, G. C., in Yeager, E. Ed., Transactions of the Symposium on Electrode Processes Wiley, New York, 1961. pp. 325—365
[5] Barker, G. C., Faireloth, R. L., Gardner, A. W.: Nature, **181,** 247 (1958)
[6] Delahay, P., Senda, M., Wels, C. H.: J. Am. Chem. Soc. **83,** 312 (1961)
[7] Van Cakenberghe, J.: Bull. Soc. Chim. Belges **60,** 3 (1951)
[8] Bauer, H. H., Elving, P. J.: Anal. Chem., **30,** 334 (1958)
[9] Bauer, H. H.: Australian J. Chem. **17,** 591 (1964)
[10] Bauer, H. H.: Australian J. Chem. **17,** 715 (1964)
[11] Smith, D. E., Reinmuth, W.: Anal. Chem. **33,** 482 (1961)
[12] Bauer, H. H., Foo, D.: Australian J. Chem., **19,** 1103 (1966)
[13] Kooijman, D., Sluyters, J. H.: Rec. Trav. Chim., **83,** 587 (1964)
[14] McCord, T. G., Smith, D. E.: Anal. Chem., **40,** 1959 (1968)
[15] McCord, T. G., Smith, D. E.: Anal. Chem., **41,** 115, 131 (1969)
[16] Dévay, J., Mészáros, L., Garai, T.: Magy. Kém. Folyóirat **74,** 403 (1969); Acta Chim. Acad. Sci. Hung. **18,** 141 (1968)
[17] McCord, T. G., Smith, D. E.: Anal. Chem., **42,** 2 (1970)
[18] McCord, T. G., Smith, D. E.: Anal. Chem., **42,** 126 (1970)
[19] Randles, J. E. B., Witehouse, D. R.: Trans. Faraday Soc., **64,** 1376 (1968)
[20] Neeb, R.: Z. Anal. Chem. **186,** 53 (1962); **181,** 401 (1962)
[21] Dévay, J., Garai, T., Mészáros, L., Palágyi-Fényes, B.: Magy. Kém. Folyóirat, **75,** 460 (1969); Hung. Sci. Instr. **15,** 1 (1969)
[22] Devanathan, M. A. V.: Electrochimica Acta, **17,** 1755 (1972)
[23] Devanathan, M. A. V.: J. Electroanal. Chem. **62,** 195 (1975)
[24] Rangarajan, S. K.: J. Electroanal. Chem. **56,** 1 (1974)
[25] Rangarajan, S. K.: J. Electroanal. Chem. **56,** 27 (1974)
[26] Rangarajan, S. K.: J. Electroanal. Chem. **62,** 31 (1975)
[27] Sathyanarayana, S.: J. Electroanal. Chem. **50,** 411 (1974)
[28] Sathyanarayana, S.: J. Electroanal. Chem. **62,** 209 (1975)
[29] Sathyanarayana, S., Srinivasan, R.: Br. Corros J., **12,** 217 (1977)
[30] Srinivasan, R., Sahyanarayana, S.: Br. Corros. J. **12,** 228 (1977)
[31] Prabhakara Rao, G., Mishra, A. K.· J. Electroanal. Chem. **77,** 121 (1977)
[32] Erdey-Gruz, T., Dévay, J., Horányi, Gy., Vajasdy, I., Mészáros, L.: Magy. Kém. Folyóirat, **67,** 378 (1961); Acta Chim. Acad. Sci. Hung., **30,** 431 (1962)
[33] Erdey-Gruz, T., Dévay, J., Vajasdy, I., Horányi, Gy., Mészáros, L.: Magy. Kém. Folyóirat, **67,** 446 (1961); Acta Chim. Acad. Sci. Hung. **32,** 363 (1962)
[34] Erdey-Gruz, T., Dévay, J., Vajasdy, I.: Magy. Kém. Folyóirat, **68,** 185 (1962); Acta Chim. Acad. Sci. Hung., **37,** 251 (1963)
[35] Erdey-Gruz, T., Dévay, J., Horányi, Gy., Vajasdy, I.: Magy. Kém. Folyóirat, **67,** 244 (1961); Acta Chim. Acad. Sci. Hung. **30,** 29 (1962)
[36] Erdey-Gruz, T., Dévay, J., Vajasdy, I., Horányi, Gy.: Magy. Kém. Folyirat, **67,** 244 (1961); Acta Chim. Acad. Sci. Hung. **30,** 29 (1962)
[37] Dévay, J., Mészáros, L.: Magy. Kém. Folyóirat, **71,** 68 (1965); Acta Chim. Acad. Sci. Hung. **43,** 25 (1965)
[38] Dévay, J., Mészáros, L.: Magy. Kém. Folyóirat, **71,** 238 (1965); Acta Chim. Acad. Sci. Hung. **45,** 119 (1965)
[39] Dévay, J., Mészáros, L.: Magy. Kém. Folyóirat **71,** 240 (1965); Acta Chim. Acad. Sci. Hung. **45,** 119 (1965)
[40] Dévay, J., Mészáros, L.: Magy. Kém. Folyóirat **71,** 277 (1965); Acta Chim. Acad. Sci. Hung. **45,** 37 (1965)
[41] Armstrong, R. D., Race, W. P.: J. Electroanal. Chem. **33,** 285 (1971)
[42] Angot, A.: Compléments de Mathématiques, Editions de la Revue d'Optique, Paris 1952
[43] Mansfeld, F.: The Polarization Resistance Technique for Measuring Corrosion Currents; in Fontana, M. G. and Staele, R. W. Ed.: Advances in Corrosion Science and Technology. vol. **6.,** Plenum 1976

József Dévay
Lajos Mészáros } H-8200 Veszprém, Schönherz Z. u. 10.

Acta Chimica Academiae Scientiarum Hungaricae, Tomus 100 (1—4), pp. 203—210 (1979)

STUDIES ON THE CONVERSIONS OF DIOLS AND CYCLIC ETHERS, XLIV*

PREPARATION OF LACTONES, SATURATED AND UNSATURATED CYCLIC ETHERS BY CONVERSION OF DIOLS WITH VARIOUS STRUCTURES ON COPPER CATALYSTS. (RELATIONSHIPS BETWEEN THE STRUCTURES OF THE DIOLS AND THE CONVERSION PATHS)

M. BARTÓK and Á. MOLNÁR

(Department of Organic Chemistry, József Attila University, Szeged)

Received July 1, 1978

Accepted for publication September 4, 1978

Conversions of six different diprimary, primary-secondary and disecondary diols (**I—VI**) were investigated on three different copper catalysts (Cu/Al, Cu, Cu/SiO_2). An explanation is forwarded for the dependence of the characteristic processes (formation of saturated and unsaturated cyclic ethers and lactones) on the structure of the starting diols, the reactivity and stability of the intermediates, as well as on the individual properties of the catalysts.

Introduction

The majority of literature data dealing with conversions of open-chain 1,4- and 1,5-diols on metals (mainly on various copper catalysts) (*e.g.*, [1—5]) report the transformations of these diols to lactones. According to other papers, however, the formation of unsaturated [6—8] and saturated cyclic ethers [9, 10] was observed on different metal catalysts (supported and Raney-type ones).

The above experimental results, owing to the use of several different catalysts, do not allow to decide which properties of the catalysts are responsible for the various characteristic reactions, and no conclusions can be drawn regarding the relationships between the structures of the starting compounds and the different reaction paths. Therefore, we limited the present studies to one single metal, copper, using, however various copper catalysts with different specific properties [Raney-type (Cu/Al), non-supported (Cu) and supported (Cu/SiO_2) copper catalysts]. This provided a possibility for the establishment of characteristic conversions brought about by the specific properties of the catalysts and for the determination of relationships between the structure and the reaction path on a given catalyst in the case of the diols **I—VI** examined.

* Part XLIII: Acta Chim. Acad. Sci. Hung. **95**, 335 (1977).

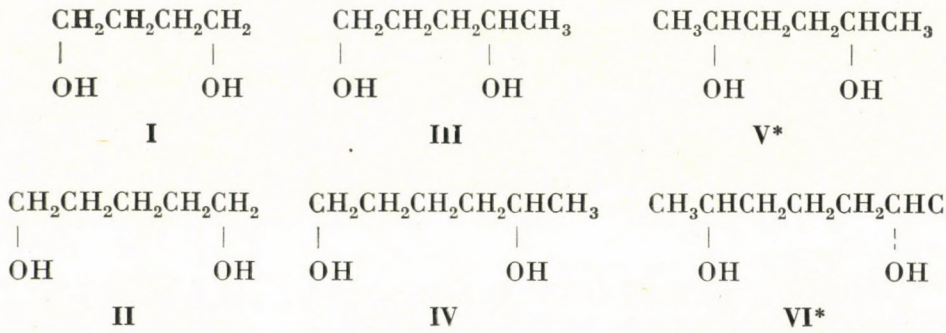

I III V*

II IV VI*

Experimental

Preparation of the model compounds

Of the compounds used, **I** and **II** were commercial products (Fluka). Compound **III** was prepared from 5-hydroxy-2-pentanone by reduction with $LiAlH_4$ (b.p. 92—96 °C/1 torr; b.p. [11] 104—105 °C/7 torr). For the preparation of **IV**, 6-hydroxy-2 hexanone was synthesized from ethylacetoacetate and 1,3-dibromopropane, and this was reduced with $LiAlH_4$ (b.p. 94 °C/1 torr; b.p. [12] 85—91 °C/0.5 torr). Compound **V** was obtained by the reduction of 2,5-hexanedione with Raney-nickel under elevated pressure (b.p. 90—91.5 °C/7 torr; b.p. [13] 114—116 °C/10 torr). Finally, 2,6-heptanedione [14] was reduced with $LiAlH_4$ to obtain **VI** (b.p. 85—86 °C/1 torr; b.p. [15] 101 °C/3 torr). The purity of the diols was checked by gas chromatography.

Experimental technique and catalysts

Description of the apparatus used and the methods of preparation of the Cu/Al and Cu catalysts has been given in our earlier papers [16, 17]. The supported copper catalyst (Cu/SiO_2) was prepared as described in the literature [18]; the support was Kieselgur (Merck). Activation was effected as follows: the catalyst (7.5 ml, 0.63—1 mm grain size) was reduced in a stream of hydrogen (10 ml/min) at 150 °C for 90 min, then treated further at 200 °C for 90 min in hydrogen (50 ml/min); finally the sample was kept at the temperature of the application for 30 min. The bulk density of the catalyst obtained was 0.54 $g \cdot cm^{-3}$.

The surface area of the catalysts used was measured by the BET method, using nitrogen for the adsorption. The acid and basic centres of the catalysts were also determined according to the method given in the literature [19]. The results obtained are shown in Table I.

Table I

Characteristic properties of the catalysts employed

Catalyst	Cu/Al	Cu	Cu/SiO_2
Specific surface ($m^2 \cdot g_{cat}^{-1}$)	12.5	3.4	27.0
Acid centres (mequ $\cdot g_{cat}^{-1}$)	0.083	0.013	0.198
Basic centres (mequ $\cdot g_{cat}^{-1}$)	0.090	—	1.008

The products of the catalytic conversions were identified by gas chromatographic comparison with reference substances; IR and NMR spectra were also utilized.

* The isomers were not separated. The isomeric ratio (± :*meso*) was: **V** = 1 : 1, **VI** = 2 : 1.

Results

The experimental results summarized in Tables II—VII have led to the following conclusions.

(1) On the Cu/Al catalyst, the characteristic reaction is the conversion into the corresponding cyclic ether.

(2) On the Cu catalyst, the main reaction is the formation of lactones in the case of **I**, **II**, **III** and **IV** (that is, for diols comprising at least one primary hydroxyl group). In addition to this, the conversion of **IV** is also accompanied by the formation of a significant amount of unsaturated cyclic ether, thus of the primary-secondary diols the conversion of **III** is more selective. Disecondary diols (**V** and **VI**) yield primarily unsaturated cyclic ethers (and a relatively high amount of oxo compound is also formed from **V**).

(3) On Cu/SiO_2 catalyst, compounds **I**—**IV** transform in the same manner as on Cu catalyst. In respect of selectivity, a similar difference can be observed also here in the conversions of **III** and **IV**, that is, with compound **IV** the process leading to the formation of the unsaturated cyclic ether is also significant.

Table II

Directions of the conversion of **I**

Catalyst Temperature (°C) Conversion (%)	Cu/Al 200 100	Cu 205 90	Cu/SiO_2 205 100
Tetrahydrofuran	100*	1	1
4-Butanolide	—	95	99
Non-identified	—	4(2)**	—

* The values are given in mole %. The space velocity employed was 0.16 ml of liquid. catalyst $ml^{-1}h^{-1}$.

** The figures in brackets given beside the mole % of the nonidentified compounds mean the number of the non-identified compounds.

Table III

Directions of the conversion of **II**

Catalyst Temperature (°C) Conversion (%)	Cu/Al 225 100	Cu 250 100	Cu/SiO_2 225 100
Tetrahydropyran	100	—	—
5-Pentanolide	—	98	99
Nonidentified	—	2(2)	1(1)

On this catalyst, the conversion of **V** is not selective either (saturated and unsaturated cyclic ether, oxo- and dioxo compounds are formed), while the unsaturated cyclic ether is the main product from **VI**.

Table IV

Directions of the conversion of **III**

Catalyst	Cu/Al	Cu	Cu/SiO_2
Temperature (°C)	200	225	200
Conversion (%)	100	100	100
2-Methyltetrahydrofuran	95	—	12
5-Methyl-2,3-dihydrofuran	—	—	8
2-Pentanone	3	—	—
4-Pentanolide	—	85	80
5-Hydroxy-2-pentanone	—	10	—
Non-identified	2(1)	5(2)	—

Table V

Directions of the conversion of **IV**

Catalyst	Cu/Al	Cu	Cu/SiO_2
Temperature (°C)	230	250	200
Conversion (%)	100	100	100
2-Methyltetrahydropyran	94	—	2
6-Methyl-3,4-dihydro-2*H*-pyran	—	25	30
5-Hexanolide	—	70	67
Non-identified	6(3)	5(2)	1(1)

Table VI

Directions of the conversion of **V**

Catalyst	Cu/Al	Cu	Cu/SiO_2
Temperature (°C)	200	200	200
Conversion (%)	100	100	85
cis-2,5-Dimethyltetrahydrofuran	49	—	23
trans-2.5-Dimethyltetrahydrofuran	47	—	6
2,5-Dimethyl-2,3-dihydrofuran	—	55	19
2-Hexanone	4	15	8
2-Hexanol	—	5	1
2,5-Hexanedione	—	—	15
Non-identified	—	25(3)	28(2)

Table VII

Directions of the conversion of **VI**

Catalyst Temperature (°C) Conversion (%)	Cu/Al 215 100	Cu 200 100	Cu/SiO_2 200 100
cis-2,6-Dimethyltetrahydropyran	57	2	3
trans-2,6-Dimethyltetrahydropyran	35	1	1
2,6-Dimethyl-3,4-dihydro-2*H*-pyran	—	61	73
Non-identified	8(2)	36(4)	23(4)

Discussion

Conversions on the Cu/Al catalyst

The formation of cyclic ethers on Cu/Al catalyst can be explained by the mechanism suggested by PINES and MANASSEN [21] for the cyclization of *trans*-1,4-cyclohexanediol in the presence of Al_2O_3 (Fig. 1). Accordingly, an intramolecular water elimination process takes place on the combined effect of the acid and basic centres of the catalyst. As suggested by the above authors, an arrangement within a sufficiently small distance of the acid and basic sites is necessary for the achievement of this reaction, allowing intramolecular concerted ring closure. The Cu/Al catalyst used by also contains aluminium oxide hydroxides, owing to the conditions of preparation (alkaline extraction) (Table I). The presence of these compounds causes the formation of cyclic ethers with this catalyst, too. This mechanism, *i.e.* intramolecular ring closure, is also supported by our earlier experiments effected with diols labelled with deuterium [17, 20].

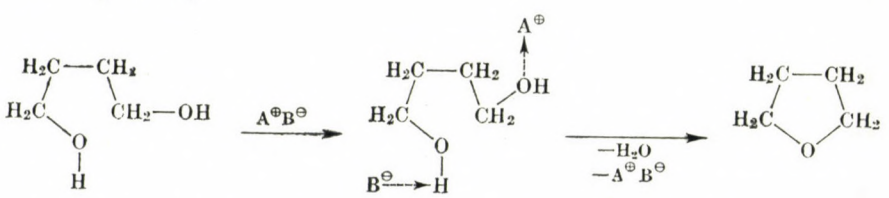

Fig. 1. Cyclization of 1,4-butanediol (I) on Cu/Al catalyst

Conversions on Cu and Cu/SiO_2 catalysts

Lactones and unsaturated cyclic ethers are formed as a result of correlated processes. A schematic diagram of the conversion is given for 1,4-pentanediol (**III**) in Fig. 2. The γ-hydroxy-oxo compounds formed by dehydrogenation

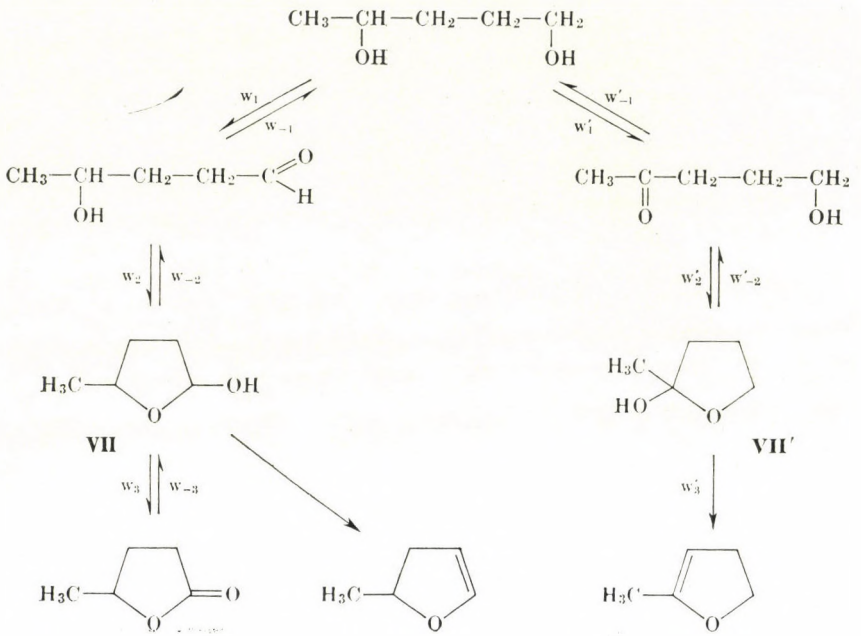

Fig. 2. Directions of the conversion of 1,4-pentanediol (III) on Cu and Cu/SiO_2 catalysts

are converted into cyclic hemiacetals, which lead to the end-products through further reactions.

The acetal **VII** formed from the γ-hydroxyaldehyde can transform into the lactone by further dehydrogenation (or the unsaturated cyclic ether is formed by the elimination of water), while the acetal **VII'** derived from the γ-hydroxyketone is capable of the water elimination reaction only. In the case of diprimary diols (**I, II**), only one type of the acetal (type **VII**) can be formed, thus these diols show only the dehydrogenation reaction yielding the lactone. On the other hand, in the primary-secondary diols (**III, IV**), there is a possibility for the development of the ketone hemiacetal of type **VII'**, too, and its conversion into the unsaturated cyclic ether may take place more readily than that of the isomeric compounds **VII**.

The corresponding lactones are the main products also in the cases of **III** and **IV**, in spite of the fact that dehydrogenation into the hydroxyketone is a process faster than the formation of the hydroxyaldehyde ($w_1' > w_1$). Literature data indicate [22—26], however, that in the hydroxyaldehydes the equilibrium between the open-chain and cyclic hemiacetal form is shifted toward the latter, while the hydroxyketones exist mainly in the open-chain form; thus $w_2 > w_2'$, and this is responsible for the predominance of lactone formation as the main direction of the conversion in these diols, too.

The differences observed on the various catalysts in the reaction directions of **III** and **IV** can be attributed to the differences in the formation and stability of the rigid five- and the flexible six-membered rings. These differences may give rise to significant deviations in the formation of cyclic ketone semiacetals (which is otherwise hindered) in the case of 5-hydroxy-2-pentanone and 6-hydroxy-2-hexanone. (In Ref. [22], such a difference can be observed in the numerical data given for hydroxyaldehydes, but the numerical values for ketone hemiacetals [24, 25] do not show differences of a similar extent. It must also be considered that the data in the two papers are controversary, and no measurements were made at the temperatures employed by us.)

Fig. 3. Formation of 2,5-dimethyl-2,3-dihydrofuran

Further differences can be established in the conversions of **V** and **VI**. In these compounds there is no possibility for a second dehydrogenation step leading to the formation of lactones, thus primarily the dehydration step yielding the unsaturated cyclic ether is expected (Fig. 3). Indeed, the main process was found to be this reaction in **VI**, on both catalysts, *i.e.* favoured formation of the six-membered ring can also be observed with this compound. In the conversion of **V** significant side reactions take place, which can be explained just by the hindrance of ring closure. Owing to this there is a possibility for other processes to occur, such as dehydrogenation (to give oxo- and dioxo compounds) and dehydration (yielding saturated cyclic ether). The formation of 2-hexanone may take place in the way substantiated by us earlier in the case of 1,3-diols : dehydration of the hydroxy-oxo intermediates and hydrogenation of the unsaturated oxo compound by hydrogen transfer [17, 20]. The formation of 2,5-dimethyltetrahydrofuran cannot be explained unambiguously on the basis of the data available as yet. Knowledge of the number of the acid and basic centres does not provide sufficient information regarding the true course of the reaction. It can only be stated that, in view of the number of the acid and basic centres of the catalyst (Table I), their presence must be responsible for this process.

*

The authors' thanks are due to Mr. F. NOTHEISZ and Mrs. Á. GREGUSS-ZSIGMOND for the surface area determinations, and to Mrs. G. BARTÓK-BOZÓKI for the determination of the active centres.

REFERENCES

[1] BALANDIN, A. A., KARPEISKAYA, E. I., TOLSTOPYATOVA, A. A.: Dokl. AN SSSR **122,** 227 (1958)
[2] Ger. Pat. 699, 945; C. A. **35,** 6977 (1941); Ger. Pat. 704, 237; Chem. Zentr. **1941,** II, 1795; Ger. Pat. 734, 568; C. A. **38,** 1248 (1944); Ital. Pat. 374, 925; Chem. Zentr. **1940,** II, 1359
[3] OKA, S.: Bull. Chem. Soc. Japan **34,** 12 (1961); **35,** 562, 986 (1962)
[4] LARKIN, D. L.: J. Org. Chem. **30,** 335 (1965)
[5] Anon.: Res. Discl. **148,** 77 (1976); C. A. **85,** 177332 (1976)
[6] DIMROTH, P., PASEDACH, H.: Angew. Chem. **72,** 865 (1960)
[7] Ger. Pat. 1.064,957; C. A. **56,** 455 (1962)
[8] U.S. Pat. 3,766,179; C. A. **80,** 14939 (1974)
[9] SHUYKIN, N. I., BARTÓK, M., KARAKHANOV, R. A., SHOSTAKOVSKII, V. M.: Acta Phys. et Chem. Szeged, **9,** 124 (1968)
[10] PINES, H., STEINGASZNER, P.: J. Catalysis **10,** 60 (1968)
[11] SHUYKIN, N. I., BELSKII, I. F., SAVEKINA, O. N.: Zh. Obshch. Khim. **29,** 874 (1959)
[12] HILL, R. M., ADKINS, M.: J. Am. Chem. Soc. **60,** 1033 (1938)
[13] SPRUNG, M. M., GUENTHER, F. O.: J. Am. Chem. Soc. **73,** 1885 (1951)
[14] RIED, W., KUNTSMANN, W.: Chem. Ber. **100,** 605 (1967)
[15] YOUNGMAN, E. A., RUST, F. F., COPPINGER, G. M., DE LA MARE, H. E.: J. Org. Chem. **28,** 144 (1963)
[16] MOLNÁR, Á., BARTÓK, M.: React. Kin. Catal. Lett. **3,** 421 (1975)
[17] MOLNÁR, Á., BARTÓK, M.: Acta Chim. Acad. Sci. Hung. **89,** 393 (1976)
[18] RUZIČKA, V., SOUKUP, J.: Czech. Pat. 91, 868; C. A. **54,** 14506 (1960); HÁJEK, M., KOCHLOEFL, K.: Collection Czeh. Chem. Commun. **34,** 2739 (1969)
[19] BORODIN, V. N.: Zh. Phys. Khim. **51,** 928 (1977)
[20] BARTÓK, M., MOLNÁR, Á.: Kémiai Közl. **45,** 335 (1976)
[21] PINES, H., MANASSEN, J.: Advances in Catal. **16,** 49 (1966)
[22] HURD, C. D., SAUNDERS, W. H.: J. Am. Chem. Soc. **74,** 5324 (1952)
[23] LÜTTKE, W.: Chem. Ber. **83,** 571 (1950)
[24] STERK, H.: Monatsh. **99,** 2107 (1968)
[25] WHITING, J. E., EDWARD, J. T.: Can. J. Chem. **49,** 3799 (1971)
[26] COTTIER, L., DESCOTES, G.: Bull. soc. chim. France **1971,** 4557

Mihály BARTÓK
Árpád MOLNÁR } H-6720 Szeged, Dóm tér 8.

Acta Chimica Academiae Scientiarum Hungaricae, Tomus 100 (1—4), pp. 211—220 (1979)

H_2 SORPTION CAPACITY OF AN UNSUPPORTED Pt CATALYST STUDIED BY DIFFERENT EXPERIMENTAL METHODS

F. NAGY, D. MÓGER, M. HEGEDÜS, Gy. MINK and S. SZABÓ

(Central Research Institute for Chemistry, Hungarian Academy of Sciences)

Received July 5, 1978

Accepted for publication August 8, 1978

Sorption of hydrogen on an unsupported, sintered platinum catalyst has been studied by means of electrochemical, volumetric and thermodesorption (TPD) techniques. Specific hydrogen sorption has been shown to depend on the thermal conditions of adsorption. If saturation with hydrogen is carried out at 0—25 °C, the amount of adsorbed H_2 corresponds to one hydrogen atom per surface Pt atom, in line with the usual findings. However, if the catalyst is cooled down gradually from a higher temperature in H_2 atmosphere, the amount of hydrogen is 4—5 times larger than in the former case. On the basis of additional experiments, we have concluded that hydrogen sorbed via activated chemisorption is probably not on the surface of the Pt catalyst.

Introduction

Since the advent of the thermodesorption technique [1, 2], especially temperature-programmed desorption, TPD, there have been numerous reports on the determination of the hydrogen sorption capacity of Pt catalysts by TPD, rather than by classical volumetric or electrochemical methods. However, only a few comparative studies [3] are available on the results of the three adsorption methods mentioned. It is not clear whether (i) they give similar results, (ii) the possible differences can be used to interpret the behaviour of the platinum-hydrogen system or to forecast the activity of a Pt catalyst. The answer to this question is not obvious, as not only the experimental techniques but also the circumstances of adsorption are strongly different.

The aim of this work was to study and compare the amounts of hydrogen sorbed on the same, unsupported Pt catalyst by electrochemical, volumetric and TPD methods. Carrying out suitable additional experiments, we wished to clarify whether or not the chemisorbed hydrogen determined under TPD conditions is located directly on the Pt surface.

Experimental

The unsupported Pt catalyst was prepared by reduction of a 0.16 mol/dm^3 aqueous solution of H_2PtCl_6 with H_2 under shaking. The fine Pt powder obtained was calcined prior to the measurements in a stream of H_2 (1 atm) at 650 °C for 2 hrs to avoid sintering on subsequent thermal treatments during adsorption.

Hydrogen and nitrogen were obtained from cylinders. Hydrogen was purified by passing through a solution containing the Cr^{2+}/Cr^{3+} redox system, and then, for drying, through a liquid N_2 trap and a column filled with molecular sieve. To remove oxygen, N_2 was diffused through copper contacts at 200 °C, then, for further purification and drying, through a trap cooled with dry ice-acetone and an adsorption column filled with molecular sieve.

In the electrochemical study of sorbed hydrogen the charging curves were recorded by means of a 3-electrode cell, whose main compartment was bottomed with a polished Pt plate. This plate ensured an electric contact with the catalyst particles placed on it. The other two, platinized platinum electrodes of the cell were immersed into the same electrolyte (0.2 mol/dm^3 HCl) as the main electrode. These electrodes served as auxiliary and reference electrodes. The central (main) electrode was connected with the reference and auxiliary electrode through uncreased stopcocks wetted with the common electrolyte; H_2 and N_2 gas inlets permitted saturation of the main electrode compartment with hydrogen and nitrogen (for removal of O_2). Polarization was performed at constant current, recording the potential of the main electrode (*vs.* the reference electrode) as a function of time curve. The measurements were made at room temperature ($\sim$ 25 °C).

In view of the low adsorbed amounts to be measured, the volumetric adsorption apparatus was equipped with a McLeod manometer, which permitted adsorption measurements in the pressure range of 100—600 Pa. The quartz adsorption vessel was maintained at the required temperature using a liquid thermostat and a temperature-controlled oven. Greaseless metal valves were employed. The adsorbent was pretreated in a high-vacuum apparatus equipped with a diffusion pump.

The TPD apparatus was the same as described earlier [4, 5] (inert gas: N_2; detector: thermal conductivity cell; gas flow rate: 16 cm^3 STP/min; heating rate: 15 °C/min). To remove impurities from the surface, the catalyst was kept alternately in a stream of O_2 and H_2 for 10 min. Saturation with H_2 was performed as follows: the catalyst was warmed gradually (in $\sim$ 10 min) to 350 °C and then pumped off to 10^{-2} Pa. Subsequently, the system was filled with H_2 and the catalyst was cooled to room temperature according to a suitable program. After subjecting the catalyst to the above treatment, the TPD runs were reproducible to within an experimental error of $\pm 5\%$.

Results

A. Electrochemical study of adsorption

The charging curves of 1.985 g Pt powder recorded at two different current intensities are shown in Fig. 1 (curves *a* and *b*). Since the reference electrode is a hydrogen electrode in the same electrolyte, the equilibrium H_2 pressure can be calculated from the Nernst equation:

$$E = 0.0285 \log \frac{1.013 \times 10^5}{P}, \tag{1}$$

where E is the electrode potential (V) and P is the pressure (Pa).

From the known amount of charge (Q) required for the reaction

$$H_2 \rightleftarrows 2\,H^+ + 2e^- \tag{2}$$

the amount of adsorbed (desorbed) hydrogen (n^E) can be calculated from Faraday's equation:

$$n^E = \frac{1}{2}\,\frac{Q}{F}, \tag{3}$$

where F is Faraday's constant,

$$F = 9.6489 \times 10^4 \text{ C/g-equ}. \tag{4}$$

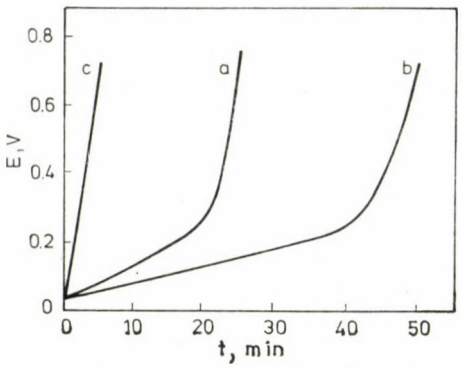

Fig. 1. Charging curve of 1.985 g Pt catalyst; *a*: $I = 0.5$ mA; *b*: $I = 0.25$ mA; *c*: after covering with Au, $I = 0.5$ mA

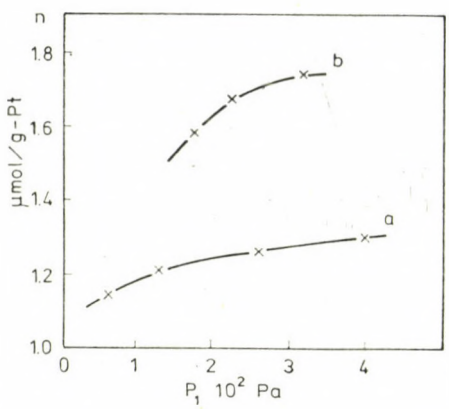

Fig. 2. Specific amount of sorbed H_2 *vs.* H_2 pressure; *a*: calculated from the charging curve, *b*: determined at 0 °C, saturated at 0 °C

Q was determined in the following way. The steep, linear section of the charging curve, where the amount of charge consumed is the function of the double layer capacitance only, was extrapolated to the abscissa. Parallels with the abscissa passing through the required potentials were then drawn, whose intercepts with the charging curve and with the straight line corresponding to the double layer section provided those points of time (t_E and t_E^0, respectively) which were used to calculate the amount of charge in Eq. (3) from

$$Q = I(t_E^0 - t_E) \quad [t] : \mathrm{s} ; \quad [I] : \mathrm{A} , \tag{5}$$

where I is the current intensity of polarization. The specific hydrogen sorption isotherm determined from the charging curve, as described above, is shown in Fig. 2 (curve *a*).

In order to investigate whether the sorbed hydrogen determined electrochemically is on the surface of the Pt catalyst, the measurements were repeated

[6] with a gold-covered catalyst (Fig. 1, curve *c*). These experiments have shown that the hydrogen sorption capacity of the gold-covered catalyst (at least under the conditions of electrochemical measurements) is close to zero.

B. TPD study of adsorption

The TPD curve of hydrogen on 2.15 g Pt catalyst recorded as described earlier is shown in Fig. 3. After calibration of the H_2 detector with a known number of H_2 pulses, the amount of hydrogen sorbed under these conditions (n^T) can be calculated from the TPD peak area:

$$n^T \approx 1\ \mu\text{mol/g-Pt}. \tag{6}$$

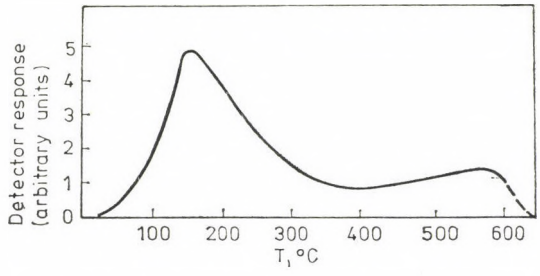

Fig. 3. TPD curve of H_2 on 2.15 g platinum

As in the electrochemical investigations, the TPD study of the platinum catalyst covered with adsorbed gold has also been carried out. According to the measurements, the shape of the TPD curve was practically identical (within $\pm 5\%$) with that of the catalyst not covered with Au. Thus, as opposed to the results of the electrochemical study of adsorption, the amount of sorbed hydrogen determined by the TPD method is not influenced by the coverage of the surface with Au.

Sorption saturation in the TPD measurements was performed — as already mentioned — by cooling the catalyst in a H_2 atmosphere from 350 °C to room temperature according to a preset program. This is necessary because at room temperature the catalyst does not adsorb, even after several hours, the amount of hydrogen which is adsorbed in a H_2 atmosphere upon cooling down from 350 °C.

C. Volumetric adsorption measurements

The TPD measurements called attention to the fact that H_2 sorption is at least partly an activated process, therefore, this problem was separately investigated in the volumetric measurements.

To determine the sorption capacity of the Pt catalyst, the following measurements were carried out. The surface of Pt was cleaned by placing the sample alternately in H_2 and O_2, then cooling it under vacuum to 0 °C. At this temperature the adsorption isotherm was recorded ($\bar{n}^V$, Fig. 2, curve *b*). For determining the equilibrium pressure corresponding to the points of the isotherm, we waited (1—2 hours) until the pressure did not change over a period of 20 min. Thus the apparent adsorption equilibrium has been reached. When attempting to determine the desorption branch of the isotherm, we have found that this lies above the adsorption branch, indicating that no real adsorption equilibrium exists.

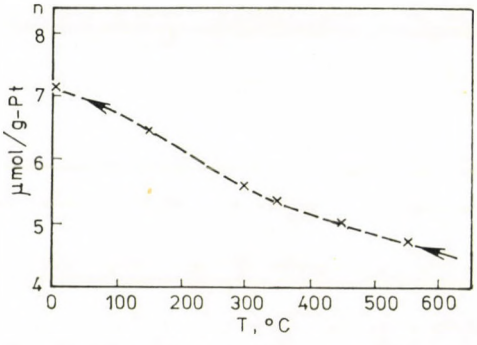

Fig. 4. Specific sorbed amount of H_2 at 2.66×10^4 Pa; temperature starts from 550 °C, and the adsorbent is cooled gradually to 0 °C in a H_2 atmosphere

In the next series of experiments, adsorption measurements were begun at 550 °C and, after obtaining an isotherm, the temperature was decreased and a new isotherm recorded in order to reach at least apparent equilibrium. The "equilibrium" adsorbed amounts at 2.66×10^2 Pa H_2 pressure are to be seen in Fig. 4. Checking the presence of a real ad- and desorption equilibrium by measuring the desorption branch, we have established that only the isotherm determined at 550 °C can be considered as referring to equilibrium.

To determine the amount of sorbed H_2 not removable by pumping at 0 °C, we carried out the following set of measurements. After the amount of sorbed hydrogen (n^V_{550}) corresponding to the given pressure (2.66×10^2 Pa) had been determined, the catalyst was cooled slowly to 0 °C in an atmosphere of H_2. At this temperature, after recording the adsorption isotherm, the amount of sorbed hydrogen (n^V_0) corresponding to the pressure of 2.66×10^2 Pa was again determined. Following this, the catalyst was pumped off to $\sim 10^{-3}$ Pa at 0 °C by a diffusion pump. After closing the adsorption vessel and heating the catalyst to 550 °C, the above set of measurements was repeated. Let $\overset{*}{n}{}^V_{550}$ and $\overset{*}{n}{}^V_0$ be, in this second case, the amounts of sorbed hydrogen correspond-

ing to the hydrogen pressure of 2.66×10^2 Pa, then the following mass balance equation can be deduced :

$$X_0 = n_{550}^V - {}^*n_{550}^V = n_0^V - {}^*n_0^V , \tag{7}$$

where X_0 denotes the amount of H_2 not removable under these conditions at 0 °C. Carrying out the above set of measurements once again, the results shown in Table I were obtained.

We determined the specific surface area of the Pt catalyst applied by low-temperature Kr adsorption (surface requirement of one Kr atom : 19.5 Å^2) at the beginning (Ω_0) and at the end (Ω_V) of the volumetric measurement series in order to be able to refer calculations to unit surface and to check subsequent sintering of the catalyst. The following values were obtained :

$$\Omega_0 = 1.39 \times 10^3 \text{ cm}^2/\text{g Pt}$$

$$\Omega_V = 1.21 \times 10^3 \text{ cm}^2/\text{g Pt.}$$

Results and discussion

Experimental results are summarized in Table I. Since the specific surface area of the catalyst determined by Kr adsorption, decreases from the initial value of 1.39×10^3 cm^2/g Pt to the final value of 1.21×10^3 cm^2/g Pt, the specific surface areas obtained by volumetric adsorption measurements are interpolated values between the initial and final surface area, corresponding to the serial number of the experiment.

Column *e* in Table I shows that the amount of sorbed hydrogen depends on whether saturation has been performed at a low (0—25 °C) temperature, or by slow cooling from a higher temperature (350—550 °C) in H_2 atmosphere. The 4- to 5-fold differences between the sorbed amounts are too large to be ascribable to experimental errors.

Taking into consideration the average distribution of the different (100), (110) and (111) crystal faces, the density of surface atoms of a platinum catalyst [7] is :

$$8.4 \text{ Å}^2/\text{active center} \approx 0.12 \times 10^{16} \text{ atom/cm}^2 \text{ Pt} \tag{8}$$

Assuming that the sorbed hydrogen is located on the surface of the catalyst, and that the H/Pt atomic ratio equals 1, the amount of adsorbed H_2 should be

$$\Omega_V = 1.21 \times 10^3 \text{ cm}^2/\text{g Pt} : 1.20 \ \mu\text{mol/g Pt}$$

$$\Omega_0 = 1.39 \times 10^3 \text{ cm}^2/\text{g Pt} : 1.38 \ \mu\text{mol/g Pt} \tag{9}$$

Table I

Results obtained by different adsorption methods
(t_a: temperature of adsorption or desorption)

Method of measurements	N°	P, $10^2 \times$ Pa	t_a, °C	n, μmol/g Pt	Ω 10^3cm²/g Pt	Remarks
a	b	c	d	e	f	g
Electrochemical	1	2.66	25	n^E: 1.27	1.21	Saturation with H_2 at room temperature. Desorption measurements.
	2.1	2.66	0	$\bar{n}_0^V$: 1.68	1.39	Saturation with H_2 at 0 °C.
Volumetric adsorption	2.2	2.66	a0	6.30 n_0^V: 6.06	1.30 1.26	Saturation in H_2 atmosphere by slow cooling from 550 °C.
	2.3	—	0	5.94 X_0: 5.40	1.30 1.26	Amount of H_2 not removable by pumping to a dynamic vacuum after run 2.2.
TPD	3	—	25–550	n^T: 7.05 5.62	1.39 1.21	Saturation in H_2 atmosphere by slow cooling from 350 °C. Desorption measurement.

The experimental adsorbed amounts listed in Table 1 show that only the hydrogen sorptions measured electrochemically and by low temperature volumetric adsorption are in satisfactory agreement with these values. Saturation with H_2 starting at higher temperatures in a H_2 atmosphere gives much higher H_2 consumptions.

As was mentioned above, upon covering the surface of the catalyst with adsorbed Au, no hydrogen is detectable by electrochemical methods, but at the same time the amount of hydrogen determined by TPD does not change. The adsorbed Au presumably remains on the surface of the platinum, because the difference in the atomic radii ($d_{Au} = 2.88$ Å, $d_{Pt} = 2.76$ Å) and the relatively low temperature (~ 25 °C) applied exclude the possibility of alloy formation. The amount of adsorbed Au from the experimental results is (a_{Au}):

$$\Omega = 1.21 \times 10^3 \text{ cm}^2/\text{g Pt}; \quad a_{Au} = 155 \times 10^{16} \text{ atom Au/g Pt} \qquad (10)$$

Supposing closest or tetragonal packing for the adsorbed Au atoms and considering the diameter of the Au atoms, the surface requirement of one Au atom is:

closest packing: $f_{Au} = 7.2$ Å²/atom Au

tetragonal packing: $f'_{Au} = 8.3$ Å²/atom Au (11)

On the basis of Eqs (10) and (11) the platinum surface "occupied" by one adsorbed Au atom (Ω_{Au}) is :

closest packing : $\Omega_{Au} = 1.14 \times 10^3$ cm^2/g Pt

tetragonal packing : $\Omega_{Au} = 1.29 \times 10^3$ cm^2/g Pt (12)

These values differ only slightly from the specific surface area of the Pt catalyst determined by Kr adsorption ($\Omega = 1.21 \times 10^3$ cm^2/g Pt).

It seems from the above data that the sorbed hydrogen determined electrochemically or by low-temperature adsorption is actually located on the Pt surface and the assumption of H/Pt = 1 [7, 8] is nearly correct.

The question of the location of the sorbed hydrogen on Pt catalysts have to be raised on the basis of the following two experimental results already mentioned : (a) the amount of sorbed H_2 is by a factor of 3 to 4 larger when saturation is started at elevated temperatures, (b) the amount of H_2 detectable by TPD is independent of the Au coverage.

A trivial explanation would be to assume the formation of a secondary pore system when the catalyst is prepared by sintering a finely dispersed Pt powder. The penetration of hydrogen into this pore system either by pore diffusion, or by dissolution and diffusion through the pore walls may require activation energy. The assumption of diffusion-controlled adsorption implies that the pores are inaccessible for the Kr atoms.

A more likely hypothesis is that the hydrogen atoms penetrate the first lattice layer and reach the Pt atoms in the second and third layers. To check the reality of this hypothesis, let us estimate the size of pores in the individual layers, considering the Pt atoms in the lattice as spheres (Table II).

The atomic diameters of the adsorptives used are given in Table III.

The data in Tables II and III show that the Au and Kr atoms are too large to penetrate the external lattice plane even if a Pt atom is missing, *i.e.* a defect site is formed. Considering its size, atomic hydrogen can only penetrate the (110) face or the defect sites. However, hydrogen in covalent bonds can penetrate the surface of the Pt catalyst — except for areas bounded by (111) faces — and can reach Pt atoms in the second or eventually also in the third lattice layer.

Table II

Diameter of holes in the various lattice; faces of platinum
ϱ' : (100) face ; ϱ'' : (110) face; ϱ''' : (111) face

Symbol	ϱ'	ϱ''	ϱ'''
ϱ, Å	1.20	2.02	0.43

Table III

"Atomic" diameters of various sorptives (d)

Symbol	Pt	Au	Kr	H_2	H_{atomic}	$H_{covalent}$
d, Å	2.76	2.88	3.50	2.36	1.62*	0.74

* Estimated from the size of the molecule ($d_{H_2} = 2.36$ Å) and from the H—H covalent bond length ($d_H^c = 0.74$ Å), using the equation: $d_H = d_{H_2} - d_H^c$

The assumption that hydrogen atoms can penetrate the surface at areas bounded by (110) faces and thus reach Pt atoms in the second and third layers, explains the difference between sorptions at low and elevated temperatures only if we suppose that the penetration of hydrogen atoms is an activated process. This may be a correct assumption, because the size of the H atom given in Table II is a rather crude estimate.

The most likely assumption seems to be the formation of a "covalent" compound [9]

$$PtH_x \tag{13}$$

the elementary steps of the process being

$$Pt \rightleftarrows \overset{*}{Pt} \qquad \text{(a)}$$

$$x(H)_{ads.} + \overset{*}{Pt} \rightleftarrows PtH_x\,, \qquad \text{(b)} \tag{14}$$

where $\overset{*}{Pt}$ is the activated state of Pt.

This would explain why the $(H)_{sorb.}$ to $(Pt)_{surf.}$ ratio is much greater than unity, and is also consistent with an activated sorption process. The reality of the formation of this Pt-H compound is also supported by our earlier results [10], according to which, the sorbed hydrogen detectable by TPD reacts but very slowly with oxygen from the gas phase at room temperature.

REFERENCES

[1] Tsuchiya, S., Amenomiya, Y., Cvetanović, R. J.: J. Catal., **19,** 245 (1970)
[2] Sokolskij, D. V., Popova, N. M., Babentiova, L. V., Solniskova, V. K.: Dokl. Akad. Nauk SSSR., **210,** 888 (1973)
[3] Bett, J., Kinoshita, K., Routsis, K., Stonehart, P.: J. Catal., **29,** 160 (1973)
[4] Móger, D., Kovács, G.: Magy. Kém. Foly., **81,** 123 (1975)
[5] Móger, D., Besenyei, G., Nagy, F.: Magy. Kém. Foly., **81,** 284 (1975)
[6] Szabó, S., Móger, D., Hegedüs, M., Nagy, F.: React. Kinet. Catal. Lett., **6,** 89 (1977)
[7] Benson, J. E., Boudart, M.: J. Catal., **4,** 704 (1965)

[8] MEARS, D. E., HANSFORD, R. C.: J. Catal., **9**, 125 (1967)
[9] CHARCOSSET, H., FRETY, R., LECLERCQ, G., NEFF, B., TARDY, B.: C. R. Acad. Sc. Paris t. 283. Série C-331. (1976)
[10] MÓGER, D., HEGEDÜS, M., BESENYEI, G., NAGY, F.: Acta Chim. Acad. Sci. Hung., **93**, 289 (1977); React. Kinet. Catal. Lett., **5**, 73 (1976)

Ferenc NAGY
Dezső MÓGER
Mihály HEGEDÜS
György MINK
Sándor SZABÓ

H-1525 Budapest, P.O. Box 17

Acta Chimica Academiae Scientiarum Hungaricae, Tomus 100 (1—4), pp. 221—228 (1979)

SPECTROCHEMICAL INVESTIGATION OF VOLATILE COMPONENTS RELEASED IN THERMOCHEMICAL PROCESSES, I

APPARATA, SYSTEM AND EXPERIMENTAL CONDITIONS

E. GEGUS, J. KREITER, L. MÉRAY and J. INCZÉDY

(Institute of Analytical Chemistry, University of Veszprém)

Received July 5, 1978

Accepted for publication August 15, 1978

A microreactor with electrical heating was designed to investigate the details of the thermochemical processes, *i.e.* evaporation and conversion processes, as well as thermal reactions occurring at temperatures up to 1350 °C. The vapour phase obtained under the heating period was introduced by an argon carrier gas into a radiation source of d.c. arc stabilized by external magnetic field. Emission intensity of a selected characteristic element was recorded as a function of the time, and temperature. The first part of the publication is concerned with the design of the apparata, as well as characteristics and function of the microreactor heating, the carrier gas stream, the external magnetic field, and the photoelectric detector and recorder system.

Introduction

In the spectroscopic emission radiation sources, and in atomic absorption cuvettes the sample to be investigated undergoes evaporation, atomization and excitation processes, on the effect of thermal, electric or laser energy. The rate of the evaporation and dissociation processes enhances with the increase of the power density of the energy introduced, thus diminishing the role of the interelement effects; the energy used for splitting lattice forces and chemical bonds forms only a negligible part of the total power of the source. However, at the same time, a number of undesirable secondary processes and reactions take place, *e.g.* the decrease of atomic emission or absorption as a consequence of the enhanced ionization, the increase of background radiation caused by electron continuum, and the shortening of residence time of the elements in question, because of high rate of particle motion, chemical reactions with electrodes, *etc.* Therefore, the investigation of thermochemical processes occurring under influence of energy introduction is of extreme importance, along with the more detailed clearing-up of secondary processes [1]. Beside d.c. arc excitation, useful information can be obtained on this subject with the aid of electrothermal atomization in atomic emission and absorption spectrometry, as well as by the application of a laser source [2—10]; theoretical in-

vestigation of the electrothermal atomization processes is carried out recently in a great number of laboratories [11]. However, atomization processes occur in the sources used with a high rate, *i.e.* the temperature changes about 2000 K between room temperature and vapour state of the sample so rapidly that no information is obtainable on fine details of processes of evaporation, several thermal reactions and dissociation. To obtain proper information, *i.e.* to follow the effects of introduction of thermal energy, a microreactor was constructed, in the form of a small-size oven with controlled heating and with very little ineffective volume. The emission signal of a known element present in the gaseous products obtained was used to detect the thermal processes, by introducing the gaseous phase from the microreactor directly into a stabilized d.c. arc source [12].

Microreactor

The design was based first in a widely adopted type of a quartz (or in an other variant stainless steel) tube thermal reactor with external heating. Better heat transfer and temperature control had been achieved by a resistance-heated graphite-tube furnace in which a sample (or a mixture with additives) was introduced in a platinum boat; the heated graphite tube was protected with argon gas, streaming in a quartz shell. Volatile components were purged

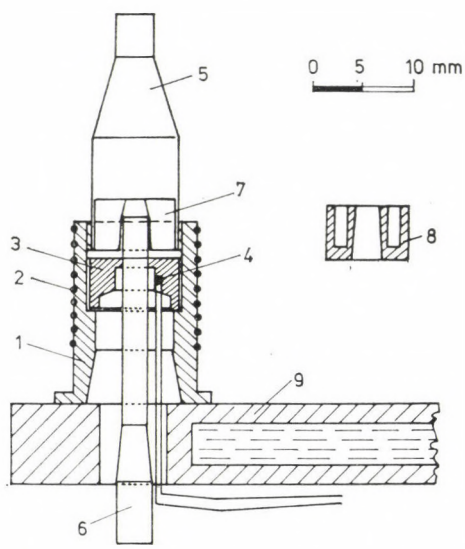

Fig. 1. Scheme of the microreactor, and crucibles; 1 — ceramic cylinder, 2 — resistor wire (PtRh, *dia.* 0.5 mm), 3 — nickel ring, 4 — thermocouple (Pt—PtRh), 5 — platinum stack (wall thickness 0.3 mm), 6 — gas introducing tube (platinum, 0.3 mm thick), 7 — platinum crucible (0.3 mm wall thickness), 8 — graphite crucible (1 mm wall thickness), 9 — water-cooled base (bronze)

at different temperatures under the heating period with a slow argon stream coming from the furnace tube.

Problems were encountered with tube furnaces due to their relatively high thermal inertia, great ineffective volume and obviously high and hardly controllable temperature gradient within the sample. To eliminate these defects, a microreactor with a platinum stack was designed (Fig. 1).

The microreactor, built on a water-cooled base, was fixed on the arc stand of a spectrograph. Samples (in μg-s or mg-s) to be investigated in solid state or solution form were weighed in a ring-shaped platinum or graphite crucible, and an argon carrier gas was conducted through the axial bore of the crucible. A temperature of 1350 °C was attained in the microfurnace in 2.5 min, at a max. power input of 12 V, 18 A on the heating wire (PtRh). Approximate temperature of the sample in the crucible was measured by a thermocouple (Pt-PtRh) and a temperature-graduated millivoltmeter or a line recorder. Crucibles are tightly fitted to the platinum stack (clearance being 0.01—0.02 mm), and the volatile components of the sample are taken by the carrier gas through the tube-electrode directly into the radiation source.

Radiation source

High-voltage spark discharge yielded suitably reproducible results but detection power of the method was not sufficient to determine micro-quantities of the volatile components. The d.c. arc source of high detection power, on the other hand, shows sufficient reproducibility only in the case of an effective stabilization. For the sake of stabilization a number of experiments were carried out with water-cooled discs, a neutral gas stream or an external magnetic field. The use of a water-cooled disc with a diameter of 2 or 3 mm axial bore necessitated the adoption of a too high electrode gap, and failed to achieve a sufficient stability in itself, at the same time hindering the application of other methods of stabilization. This is why it was scrapped. Argon gas stream was introduced at both electrodes axially but no optimal streaming ratio was found at which plasma dynamics would not be disturbed; therefore, only the carrier gas stream of the microreactor was adopted, introduced axially into the plasma through the lower tube-electrode.

For the purpose of magnetic stabilization, both water-cooled aluminium discs were provided with magnetic coils at first; since the magnetic coils were series-connected, a homogeneous external magnetic field was obtained. Later on, the lower magnetic coil was eliminated, because the water-cooled disc of the coil lowered the temperature of the platinum stack, being in contact with it, as a consequence of which several components of the vapour phase deposited from the carrier gas on the stack. Supplying power through a platinum wire

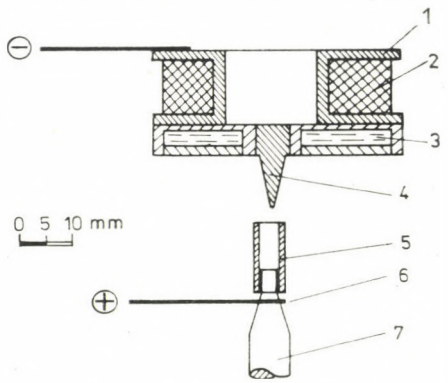

Fig. 2. Structure of the radiation source; 1 — aluminium disk, 2 — magnetic coil, 3 — water-cooled electrode holder, 4 — conical graphite cathode, 5 — graphite tube-electrode, 6 — connection to the anode (platinum wire of *dia.* 0.7 mm), 7 — platinum stack

0.7 mm in diameter, no significant temperature gradient was observable along either the platinum stack or the graphite tube-electrode; the magnetic field turned inhomogeneous in this manner is sufficient to stabilize the radiation source. The arrangement of the radiation source is shown on Fig. 2; this was found to be most suitable for further tests.

Radiation detector and recorder

For selecting the spectral line of the analysis element a plane-grating spectrograph was used. By recording line intensities on a spectral plate, only an integrated information of suitably long time intervals could be obtained (for the given microsamples and low concentrations of approx. 20—30 s periods). Detecting and recording spectral line intensities on periodically forwarded spectral plates, only coarse steps of thermal processes could be followed, and, moreover, the reproducibility of the measurement was limited by the emulsion characteristics. A suitable time-resolution and reproducibility could be achieved only by photoelectric detection. For this purpose, the cassette of spectrograph was replaced by an adapter, consisting of an exit slit, horizontally split at the middle (slit block of TB 3 spectroscope — with the permission of T. TÖRÖK), and of two photomultipliers, complete with the necessary stabilized supply units. The bottom section of the slit can be shifted off the top section along the wavelength axis by a micrometer-screw, and by means of both multipliers directly a background-corrected signal can be obtained.

System of apparata and experimental conditions

Block scheme of the system consisting of the units treated before is shown on Fig. 3. Experimental conditions established in the course of the investigations, and adopted for the further tests are as follows.

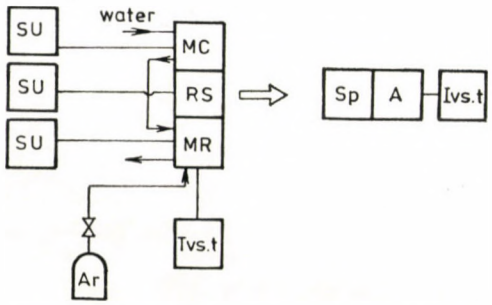

Fig. 3. Block scheme of the apparata system; SU — supply unit, MC — magnetic coil, RS — radiation source, MR — microreactor, Sp — spectrograph, A — photoelectric adapter, "*I vs. t*" and "*T vs. t*" — recorders

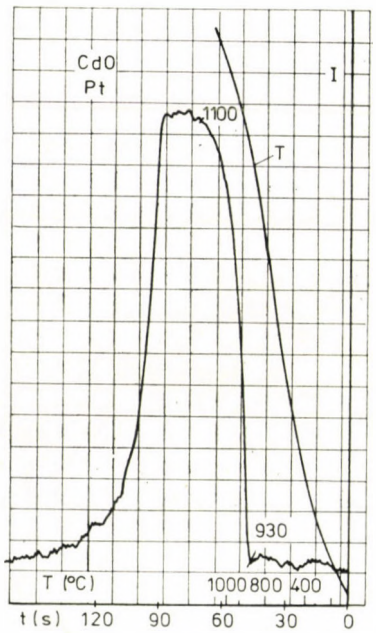

Fig. 4. Spectral line intensity and temperature (T) records with determined identification and peak temperatures

Heating rate of the microreactor was controlled manually so as to attain a temperature of 1000 °C in about one minute. Thermal processes taking place during the heating can be identified in this case in the form of apparent peaks or distinct points on the emission intensity signal recorded by means of a line recorder. Temperature of the microreactor was also recorded at the same time (double-line recorder), as apparent from Fig. 4. Temperature measured by the

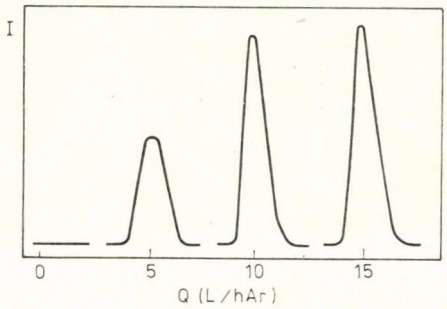

Fig. 5. Effect of the volume rate of the carrier gas streaming on the peak height (solution of $CdSO_4$, platinum crucible)

built-in thermocouple was controlled by a second thermocouple introduced for this purpose into the crucible, as well as by recorded peaks of well-known modification temperatures, and deviations of max. ± 20 °C were observed.

The rate of the carrier gas passing the crucible of the microreactor was selected so as to achieve optimal emission intensity (Fig. 5), without upsetting plasma dynamics of the source; optimum value of gas stream velocity was obtained as 10 L/h*.

Charged particles of a d.c. arc plasma in an external magnetic field are forced to rotate, thereby source stability being enhanced. At the same time, residence time of emitting particles is also prolonged, and detection power improved.

Under the influence of the sample material introduced into tha plasma the rate of rotation changes [13]; in the case of investigation of solutions, vapours of water and acids leave the reactor at a temperature between 60—150 °C, and plasma rotation takes place at a low value of magnetic induction (1,2 mT), moreover, in this period of intensive evaporation, at higher induction values the arc also burns out. According to this, in our investigations at the lower temperature interval a suitable low induction was applied but after that a more convenient higher induction value (12 mT) was adopted. In these conditions the stability of the d.c. arc approaches that of a mercury spectral lamp (intensity fluctuations of the stabilized d.c. arc were about 1.5 times as high as those of a mercury lamp), according to the undamped curves on Fig. 6.

A plane-grating spectrograph (C. Zeiss, Jena, type PGS 2) was used to select the analysis line of a characteristic element of vapours volatilized in the microreactor, and excited in the source. Grating characteristics were: 651

* It can be noted that experiments were carried out with periodically pulsed introduction of sample vapours but, in this case, an enhanced rate of passing the plasma resulted a reduction of residence time and therefore a decrease of detection power.

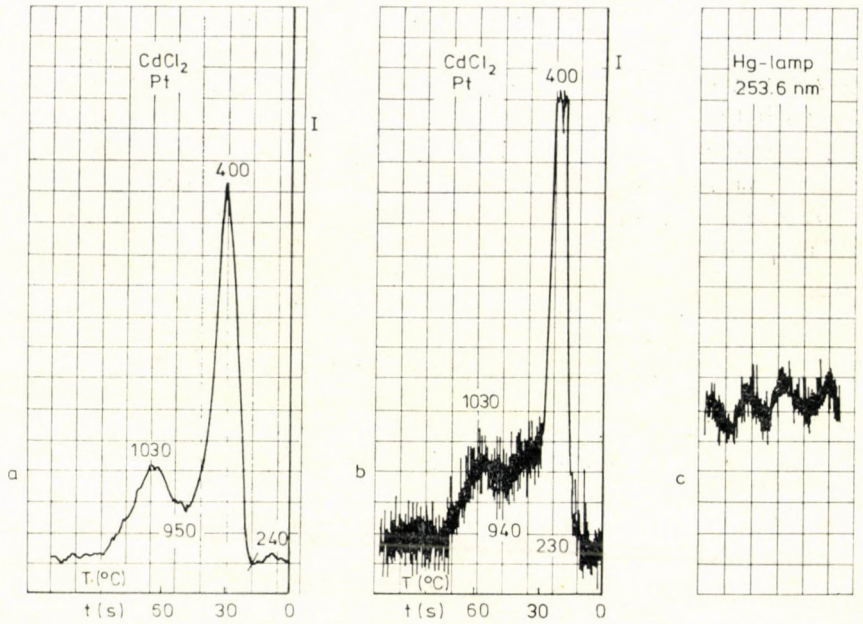

Fig. 6. Recorded emission signal of the evaporation process of $CdCl_2$, *a)* condenser-damped, and *b)* undamped; *c)* signal of a mercury lamp, undamped

grooves/mm, $\alpha_{blaze} = 5.23°$, reciprocal linear dispersion in the ultraviolet range ($m = 1$) 0.76 nm/mm. Radiation detector consists of two photomultipliers (EMI 6256S), on the working resistor (8 MOhm) of which, connected into the anodic circuit of both multipliers, appears a voltage signal which controls the gride voltage of an electrometric valve playing the role of impedance matching between the multiplier and the transistorized two-step differential amplifier. Both valves are provided with independent amplifier systems. Background-free spectral line intensities can be measured directly by means of a recorder connected with the output hot points of the amplifiers so as to set up (by means of an oscilloscope) the fixed half of the output slit of the adapter at the wavelength of the selected spectral line, adjusting the angle of the grating, and to shift the movable half of the slit onto the wavelength of the background radiation. A voltage divider was used at one of the outputs to balance the difference between both multipliers. To compensate fluctuations of the radiations of the radiation source, the signal obtained on the outputs was smoothed by a condenser ($C = 1000\ \mu F$) which caused only a negligible delaying effect (it resulted a relaxing time $T = \sqrt{RC} = 1$ s, at an output impedancy of 1 kOhm).

Conclusions

By using this system of apparata, under the experimental conditions established before, evaporation and conversion processes or thermal reactions carrying out at different rates in the microreactor could be followed on the base of intensity changes of the emitting element. Experimental results obtained with several sample types will be dealt with and discussed in the second part of the publication.

REFERENCES

[1] NICKEL, H.: Proc. XX. Coll. Spectr. Inter., Prague, 1977. Invited Lect. I, p. 27
[2] JONES, J. L., DAHLQUIST, R. L., HOYT, R. E.: Appl. Spectr., **25,** 628 (1971)
[3] RAJIĆ, S. R., VRGA, V., PAVLOVIĆ, A. R.: Mikrochim. Acta, **1976,** 93
[4] STURGEON, R. E., CHAKRABARTI, C. L., LANGFORD, C. H.: Anal. Chem., **48,** 1792 (1976)
[5] STURGEON, R. E., CHAKRABARTI, C. L.: Spectrochim. Acta, **32B,** 231 (1977)
[6] VAN den BROEK, W. M. G. T., de GALAN, L.: Anal. Chem., **49,** 2176 (1977)
[7] KÁNTOR, T., PUNGOR, E.: Spectrochim. Acta, **29B,** 139 (1974)
[8] MOSSOTTI, V. G., LAOUA, K., HAGENAH, W.-D.: Spectrochim. Acta, **23B,** 197 (1967)
[9] KÁNTOR, T., PUNGOR, E.: Proc. XIX Annual Hung. Symp. on Spectral Anal., Győr, 1976. II/17 p. (in Hung.)
[10] POSTA, J., PAPP, L.: Proc. XIX. Annual Hung. Symp. on Spectral Anal., Győr, 1976. IV/9 p. (in Hung.)
[11] XX. Coll. Spectr. Inter., Prague, 1977. Abstracts Nr. 136, 150, 151, 152; 540—551, 553—562, 565.
[12] KREITER, J.: Dissertation. Veszprém, 1977 (in Hung.)
[13] MÉRAY, L.: XX. Coll. Spectr. Inter., Prague, 1977. Abstract Nr. 74

Ernő GEGUS
József KREITER
László MÉRAY
János INCZÉDY
H-8200 Veszprém

Acta Chimica Academiae Scientiarum Hungaricae, Tomus 100 (1—4), pp. 229—242 (1979)

ON THE ROLE OF THE STRONG CHEMISORPTION IN THE STEADY STATE ANODIC POLARIZATION BEHAVIOUR OF SIMPLE ORGANIC COMPOUNDS AT PLATINIZED PLATINUM ELECTRODES

G. HORÁNYI and G. INZELT[1]

(Central Research Institute for Chemistry of the Hungarian Academy of Sciences,

[1] *Department of Physical Chemistry and Radiology L. Eötvös University, Budapest)*

Received July 5, 1978

Accepted for publication August 2, 1978

Views on the role of strongly chemisorbed species in the electrooxidation of simple organic compounds were surveyed. Instead of methanol oxidation, oxidation of ethylene glycol and its oxidation products was proposed as model system for the elucidation of the problems. It has been shown that in this case the chemisorption plays a subordinate role in comparison with the main oxidation reactions. Despite of this situation the shape of the initial section of the polarization curves is determined by the behaviour of the strongly chemisorbed species. The validity of mechanistic assumptions were supported by experimental results obtained by the use of radiotracer adsorption method.

In the last twenty years several efforts have been made to give a generalized picture of the chemisorption and the electrooxidation of simple organic compounds on platinum group metals [1]—[3]. In a recent paper by BAGOTSKII *et al.* [4] an attempt was made to explain the fundamental phenomena observed in the course of the chemisorption and electrooxidation of simple organic compounds. A generalized scheme involving both chemisorption and oxidation was proposed for the compounds containing one carbon atom. The different reaction paths starting from methane, methanol, formaldehyde, formic acid were analysed. The validity of the considerations was assumed in the case of more complicated systems, too.

In the case of the chemisorption and oxidation of methanol the corresponding part of the scheme given in [4] is as follows:

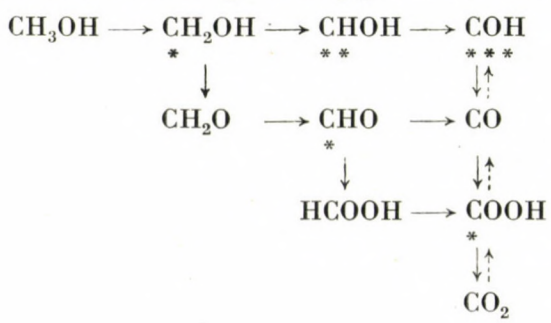

For the formation of formaldehyde and formic acid the following equations are given

$$\overset{*}{CH_2OH} + OH_{ads} \longrightarrow CH_2O + H_2O$$

$$\overset{**}{CHOH} + 2\,OH_{ads} \longrightarrow HCOOH + H_2O\,.$$

In connection with the scheme proposed some remarks should be made as it is at variance with previous considerations and experimental results [5]—[8]. In the works cited it is assumed that the formation of formaldehyde and formic acid occurs *via* weakly adsorbed species. It has been shown in [9] that formaldehyde found in the solution phase is the main primary product of the methanol oxidation at a smooth platinum electrode. (The current efficiency with respect to CH_2O was 95%.) This means that the desorption of CH_2O and HCOOH should be taken into consideration. On the other hand it is a fact that formaldehyde and formic acid dissolved in the bulk solution phase adsorb and chemisorb on the surface of the electrode. Thus the adsorption and desorption of both species should be taken into account in mechanistic considerations. The existence of simultaneous adsorption and desorption processes can not, however, be explained without the assumption of weakly bounded adsorbed species as it is pointed out in [5], [7]. Another problem with the methanol oxidation is the very fact, that the steady state polarization curves presented in the literature are regular Tafel lines. This observation is at variance with different mechanistic considerations and other experimental results. The existence of parallel paths, the poisoning effect of strongly chemisorbed species on the oxidation rate, the potential dependence of the product composition cannot be reconciled with a regular Tafel-line, thus the origin of the experimental Tafel relationship is not easily interpretable in the case of these reactions [1].

Regarding the problems outlined above it seems to us that the chemisorption and oxidation of methanol, formaldehyde and formic acid cannot be considered as an adequate model for the generalization of chemisorption and oxidation of simple organic compounds.

In previous communications [10]—[14] results on the electrochemical behaviour of ethylene glycol and its oxidative derivatives were reported. The results obtained suggest the assumption that the link of chemisorption and oxidation is more easily interpretable in this case that in the case of the methanol.

This assumption is based on the following main experimental observations
i) No Tafel lines were obtained from steady state polarization measurements.
ii) Changes in the composition of the products are reflected in the shape of the polarization curves.
iii) In certain potential range the rate of the oxidation of strongly chemisorbed

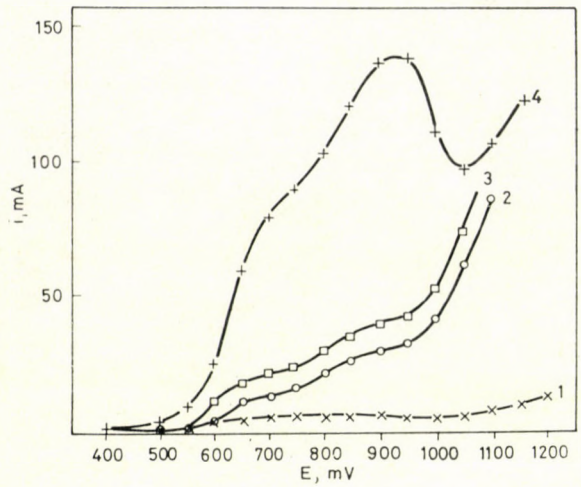

Fig. 1. Polarization curves: (1) glycolic acid, (2) glyoxalic acid, (3) glyoxal, (4) ethylene glycol

molecules resulting in CO_2 may be neglected in comparison with the rate of the formation of intermediates migrating into the solution phase.

In Table I the main products of the oxidation of the compounds studied at different potentials are tabulated.

The polarization curves are shown in Fig. 1. The chemisorption of these compounds was studied by several authors [15]—[20]. From these studies it is known that the coverage with respect to strongly chemisorbed molecules is negligible above 800 mV (rhe). Thus it is the first section of the polarization curves which may reflect the effect of chemisorbed molecules on the oxidation rate. (Bearing in mind the results presented in Table I the second increasing section of the polarization curves may be explained by the increasing of the formation rate of CO_2.) In the potential range corresponding to the first section of the polarization curves there are no significant changes in the composition of the products of the reaction. This means that the potential has no effect on the relative rates of the different reaction steps at least in the potential range considered. At the same time there is a plateau-like section following the first increasing part of the polarization curves *i.e.* the rate of the overall reaction does not depend significantly on the potential in this potential region. As the first increasing section on the polarization curve corresponds to the potential range where the decrease of the steady state coverage with respect to strongly chemisorbed molecules occurs it may be assumed that the shape of the polarization curves may be explained by this phenomenon assuming that the rate of the main reactions resulting in oxalic acid end-product does not depend on the potential. On the basis of the above considerations the

Table I

Compound	Potential (mV)	Products (current efficiency)*			
		HOOC—COOH		CO_2	
	700 mV	95%		5%	
OHC—COOH	800 mV	80%		20%	
	900 mV	45%		55%	
	1000 mV	5%		95%	
		HOOC—COOH		CO_2	
	600 mV	50%		8%	
$HOCH_2$—COOH	700 mV	50%		5%	
	800 mV	40%		8%	
	900 mV	10%		30%	
	1000 mV	4%		45%	
		HOOC—COOH		CO_2	
OHC—CHO	650 mV	50%		5%	
	900 mV	40%		20%	
	1000 mV	20%			
$HOCH_2$—CHO	600—	OHC—CHO	$HOCH_2$—COOH	HOOC—COOH	CO_2
	700 mV	80—90%		1—2%	5%
		$HOCH_2$—CHO	CO_2	OHC—CHO	
	575 mV	85%	5%		
$HOCH_2$—CH_2OH	625 mV	75%	5%		
	675 mV	60%	5%		

* Conversion of the primary compound is lower than 10%

following generalized scheme may be given for the oxidation of ethylene glycol and its derivatives. The scheme involves

a) Ad- and desorption processes of weakly adsorbed species

b) The strongly chemisorbed species are formed from the weakly adsorbed ones

c) There is no strong chemisorption in the case of glycolic and oxalic acids. (The reversibility of the adsorption of these compounds was shown in [21], [22].)

d) The oxidation process takes place stepwise, via weakly adsorbed species.

It is known that the strong chemisorption is a dehydrogenation (oxidation process). During the chemisorption process an adsorption product of high

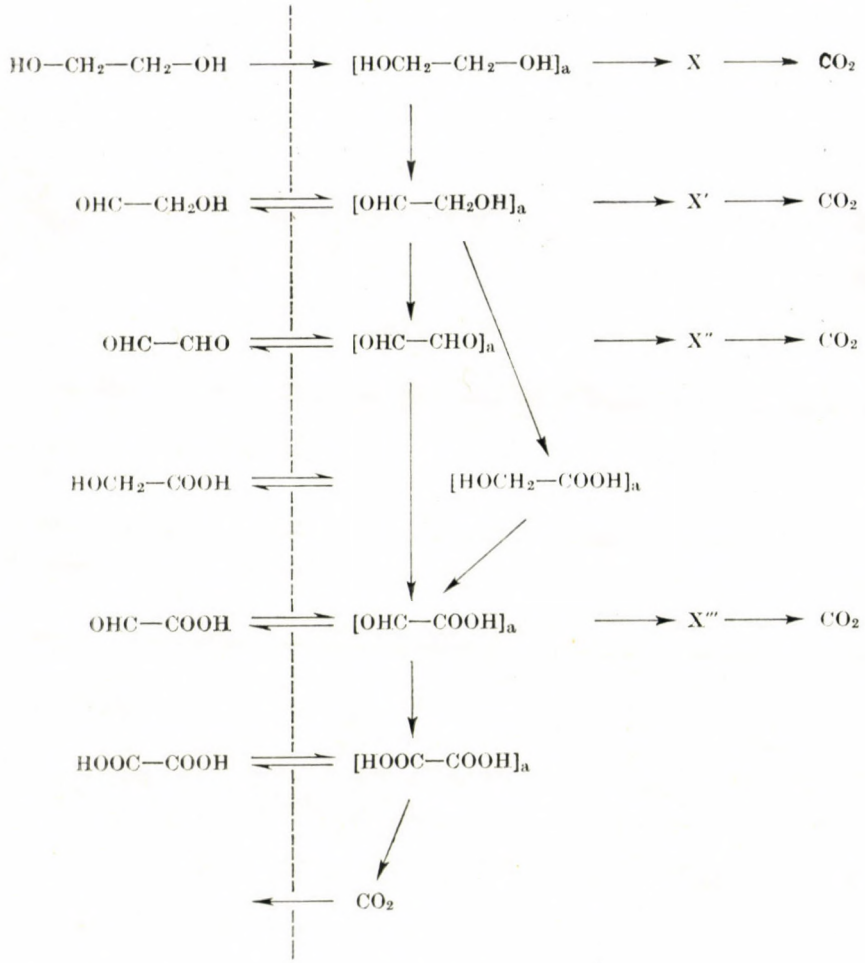

Scheme 1

degree of oxidation is obtained [15]—[20]. It would be impossible to observe all the intermediates in the solution phase if the process occurred via strongly chemisorbed species. More detailed mechanistic and kinetic considerations in the case of glyoxalic acid are given in [12]. The scheme presented above may be accepted as a first approximation only, more detailed studies are needed in order to have a deeper insight in the processes. One of the most important problems is to examine the validity of the assumption that the rate of the oxidation process in the potential range corresponding to the first section of the polarization curves is governed by the coverage with respect to the strongly chemisorbed species. To this end a radiotracer adsorption method was used. The results of these studies are presented in the following part of the paper.

Indirect radiotracer study of the adsorption of organic compounds

In a previous communication [23] it has been shown that the study of the adsorption of labelled non-reacting species which are present in low concentration may furnish informations concerning the processes taking place on the surface of the electrode in the course of the electrooxidation of organic compounds. As the study of the adsorption of the labelled reacting species encounters several problems the use of this method may be suggested for the indirect study of the adsorption of the reacting organic compounds. Anions (Cl^- labelled with Cl-36, $H_2PO_4^-$ labelled with P-32) simple organic compounds

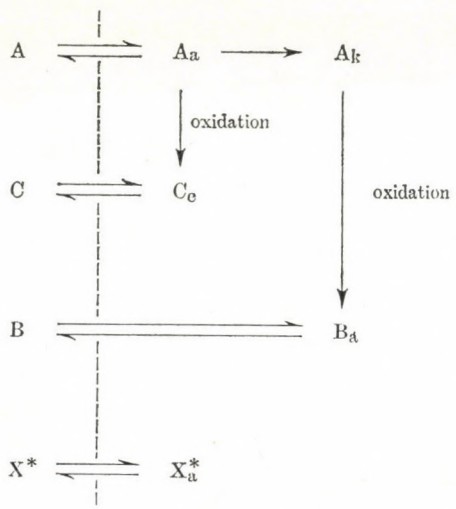

Scheme 2

(urea labelled with C-14) may be chosen as labelled partners. The reversibility of the adsorption of these species is a very important criterion of the choice. First of all it should be examined what kind of relationships between count rate, time, current may be expected on the basis of previous consideration in a system containing labelled nonreacting species.

To this end let us consider a simplified version of the reaction scheme proposed above involving a single main reaction only (for instance the conversion of glyoxylic acid to oxalic acid).

In Scheme 2 A is the compound studied, C is the product of the main reaction. By A_k is denoted the strongly chemisorbed form of A and B is the oxidation product of A_k, A_a, C_a, B_a are the weakly adsorbed forms of the species considered. X* is the labelled nonreacting species added to the system for the study of the adsorption phenomena.

Assuming Langmuir equilibrium conditions with respect to A, B, C and X* the following equations may be given

$$k_i c_i(1 - \Sigma\theta_i - \theta_k - \theta^*) = k_d^i \theta_i \tag{1}$$

$$k^* c^*(1 - \Sigma\theta_i - \theta_k - \theta^*) = k_d^* \theta^* \tag{2}$$

where i = A, B, C, θ_i-s are the coverage values with respect to the A, B and C components, θ_k and θ^* refer to chemisorbed and labelled species, respectively. By c is denoted the concentration.

From eqs (1) and (2) it follows that

$$\theta_i = \alpha_i \theta^*, \tag{3}$$

where

$$\alpha_i = \frac{k_d^* k_i c_i}{k_d^i k^* c^*}.$$

For θ_k the following relationship is obtained:

$$\theta_k = 1 - \beta\theta^*, \tag{4}$$

where

$$\beta = \left(\Sigma\alpha_i + 1 + \frac{k_d^i \alpha_i}{k_i c_i}\right) = 1 + \frac{k_d^*}{k^* c^*}\left(\Sigma \frac{k_i c_i}{k_d^i} + 1\right).$$

According to the scheme proposed the strongly chemisorbed species are formed from weakly adsorbed ones. On the other hand the oxidation rate of the chemisorbed molecules is proportional to θ_k (at a given potential). According to this

$$\frac{d\theta_k}{dt} = k\theta_A - k_0\theta_k. \tag{5}$$

At steady state conditions $\left(\frac{d\theta_k}{dt} = 0\right)$

$$\theta_k = \frac{\alpha_A k}{k_0}\theta^*. \tag{6}$$

The attainment of the steady state with respect to θ_k and current after a potential change is, generally, a slow process and using eq. (5) there is a possibility to study the transient phenomena.

From eq. (5) we obtain

$$\frac{d\theta^*}{dt} = A - B\theta^*, \tag{7}$$

where $A = \frac{k_0}{\beta}$. $B = k_0 + \frac{k\alpha_i}{\beta}$,

Solving eq. (7) assuming that at $t = 0$, $\theta^* \approx 0$ ($\theta_k \approx 1$)

$$\theta^* = \frac{A}{B}(1 - e^{-Bt}) \tag{8}$$

is obtained.

For the rate (i) of the A → C transformation the following equation may be given:

$$i = k_r \theta_A = k_r \alpha_A \theta^* \tag{9}$$

The radiation measured (I) is proportional to θ^* ($\theta^* = pI$) and eqs (8), (9) take the following form

$$I = \frac{A}{Bp}(1 - e^{-Bt}) \tag{10}$$

$$i = k_r \alpha_A p I \tag{11}$$

Summarizing our considerations the following features between count rate time and current may be expected at a given potential:

i. In transient measurements starting from $\theta_k \sim 1$ the validity of eq. (10) should be found.

ii. Linearity should be found between the count rate and the current measured.

The experimental results obtained with different systems are in good accordance with these expectations.

The experiments were carried out using Cl-36 labelled HCl, P-32 labelled phosphoric acid and C-14 labelled urea.

The experimental procedure was the same described in previous publications [21]—[25]. The labelled species were used in low concentration ($< 10^{-3}$ M). All measurements were carried out in M $HClO_4$ supporting electrolyte.

In the first run of experiments the transition phenomena were studied switching the potential from a value where no oxidation occurs to a given value where a measurable steady-state oxidation rate may be expected. This means that at the initial conditions the surface of the electrode is occupied by chemisorbed particles and the coverage (count rate) with respect to the labelled compound is very low. After the switching both count rate and current increase simultaneously as it is shown in Fig. 2.

It is easy to show that there exists a proportionality between the measured i and count rate values, *i.e.* the expectations corresponding to eq. (9) are fulfilled. This is shown in Fig. 3.

In order to analyse more easily the time dependence of the count-rate eq. (10) should be transformed into the form

$$\Delta I = \frac{A}{Bp} e^{-Bt_2}(1 - e^{B\Delta t}), \tag{12}$$

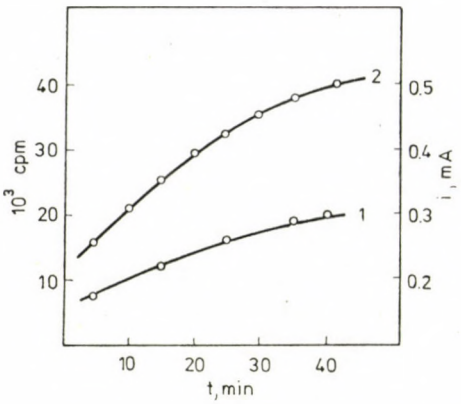

Fig. 2. Simultaneous measurement of the adsorption of Cl^- ions (2) and current (1) in the course of the electrooxidation of glyoxalic acid $E = 600$ mV, $c_{HCl} = 10^{-4}$; $c_{\text{glyoxalic acid}} = 10^{-1}$ mol dm^{-3}

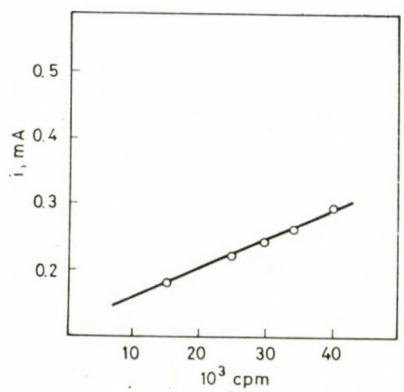

Fig. 3. Count rate — current relationship in the case presented in Fig. 2

where

$$\Delta I = I(t_2) - I(t_1)$$

$$\Delta t = t_2 - t_1 .$$

Plotting the logarithm of ΔI values belonging to an arbitrary chosen Δt = constant against the t_2 values a linear relationship should be found in the case of the validity of eq. (10). Some curves obtained from the experimental results are shown in Fig. 4. Linearity may be observed according to the expectations.

The adsorption competition of weakly adsorbed species and anions may be shown in the case of oxalic acid. Oxalic acid forms weakly adsorbed species, only in the potential range of its oxidation [21], [24]. In the experiments with oxalic acid labelled phosphoric acid was used for the indirect adsorption studies.

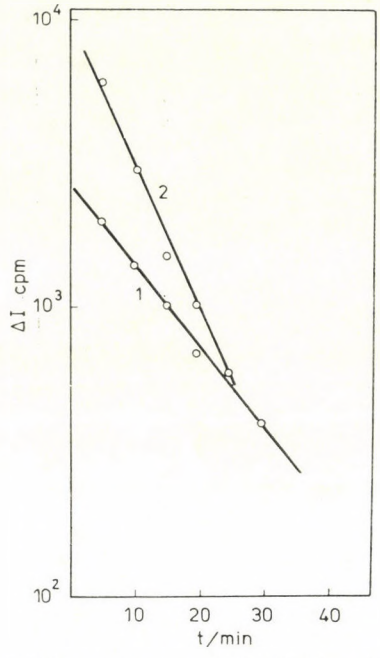

Fig. 4. lg ΔI—t curves [according to the eq. (12)]; (1) Glyoxal 10^{-1} mol dm^{-3}, (2) Ethylene glycol 0.3 mol dm^{-3}, $c_{HCl} = 10^{-4}$ mol dm^{-3}

In Fig. 5 the potential dependence of phosphoric acid adsorption is shown in the presence of oxalic acid at different oxalic acid concentrations. The maximum observed in the presence of pure supporting electrolyte, *i.e.* the decrease of the adsorption above 800 mV is a result of the oxygen adsorption. In the presence of oxalic acid the position of the maximum shifts to more positive potentials. This phenomenon is connected with the existence of simultaneous processes:

a) chemisorption of oxygen,

b) adsorption of oxalic acid and phosphoric acid on the sites not occupied by adsorbed oxygen, and

c) oxidation of adsorbed oxalic acid.

There is a competition between phosphoric and oxalic acids for the sites not occupied by oxygen.

As the adsorbability of oxalic acid is greater than that of phosphoric acid a significant part of the latter is displaced by the former even at low oxalic acid concentration. With increasing potential the oxidation rate of oxalic acid increases. It has been shown in a previous communication [24] that the rate of the oxidation of oxalic acid (i) obeys the following equation:

$$i = k_a \theta_a 10^{bE}, \tag{13}$$

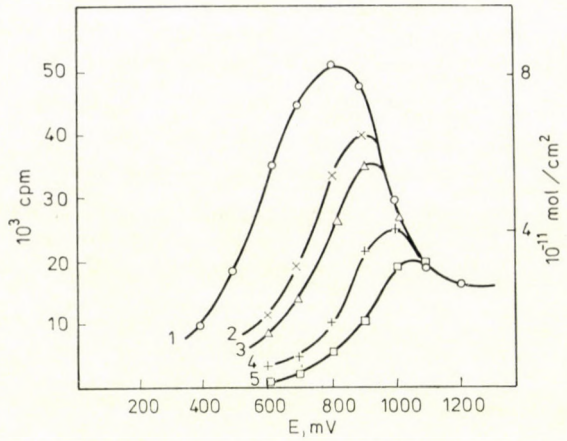

Fig. 5. The potential dependence of the adsorption of labelled phosphoric acid; $c_{H_3PO_4} = 5 \times 10^{-4}$ mol dm^{-3}. $c_{C_2H_2O_4}$: (1) 0; (2) 5.8×10^{-5}; (3) 1.7×10^{-4}; (4) 7.3×10^{-4}; (5) 2.6×10^{-3} mol dm^{-3}

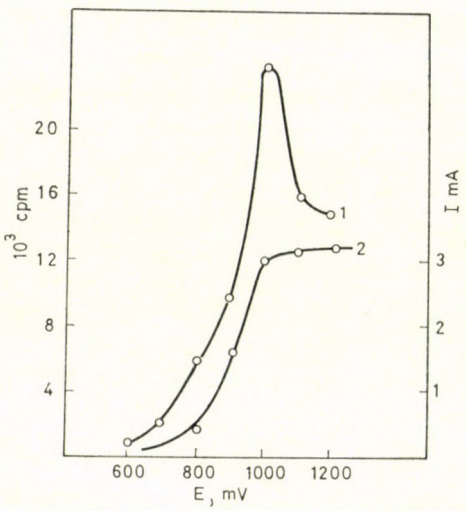

Fig. 6. Simultaneous measurement of the adsorption of labelled phosphoric acid ($c = 5 \times 10^{-4}$ mol dm^{-3}) and the oxidation rate of oxalic acid ($c = 2.6 \times 10^{-3}$ mol dm^{-3}); (1) count rate, (2) current

where k_a and b are constants, θ_a is the coverage with respect to the oxalic acid, E is the potential.

In Fig. 6. the i and $\Gamma_{H_3PO_4}$ *v.s.* potential curves are presented at a given H_3PO_4 and $H_2C_2O_4$ concentration. As the concentration of oxalic acid is low, a limiting diffusion current is obtained with increasing potential. According to eq. (13) θ_a should decrease in the potential range corresponding to the limiting current (i = const). This means that the number of the sites available for the

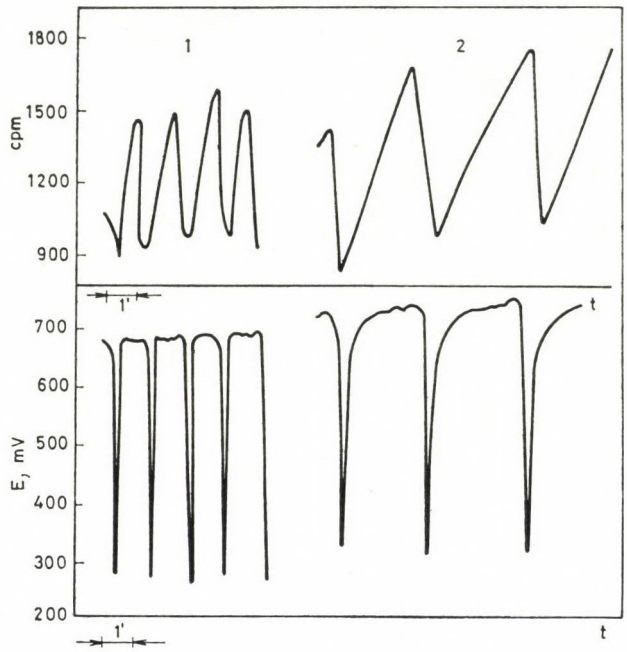

Fig. 7. Simultaneous potential and urea adsorption oscillation in the course of the galvanostatic electrooxidation of glyoxal; (1) $c_{\text{glyoxal}} = 2.5\times10^{-2}$ mol dm^{-3}; $c_{\text{urea}} = 6.8\times10^{-5}$ mol dm^{-3}; $i = 7.5$ mA. (2) $c_{\text{glyoxal}} = 10^{-1}$ mol dm^{-3}; $c_{\text{urea}} = 4.5\times10^{-5}$ mol dm^{-3}; $i = 5$ mA

adsorption of labelled phosphoric acid should increase. This is reflected by the increase of the count rate with increasing potential as it is shown in Fig. 6. The decrease following the maximum is connected with the oxygen chemisorption. As θ_a with increasing potential tends to zero, the $\Gamma_{H_3PO_4} - E$ curves taken in the presence of oxalic acid approach to the curve taken without addition of oxalic acid and they coincide with the latter at potentials where the stationary coverage with respect to oxalic acid is practically zero. This coincidence may be seen in the case of the curves 2, 3, 4 and 5 of Fig. 5. Previous experiments with labelled oxalic acid [24] are in agreement with these statements.

Another interesting feature should be mentioned here. It is known from the literature that potential oscillations are produced in the course of the galvanostatic oxidation of different fuels [26]. This phenomenon presumably may be attributed to the inhibiting effect of chemisorbed molecules and to the existence of parallel reaction paths. In this respect too ethylene glycol and its derivatives behave similarly to the other compounds studied in the literature. The radiotracer method used here offers some possibility to gain more insight into the adsorption phenomena occurring in the course of potential oscillations. Some preliminary results were presented in a previous communi-

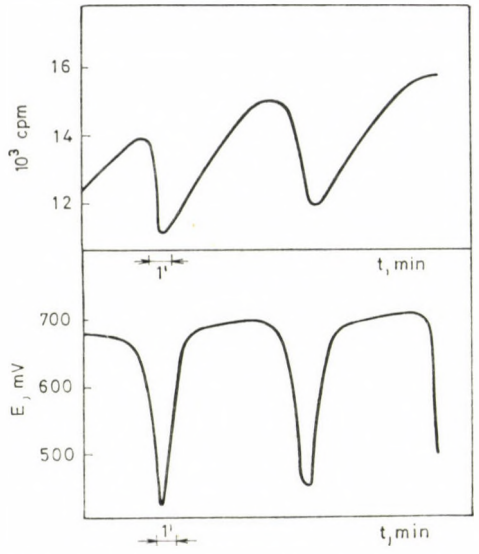

Fig. 8. Potential oscillations and periodical changes in the count rate in the course of electro-oxidation of ethylene glycol under galvanostatic experimental conditions $i = 2$ mA; ethylene glycol concentration $= 0.3$ mol dm^{-3}; $c_{HCl} = 10^{-4}$ mol dm^{-3}

cation [23]. In this paper it has been shown that the potential oscillations are accompanied by periodical changes in the adsorption of the non-reacting labelled species. In the case studied labelled Cl^- ions were used. Similar results were obtained using C-14 labelled urea as it is shown in Fig. 7.

On the basis of the considerations outlined above it would be very easy to assume that the periodical changes observed in the adsorption of the weakly adsorbed component reflect the changes in the number of surface sites freed from strongly chemisorbed species. It should, however, be taken into account that the extent of the adsorption of the labelled partner depends on the potential, and the sharp decrease of the adsorption following the decrease of the potential may be connected not only with the increase of the coverage with respect to the chemisorbed molecules, but with the decrease of the potential, too. Thus the interpretation of the experimental results considering the decrease of the adsorption encounters difficulties. In contrast to this the increasing section of the adsorption — time curve may be explained with the oxidation of chemisorbed species.

For example in the case of ethylene glycol the adsorption of Cl^- ions continues to increase while the potential does not change as it is shown in Fig. 8. The slow increase in the adsorption may reflect the slow elimination of chemisorbed particles. Finally, this process results in the increase of the "activity" (more available sites for a reaction) of the electrode with respect to the main reaction proceeding *via* weakly adsorbed species. As there are galvanostatic

experimental conditions the increase of "activity" should result in the decrease of the potential. It should be mentioned here that the desorption of anions with decreasing potential may accelerate the activation process resulting in more and more free sites. It is possible that the sharp decrease of the potential is connected with this phenomenon.

There is no possibility to give an unambigous explanation of the phenomena, but whatever the explanation may be it follows from the experimental results that the potential oscillations occur about the potential values where significant changes in the coverage with respect to the chemisorbed species may be expected.

REFERENCES

[1] BREITER, M. W.: Electrochemical Processes in Fuel Cells. Springer Verlag Berlin—Heidelberg—New York 1969
[2] DAMASKIN, B. B., PETRII, O. A., BATRAKOV, V. V.: Adsorptsiya organicheskikh soedinenii na elektrodakh. Nauka, Moscow 1968
[3] BREITER, M. W.: Adsorption of organic species on platinum metal electrodes in "Modern Aspects of Electrochemistry" Ed. by J. O'M. BOCKRIS and B. E. CONWAY Vol. 10. p. 161. Plenum Press. New York 1973
[4] BAGOTZKY, V. S., VASSILIEV, YU. B., KHAZOVA, O. A.: J. Electroanal. Chem. **81,** 229 (1977)
[5] BREITER, M. W.: Disc. Faraday Soc. **45,** 79 (1968)
[6] PODLOVCHENKO, B. I., FRUMKIN, A. N., STENIN, V. F.: Elektrokhimiya **4,** 339 (1968)
[7] PODLOVCHENKO, B. I., PETUKHOVA, R. P.: Elektrokhimiya **8,** 899 (1972)
[8] PODLOVCHENKO, B. I., PETUKHOVA, R. P.: Elektrokhimiya **9,** 273 (1973); **10,** 489 (1974)
[9] PETUKHOVA, R. P., STENIN, V. F., PODLOVCHENKO, B. I.: Elektrokhimiya **14,** 755 (1978)
[10] HORÁNYI, G., INZELT, G., SZETEY, É.: Acta Chim. Acad. Sci. Hung., **97,** 313 (1978)
[11] HORÁNYI, G., INZELT, G., SZETEY, É.: Acta Chim. Acad. Sci. Hung., **98,** 49 (1978)
[12] INZELT, G., HORÁNYI, G.: Acta Chim. Acad. Sci. Hung. (In press)
[13] INZELT, G., HORÁNYI, G.: Acta Chim. Acad. Sci. Hung. (In press)
[14] INZELT, G., HORÁNYI, G.: Acta Chim. Acad. Sci. Hung. (In press)
[15] BAGOTZKY, V. S., VASSILIEV, YU. B.: Electrochim. Acta **11,** 1439 (1966)
[16] TRASATTI, S., FORMARO, L.: J. Electroanal. Chem. **17,** 343 (1968)
[17] FORMARO, L., CASTELLI, G.: J. Electroanal. Chem. **28,** 363 (1970)
[18] SIDHESWARAN, P.: J. Electrochem. Soc. India **81,** 24 (1975)
[19] SIDHESWARAN, P.: Ind. J. Chem. **12,** 1077 (1974)
[20] BIANCHI, G., FORMARO, L., TRASATTI, S.: Chim. Ind., **50,** 26 (1968)
[21] HORÁNYI, G., HEGEDÜS, D., RIZMAYER, E. M.: J. Electroanal. Chem. **40,** 393 (1972)
[22] HORÁNYI, G., VÉRTES, G., RIZMAYER, E. M.: J. Electroanal. Chem. **48,** 207 (1973)
[23] HORÁNYI, G., INZELT, G.: J. Electroanal. Chem. **87,** 423 (1978)
[24] HORÁNYI, G., VÉRTES, G.: J. Electroanal. Chem. **43,** 225 (1973)
[25] HORÁNYI, G., SOLT, J., NAGY, F.: J. Electroanal. Chem. **31,** 87 (1971)
[26] WOJTOWICZ, J.: Oscillatory Behaviour in Electrochemical Systems, in Modern Aspects of Electrochemistry Vol. **8.** Plenum Press. New York 1972

György HORÁNYI H-1025 Budapest, Pusztaszeri út 59—67.
György INZELT H-1088 Budapest, Puskin u. 11—13.

Acta Chimica Academiae Scientiarum Hungaricae, Tomus 100 (1—4), pp. 243—256 (1979)

CONNECTION BETWEEN ELECTRIC CONDUCTIVITY AND VISCOSITY IN AQUEOUS AND HYDROCHLORIC METAL CHLORIDE SOLUTIONS

E. BERECZ and I. BÁDER

(Department of General and Physical Chemistry, Technical University for Heavy Industries, Miskolc)

Received July 5, 1978

Accepted for publication July 31, 1978

Systematic investigations were carried out for a more thorough understanding of the behaviour of solution systems of type $MCl_x - H_2O$ and $MCl_x - HCl - H_2O$ on the basis of the experimental results and the functions of activation ($\Delta H_\eta^\ddagger$, $\Delta H_\Lambda^\ddagger$, $\Delta H_\eta^\ddagger/\Delta H_\Lambda^+$), as well as on some other useful functions (Λ_η, $\varkappa_\eta$, $\Lambda - \vartheta$) calculated from them. Conclusions have been drawn for the mutual connection of the electric conductance and the viscosity and for its dependence on the concentration. It was attempted also to interpret and to reconcile the results with the structural changes occurring by the change of concentration in the solution systems investigated.

Within the scope of our investigations connected with the aqueous and acidic solutions of strong electrolytes the authors investigated some physicochemical properties of the systems of types $MCl_x - H_2O$ and $MCl_x - HCl - H_2O$. These systems can be well measured, they are sensitive to changes in the structure, and important also for the practice. The main aim of the investigations was to get a deeper insight into the structural conditions mainly of the concentrated solutions on the basis of the interpretation and possible theoretical generalization of the experimental data obtained.

It was considered that besides the present state of research on the structure of ternary solutions the best possibilities are provided by suitable, comparative examinations permitting a uniform systematization on a fixed experimental basis.

At the same time, the study of ternary solutions was treated by us as a method of obtaining more detailed information on the structure of the constituent binary systems on the basis how the addition of a third component affects the properties of the original binary system.

The investigated properties were the following: the two main transport properties, the viscosity and the electric conductivity (and the adequate thermodynamic functions of activation calculated on their basis), the density (and the molar and excess volume calculated from the density), the vapor pressure conditions, in some systems the dielectric properties measured in the microwawe region, the solubilities of the appropriate salts, as well as their concentration and temperature dependence in the temperature range of

10—55 °C, and in the saturated and unsaturated solutions stable at given temperatures (except the concentration range of dilute solutions $m < 0.02$). During our previous work we examined and studied in detail the alkaline and alkaline earth metal chloride—HCl—H_2O, the $LaCl_3$—HCl—H_2O, and the $MnCl_2$—H_2O systems.

In our present paper we are dealing only with the electric conductivity and viscosity of the binary and ternary chloride systems under isothermic conditions, on this basis with their interrelation, and with their dependence on the structure.

In order to study the interrelation between the electric conductivity and viscosity in the binary and ternary solutions of metal chlorides in the first place we have to know the general line of their isothermal concentration dependence. We are referring to our earlier papers in regard to this, in which we have proved that the viscosity *vs.* molality curves of binary aqueous metal chloride solutions exhibit several bands [1]. The position of the bands is determined by the charge of cations, within the bands the sequence of the curves is determined by the size of the cations. Similarly it was shown [2] that the isothermic temperature dependence of the electric conductance in the solutions of binary aqueous metal chlorides differs from each other, as well as from that of the HCl, and it pointed to the different behaviour of the chlorides of transition metals with d-electrons concerning the dependence of the conductance on the concentration.

Namely, while the extent and the width of bands of specific conductivity and the slope and the width of bands of molar conductivity are the function of the cation charge within the bands according to the different cation charges the lines of the curves of specific conductivity *vs.* molality do not correspond to the adequate ionic size. The line of curves approaches to that of charged cations at smaller molalities and to that of triply charged cations at greater molalities. Consequently, the curve of $MnCl_2$ deviates practically from the adequate band, in spite of the fact that the size of the cation is between that of the Mg^{2+} and Ca^{2+}.

In the ternary solutions it was shown that the viscosity *vs.* molality diagrams of the systems of type MCl_x—HCl—H_2O can be classified in three characteristic types according to the cations of metal chlorides hydrating weekly positively (Na^+), strongly positively (Li^+, Mg^{2+}, Ca^{2+}, La^{3+}) and negatively (K^+, Rb^+, Cs^+).

At the same time the specific conductivity *vs.* molality diagrams can be classified in two characteristic types; in the case of both types occurs a so-called isothermal inversion acid concentration ($m_{HCl}^{inv,\varkappa}$). These data and other ones referring to this phenomenon (the cation radius the $\varkappa$-values belonging to the inversion acid concentration, the extent of the line $m_{HCl}^{inv,\varkappa}$ = constant, the hydration enthalpies giving information about the effectiveness of the hydra-

tion of ions [3]) can be seen in Table I. According to the data of Table I the inversion acid concentration increases with increasing cation size at identical cation charge, and its value can give information about the relative hydration power of the cations of the salt, like the hydration enthalpies.

On the structural relations developed in *ternary* solutions and determined decisively by ion-ion and ion-solvent interactions, and on the changes of these relations as a function of concentration, a certain information may be obtained also from the measure and direction of the shift of the maximum conductivity value $\varkappa_{max}$ found for binary $HCl-H_2O$ solutions, caused in ternary solution

Table I

Some characteristic data of aqueous metal chloride solutions

MCl_z	LiCl	NaCl	KCl	NH_4Cl	CsCl	$MgCl_2$	$CsCl_2$	$LaCl_3$
r_{cation}, nm	0.060	0.095	0.133	0.143	0.169	0.065	0.099	0.115
$m_{HCl}^{inv.\varkappa}$, 25 °C	1.0	1.5	3.4	3.5	3.8	0.6	0.9	0.98
$\varkappa_{inv.}^{25°}$, S cm^{-1}	0.30	0.45	0.72	0.73	0.75	0.18	0.30	0.31
$m_{HCl}^{inv.\varkappa} = \text{const.}$ m_{salt}	2.5	1.0	0.5	1.3	1.5	1.5	1.2	0.75
ΔH_{hidr}, J mol^{-1}	507	410	335	331	264	1968	1570	3215
$m_{salt, sat.}^{25°C}$	19.8	6.1	4.9	8.0	11.5	5.8	6.8	3.3

by the action of various salt components, and from the shape and features of the curves representing the course of the $\varkappa$-maximum in ternary systems [2].

It is evident from the curves that both the shape and direction of the slope of the curves, corresponding to cations with different hydration character, are very different. Moreover, the curve is sectioned similarly as has been found [4] in the investigation of the concentration dependence of various properties measured and calculated (thermodynamic functions of activation, molar volume, *etc.*) of the corresponding binary salt solutions. On the basis of comparative evaluation of these phenomena we have concluded that the change of the structure of binary aqueous salt solution is not monotonous, not uniform even on adding the salt to the solutions uniformly, and in each concentration interval of the nearly linear sections of the curves different dominating structural types exist, which turn into one another in the narrow surroundings of given values of concentration. Namely, the structure does not change monotonously in the function of concentration.

In the case of electrolyte solutions — certainly also in the case of solutions of other type — the close interconnection of electric conductivity and

the viscosity is absolutely evident being the mechanism of displacement of the moving unit (in the case of electrolyte solutions these can be simple or aqua-complex ions, or more complicated formations surrounded with solvent shell) similar in the case of both transport processes [5].

In one of the cases the electric field in the other case the mechanical, and gravitational one, respectively, is that, which makes the moving unit to leave its place through series of transitions from one equilibrium position to the other in a measure depending on its free enthalpy of activation determined by the structure of the solution. Clearly, the moving units with opposite changes move to opposite directions applying electric field, but meanwhile, the viscosity always counteracts the displacement of the moving units. But in the case of the displacement, caused by the influence of mechanical or gravitational field only (when the moving units with opposite charges move to the same direction) electric force reacting against the displacement does not arise (we can neglect the electroviscous effect in the electrolyte solutions), the viscosity can be regarded as an independent variable.

Properly, even the Falkenhagen and Wishaw-Stokes equations developed for the electric conductivity on the strength of Debye-Hückel theory denote the viscosity-electric conductivity relation, because the viscosity appears in it explicitly. But the given equations are valid only for dilute solutions, therefore several empirical equations were also developed which are valid more or less up to high concentrations [8].

In the course of our studies directed to reveal the relation toward the between viscosity and electric conductivity we came to the conclusion that the coupling of the viscosity and the specific electric conductivity can be made with more reason than that of the viscosity and molar electric conductivity, because the formers are both specific properties. At the same time the molar electric conductivity can be coupled more profitably with a $\frac{\eta}{c} = \vartheta$ molar function introduced by us the so-called molar viscosity [9].

Our idea to apply the product of specific conductivity and viscosity has been stimulated by the fact established by us that the shape of the molar conductivity — ternary molality surface is relatively complicated, and for this reason its interpretation is difficult. The shapes of the specific conductivity — ternary molality surface are much more simple, its interpretation is much easier which made possible to obtain the interconnection between the two transport properties and to predict the numerical values of electric conductivity and viscosity in the ternary system from the suitable data of both constituent binary systems.

It can be seen from Fig. 1 demonstrating the concentration dependence of several metal chloride systems and hydrogen chloride that the specific electric conductivity—viscosity product changes practically linearly under

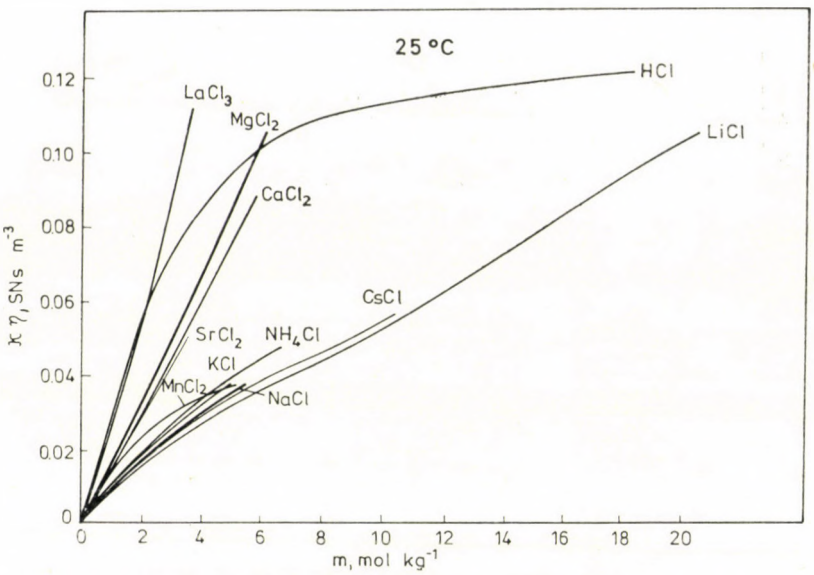

Fig. 1. $\varkappa\eta$-product of binary aqueous metal chloride solutions in the dependence on the composition

the influence of the concentration in the case of aqueous solutions of metal chlorides containing strongly positively hydrating cations, mainly in the case of $MgCl_2$, $CaCl_2$ and $LaCl_3$, but practically also in the case of LiCl, contrasted with the solutions of metal chlorides containing negatively, or slightly positively hidrating cations (*e.g.* Na^+), and much more contrasted with that of the hydrogen chloride. The lines of curves of the latter systems show negative deviation from the linearly extrapolated straight line of dilute solutions increasing with the increase of concentration.

The line of the curves of Fig. 1 is referring to the fact, that the role of the viscosity in the determination of the electric conductance becomes more and more considerable with the increase of the concentration. It seems that the increase of ion-ion interactions has a relatively greater effect on the viscosity than on the conductance. Especially, the situation is similar in the case of metal chlorides containing strongly positively hydrating, mainly double and triply charged cations, where the curves according to the specific conductivity and viscosity product straighten out practically completely. The situation is nearly similar also in the case of the metal chlorides containing cations with opposite hydrating properties.

The analyses of Fig. 2 shows very well, that the concentration dependence of the lines according to the $\Lambda\eta$ product, as well as to the $\Delta H_\eta^\ddagger$ of viscous flow, respectively, are very similar in the given binary systems. It seems to support that — on one hand — the viscosity takes the dominating effect on the con-

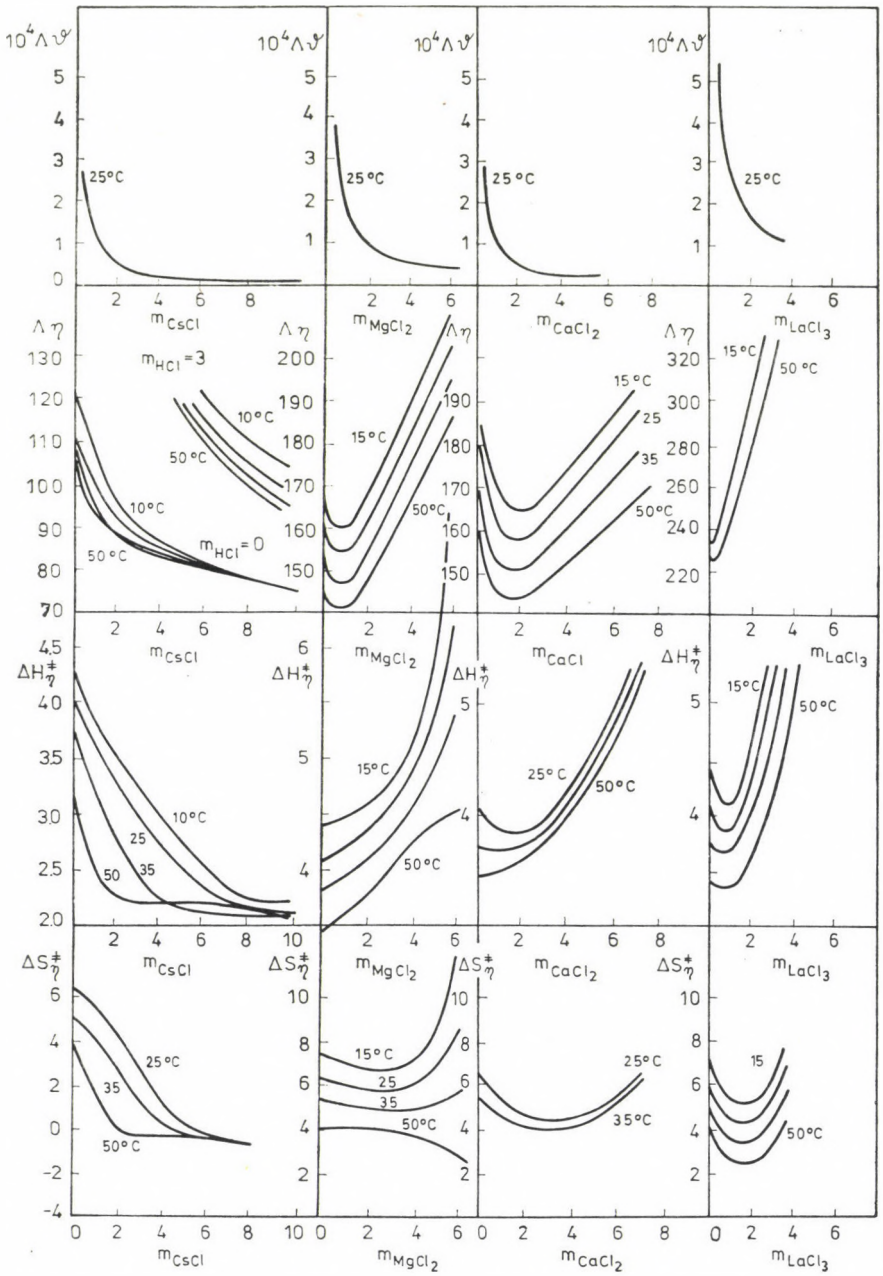

Fig. 2. $\Lambda\vartheta$,$\Lambda\eta$-products and the $\Delta H_\eta^\ddagger$- and $\Delta S_\eta^\ddagger$-values of binary aqueous metal chloride solutions in the dependence on the composition

ductance in the given system and in the case of given external electric field — on the other hand — the product of molar conductivity and viscosity is likewise characteristic of the structure respectively the ordering as the entropy of activation is characteristic of that. Because the viscosity is determined by the structure arising mainly as the result of ion-ion and ion-solvent interactions, thus the structure effects the electric conductivity practically through the viscosity in the case of a given number of charged particles.

It can be seen from Fig. 2 that the $\Lambda\vartheta$ *vs.* composition curves have less specific lines than the $\Lambda\eta$ *vs.* composition lines, and also its dependence on the type of salts is less characteristic. Namely, the division with c makes the concentration dependence of the conductivity—viscosity product so to say uniform in each metal chloride—water system.

The Λ—ϑ diagrams yield the most remarkable relation to the interconnection of the conductivity and viscosity both in binary and ternary systems.

Figure 3 demonstrates comprehensively the molar viscosity values belonging to the molar conductivity ones in the various binary systems. The values of both molar properties decrease with increasing concentration of the solution. But the influence of ion-ion interaction increasing the viscosity becomes more and more dominant in more concentrated solutions, than that decreasing the specific conductivity. Consequently the curve turn back.

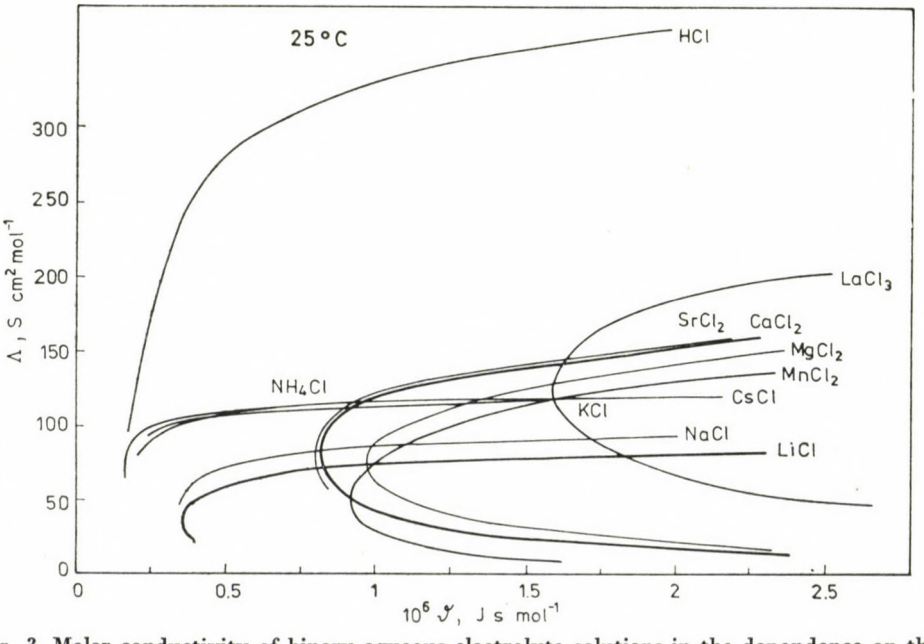

Fig. 3. Molar conductivity of binary aqueous electrolyte solutions in the dependence on the molar viscosity

So the dependence of Λ on ϑ can be given by a function of type

$$\Lambda = A\sqrt{\vartheta + B} + C.$$

For metal chlorides, where the effect increasing the viscosity becomes properly great, the values of the constants are given in Table II.

Table II

The values of the constants B and C of the equation for different aqueous metal chloride solutions

Electrolyte	B	C
LiCl	−0.350	33
$MgCl_2$	−0.955	74
$CaCl_2$	−0.815	82
$SrCl_2$	−0.790	83
$LaCl_3$	−1.590	123
$MnCl_2$	−0.920	51

The separation of curves according to the valency of cations can be well observed from the deviation into the ϑ-direction of the curves (the coefficient B of the equation is characteristic of this phenomenon), as well as the dependence on the size of cations within this. The coefficient C of the equation (this is the Λ-value belonging to the cusp of the curves, *i.e.* to the minimum of ϑ) increases slightly with an increase of the cation size at a given cation charge, as a proof that the influence of the increase of viscosity decreasing the conductivity predominate more stronger even at relatively greater conductivity (in the more dilute solutions).

The curve of HCl separates from the set of curves evidently very remarkably. This is the result of the protonic conductance and the turning back can not occur even in concentrated solutions. The reason for this is that the role of viscosity influencing the conductance is much smaller than in the case of ions conducting by hydrodynamic migration.

The diagram demonstrates, that the slope of the curve of the $MnCl_2$ differs from that of other metal chlorides investigated. Although the ϑ-value at the cusp corresponds to the series determined by the cation size, but the value in the Λ-direction is smaller than that required by the ion size. This refers also to the fact, that the Mn^{2+}-ion with an electron configuration of [Ar] $(3d)^5$ affects the conductivity in another way and more stronger, than an ion with the same size but with an electron configuration of s^2p^6.

Even a relatively small quantity of HCl added to the binary metal chloride solution has a great influence on the slope of the molar conductivity *vs.* molar viscosity curves, cusp of the curves is shifted toward higher molar con-

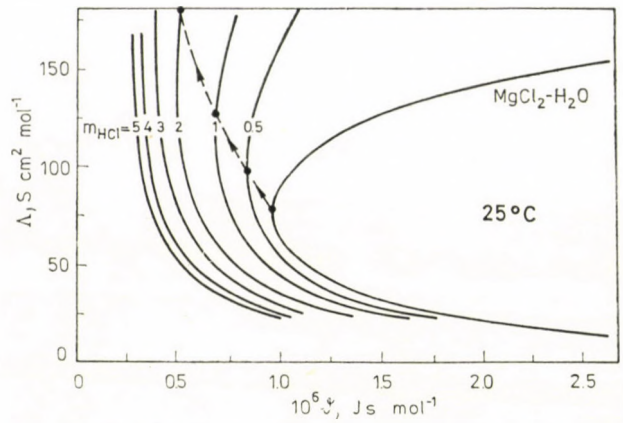

Fig. 4. Molar conductivity of the $MgCl_2$—HCl—H_2O system in the dependence on the molar viscosity

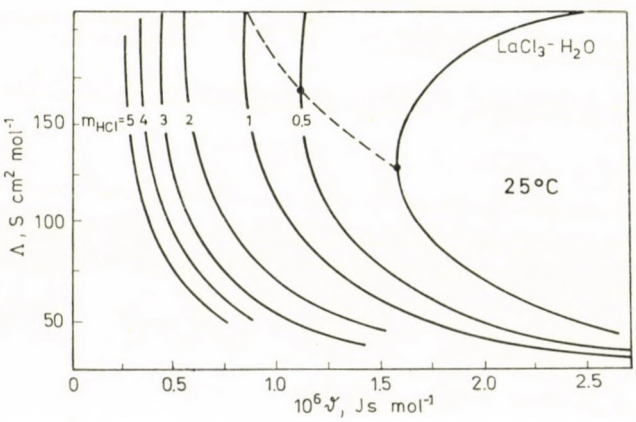

Fig. 5. Molar conductivity of the $LaCl_3$—HCl—H_2O system in the dependence on the molar viscosity

ductivity values, moreover, the cusp disappears if more HCl is added. This phenomenon can be seen very well on Figs 4 and 5 referring to $MgCl_2$ and $LaCl_3$, respectively. The diagrams show that the minimum of ϑ disappears at smaller amounts of HCl in the case of $LaCl_3$, than in the case of $MgCl_2$ and the curve indicating the path of the shift of the minimum is less steep in the case of $LaCl_3$.

In the course of our further investigations in the systems mentioned above we have tried to compare the concentration dependence of the enthalpies of activation of viscous flows (Fig. 6) and that of electric conduction (Fig. 7) as well as that of their ratio in order to get further informations from a new

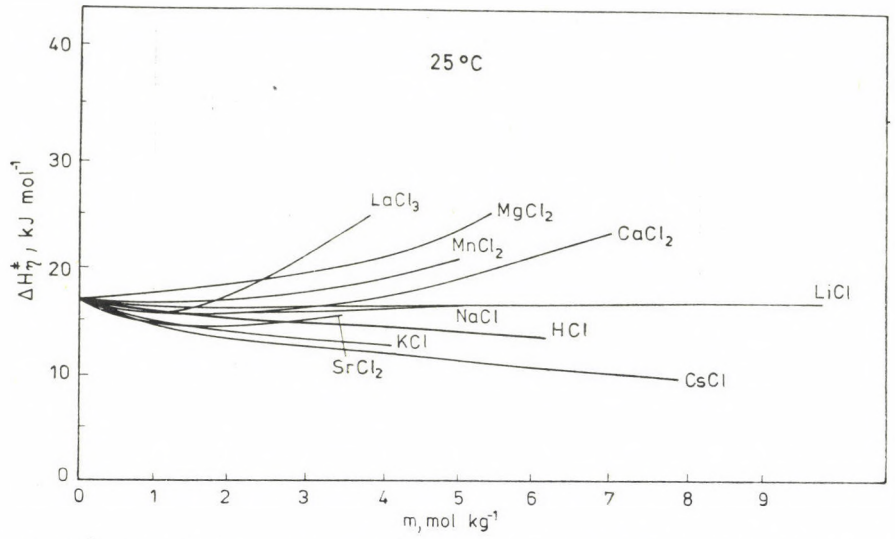

Fig. 6. $\Delta H_\eta^\ddagger$**-values of binary aqueous solutions of some chlorides in the dependence on the composition**

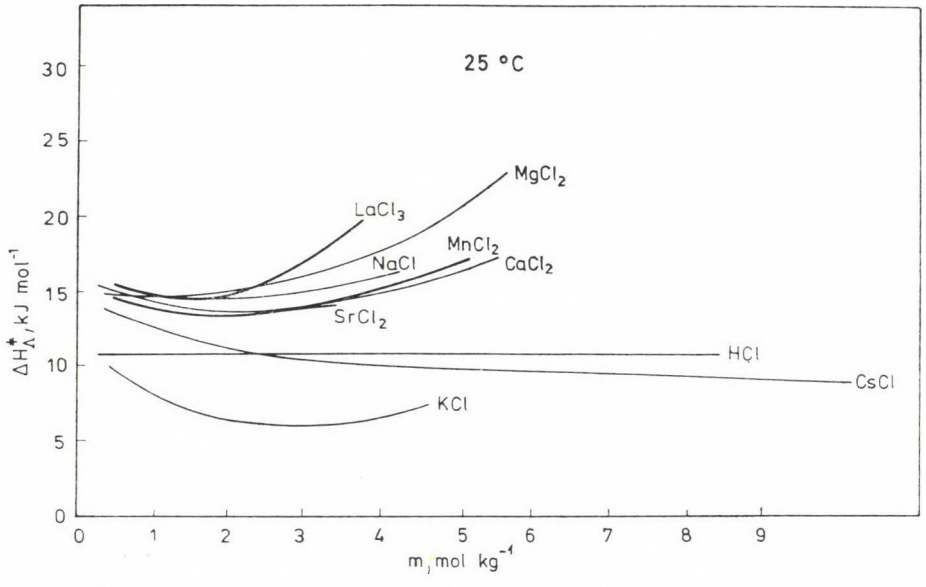

Fig. 7. $\Delta H_\Lambda^\ddagger$**-values of binary aqueous solution of some chlorides in the dependence on the composition**

side about the interconnection of two transport processes and about their concentration dependence.

From the diagram of enthalpy of activation of the viscous flow it can be established that

— the enthalpy of activation decreases compared to that of the pure water in the concentration range of dilute solutions, except in the case of the $MgCl_2-H_2O$ system, where the enthalpy of activation of the dilute solutions equals practically to that of the water. The cause of this can be searched in the strong effect of the Mg-ions hydrating very positively;

— in the case of given valency of cations and at given concentration the enthalpy of activation decreases monotonously with the increase of the size of the cations. This statement is valid also for $MnCl_2$, where the electron configuration of the cation is no of the s^2p^6 type. In this case the curve of enthalpy of activation falls between those of $MgCl_2$ and $CaCl_2$ similar to the case of the $\eta-m$ curves.

The line of curves and their mutual position is different in the case of the enthalpy of activation of electric conduction. Figure 7 shows that for all metal chlorides the enthalpy of activation values decrease compared to those in the infinitely dilute solutions (which occur because of the increasing number of charged particles), but neither with univalent nor with bi- and trivalent cations the interconnection is not unequivocal between the ionic size and the position of the enthalpy of activation curves. Among the alkaline metal chlorides KCl excels with its very small requirement of enthalpy of activation. Among the metal chlorides containing bivalent cation $MnCl_2$ is remarkable, the curve of which falls into the proper place corresponding to the size of the Mn^{2+}-ion only in the concentrated solutions. In dilute solutions the position of the $\Delta H_\Lambda^\ddagger$-curve of the $MnCl_2$ does not correspond to the size of the Mn^{2+}, like in the case of the $\Lambda-m$ and $\varkappa-m$ curves.

Figure 8 demonstrates the change in the $\Delta H_\eta^\ddagger/\Delta H_\Lambda^\ddagger$ ratio with the concentration under isothermal conditions (25 °C) in the case of HCl and metal chlorides containing single-charged cations, as well as in the case of metal chlorides containing double- and triply-charged ones, respectively.

Figure 8 shows, that values of $\Delta H_\eta^\ddagger/\Delta H_\Lambda^\ddagger$ ratio relating to metal chloride solutions containing double- and triply charged cations fall into a relatively narrow interval, the $\Delta H_\eta^\ddagger/\Delta H_\Lambda^\ddagger$ values of the metal chloride solutions containing single-charged cations fall also in a narrow interval, but only in concentrated solutions. Consequently, the $\Delta H_\eta^\ddagger/\Delta H_\Lambda^\ddagger$ values are close to each other supporting also our opinion that the two transport mechanisms are similar, essentially the same. There are two exceptions. From the figure it can be seen, that the $\Delta H_\eta^\ddagger/\Delta H_\Lambda^\ddagger$-values of the $KCl-H_2O$ system are much greater than those in the solutions of the other metal chlorides. At the same time also the $\Delta H_\eta^\ddagger/\Delta H_\Lambda^\ddagger$ — values referring to the $HCl-H_2O$ system are also somewhat greater than those of the metal chloride solutions (except KCl).

In the case of the $HCl-H_2O$ system this fact can be interpreted by the much smaller demand of enthalpy of activation of the protonic conduction than that of the hydrodynamic one, at the same time from the point of view

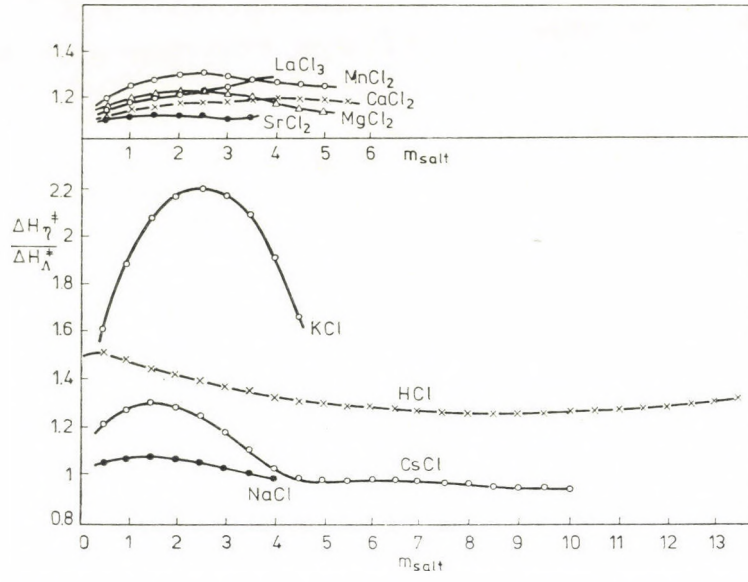

Fig. 8. Values of the $\Delta H_{\Lambda}^{\ddagger}/\Delta H_{\Lambda}^{\ddagger}$-ratio of binary aqueous solutions of some chlorides in the dependence on the composition

of the viscosity the H_3O^+-ion behaves like a simple cation with common properties [1].

For the very different behaviour of KCl we could not find a suitable interpretation so far.

The curves of Fig. 8 can be divided into linear sections with different slopes, which support our opinion mentioned earlier on the non-monotonous change of the structure.

The more detailed analysis of the dependence on the structure from the line of the curves is very difficult because of the very complex interactions and it requires further studies. But some statements can be made at present.

The curves of Fig. 8 demonstrate, that the value of the $\Delta H_{\eta}^{\ddagger}/\Delta H_{\Lambda}^{\ddagger}$ ratio increases in the dilute solutions compared to those referring to the infinite dilute solutions. Obviously, this is caused by the decrease of the enthalpy of activation of the electric conduction occurring because of the getting of the ions into the solution.

The beginning increasing section of the curves continues until $m \approx 1.5$ in the case of NaCl and CsCl, then it decreases to a value of about 1.

In the case of the 2 : 1 metal chlorides it increases until $m \approx 2.5$ then the extent of the decrease is smaller. In the case of the 3 : 1 type $LaCl_3$ the decrease can not be observed.

It is characteristic that in the case of CsCl hydrating very negatively the $\Delta H_{\eta}^{\ddagger}/\Delta H_{\Lambda}^{\ddagger}$-ratio is smaller than 1, and practically independent on the con-

centration. This means, that the $\Delta H_{\Lambda}^{\ddagger}$ decreasing with the concentration will be greater throughout in identical degree as the $\Delta H_{\eta}^{\ddagger}$ decreasing also with the concentration. Thus a third section appears on the curve continuing until saturation, and indicating that the structural conditions hardly change here. In this interval only the successive and monotonous dehydration and the redistribution of the water molecules around the entering ions occur as a result of the increasing salt concentration.

In the case of $MgCl_2$ the extents of the three concentration intervals are different from those of the CsCl. In the first section $\Delta H_{\eta}^{\ddagger}$ increases strongly, but $\Delta H_{\Lambda}^{\ddagger}$ decreases. In the second section $\Delta H_{\eta}^{\ddagger}$ increases because of the strong destruction of water and building of its own structure. The value of $\Delta H_{\Lambda}^{\ddagger}$ does not decrease any more but remains practically constant. This section continues until the concentration is somewhat above the boundary of complete hydration. But beginning from this as a result of the stronger increase of ion-ion interactions due to the double charged Mg^{2+}-ions and to double quantity of Cl^--ions the value of $\Delta H_{\Lambda}^{\ddagger}$ begins to increase stronger than the value of $\Delta H_{\Lambda}^{\ddagger}$. (The value of $\Delta H_{\eta}^{\ddagger}$ increases to a lesser degree, since the influence of the decrease of the measure of ions decreasing $\Delta H_{\eta}^{\ddagger}$ as a result of successive dehydration counteracts the influence of ion-ion interactions increasing the viscosity and the value of $\Delta H_{\eta}^{\ddagger}$.) Thus after all the $\Delta H_{\eta}^{\ddagger}/\Delta H_{\Lambda}^{\ddagger}$ ratio has a diminishing tendency as long as a new section appears with other slope near the saturation, like the case of the V_m-curves already observed by us [11].

In the course of the study of molar volume, the functions of activation and the solubilities the structural conditions in the solution for this section were interpreted in out earlier paper [11] as the formation of a preordering in the solution tending towards the structure of the solid phase being inequilibrium with the saturated solution. It seems, this transformation in the solution is supported by the lines of curves due to the concentration dependence of the $\Delta H_{\eta}^{\ddagger}/\Delta H_{\Lambda}^{\ddagger}$ ratio.

In the case of the chloride of lanthanum ion having a greater charge and nearly two times greater size than the Mg^{2+}-ion the $\Delta H_{\eta}^{\ddagger}/\Delta H_{\Lambda}^{\ddagger}$ ratio increases almost until to saturation. This is connected doubtless with the permanent increase of the $\Delta H_{\eta}^{\ddagger}$ due to the big charge of cation and to the bigger number of ions compared to other metal chlorides with single and double charged cations, which excel the increase of the value of $\Delta H_{\Lambda}^{\ddagger}$ throughout. The regression of the curve of the $\Delta H_{\eta}^{\ddagger}/\Delta H_{\Lambda}^{\ddagger}$ ratio occurring near the saturation can be interpreted also with the formation of uncharged ion pairs, which increases strongly the value of $\Delta H_{\Lambda}^{\ddagger}$, thus the increase of the $\Delta H_{\eta}^{\ddagger}/\Delta H_{\Lambda}^{\ddagger}$ ratio will lessen.

In the $HCl-H_2O$ system the line of the curve of the $\Delta H_{\eta}^{\ddagger}/\Delta H_{\Lambda}^{\ddagger}$ ratio can be interpreted by the repression of the protonic conductance in the dependence on the concentration, *i.e.* it is characteristic of the latter. But the line of the curve show also, that the repression of the protonic conductance

with increasing concentration begins still at concentrations $m_{HCl} > 1$, and increases slowly. The second decreasing section of the curve referring to this fact continues to the concentration of $m_{HCl} \approx 8-9$, where the value of $\Delta H_\eta^\ddagger/\Delta H_\Lambda^\ddagger$ of the $HCl-H_2O$ solution reaches the highest value of $\Delta H_\eta^\ddagger/\Delta H_\Lambda^\ddagger \approx 1.2$ possible at metal chloride solutions conducting with hydrodynamic migration. But contrasted with the behaviour of the metal chlorides in the case of the $HCl-H_2O$ system the value of the $\Delta H_\eta^\ddagger/\Delta H_\Lambda^\ddagger$ ratio is never less than 1.2 further it begins to increase again as a result of a slight increase in $\Delta H_\eta^\ddagger$, and the practical constant value of $\Delta H_\Lambda^\ddagger$. This latter phenomenon indicates that — it seems — the protonic conductance does not cease to exist entirely even in the most concentrated solutions, although it will be repressed strongly.

REFERENCES

[1] BERECZ, E.: Magy. Kém. Folyóirat, **79,** 404 (1973)
Acta Chim. Acad. Sci. Hung., **84,** 353 (1975)
[2] BERECZ, E.: Magy. Kém. Folyóirat, **81,** 292 (1975)
Acta Chim. Acad. Sci. Hung., **87,** 371 (1975)
[3] МИЩЕНКО, К. П. РАВДЕЛЬ, А. А.: Краткий Справочник Физико-Химичезких Величин. Изд. ГХИ, Ленинград 1955
[4] BERECZ, E., BÁDER, I.: Acta Chim. Acad. Sci. Hung., **74,** 213 (1972)
[5] GLASSTONE, S., LAIDLER, K. L., EYRING, K. L., H.: The Theory of Rate Processes. New York 1941
[6] FALKENHAGEN, H., LEIST, M., KELBG, G.: Z. Phys. Chem: **205,** 16 (1955)
[7] WISHAW, B. F., STOKES, R. H.: J. Am. Chem. Soc., **76,** 2065 (1954)
[8] Максимова, И. Н.: Ж. Физ. Химии, **38,** 277 (1964)
[9] BERECZ, E., BÁDER, I., TÖRÖK, T.: Magy. Kém. Folyóirat, **82,** 51 (1976); Acta Chim. Acad. Sci. Hung., **91,** 119 (1976)
[10] BERECZ, E.: Acta Chim. Acad. Sci. Hung., **77,** 285 (1973)
[11] BERECZ, E.: Magy. Kém. Folyóirat, **83,** 448 (1977)

Endre BERECZ
Imre BÁDER
H-3515 Miskolc-Egyetemváros

Acta Chimica Academiae Scientiarum Hungaricae, Tomus 100 (1—4), pp. 257—264 (1979)

POLYETHYLENE GLYCOL DERIVATIVES AS COMPLEXING AGENTS AND PHASE-TRANSFER CATALYSTS, II

COMPLEXING BEHAVIOUR OF POLYETHYLENE GLYCOLS AND THEIR DERIVATIVES

L. TŐKE, G. T. SZABÓ and K. ARANYOSI

(Department of Organic Chemical Technology, Technical University, Budapest)

Received July 5, 1978

Accepted for publication August 7, 1978

End-group substitutions were carried out on polyethylene glycols. The complexing power of the polyoxyethylene compounds was found to depend on the nature of the end-group and on the average chain length.

Introduction

In a previous paper we reported our experiments on the complexing ability of polyethylene glycols and their derivatives toward sodium ion. It has been shown that the complexing power depends upon the average molecular weight of the polyethers and the nature of the end-groups attached to the chains; evidence has been given for the potential use of these materials in phase-transfer catalytic reactions [1].

Papers dealing with the complexing power of noncyclic compounds are known in the literature [2—12], but most of them report only on homogeneous compounds of a low molecular weight. No detailed examinations have been published on the relationship between the complexing ability and the average molecular weight of polyethers; thus we decided to continue our researches in this field.

Results and Discussion

Polyethylene glycols

Using the method described earlier [1] we calculated the complex stability constants (K_1) of the samples shown in Table I.

A stable 1 : 1 complexing stoichiometry was found to exist between the polyethers and sodium ion.

Table I

Logarithms of the stability constants of polyethyleneglycol — Na^+ complexes

Average molecular weight	lg K_1
200	1.64
300	2.02
400	2.26
600	2.59
1000	2.88
1500	3.09
2000	3.28

An interesting curve can be obtained in a K_1 *vs.* M diagram (Fig. 1) where n = the average n number of CH_2CH_2O units, M = the average molecular weight of the sample.

The complexing ability pro unit increases steeply in the range of low average molecular weights, later the slope of the curve diminishes.

Obviously, the conformer needed for complexation can be produced easier if the chain is longer.

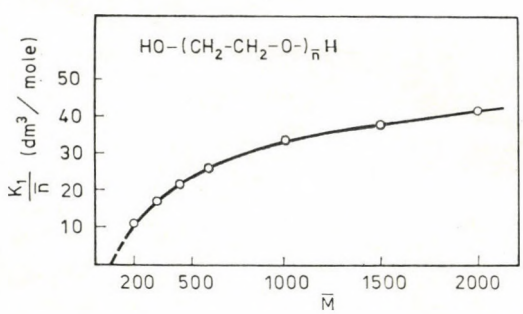

Fig. 1. Stability constants calculated per —CH_2CH_2O— units as a function of the average molecular weight

Derivatives of polyethylene glycols

To investigate the effect of the end-groups on the behaviour of the polymers, a number of derivatives were prepared by substituting the hydroxyl groups at both ends of the polyethylene glycols. The stability constants of the derivatives thus obtained are listed in Table II.

The values of the stability constants calculated for one — CH_2CH_2O–unit $\frac{K_1}{n}$ are plotted against the molecular weight of the polyethylene glycols used for the preparation (Figs 2—5).

Table II

*Logarithms of the stability constants of Na^+ complexes of polyoxyethylene compounds**

$\overline{M}$*	lg K_1			
	CH_3O-	C_2H_5O-	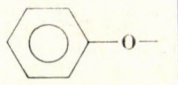	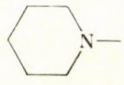
200			0.50	
300	1.55	1.25	1.05	1.16
400			1.49	1.51
600	2.09	1.99	1.87	
1000	2.55	2.48	2 37	2.46
1500	2.86	2.80	2.68	
2000	3.08	3.05	2.81	3.08

* The columns $\overline{M}$ of this and the next tables show the average molecular weight of the *polyethylene glycol* used for the preparation.

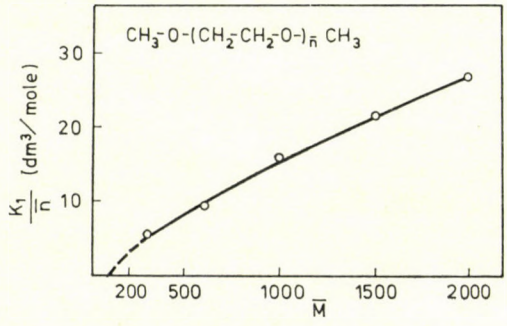

Fig. 2. Stability constants calculated per $—CH_2CH_2O—$ units as a function of the average molecular weight

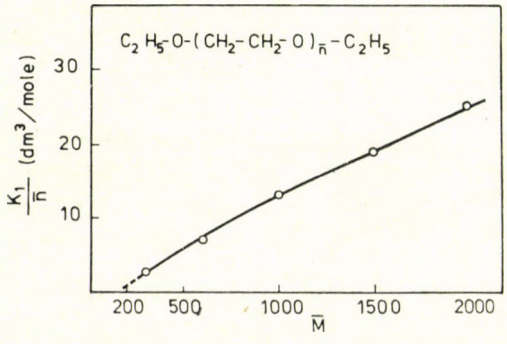

Fig. 3. Stability constants calculated per $—CH_2CH_2O—$ units as a function of the average molecular weight

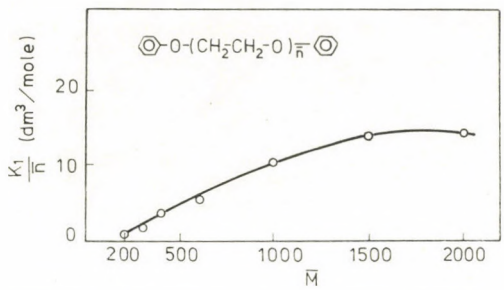

Fig. 4. Stability constants calculated per —CH_2CH_2O— units as a function of the average molecular weight

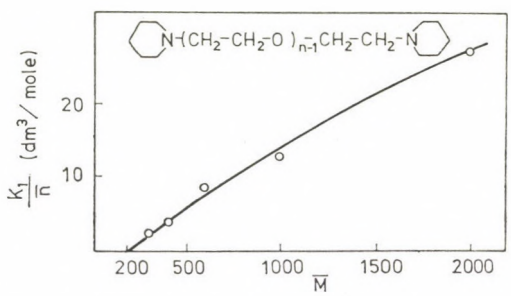

Fig. 5. Stability constants calculated per —CH_2CH_2O— units as a function of the average molecular weight

It is seen that each derivative prepared here has a lower K_1 value than the polyethylene glycol starting material. If the starting sections of the diagrams in Figs 1—5 is extrapolated, an intersection is formed at an $\overline{M}$ value of about 150—200 (except for the methylethers of the polyethylene glycols), which can be interpreted as the minimal molecular weight required for complex formation. It gives a coordination number of four.

$$-H > -CH_3 > -C_2H_5 > -C_6H_5$$

Notably, the stability constants decrease in the following order of the end-groups showing that the electronic effect of the end-groups in such a long chain does not play a decisive role in the complex formation process. The same result was obtained in measurements on derivatives with ring-substituted phenoxy end-groups (Table III).

Table III

Logarithms of the stability constants of Na^+ complexes of symmetrically substituted $\overline{M} = 300$ *polyoxyethylene compounds*

Substituent	log K_1	
	$\overline{M} = 300$	$\overline{M} = 1000$
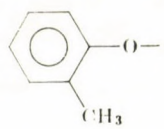	1.08	2.40
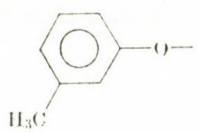	1.04	
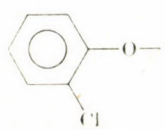	0.97	
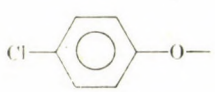	0.94	
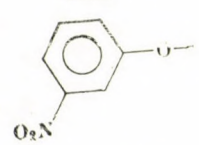	1.04	2.34
	0.95	2.30

Experimental

The stability measurements were carried out as described previously [1]. The solvent was 96% aqueous ethanol, the temperature 25 °C. The stability constants are given in $\frac{dm^3}{mole}$. Calculated error of logarithms = ± 0.08 logarithmic units.

The polyethylene glycol samples were commercial products supplied by Fluka, dried over P_2O_5.

The derivatives were prepared as described below.

Notes: (a) All preparations and evaporations were carried out in N_2 atmosphere.

(b) When referring to any average molecular weight in this paper, we always mean the average molecular weight of the polyethylene glycol starting material.

(c) Each product was analyzed by atomic absorption spectrometry and their Na content was found to be less than 0.1 mole percent.

Preparation of α, ω-dichloropolyoxyethylenes

Into a 100 cm³ flask fitted with a stirrer, thermometer, reflux condenser, dropping funnel, gas inlet and outlet, 30 g (0.015—0.15 moles) of polyethylene glycol and 0.1 ml of pyridine were placed.

When using solid polyethylene glycols, the temperature was raised above the melting point; otherwise at room temperature, with stirring, freshly distilled $SOCl_2$ (3 moles) was added to 1 mole of polyethylene glycol in small portions. After the addition had been completed, the reaction mixture was heated to 90 °C and stirred at this temperature for 2 h.

The unchanged $SOCl_2$ was then removed in vacuum. Suction was continued until the product became free of SO_2.

The quality of the product was checked by determining the total chlorine content. We used only the products with chlorine contents of 98—102% of the theoretical.

Preparation of α, ω-bis-(*N*-piperidyl)-polyoxyethylenes

Using a 250 cm³ flask fitted with a stirrer, reflux condenser, thermometer, gas inlet and outlet, 30 g (0.015—0.13 moles) of α, ω-dichloropolyoxyethylene was dissolved in dry acetonitrile. The quantity of solvent depended upon the average molecular weight of the intermediate. In the case of $\overline{M} = 200$ 70 cm³, whereas for $\overline{M} = 2000$ only 10 cm³ of acetonitrile was used. To the solution 0.1 cm³ of methyl iodide, and for 1 mole of polyether 6 moles of dry piperidine were added.

The reaction mixture was stirred at 85—90 °C for 8 h. The solvent was removed in vacuo and the residue dissolved in 80 cm³ of benzene. The precipitate was filtered off and washed with 20 cm³ of benzene. The workup of the benzene solution depended upon the average molecular weight of the product.

Purification of α, ω-bis-(*N*-piperidyl)-polyoxyethylenes ($\overline{M}$ = 300—1000)

The benzene solution of the product (100 cm³) was extracted with 3×20 cm³ portions of distilled water and the organic phase was evaporated in vacuum.

The residue was dried in a vacuum desiccator over solid paraffin, *conc.* H_2SO_4 and P_2O_5.

Purification of α, ω-bis-(*N*-piperidyl)-polyoxyethylenes ($\overline{M}$ = 1500—2000)

The benzene solution of the product (100 cm³) was extracted with 3×30 cm³ portio n of distilled water.

Table IV

Refractive indices of polyethylene glycols and α, ω-bis-(N-piperidyl)-polyoxyethylenes

$\overline{M}$	n_D^{40}	
	HO—	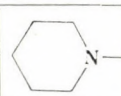
200	1.4461	1.4639
300	1.4510	1.4620
400	1.4529	
600	1.4544	1.4612
1000	1.4562	1.4600
1500	1.4570	
2000	1.4572	1.4594

The combined aqueous solution was mixed with 30 cm^3 of *n*-butanol and successively extracted with 15 cm^3 of benzene and 15 cm^3 of 1,2-dichloroethane. The combined organic extracts were evaporated in vacuum and the residue was dried in a vacuum desiccator over P_2O_5, H_2SO_4 and solid paraffin. The product was characterized by acid titration. The amine content of a satisfactory product was 95—105%.

The refractive indices of materials together with those of the starting polyethylene glycols are listed in Table IV.

Preparation of α, ω-bis-(alkoxy)-polyoxyethylenes

Into a 250 cm^3 flask fitted with a stirrer, thermometer, reflux condenser, gas inlet and outlet, 50 cm^3 of the appropriate dry alcohol, corresponding to the desired end-group, was placed. For 1 mole of the polyether 2 moles of sodium was added. After the sodium had dissolved, the mixture was cooled to 25 °C and 0.5 g of dry NaI and 30 g of dichloropolyoxyethylene were added. The mixture was stirred for 1 h at 25 °C and 8h at reflux temperature.

The alcohol was evaporated, and the residue taken up in 80 cm^3 of freshly distilled, phosgene-free chloroform. The solid was filtered off and washed with 20 cm^3 of chloroform. The combined chloroform solutions were successively extracted with 10 cm^3 portions of water until the last extract was free of chloride ions and neutral. The chloroform solution was then evaporated and the residue dried in a vacuum desiccator over solid paraffin and P_2O_5.

The alkoxy products could be characterized by determining their OH end-group impurities. The conversion was established by determining the hydroxide and chloride ion contents of the solid and the collected washing water. The refractive indices of the alkoxyl products are listed in Table V.

Table V

Refractive indices of α,ω-bis-(alkoxy)polyoxyethylenes

$\overline{M}$	n_D^{40}	
	CH_3—O—	C_2H_5—O—
300	1.4334	1.4319
600	1.4461	1.4445
1000	1.4505	1.4496
1500	1.4536	1.4532
2000	1.4561	1.4540

Preparation of α, ω-bis-(phenoxy)-polyoxyethylenes

In a 250 cm^3 flask fitted with a stirrer, reflux condenser, thermometer, gas inlet and outlet, 2 moles of sodium for 1 mole of polyether was dissolved in 50 cm^3 of dry ethanol, then 2 moles of phenol and 0.5 g of NaI were added.

Dichloropolyoxyethylene (30 g; 0.015—0.13 moles) was added to the mixture and it was stirred for 1 h at 25 °C and 8 h at reflux temperature.

The solvent was evaporated, the residue taken up in 80 cm^3 of benzene, the solid filtered off and washed with 20 cm^3 of benzene.

The product dissolved in benzene was purified in a way depending upon the chain length.

Purification of α, ω-bis-(phenoxy)-polyoxyethylenes ($\overline{M}$ = 200—600)

The benzene solution (100 cm^3) was successively extracted with 10 cm^3 portions of water until the last extract contained no chloride ion, and was neutral. The organic solution was evaporated to dryness and the residue dried in a vacuum desiccator over NaOH, solid paraffin and P_2O_5.

Purification of α, ω-bis-(phenoxy)-polyoxyethylenes ($\overline{M}$ = 1000—2000)

The solvent from the benzene solution was evaporated, the residue dissolved in 100 cm^3 of phosgene-free chloroform, and worked up as described earlier.

Characterization of the products was done similarly to that of the alkoxy compounds. The refractive indices of the products are listed in Table VI.

Table VI

Refractive indices of α,ω-bis-(phenoxy)polyoxyethylenes

$\overline{M}$	n_D^{60}
200	1.5070
300	1.5012
400	1.4952
600	1.4869
1000	1.4700
1500	1.4686
2000	1.4651

Preparation of α, ω-bis(ring substituted phenoxy)-polyoxyethylenes

In the preparation of tolyloxy and chlorophenoxy-substituted products the same method was used as described for the phenoxy compounds. For the preparation of nitrophenoxy-substituted products the following procedure is suggested.

In a 100 cm^3 flask, fitted with a stirrer, thermometer, reflux condenser, gas inlet and outlet, 30 g of α,ω-dichloropolyoxyethylene was allowed to react with solid sodium nitrophenolate (2 moles for 1 mole of polyether) at 90 °C for 8 h.

To isolate the product the same method was used as described for the phenoxy compounds.

*

The authors are indebted to Prof. I. Rusznák, Head of the Department, for his help in this work in every respect, to Mr. S. Bozsó for technical assistance, and to the National Committee for Technical Development for a financial support of this work.

REFERENCES

[1] Tőke, L., Szabó, G. T.: Acta Chim. Acad. Sci. Hung. **93,** 421 (1977)
[2] Parker, J. M., Wright, P. V.: Polymer **14,** 589 (1973)
[3] Takaki, U., Smid, J.: J. Am. Chem. Soc. **96,** 2588 (1974)
[4] Davidova, S. L., Barabanov, V. A., Alimova, N. V., Plate, N. A.: Izv. Akad. Nauk. USSR, **1975,** 1441
[5] Weber, E., Vögtle, V.: Tetrahedron Lett. **1975,** 2415
[6] Vögtle, F., Sieger, H.: Angew. Chem. **89,** 410 (1977)
[7] Rasshofer, W., Oepen, G., Müller, W. M., Vögtle, F.: Ber. **111,** 1108 (1978)
[8] Heimann, U., Vögtle, F.: Angew. Chem. **90,** 211 (1978)
[9] Buhleier, E., Wehner, W., Vögtle, F.: Synthesis **1978,** 155
[10] Rasshofer, W., Vögtle, F.: Tetrahedron Lett. **1978,** 309
[11] Tümmler, B., Maass, G., Weber, E., Wehner, W., Vögtle, F.: J. Am. Chem. Soc. **99,** 4683 (1977)
[12] Lehmkuhl, H., Rabet, F.: Ger. Offen. 25 34 851 (1977)

László Tőke
Gábor Tamás Szabó
Katalin Aranyosi
H-1521 Budapest, Műegyetem

Acta Chimica Academiae Scientiarum Hungaricae, Tomus 100 (1—4), pp. 265—273 (1979)

CHARACTERIZATION AND CHROMATOGRAPHIC BEHAVIOUR OF CYCLODEXTRIN POLYMERS

B. ZSADON,* M. SZILASI, K. H. OTTA, F. TÜDŐS, É. FENYVESI[1] and J. SZEJTLI[1]

(Eötvös Loránd University, Department of Chemical Technology, Budapest
[1] Biochemical Laboratory of Chinoin Pharmaceutical and Chemical Works, Budapest)

Received July 5, 1978

Accepted for publication September 27, 1978

Cyclodextrin polymers (α-CDP, β-CDP and γ-CDP) have been prepared in the form of regular beads by cross-linking cyclodextrins (α-CD, β-CD and γ-CD); the products were characterized, besides by their chemical composition, on the basis of their swelling properties and grain size. Cyclodextrin polymers with medium swelling capacity and well defined composition proved to be useful column packings for inclusion chromatography. They swell rapidly, retain their form and are elastic; they can be stored even in the swelled state for a long time without decomposition, and maintain their original properties after repeated regenerations. Chromatograms obtained on the swelled CDP gels can be readily reproduced.

Using 20 natural amino acids as model substances, the chromatographic behaviour of α-CDP, β-CDP and γ-CDP, the resolution and its dependence on the experimental conditions have been studied. Retention data of the amino acids and several data on the height equivalent of a theoretical plate (HETP) are given. Investigations showed that a good separation of aromatic amino acids from one another and from other amino acids can be achieved primarily on a column packed with β-CDP. In the case of tryptophan α-CDP gave the best separation.

An interesting field of application of polymers prepared by cross-linking cyclodextrins (CD) [1, 2] is the inclusion chromatography [3]. In cyclodextrin polymers (CDP) the ability of cyclodextrins to form inclusion complexes is combined with the characteristic properties of a cross-linked polymeric structure. Used as swelled gels, these polymers reversibly bind from solutions certain substances in the form of inclusion complexes, and retention during chromatographic separation is determined, besides other effects (*e.g.* gel permeation, adsorption), by the complex formation. Thus, *e.g.*, simple aromatic isomers [1, 3], tryptophan and phenylalanine [1], or tryptophan and tyrosine [3] could be separated from one another.

We reported recently [5] that using bead-form β-cyclodextrin polymer (β-CDP) as column packing, several natural amino acids could be separated. Therefore amino acids were thought to be suitable model compounds for a comparative investigation of the chromatographic behaviour of CDP column packings. In the following the results of relevant systematic investigations are reported, complemented by a brief description of methods for the characterization of these polymers.

Materials

For the preparation of the polymers, crystalline cyclodextrins, manufactured by Chinoin, were used. Their main characteristics are summarized in Table I.

Table I

Characteristics of the cyclodextrins used for the preparation of the polymers

	$[\alpha]_D^{25}$
α-Cyclodextrin (α-CD)	$+150 \pm 2°$ (in water)
β-Cyclodextrin (β-CD)	$+163 \pm 2°$ (in water)
γ-Cyclodextrin (γ-CD)	$+177 \pm 2°$ (in water)
α-CD-acetate	+108° (in chloroform)
β-CD-acetate	+124° (in chloroform)
γ-CD-acetate	+138° (in chloroform)

In the chromatographic investigations standard amino acids marketed by Merck Co. were employed.

Characterization of the cyclodextrin polymers

The cyclodextrin polymers for chromatographic purposes were prepared in the presence of polyvinyl acetate, according to our process developed recently [6]; α-CD, β-CD and γ-CD were cross-linked with ethyleneglycol-di(epoxypropyl)-ether, to obtain regular beads (Fig. 1).

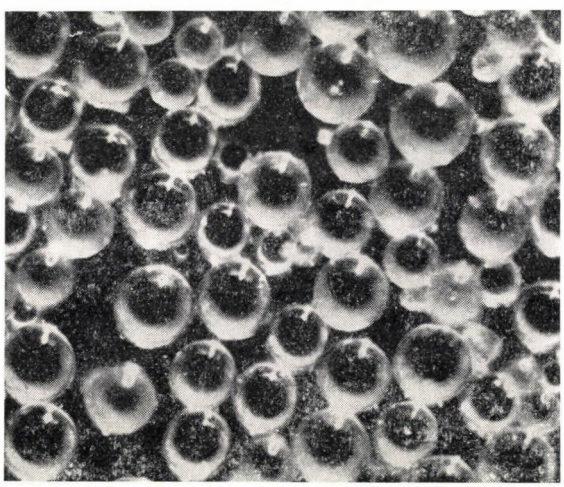

Fig. 1. Microscopic picture of β-cyclodextrin polymer (β-CDP) prepared in the form of beads

These polymers are well-characterized by their CD content, polyvinyl alcohol (PVA) content, by the solvent retention of the swelled polymer and the volume of the gel bed obtainable by sedimentation, further by the average grain size or grain size distribution.

The CD content was determined essentially by the method recommended by WIEDENHOF [7] : the polymer sample was hydrolyzed by boiling in 1*N* hydrochloric acid for 2 h. The liberated reducing sugars were determined by iodometry according to Willstätter. Cyclodextrin was used for calibration.

For the determination of the PVA content, the polymer sample was hydrolyzed by boiling in 1*N* hydrochloric acid for 2 h. The hydrolyzate was then neutralized and the PVA content determined by the method of FINLEY [8] : boric acid and iodine solution containing potassium iodide were added to the solution, and the colour intensity of the complex formed by PVA with iodine was measured at 690 nm. PVA was used for calibration.

For the determination of solvent retention, the polymer sample was swelled in the solvent (in our present investigations in water), the swelled gel particles were filtered off with mild suction on a sintered glass filter G4, and any residual solvent adhering to the surface was removed by centrifuging. The centrifuged sample was weighed, the remaining solvent was removed by drying, and the dried sample was weighed again. The difference of the two weighings is the solvent retention, which is given in units of g solvent per g dry polimer.

For the determination of the gel bed volume, the weighed dry polymer was placed into a measuring cylinder, solvent was added in excess, and periodically shaking the cylinder, the gel was allowed to swell. The gel phase was then sedimented and after the swelling equilibrium had been attained, the volume of the gel bed was read, and given in ml per g dry polymer.

Average grain size and grain size distribution were determined by sieve analysis or (in the case of small quantities) by microscopic analysis.

For chromatography, medium swelling cyclodextrin polymers of 90—200 micron grain size were used : the main characteristics are summarized in Table II.

Table II

Main characteristics of the polymers used for chromatography

	α-CDP	β-CDP	γ-CDP
CD-content, %	46	48	50
PVA-content, %	0.3	0.4	0.4
Water retention,* g/g	1.8	1.7	1.6
Gel bed volume,* ml/g	4.0	4.2	4.1

* Measured at room temperature

Chromatographic procedure

In the present experiments cyclodextrin polymers were allowed to swell in aqueous phosphate buffer solutions (pH 5—6), and packed into chromatographic columns of 1.6 cm diameter and 100 cm length (Pharmacia K 16/100), equipped with adapter and thermostating jacket.

The schematic diagram of our chromatographic equipment is shown in Fig. 2. The solution of the sample (**A**) and the eluent (**B**) were sucked in through a distributor valve (**C**) by a peristaltic pump (**D**) and fed into the chromatograph-

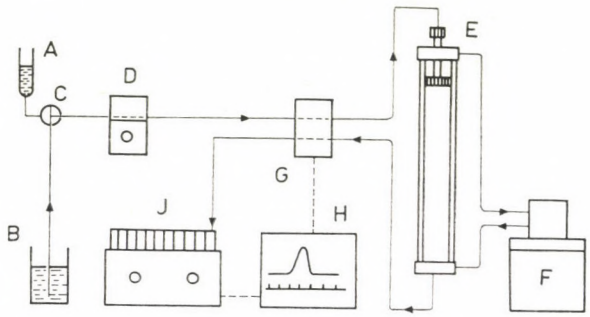

Fig. 2. Schematic diagram of the chromatographic equipment. A: sample; B: eluent; C: distribution valve; D: peristaltic pump; E: chromatographic column; F: thermostat; G: Uvicord III UV absorptiometer; H: recorder; I: automatic fraction collector

ic column (**E**). The temperature of the latter was controlled by a circulating thermostat (**F**). The concentration of the amino acids in the eluate was continuously measured against the eluent on the basis of the light absorption at 206 nm, using an LKB Uvicord III absorptiometer (**G**). The change in concentration was continuously recorded (**H**), and fractions were taken with an automatic fraction collector (**I**).

Discussion

Cyclodextrin polymers of medium swelling capacity and well defined composition, prepared in the form of regular beads, proved advantageous as packings for chromatographic columns. They swell rapidly (in 40—60 min) even at room temperature, and can be readily packed and settled. The swelled particles do not deform and are elastic. They retain their original form, dimensions and properties even after repeated drying (at 105 °C) and swelling. They have the further advantage of being resistent to damage by microorganisms even when moist, thus they can also be stored for a long period without decomposition when swelled in water.

For a study of the properties of cyclodextrin polymers as packings for chromatographic columns, systematic investigations were made using 20 natural amino acids as model substances. According to our preliminary experiments, chromatograms easy to evaluate and reproduce could be obtained in weakly acid solutions. Therefore, our investigations were carried out in weakly acid (pH between 5 and 6) phosphate buffer solutions.

The statistically evaluated relative elution volumes (V_e/V_t) of 20 natural amino acids measured on columns packed with the different cyclodextrin polymers (α-CDP, β-CDP and γ-CDP) at room temperature, using an elution rate of 40 ml/h between pH 5 and 6, are summarized in Table III. (There was no significant difference in the values measured at pH 5 or 6.)

On the basis of the differences in the relative elution volumes, the β-cyclodextrin polymer (β-CDP) proved to be the most suitable for the separation of amino acids. In this case, the retentions of the aromatic amino acids considerably differ from one another, while on the other hand they are characteristically larger than the retentions of the non-aromatic amino acids. Of the latter, lysine has the smallest value. Of aromatic amino acids, the difference in retention between tryptophan and all the other amino acids is the greatest in the case of α-CDP.

The differences in the retentions of amino acids are even easier to discern by a comparison of the volumetric partition coefficients $\left(K_{av} = \dfrac{V_e - V_0}{V_t - V_0}\right)$.

Table III

Relative elution volumes (V_e/V_t) of amino acids on columns packed with CDP gels
(room temperature, pH 5—6, elution flow velocity 40 ml/h, column packing 1.6×88 cm)

Amino acids	V_e/V_t		
	β-CDP	α-CDP	γ-CDP
Tryptophan	1.90±0.10	2.20±0.10	1.35±0.05
Tyrosine	1.15±0.05	1.05±0.05	0.95±0.05
Phenylalanine	0.95±0.05	1.05±0.05	0.85±0.05
Alanine	0.74±0.02	0.77±0.02	0.72±0.02
Further 11 amino acids*	0.75±0.05		
Aspartic acid	0.69±0.02		
Glutamic acid	0.69±0.02		
Arginine	0.69±0.02		
Histidine	0.69±0.02		
Lysine	0.63±0.02	0.72±0.02	0.68±0.02

* Cysteine, Glycine, Leucine, Isoleucine, Methionine, Proline, Serine, Threonine, Valine as well as Asparagine and Glutamine

Table IV contains the values calculated from data measured for a few amino acids on a column packed with β-CDP. The void volume of the column was, determined with water-soluble proteins of high molecular weight. ($V_0/V_t = 0.38$.)

Table IV

Volumetric partition coefficients (K_{av}) of a few amino acids on columns packed with β-CDP (room temperature, pH 5—6, elution flow velocity 40 ml/min, column packing 1.6×88 cm)

	$K_{av} = \frac{V_e - V_0}{V_t - V_0}$
Tryptophan	2.45±0.15
Tyrosine	1.25±0.10
Phenylalanine	0.92±0.10
Alanine	0.58±0.04
Lysine	0.40±0.03

The resolution of a chromatographic column is determined, besides the difference in retention, also by the efficiency of separation. For the characterization of the latter, the height equivalent of a theoretical plate (HETP) was determined for a column packed with β-CDP with a few amino acids under different conditions. It can be seen from the data summarized in Table V that on a column packed with β-CDP, separation at room temperature is most efficient at an elution rate of 10—20 ml/h.

Table V

Change of the height equivalent of a theoretical plate with the elution flow velocity (room temperature, pH 5—6, column packing 1.6×88 cm)

	Height of a theoretical plate (HETP), mm			
	10 ml/h	20 ml/h	40 ml/h	80 ml/h
Tryptophan (0.2 mg)	0.7—0.8	0.7—0.8	1.7—1.9	3.0—3.2
Tyrosine (0.1 mg)	0.7—0.8	0.7—0.8	1.0—1.2	2.0—2.2
Phenylalanine (0.1 mg)	0.7—0.8	0.7—0.8	1.3—1.5	2.1—2.3
Alanine (2 mg)	0.4—0.5	0.4—0.5	0.7—0.8	

The HETP depends to a considerable extent also on the temperature. As can be seen from Fig. 3, the most efficient separation (the smallest theoretical plate height) is to be expected at room temperature. On the basis of the data obtained for aromatic amino acids at room temperature and at an elution rate of 10—20 ml/h, the expected number of theoretical plates of a 1 m column packed with β-CDP is 1200 to 1400.

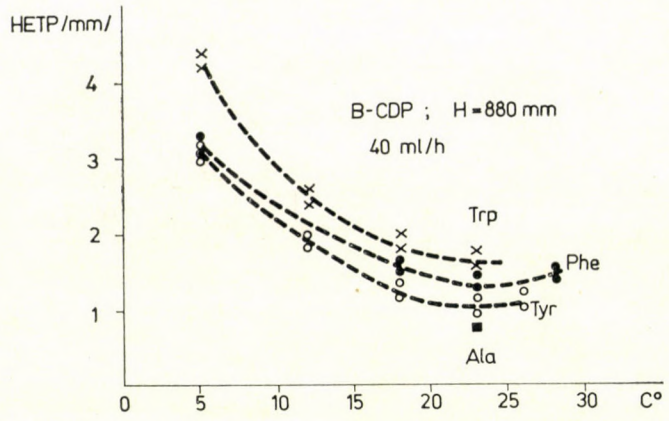

Fig. 3. Dependence of the height equivalent of a theoretical plate (HETP) on the temperature. (1.6×88 cm column packing, pH 5—6, elution rate 40 ml/h.)

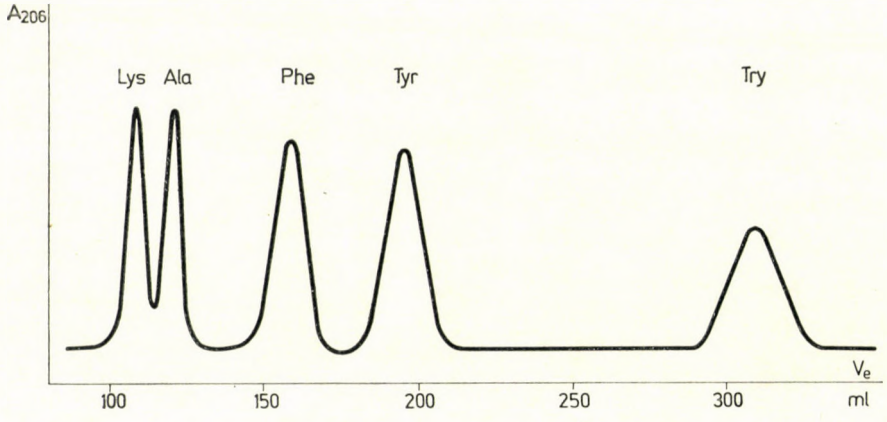

Fib. 4. Separation of amino acids on a column packed with β-CDP. (1.6×88 cm, pH 5—6, elution rate 10 ml/h, room temperature.)

By way of example, the chromatographic separation of tryptophan, tyrosine, phenylalanine, alanine and lysine is shown on columns packed with β-CDP (Fig. 4), α-CDP (Fig. 5) and γ-CDP (Fig. 6). As was to be expected, the best resolution (complete separation) could be achieved on a column packed with β-CDP.

For comparison, a mixture of the above 5 amino acids was chromatographed under identical conditions on a column packed with Sephadex G-25 gel, which binds the amino acids by adsorption according to data in the literature [9]. As can be seen from the chromatogram shown in Fig. 7, the sequence of elution is the same as that obtained on columns packed with CDP, but resolution is poorer than on the column packed with β-CDP, or (in the case of tryp-

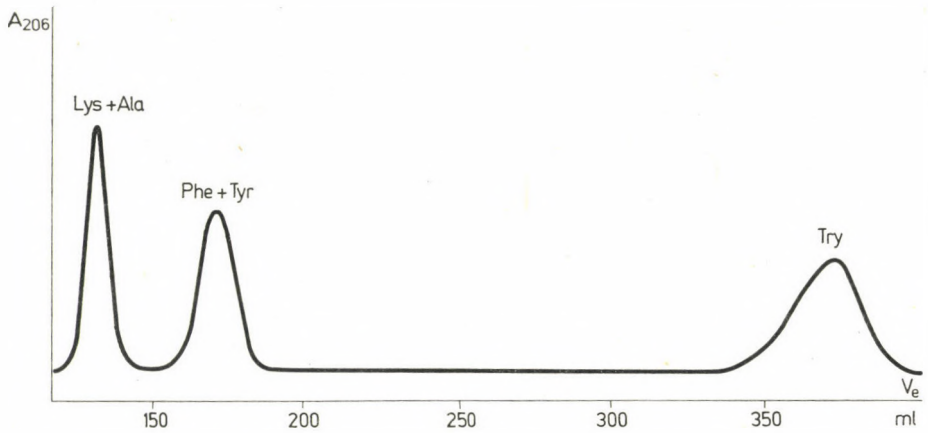

Fig. 5. Separation of amino acids on a column packed with α-CDP. (1.6×88 cm, pH 5—6, elution rate 10 ml/h, room temperature.)

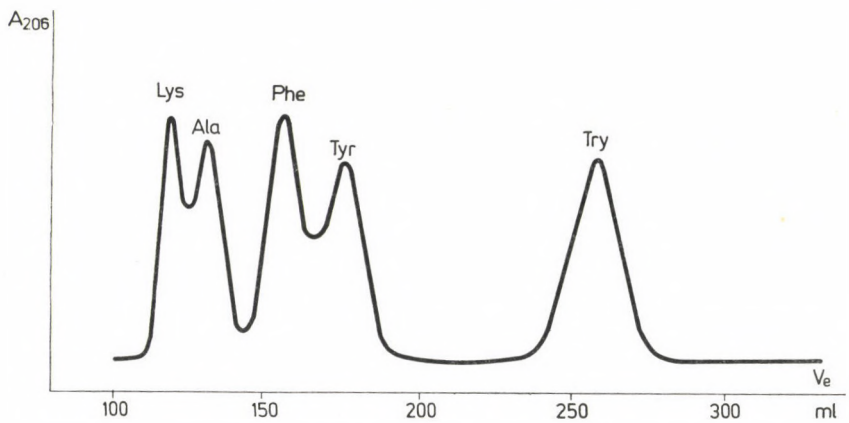

Fig. 6. Separation of amino acids on a column packed with γ-CDP. (1.6×88 cm, pH 5—6, elution rate 10 ml/h, room temperature.)

tophan) with α-CDP. The relative elution volumes (V_e/V_t) of the chromatographic peaks on the column packed with Sephadex G-25 gel are 1.56, 1.08, 1.02, 0.86 and 0.83.

The results described above are consistent with the conception that in the separation of the amino acids discussed, at least in the cases of β-CDP and α-CDP, the formation of inclusion complexes has also played a role besides adsorption. It seems justified to assume that the considerable increase in retention of mainly tryptophan and tyrosine on β-CDP gel, and of tryptophan on α-CDP gel, as compared with their retention on Sephadex G-25 gel, is due to complex formation. (This statement is consistent with earlier chromatographic

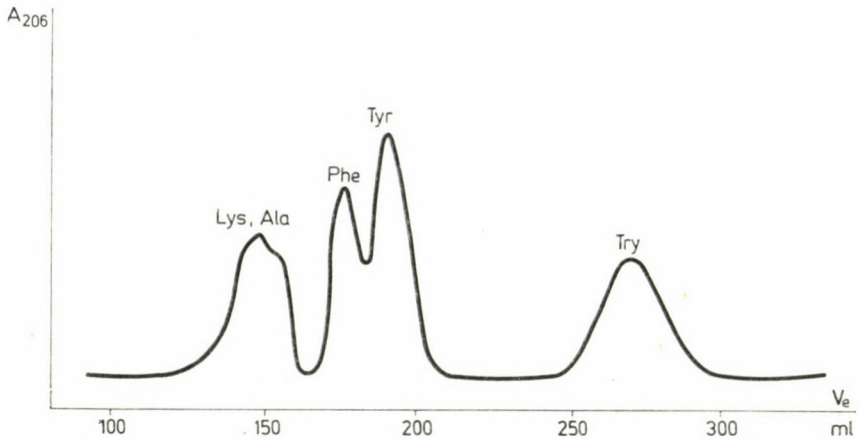

Fig. 7. Separation of amino acids on a column packed with Sephadex G-25 gel. (1.6×88 cm pH 5—6, elution rate 10 ml/h, room temperature.)

observations [1, 3, 4] and with the experience that from solutions primarily those aromatic compounds can be bound with cyclodextrin polymers, which demonstrably form inclusion complexes with the respective cyclodextrins.) Moreover, it should be added that in the case of non-aromatic amino acids (in the present case, alanine and lysine) complex formation is less to be expected, and indeed, retention based on adsorption is somewhat poorer than on Sephedex G-25 dextran gel.

REFERENCES

[1] Solms, J., Egli, R. H.: Helv. Chim. Acta **48,** 1225 (1965)
[2] Szejtli, J., Fenyvesi, É., Zsadon, B.: Stärke **30,** 127 (1978)
[3] Wiedenhof, N.: Stärke **21,** 163 (1969)
[4] Hoffman, J. L.: Anal. Chem. **33,** 209 (1970)
[5] Zsadon, B., Szilasi, M., Tüdős, F., Fenyvesi, É., Szejtli, J.: Stärke **31,** 11 (1979)
[6] Hung. Pat. Appl. (1978) CI 18—45.
[7] Wiedenhof, N., Lammers, J. N. J. J., Van Eck, C. L.: Stärke **21,** 119 (1969)
[8] Finley, J. H.: Anal. Chem. **33,** 1925 (1961)
[9] Gelotte, B.: J. Chromatography **3,** 330 (1960)

Béla Zsadon
Mária Szilasi
Klára H. Otta
Ferenc Tüdős
H-1088 Budapest, Múzeum krt. 6—8.

Éva Fenyvesi
József Szejtli
H-1026 Budapest, Endrődi Sándor u. 38—40.

Acta Chimica Academiae Scientiarum Hungaricae, Tomus 100 (1—4), pp. 275—288 (1979)

NEW METHOD FOR THE EVALUATION OF OVERLAPPING PROTONATION EQUILIBRIA OF POLYFUNCTIONAL LIGANDS

EFFECT OF SOLVENT ON THE PROTONATION OF THE FUNCTIONAL GROUPS OF CORTICOTROPINE

B. NOSZÁL and K. BURGER

(Institute of Inorganic and Analytical Chemistry, L. Eötvös University, Budapest)

Received July 5, 1978

Accepted for publication August 7, 1978

A method has been developed for the simultaneous determination of the protonation constants characteristic of the single functional groups and of pairs of groups forming hydrogen bonds, and of the number of hydrogen bonds in systems of overlapping protonation equilibria. The group and structural constants of the polyfunctional ligands, $ACTH_{1-4}$ and $ACTH_{1-32}$ polypeptides in 50% propylene glycol solution have been determined by the method, and from the constants conclusions are drawn concerning the interaction of the functional groups with one another and with the solvent.

Introduction

The interpretation of the protonation equilibria of ligands containing several donor groups of similar basicity is made rather difficult by overlapping processes. No evaluation method was elaborated so far suitable for characterizing the single functional groups in systems showing the overlap of more than two protonation steps. This is rather surprising as the basic relationships between macroconstants, characteristic of the stepwise protonation of the molecule, and microconstants, describing the protonation of a certain group of the molecule in a given state of protonation, were established by Niels BJERRUM in his classical work as early as 1923 for systems containing molecules of two and three groups without hydrogen bonding [1]. Since that time the literature on methods for the determination of macroconstants has vastly expanded [2—4] and the accumulated results fill several volumes [5]. This much less applies to microconstants, because in spite of the fact that several complex measuring methods including UV, Raman, NMR spectroscopy, *etc.* and methods of evaluation are known [6—10], the performance of these methods is limited to four microconstants characteristic of two groups, or to two times two groups contained in the molecule, thus to eight microconstants [11]. This is to be attributed primarily to the fact that the number of both the possible species of different protonation and the microconstants characteristic of

these particles increases rapidly with an increasing number of functional groups, causing difficulties in evaluation, insurmountable so far.

Polyfunctional bioligands, playing an important role in vital processes, can exert their action only at a suitable protonation of their groups. Therefore, the knowledge of the protonation constants of these groups is very important also from the aspect of the understanding and influencing biological systems. In the following the results of a work are summarized, the object of which was the elaboration of a method permitting in principle the simultaneous determination of the protonation constants of the functional groups and of the number of hydrogen bonds between these groups. The method is illustrated on the example of a protonation study of two fragments of the corticotropine (ACTH) molecule in propylene glycol—water mixture, where the effect of interaction of the functional groups with one another and with the solvent on the group protonation constants can be observed.

Principles of the Method

A molecule containing two functional groups, in which the sites of coordination are not equivalent, is characterized by the protonation equilibria shown in Fig. 1.

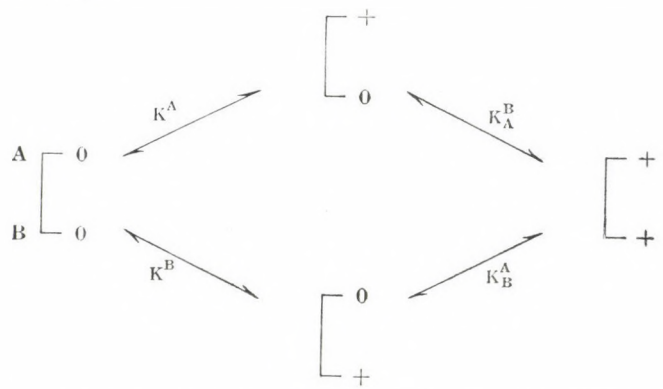

(1)

Fig. 1. Protonation equilibria of molecules containing two groups, without formation of hydrogen bonds

The microconstants relevant to this system are:

$$K^A = \frac{[\square_0^+]}{[H^+][\square_0^0]} \qquad K_A^B = \frac{[\square_+^+]}{[H^+][\square_0^+]}$$

$$K^B = \frac{[\square_+^0]}{[H^+][\square_0^0]} \qquad K_B^A = \frac{[\square_+^+]}{[H^+][\square_+^0]}, \tag{2}$$

where the upper index denotes the group being protonated in the process, while the lower index the already protonated group.

Material balances can be written as

$$C_L = [l_0^0] + [l_0^+] + [l_+^0] + [l_+^+] \tag{3}$$
$$C_H = [H^+] + [l_0^+] + [l_+^0] + 2[l_+^+],$$

where C_L is the total ligand concentration and C_H the total hydrogen ion concentration.

Rearrangement of Eqs (2) and their substitution into Eq. (3) gives;

$$C_L = [l_0^0] + (K^A + K^B)[l_0^0][H^+] + K^A K_A^B [l_0^0][H^+]^2 =$$
$$= [l_0^0] + (K^A + K^B)[l_0^0][H^+] + K^B K_B^A [l_0^0][H^+]^2$$
$$C_H = [H^+] + (K^A + K^B)[l_0^0][H^+] + 2K^A K_A^B [H^+]^2 [l_0^0] =$$
$$= [H^+] + (K^A + K^B)[l_0^0][H^+] + 2K^B K_B^A [H^+]^2 [l_0^0]. \tag{4}$$

It can be seen from Eqs (4) that on the basis of the material balance written for any of the total concentrations, the constant to be obtained from potentiometric data by the various known evaluation methods as the coefficient of hydrogen ion activity, is the sum of microconstants characterizing the different functional groups, while the constant obtained as the coefficient of the square of hydrogen ion activity is the product of corresponding microconstants (one of them is, however, different from the former microconstants):

$$\beta_1 = K^A + K^B$$
$$\beta_2 = K^A K_A^B = K^B K_B^A, \tag{5}$$

where β_1 and β_2 are complex products obtainable by the usual evaluation methods.

The same type of relationship for a system containing molecules with three groups is:

$$\beta_1 = K^A + K^B + K^C$$
$$\beta_2 = K^A K_A^B + K^A K_A^C + K^B K_B^C = K^B K_B^A + K^C K_C^A + K^C K_C^B$$
$$\beta_3 = K^A K_A^B K_{AB}^C = K^B K_B^C K_{BC}^A = K^C K_C^B K_{BC}^A. \tag{7}$$

The corresponding equilibria are shown in Fig. 2.

Models shown in Figs 1 and 2, and relationships (5) and (7) which can be derived from them, are characteristic of the protonation processes of molecules, in which the functional groups do not form intramolecular H-bonds with one another, and influence one another's protonation processes only by inductive and mesomeric effects, or possibly by hydrophobic interaction.

Two functional groups (A and B) form an H-bond only if this is energetically favourable for the system. Since the H-bond between A and B represents

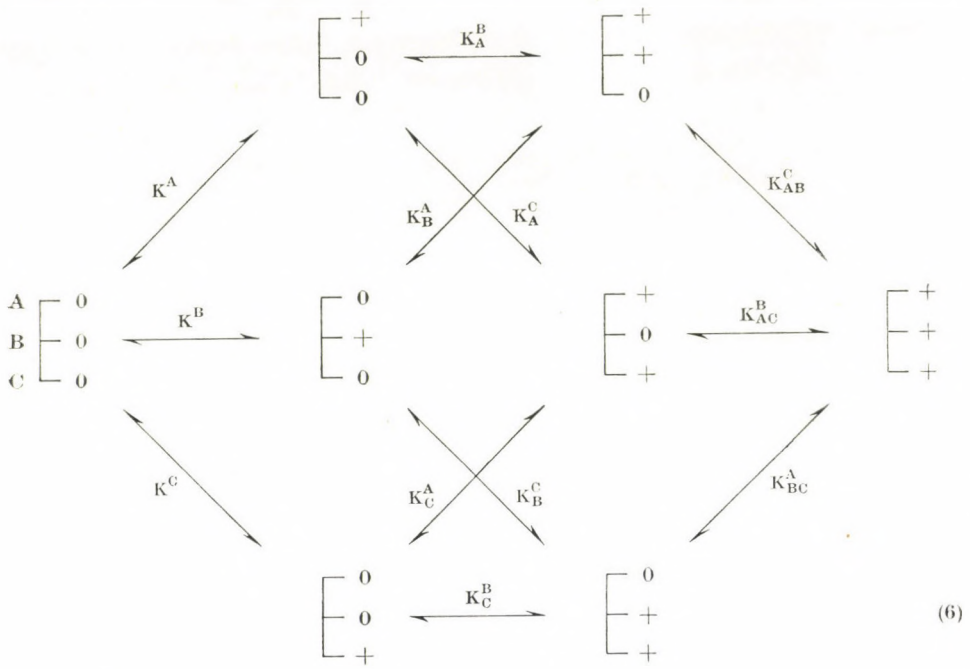

(6)

Fig. 2. Protonation equilibria of molecules containing three groups, without formation of hydrogen bonds

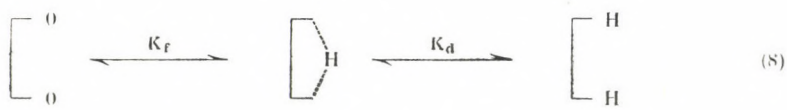

(8)

Fig. 3. Protonation equilibria of molecules containing two groups in the case of hydrogen bond formation

the singly protonated state of the lowest energy level, the H-bond is formed regardless of whether the proton approaches the molecule from group A or B. This reduces the possible number of particles occurring in the system (Fig. 3). In this case

$$\beta_1 = K_f; \quad \beta_2 = K_f \cdot K_d, \tag{9}$$

where K_f is the micro- and at the same time group constant (to be introduced in the following), characteristic of hydrogen bond formation, while K_d that characteristic of its rupture and the uptake of the second proton.

For molecules containing three functional groups (A, B and C), the scheme of protonation in the case of H-bond formation between groups A and B is

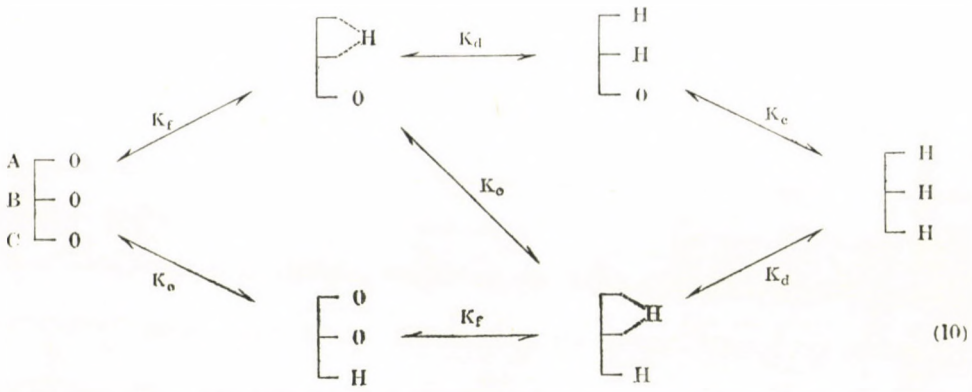

(10)

Fig. 4. Protonation equilibria of molecules containing three groups in the case of hydrogen bond formation

shown in Fig. 4 [where the symbols according to Eqs (16) are indicated in a simplified form]. From this the following relationships are obtained:

$$\beta_1 = K^f + K^C$$

$$\beta_2 = K^f K_f^C + K^f K_f^d = K^C K_C^f + K^f K_f^d$$

$$\beta_3 = K^f K_f^C K_{fC}^d = K^C K_C^f K_{fC}^d = K^f K_f^d K_{fd}^C . \qquad (11)$$

Tables I and II show the relationships between the number of groups (n) to be found in the molecule, the number of hydrogen bonds (k) linking the groups, and the number of species and microconstants, respectively.

It becomes evident from a comparison of Eqs (5) and (9) as well as (7) and (11) the protonation schemes (6) and (10) and data in Table I, that in the case of hydrogen bond formation the number of species formed is less than without H-bond formation, and thus, the number of microconstants needed for the characterization of the whole equilibrium system is also inversly proportional to the number of hydrogen bonds (Table II).

Table I

Number of species in the system as a function of the number of groups (n) contained in the molecule, and of the number of hydrogen bonds (k) linking the groups

k \ n	1	2	3	4	5	6
0	2	4	8	16	32	64
1	—	3	6	12	24	46
2	—	—	—	9	18	35
3	—	—	—	—	—	27

Table II

Number of microconstants serving for the complete equilibrium characterization of the system as a function of the number of groups (n) contained in the molecule and of the number of hydrogen bonds (k) linking the groups

k \ n	1	2	3	4	5	6
0	1	4	12	32	80	192
1	—	2	7	20	52	128
2	—	—	—	12	33	84
3	—	—	—	—	—	54

On comparison of the system of Eqs (5) and (9), as well as (7) and (11), it is remarkable and of basic importance for the determination of the number of hydrogen bonds to be described later, that for any of the systems the number of terms in the i-th β constant is equal to the number of i-times protonated species present in the solution.

The difference between the microconstants relevant to the same group in different surroundings can be traced back to two basic factors. One of these is the electron-attracting, (*i.e.* basicity-reducing) effect, occuring on protonation of the adjacent group, and perceptible also on the selected group. This effect is operative when the adjacent group is separated by an adequately low number of carbon (or other) atoms from the group in question, *i.e.* the static inductive effect actually reaches the given functional group.

The other essential effect to be taken into account is the steric proximity established by the protonation more often of the adjacent and more seldom of the more distant functional group, causing changes in rotational energy levels, which results in the formation of a hydrogen bond, ensuring a lower energy level for the system.

In the case of molecules having unknown structure in the solution, the first effect cannot be investigated separately from the second effect by the potentiometric method, because the change of the protonation constant observed cannot be separated into static inductive effect and H-bond formation. Therefore, independent experimental data are needed to establish electron attraction and electron release through the chain. Data of this kind are furnished by the proton resonance measurements of SUDMEIER and REILLEY [12]. These authors have found that the change in chemical shift occurring on protonation of the primary amino group can still be perceived at the third (γ) carbon atom from the amino group, but not at more distant atoms. In the case of carboxylate the effect cannot be measured any more at the third (γ) carbon atom. This means that, with the exception of conjugated systems, electron attraction occurring on protonation of group B (or electron donation on loss of a proton) will cause a perceptible change in the electron density of

group A only if not more than 2 atoms are located between the two functional groups. In peptides this occurs only in the single case when the *C*-terminal amino acid is aspartic acid. In the case of *C*-terminal glutamic acid the number of intermediate carbon atoms is already three, while in the next interchain case, when the — Asp — Asp sequence is present, the number of intermediate atoms is already six.

Thus, disregarding those peptides the *C*-terminal amino group of which is aspartic acid, or to be on the safe side, glutamic acid, it can be established that the basicity of the functional groups in the side chain of peptides occurring in practice, and thus the value of the protonation microconstants of the said functional groups cannot be affected by electron shifts through the chain even due to the nearest functional group. This means that microconstants relevant to identical groups are to be considered as identical, independently of the protonation of the molecule in the environment of the group. Accordingly, in the case of a molecule with two groups it follows from Eqs (2) that

$$K^{\mathrm{A}} = K_{\mathrm{B}}^{\mathrm{A}} = K_{\mathrm{A}}$$
$$K^{\mathrm{B}} = K_{\mathrm{A}}^{\mathrm{B}} = K_{\mathrm{B}} \tag{12}$$

and substituting Eqs (12) into Eq. (5):

$$\beta_1 = K_{\mathrm{A}} + K_{\mathrm{B}}$$
$$\beta_2 = K_{\mathrm{A}} K_{\mathrm{B}} \,. \tag{13}$$

In an analogous way, in a molecule containing three groups, in the absence of H-bonds:

$$K^{\mathrm{A}} = K_{\mathrm{B}}^{\mathrm{A}} = K_{\mathrm{C}}^{\mathrm{A}} = K_{\mathrm{BC}}^{\mathrm{A}} = K_{\mathrm{A}}$$
$$K^{\mathrm{B}} = K_{\mathrm{A}}^{\mathrm{B}} = K_{\mathrm{C}}^{\mathrm{B}} = K_{\mathrm{AC}}^{\mathrm{B}} = K_{\mathrm{B}}$$
$$K^{\mathrm{C}} = K_{\mathrm{A}}^{\mathrm{C}} = K_{\mathrm{B}}^{\mathrm{C}} = K_{\mathrm{AB}}^{\mathrm{C}} = K_{\mathrm{C}} \tag{14}$$

and upon substitution of Eqs (14) into Eqs (7):

$$\beta_1 = K_{\mathrm{A}} + K_{\mathrm{B}} + K_{\mathrm{C}}$$
$$\beta_2 = K_{\mathrm{A}} K_{\mathrm{B}} + K_{\mathrm{A}} K_{\mathrm{C}} + K_{\mathrm{B}} K_{\mathrm{C}}$$
$$\beta_3 = K_{\mathrm{A}} K_{\mathrm{B}} K_{\mathrm{C}} \,. \tag{15}$$

In the case of H-bond formation in a molecule containing two groups the reductions are not feasible.

In the case of H-bond formation in a molecule containing three groups:

$$K^{f} = K_{\mathrm{C}}^{f} = K_f$$
$$K^{\mathrm{C}} = K_f^{\mathrm{C}} = K_{fd}^{\mathrm{C}} = K_{\mathrm{C}}$$
$$K_f^d = K_{f\mathrm{C}}^d = K_d \,, \tag{16}$$

where K^f is a constant characteristic of hydrogen bond formation, K^d a constant characteristic of the rupture of the same by protonation; upon substituting Eqs (16) into (11) one obtains

$$\beta_1 = K_f + K_C$$

$$\beta_2 = K_f K_C + K_f K_d$$

$$\beta_3 = K_f K_C K_d. \tag{17}$$

In general formulation for the case of n groups and k hydrogen bonds:

$$\beta_1 = \sum_{i=0}^{n-k} K_i$$

$$\beta_2 = \sum_{\substack{a=0 \\ b=a+1}}^{\substack{n-k \\ n-k-1}} \prod_{i=a}^{b} K_i + \sum_{s=0}^{k} K_s K_{s+n-k}$$

$$\beta_3 = \sum_{\substack{a=0 \\ b=a+1 \\ c=b+1}}^{\substack{n-k \\ n-k-1 \\ n-k-2}} \prod_{i=a}^{c} K_i + \sum_{s=0}^{k} K_s K_{s+n-k} \sum_{\substack{t=0 \\ t=s+1}}^{\substack{n-k \\ s-1}} K_t$$

$$\vdots$$

$$\beta_n = \prod_{i=1}^{n} K_i, \tag{18}$$

where K_i and K_s are group constants carrying the symbols of current indexes i and s. Constants denoted from K_1 till K_k are the structural constants characterizing the formation of H-bonds, those from K_{k+1} till K_{n-k} are the protonation constants of groups without H-bond formation, while constants from K_{n-k+1} till K_n refer to rupture of H-bonds by protonation.

It can be seen from equations (13), (15) and (16) that the number of unknown group constants (K_A, K_B, K_C) and that of the group + structural constants (K_f, K_d), respectively, is equal to that of the known macroconstants (β_1, β_2, β_3) to be determined from potentiometric data. Thus, knowing the H-bond forming properties of the molecule, protonation constants characteristic of the groups and of the structural elements can be determined.*

* It should be noted that the simplifying reductions in systems of equation (12), (14) and (16) can be performed only in the case of adequately distant groups, because otherwise incorrect results (like those described in Ref. [14]) will be obtained.

Simultaneous determination of group constants and the number of hydrogen bonds from protonation macroconstants

If the number of hydrogen bonds in the molecule investigated is known, from relationships (13), (15) or (16), though they cannot be made explicite both for group and structural constants, the values of K_A, K_B, K_C, K_f, K_d can be obtained.

However, in the majority of cases, particularly for complicated molecules, the number of H-bonds in unknown.

As becomes evident from the comparison of equations (9) and (12) as well as (15) and (17) and from the interpretation of (18), the corresponding complex products (β) are determined by the group constants and by the number of species (which depends, besides the known number of functional groups, on the usually unknown number of hydrogen bonds ; see also Table I). This offers at the same time a possibility for the simultaneous determination of the group constants and the number of hydrogen bonds, when the β values are known.

It can be seen that from the n complex products of a molecule containing n groups, the n group or structural constants can be obtained in any case as the roots of the system of equations by a suitable mathematical (*e.g.* Newton—Raphson iteration) method, whichever relationship is used. Naturally, reality is correctly reflected only by those group and structural constants, in the calculation of which the number of the assumed H-bonds has been the same as in reality.

If the chemical model is not correct (incorrect number of H-bridges) some of the roots of the equation system may be complex or negative. In view of the fact that a protonation constant is always a real positive number, this in itself would be sufficient proof of the incorrectness of the model, if the macroconstants obtained from measured data were not subject to random errors, which are similarly sources of distortion in the type and particularly in the value of the roots obtained. Thus, the most suitable method of determination of the group (or structural) constants of a molecule containing an unknown number of hydrogen bonds, and of the number of hydrogen bonds in real systems is the following.

From the difference of the complex products, obtained from data measured, and from the group constant combinations yielding the same, a quadratic error function is generated in each member of the equation system. Constants obtained at zero value (which is the minimum of the error function) of the partial derivatives with respect to all the group constants of all the members of the equation system will give the group or structural constants with the best fit to the data.

For example, for a molecule with three groups and no H-bond the error functions are:

$$Z_1 = [\beta_1 - (K_A + K_B + K_C)]^2$$
$$Z_2 = [\beta_2 - (K_A K_B + K_A K_C + K_B K_C)]^2$$
$$Z_3 = [\beta_3 - (K_A K_B K_C)]^2 \qquad (18)$$

The quadratic matrix obtainable from the partial derivatives is:

$$\left.\begin{array}{lll} \frac{\partial Z_1}{\partial K_A} = 0; & \frac{\partial Z_1}{\partial K_B} = 0; & \frac{\partial Z_1}{\partial K_C} = 0 \\ \frac{\partial Z_2}{\partial K_A} = 0; & \frac{\partial Z_2}{\partial K_B} = 0; & \frac{\partial Z_2}{\partial K_C} = 0 \\ \frac{\partial Z_3}{\partial K_A} = 0; & \frac{\partial Z_3}{\partial K_B} = 0; & \frac{\partial Z_3}{\partial K_C} = 0 \end{array}\right\} \begin{array}{l} K_A \\ K_B \\ K_C . \end{array} \qquad (19)$$

A proof of the validity of the model reflecting the equilibrium constants and the number of H-bonds thus calculated is a good agreement between the experimental β values and those calculated from the group constants; the measure of this agreement can be characterized by the mean quadratic error. Another possibility for the selection of the models and thus of the number of hydrogen bonds is to follow the protonation of one of the functional groups by selective spectroscopy. If the constant calculated in this way is in exclusive agreement (whithin the limits of error) with one of the group constants of one of the models, this is also proof of the correctness of the given H-bond number.

The applicability in practice of the evaluation method described above is shown on the example of the protonation equilibria of corticotropin fragments consisting of 32 amino acids (henceforth $ACTH_{1-32}$) and its *N*-terminal tetrapeptide fragment ($ACTH_{1-4}$), measured in 50 vol. % propylene glycol.

Experimental

The *N*-terminal fragment of the α_H adrenocorticotropic hormone consisting of 32 amino acids ($ACTH_{1-32}$), and $ACTH_{1-4}$ consisting of the *N*-terminal four amino acids of this hormone were twice lyophilized, perprotonated preparations of G. Richter Chemical Works (Budapest). The solvent mixture was a homogenous 50 vol. % mixture of distilled propylene glycol and water, in which the ionic strength has been adjusted with $NaClO_4$ to 0.3 *M*. Devices used for the measurements: digital pH-meter Model Radiometer PHM 64 (precision of display + 0.1 mV), automatic burette Model Radiometer ABU 12 (precision of reading 0.001 ml); measuring electrode: glass electrode Radiometer G202B, reference electrode: Ag electrode Model Radiometer P 401, which was immersed into 0.01 *M* $AgNO_3$ solution (ionic strength adjusted with $NaClO_4$ to 0.3 *M*) and was connected through 0.3 *M* $NaClO_4$ dissolved in 50% propylene glycol with the measuring cell.

The macroconstants (β complex products) were calculated by the well known computerized evaluation. For the checking of the accuracy of the constants, the experimental mV *vs.* cm^3 0.01 *M* NaOH curves were recalculated with their aid. The good fit of the experimental

points to the calculated curves was considered as proof of the reliability of the data. From the macroconstants obtained in this way the group constants and structural constants characteristic of the single functional groups have been calculated with the evaluation method described above.

Results and discussion

Constants obtained in the protonation investigation of $ACTH_{1-4}$, a Ser-Tyr-Ser-Met tetrapeptide, are summarized in Table III. The protonation

Table III

Protonation constants of the tetrapeptide $ACTH_{1-4}$ in a **50**% *mixture of* **1,2**-*propylene glycol and water*

Complex product	Macroconstant	Group constant
$\lg\beta_1 = 10.04$	$\lg K_1 = 10.04$	$\lg K_A = 10.04$
$\lg\beta_2 = 16.91$	$\lg K_2 = 6.87$	$\lg K_B = 6.87$
$\lg\beta_3 = 20.75$	$\lg K_3 = 3.84$	$\lg K_C = 3.84$

macroconstants (K_1, K_2, K_3) belonging to the tetrapeptide and the values of the group constants obtainable from them are the same. The reason for this is that between the macroconstants there is a difference of at least 3 orders of magnitude, which at an accuracy of ± 0.06 lg K in the alkaline range and of ± 0.04 lg K in the acid range does not permit a distinction between the numerical values of the macroconstants and of the group constants. Moreover, the overlap of such distant equilibria is also too small for significantly changing the constants.

When the values of the protonation constants of the functional groups (phenolic hydroxy, terminal amino, terminal carboxy) obtained in the given solvent are compared with values obtained in aqueous solution [13], conclusions can be drawn on solvent — solute interactions.

Evidently, the value of lg $K_C = 3.84$ can be assigned to the terminal carboxylate group. As compared to the value of lg $K = 3.20$ measured in water, here primarily a decrease in permittivity ($\varepsilon = 59$), favourable for the formation of neutral particles, exerts its action.

The lg $K_B = 6.87$ value, belonging to the terminal amino group, is somewhat decreased, as compared to the respective constants measured in water (lg $K = 7.17$), which can be attributed to the specific solvation of the unprotonated amino group. In the value of lg $K_A = 10.4$ to be assigned to the phenolic hydroxy group (of lower value than that found in water), most different type of forces play a role, of which the interaction between propylene glycol and phenolate oxygen, leading probably to the formation of an H-bonded chelate is dominant.

Table IV

Various protonation constants obtained in **50%** **1,2-propylene glycol**

Macroconstant	Group constants				
	$k=$	0	1	2	3
$\lg K_1 = 10.27$	$\lg K_A$	9.70	9.75	9.85	9.84
$\lg K_2 = 10.13$	$\lg K_B$	9.70	9.75	9.84	9.84
$\lg K_3 = 9.89$	$\lg K_C$	9.70	9.75	9.83	9.84
$\lg K_4 = 9.50$	$\lg K_D$	9.70	9.74	9.75	9.84
$\lg K_5 = 9.28$	$\lg K_E$	9.70	9.73	9.71	9.73
$\lg K_6 = 8.58$	$\lg K_F$	9.20	8.88	8.80	8.56
$\lg K_7 = 6.90$	$\lg K_G$	6.81	6.81	6.80	6.82
$\lg K_8 = 6.11$	$\lg K_H$	6.09	6.06	6.17	6.06
$\lg K_9 = 5.41$	$\lg K_I$	5.15	5.29	5.16	5.29
$\lg K_{10} = 4.98$	$\lg K_J$	5.00	5.00	5.06	5.02
$\lg K_{11} = 4.61$	$\lg K_K$	4.68	4.46	4.45	4.46
$\lg K_{12} = 4.07$	$\lg K_L$	4.07	4.21	4.40	4.21
$\lg K_{13} = 3.95$	$\lg K_M$	4.00	4.07	4.00	4.00
	$\hbar_{OH}$	0.107	0.091	0.042	0.043
	$\hbar_H$	0.057	0.045	0.043	0.044

where $\hbar_{OH}$ and $\hbar_H$ denote the means of the absolute error in solutions of pH $>$ 7.5 and pH $<$ 8.0, respectively.

The results of the investigation of $ACTH_{1-32}$ protonation are summarized in Table IV. The first column of Table IV contains the macroconstants of stepwise protonation, while the other columns the group and structural constants, under the assumption of $k = 0, 1, 2, 3$ H-bonds both in the acid and alkaline regions, divided by a broken line. The means of the absolute error ($\hbar$) of recalculation are given below these columns. The division of the complete protonation pH-range into two parts was made because of computational considerations. The division into constant series below K_7 and above K_6 is made possible by the fact that the difference between the logarithms of these two constants is 1.68, owing to which there is only an overlap of about 2% between the two protonation processes. Differences between the logarithms of the macroconstants vary between 0.12 and 1.68, so that their value exceeds in all the cases the limits of error. It can be seen at the same time that group and structural constants, particularly in the alkaline region, are very similar whichever model is used for their calculation. The best agreement, both in the alkaline and acid regions can be observed when calculating with two and three hydrogen bonds. The difference between these latter two cannot be considered

significant any more. This is due partly to the fact that as yet the accuracy of measurements does not make possible the determination of equilibrium constants, correct to 3—4 decimal logarithmic units. On the other hand, in the acid region there are differences even of an order of magnitude between the various constants, so that their sum reflects mainly the value of the larger constant. Nevertheless, both in the acid and alkaline regions the model with two hydrogen bonds reveals the smallest (though not significantly smallest) error, and the appropriateness of this variant is supported also by chemical evidences.

Chemical conclusions to be drawn on the basis of the $k = 2$ model

The method of calculation presented here does not give direct information on the assignment of the individual constants to the functional groups, and even less so on the location of the hydrogen bonds in the peptide sequence. However, the method yields the number of hydrogen bonds between the functional groups, and the constants characterizing the structural elements forming hydrogen bonds with one another. The participation in other intramolecular hydrogen bonds (or possibly in hydrophobic interaction) of those groups forming no hydrogen bonds with one another but having constants different from that expected for the functional group, is highly likely.

The constants referring to the formation and rupture of hydrogen bonds between the appropriate pairs of groups in the alkaline region for $k = 2$ are 9.85 and 9.71, and 9.84 and 9.75, respectively. In view of the fact that there is a group in the same region which does not participate in a hydrogen bond and has a constant of 9.83, it can be established that all the hydrogen bonds formed are very weak, and their formation means only a slight gain in energy for the system. Since the deprotonation of the phenolic hydroxy group and of the ε-ammonium group of lysine proceeds in a very close pH-range, the above constants cannot be exactly assigned to groups and pairs of groups.

The structural constant of 8.80, similarly in the alkaline region, has no hydrogen bonding pair in this region. However, its unusually low value, as compared to both the phenolic hydroxy and the ε-amino group, indicates that the deprotonated form of one of the groups (presumably of the ε-amino group of lysine) forms a strong hydrogen bond with a group (*e.g.* the alcoholic hydroxy group of serine or the guanidino group of arginine), the deprotonation of which proceeds only at very high pH-values.

The lg K values in the acidic region in the absence of hydrogen bonding are : 6.80, 6.17 and 4.00. These can be safely assigned to terminal amino, histidine imidazole and terminal carboxy group, respectively. Their values reflect the same effects that have been observed (with the exception of imidazole) also in the case of the tetrapeptide.

The structural constants of formation and rupture of hydrogen bonds belonging together are: 5.16 and 4.40, and 5.06 and 4.45, respectively. Since the solvent mixture (similarly as in the case of the tetrapeptide) increases the protonation constants of the carboxylate group by about 0.7 lg units as compared to that in water [13], it can be established that each of these H-bonds has aspartic acid-glutamic acid carboxylate bridgehead groups. In 50% propylene glycol-water glutamic acid γ-carboxylate should have a protonation group constant of about $\lg K = 4.95$, while that of aspartic acid is approximately $\lg K = 4.60$. The differences of $\sim \pm 0.20$ and $\sim \pm 0.15$ lg K units from these values are proportional to the gain in energy by H-bond formation and to the loss in energy by H-bond rupture, respectively.

*

The authors thank G. Richter Chemical Works (Budapest) for making available the ACTH substances and propylene glycol, and Dr. Sándor B. Nagy for the determination of the relative permittivity of the solvent.

REFERENCES

[1] Bjerrum, N.: Z. phys. Chem., **106,** 219 (1923)
[2] Rosotti, F. J. C., Rosotti, H. S.: The Determination of Stability Constants. McGraw Hill, New York 1961
[3] Butler, J. N.: Ionic Equilibrium. Addison—Wesley, Reading 1964
[4] Beck, M. T.: Chemistry of Complex Equilibria. Van Nostrand, London 1970
[5] Sillén, L. G., Martell, A. E.: Stability Constants of Metal-Ion Complexes. Special Publication No. 17. The Chemical Society, London 1964; Supplement No. 1, Special Publication No. 25. The Chemical Society, London 1971
[6] Edsall, J. T., Wyman, J.: Biophysical Chemistry, p. 474. Academic Press, New York 1958
[7] Sarneski, J. E., Reilley, C. N.: The Determination of Proton-Binding Sites by "NMR Titrations", in Analytical Chemistry, Essays in Memoriam of Anders Ringbom. (Ed. E. Wänninen.) Pergamon Press, p. 35—49. 1977
[8] Shrager, R. J., Cohen, J. S., Heller, R. S., Sachs, D. H., Shechter, A. N.: Biochemistry, **1,** 541 (1972)
[9] Benesch, R. E., Benesch, R.: J. Am. Chem. Soc., **77,** 5877 (1955)
[10] Martin, R. B.: J. Phys. Chem., **75,** 2657 (1971)
[11] Rabenstein, D. L.: J. Am. Chem. Soc., **95,** 2797 (1973)
[12] Sudmeier, J. L., Reilley, C. N.: Anal. Chem., **36,** 1698 (1964)
[13] Burger, K., Gaizer, F., Noszál, B., Pékli, M., Takácsi-Nagy, G.: Bioinorg. Chem., **7,** 335 (1977)
[14] Jameson, R. F.: J. Chem. Soc. Dalton Trans., **1978,** 43

Béla Noszál
Kálmán Burger } H-1088 Budapest, Múzeum krt. 4/b.

Acta Chimica Academiae Scientiarum Hungaricae, Tomus 100 (1—4), pp. 289—303 (1979)

ON THE ESTIMATION OF ADSORPTION CAPACITIES FROM *L/S* EXCESS ISOTHERMS OF DILUTE SOLUTIONS

G. SCHAY,[1] L. G. NAGY[1,2] and G. FÓTI[2]

([1] *Central Research Institute for Chemistry, Hungarian Academy of Sciences, Budapest,*

[2] *Technical University of Budapest, Department of Applied Chemistry)*

Received July 5, 1978

Accepted for publication August 14, 1978

The usefulness of the isotherm transformation according to $\frac{x_1' x_2^l}{\Delta n_2^{(n)}} = \frac{1}{S n_{1,0}^s} + \frac{x_2}{n_{2,0}^s}$ in connection with dilute solutions of strongly adsorbed solutes is demonstrated. In favourable cases it provides means for a more reliable estimate of the adsorption capacity than the isotherms in their usual form and it is in general more informative concerning solute—solid interactions and the nature of the adsorbed layer. The following systems were studied: stearic acid from cyclohexane on carbon black; benzoic acid and *n*-butanol from water, and anthracene from cyclohexane on different activated carbons.

Introduction

It is well known that adsorptive enrichment of one or more molecular species at the surface or in the pores of an adsorbent can be characterized operationally, that is by relying only on directly measurable quantities, in an unambiguous quantitative way only through suitably defined surface excess amounts. In connection with S/L interfaces, the mostly used such quantity is the so-called reduced surface excess amount, $\Delta n_i^{(n)}$, the definition of which is [1]:

$$\Delta n_i^{(n)} = n_i - n x_i^l , \tag{1}$$

where n is the total amount of liquid in contact with the solid adsorbent of mass m_a, n_i the amount of component i present in it, and x_i^l the mole fraction of this component in the bulk liquid when adsorption equilibrium is established. The values of $\Delta n_i^{(n)}$ are usually determined by immersion experiments in which an amount n of liquid mixture or solution with mole fraction x_i^0 of component i in it is brought into contact with the adsorbent. The definition (1) transforms then into

$$\Delta n_i^{(n)} = n(x_i^0 - x_i^l) = n \Delta x_i \tag{2}$$

Δx_i is the apparent depletion of component i in the solution, caused by adsorption (in the case of negative adsorption, *i.e.* displacement of i by another

more strongly adsorbing component, Δx_i will be negative and corresponding to an apparent enrichment).

In order to get intercomparable data, it is usual to refer $\Delta n_i^{(n)}$ to unit mass of the adsorbent (specific reduced surface excess amounts):

$$n_i^{\sigma(n)} = \Delta n_i^{(n)}/m_a = n\Delta x_i/m_a \tag{3}$$

(the superscript σ is used to designate excess quantities). The function $n_i^{\sigma(n)}(x_i^l)$ at constant temperature and pressure is the reduced surface excess isotherm (in multicomponent systems this function is univalued only when the ratios of the mole fractions of the components other than i are kept constant).

The reduced surface excess isotherms can be defined, in the absence of chemical reactions, by the same right in terms of masses and mass fractions instead of amounts and mole fractions, by simple replacements in Eqs (1)—(3) (for the relevant conversion formulae, see *e.g.* [2]).

Any attempts at the interpretation of experimentally determined surface excess isotherms are based on the idea that the total amount of liquid present in the equilibrium system can be split into two parts: $n = n^s + n^l$, where $n^s = \Sigma n_i^s$ is the amount contained in the adsorption space (the layer adjoining the solid surface or eventually the total volume of the narrower pores of the adsorbent) in which the liquid is subjected to the force field of the adsorbent; the remaining part, $n^l = \Sigma n_i^l$ constitutes the homogeneous bulk liquid.

In the following, we shall concern ourselves only with dilute binary solutions, and designate by $i = 1$ the solvent, and by $i = 2$ the solute. We can write in this case for Eq. (1):

$$\Delta n_2^{(n)} = n_2 - nx_2^l = n_2 - (n_1 + n_2)\,x_2^l = n_2 x_1^l - n_1 x_2^l \tag{4}$$

and by subtracting the identity $0 = n_2^l x_1^l - n_1^l x_2^l$, we get the well-known equation of OSTWALD and IZAGUIRRE [3]:

$$\Delta n_2^{(n)} = n_2^s x_1^l - n_1^s x_2^l. \tag{5}$$

Evidently, if the relative accumulation by adsorption of *2* is considerable enough, then at sufficiently low equilibrium concentrations, x_2^l, the second term on the right hand side of Eq. (5) may become negligibly small so that, because of $x_1^l \approx 1$, $\Delta n_2^{(n)}$ can be approximately equated with n_2^s, the amount of *2* bound by adsorption. Nothing can be stated, however, concerning n_1^s, the amount of solvent present at the same time in the adsorption space, without recurring to more or less well-founded model assumptions. In practice we are interested in the maximum value of n_2^s, the adsorption capacity of the adsorbent for the given solute. In cases of strong preferential adsorption, the isotherms often appear to reach a plateau already at very low values of x_2^l, and it is usual to identify the height of this plateau with the adsorption capacity. This is in fact justified in some instances (an example is the system stearic acid

— cyclohexane — Spheron 4, examined by KIPLING and WRIGHT [8], see in the experimental section), but the plateau might often correspond in reality to a protracted maximum which would be followed by a decrease if the measurements were (or could be, if the solubiliy limit allowed it) extended to higher concentrations. In this case the apparent plateau does not represent the true adsorption capacity. In his book "Adsorption from Solutions of Non-Electrolytes" [4], KIPLING quotes several examples corroborating this statement, but we may also refer to SCHAY—NAGY type II isotherms [5] of completely miscible liquid pairs, the analysis of which shows conclusively that the maximum of this type of isotherms occurs at a value smaller than the true adsorption capacity for any strongly preferred component of the mixture.

We propose in the following a mode of evaluation of the isotherms of strongly adsorbing solutes which ensures a more reliable estimation of adsorption capacities.

Theoretical considerations

Two main assumptions are currently used as models for the structure of liquid adsorption layers : *a)* the layer model, applicable if the concept of surface area can be given a clear and more or less unambiguous meaning, and *b)* the pore filling model for adsorbents with narrow, mainly micropores, in the case of which the notion of surface area as relevant to adsorption becomes blurred.

a) Layer model [6]. In connection with this model it may be assumed that the adsorption space contains t layers of molecules (this is evidently a more or less crude idealization because no discrete molecular layers can be distinguished in real, non-crystalline liquids). The condition that the accessible surface of the solid is always completely covered can be expressed then as

$$n_1^s a_1 + n_2^s a_2 = A_s \,, \tag{6}$$

where A_s is the surface area of the adsorbent, while a_1 and a_2 are the respective partial molar areas in the surface layer; they are approximately equal to a_1^0/t and a_2^0/t, where a_1^0 and a_2^0 are the molar equivalents of the cross-sectional areas of the molecules. It has to be emphasized, however, that in the case of molecules of markedly asymmetrical shape, these effective cross-sectional areas will depend on the orientation of the molecules with respect to the surface (*e.g.* lying flat or standing erect) and this orientation may vary along an isotherm so that the values of a_i and a_i^0 should not necessarily remain constant, and even the constancy of t may not be warranted.

The adsorption capacities, $n_{1,0}^s$ and $n_{2,0}^s$, for the two components are the values of n_1^s and n_2^s extrapolated to the state where the adsorption space contains the respective pure component, in the molecular arrangement corresponding to the structure of the adsorption layer. Evidently

$$n_{i,0}^s = A_s t / a_i^0 \tag{7}$$

so that Eq. (6) can be transformed into

$$n_1^s/n_{1,0}^s + n_2^s/n_{2,0}^s = 1 \tag{8}$$

a form which can be retraced to WILLIAMS [4].

A widely used assumption is that of $t = 1$, *i.e.* of monolayer adsorption. There are strong arguments, however, partly intuitive, but more precisely based on considerations of thermodynamic stability, supporting the view that in general there must be a gradual transition in composition from the first layer adjoining the solid surface towards the bulk equilibrium liquid. Actual theoretical calculations show that at least two layers may be involved [6], but in many cases, mainly with marked preferential adsorption of one of the components, the monolayer model seems a quite satisfactory approximation.

Multilayer adsorption may be characterized by mean mole fractions, according to the following relations:

$$n_i^s = \sum_{j=1}^{t} n_i^{s,j}, \quad n^s = \sum_{j=1}^{t} n^{s,j}, \quad \bar{x}_i^s = n_i^s/n^s \tag{9}$$

and Eq. (6) can be transformed then into

$$n^s(\bar{x}_1^s a_1 + \bar{x}_2^s a_2) = A_s \tag{10}$$

while Eq. (8) remains unchanged. It has to be noted that n^s is not constant either in the monolayer or in the multilayer case, if the components are of markedly different size.

Combination of Eqs (5) and (8) allows to derive:

$$n_1^s = \frac{n_{1,0}^s(n_{2,0}^s x_1^l - \Delta n_2^{(n)})}{n_{2,0}^s x_1^l + n_{1,0}^s x_2^l}, \quad n_2^s = \frac{n_{2,0}^s(n_{1,0}^s x_2^l + \Delta n_2^{(n)})}{n_{2,0}^s x_1^l + n_{1,0}^s x_2^l}. \tag{11}$$

It may be born in mind that, owing to possible changes in orientation, $n_{1,0}^s$ and $n_{2,0}^s$ are not necessarily constant along the whole range of an isotherm.

The separation of the components brought about by adsorption can be characterized (similarly as in connection with the separation of liquids by distillation) by a separation factor S, defined as

$$S = \frac{\bar{x}_2^s x_1^l}{\bar{x}_1^s x_2^l} = \frac{n_2^s x_1^l}{n_1^s x_2^l} \tag{12}$$

($S > 1$ means preferential adsorption of *2*). Upon simple rearrangement:

$$\bar{x}_2^s = \frac{x_2^l/x_1^l}{1/S + x_2^l/x_1^l} \tag{13}$$

which is formally an expression of the Langmuir type, with the variable x_2^l/x_1^l going from zero to infinity over the whole composition range. In the domain of very dilute solutions, where $x_1^l \approx 1$, Eq (13) simplifies to

$$\bar{x}_2^s = \frac{x_2^l}{1/S + x_2^l}. \tag{14}$$

However, these equations would represent a real Langmuir isotherm only when S could be assumed to be equivalent to a true equilibrium constant. With the exception perhaps of practically ideal liquid mixtures, composed of molecules of nearly equal size, and of adsorbents whose surface is sufficiently homogeneous from the energetic point of view, S is in general certainly not an equilibrium constant and even not constant at all: in the case of preferential adsorption of *2*, S usually decreases decidedly with increasing x_2^l. In the following we shall restrict our considerations to highly and consequently ideally dilute solutions, and in this case it is the energetic heterogeneity of the adsorbent which is responsible for the decrease of S. This is well known nowadays from the experience accumulated in the practice of *HPLC* (for details, *cf.* the monography of SNYDER [7]).

By combination of Eqs (12) and (11) and rearrangement, we can derive (see EVERETT [6]):

$$\frac{x_1^l x_2^l}{\Delta n_2^{(n)}} = \frac{x_1^l}{(S-1)\, n_{1,0}^s} + \frac{S x_2^l}{(S-1)\, n_{2,0}^s} \,. \tag{15}$$

Multiplied on both sides by m_a, the mass of adsorbent used, this equation will refer to specific quantities: $n_2^{\sigma(n)} = \Delta n_2^{(n)}/m_a$ and the respective, specific adsorption capacities, $n_{1,0}^s/m_a$ and $n_{2,0}^s/m_a$. It may be noted further that the numerical value of S remains unchanged when we use masses and mass fractions instead of amounts of substance and mole fractions so that Eq. (13) is valid also when we replace the x_i by w_i and the n_i by the corresponding m_i.

Equation (15) can be used for the computation of $n_{2,0}^s$, the *adsorption capacity* of the adsorbent for *2*, if the adsorption of the latter is strongly preferred so that $S \gg 1$ and further $n_{1,0}^s$ is greater (or at least not substantially smaller) then $n_{2,0}^s$. In this case $S/(S-1) \approx 1$ and $1/(S-1)\, n_{1,0}^s \ll 1/n_{2,0}^s$, and in the domain of high dilutions $x_1^l \approx 1$ so that Eq. (13) simplifies to

$$\frac{x_1^l x_2^l}{\Delta n_2^{(n)}} = \frac{1}{S n_{1,0}^s} + \frac{x_2^l}{n_{2,0}^s} \,. \tag{16}$$

This means that the graph of the left-hand side against x_2^l is a straight line the slope of which gives the absolute value of the reciprocal of $n_{2,0}^s$. S has not to be strictly constant, only great enough throughout the range of compositions considered, because in this case an eventual moderate variation of S will not impair the linearity within the error limits of the experimental determination of the excess isotherm. The criterion for the fulfillment of this requirement is that the ratio of the intercept of the practically straight line with the ordinate at $x_2^l = 0$ to its slope should be very small, less than say 10^{-2}. An example of this kind of computation, taken from the literature, is shown in Fig. 1 which refers to the adsorption of stearic acid from cyclohexane solution on Spheron 6 the surface of which is fairly homogeneous. The graph is constructed from

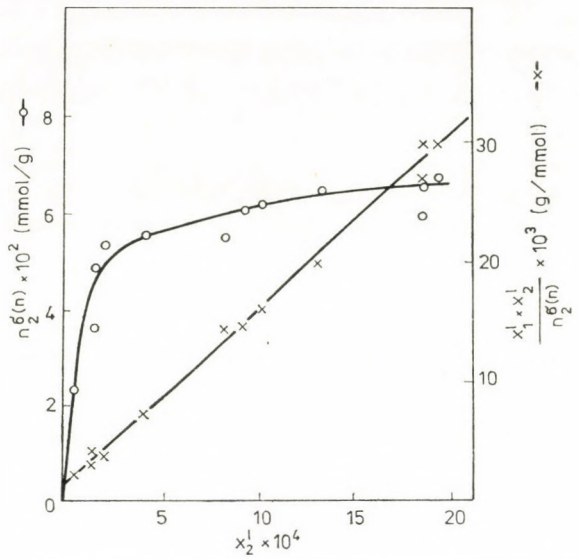

Fig. 1. Adsorption of stearic acid *(2)* from cyclohexane *(1)* on *Spheron 6* (see Ref. [8]). Intercept: 1.3×10^{-3} g/mmol; slope: 14.8 g/mmol; $n_{2,0}^s = 67.6$ μmol/g

data of KIPLING and WRIGHT [8]: the intercept of the straight line drawn through the experimental points is 1.3×10^{-3} g mmol^{-1}, whereas its slope 14.8 g mmol^{-1}. The latter value corresponds to $n_{2,0}^s = 67.6$ μmol g^{-1}, which is, according to KIPLING, compatible with the picture of a compact monolayer of hydrogen-bonded dimeric stearic acid molecules lying flat on the surface of the adsorbent. KIPLING came to this conclusion by considering the plateau of the excess isotherm itself which begins just at the last values shown in his Fig. 1 in [4] p. 98. Evidently, the computation according to Eq. (16) is a more reliable procedure, because it makes use of much more experimental points.

It must be noted, however, that the above arguments have to be somewhat modified in cases of strong surface heterogeneity.

The latter is mostly of a character that the surface contains a comparatively small amount of very active sites, the rest being much nearer to uniformity. This entails a sharp drop of S at the very beginning and consequently an initial increase of the first term on the right-hand side of Eq. (16). This may become ostensible on the graph by a departure from practical linearity at the lowest concentrations. It goes without saying that in such cases only the subsequent practically linear part of the representation is relevant for the computation of $n_{2,0}^s$. An example of such behaviour is shown in Fig. 6.

b) Pore filling model. In the case of adsorbents with narrow pores, especially micropores, where the clear meaning of the concept of surface area of the pores and the picture of a monolayer or multilayer coverage become

problematic or even meaningless, it seems more appropriate to consider the pore volume V_s as the adsorption space. Equation (6) has then to be replaced by

$$n_1^s V_1^s + n_2^s V_2^s = V_s \tag{17}$$

where V_1^s and V_2^s are the partial molar volumes of the components in the adsorbed portion of the solution. It may be remarked that in this picture equilibrium bulk liquid is not supposed to be present within, but only outside the pores, a circumstance which does not affect, however, the phenomenological definition of the reduced excess by Eq. (1). Since the composition of the liquid contained in somewhat wider pores may not be uniform throughout the whole volume of the pore and the average composition may depend on pore width, mole fractions characterizing the amounts contained in the adsorption space are to be considered as mean values, much in the same way as explained in connection with the layer model.

Considering that

$$V_s/V_1^s = n_{1,0}^s \quad \text{and} \quad V_s/V_2^s = n_{2,0}^s \tag{18}$$

Eq. (17) is equivalent to Eq. (8). It follows then that all the conclusions arrived at by combination of Eqs (5) and (8) and by making use of the definition of the separation factor S are valid also for the pore filling model. It appears, therefore, that the possbility of a reliable computation of $n_{2,0}^s$, the adsorption capacity of the adsorbent for a strongly preferred component is independent of any detailed model conception.

Some examples of application and discussion of the results

Experimental

Excess adsorption isotherms were determined at 25 °C according to the considerations and measuring principles described previously [2]. Each measurement was performed on a separate sample taken from the same batch of the adsorbent in question.

Adsorbents were four kinds of Hungarian active carbon prepared from nutshell: Nuxit A I, Nuxit A III, Nuxit Al III and Nuxit LBS. According to the manufacturers, the specific surface areas were, as determined by the *BET* method from nitrogen isotherms, equal to 620, 840, 860 and 510 m^2/g. Our own determinations by the method of NAGY and SCHAY [2, 5, 6, 9, 10] from excess isotherms of ethanol-benzene mixtures gave satisfactory agreement, *viz.* 590, 870, 850 and 530 m^2/g, respectively.

The adsorbent for the determination of the excess isotherm of anthracene in cyclohexane was the commercial activated carbon *Chemviron Type CAL*, designed for sugar refinery and similar purposes, with a specific surface area (*BET*, N_2) of 1000—1100 m^2/g and a total pore volume of 0.94 cm^3/g, and the pore size distribution shown in Fig. 7, according to the specification of the producing firm. Our own measurements with methanol—benzene and ethanol—benzene mixtures gave 900—1000 m^2/g for the specific surface area, again in fair agreement with the specification.

The chemicals used were of analytical grade; anthracene was of scintillator grade purity. The active carbons were pretreated each time by extraction with the respective solvent for six hours in a Soxhlet apparatus, then dried at 110—120 °C for twelve hours in a vacuum desiccator. The time for equilibration in the adsorption experiments was 24 hours under shaking the amount of adsorbent sample used for each experiment between 0.2 and 1 g, with an L/S weight ratio between 10 and 30 (30—300 in the case of *Chemviron Type CAL*).

Results

As can be seen from Tables I and II, the excess isotherms of benzoic acid in water level off after a sharp increase and appear then to tend towards a limiting value, but evidently do not reach what could be called a plateau, so that in their original form they are not suited for estimating the adsorption

Table I

Adsorption of benzoic acid **(2)** *from water* **(1)** *on Nuxit LBS at* **25** °*C* ($a_{s,\,BET}$ = **510** m^2/g), *compare Fig. 2*

$x_2^l \times 10^5$	1.10	2.30	4.38	9.20	18.01	23.00	39.90
$n_2^{\sigma(n)}$(mmol/g)	1.55	1.79	1.87	2.01	2.13	2.20	2.31

Table II

Adsorption of benzoic acid **(2)** *from water* **(1)** *on Nuxit Al III at* **25** °*C* ($a_{s,\,BET}$ = **860** m^2/g), *compare Fig. 3*

$x_2^l \times 10^5$	1.02	2.14	4.30	8.81	17.82	24.20	40.01
$n_2^{\sigma(n)}$(mmol/g)	1.96	2.28	2.66	2.70	2.80	2.91	3.04

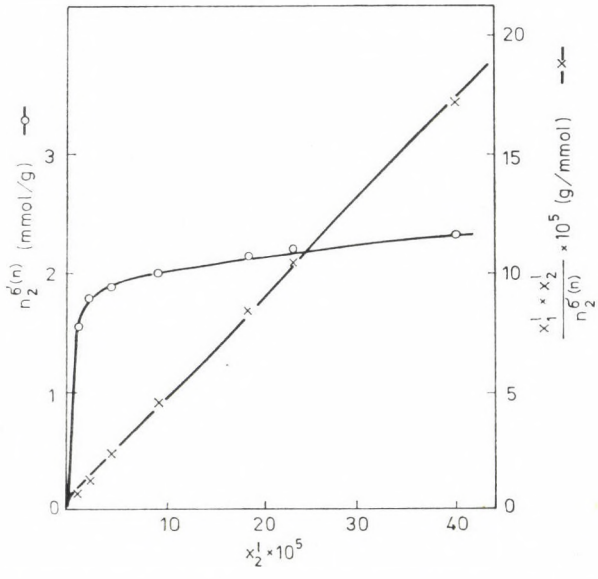

Fig. 2. Adsorption of benzoic acid *(2)* from water *(1)* on *Nuxit LSB* type activated carbon. Intercept: 5.0×10^{-6} g/mmol; slope: 0.425 g/mmol; $n_{2,0}^s$ = 2.36 mmol/g

capacities $n^s_{2,0}$. The transformations according to Eq. (16) reveal, on the other hand, very satisfactory linearity, as shown by Figs 2 and 3. The straight line in Fig. 2 has a slope of 0.425 g/mmol, to which corresponds a value of $n^s_{2,0} = 2.36$ mmol/g. If referred to the specific surface area of 510 m^2/g of *Nuxit LBS*, $a^0_2 = 216$ m^2/mmol benzoic acid results (0,36 nm^2/molecule), and this is a reasonable value when we take into account that surface area determinations according to the method of NAGY and SCHAY give good agreement with *BET* N_2 surface areas when using a value of $a^0_B = 0{,}30$ nm^2/molecule for benzene.

A similar calculation from the graph shown in Fig. 3 gives, however, on the basis of the slope 0.325 g/mmol in this case, an apparent value of 280 m^2/mmol (0,47 nm^2/molecule) for benzoic acid, a value markedly higher than the former one. The explanation for this finding might be sought in the fact that *Nuxit Al III* has a higher specific surface area, 860 m^2/g, and consequently contains a higher proportion of micropores, accessible only to the small water molecules, but not to those of benzoic acid. Thus, if the maximally adsorbable amount of the latter is referred to the total surface area and not only to the accessible part of it, the area per molecule will be overestimated. A quantitative description of this effect might be attempted in the following way.

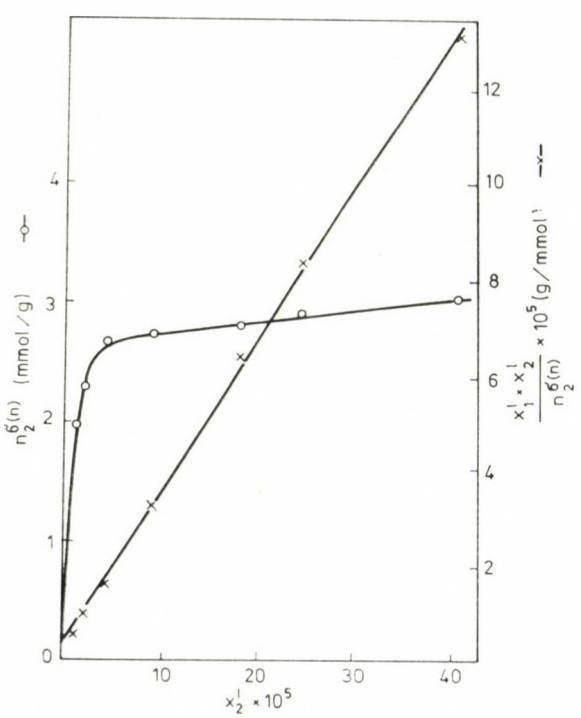

Fig. 3. Adsorption of benzoic acid *(2)* from water *(1)* on *Nuxit Al III* type activated carbon. Intercept: 3.5×10^{-6} g/mmol; slope: 0.325 g/mmol; $n^s_{2,0} = 3.08$ mmol/g

Let us reserve the superscript s for that part of the surface which is equally accessible for both components, and designate by superscript p the amount of matter contained in the micropores. We have then to write instead of Eq. (5):

$$\Delta n_2^{(n)} = n_2^s x_1^l - (n_1^s + n_1^p) x_2^l \tag{19}$$

and for the separation factor S instead of Eq. (12):

$$S = \frac{n_2^s x_1^l}{(n_1^s + n_1^p) x_2^l} \tag{20}$$

while Eq. (8) remains unchanged. From these relations there follows then

$$\frac{x_1^l x_2^l}{\Delta n_2^{(n)}} = \frac{x_1^l}{(S-1)(n_{1,0}^s + n_1^p)} + \frac{S x_2^l n_{1,0}^s}{(S-1) n_{2,0}^s (n_{1,0}^s + n_1^p)} \tag{21}$$

instead of Eq. (15) and

$$\frac{x_1^l x_2^l}{\Delta n_2^{(n)}} = \frac{1}{S(n_{1,0}^s + n_1^p)} + \frac{x_2^l}{n_{2,0}^s (1 + n_1^p / n_{1,0}^s)} \tag{22}$$

instead of Eq. (16). This result is somewhat surprising, because it indicates that the evaluation of $n_{2,0}^s$ from the slope of the graph leads to a more or less overestimated value, apparently contradicting the argument of the foregoing paragraph. The explanation might be that the "segregation" of n_1^p has the effect as if a reference amount of solution which is richer in component *2* were considered so that any measured point of the isotherm corresponds to a higher fictive x_2^l. Since, however, the surface area to pore volume ratio increases with decreasing pore width, the overall effect of the inaccessibility of the micropores for the solute molecules will manifest itself in an apparently increased value of the surface area per molecule if the maximal adsorbed amount is referred to the total surface area of the adsorbent (0,47 against 0,36 nm^2 in our case).

As can be judged from Tables III and IV, and Figs. 4 and 5, respectively, the isotherms of butanol in water and the representation of $x_1^l x_2^l / n_2^{\sigma(n)}$ are of a similar character as for benzoic acid. The slope of the straight line shown in Fig. 4 is 0.29 g/mmol, corresponding to a value of $n_{2,0}^s = 3.45$ mmol/g. If referred to the specific surface area of 620 m^2/g of *Nuxit AI*, $a_2^0 = 179$ m^2/mmol

Table III

Adsorption of n-butanol (**2**) *from water* (**1**) *on Nuxit A I, at* **25** °*C* ($a_{s,\,BET}$ = **620** m^2/g), *compare Fig. 4*

$x_2^l \times 10^3$	0.31	1.49	3.71	5.48	9.27	11.18	12.99	15.66
$n_2^{\sigma(n)}$(mmol/g)	1.40	1.77	2.44	2.88	2.93	3.03	3.05	3.18

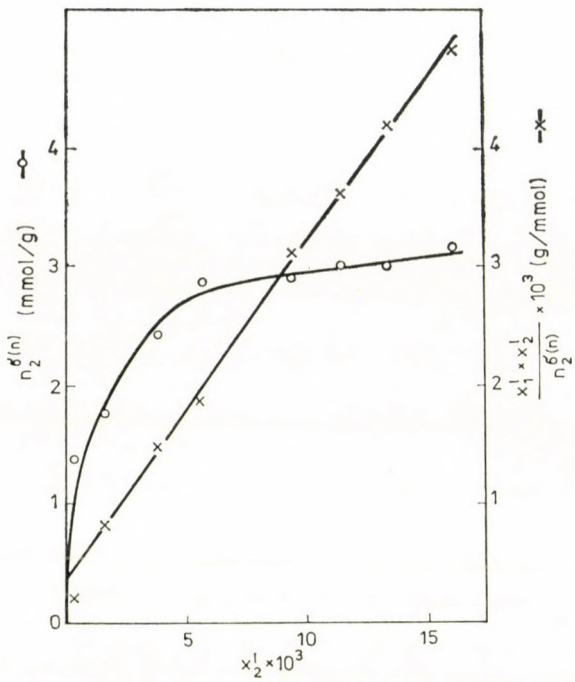

Fig. 4. Adsorption of *n*-butanol *(2)* from water *(1)* on *Nuxit A I* type activated carbon. Intercept: 4.0×10^{-4} g/mmol; slope: 0.29 g/mmol; $n_{2,0}^s = 3.45$ mmol/g

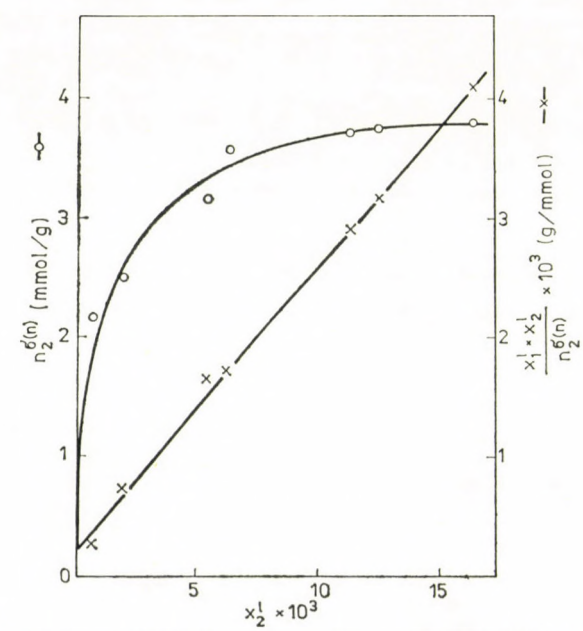

Fig. 5. Adsorption of *n*-butanol *(2)* from water *(1)* on *Nuxit A III* type activated carbon. Intercept: 2.0×10^{-4} g/mmol; slope: 0.244 g/mmol; $n_{2,0}^s = 4.1$ mmol/g

Table IV

Adsorption of n-butanol **(2)** *from water* **(1)** *on Nuxit A III, at* **25** °C ($a_{s,\,BET}$ = **840** m^2/g), *compare Fig. 5*

$x_2^l \times 10^3$	0.60	1.84	5.33	6.21	11.08	12.23	16.17
$n_2^{\sigma(n)}$(mmol/g)	2.16	2.50	3.17	3.56	3.74	3.78	3.83

(0,30 nm^2/molecule) results, again a reasonable value. The corresponding values which can be deduced from Fig. 5 are : slope = 0.244 g/mmol ; $n_{2,0}^s$ = 4.1 mmol/g ; a_2^0 = 204 m^2/mmol (0,34 nm^2/molecule), if referred to 840 m^2/g as the specific surface area of *Nuxit A III*. The difference between 0,30 and 0,34 nm^2 is only slight (it might be considered even as lying within the limits of experimental error), indicating that the less voluminous and more flexible molecules of *n*-butanol are not markedly excluded from the micropores, so that the value of $n_{2,0}^s$ represents in this case fairly well the true adsorption capacity also for the partly microporous activated carbon.

The last example we show here refers to the adsorption of anthracene *(2)* from cyclohexane *(1)* as the solvent, on granulated activated carbon *Chemviron Typ CAL*. The isotherm points listed in Table V (incidentally, these data reflect the somewhat poor accuracy, ±10%, of the fluorometric concentration determinations in this region of high dilutions) can be represented fairly well by a *Freundlich* type equation up to about $m_2^{\sigma(m)}$ = 75 mg/g, but then the isotherm levels off and tends apparently towards a plateau. With the exception

Table V

Adsorption of anthracene **(2)** *from cyclohexane* **(1)** *on Chemviron Typ CAL at* **25** °C ($a_{s,\,BET}$ = **1000—1100** m^2/g), *compare Fig. 6*

m/m_a (g/g)	$w_2^l \times 10^6$	$m_2^{\sigma(m)}$ (mg/g)
30	0.21	5.34
30	0.65	11.1
75	1.43	13.1
30	4.42	27.9
75	6.23	27.5
30	30.3	60.2
300	45.5	76.8
75	70.1	65.1
75	519	118
130	519	128
38	1720	133

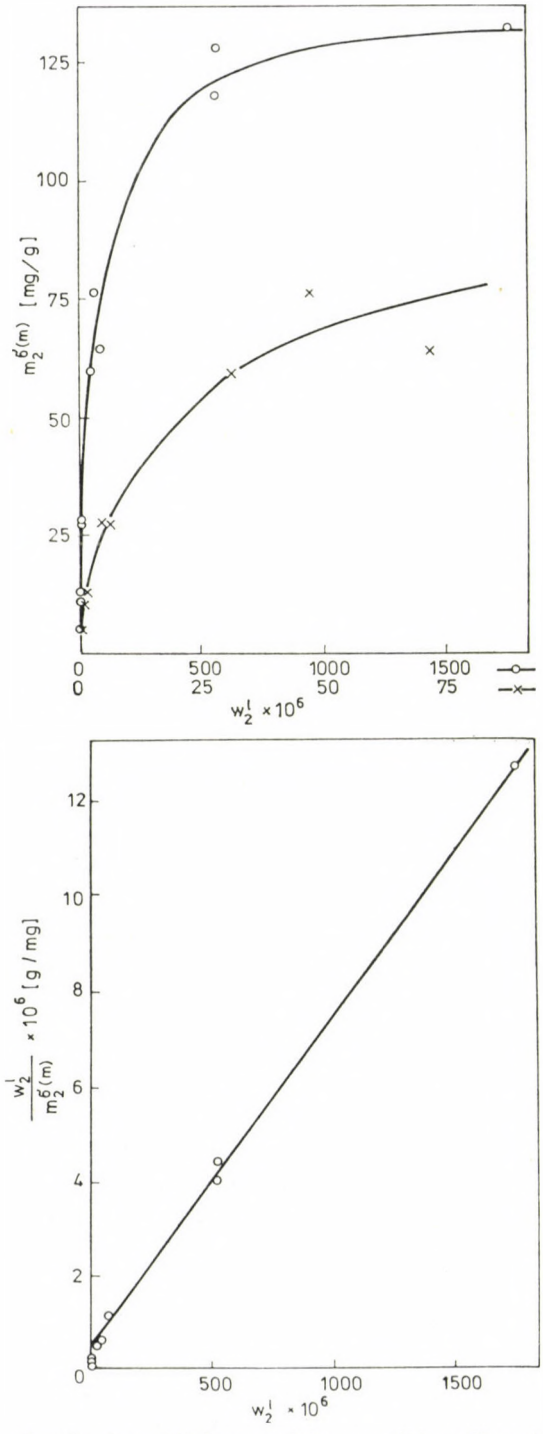

Fig. 6. Adsorption of anthracene *(2)* from cyclohexane *(1)* on *Chemviron type CAL* activated carbon. *a)* $m_2^{\sigma(m)}$ plotted *vs.* w_2^l. *b)* $w_2^l/m_2^{\sigma(m)}$ plotted *vs.* w_2^l; intercept: 0.5×10^{-6} g/mg; slope: 7.2×10^{-3} g/mg; $m_{2,0}^s = 139$ mg/g

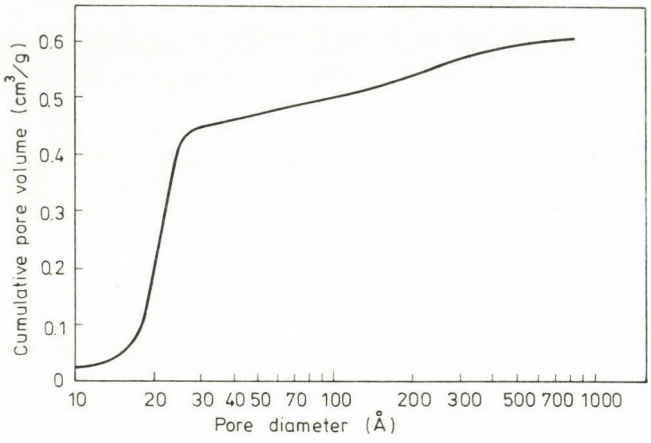

Fig. 7. Cumulative pore size distribution of *Chemviron type CAL* from data sheet supplied by the manufacturer firm

of its very first part, the plot of $w^l/m_2^{o(m)}$ *vs.* w_2^l (Fig. 6) is fairly linear; the straight line drawn in the figure has an intercept of 0.5×10^{-6} g/mg and a slope of 7.2×10^{-3} g/mg, the latter corresponding to $m_{2,0}^s = 139$ mg/g $= 0.78$ mmol/g. If referred to the specific surface area of about 1000 m²/g of the adsorbent, this value of $m_{2,0}^s$ would correspond to a molar surface area of antracene $a_2^0 = 1280$ m²/mmol, a quite unreasonable value, since 440 m²/mmol would be the maximum value for a close-packed layer of anthracene molecules lying flat on the surface. This great discrepancy between the two values cannot be explained by the exclusion of the anthracene molecules from micropores, as in the case of benzoic acid on *Nuxit Al III*, because on the one hand, according to Fig. 7, *Chemviron CAL* does not contain any considerable amounts of narrow micropores and, on the other hand, with cyclohexane as the solvent there is not such a great difference in size between solvent and solute molecules.

In order to explain our results we may suspect that the adsorption of anthracene is of mainly the pore filling type in this case. As can be seen in Fig. 7, a decisive part of the pores of *Chemviron CAL* has a size around 2 nm, a pore volume of about 0.3 cm³/g in this size region. The adsorption value we have found, 139 mg/g, corresponds to a volume of 0.111 cm³ of solid anthracene (density 1.25 g/cm³). If we adopt the pore filling model, then it is evident that in the pores, which have certainly irreguar shapes, the packing of the anthracene molecules cannot be by far so regular as in the solid state so that we have to reckon with a two to three times greater effective volume and this corresponds to that of the pores of around 2 nm size, in which strong adsorption of anthracene is to be expected. On inspection of Fig. 6 one can see that at its very beginning the plot deviates markedly from linearity. According to the argument in the last paragraph under *a)* in the foregoing section, such a be-

haviour points to a sharp initial decrease of the separation factor S. Now, evidently, the adsorption of anthracene molecules will be the strongest if they can lie flat on the surface. Such a position requires, however, in view of the size and rigidity of the anthracene molecules, a portion of about 0,80 nm^2 of smooth surface. Evidently the surface of the activated carbon will not contain many smooth sites of such extension so that only a small part of the anthracene molecules will adsorb in this way, while the main part will be bound by pore filling. This is the only explanation we can imagine for the behaviour we have found, but in spite of the uncertainty of the interpretation, we think that the value deduced from the graph of Fig. 6 is a reliable estimate of the adsorption capacity.

Concluding remarks

In our opinion, the examples shown above prove in an incontestable way the usefulness of the isotherm transformation according to Eq. (16), in connection with dilute solutions of strongly adsorbed solutes. In favourable cases it provides means for a more reliable estimate of the adsorption capacity than the isotherms in their usual form and is in general more informative concerning solute-solid interactions and the nature of the adsorbed layer. On the other hand however, any mechanical application without due criticism might lead to erroneous conclusions. Such a criticism has to rely mostly also on further relevant data concerning the system under question.

REFERENCES

[1] IUPAC Manual of Symbols and Terminology for Physico-chemical Quantities and Units, Appendix II, Definitions, Terminology and Symbols in Colloid and Surface Chemistry, Part I, Pure Applied Chem., **31,** 579 (1973)
[2] SCHAY, G., NAGY, L. G.: J. Colloid Interface Sci., **38,** 302 (1972)
[3] OSTWALD, Wo., de IZAGUIRRE, R.: Kolloid-Z. **30,** 279 (1922)
[4] KIPLING, J. J.: Adsorption from Solutions of Non-Electrolytes, Acad. Press, London and New York 1965
[5] NAGY, L. G., SCHAY, G.: Acta Chim. Acad. Sci. Hung., **39,** 365 (1963)
[6] EVERETT, D. H.: in Colloid Science, Ed. D. H. EVERETT, Vol. **1,** p. 49, The Chemical Society, Burlington House, London 1973
[7] SNYDER, I. R.: Principles of Adsorption Chromatography, Marcel Dekker Inc., New York 1968
[8] KIPLING, J. J., WRIGHT, E. H. M.: J. Chem. Soc., **1963,** 3382
[9] SCHAY, G., NAGY, L. G.: Acta Chim. Acad. Sci. Hung., **50,** 207 (1966)
[10] FÓTI, G., NAGY, L. G., SCHAY, G.: Acta Chim. Acad. Sci. Hung. **80,** 25 (1974)

Géza SCHAY H-1025 Budapest, Pusztaszeri út 59—67.

Lajos György NAGY
György FÓTI } H-1521 Budapest, Egri J. u. 20—22.

Acta Chimica Academiae Scientiarum Hungaricae, Tomus 100 (1—4), pp. 305—310 (1979)

CONTINUOUS ELECTROLYSIS OF ORGANIC COMPOUNDS

G. KORÁNYI, L. RÉDEY and E. GAGYI PÁLFFY

(Department of Applied Chemistry, Technical University, Budapest)

Received July 5, 1978

Accepted for publication July 31, 1978

A filterpress-type multi-purpose electrolysis equipment has been constructed to perform electrolytic reactions of organic compounds in a continuous process. Tests with reduction of benzoic acid to benzyl alcohol showed that the process can be performed continuously with appropriate efficiencies of reduction and current.

I

Theoretical and practical research in electrochemistry of organic compounds increased in the past 10 years and in a few cases the methods developed has been introduced to large scale manufacturing. Publications in this field include mainly descriptions of experiments discussing oxidation-reduction reactions as well as different types of cells [1—9].

Scaling up of processes depends on the application of adequate cell construction and soon after the first trials on pilot scale it became obvious that in order to obtain satisfactory yields, cells have to work continuously.

Utilization of electrochemical synthesis methods to manufacture organic compounds is considered most advantageous to cover medium volume (1—100 t/y) needs of relatively high priced products. A multi-purpose continuous cell construction would provide the opportunity to treat different materials and obtain different products in the same apparatus. Therefore constructing a single equipment with exchangeable electrodes and controls, production capacity for different products could be established.

The task of the work done was to create a model for a multi-purpose continuous electrolysis equipment.

The classical electrolysis equipment consisted of a tank, where the motion of the electrolyte has been sustained by pumping, mixig or using a rotating cathode. Temperature control needed the application of heating of refrigerating coils. The tank type cells however could not provide high productivity because of difficulties in controlling transport-processes.

Good results have been reported in using filterpress type cells. This type of equipment is utilized to the large scale production of adiponitryle by hydrodimerization of acrylonitrile [10—12], periodic acid [10], cyanogen bromide [13] and tetraethylammonium hydroxide [14].

II

The multi-purpose, continuous filterpress-type laboratory electrolysis equipment ensures the investigation of different electrochemical oxidation-reduction reactions, optimization of yields and evaluation of troubles that may arise in large scale manufacturing. Anodes, cathodes and diaphragmas can be exchanged and thus different types of materials can be tested. Space velocities of anolyte and catholyte can be varied as well as voltage input and pattern. The number of the cells can be modified and they can be switched to cascade or parallel exploitation. Volumes of gases generating during the process can be measured. Electrolyte temperatures can smoothly be regulated and owing to small distance between the electrodes no problem arises in keeping temperatures constant.

The cell system is shown in Fig. 1. The electrode plates are separated by plastic frames. Anolyte and catholyte are streaming in the space enclosed by the frames. Between anode and cathode two frames are placed which hold the diaphragm. In case of necessity, each cell may be heated or cooled inserting a neighbouring empty space, built of the same frame elements, where cooling or heating liquid can be circulated, ensuring direct contact with the non-working side of the electrode.

According to the number of cells and cooling/heating spaces, the system is coupled and compressed by longitudinal bolts of varying length.

Additional equipment of the cell system consists of voltage input, electrolyte pumps, heating/cooling equipment, degasifiers, electrolyte reservoirs, as shown in Fig. 2.

The use of variable speed peristaltic pump ensured the variation possibility in electrolyte velocities (5). To separate and measure gases leaving the

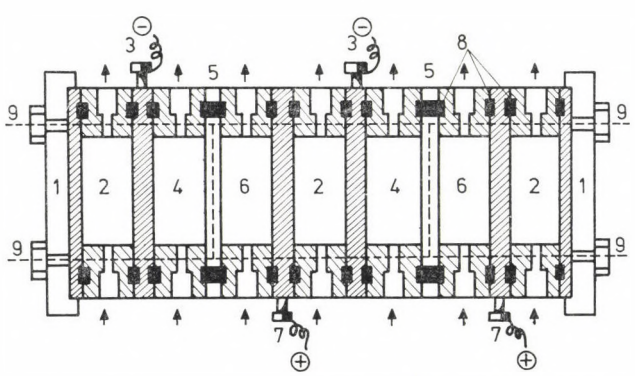

Fig. 1. Multi-purpose filterpress-type electrolysis cell; (1) Covering heads, (2) cooling/heating space, (3) cathode, (4) cathode space, (5) diaphragm, (6) anode space, (7) anode, (8) fittings, (9) bolts

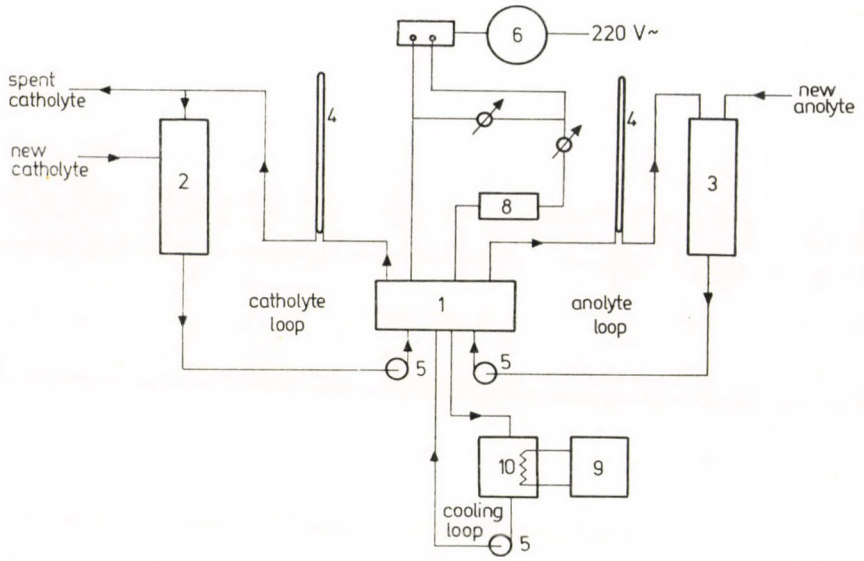

Fig. 2. Working scheme of the continuous laboratory-scale electrolysis; (1) filterpress cell, (2) tank for catholyte, (3) tank for anolyte, (4) gasholder, (5) pump, (6) voltage regulator, (7) rectifyer, (8) coulombmeter, (9) refrigeration equipment, (10) cooling liquid

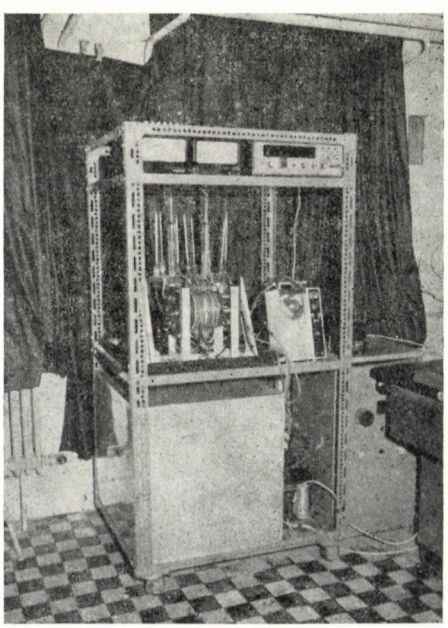

Fig. 3. Filterpress-type electrolysis cells

cells, calibrated tubes have been inserted (4) directly to the cell-interior. The anolyte and catholyte, after leaving the cell is pumped into tanks (2) and (3) from where they can be recirculated or extracted from the system. In continuous electrolysis new electrolyte can be added to the system in replacement of the exhausted and extracted electrolyte.

The heating/cooling liquid circulates in an independent system through the appropriate chambers adjacent to the cells (10).

The filterpress-type cell arrangement is shown in Fig. 3.

III

In testing the equipment, the electrolytic reduction of benzoic acid to benzyl alcohol has been investigated. This process has throroughly been investigated by K. NATARAJAN and al. [15], so the present work exclusively aims determining the applicability of the filterpress-type equipment to perform this kind of processes.

In the chemical process benzyl alcohol is produced by the hydrolysis of benzoyl chloride and the resulting alcohol needs purification. Advantage of the electrochemical reduction is that the end product is free of chlorine. Beside benzyl alcohol hydrogen is generated on the cathode:

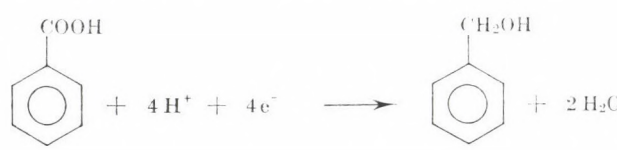

The generation of hydrogen is influenced by the concentration of benzoic acid and benzyl alcohol in the catholyte, the temperature of the catholyte, and the current density. The appropriate selection of the cathode material having a hydrogen overvoltage, prevents the hydrogen generation and promotes reduction of the benzoic acid. Contaminating metals in the cathode material or on the surface of the cathode influence also hydrogen generation, their presence may increase hydrogen generation and decrease current yield. Hydrogen volume measurement therefore is an important indication in controlling cathodic processes.

Because of oxygen evolution on the anode, to prevent its oxidation, an indifferent metal with a low oxygen overvoltage has to be applied. The purity of the anode is equally important as eventual metallic contaminations may be dissoluted into the anolyte, and passing through the diaphragm may contaminate the surface of the cathode.

A diaphragm with ion-exchange properties has been used in the electrolytic reduction experiments. Its selectivity supported to attain the overall net reaction corresponding to the equation

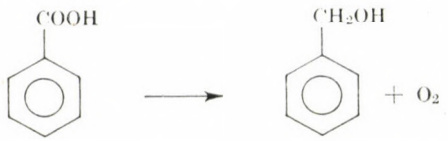

Based on the previous considerations and on experiences gained in former studies [15] lead anode and cathode of 99.99% purity has been used. A 10% sulphuric acid anolyte included addition of some ethyl alcohol in order to increase the solubility of the benzyl alcohol. The cells and the voltage has been switched in series.

1 liter 2.5% benzoic acid solution was electrolysed during 80 minutes using a current density of 40 A/dm^2 and an electrolyte velocity of 0.8 l/min. The necessary current amount was measured by using a coulombmeter. Solid benzoic acid has continuously been added to the electrolyte in order to replace consumed quantities, thus the benzoic acid concentration could be kept constant throughout the experiment. After this period electrolysis has been continued for another 60 minutes putting aside 800 ml of the used electrolyte and adding the same amount of fresh catholyte into the system.

Maintaining a temperature of 35 °C current efficiency was 48% and the yield 70%. Gas measurements showed hydrogen evolution corresponding to the current efficiency. By increasing the yield, current efficiency decreased. The optimal conditions for the electrochemical reduction process can be determined by taking into account prices of the raw material, eletrolyte, product and current.

The experiment demonstrated that a continuous reduction of benzoic acid to benzyl alcohol can be realized in the filterpress-type electrolyser equipment with the same current and reduction efficiences as in non-continuous electrolysis.

REFERENCES

[1] Fitzjohn, J. L.: Chem. Eng. Progr., **71,** 85 (1975)
[2] Fleischmann, M., Pletcher, D.: Chemistry in Britain, **11,** 50 (1975)
[3] Tomilov, A. P., Fioschin, M. Ya.: Brit. Chem. Eng., **16,** 154 (1971)
[4] Clarke, R.: Chemistry in Britain, **11,** 59 (1975)
[5] Frumkin, A. N., Ershler, A. B.: Progress In Electrochemistry of Organic Compounds, Plenum Press, London, N.Y. 1971
[6] Organic Electrochemistry. (Ed.: Baizer, M. M.) Marcel Dekker Inc. N. Y. 1973
[7] Weinberg, N. L.: Technique of Electroorganic Synthesis. I. II. Vol. **5.** Part I. J. Wyley Sons. 1974
[8] Fry, A. J.: Synthetic Organic Electrochemistry, Harper Row. N.Y. 1972
[9] Rédey, L., Szebényiné Győri, E., Gagyi Pálffy, E.: Magyar Kémikusok Lapja, **32,** 17 (1977)

[10] PRESCOTT, J. H.: Chem. Eng., **1965**, 238
[11] Fr. Pat. No. 1 503 244. Oct. 16, 1967
[12] BECK, F., GUTHKE, H.: Chem. Ing. Techn., **41**, 943 (1969)
[13] FOREMAN, R. W., SPRAGUE, J. W.: Ind. Eng. Chem. Prod. Res. Develop., **2**, 303 (1963)
[14] Brit. Pat. No. 1066930. April 26, 1976
[15] NATARJAN, K., UDUPA, K. S., SUBRAMANIAN, G. S.: Electrochem. Techn., **2**, 151 (1964)

György KORÁNYI
László RÉDEY
Edit GAGYI PÁLFFY
H-1502 Budapest, Egry József u. 20—22.

Acta Chimica Academiae Scientiarum Hungaricae, Tomus 100 (1—4), pp. 311—317 (1979)

NEW USES OF AMINALS IN ORGANIC SYNTHESIS*

SELECTIVE NUCLEAR ALKYLATION AND ARALKYLATION OF ACETOPHENONES

F. KÁLLAY,[1] G. JANZSÓ,[1] I. EGYED,[1] E. BAITZ-GÁCS and J. TAMÁS

([1] Research Institute for Organic Chemical Industry, Budapest, Central Research Institute for Chemistry of the Hungarian Academy of Sciences, Budapest)

Received July 10, 1978

Accepted for publication October 10, 1978

Benzylidene-bis-piperidine (**2a**) effects the nuclear aminoalkylation of 2',4'-dihydroxy- (**1a**) and 2',4',6'-trihydroxyacetophenone (**1b**) to give the 3'- (**3a**) and 3',5'-(phenyl-1-piperidinomethyl) (**3b**) derivatives, respectively. Similarly, **1a** with methylene-bis-piperidine (**2b**) gives 2',4'-dihydroxy-3'-(1-piperidinomethyl)acetophenone (**3c**). Reduction of the aminomethyl derivatives offers a selective route to *C*-benzyl- and *C*-methyl-acetophenones.

Aminals, the condensation products of aldehydes with two moles of a secondary amine, are known to react with the activated hydrogen atoms of organic compounds. There are several reports in the literature on the use of, *e.g.*, *N,N'*-benzylidene-bis-piperidine [1—4] and methylene-bis-piperidine [5—7] in syntheses of the Knoevenagel, Leuckart—Wallach and Mannich types.

Very often the same products are obtained when the aminal is used in a reaction instead of the corresponding aldehyde and secondary amine catalyst. This suggested questioning of the actual catalytic function of the amine [1].

Our experiments have shown that aminals act, in general, more powerfully than the components from which they are derived [8]. This is evidenced by better yields, or shorter reaction times, or in the practicability of a reaction otherwise failing to occur. In consequence of this higher activity, compounds containing less activated hydrogen atoms can also be brought into reaction. The examples herein reported are the interaction of 2',4'-dihydroxyacetophenone (resacetophenone) with *N,N'*-benzylidene-bis-piperidine and methylene-bis-piperidine, and the reaction of 2',4',6'-trihydroxyacetophenone (phloracetophenone) with the former aminal.

Treatment of resacetophenone (**1a**) in ethanol or benzene solution with an equimolar quantity of benzylidene-bis-piperidine (**2a**) or methylene-bis-piperidine (**2b**) gives 2',4'-dihydroxy-3'-(phenyl-1-piperidinomethyl)acetophe-

*For a preliminary communication, see Ref. [8].

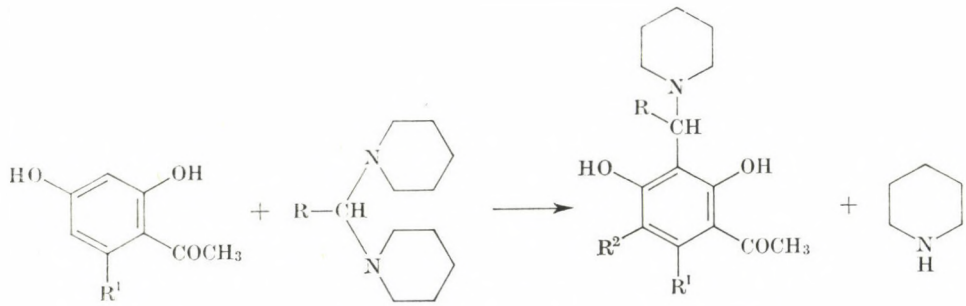

	R^1		R		R	R^1	R^2
1a	H	**2a**	Ph	**3a**	Ph	H	H
1b	OH	**2b**	H	**3b**	Ph	OH	CHR—N
				3c	H	H	H

none (**3a**) and 2',4'-dihydroxy-3'-(1-piperidinomethyl)acetophenone (**3c**), respectively, in good yields.

The corresponding product from 2',4',6'-trihydroxyacetophenone (**1b**) and **2a** is 2',4',6'-trihydroxy-3',5'-di(phenyl-1-piperidinomethyl)acetophenone (**3b**).

The fact that nuclear aminoalkylation had occurred selectively was proved by IR, NMR and MS investigations and chemical reactions of the products.

The IR spectra of **3a**—**3c** showed the presence of piperidine and the carbonyl group in hydrogen bridge. NMR revealed the acetyl-methyl group (excluding a condensation of the Claisen—Schmidt type) and that the acetophenone ring contained only two, neighbouring protons in **3a** and **3c** and none in **3b**. The presence of two piperidine-containing substituents in **3b** was evident. The mass spectrum of **3a** (see Experimental) gave the correct molecular weight for $C_{20}H_{23}NO_3$.

The fragmentation pathways of the molecular ions of **3a** leading to abundant peaks in the mass spectrum are connected with the presence of the piperidine part in the molecule: loss of a H atom and a neutral piperidine molecule (resulting in a peak at *m/e* 239); formation of piperidine molecular ion (*m/e* 85) and its $(M-H)^+$ ion (*m/e* 84); furthermore, ions at *m/e* 282 are at least partly due to elimination of a C_3H_7 radical from the piperidine moiety.

The mass spectrum of **3b** (see Experimental) exhibits ions attributable to a gas phase mixture of piperidine molecules and a compound with the molecular weight of 344. Chemical composition of the latter can be deduced from **3b** by substraction of two piperidine molecules.

The appearance of these compounds in the ion source under the experimental conditions applied is attributed to thermal decomposition of **3b** taking place during the sample evaporization.

3-(Phenyl-*N*-piperidinomethyl)resacetophenone (**3a**) gives a phenylhydrazone (**4**). Mild acetylation results in the removal of the piperidine moiety and the product is 2'-hydroxy-3'-(phenylacetoxymethyl)-4'-acetoxyacetophenone (**5**). Methanolysis of this product in the presence of dilute hydrochloric acid yields 2',4'-dihydroxy-3'-(phenylmethoxymethyl)acetophenone (**6**), which compound has also been prepared by refluxing **3a** in a 1 : 1 mixture of methanol and acetic acid, or by its hydrolysis in 1% methanolic sodium hydroxide.

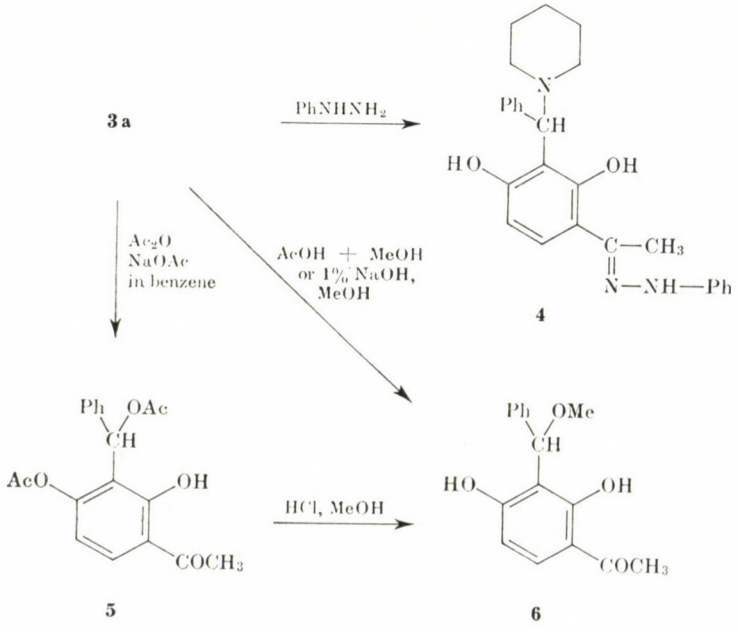

Additional and final chemical proof of the structures has been obtained by the hydrogenation of **3a** and **3c** in the presence of palladium-on-carbon catalyst which gives 2',4'-dihydroxy-3'-benzylacetophenone and 2',4'-dihydroxy-3'-methylacetophenone, respectively.

Instead of catalytic hydrogenation, tetraline in the presence of palladium-on-carbon has also successfully been used as the source of hydrogen.

These hydrogenations complete a reaction route affording now a new method of convenient selective nuclear alkylation or aralkylation of phenolic compounds, which reactions are known to be notoriously difficult to accomplish otherwise [9, 10] because of the formation of a mixture of the partial or complete *O*-alkyl or -aralkyl ethers.

The structures of all products have been confirmed by IR, NMR and elemental analysis. 3-Benzylresacetophenone [11] and 3-methylresacetophenone [12] have been reported in the literature, prepared by the usual methods.

Activation of the hydrogen atom in resacetophenone must be clearly due to a resonance structure [9] which undergoes re-aromatization after the reaction with the aminal.

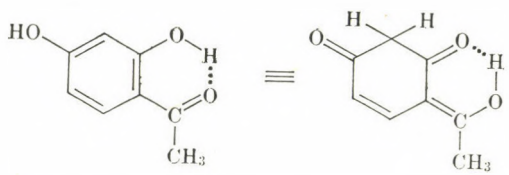

The resorcinol and phloroglucinol hydroxylation pattern is thus singularly suitable for reaction with aminals. As many naturally occurring flavonoids contain just this pattern and 6- or 8- or 6,8- *C*-methyl groups, a convenient synthesis of such substances also seems to be now accessible by the reaction of the parent flavonoid with methylene-bis-piperidine and subsequent reduction [8].

The scope of the reactions of various aminals with suitably hydroxylated acetophenones, flavonoids and other compounds containing activated hydrogen atoms is under investigation in our laboratory and the results will be reported in the future.

Experimental

All m.p.'s are uncorrected. NMR spectra were obtained at 100 MHz on a Varian XL-100 spectrometer; chemical shifts are given in δ ppm. Infrared spectra were measured on a Perkin—Elmer 577 instrument and mass spectra were taken and the exact mass measurements were carried out using an AEI MS-902 double focussing mass spectrometer operating at 70 eV ionizing electron energy. The samples were introduced *via* a direct inlet system.

Benzylidene-bis-piperidine

Analogously to literature methods [2,3], this starting material was synthesized by mixing a solution of piperidine (170 g) in ethanol (100 ml) with benzaldehyde (106 g) in ethanol (200 ml). The mixture was allowed to stand at room temperature for 6 h, then in a refrigerator overnight. The crystalline mass was broken up, filtered off, washed with ethanol (4×60 ml), and dried over $CaCl_2$ to obtain 210 g of chromatographically homogeneous benzylidene-bis-piperidine, m.p. 80—81 °C (*lit.* [2] m.p. 80.5—81 °C).

Methylene-bis-piperidine

Essentially following the literature method [5], this aminal was prepared by adding paraformaldehyde (30 g) in small portions to piperidine (170 g), maintining the temperature between 60 and 80 °C. When dissolution was complete, the mixture was filtered from any solid impurity, the water formed was separated, and the crude product dried over Na_2SO_4. Distillation in vacuum gave, after a short forerun, methylene-bis-piperidine (b.p. 107—108° at about 16 torr) in 90—95% yield; n_D^{18} 1.4835 (*lit.* $n_D^{18.5}$ 1.4830).

2',4',-Dihydroxy-3'-(phenyl-1-piperidinomethyl)acetophenone (3a)

2',4'-Dihydroxyacetophenone (**1a**) (19.2 g; 0.127 mole) in 63 ml of ethanol was mixed with a hot solution of 33.6 g (0.130 mole) of benzylidene-bis-piperidine (**2a**) in 130 ml of ethanol. The solution was refluxed for 4 h and then allowed to stand overnight. The yellow crystals which precipitated were filtered off, washed with ethanol and dried (P_2O_5) to obtain 27.7 g of the crude product, m.p. 162—166 °C. Recrystallization from methanol (45 ml MeOH/g) gave 23.4 g of **3a**; m.p. 168—171 °C.

IR (KBr): 2980 (CH), 2940, 2860, 2830 (piperidine), ~1620 cm^{-1} (CO).

PMR ($CDCl_3/Me_4Si$): δ 6.39(1H, d, C5-H), 7.48(1H,d,$J_{5,6}$ = 9 Hz, C6-H), 4.90(1H,s, C3-CH), 2.40(3H,s,C1-$COCH_3$), 13.08(1H,s,C2-OH), 7.2—7.55(5H,m,Ph), 1.58 + 2.42(10H, m, piperidine).

MS (source temperature: 120 °C) *m/e* (%): 325.1680 (24, $C_{20}H_{23}NO_3$, M^+; 324 (6.3); 308 (1.5); 282 (10); 239 (23); 221 (10); 197 (5.0); 115 (4.7); 85 (32); 84 (100).

$C_{20}H_{23}NO_3$ (325.41). Calcd. C 73.8; H 7.12; N 4.30. Found C 73.7; H 7.2; N 4.4%.

The same product was obtained in similar yields when effecting the reaction in benzene instead of ethanol.

2',4',6'-Trihydroxy-3',5'-di(phenyl-1-piperidinometyl)acetophenone (3b)

2',4',6'-Trihydroxyacetophenone (**1b**) (1.68 g; 0.01 mole) was dissolved in 35 ml of ethanol, filtered and mixed with a solution of 2.58 g (0.01 mole) of benzylidene-bis-piperidine (**2a**) in 35 ml of ethanol. Within 3 min the deposition of glistening pale yellow crystals started at room temperature. The mixture was allowed to stand overnight, the product was filtered off, washed with ethanol and dried (P_2O_5) to obtain 2 g of **3b**; m.p. 241—243 °C. A small sample recrystallized from ethyl acetate had m.p. 248 °C.

IR (KBr): 2970 (CH), 2940, 2858, 2830 (piperidine), 1623 cm^{-1} (CO).

PMR ($CDCl_3/Me_4Si$): δ 7.06 (5H, bs, Ph), 7.2—7.5 (5H, m, Ph), 4.82 (1H, s, C5-CH), 4.90 (1H, s, C3-CH), 2.62 (3H, s, C1-$COCH_3$), 14.15 (1H, s, C2-OH), 1.58 + 2.38 (20H, m, piperidine).

MS (source temperature: 160 °C) *m/e* (%): 344.1045 (84, $C_{22}H_{16}O_4$, M-2 x 85); 343 (81); 325 (8.8); 162 (10); 85 (90); 84 (100); 70 (16).

$C_{32}H_{38}N_2O_4$ (514.74). Calcd. C 74.67; H 7.44; N 5.44; O 12.43. Found C 74.43; H 7.25; N 5.62; O (direct) 13.37%.

2',4'-Dihydroxy-3'-(phenyl-1-piperidinomethyl)acetophenone phenylhydrazone (4)

A solution of **3a** (975 mg; 0.003 mole) in 40 ml of methanol was refluxed for 8 h with 0.6 ml (0.006 mmole) of phenylhydrazine. The product which separated after concentrating the solution was recrystallized from 1 : 6 $CHCl_3$/EtOH to obtain 460 mg of the phenylhydrazone (**6**); m.p. 214—217 °C.

IR (KBr): 3345 (NH), 2940, 2930, 2860, 2830 cm^{-1} (piperidine).

$C_{26}H_{29}N_2O_2$ (415.54). Calcd. C 75.2; H 7.0; N 10.1. Found C 75.5; H 6.9; N 10.1%

2'-Hydroxy-3'-(phenylacetoxymethyl)-4'-acetoxyacetophenone (5)

A mixture of **3a** (1.95 g), acetic anhydride (1 ml) and sodium acetate (222 mg) was refluxed for 10 h, then poured into water (100 ml) and the benzene phase was separated, dried over Na_2SO_4, and concentrated to give a deposit of crystals on standing; these were washed with cold benzene and recrystallized from the same solvent to obtain 400 mg of the acetyl derivative **5**, m.p. 176—178 °C.

IR (KBr): 1770, 1740 (CO (Ac)); 1620 cm^{-1} (CO).

PMR ($CDCl_3/Me_4Si$): δ 6.63 (1H, d, C5-H), 7.72 (1H, d, $J_{5,6}$ = 9 Hz, C6-H), 7.30 (5H, bs, Ph), 2.58 (3H, s, C1-$COCH_3$), 2.10 (3H, s, $OCOCH_3$), 2.21 (3H, s, $OCOCH_3$), 7.51 (1H, s, C3-CH), 13.05 (1H, s, C2-OH).

$C_{19}H_{18}O_6$ (342.35). Calcd. C 66.7; H 5.27. Found C 67.0; H 5.3%.

2',4'-Dihydroxy-3'-(phenylmethoxymethyl)acetophenone (6)

This compound was prepared in three ways. The acetyl derivative **5** (98 mg) was dissolved in methanol (3.5 ml), *conc.* hydrochloric acid (0.7 ml) was added, and the mixture refluxed for 1.5 h. On the addition of water, the product crystallized, m.p. 83—85 °C.

The same compound was obtained when 3.25 g of **3a** was refluxed in a mixture of methanol and acetic acid (50 ml each) for 24 h, and the hot reaction mixture was diluted with hot water (150 ml). Recrystallization from methanol (2.5 ml MeOH/g) gave 1.4 g of **6**, m.p. 84.5—86 °C.

IR (KBr): 2830 (OCH_3), 1620 cm^{-1} (CO).

PMR ($CDCl_3/Me_4Si$): δ 6.44 (1H, d, C5-H), 7.59 (1H, d, $J_{5,6} = 9$ Hz, C6-H), 7.2—7.55 (5H, m, Ph), 3.49 (3H, s, OCH_3), 5.94 (1H, s, C3-CH), 2.49 (3H, s, C1-$COCH_3$), 13.12 (1H, s, C2-OH).

$C_{16}H_{16}O_4$ (272.30). Calcd. C 70.5; H 5.9. Found C 70.0; 5.8%.

The compound was also isolated in a low yield from the hydrolysis (4 h at about 80 °C) of **3a** (1 g) in MeOH (50 ml) and 1% NaOH solution (20 ml); m.p. 81—82 °C; identification was made by IR.

2',4'-Dihydroxy-3'-benzylacetophenone

A suspension of 0.5 g of 10% palladium-on-carbon catalyst suspended in 25 ml of acetic acid was prehydrogenated; then 650 mg (0.002 mole) of the phenylpiperidinomethylresacetophenone **3a** in 30 ml of acetic acid was added and hydrogenation continued. After the absorption of 0.002 mole of hydrogen the rate of hydrogenation became very slow. The catalyst was filtered off, and the solution was diluted with 100 ml of hot water; on cooling white crystals separated (331 mg), m.p. 207—208 °C (slight sublimation started at 180 °C) (*lit.* [11] m.p. 195—197 °C).

IR (KBr): 1620 cm^{-1} (CO).

PMR ($CDCl_3/Me_4Si$): δ 6.49 (1H, d, C5-H), 7.49 (1H, d, $J_{5,6} = 9$ Hz, C6-H), 7.0—7.40 (5H, m, Ph), 3.99 (2H, s, C3-CH_2), 2.49 (3H, s, C1-$COCH_3$), 12.98 (1H, s, C2-OH).

$C_{15}H_{14}O_3$ (242.27). Calcd. C 74.36; H 5.8. Found C 74.4; H 5.9%.

An alternative route of reduction consisted in heating **3a** (650 mg) and palladium-on-carbon (300 mg) in tetraline (10 ml) between 140° and 150 °C for 8 h. The reaction mixture was then extracted with cold 5% NaOH solution (3×10 ml); the extracts were immediately acidified with 1 : 1 HCl. The product which precipitated was filtered off and dried to obtain 278 mg of 3-benzylresacetophenone, m.p. 197—202 °C. Recrystallization from aqueous EtOH raised the m.p. to 207—209 °C.

2',4'-Dihydroxy-3'-(1-piperidinomethyl)acetophenone (3c)

To 12.2 g (0.08 mole) of 2',4'-dihydroxyacetophenone (**1a**) in 40 ml of ethanol was added a solution of 14.6 g (0.08 mole) of methylene-bis-piperidine (**2b**) in 20 ml of ethanol. Refluxing for 1 h followed by cooling overnight in a refrigerator gave the almost pure product, which was recrystallized from ethanol to obtain 14.2 g of pure **3b**, m.p. 98.5—100 °C.

IR (KBr): 2950, 2930, 2855, 2830 cm^{-1} (piperidine), ~1620 (CO).

PMR ($CDCl_3/Me_4Si$): δ 6.32 (1H, d, C5-H), 7.53 (1H, d, $J_{5,6} = 9$ Hz, C6-H), 3.82 (2H, s, C3-CH_2), 2.49 (3H, s, C1-$COCH_3$), 12.60 (1H, s, C2-OH), 1.60 + 2.60 (10H, m, piperidine).

$C_{14}H_{19}NO_3$ (249.34). Calcd C 67.4; H 7.5; N 5.6. Found C 67.5; H 7.5; N 5.5%.

2',4'-Dihydroxy-3'-methylacetophenone

The piperidinomethylresacetophenone **3c** (2.5 g; 0.01 mole) was hydrogenated in the presence of prehydrogenated 10% palladium-on-carbon catalyst (1.0 g) in a total of 80 ml of methanol until the absorption of hydrogen stopped (uptake of about 0.01 mole of H_2). The catalyst was filtered off, the solution was adjusted to pH 3 with 15% HCl and concentrated to about 15 ml. Dilution with water (100 ml) induced the precipitation of white needles (1.1 g; 65%), m.p. 157—158 °C (*lit.* [12] m.p. 156—157 °C).

IR (KBr): 1620 cm^{-1} (CO).

PMR ($CDCl_3/Me_4Si$): δ 2.09 (3H, s, C3-CH_3), 2.50 (3H, s, C1-$COCH_3$), 6.45 (1H, d, C5-H), 7.45 (1H, d, $J_{5,6} = 9$ Hz, C6-H), 12.92 (1H, s, C2-OH).

$C_9H_{10}O_3$ (166.18). Calcd. C 65.05; H 6.0. Found C 64.5; H 6.2%.

*

The authors thank Mr. Kornél SZIJÁRTÓ for his valuable help in the experiments.

REFERENCES

[1] DILTHEY, W., STAHLMANN, B.: Ber. **62,** 1603 (1929)
[2] STEWART, Jr., A. TH., HEUSER, CH. R.: J. Am. Chem. Soc. **77,** 1098 (1955)
[3] LEONARD, N. L., LITTLE, J. C., KRESGE, A. S.: J. Am. Chem. Soc. **79,** 6436 (1957)
[4] STAPLE, E., WAGNER, E. C.: J. Org. Chem. **14,** 559 (1949)
[5] KNOEVENAGEL, E.: Ber. **31,** 2585 (1898)
[6] FELDMAN, J. R., WAGNER, E. C.: J. Org. Chem. **7,** 31 (1942)
[7] RAPAPORT, H.: J. Am. Chem. Soc. **73,** 2718 (1951)
[8] KÁLLAY, F., JANZSÓ, G.: Tetrahedron Lett. **1978,** 1443
[9] JAIN, A. C., SESHADRI, T. R.: J. Sci. Ind. Research (India), **14A,** 227 (1955)
[10] SESHADRI, T. R.: "The Chemistry of Flavonoid Compounds", (Geissman, T. A. Ed.) pp. 180. Pergamon Press, Oxford, 1962
[11] MULLAJI, B. Z., SHAH, R. C.: Proc. Indian Acad. Sci. **34A,** 88 (1951)
[12] RANGASWAMI, S., SESHADRI, T. R.: Proc. Indian Acad. Sci., **8A,** 214 (1938)

Ferenc KÁLLAY
Géza JANZSÓ
Ildikó EGYED
H-1085 Budapest, Stáhly u. 13.

Eszter BAITZ-GÁCS H-1025 Budapest, Pusztaszeri út 59—67.
József TAMÁS H-1088 Budapest, Puskin u. 11—13.

Acta Chimica Academiae Scientiarum Hungaricae, Tomus 100 (1—4), pp. 319—339 (1979)

INFLUENCE OF PHOTOGRAPHIC AND PHOTOMETRIC EFFECTS ON SPECTROGRAPHIC EVALUATION, I

PROBLEMS IN THE EVALUATION OF EMISSION SPECTRA; EFFECT OF THE MICRODENSITOMETER TYPE ON THE RESULTS OF DENSITY MEASUREMENTS

K. ZIMMER* and Gy. HELTAI[1]

(Institute for Inorganic and Analytical Chemistry of L. Eötvös University, Budapest,
[1] Department of Chemistry of the University of Agricultural Sciences, Gödöllő)

Received July 10, 1978

Accepted for publication August 14, 1978

In the first paper of this series problems connected with photometric evaluation of spectrograms, first of all error sources of density measurements and terms of extending measuring range are dealt with. When comparing various types of microdensitometers it has been established that the density measuring range of traditional microdensitometer type C. Zeiss Jena G II can be extended to about its twice, to $S = 4$, by building in a modern low-noise detection system linear in wide-range and by reducing simultaneously the scattered light in a considerable measure.

1. Introduction

In the past decade the development of analytical chemical methods has resulted in the elaboration of new techniques meeting the requirements of modern optical emission spectral analysis, too. Especially rapid progress can be observed in the field of spectrochemical radiation sources primarily due to the introduction of new excitation methods (*e.g.* ICP) [1, 2, 3, 4]. With the help of novel sensors (*e.g.* chevron shaped electron multiplier, semiconductor sensors) promising experiments are performed also in the domain of spectrometric methods measuring directly the radiation [5, 6]. This progress, as well as the wide use of computerization made possible the development of automatic analyzers of new types and high performance [7].

However, the spectrographic methods continue to be of great importance, since even the most up to date spectrometers do not have such a great information fixing and storing capacity as the photographic emulsion method does. Computerization and the introduction of modern automatic microdensitometers have opened up new possibilities also in spectrography [8]. With their help the big amount of information fixed on spectrograms can be better utilized and

the evaluation can be automated. The advantages offered by mathematical statistical methods may be exploited and thus the most complicated calibration and correction calculations do not cause any problem. Further on, with the modernization of microdensitometers, the measuring range can be widened and errors of measurement can be reduced, as well. However insufficient attention has been paid so far to the theoretical and practical results of these achievements in analytical chemistry.

Our series, starting with this paper, intends to deal with the development of spectrographic evaluation using the above mentioned possibilities. Error sources of density measurements, theoretical requirements and practical aspects of the instrumental technical realization of increasing the measured range will be treated. Relationships between photographic and photometric factors influencing the shape of blackening curve are examined in detail by the help of conventional and modern microdensitometers of wide measuring range. The applicability and precision of *l*-transformation in the case of various microdensitometers are compared. The influence of the characteristics of photographic emulsion and that of the microdensitometer on the shape and parameters of the analytical curve is discussed, too. Our main aim was to explore new analytical chemical possibilities deriving from the increased range of density measurements: to increase the measurable concentration range, to improve the precision, reliability and power of detection in analytical practice.

2. Problems of photographic evaluation of emission spectra

2.1. Role of blackening curve and blackening transformation in spectrographic evaluation

The main aim of quantitative spectral analysis is to determine concentration c from the intensity I of spectral lines. The practical methods are based on the empirical SCHEIBE—LOMAKIN [9, 10] equation, $I = ac^b$, which is used in spectrographic analysis as follows [11, 12]:

$$\Delta Y_{X\,R} = A_{X,R} + B_X \lg c_X ,$$

where $\Delta Y_{X,R}$ is the logarithm-intensity ratio of the pair of line,

c_X is the concentration of element to be determined.

$A_{X,R}$ and B_X are constants depending on experimental conditions.

In practice the above correlation was found to be linear in certain concentration limits. At low concentrations disturbing effects (background, blank value) comparable to the I_X intensity, while at high concentrations due to self-absorption the slope of the curve decreases. $\Delta Y_{X,R}$ values are influenced also by the photographic radiation measuring method. From the point of view of precision and reliability of analysis correct determination of the characteristic

curve of photographic emulsion [13, 14] (the blackening curve) and the precise limits of intensity range to be measured photographically are of decisive significance.

Photographic emulsion is an irreversibly operating radiation detector. Upon exposure in the silver-halogenide grains photolysis occurs in a small degree which is then in course of the development multiplied by its 10^7-10^8 producing a photographic image. The amount of silver formed on the exposed spots depends on the energy of radiation E falling on one surface unit of photographic emulsion, which can be given as the mean value of intensity I of radiation depending on time multiplied by the time of exposure: $E = I \cdot t$. The amount of silver formed determines density S:

$$S = -\lg T = \lg \frac{i_0}{i},$$

where T is transmittance,

i_0 the intensity of light falling on the developed photographic emulsion,

i the light intensity transmitted through photographic emulsion.

Intensity decrease of incident light is due to the light absorption, reflection and scattering of silver grains.

In spectrography the logarithm-intensity-ratio of analytical lines is determined indirectly on the basis of density measurements. For this reason it is essential to establish the correlation between density and intensity of exposing light (emulsion calibration). Density is plotted against the logarithm of the amount of radiation, thus the characteristic curve of photographic emulsion, that is the blackening curve is obtained [13]. For spectrographic purposes the blackening curve relating to constant exposure time is suitable (Fig. 1). For spectrographic analysis only the densities found in the underexposed and the straight part can be used reliably. An important feature of photographic emulsion is the slope of the straight part that is the γ-value.

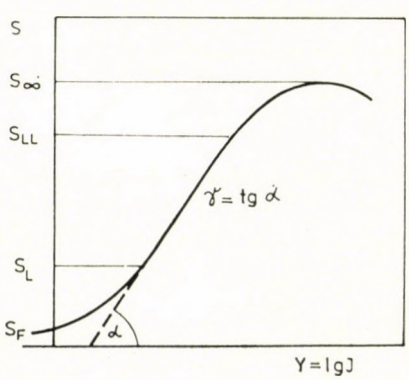

Fig. 1. The blackening curve relating to constant exposure time

S_F is the fog density developed without exposure, S_L and S_{LL} are values belonging to the lower and upper limits of the linear section. S_∞ is the highest density to be reached, termed saturation density.

The fundamental processes of spectrographic evaluation can be demonstrated as follows:

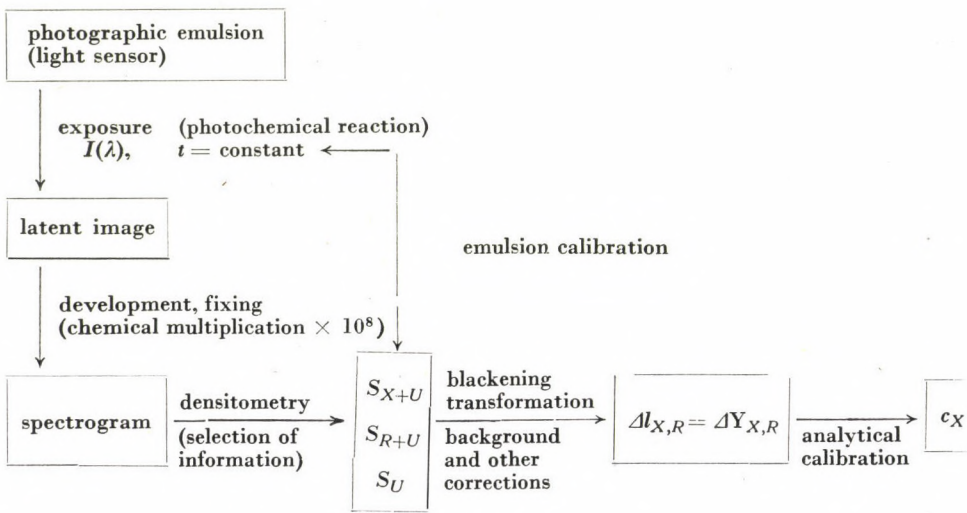

In the above diagram S_{X+U} and S_{R+U}, resp., mean the common density of the lines and their background, while S_U means the density only of the background.

Since spectrographic evalution is based on the complex processes of photographic detection, therefore the results obtained are influenced by those factors which may play a role in forming the image and in its evaluation, resp. Beside photographic and photometric parameters, the reliability and accuracy of calculations of emulsion calibration (*e.g.* blackening transformation) play a role in the evaluation [15]. Later on, these parameters and their role in spectrographic evaluation will be surveyed, without any claim for completeness. First of all, however, the problems of density measuring will be dealt with, the other questions will only be treated to the extent as they are necessary from the point of view of the relationships investigated in our work.

2.2. Photographic emulsion as a detector of spectrographic photometry

The shape of the blackening curve, and through this the intensity range to be measured spectrographically, as well as the precision and reliability of light intensity measurements depend primarily on the properties of the pho-

tographic emulsion and on the conditions of its processing. The theoretical description of blackening curve on the basis of emulsion properties is quite difficult and usually it is possible only by making use of simplifying assumptions. Most theories describing the properties of photographic emulsion interpret the characteristics of practical emulsions by describing the thin layers containing silver-halide crystals of similar size and taking into consideration the size distribution and superposing of layers [16, 17].

For spectrographic purposes fine-grained, anti-halation emulsions of appropriate γ-value, having suitable sensitivity [18, 19] in the wave-length range to be measured should be used [20]. The layer thickness of spectrographic emulsions is great compared to grain sizes, thus their useful exposure range is also quite wide. The properties of spectral plates are given for the employers by manufacturers, and unfortunately these days the assortment is regrettably narrow. Recently, however, fruitful experiments have been performed for the spectrographic application of holographic emulsions [21]. The quality of the product changes during storage owing to internal structural rearrangement (ageing) and to external chemical effects (Ag-centre forming) as well. The fog density increases, the γ-value decreases and the uniformity of emulsion properties deteriorates [22, 23].

The most important advantage of photographic emulsion over photoelectric light detectors lies in its high resolving power and, due to this, its huge information fixing and storing capacity. So, *e.g.* the information capacity of different types of spectral plates produced by ORWO is about 10^4 bit/mm^2 [24]. The photographic emulsion fixes the spectrum in the whole wave-length range of the spectrograph applied, thus enabling the comparison and survey of spectrograms and making possible the utilization of any useful information for analytical purposes. Photoelectric methods do not yet ensure this possibility, measurements can only be carried out at previously selected and precisely determined wave-lengths. In addition, the spectrogram may be regarded as a document that can be stored as long as desired and at any time it can be evaluated from new points of view. Photographic detection possesses another significant advantage, namely that the density is dependent on the average value of exposing light intensity (averaging effect).

2.3. Exposure, formation of latent image

During exposure an absorbed quantum raises an electron to the conduction band of the silver-halide crystal, then this electron is trapped at a Frenkel Ag^+-ion situated in a defect centre. During the following diffusion period this silver atom attracts another Frenkel Ag^+-ion. This process is repeated several

times and thus the developable silver centres constituting the latent image [25, 26] are formed.

This mechanism provides at least a qualitative explanation for the effects connected with the variations of exposure time. Because of the deviation from the law of reciprocity equality of light quantities at two different exposures $I_1t_1 = I_2t_2$ does not mean equality of the photochemical effect (density). There are quite significant differences both in the ranges of low and high intensities, when exposure time is too short or too long for the undisturbed operation of the mechanism of latent image formation. The above difference can be taken into consideration by applying the SCHWARZSCHILD formula [27] $E = I \cdot t^p$. On this basis one can see that the slope of time-scale and that of intensity scale blackening curve are different : $\gamma_y = p\gamma_t$. According to ZIMMER's investigations, if spectrograms are made using a step filter, an intensity-scale blackening curve can be plotted also by varying the exposure time [28]. The intermittance effect can similarly be interpreted, which means that continuous or interrupted exposures result in different photochemical effect [29]. The connection between the above two effects is evident ; by the use of rotating sector the intermittance effect may equalize in some cases the SCHWARZSCHILD effect of opposed sign occurring simultaneously [29, 30, 31].

The explanation of the sensitivity increasing effect of the so-called supplementary exposure is similar to that of intermittance effect. This supplementary exposure has successfully been employed in spectrography for decreasing detection limit [32]. Grains that have been exposed already, are much more sensitive to the effect of repeated exposure, since the number and sizes of crystal defects have increased. According to DENISOFF [33] supplementary exposure is most effective when done simultaneously with the main exposure. As a matter of fact, the photographic effect of background radiation can also be explained with the above, if it is regarded as supplementary exposure and the line providing analytical information as main exposure. Both supplementary exposure and background radiation decrease the γ-value of the photographic emulsion, because the slope of the blackening curve of continuous spectra is always less than that of line spectra [34, 35].

The shape of the blackening curve is influenced by the conditions of exposure of spectrum. So, *e.g.* the slope of a blackening curve plotted on the basis of spectrograms made with prism spectrograph is less than that obtained with grating spectrographs. The angle of incidence of the radiation on the spectral plate, as well as the shape of the lines are different in the two cases [36, 37, 38]. With a given spectrograph the γ-value is also influenced by slit width [34, 36, 39]. γ-values also depend on the method of constructing the blackening curve, whether it is made by two-step, multi-step or other radiation varying method [11].

2.4. Development

Evenness of development highly influences the precision and reliability of light intensity measurement, Agitation of the developer by rocking the dish which is still quite widely used has a rather great macro-error — *i.e.* the standard deviation of density of the photographic emulsion exposed uniformly is relatively high [40, 41]. With strict observance of the composition of the developer, the time period and temperature of development, the turbulent interrupted mixing of the developing solution gives a significant improvement in this field. These problems have been dealt with in detail by TÖRÖK and coworkers, and developing methods of practical applicability have also been reported by them [42, 43, 44, 45].

2.5. Density measurement

2.5.1. General considerations

With microdensitometers density is measured in spectrally complex light determined by the light source of the apparatus and not in monochromatic light. In spectrography densities of very small areas (spectral lines), in the order of 10^{-2} mm^2, are be measured. In these conditions the results of measurements are equally influenced by the geometry of the measuring system, the granularity of the emulsion to be measured and the character (line or continuous spectrum) and surroundings of the image part to be examined. The standard deviations of measuring results are also due to different causes; one has to distinguish between standard deviation caused by the granularity of the developed photographic layer (fluctuation noise) and the other noises arising in the measuring system. In the case of a given instrument, of course, the combined effects of these above factors determine the standard deviation of the measured density.

Apparatuses developed for density measurements can measure — according to their geometry — specular, diffuse and double-diffuse densities. In the first two cases, the photographic emulsion is illuminated by radiation beam from a small angular aperture and of normal incidence (approximately parallel). Diffuse density is measured by detecting the total amount transmitted, while if we measure only the light transmitted normally, specular density is obtained. Double-diffuse density is obtained by measuring the total quantity of light transmitted through a photographic emulsion illuminated with diffuse light [46]. Microdensitometers manufactured for spectrographic purposes are constructed to measure specular density. However, the geometric conditions of this are only partially met by the different types of instruments. The difference between the two kinds of densities can be explained by light scattering on the grains of the developed photographic emulsion. According to CALLIER's [46] investigations, disregarding the range of small densities, the ratio of spec-

ular and diffuse densities S_{sp} and S_d is constant:

$$\frac{S_{sp}}{S_d} = Q$$

Q is a number dependent on grain size. As a consequence of this, the ratios of densities measured with two apparatuses of different construction, are theoretically constants. The value of fluctuation noise caused by the granularity of the photographic emulsion is also dependent upon the construction and adjustment of the apparatus. The smaller the area measured, the greater the part of standard deviation caused by granularity [47]. The relationship of noises coming from the measuring system and fluctuation noises have been thoroughly dealt with by BURGUDJIEV and coworkers [48, 49, 50, 51]; considering the type of photographic emulsion, the area measured and value of mean density. They have found that from the point of view of signal-noise ratio the optimal area is 0.0100—0.0125 mm² in the case of commonly used microdensitometers *e.g.* Zeiss G II. On this basis, taking into account enlargement of the microdensitometer, the value of optimal slit width of the microdensitometer and the corresponding slit width of the spectrograph, respectively, can be calculated. In practice, however, the slit width of the spectrograph is usually given, and the slit width of the microdensitometer is adjusted so, as to cover 1/2—2/3 of the spectral line width [39]. However, the above requirement can generally be fulfilled, consequently fluctuation noise is not significant. Therefore in the following only noises produced in the measuring system will be discussed.

In photometric evaluation of spectrograms it is important to process the great amount of information available on the photographic emulsion and to extract from it the useful information. With traditional microdensitometers information selection and finding of spectral lines are to be done by the operator of the apparatus. For an experienced operator it does not mean any problem, although the measurement is slow and tiring, thus the amount of information that can be processed is highly limited.

The Zeiss Schnellphotometer generally used in Europe is able to measure density in a range of 0—2.0 and the narrow measuring range also decreases the efficiency of information acquisition. In modern microdensitometers, however, information utilization has been increased by automating the measurement and by computerizing control and data processing [8, 52, 53, 54, 55]. Total automation would require, however, extremely delicate solution of the mechanical system and in addition to this the selection and identification of lines demands very complicated programming. Therefore these instruments are still highly complicated and expensive, their application is mostly not worth the costs. At present in most laboratories it is expedient to employ semi-automatic systems which, supplied with up-to-date digital measuring systems and data fixing and storing facilities, facilitate the operator's work [56, 57, 58, 59].

Another field of information utilization still barely exploited is the expansion of the range of density measurement. Because of the narrow measuring range of traditional microdensitometers, in the practice of spectrography the formation of high densities is eliminated by step-filter radiation weakening. This process is, however, quite difficult to perform, since the shape of the blackening curve depends also on the number of filter-steps. Beside this, due to the greater place demand of spectrum the process is uneconomical [11]. At the same time, VECSERNYÉS and ZÁRAY [60, 61] have recently pointed out that modern wide-range microdensitometers *e.g.* Joyce-Loebl MK III CS produce a much longer linear section of the blackening curve of the spectral plate in the direction of high densities (frequently to density 4.0) than traditional microdensitometers do. In the latter case, inclination of curve at great densities is due to the scattered light produced in the apparatus causing systematic error and not to the saturation exposure of the photographic emulsion [62, 63, 64, 65, 66, 67]. The above experiments prove that at present the useful exposure range of spectral plates is restricted not by the photographic emulsion, but by the properties of the microdensitometer.

Efficiency of information utilization is influenced by the slit width of the microdensitometer, too. Analytical information contained by the shape of spectral lines is not exploited at all, because of the great slit width that is necessary to reduce the fluctuation noise. In this field further progress can be expected from the measuring of the area below the curve or of the line width [68].

The results of density measurement, the shape of the blackening curve and the efficiency of information utilization are greatly influenced by the properties of the microdensitometer. In the following error sources of density measurement will be dealt with, primarily from the point of view of increasing the measuring range of traditional microdensitometers. Table I briefly summarizes the requirements set up for the main parts of microdensitometers, and their role in standard deviation and systematic error of measurements as well. The table and the further discussion relate to the single-beam apparatuses in general use.

2.5.2. Statistical errors of density measurement

Transmittance is expressed by the relation $T = \frac{j}{j_0}$, where j_0 is the electric signal (mostly current) caused by light of i_0 intensity transmitted through an unexposed part of photographic emulsion, while j is the electric signal caused by weakened light having intensity i transmitted through the blackening to be measured. Transmittance fluctuation σ_T observed in the measuring system is caused by addition of noises originating from different sources according to the error propagation law. In the σ_T value noises coming from the light source

and detection system are added, thus it expresses the degree of stability of the measuring system. σ_S density deviations belonging to different σ_T stability levels have been calculated in the function of density on the basis of the correlation $\sigma_S = \frac{\sigma_T}{\ln 10} \cdot 10^S$ considering the logarithmic transformation. The results of these calculations are presented in Table II.

Table II

Values of density deviation σ_S belonging to different σ_T transmittance fluctuations

S	σ_S				
	$\sigma_T = 0.1$	$\sigma_T = 0.01$	$\sigma_T = 0.001$	$\sigma_T = 0.0001$	$\sigma_T = 0.00001$
0.010	0.045	0.0045	0.00045	0.000045	0.0000045
0.050	0.050	0.0050	0.00050	0.000050	0.0000050
0.434	0.120	0.0120	0.00120	0.000120	0.0000120
1.000	0.434	0.0434	0.00434	0.000434	0.0000434
2.000	4.340	0.4340	0.04340	0.004340	0.0004340
3.000	43.400	4.3400	0.4340	0.043400	0.0043400
4.000	434.000	43.4000	4.3400	0.434000	0.0434000

From the table it can be seen that the stability of the system determines also the upper limit of measurement in addition to the standard deviation of density measurement. In measuring density 2.0 the permitted maximal transmittance fluctuation is ± 0.001, while in the case of density 4.0, this value is only ± 0.00001.

From the point of view of instrumentation it must be taken into consideration that transmittance fluctuation caused by power fluctuations of the light source always reaches the detector weakened according to the transmittance to be measured, thus here less strict stability requirements are needed. A stability $\sigma_T = 0.01$ of the light source makes namely possible the sufficiently precise measurement of small densities, and at the same time at a density 2.0 it causes only transmittance fluctuation ± 0.0001. Noise coming from it, does not disturb the measurement of high densities. On the other hand, the above strict demands are valid for noises occurring in the detection system and for the accuracy of display, since they directly influence the σ_T value. For traditional microdensitometers signal stability $\sigma_T = 0.001$ corresponding to density 2.0 (the upper measuring limit) should be reduced to $\sigma_T = 0.00001$ in order to extend the measuring range to density 4.0. In transmittance measurement this task requires extremely great scale extension, and in digital indication at least six digits are required, which causes already technical difficulties.

Table I

The error sources of density measurement

Unit	Task — Requirement	Source of systematic errors	Source of random standard deviation
Light source	To ensure a stable, low noise light intensity (i_0) by keeping the heating filament at constant temperature.	During long operation the one-way change (usually decrease) of light intensity causes displacement of zero-point. All density values are either increased or reduced. It can be eliminated by frequent zero control.	Due to unsufficient current and voltage stability the value of i_0 fluctuates which causes considerable standard deviation at small densities, as this effect appears indirectly in the noise level of the signal on the detector.
Focussing system	To let the light of light source get to the detector through the surface to be measured of photographic emulsion. The correct and sharp focussing and elimination of scattered light should be ensured. In usual micro-densitometers preslit on photographic emulsion and the latter on the entrance slit of light detection system is focussed.	Scattered light coming from defective, diffusely reflecting surfaces or optical elements may reach the detector without getting through the surface to be measured. Its intensity is added to the intensity to be measured and reduces the density value measured. Its effect increases with density. Deflection of plate, displacement and play of mechanical parts may weaken sharpness of focussing which results in reducing the value of line blackenings.	
Detection — (Amplifying) — Display System	The light sensitive detector has to produce an electric signal strictly proportional to its illumination. When this is amplified and logarithmized, the density value is obtained. Important demands are: linearity of characteristics of sensor and amplifier, correctness of logarithmation and low noise level and inertia, as well.	Linearity faults of detector and amplifier influence the density values in the whole measuring range. Values and signs of deflections can vary depending on density.	Noises produced in detection and electric system, resp., exert direct influence on standard deviation of density measurement. It is important that accuracy of reading should be in accordance with noise level.

However, with logarithmic transformation four digits are sufficient for the display of density values which considerably simplifies also the digital system needed.* The power supply unit connected to Zeiss G II microdensitometer has a voltage stability $\pm 3\%$, which does not always ensure the necessary radiant power stability. At the same time transmittance can not be read with a precision higher than 0.001, thus density measurements above 2.0 — due to this lack of precision — are not reliable.

With a double-beam solution, in the case even of lower stability, densities above 2.0 can reliably be measured with the compensation method. So, *e.g.* the measuring range of Joyce-Loebl MK III CS microdensitometer using double-beam, neutral wedge optical compensation is exceptionally wide (0—6.0). However, in spite of its advantages the double-beam method was not generally adapted because extremely delicate optical and mechanical instrumentation is required.

2.5.3. Systematic errors of density measurement

The systematic errors in density measurement are presented in deviation from linearity. These are originated partly from optical sources, partly from the linearity defects of detection system.

In the case of conventional microdensitometers the most important error source is the scattered light [46, 62]. The intensity i_s of the scattered light is added to intensity i, consequently the value of transmittance is found to be higher, while that of blackening to be smaller than the actual value:

$$T_{\text{measured}} = \frac{i + i_s}{i_0} \qquad S_{\text{measured}} = \lg \frac{i_0}{i + i_s} .$$

From these equations it can be seen that the disturbing effect becomes significant if intensity i_s of scattered light is comparable with intensity i. In order to decrease the intensity of scattered light a preslit used to be applied in microdensitometers. According to KÁNTOR's [63] investigations performed on Zeiss G II microdensitometer, the green glass preslit built into the device scarcely decreases the amount of scattered light, owing to which this scattered light causes quite significant negative systematic error in density measurement. Numerical data are also given to error correction. He exchanged the jaws of the green glass preslit with metal plates, thus be succeeded in decreasing the amount of scattered light. Most favourable result can be achieved if the image of preslit appearing on photographic emulsion covers the margin of spectral lines. Similarly for correction of scattered light occurring in Zeiss G II microdensito-

* In practice below density 2.0 three decimals, above it two decimals are satisfactory for the precision of the display of density values.

meter calculation and other methods have been published by TÖRÖK and HÁFENSCHER [64]. It has been stated that the density measurement above 1.4 is strongly disturbed by scattered light in conventional operation, and therefore the upper section of the blackening curve is distorted. In Joyce-Loebl MK III CS microdensitometers applying complementary filtration the blackening curve is linear even up to 4.0. For the blue sensitive detector (photoelectron multiplier) the orange glass slit is opaque, so the amount of scattered light is very low. At the same time the preslit does not hinder the orientation on the spectrum [55]. The density range measurable without disturbance can be increased by complementary filtration and by applying opaque preslit also at Zeiss G II microdensitometers.

In the above calculations it was presumed that intensity i_S of scattered light is constant in different experimental conditions. However, it does not exist strictly, since the other parameters of measurement (slit width, magnification, deposit of aerial dust in surface of optical elements), further on the character of the image part to be measured (line, continuous spectrum, line spectrum with significant background density) may influence the intensity of scattered light falling on the detector. Consequently, these kinds of corrections are not commonly applicable even in the case of an instrument. From the point of view of increasing the measuring range a better method is suggested also by above authors, that is the methods decreasing the amount of scattered light. As a matter of fact, the intensity of scattered light optically determines — as seen earlier — the density range to be measured without disturbance and the upper limit of measurement, as well. The least measurable transmittance is $T_{\min} = \frac{i_S}{i_0}$, the maximal density is $S_{\max} = \lg \frac{i_0}{i_S}$.

In density measurements other errors of optical origine* may also play role. So, it is very important — especially in automatic densitometry — *e.g.* to focus sharply the whole surface range to be examined of photographic emulsion onto the entrance slit of detection system. Generally it does not agree with the visual finest focussing. This requires a very precise manufacturing of the mechanical system serving for fixing and moving of spectral plate. At conventional microdensitometers bending of spectral plate fixed horizontally can not be eliminated. An up-to-date instrument solution filling the requirements of automation is reported by WITMER and co-workers [53] and KOVALJEV and KONONOV [70].

The detection system has to provide for linear data up to the upper limit of density measurement, which is determined by scattered light. The primary

* Those nonlinearity errors of optical origin, however, are not dealt with, which come from the comparison of the size of examined part of image with wave-length of light. Namely in practical spectral analysis the measured surface elements are greater than that [48, 49, 50, 51, 69].

source of non-linearity is the fact that the electric signal produced on the light sensitive detector is not strictly linear with the intensity of the falling light. These differences depend on the type of detector (photoelectric cell, photovoltaic cell, photomultiplier, photodiode, *etc.*) on its characteristics and frequently on its age, too, and also numerous other experimental conditions, so their correction would only be possible if repeatedly checked. However, in this case, too, the application of a detector having optimal properties is the most expedient. The linearity of the amplifying system and that of the display may play a role, too. Linearity errors of the detection system may influence the measurement results in the whole measuring range, and the differences caused vary depending on density. According to KÁNTOR's investigations the linearity error of detection system consisting of selenium photovoltaic cell and galvanometer of the Zeiss G II microdensitometer causes positive differences increasing with density [63].

2.6. Conversion of density data to Y-values, density transformation

The fundamental data of spectrographic evaluation are density values. In the practice from these are gained the *Y*-values by different blackening-transformations. The reliability of these calculations highly depends on the validity of equations applied and on the correct determination of parameters contained in them. In order to obtain more reliable data, computerized data processing should be used for the evaluation of the great amount of data by replacing the conventional densitometry with modern automated or semi-automated measurement. Perfect density transformation fulfilling all demands is not known yet. The approximation of the blackening curve with polynoms does not seem feasible, since these methods do not have physical meaning, they are inevitably complicated and require frequent calibration. Considering the many kinds of factors influencing the precision of density measurement, it is evident, that within the precision limits determined by them a number of different functions can be fitted to the blackening curve [8]. However, these do not produce better results than the commonly used density transformations, except some special cases. We have decided on the application of the *l*-transformation [15] taking into account the above-mentioned advantages, and also with a view to the possibility of computerized evaluation [71].

3. Influence of the type of microdensitometer on the results of density measurement

From the point of view of errors of density measurement and extension of measuring range, the conventional and modernized Zeiss G II microdensitometers have been compared. Modernization of the instrument was done in the

Research Institute of Technical Physics of the Hungarian Academy of Sciences [58, 65]. The light detection system consisting of selenium photovoltaic cell and galvanometer was completely changed. Density values are obtained by amplifier of logarithmic characteristic and digital display from the signal of silicon photo-diode detector, sometimes ready for data processing (recorded on punched tape). To reduce the scattered light, the green glass jaws of the preslit have been replaced by metal plates. Detailed description of the apparatus will be given in our next paper. In the following (in Figures and Tables) this instrument will be referred to as G II-MFKI. In some cases comparison was also made with other Zeiss G II, conventional MF 2 and the modern Joyce-Loebl MK III CS-type microdensitometers.

3.1. Statistical errors

With the help of a deuterium lamp and a Q 24 spectrograph a series of continuous spectrograms have been made by varying the exposure time. Spectrograms have been photometried 8 times at a wave-length 300 nm with microdensitometers of the Zeiss G II and G II-MFKI type resp. The relative standard deviation of density values ($\sigma_S/\overline{S}$) has been plotted in the function of

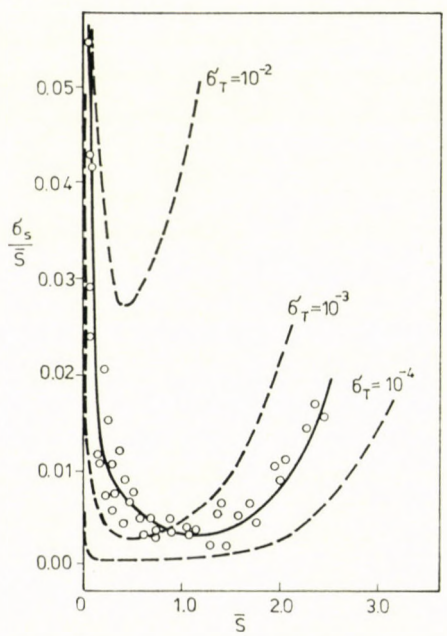

Fig. 2. **The relative standard deviation values ($\sigma_S/\overline{S}$) in the function of mean density in the case of Zeiss G II microdensitometer**

mean density $\overline{S}$ (Figs 2 and 3). Calculated changes of σ_S/S values belonging to different σ_T stability levels are also presented in the Figures.

From the Figures the standard deviation of measurements seem to be $10^{-3} < \sigma_T < 10^{-2}$ in the case of low densities ($S < 1.0$) using microdensitometers of the Zeiss G II and G II-MFKI types. However, the value of 10^{-3} is better approached by σ_T if the G II-MFKI microdensitometer is employed. As described above, this shows a power fluctuation in the light source. At high densities the following values are obtained: with the Zeiss G II instrument $10^{-4} < \sigma_T < 10^{-3}$; with the G II-MFKI apparatus $\sigma_T \approx 10^{-5}$. These data indicate the precision of reading and stability of the measuring system, resp. Regarding stability, the upper measuring limit of the traditional instrument lies between the density value 2 and 3, while the G II-MFKI microdensitometer is able to measure density even up to 4.0.

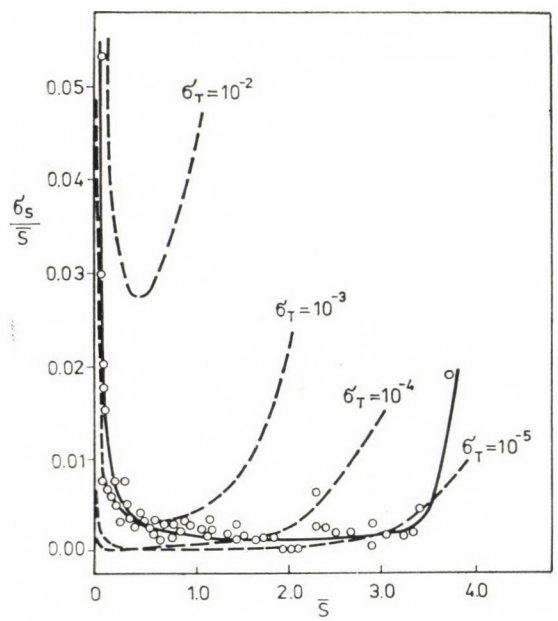

Fig. 3. The relative standard deviation values ($\sigma_S/\overline{S}$) in the function of mean density in the case of G II—MFKI microdensitometer

3.2. Systematic errors

The intensity of scattered light falling on the detector of a given microdensitometer cannot be determined unambiguously. As follows from the above, its amount depends upon the slit width and also on the character of the measured image. For comparison of the intensity of scattered light the apparent

density of a thin wire of theoretically infinite density is measured [72]. It was experienced that within certain limits the width of the entrance slit situated before the detector, did not influence the results obtained if it was smaller than the width of wire image produced on it. On the contrary, adjustment of preslit had significant influence [63]. Reducing its width, the density of wire increased until the image of the preslit covered the two margins of the wire image. This observation confirms that the major part of scattered light gets onto the detector from the direct neighbourhood of the spectral line [62]. Therefore, in photometrying spectra the margins of lines should be excluded. Wire densities S_{max} measured in the above way with different apparatuses are summarized in Table III. Measuring ranges given by the manufacturer are also demonstrated in Table III.

Table III

Apparent density S_{max} of a tungsten wire of **40** *μm diam. in the case of various types of microdensitometers, and the measuring range of apparatuses*

Type of microdensitometer	Measuring range	S_{max}
Zeiss G II	0—2.0	2.0—2.2
MF 2	0—2.0	1.5—1.8
G II—MFKI with green glass preslit	—	~3.0
G II—MFKI with metal preslit	—	~4.0
Joyce—Loebl MK III CS	0—6.0	~4.0

From the table it can be seen that the amount of scattered light is determined first of all by the type of apparatus. Having examined several apparatuses of same Zeiss G II and MF 2 types, respectively, it has been stated that measuring results — although in a smaller degree — are also influenced by the condition of instrument. In these cases the extreme values of S_{max} obtained with several apparatuses have been presented.

Above data represent such limits, above which density measurement is unreasonable with microdensitometer in question, and even in its vicinity one has to count with significant nonlinearity. It is also visible that density value S_{max} corresponding to the scattered light is to be found near the upper density limit given by manufacturer.

In the knowledge of above limits linearity of detection systems has been controlled, too, at microdensitometers Zeiss G II, MF 2 and G II-MFKI. We had no opportunity to do the same with Joyce-Loebl MK III CS instrument. According to producer's data linearity error of the instrument in density measurement is not higher than 1% [55]. Measurements have been performed

by varying the entrance slit of the detection system transilluminated evenly. The theoretically correct density is given by $S_{theor} = \lg \frac{d_0}{d}$; where d_0 is the initial, and d is the actual slit width. The difference $\Delta S = S_{theor} - S_{meas}$ is plotted in function of S_{theor} density (Fig. 4). The figure clearly shows that

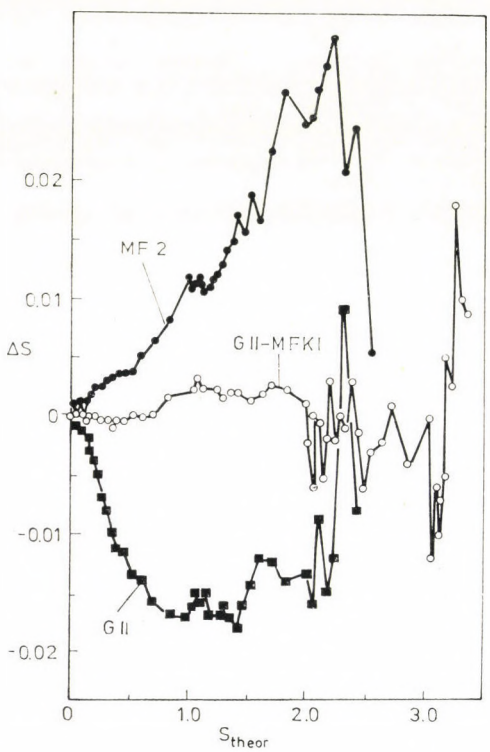

Fig. 4. The difference $\Delta S = S_{measured} - S_{theoretical}$ in the function of theoretical density

in the case of conventional Zeiss G II and MF 2 microdensitometers a minimum or maximum curve has been obtained owing to endpoint calibration ($T = 0.000$ and $T = 1.000$ adjusting). The highest deviations got by Zeiss G II -0.017 and by MF 2 $+0.033$ are by no means values to be neglected. These values are characteristic of apparatuses examined, the numerical values of deviations in the case of other apparatuses of the same type differ, although the character of the curve remains unchanged. With G II-MFKI instrument the sign of deviations is changing, in density range 0—2.0 it does not reach the value 0.003, and only at density higher than 3.0 is more than 0.005. Linearity error of detection system scarcely exceeds 0.1%.

3.3. Conclusions, preconditions of extending measuring range

Comprehensively it can be stated that the measurable density range is determined by the properties (stability, scattered light, linearity) of microdensitometer. In order to extend, that is to double the density range to 0—4.0 of conventional, single-beam microdensitometer Zeiss G II it was necessary to build in a modern detection system being linear in wide-range and of low noise-level and to reduce simultaneously the intensity of scattered light in a significant measure. At the same time both systematic error and standard deviation of measurement can considerably be decreased.

Generalized foregoing experiences one can state that the measuring range limited by optical system of microdensitometer can be utilized, when the noise level of the detection system σ_T is lower or equal to transmittance $T_{\min} = \frac{i_s}{i_0}$ corresponding to intensity i_s of scattered light:

$$\sigma_T \leq T_{\min} = \frac{i_s}{i_0}.$$

Detection system is required to dispose suitable linearity up to density $S_{\max} = -\lg T_{\min}$ corresponding to transmittance $T_{\min}$. These preconditions are fulfilled in the case of both Zeiss G II and G II-MFKI microdensitometers.

REFERENCES

[1] Barnes, R. M.: Anal. Chem., **46,** 150 R (1974)
[2] Boumans, P. W. J. M., de Boer, F. J.: Spectrochim. Acta, **27B,** 391 (1972)
[3] Greenfield, S., Jones, I. Ll., McGeachin, H. McD., Smith, P. B.: Anal. Chim. Acta, **74,** 225 (1975)
4. Zimmer, K.: Proc. XIX. Annual Hung. Symp. on Spectral Analysis, Győr, 1976, p. I/13.
[5] Colson, W. B., McPherson, J., King, F. T.: Review of Scientific Instrum. **44,** 1694 (1973)
[6] Boumans, P. W. J. M., Rumphort, R. F., Willensen, L., de Boer, F. J.: Spectrochim. Acta, **28B,** 227 (1973)
[7] Török, T., Vecsernyés, L.: Proc. XIX. Annual Hung. Symp. on Spectral Analysis, Győr, 1976, p. I/3.
[8] Török, T.: Kém. Közlem., **37,** 167 (1972)
[9] Scheibe, G., Linström, C. F., Schnettler, O.: Z. angew. Chem., **49,** 145 (1931)
[10] Lomakin, A.: Z. anorg. u. allg. Chem., **187,** 75 (1930)
[11] Zimmer, K.: Dissertation D. Sc., Budapest, 1970, p. 17.
[12] Filo, O., Lavrin, A., Matherny, M.: Acta Geol-Geograph. Univ. Comenianae, Geologica, **15,** 219 (1968)
[13] Hurter, F., Driffield, V. C.: J. Soc. Chem. Ind., **9,** 455 (1890)
[14] Török, T.: Proc. 14th Coll. Spectrosc. Int., Debrecen, 1967, Vol. I., p. 155. Hilger, London 1968
[15] Török, T., Zimmer, K.: Quantitative Evaluation of Spectrograms by Means of *l*-Transformation, ed. Akadémiai Kiadó, Budapest, and Heyden and Son, London 1972
[16] Mees, C. E. K., James, T. H.: The Theory of the Photographic Process, 3rd edition The Macmillan Co. New York and Collier Macmillan Ltd. London, 1966, p. 72—85.
[17] Kántor, T.: Magy. Kém. Folyóirat, **70,** 541 (1964)

[18] Deutsche Industrie Normen, 4512
[19] American Standard 238.2.1. — 1947
[10] MIKA, J., TÖRÖK, T.: Analytical Emission Spectroscopy, ed. Akadémiai Kiadó Budapest and Butterworths London, 1973, p. 430.
[21] BURGUDJIEV, Z., ZIMMER, K., BOBOLINA, E.: Magy. Kém. Folyóirat, **83,** 110 (1977)
[22] ZIMMER, K., TÖRÖK, T., ASZTALOS, I.: Chem. Analityczna, **11,** 1065 (1966)
[23] ZIMMER, K., TÖRÖK, T., ASZTALOS, I.: Magy. Kém. Folyóirat, **72,** 417 (1966)
[24] DANZER, K., SONNTAG, A.: Acta Chim. Acad. Sci. Hung., **93,** 357 (1977)
[25] GURNEY, R. W., MOTT, N. F.: Proc. Roy. Soc. (London), Ser, A., **164,** 151 (1938)
[26] MITCHELL, J. W.: Rept. Progr. Phys., **20,** 433 (1957)
[27] SCHWARZSCHILD, K.: Astrophys. J., **11,** 89 (1900)
[28] ZIMMER, K.: Magy. Kém. Folyóirat, **72,** 415 (1966)
[29] WEBB, J. H.: J. Opt. Soc. Am., **23,** 157 (1933)
[30] TÖRÖK, T., ZIMMER, K., BIEDL, J., ASZTALOS, I.: Magy. Kém. Folyóirat, **72,** 430 (1966)
[31] TÖRÖK, T., ZIMMER, K., BIEDL, J., ASZTALOS, I.: Acta Chim. Acad. Sci. Hung., **50,** 23 (1966)
[32] INTONTI, R., TADDEUCCI, A.: Spectrochim. Acta, **18,** 379 (1962)
[33] DENISOFF, A.: Z. Wiss. Phot., **27,** 128 (1929)
[34] ARRAK, A.: Appl. Spectr., **16,** 124 (1962)
[35] ZIMMER, K., SZABÓ, É.: Proc. 15th Coll. Spectrosc. Int., Madrid 1969 Vol. IV., p. 55., Ibérica, Madrid, Tarragona 1970
[36] STRASHEIM, A., DE VILLIERS, D. B.: Acta Chim. Acad. Sci. Hung., **58,** 61 (1968)
[37] ZIMMER, K., TÖRÖK, T., BIEDL, J.: Acta Chim. Acad. Sci. Hung., **51,** 17 (1967)
[38] ZIMMER, K., TÖRÖK, T., BIEDL, J.: Magy. Kém. Folyóirat, **72,** 425 (1966)
[39] ZIMMER, K., SZABÓ, É.: Spectrochim. Acta, **24B,** 649 (1969)
[40] TÖRÖK, T., HELTAI, GY., MOHAROS, I.: Spectrochim. Acta, **27B,** 215 (1972)
[41] TÖRÖK, T., HELTAI, GY., MOHAROS, I.: Acta Chim. Acad. Sci. Hung., **77,** 11 (1973); Magy. Kém. Folyóirat, **78,** 594 (1972)
[42] TÖRÖK, T., HELTAI, GY.: Acta Chim. Acad. Sci. Hung., **77,** 19 (1973); Magy. Kém. Folyóirat, **78,** 598 (1972)
[43] TÖRÖK, T., HELTAI, GY., MOHAROS, I.: Acta Chim. Acad. Sci. Hung., **77,** 117 (1973); Magy. Kém. Folyóirat, **78,** 608 (1972)
[44] HELTAI, GY., TÖRÖK, T.: Spectrochim. Acta, **32B,** 107 (1977); Magy. Kém. Folyóirat, **82,** 469 (1976)
[45] HELTAI, GY.: Dissertation, Budapest 1973
[46] CALLIER, A.: Z. Wiss. Phot., **7,** 257 (1909)
[47] SELWYN, E. W. H.: Phot. J., **82,** 208 (1942)
[48] BURGUDJIEV, Z.: Bulg. J. Phys., II **2,** 117 (1975)
[49] BURGUDJIEV, Z., BELCHEV, ST., NIKOVA, R., ALEKSANDROV, A.: Bulg. J. Phys., II **4,** 399 (1975)
[50] BURGUDJIEV, Z., LYOCHKOVA, M., VOYKOVA, T.: Bulg. J. Phys., II **5,** 492 (1975)
[51] BURGUDJIEV, Z., LYOCHKOVA, M., STEFANOVA, D., KOLEVA, I.: Mikrochim. Acta (Wien), I, 441 (1976)
[52] MARGOSHES, M.: Spectrochim. Acta, **25B,** 113 (1970)
[53] WITMER, A. W., JANSEN, J. A. J., VAN GOOL, G. H., BROUWER, G.: Philips Tech. Rev., **34,** 322 (1974)
[54] BOUMANS, P. W. J. M.: Preprints 16th Coll. Spectrosc. Int., Heidelberg, 1971, Vol. II. p. 247. Hilger, London 1971
[55] WEST, G. J.: The Joyce—Loebl digitised microdensitometer, Ilford Ltd., England, CRF No 3165 (1970)
[56] MAI, H., STAHLBERG, U.: Jenaer Rundschau, **21,** 316 (1976)
[57] TEUSCHEL, W., HÜTTIG, W.: Jenaer Rundschau, **22,** 216 (1977)
[58] KOZMA, L., BARTHA, L., ZIMMER, K., HELTAI, GY.: Proc. XIX. Annual Hung. Symp. on Spectral Analysis, Győr, 1976, p. VI/3.
[59] VICZIÁN, M., PETIK, P.: Proc. XX. Annual Hung. Symp. on Spectral Analysis, Gyula, 1977, p. 183.
[60] VECSERNYÉS, L., ZÁRAY, GY.: Proc. XV. Annual Hung. Symp. on Emission Spectral Analysis, Tatabánya, 1972, p. 155.
[61] VECSERNYÉS, L., ZÁRAI, GY.: Abstracts of Euroanalysis II., Budapest, 1975, p. 32.
[62] SCHWARZSCHILD, K., WILLIGER, W.: Astrophys. J. **23,** 284 (1906)
[63] KÁNTOR, T., ERDEY, L.: Acta Chim. Acad. Sci. Hung., **65** (1), 21 (1970)
[64] TÖRÖK, T., HÁFENSCHER, I.: Magy. Kém. Folyóirat, **84,** 183 (1978); Spectrochim. Acta, **33B,** 283 (1978)

[65] HELTAI, GY., ZIMMER, K., KOZMA, L.: Proc. XX. Annual Hung. Symp. on Spectral Analysis, Gyula, 1977, p. 19.
[66] HELTAI, GY., FLÓRIÁN, K., MATHERNY, M., ZIMMER, K.: Abstracts of 20th Coll. Spectrosc. Int., Prague, 1977, No 517 (1977)
[67] ZIMMER, K., HELTAI, GY.: Spectrochim. Acta, **33B**, 417 (1978)
[68] VECSERNYÉS, L.: Proc. XX. Annual Hung. Symp. on Spectral Analysis, Gyula, 1977, p. 171.
[69] SWING, R. E.: J. Opt. Soc. Am., **62**, 199 (1972)
[70] KOVALJEV, V. I., KONONOV, E. J.: Prib. Tech. Exp., **3**, 241 (1977)
[71] MATHERNY, M.: Kém. Közlem., **48**, 363 (1977)
[72] KECK, P. H.: Zeiss Nachr., **10**, 1 (1936)

Károly ZIMMER H-1443 Budapest, Pf. 123
György HELTAI H-2103 Gödöllő

Acta Chimica Academiae Scientiarum Hungaricae, Tomus 100 (1—4), pp. 341—352 (1979)

DESCRIPTION OF TRANSIENT POTENTIOMETRIC SIGNALS MEASURED IN INJECTION ANALYSIS SYSTEMS

M. GRATZL, Zs. FEHÉR, G. NAGY, K. TÓTH and E. PUNGOR

(Institute for General and Analytical Chemistry, Technical University, Budapest, Hungary)

Received July 10, 1978

Accepted for publication August 24, 1978

Concentration-time signal curves developed by coulometric as well as manual injection into a continuous carrier stream of a serial analysis' setup, are described mathematically. The effects of the design parameters on the validity of the mathematical models derived are discussed in the case of potentiometric detection.

Introduction

The technique of injection of samples into a flowing solution with the aim of direct analysis has been developed and the principle of the method has been described by PUNGOR and coworkers in 1969 [1]. Their measuring setup was the first continuous analysis' design which allowed to carry out rapid serial analyses of samples in small volumes by using continuous carrier flow. The new analytical method, called injection techniques, was used in its first applications in combination with voltammetric detection [1, 2]. Later, BERGMEYER and HAGEN have used the same technique in combination with spectrophotometric detection and reagent circulation [3]. Then some new voltammetric [4—7], and potentiometric [8—10] applications using ion-selective electrodes for detection have followed. Later on, MOTTOLA *et al.* developed a flow-through measuring setup in which the injection was done directly into the detector cell [11]. While in most of the works cited above a mixing unit was used for the homogenization of the injected sample in the direction perpendicular to that of the carrier stream [1, 2, 4—11], RŮZIČKA and coworkers constructed a flow injection system without mixing chamber [12, 13].

In the last few years a number of further publications have been reported on the injection techniques using a wide variety of injectors, flow patterns and detector cells [14—20], the performances of which proved the high analytical value of the injection principle, *i.e.* the principle of direct sample injection into a continuous carrier flow [1].

The block diagram of a measuring setup used in this work for carrying out injection analysis is shown in Fig. 1. Small volumes of the sample solutions

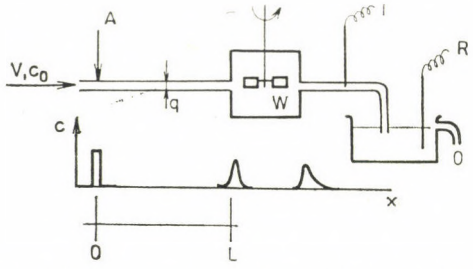

Fig. 1. Schematic diagram of the measuring system with manual injection together with the indication of the local shape of the concentration profile along the flow way. I: indicator electrode; R: reference electrode; *x:* length coordinate; 0: outlet (For the other symbols see the text.)

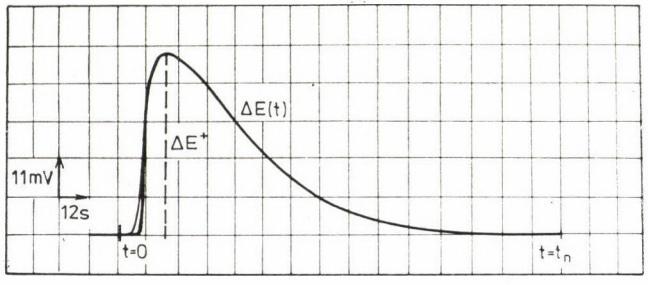

Fig. 2. Measured and calculated potentiometric signal at volumetric manual injection (thick line: measured, thin line: calculated shape) $C_0 = 10^{-4}$ *M* KI, $M = 3 \cdot 10^{-6}$ mole KI, $S =$ $= 58$ mV (For the other data see the Experimental in the text)

are injected into the carrier solution streaming at a constant rate. The sample injected is then mixed with the flowing solution and after a homogenization in the mixing chamber, it is carried into the detector cell.

Every injected solution portion, passing through the detector cell produces a peak-type dynamic signal-time curve. Such a curve is shown in Fig. 2 if potentiometric detector cell is used. The area as well as the height of such peaks were used earlier as the analytical readout of injection measurements [1, 2, 4—10].

In the present work potentiometric detection involving ion-selective electrodes is used. Hence, owing to the nonlinear response of the sensor, the signal obtained depends on the concentration of the appropriate material in both the injected and the carrier solution. Therefore, the potentiometric injection method is able to analyze not only injected samples, but also the carrier flow [19].

A further variety of analytical techniques can be achieved if a chemical reaction between the injected sample and the constituents of the carrier flow is superimposed on the simple dilution of the injected material [2, 18, 19]. In this case either the appropriate species of the carrier stream is measured and

hence a negative peak can be detected, or the injected reagent is measured giving a positive peak. In this way also both injected and carrier solutions can be analyzed.

In the former, more important case, when injected samples are analyzed, the carrier solution generally contains a certain, relatively small amount of primary ion, in order to ensure a stable baseline, while if the carrier stream is to be analyzed, standard amounts of the primary ion or a reagent are injected.

The standard or reagent injection itself can be done either volumetrically or coulometrically.

Volumetric injection can be carried out *e.g.* manually, using a Hamilton syringe as shown in Fig. 1 [1, 2, 4—10], but also in a mechanized way with an appropriate injector (see *e.g.* [14, 20]).

A coulometric injection system, the signals of which are used in this work is described in [18].

The understanding of the resulting detectable signals requires the mathematical modelling of the flow injection system employed. This understanding is, however, necessary, if the injection measuring setup is used to solve different analytical problems. By applying the volumetric manual or the coulometric standard or reagent injection technique combined with potentiometric sensors, a large variety of advantageous analytical procedures could [5, 19], and can certainly be worked out in the future. Therefore, the best understanding of the detected signals is important.

If a simple dilution or a dilution combined with an instantaneous chemical reaction of the injected species occurs, then the concentration at the detector in function of time can be described on the basis of the following differential equation (1) considering the mass balance in the mixing chamber:

$$\frac{\mathrm{d}\Delta c(t)}{dt} = \frac{V}{W}\left[\Delta c_s(t) - \Delta c(t)\right], \tag{1}$$

where

$$\Delta c_s(t) = \frac{M}{V\tau} \quad \text{if} \quad t_L < t \leq t_L + \tau \tag{2}$$

and

$$\Delta c_s(t) = 0 \quad \text{if} \quad t \leq t_L \quad \text{or} \quad t > t_L + \tau\,. \tag{3}$$

Here

t is time (sec) $t = 0, \ldots$
$\Delta c(t)$ is equal to $c(t) - c_0$ (M)
$c(t)$ is the actual concentration at the detector (M)
$\Delta c_s(t)$ is the concentration change due to the injected "plug", just at the entrance of the mixing unit (M)
c_0 is the concentration of the flowing carrier solution (M)
V is volumetric flow rate (ml/sec)

W is the volume of the mixing chamber (ml)

M is the injected amount (mole)

t_L is the time delay between injection and detection due to the finite flow rate of the carrier stream : a time t_L is required by the injected "plug" to reach the detector ($t_L = Lq/V$, where L is the length and q is the cross section area of the connecting tube, see Fig. 1).

τ is the time required by the solution "plug" containing the injected material to pass the entrance section of the mixing chamber. If the dispersion is negligible then τ is equal to the time of injection, τ_{inj}.

It has been stated [1, 18] that equations (1) and (3) are valid under ideal conditions *i.e.* if

1. no concentration gradient is formed in the direction of flow inside the "plug" of liquid containing the injected material, and

2. the mixing of the solution in the stirrer is instantaneous.

By substituting the solution $\Delta c(t)$ of equations (1—3) into the signal-concentration relationship characteristic for the sensor, the signal-time relationship *i.e.* the mathematical description of the detected peak can be obtained. As in the present work potentiometric detection is dealt with, the appropriate signal transformation equation is :

$$\Delta E(t) = S \cdot \ln\left[1 + \frac{\Delta c(t)}{c_0}\right] \tag{4}$$

assuming that only univalent ions take part in the electrode reaction, and neglecting the effects of the interfering ions. Here S is the slope of the electrode calibration graph, and $\Delta E(t)$ is the potential change in time as an effect of the injection.

In the present paper the validity of the simple peak-type model derived earlier on the basis of equations (1—4) shall be examined in function of the time of injection in the case of coulometric injection, and a new model will be derived and checked for describing the peaks obtained by volumetric manual injection under certain conditions. In both cases potentiometric detection [equation (4)] will be considered. Furthermore, the application of the models for analytical purposes will be outlined.

Experimental

Apparatus

a) Volumetric manual injection system (see Fig. 1)

The carrier solution is streamed at a constant volumetric flow rate (0.13 ml/sec) with the help of a peristaltic pump (LKB Varioperplex Type 12000). One section of the flow-through channel, made of a silicone rubber tube of a diameter of 2.5 mm and length of about 20 cm ($L = 20$ cm on Fig. 1), was specially prepared for injection. The injection was done with a syringe (*e.g.* Hamilton 710) into this section. Small volumes of sample were injected (30—50 μl) in every 3—4 min.

A flow-through mixing unit of volume 2.7 ml between the place of injection and the detector cell serves for delivering into the detector cell a solution homogeneous in the cross section of the tube.

The flow-through detector cell involved the potentiometric indicator electrode (*e.g.* a semi-micro iodide selective electrode, prepared in our Laboratory) and a calomel reference electrode (Radelkis Type OP-8302) which was placed far downstream from the indicator electrode.

For potential measurements a Keithley differential electrometer, Type 604, while for recording a Radelkis potentiometric strip chart recorder (Type OH-814/1) have been employed. For fitting the dynamic model, a Hewlett—Packard calculator (Type 9100 B) equipped with a digital plotter was used.

b) Coulometric injection system

The coulometric injection system, the signals of which are used in this work, is described in paper [18].

Chemicals

All reagents used were of analytical grade. The streaming carrier solution contained in addition to the primary ion, an ionic strength adjusting salt *e.g.* KNO_3 in 10^{-1} *M* concentration. The injected samples in the case of volumetric manual injection were prepared similarly.

Results and Discussion

a) Description of the signals obtained in the coulometric injection system

Coulometric injection can be done with precisely determined injection times under well controllable conditions. Therefore, the signals of a coulometric injection system are favourable for studying the validity of the relatively simple peak model derived earlier and implicity given by equations (1—4).

The solution of equations (1—4) is as follows:

$$\text{if} \quad 0 \leq t \leq t_L, \qquad \text{then}$$

$$\Delta E(t) = 0 \tag{5}$$

$$\text{if} \quad t_L < t \leq t_L + \tau_{\text{inj}}, \quad \text{then}$$

$$\Delta E(t) = S \cdot \lg\left[1 + \frac{M}{V \tau_{\text{inj}} c_0}\left(1 - e^{-\frac{V}{W}(t - t_L)}\right)\right] \tag{6}$$

$$\text{and if} \quad t_L + \tau_{\text{inj}} < t, \quad \text{then}$$

$$\Delta E(t) = S \cdot \lg\left[1 + \frac{M}{V \tau_{\text{inj}} c_0}\left(1 - e^{-\frac{V}{W}\tau_{\text{inj}}}\right) e^{-\frac{V}{W}(t - t_L - \tau_{\text{inj}})}\right]. \tag{7}$$

Although in the case of coulometric injection the injection is done directly into the mixing chamber and the only connecting tube being in the system is placed after the mixing unit, equations (5—7) give a reasonably good approach to the description of the signals developed because only one tube process, *i.e.*

a time delay is involved in equations (5—7) for which the place of the connecting tube (before or after the stirrer) is indifferent. If injector, stirrer and detector are placed very near to each other, then $t_L = 0$, and equation (5) expressing the delay can be even neglected.

Figure 3 shows some peak-type curves calculated with equations (5—7) when the time of injection is relatively large ($\tau_{inj} = 33$ sec). It can be observed that the calculated and experimental peaks coincide very well not only in shape but also numerically.

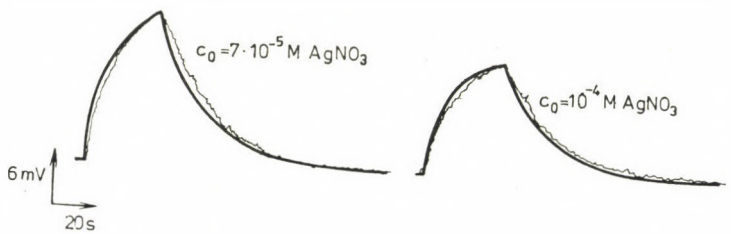

Fig. 3. Detected and calculated potentiometric signal at coulometric injection (thick line: calculated, thin line: measured shape) $\tau = 33$ sec, for the other parameters see [18]

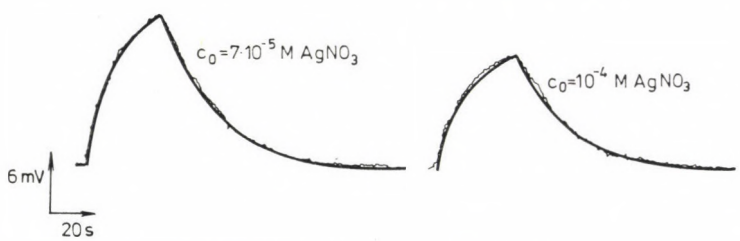

Fig. 4. Detected signal and calculated signal fitted to the measured one with respect to the mixing volume, W (coulometric injection, potentiometric detection) $\tau = 33$ sec, for the other parameters see [18]

The relatively simple model expressed by equations (5—7), however, can offer an even more accurate description of the peaks as compared with that shown in Fig. 3, if the value of the stirrer volume, W is corrected by the additional volumes of the small mixing rooms which appear unavoidably at the tube connections being after the outlet of the mixing chamber. As these volume increments would be difficult to measure, such a correction can be done most easily by fitting the model to the experimental peaks with respect to W. Such a fitting can be done by varying the value of W until best coincidence is obtained. Figure 4 shows the peaks calculated after the appropriate correction of W, and proves a perfect coincidence of the measured and calculated signals, though the value of W had to be corrected only by 12 per cent.

If the model is intended to be used for quantitative analytical purposes, it is always worth-while to carry out its fitting, and to compute the peak-type

curves with the such obtained effective value of the mixer volume, W_{eff}', instead of its nominal value, W. Once W_{eff} is determined for a given injection setup, the model expressed by equations (5—7) nicely follows the changes of the other parameters such as S, c_0 and M, according to our experiences.

If the time of coulometric injection, τ_{inj} is large enough, the dispersion of the injected material in the connecting tube sections between the place of injection and the detector cell is relatively small as compared with the length

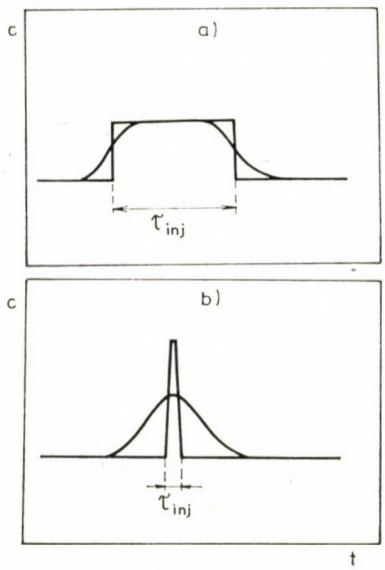

Fig. 5. Dispersion of the injected material at large injection time (a) and at small injection time (b), τ_{inj} (thick line represents the injected material "plug", and thin line illustrates its dispersion)

of the "plug" (see Fig. 5). Hence, the injected substance enters the mixing unit shown in Fig. 1 under a time period, τ being approximately equal to the time of injection, τ_{inj}.* In addition, the coulometric injection can be carried out accurately at a very constant rate, which results in the fact that in the injected "plug" practically no concentration gradient occurs. The only process taking place in the connecting tube sections which cannot be neglected is the time delay, t_L between injection and detection, due to the finite flow rate.

Thus, as the basic assumptions derived earlier [1] are valid, equations (1—4) give a good approach to the description of the signals of the coulometric injection system. This fact is illustrated by the results treated so far (Fig. 4).

* It must be mentioned that in the setup generally used the interconnecting tube length between the stirrer and detector is longer than it is between the place of injection and the stirrer. Just the opposite is shown in Fig. 1. However, this does not affect the derivation given.

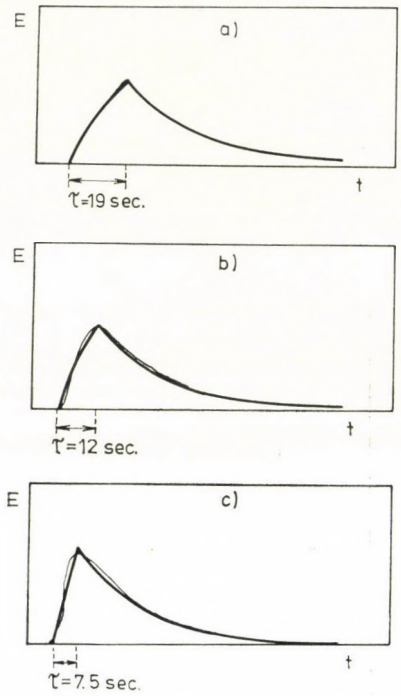

Fig. 6. Detected and calculated signals at various injection times: (a) $\tau_{inj} = 19$ sec, (b) $\tau_{inj} = 12$ sec, (c) $\tau_{inj} = 7.5$ sec. (Coulometric injection, potentiometric detection)

If, however, the time of injection, τ_{inj} is decreased, the dispersion of the injected substance relatively increases and a gradient is formed, as it is illustrated by Fig. 5. Hence, by decreasing τ_{inj}, the model discussed so far gradually loses its validity. It is then important to know for a given injection setup and flow rate, the minimum time of injection at which the model still remains valid.

Figure 6 shows the influence of the decreasing τ_{inj} values on the measured and calculated signals. On the basis of these curves it can be concluded that under the experimental conditions examined (see [18]) the performance of equations (5—7) is still good at $\tau_{inj} = 19$ sec, while at $\tau_{inj} = 12$ sec it becomes less accurate, and at $\tau_{inj} = 7.5$ sec it is no longer acceptable.

This tendency of devaluation of the model (5—7) by decreasing τ_{inj}, however, does not occur if the length of the connecting tubes, L, is very small because in this case no considerable dispersion can occur in the short tube sections involved. Thus, in this case of short connecting tubes the simple model discussed so far [1] can remain valid even if an impulse type (volumetric manual) injection is done, as it has been stated earlier [1, 9]. In this case, however, the fitting of the model has to be carried out with respect to not only the volume of the mixing chamber, W, but in general also the time of injection, τ_{inj} [9].

b) Description of the signals obtained in the volumetric manual injection system

If the volumetric injection is carried out manually with a syringe (see Fig. 1), the injection must be done in a very short time period in order to ensure the rate of injection to be constant and hence, the reproducibility of the signals. This means that if the peak-type signals obtained by manual injection should be described mathematically, an impulse type injection must be considered ($\tau_{inj} \to 0$).

In this case, as it has been said before, the model expressed by equations (5—7) can be used only if short connecting tubes are incorporated in the measuring system [1, 9]. If, however, the length of the connecting tubes is relatively large (see Experimental), a new mathematical model may describe the experimental transient signal more accurately than the model (5—7) does.

For this, our derivation can be started from the same equations as in the former case, *i.e.* from equations (1—4). Only the generator function of the differential equation (1), $\Delta c_s(t)$, given in the case of coulometric injection or of volumetric manual injection with small tube length by equations (2, 3), should be substituted by a more complicated one. This new function, $\Delta c_s(t)$ should describe not only the time delay elapsed between injection and detection, but also the dispersion of the injected material "plug" and the formation of a concentration gradient in the connecting tubes.

Since these phenomena cannot be due solely to the molecular diffusion of the injected species, but also to the longitudinal mixing of the sample "plug" in the analysis channel because of the nearly laminar carrier flow, thus the function $\Delta c_s(t)$ which expresses the concentration peak constituting the input signal of the mixing chamber cannot be derived directly on the basis of Fick's second law. This law, however, can be employed if an effective diffusion coefficient, D_{eff}, is inserted instead of the respective ionic or molecular one. (This is a very common practice in modelling chemical plant units, see *e.g.* [21].)

If the concentration impulse is assumed to be confined to an infinitely thin cross section layer at the point of injection, then from Fick's second equation there follows (see *e.g.* [22]):

$$\Delta c_s(t) = \frac{M}{2q(\pi D_{eff} \cdot t)^{1/2}} \exp\left[\frac{-1}{4D_{eff}}\left(\frac{L}{\sqrt{t}} - \frac{V\sqrt{t}}{q}\right)^2\right]. \tag{8}$$

Thus, the new model proposed for describing volumetric manual injection peaks developed at larger tube length consists of equations (1) and (8); thus, it follows that:

$$\frac{d\Delta c(t)}{dt} = \frac{V}{W}\left\{\frac{M}{2q(\pi D_{eff} \cdot t)^{1/2}} \exp\left[\frac{-1}{4D_{eff}}\left(\frac{L}{\sqrt{t}} - \frac{V\sqrt{t}}{q}\right)^2\right] - \Delta c(t)\right\}. \tag{9}$$

Equation (9) cannot be solved directly for $\Delta c(t)$ by the standard methods of mathematical analysis, but a number of appropriate numerical methods exist for its computational solution. The most simple integration procedure, the so called Euler integration scheme (23) which for example can be used for this purpose, is as follows:

$$\Delta c(t_0) = \Delta c(t_1) = 0, \tag{10}$$

while for $i = 2, 3, \ldots, n$:

$$\Delta c(t_i) = \left[\frac{V}{W}\Delta c_s(t_{i-1}) + \left(1 - \frac{V}{W}\right)\Delta c(t_{i-1})\right]\Delta t_i \tag{11}$$

where $\Delta t_i = t_i - t_{i-1}$, and the function $\Delta c_s(t)$ is defined by equation (9) At $t = t_n$, $\Delta c(t_n) \cong 0$, which means that the peak-type curve calculated comes to its end by reaching again the baseline.

Thus, the function $\Delta c(t)$ can be obtained, and by inserting it into equation (4), the potential-time curve *i.e.* the detected peak-type curve can be numerically computed.

In using the above model, however, a problem appears concerning the value of the model parameters. Namely, the effective diffusion coefficient, D_{eff} is not a simple physical constant defined by a single process, but an effective parameter which describes the effect of several simultaneous processes such as molecular diffusion and convective mixing. Thus, it depends on the diameter of the analysis channel and on the flow rate among others, mostly microscopic properties of the streaming and injected solution. Hence, the most simple and straightforward way of determining D_{eff} is that of fitting the model represented by equation (9) to some experimentally recorded peak-type curve. However, as the model is intended to use for quantitative analysis, the other model parameters are also worthy of being varied until best fitting is obtained. In this way the best possible description of the peak-type curves detected can be achieved (just as well as also in the case of the former simple model).

The fitting procedure has been carried out with respect to four independent model parameters, namely the effective diffusion coefficient D_{eff}, the volume of the mixing chamber W, the flow rate V, and the tube diameter d; the fitting was done by a simple "trial and error" method [23].

Once the fitting has been carried out, the model represented by equation (9) follows the variations in the detector electrode slope, S, carrier flow concentration, c_0, and injected amount, M.

For given values of S, c_0 and M a peak-type signal detected and its computed version are shown in Fig. 2. It can be seen in this figure that shape of the signal calculated with the model and that recorded coincide very well, except at the rising part of the signal where the fit is not so satisfactory.

This may be due to the fact that the electronic detector network which incorporates an ion-selective electrode as a sensor does not respond instanta-

neously to the sudden rise of concentration which is caused by the arrival of the fore-part of the injected "plug" to the detector cell. This response delay is, however, ignored in the model [see equation (4)], and this fact may account for the small deviation occurring at the first seconds between measured and computed signals.

Conclusion

As it has been shown, the model of coulometric injection peaks or peaks developed at manual injection into a system with short connecting tubes equations (5—7) gives good results if either the time of injection, τ_{inj}, is large enough ($\tau_{inj} > 15$ sec in the experimental setup described in [18]), or the connecting tubes are short enough [1, 9], while the model derived first of all for an impulse type volumetric manual injection [equations (9—11) gives good performance in the opposite case, *i.e.* if the injection is done suddenly $\tau_{inj} \to 0$], and the length of the connecting tubes is considerable.

Both models can be used for the following purposes:

1. The characteristics of the transient signals detected can be optimized with respect to the parameters of the measuring setup on the basis of the models discussed, in order to solve given analytical problems in the best way.

2. New numerical methods of injection analysis can be developed by using the models reported.

3. The linear range of the calibration graphs can be enhanced by considering the models, if the analysis is carried out by using calibration graphs instead of numerical methods [1, 2, 4—10, 18—20].

These applications will be reported in a following paper.

REFERENCES

[1] NAGY, G., FEHÉR, ZS., PUNGOR, E.: Anal. Chim. Acta **52,** 47 (1970)
[2] FEHÉR, ZS., PUNGOR, E.: Anal. Chim. Acta **71,** 425 (1974)
[3] BERGMEYER, H. U., HAGEN, A.: Fresenius' Z. Anal. Chem. **261,** 333 (1972)
[4] FEHÉR, ZS., NAGY, G., TÓTH, K., PUNGOR, E.: Analyst **99,** 699 (1974)
[5] PUNGOR, E., FEHÉR, ZS., NAGY, G.: Pure and Appl. Chem. **44,** 595 (1975)
[6] TÓTH, K., NAGY, G., FEHÉR, ZS., PUNGOR, E.: Z. Anal. Chem. **282,** 379 (1976)
[7] PUNGOR, E., NAGY, G., FEHÉR, ZS.: J. Electroanal. Chem. **75,** 241 (1977)
[8] PUNGOR, E., TÓTH, K.: Vom Wasser **42,** 43 (1974)
[9] PUNGOR, E., TÓTH, K., NAGY, G.: Hung. Sci. Instr. **35,** 1 (1975)
[10] NAGY, G., PUNGOR, E.: Hung. Sci. Instr. **32,** 1 (1975)
[11] ESWARA DUTT, V. V. S., MOTTOLA, H. A.: Anal. Chem. **47,** 357 (1975)
[12] RŮŽICKA, J., HANSEN, E. H.: Anal. Chim. Acta **78,** 145 (1975)
[13] RŮŽICKA, J., HANSEN, E. H., ZAGATTO, E. A.: Anal. Chim. Acta **88,** 1 (1977)
[14] STEWART, K. K., BELCHER, G. R., HARE, F.: Anal. Biochem. **70,** 167 (1976)
[15] WATSON, B., KEYES, M. H.: Anal. Lett. **9**(8), 713 (1976)
[16] RŮŽICKA, J., HANSEN, E. H., MOSBAECK, H.: Anal. Chim. Acta **92,** 235 (1977)

[17] BETTERIDGE, D., RŮŽICKA, J.: Talanta **23**, 409 (1976)
[18] FEHÉR, ZS., NAGY, G., TÓTH, K., PUNGOR, E.: Anal. Chim. Acta **98**, 193 (1978)
[19] PUNGOR, E., TÓTH, K., NAGY, G., FEHÉR, ZS.: Ion-Selective Electrodes, Ed. E. PUNGOR, Akadémiai Kiadó, Budapest 1977.
[20] TÓTH, K., FEHÉR, ZS., NAGY, G., LINDNER, E., PUNGOR, E.: Magyar Kémikusok Lapja 34 (1), 17 (1979); 34 (2), 77 (1979)
[21] TREYBAL, W.: "Mass Transfer Operations", Mc Graw Hill Co., New York (1970)
[22] CRANK, J.: "The Mathematics of Diffusion", Clarendon Press, Oxford (1975)
[23] GILOI, W. K.: "Principles of Continuous System Simulation", B. G. Teubner, Stuttgart (1975)

Miklós GRATZL
Zsófia FEHÉR
Géza NAGY
Klára TÓTH
Ernő PUNGOR

H-1521 Budapest, Műegyetem

Acta Chimica Academiae Scientiarum Hungaricae, Tomus 100 (1–4), pp. 353–363 (1979)

IONIC SOLVATION IN MEDIA WITH ANOMALOUS ELECTRICAL EQUATION OF STATE

I. RUFF, Z. G. SZABÓ and J. LISZI

(Institute of Inorganic and Analytical Chemistry, L. Eötvös University, Budapest,

Department of Physical Chemistry, The University of Chemical Industries, Veszprém)

Received July 10, 1978

Accepted for publication August 7, 1978

By approximating the electrostriction of the dielectric around an ion, an equation can be deduced for the electrostatic solvation free enthalpy which explicitely contains the density dependence of the relative permittivity of the solvent. For liquids with non-linear relationship between relative permittivity and mass density (*i.e.* anomalous with respect to their electrical equation of state), the Born charging up integral for ions immersed in the dielectric is multiplied by a factor d ln ε/d ln g where g is mass density. The combination of this result with the Grahame equation, which accounts for dielectric "saturation effects", indicates that the above factor gives the greatest correction in the high field region around the ion where the relative permittivity is reduced to the square of the internal refraction index, n^2. Calculations of the density dependence of n^2 based on molar refraction data show that most polar solvents behave anomalously. Numerical calculations for alkali halides in dimethylformamide, 1-propanol, and water are in fair agreement with experimental data.

1. Introduction

Since the time it has got known that the application of the BORN equation [1] with the assumption of field-independent relative permittivity gives an overestimate of the solvation free enthalpies of ions, a very large number of papers have appeared in which attempts were made to improve the model and to obtain better agreement with experiments [2]. These modifications are centered around three problems: (i) the liquid is molecularly "granulated" and its structure may change under the effect of the high field and/or non-fitting size of the ions, whereas the model is a continuum approach; (ii) the real solution radii of ions are unknown, and there are many solvents in which the dipole centre and the mass center of the molecules do not coincide, thus there is a great variety of possible but more or less unjustified corrections for all radii or even different corrections for cations and anions; (iii) no exact theoretical solution is known for the non-linear "saturation" effects in dielectrics under high field, and no experimental results are available for nonlinear effects under very high fields such as those in the close vicinity of relatively

small ions, thus there are almost arbitrary choices of continuous or discontinuous models for dielectric saturation effects.

Considering these possibilities of, in some cases quite optional, in some others more or less justified corrections, one can conclude that agreement with experiments must not be the sole criterion for the acceptance of a model. It is the present authors' opinion that the self-consistence of a treatment should at least be one of the additional criteria in the sense that, if, say, classical macroscopic electrostatics is intended for use, it is to be applied throughout with no arbitrary manipulations with ionic radii, refraction index, or with the breakdown of the solvation free enthalpy of salts into single ion quantities. Hence, the model outlined in the present paper — although approximate — is based on classical electrostatics, and is semiempirical in that it uses (i) the empirical density dependence of the relative permittivity and refraction index as quantities reflecting structural effects in solvents, (ii) crystallographic GOURARY—ADRIAN radii [3] which have more experimental justifications as opposed to the Pauling or Goldschmidt radii, and (iii) the GRAHAME equation [4] for non-linear effects under high fields with empirical (and macroscopic) non-linearity coefficients.

2. Calculation of the "experimental" value of the electrostatic free enthalpy of solvation

The various portions of the total free enthalpy of ionic solvation that must be distinguished separately have been discussed recently by ABRAHAM and LISZI [5]. By analogy to their and NOYES' treatment [6], the nonelectrostatic free enthalpy of solvation can be approximated by extra- or interpolating the free enthalpy of dissolution of noble gases and simple hydrocarbons. In Figs 1—3 the sum of the electrostatic free energy of solvation of both ions of alkali halides is plotted as a function of the sum of their reciprocal Gourary—Adrian radii. Except fluorides in water, all values fall on straight lines. (The deviation of fluorides may be due partly to a systematic error in the radius of the fluoride ion [3], and partly to the pronounced hydrogen bonding ability of this ion with water.) If Noyes' single ion hydration free enthalpies are used, after a correction for the nonelectrostatic part, the points corresponding to anions and cations also lie on the same straight line with an intercept half of that in Fig. 3. Since the differences between Pauling and Gourary—Adrian radii are almost the same as the correction used by MISHCHENKO *et al.* [2b], the coincidence of the cation and anion curves is quite evident.

In some papers [2] the correction of Pauling radii is thought to be justified by the argument that, even if crystallographic and solution radii are equal, there is an expansion of the ions in gas phase, and, — since the gas phase electrostatic energy of the ion is the major term in the solvation free enthalpy —

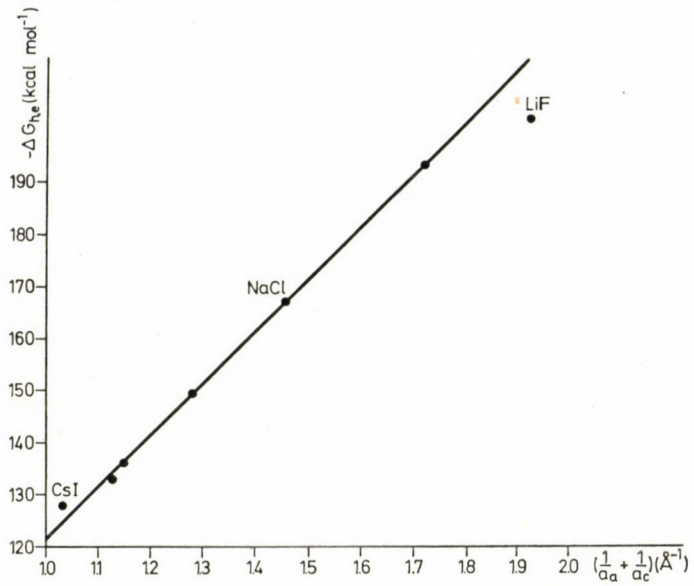

Fig. 1. Dependence of the electrostatic free enthalpy of solvation of alkali halides in dimethylformamide on the sum of the reciprocal Gourary—Adrian radii of ions

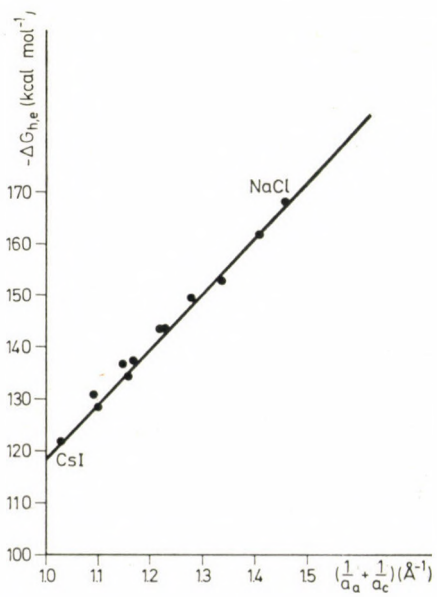

Fig. 2. Dependence of the electrostatic free enthalpy of solvation of alkali halides in 1-propanol on the sum of the reciprocal Gourary—Adrian radii of ions

a relatively small positive correction for the gas phase radii would sufficently reduce the error of the Born equation. On the ground of the Born—Haber cycle in Fig. 4, however, it seems that no such correction is justified, owing to the fact that, after the expansion of the ionic crystal lattice to infinity which

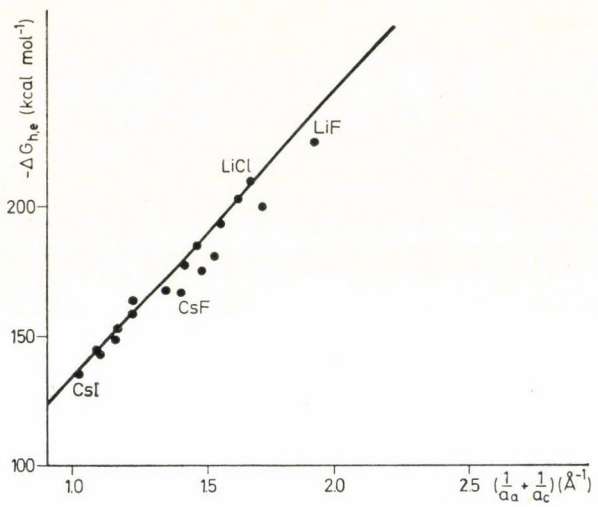

Fig. 3. Dependence of the electrostatic free enthalpy of solvation of alkali halides in water on the sum of the reciprocal Gourary—Adrian radii of ions

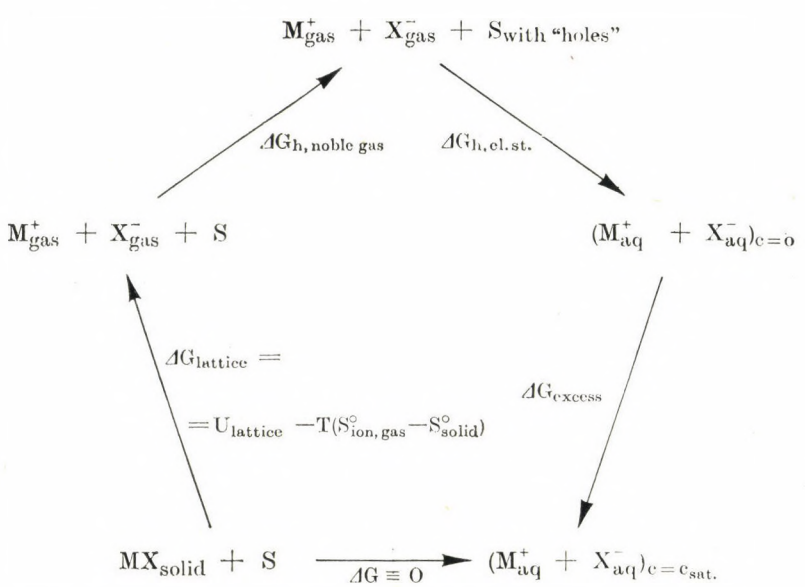

Fig. 4. The Born—Haber cycle of solvation showing the breakdown of the solvation free enthalpy into electrostatic and non-electrostatic parts

requires the supply of the lattice energy, one ends up with a fictive gas of ions preserving their original size. Even if the corresponding entropy of a monoatomic gas is added which accounts for the randomization of the infinitely expanded lattice, still no allowance is made for the expansion of the electron shell of ions. Then, in the dissolution step, the ions possessing still their crystallographic size are immersed into the solvent. In addition, if it is taken into consideration that lattice energies can be calculated without the assumption of larger gas phase ions in very good agreement with Born—Haber cycles involving ionization potentials and standard elementary states, there seems to be no real reason for radius corrections.

While it is doubtless that the step accounting for non-electrostatic effects, labelled by $\Delta G_{\mathrm{h,\ noble\ gas}}$, is to be introduced into the cycle, the additivity of this term and the electrostatic one will only apply, when specific interactions such as hydrogen bonding or coordination bonds between the solvent and the ions do not interfere. These specific forces are certainly inactive between noble gas or a hydrocarbon and the solvent, and thus they do not alter the own structure of the solvent in the same way as would "uncharged alkali or halide ions". The correct term on the upper left hand side of the cycle should be the free enthalpy change due to the appropriate hole formation in the solvent with a solvent structure around it that corresponds to the solvate of the ion. Although the error committed by approximating this quantity by the free enthalpy of dissolution of neutral molecules may be only a few kcal/mol, it can be commensurable with $\Delta G_{\mathrm{excess}}$ and, thus, result in appreciable error in predicting the concentration of saturated solutions.

The straight lines in Figs 1—3 correspond to the following equation:

$$\Delta G_{\mathrm{h,e}} = -A - B\left(\frac{1}{a_{\mathrm{a}}} + \frac{1}{a_{\mathrm{c}}}\right), \tag{1}$$

where a_{a} and a_{c} are the radius of the anion and cation, respectively, measured in Å, and the numerical values of the constants are given for kcal/mol units as follows: $A = 20$, 10, and 13, $B = 100$, 108 and 110 for dimethylformamide, 1-propanol, and water, respectively.

3. Calculation of solvation free enthalpies via the volume force acting on a dielectric

The basic equation usually applied in the calculation of the electrostatic free enthalpy of solvation is:

$$w = \frac{1}{8\pi}\int \mathbf{E} \cdot \mathbf{D}\, \mathrm{d}v, \tag{2}$$

where **E** is the electric field vector, **D** the dielectric displacement, and dv is an infinitesimal volume element. If a single ion immersed in a dielectric with constant (*i.e.* field independent) relative permittivity ε_0 is considered, the integration leads to the following equation:

$$w = \frac{(ze)^2}{2\varepsilon_0 a_i}, \tag{3}$$

where ze is the charge of the ion, and a_i is its radius.

On the other hand, w can be calculated also by the equation:

$$\delta w = -\int \mathbf{F}_v \cdot \delta \mathbf{x} \mathrm{d}v, \tag{4}$$

where $\mathbf{F}_v$ is the volume force acting on unit volume and $\delta\mathbf{x}$ is the variation of the position coordinates of the volume element dv. By utilizing the hydrodynamic equations of continuity it can be shown [8] that Eq. (4) is equivalent to Eq. (2), if $\mathbf{F}_v$ has the form:

$$\mathbf{F}_v = \varrho\mathbf{E} - \frac{1}{8\pi}\mathbf{E}^2\nabla\varepsilon + \frac{1}{8\pi}\nabla\left(\mathbf{E}^2\frac{\mathrm{d}\varepsilon}{\mathrm{d}\ln g}\right), \tag{5}$$

where ϱ is the charge density and g the mass density. Again, assuming that the relative permittivity ε is field-independent but not independent of position coordinates, due to changes in solvent density through electrostriction, and considering the case of a charged sphere of radius a_i, from Eqs. (4) and (5) we arrive at the result:

$$w = \frac{\mathrm{d}\ln\varepsilon_0}{\mathrm{d}\ln g}\frac{(ze)^2}{2\varepsilon_0 a_i} \tag{6}$$

which transforms into Eq. (3) if $\mathrm{d}\ln\varepsilon_0/\mathrm{d}\ln g = 1$, *i.e.* if the dielectric behaves "normally" having a linear relative permittivity dependence on mass density. The advantageous feature of Eqs. (4)—(5) as opposed to Eq. (2) is that it explicitely involves the term containing the density dependence of relative permittivity. When obtaining Eq. (6), we assumed that $\mathrm{d}\ln\varepsilon_0/\mathrm{d}\ln g$ is constant.

For liquids whose relative permittivity follows the Onsager equation, the $\mathrm{d}\ln\varepsilon_0/\mathrm{d}\ln g$ factor is unity, since it implies the assumption that the dipole density increases linearly with mass density. This is also justified by experimental results on the pressure dependence of relative permittivity and that of density, which run in parallel [9], giving the following approximate correlation valid for many organic liquids:

$$\frac{\mathrm{d}\ln\varepsilon_0}{\mathrm{d}\ln g} = 1.8g^2. \tag{7}$$

If g is around 0.75 g/cm^3, the right hand side of Eq. (7) is about unity.

Liquids with non-unity Kirkwood factor may or may not be anomalous from the point of view of the density dependence of relative permittivity. If there are structural effects that make the Onsager equation invalid, but this structure is not broken down by increasing the pressure in the region around 1 atm, the density dependence may be linear. If, however, structural changes occur due to the change in density, the $d \ln \varepsilon_0 / d \ln g$ factor may be less then unity — when the higher density structure has a lower Kirkwood g-factor — or greater than unity in the opposite case. Of the solvents we will discuss below, 1-propanol behaves normally [10], while water seems to have a $d \ln \varepsilon_0 / d \ln g$ factor lower than unity. (It must be stated conditionally, since from the polynomial given by SILVESTER and PITZER [11] a value of 0.707 can be calculated for 25 °C, but the constants of this equation are misprinted someplace, because it yields only 70.8 for ε_0 at 25 °C instead of 78.54. In the derivative with respect to density, the constants of the terms not containing the density cancel out. Thus, if the misprint happens to be among those constants, the derivative can still be calculated correctly.)

In the close vicinity of the ions the very high electric field affects the dielectric so that the relative permittivity is reduced to its high frequency value. In this region the charging up integral will take a similar form as that in Eq. (6) with n^2 in place of ε_0. Thus we have to estimate the density dependence of the internal refraction index too. For this purpose we can use the expression of molar refraction:

$$R_M = \frac{n^2 - 1}{n^2 + 2} \cdot \frac{M}{g} \neq \mathrm{f}(g)\,, \tag{8}$$

where M is the molecular weight and R_M is the so-called molar refraction which is strictly independent of density so that even phase changes leave it unaltered. The differentiation of eq. 8 yields:

$$\frac{d \ln n^2}{d \ln g} = \frac{3 R_M M/g}{(R_M - M/g)^2} \cdot \frac{1}{n^2}\,. \tag{9}$$

Many polar liquids have $d \ln n^2 / d \ln g$ values lower than unity, while most nonpolar ones show "normal" behaviour. For example Eq. (9) gives 0.685 for dimethylformamide, 0.672 for 1-propanol, and 0.556 for water, while 1.02 for carbon disulfide at 25 °C. (It seems interesting to note here that Eq. (9) would yield unity for water, if its density were 1.84 g/cm^3 which would be the density of body-centered close-packed water with a molecular diameter of 2.76 Å.)

4. Calculation of nonlinear effects

The electrostatic free enthalpy of solvation is:

$$\Delta G_{h,e} = w - \frac{(ze)^2}{2a_i}, \tag{10}$$

where the second term is the free enthalpy of the gaseous ion. It can be seen on the basis of the foregoing section that calculations using a field-independent relative permittivity would give no appreciably different results for either Eq. (4) or Eq. (3) — and large overestimates in both cases —, since w would be very small in comparison with the second term above. Nonlinear dielectric effects, however, would increase w due to the fact that some lower relative permittivity regions would come into account in the close vicinity of ions.

According to the GRAHAME equation [4], which can be regarded as an approximation to the theoretically more adequate but mathematically less convenient BOOTH equation [12], the relative permittivity can be calculated from the following two equations:

$$\varepsilon = n^2 + \frac{\varepsilon - n^2}{1 + b\mathrm{E}^2} \tag{11}$$

and

$$\mathrm{D} = n^2\,\mathrm{E} + \frac{\varepsilon_0 - n^2}{\mathrm{E}\sqrt{b}} \arctan \mathrm{E}\sqrt{b}, \tag{12}$$

where b is the nonlinearity coefficient determined experimentally or — for regular solvents for which the Onsager model is correct — it can be calculated as follows:

$$b = \frac{\mu^2(n^2+2)^2}{60k^2T^2}, \tag{13}$$

where μ is the gas phase dipole moment.

Equations (11)—(12) can be used to calculate the dependence of relative permittivity as a function of the distance from the centre of an ion. The usual result is that the relative permittivity is practically equal to n^2 of the solvent up to a radius a, then it increases monotonously to the bulk value ε_0. It seems to be a very good approximation, if one assumes that at distances larger than or equal to a the $n^2\mathrm{E}$ term in Eq. (12) can be neglected in comparison with the arctan term which enables us to write the following explicite equation for ε:

$$\varepsilon = \varepsilon_0 - (\varepsilon_0 - n^2)\sin^2 \frac{\mathrm{D}\sqrt{b}}{\varepsilon_0 - n^2} \quad (\text{for } r \geq a) \tag{14}$$

and

$$\varepsilon = n^2 \quad (\text{for } r < \mathrm{a}). \tag{15}$$

In this way we can separate w into two terms: one is a simple charging up integral for a medium with relative permittivity n^2 in the spherical layer from the radius of the ion a_i to a:

$$w_1 = \frac{\mathrm{d} \ln n^2}{\mathrm{d} \ln g} \left(\frac{1}{a_i} - \frac{1}{a} \right) \frac{(ze)^2}{2n^2} \tag{16}$$

which can be obtained by analogy to the reactive field approximation used by ABRAHAM and LISZI [5], while another term will be independent of the radius and represents only the non-linear characteristics of the solvent:

$$w_2 = -4\pi \int_a^\infty r^2 \int_{r'}^\infty \mathbf{F}_v \, \mathrm{d}r \, \mathrm{d}r' , \tag{17}$$

where $\mathbf{F}_v$ is given now for the radially symmetrical case of a charged sphere into which Eq. (14) and the corresponding equation for the field:

$$\mathrm{E} = \frac{1}{\sqrt{b}} \operatorname{tg} \frac{\mathrm{D} \sqrt{b}}{\varepsilon_0 - n^2} \tag{18}$$

are to be inserted.

The final equation for electrostatic free enthalpy of solvation is:

$$\Delta G_{h,e} = w_2 - \frac{\mathrm{d} \ln n^2}{\mathrm{d} \ln g} \cdot \frac{(ze)^2}{2an^2} - \left(1 - \frac{\mathrm{d} \ln n^2}{\mathrm{d} \ln g} \cdot \frac{1}{n^2} \right) \frac{(ze)^2}{2a_i} . \tag{19}$$

It can be seen that the first two terms are independent of ionic radius, *provided that none of the ionic radii considered exceed the value of a*, and thus Eq. (19) leads to the type of linear relationship written in Eq. (1).

5. Numerical calculations

We have chosen three solvents for which the test of Eq. (19) could be carried out: dimethyl formamide which conforms well with the Onsager model and in which there are probably no specific interactions between the molecules that would make the nonlinearity coefficient [Eq. (13)] differ from theoretical; 1-propanol which does not conform with the Onsager model, and its nonlinearity coefficient is anomalous [13]; and water which is anomalous in all aspects considered here [14].

The most important quantities of the computations are shown in Table I. Taking into account that the calculations are less precise in the intercept, the agreement with experiment is quite good with one exception, *viz.* the slope for dimethyl formamide.

It is interesting to note that the individual characteristics of the solvent are mainly represented by the ε_0, b, and a values, still a sort of inner compen-

Table I

Comparison of calculated and observed electrostatic free energies of solvation of alkali halides in dimethylformamide, 1-propanol and water

Quantity	Solvent		
	Dimethylformamide	1-Propanol	Water
ε_0	36.71	20.45	78.54
n^2	2.15	2.01	1.78
$\frac{\mathrm{d} \ln \varepsilon_0}{\mathrm{d} \ln g}$	1*	1**	0.707
$\frac{\mathrm{d} \ln n^2}{\mathrm{d} \ln g}$	0.685	0.672	0.556
b/(el.st.u.)^2	2.51×10^{-9}	1.34×10^{-8}	1.14×10^{-8}
a/Å***	2.4	2.3	2.2
w_2/kcal · mol^{-1}	13.9	19.7	14.5
$A_{\text{calcd.}}$/kcal · mol^{-1}	18.3	8.8	18.0
$A_{\text{expl.}}$/kcal · mol^{-1}	20	10	13.0
$B_{\text{calcd.}}$/kcal · mol^{-1}	110	110	113.9
$B_{\text{expl.}}$/kcal · mol^{-1}	100	108	109.3

* Assumed.

** Approximated by the assumption that the density dependence parallels those of other organic liquids [9] and using experimental data [10] for the pressure dependence of relative permittivity.

*** The parameter a was chosen in such a way that this distance correspond to $\varepsilon \sim 2n^2$.

sation make the w_2 values rather uniform. Similar inner compensation results in the fact that, if electrostriction is calculated through a computation of inner pressure as a function of the distance from the centre of the ion — which was done for 1-propanol and water —, the final results were practically the same, since the electrostriction effect is smoothed out in w_2 and the increase in n^2 is compensated by an increase in $\mathrm{d} \ln n^2 / \mathrm{d} \ln g$.

REFERENCES

[1] BORN, M.: Z. Physik, **1,** 45 (1920)
[2] *a)* ROSSIENSKY, D. R.: Chem. Revs., **65,** 467 (1965)
b) MISHHENKO, K. P., POLTORATSKII, G. M.: "Termodinamika i stroenie vodnikh i nevodnikh rastvorov elektrolitov", Khimia, Leningrade, 1976, and references therein
c) LENGYEL, S., KEMPELEN, M.: MTA Alk. Mat. Int. Közl., **2,** 489 (1952)
[3] GOURARY, B. S., ADRIAN, S. J.: Solid state Physics, **10,** 127 (1960)
[4] GRAHAME, D. C.: J. Chem. Phys., **18,** 903 (1950), **21,** 1054 (1953)
[5] ABRAHAM, M. H., LISZI, J.: JCS Faraday Trans. I, **74,** 1604 (1978)
[6] NOYES, R. M.: J. Chem. Soc., **84,** 513 (1962)
[7] LAIDLER, K. J., MUIRHEAD-GOULD, J. S.: Trans. Faraday Soc., **63,** 953 (1967) and references therein

[8] PANOFSKY, W. K. H., PHILIPS, M.: "Classical Electricity and Magnetism", Addison—Wesley, Cambridge, Mass., 1955, pp. 92—95.
[9] HARNED, H. S., OWEN, B. B.: "The Physical Chemistry of Electrolyte Solutions", Reinhold, Princeton 1958
[10] CHEN, T., DANNHAUSER, W., JOHARI, G. P.: J. Chem. Phys., **50,** 2046 (1969); the data from this paper were fitted to the equation given in ref. [9], and the constants were found to be reasonably close to those for "many organic liquids"
[11] SILVESTER, L. F., PITZER, K. S.: J. Phys. Chem., **81,** 1822 (1977)
[12] BOOTH, F.: J. Chem. Phys., **19,** 391, 1327, 1615 (1951)
[13] BROWN, B. L., PARRY JONES, G.: JCS Faraday Transactions II, **71,** 1657 (1975)
[14] KOŁODZIEJ, H. A., PARRY JONES, G.: JCS Faraday Transactions II, **71,** 269 (1975)

Imre RUFF
Zoltán G. SZABÓ } H-1443 Budapest, P.O. Box 123
János LISZI H-8200 Veszprém

Acta Chimica Academiae Scientiarum Hungaricae, Tomus 100 (1—4), pp. 365—376 (1979)

SYNTHESIS OF 7-[(HETEROARYL-THIO)ACETAMIDO]-3-DEACETOXYCEPHALOSPORANIC ACID DERIVATIVES, I

F. SZTARICSKAI, I. MISKOLCZI[1] and R. BOGNÁR

(Research Group for Antibiotics of the Hungarian Academy of Sciences and Institute of Organic Chemistry, Kossuth Lajos University, Debrecen
[1] Biogal Pharmaceutical Works, Debrecen)

Received July 11, 1978

Accepted for publication September 8, 1978

The preparation of nineteen new 7-[(heteroaryl-thio)-acetamido]-3-deacetoxy-cephalosporanic acids (**IVa—t**) *via* the nucleophilic substitution of 7-chloroacetamido-3-deacetoxycephalosporanic acid (**II**) with various mercapto-heteroaryl compounds (**III—t**) is described. A new convenient method, including the acylation of 7-ADCA with the chemically "active" 8-quinolyl esters of heteroaryl-thioacetic acids (prepared *in situ* in the reaction mixture) has been elaborated for the synthesis of these compounds. The transformation reactions of **XIIIe,p,r** — obtained from 6-chloroacetamidopenicillanic acid-sulfoxide (**XI**) — into the corresponding dihydrothiazine ester derivatives (**XVe,p,r**) have also been studied.

In both *in vitro* and *in vivo* experiments, the synthesized compounds showed antibiotic activity only against Gram-positive bacteria. Compound **IVn** proved to be more effective than cephalexin, whereas **IVd** — exhibiting a significant *in vitro* biological activity — was found to be ineffective in experiments on mice infected by *Mycobact. tuberculosis typ. bovinus* (RAVENEL).

Semisynthetic penicillin derivatives with sulfur-containing side chain have been long known in the literature [1, 2, 3]. Therefore it is not surprising that efforts have been made to synthesize the corresponding cephalosporin analogues, as well.

In the case of some natural cephalosporins both the exchange of the *C*-3 acetoxy group and the substitution of the 7-*N*-acylamido side chain with mercaptoalkyl-, mercaptoaryl- or mercapto-heteroaryl groups have been accomplished [4—8]. In several cases the analogues contain the sulfur atom of the side chain in the form of a sulfoxide or sulfone [9, 10].

Recently an increasing number of semisynthetic cephalosporin derivatives containing a similar structural element (Cephapirin, Cephazaflur, Cefazolin, Cephanone) have been applied in the clinical practice [6, 11].

During the past few years MISIEK *et al.* [12, 13] have reported the biological investigation of more than six hundred 7-[(2-S-substituted-thio)acetamido]cephalosporanic acid derivatives. The most active compound, 7-[(2,6-dichloropyrid-4-yl-thio)acetamido]cephalosporanic acid, inhibited the *in vitro* reproduction of *Mycobact. tbc.* at a concentration of 1.4 μg/ml.

In the present communication we describe the synthesis and biological investigation of several 7-[(heteroaryl-thio)acetamido]-3-deacetoxycephalosporanic acid derivatives. For the preparation of these compounds the method elaborated in our laboratory [14], including acylation with 8-hydroxyquinoline "active" esters, has been applied.

Synthesis

The starting material of one of the synthetic routes (Fig. 1, route A) was 7-chloroacetamido-3-deacetoxycephalosporanic acid (**II**) which was prepared by the acylation of 7-amino-3-deacetoxy-cephalosporanic acid (**I**, 7-ADCA) with the 8-hydroxyquinolyl ester of chloroacetic acid [14]. It is to be referred that Ho [15] also successfully applied 8-acyloxyquinolines for the selective *N*-acylation of several simple amino compounds. Nucleophilic substitution of chloro atom of **II** by various mercapto-heteroaryl compounds (**IIIa—t**) in *N*,*N*-dimethylformamide in the presence of triethylamine (20 °C, 12 h) resulted in the corresponding 7-[(heteroaryl-thio)acetamido]-3-deacetoxy-3-cephem-4-carboxylic acids (**IVa—t**, Table I). For the synthesis of Cephapirin and its analogues, CRAST *et al.* [8] made 7-bromoacetamidocephalosporanic acid to react with mercapto compounds in chlorinated hydrocarbons or in aqueous medium. Our compound **II**, however, did not react with mercapto compounds in chlorinated hydrocarbons or alcohols even in hot solution. The application of aqueous medium is strongly limited due to the low solubility of the mercapto compounds. On the other hand, the reactions readily occurred in *N*,*N*-dimethylformamide at room temperature. This letter observation can be explained by the different reactivity of the halogen atoms in protic and dipolar aprotic solvents. The details of the preparation and crystallization of synthetic **IVa—t**, as well as the measured physical data (m.p., analytical data and yields) are summarized in Table I. The νC=O (β-lactam) band of all products was observed between 1767—1780 cm^{-1} (KBr).

The preparation of the products mentioned above was also effected in another way (see Fig. 1). Heteroarylthioacetic acid 8-quinolyl esters (**VIIIc, l, p**) were prepared either from a heteroaryl-thioacetic acid (**VI**) and 8-hydroxyquinoline (**VI**) in dichloromethane (20 °C; 1 h) in the presence of *N*,*N*'-dicyclohexylcarbodiimide, or from chloroacetic acid 8-quinolyl ester (**VII**) and the corresponding heteroaryl-mercapto compound (**IIIc, l, p**) in *N*,*N*-dimethylformamide (20 °C, 3 h). Thus as a variation of the method represented by route A, the desired antibiotic analogues (**IVc, l, p**) were also obtained by synthesizing first the side chain, followed by the reaction of the resulting esters (**VIIIc, l, p**) with 7-ADCA in *N*,*N*-dimethylformamide (20 °C, 12 h) in the presence of triethylamine (route B). The physical data (IR spectrum, m.p., mixed m.p. and

Table I

Physical data of semisynthetic deacetoxycephalosporanic acids

Compound	Dec. point °C	Formula	Method	Yield %	Crystallization	Analysis			
						Calcd.		Found.	
						S %	N %	S %	N %
IVe	195	$C_{14}H_{15}O_4N_3S_3$	A	42	CH_3OH	24.95	10.90	24.69 24.65	10.80 11.00
IVb	160	$C_{19}H_{17}O_4N_3S_3$	A	76	EtOAc petroleum ether	21.48	9.38	21.04 20.74	9.33 9.29
IVc	208	$C_{17}H_{15}O_4N_3S_3$	A B	99 95	DMFA-H_2O	22.80	9.96	22.72 22.67	9.82 10.02
IVd	195	$C_{17}H_{14}O_4N_3S_3Cl$	A	43	DMFA-H_2O	21.08	9.21	21.09 21.03	9.31 9.50
IVe	211	$C_{17}H_{15}O_5N_3S_2$	A	80	DMFA-H_2O	15.80	10.35	15.76 15.74	10.40 10.16
IVf	204	$C_{16}H_{18}O_4N_4S_2$	A	60	DMFA-H_2O	16.26	14.20	16.06 16,00	14.07 14.37
IVg	185	$C_{19}H_{17}O_4S_2Cl$	A	43	DMFA-H_2O	13.79	12.04	13.74 13.49	12.21 12.37
IVh	193	$C_{18}H_{17}O_4N_5S_2$	A	46	acetone	14.85	16.23	14.86 14.73	16.21 16.32
IVi	207	$C_{16}H_{14}O_5N_5S_2$	A	80	DMFA-H_2O	15.21	16.62	15.35 15.66	16.68 16.56
IVj	181	$C_{24}H_{21}O_4N_5S_2$	A	80	EtOAc	12.63	13.80	12.66 12.46	13.76 13.52
IVk	195	$C_{17}H_{16}O_4N_6S_2$	A	42	EtOAc	14.82	19.43	14.87 15.01	19.76 19.95
IVl	185	$C_{18}H_{18}O_4N_6S_2$	A B	76 45	CH_3OH	14.38	18.85	14.35 14.68	19.02 19.03
IVm	175	$C_{17}H_{15}O_4N_6S_2Br$	A	47	EtOAc-petroleum ether	12.54	16.43	12.24 12.62	16.39 16.12
IVn	172	$C_{18}H_{18}O_4N_6S_2$	A	50	EtOAc-petroletum ether	14.38	18.85	14.27 14.19	18.84 18.55
IVo	205	$C_{18}H_{18}O_5N_6S_2$	A	30	CH_3OH	13.88	18.20	13.88 13.97	17.83 17.53
IVp	185	$C_{17}H_{15}O_4N_6S_2Cl$	A B C	51.5 45.0 35.39	CH_3OH	13.73	18.00	13.68 13.49	17.81 17.79
IVr	178	$C_{18}H_{18}O_5N_6S_2$	A C	56.5 28.13	CH_3OH	13.88	18.20	13.85 13.79	18.18 18.05
IVs	173	$C_{12}H_{14}O_4N_6S_2$	A	35	ether	17.31	22.69	17.38 17.20	22.22 22.16
IVt	165	$C_{18}H_{18}O_5N_6S_2$	A	50	CH_3OH	13.88	18.20	13.73 13.66	18.08 18.06

chromatographic mobility) of the products **IVc, l, p** synthesized in the two different ways were identical. The yields obtained by routes A and B were also almost identical (51—99% and 45—99%, respectively, calculated for the pure products).

Moreover, method B could be simplified by elaborating a one-pot process for steps **VII** → **VIIIc, l** → **IVc, l**, and only the end-products were isolated. This simplification had no effect on the overall yields.

The ring expansion method elaborated by MORIN *et al.* [16] offered a possibility for synthesizing new 7-[(heteroaryl-thio)acetamido]-3-deacetoxy-cephalosporanic acid derivatives (Fig. 2) starting from 6-aminopenicillanic acid (**IX**, 6-APA). Acylation of 6-APA with the 8-quinolyl ester of chloroacetic acid led to 6-chloroacetamidopenicillanic acid (**X**) which was oxidized with potassium periodate in aqueous solution (20 °C, 2.5 h) to obtain the corresponding *S*-sulfoxide (**XI**). Precedential oxidation of the sulfur atom of the thiazolidine ring was necessary to avoid the simultaneous oxidation of the sulfur atom of the side chain to be coupled in the following step. Nucleophilic substitution of the chlorine atom of **XI** by **IIIe** gave the sulfoxide of 6-[(benzoxazole-2-yl-thio)acetamido]-penicillanic acid (**XIIIe**) in a good yield.

To avoid the non-desired decarboxylation of **XIIe** under the conditions of the ring enlargement reaction, it was esterified with bromomethyl acetate in *N*,*N*-dimethylformamide in the presence of triethylamine, whereupon the sulfoxide-acetoxymethyl ester (**XIIIe**) was obtained. The trichloroethyl ester protecting group has also been successfully applied for this purpose.

Compounds **XIIIp, r** were also synthesized by performing first the esterification with trichloroethanol, followed by the nucleophilic displacement of the resulting ester (**XIV**).

Ring enlargement of compounds **XIIIe, p, r** was effected (Fig. 2, route C) in boiling abs. dioxane using a polyphosphoric acid-pyridine-calcium oxide catalyst [17]. The product, 7-[(benzoxazole-2-yl-thio)acetamido]-3-deacetoxy-3-cephem-4-carboxylic acid acetoxymethyl ester (**XVe**), was isolated after the evaporation of the reaction mixture, followed by purification on a Kieselgel G column using a 7 : 3 benzene-ethyl acetate mixture as the eluant. The structure of the product was confirmed by comparing its physical data with those of compound **XVe** prepared from **IVe** with bromomethyl acetate in *N*,*N*-dimethylformamide (20 °C, 1 h).

The trichloroethyl ester protecting group of **XVp, r** — obtained by analogous ring enlargement reactions — was removed with zinc dust in *N*,*N*-dimethylformamide-acetic acid (0 °C, 1.5 h). The products **IVp, r** were completely identical with those obtained by route A. The total yield of the successive ring expansion and de-esterification reaction was 28—36%.

Biological activities

The *in vitro* antibacterial activities of compounds **IVa-o** were tested by the serial agar dilution technique using Cephalexin and Kanamycin sulfate as reference compounds. The minimal inhibitory concentrations (MIC) against a variety of Gram-positive and Gram-negative bacteria and *Mycobact. tbc.* are shown in Table II. From the data in Table II it is apparent that the compounds are inactive against Gram-negative organisms, but significant activities against Gram-positive bacteria were observed. In particular, 7-[(*m*-methylphenyltetrazole-5-yl-thio)acetamido]-3-deacetoxycephalosporanic acid (**IVn**) was not only as active as Cephalexin, but it was superior to the latter in most cases. Compounds **IVc**, **IVe**, **IVf** and **IVg** were more active against the penicillin-resistant *Staphylococcus aureus* 1100 and *Staphylococcus aureus* 53 than the reference compounds. It is interesting that 7-[(4-chlorobenzthiazole-2-yl-thio)acetamido]-3-deacetoxycephalosporanic acid (**IVd**) possessed a MIC of 3.1 μg/ml against *Mycobact. tbc.* $H_{36}R_V$, but it was less active against other bacteria.

The antibacterial activities of the products were investigated in *in vivo* experiments on mice, as well. The *in vitro* data summarized in Table II are in good agreement with those obtained in the *in vivo* experiments on mice infected *i.p.* by *Staphylococcus aureus SMITH* and *Proteus vulgaris-XL*. At the same time, numerous compounds with a large structural variety, including **IVd** possessing significant *in vitro* activity, were found to be inactive (Table III) in experiments on mice infected by *Mycobact. tuberculosis typ. bovinus* (RAVENEL).

Experimental

M.p.'s were determined by the capillary tube method, and are uncorrected. The IR spectra were obtained in KBr pellets with a UNICAM SP 200 G instrument. Thin-layer chromatographic investigations were made on 0.4 mm thick Kieselgel G layer on glass in benzene-ethyl acetate (7 : 3) (system A), or in benzene-ethyl acetate-acetic acid (7 : 3 : 1) (system B); the spots were visualized by means of iodine vapour.

8-Quinolyl ester of chloroacetic acid (VII)

A solution of 8-hydroxyquinoline (2.17 g; 0.015 mole), chloroacetic acid (1.4 g; 0.015 mole) and *N,N'*-dicyclohexylcarbodiimide (3.1 g; 0.015 mole) in dichloromethane (50 ml) was allowed to stand at room temperature for 1 h. The *N,N'*-dicyclohexylurea which precipitated was filtered off and the filtrate evaporated to dryness. The residue was crystallized from isopropyl ether to obtain 1.9 g (58.3%) of **VII**, m.p. 77—78 °C.

$C_{11}H_8O_2NCl$ (221.62). Calcd. Cl 16.02; N 6.32. Found Cl 16.36, 16.37; N 6.29, 6.24%.

Indian authors [18] prepared the hydrochloride of **VII** (m.p. 127 °C) by the reaction of chloroacetyl chloride and 8-hydroxyquinoline in boiling chloroform. However, the structural formula and data of analysis were given for **VII**.

Table II

In vitro antibacterial activities of

Microorganisms	MIC (μg/ml) **IV**							
	a	b	c	d	e	f	g	h
Bordetella bronchiseptica	500	500	500	500	500	500	500	500
E. Coli K_{12}								
E. Coli **6R**								
E. Coli polirez.								
Klebsielle								
Proteus vulgaris XL								
Proteus morgani								
Pseudomonas pyocyanea								
Pseudomonas seruginosa NTCT								
Salmonella tiphimurium								
Shigella sonnai	500	500	500	500	500	500	500	500
Bacillus subtilis ATCC **6633**	0.15	0.15	0.15	1.2	0.6	1.2	2.5	2.5
Staph. aureus **1110** *pen. rez.*	500	250	62.5	250	125	10.0	5.0	500
Staph. aur. **53** *pen. rez.*	5.0	1.2	1.2	250	2.5	10.0	5.0	5.0
Staph. aur. SMITH	0.6	0.15	0.3	1.2	0.3	5.0	1.2	2.5
Staph. epiderm. ATCC **12 228**	0.3	0.3	0.6	0.6	0.6	5.0	1.2	2.5
Streptococcus foecalis	500	500	125	250	125	—	—	500
Strept. haemolyticus A **117**	3.1	0.7	0.7	2.5	1.5	0.6	1.2	1.2
Strept. haemolyticus A_1 **118**	6.2	0.7	0.7	1.2	0.7	0.6	0.6	1.2
Pneumococcus	1.2	0.7	0.3	2.5	0.7	1.2	0.6	1.2
Mycobact. tuberculosis $H_{37}R_V$	50.0	25.0	25.0	3.1	25.0	25.0	25.0	100

7-Chloroacetamido-3-deacetoxy-3-cephem-4-carboxylic acid (II)

A mixture of **VII** (1.1 g; 0.005 mole), 7-amino-3-deacetoxy-3-cephem-4-carboxylic acid (1.07 g; 0.005 mole) and sodium hydrogen carbonate (0.5 g) in tetrahydrofuran (60 ml) and water (15 ml) was stirred at room temperature for 12 h. The solution was then diluted with 50 ml of 2% aqueous sodium hydrogen carbonate and extracted with ethyl acetate (2× 20 ml). The pH of the aqueous layer was adjusted to 2 with dilute hydrochloric acid and extracted again with ethyl acetate. The resulting organic layer was dried over $MgSO_4$ and evaporated to dryness. The residue was crystallized from acetone-petroleum ether to yield 0.8 g (55.5%) of **II**, m.p. 174 °C (dec.);

R_f(B) = 0.41; $[\alpha]_D^{20}$ + 127° (c = 1, DMFA). *Lit.* [19] $[\alpha]_D^{20}$ + 127° (c = 0.96, DMFA).

semisynthetic deacetoxycephalosporanic acids

MIC (μg/ml) IV								Cephalexin	Kanamycin
i	j	k	l	m	n	o	p		
500	500	500	500	500	500	500	500	500	
								32	
								16	
								500	
								16	
								500	
								500	
								500	
								16	
								16	
500	500	500	500	500	500	500	500	16	
10.0	0.6	0.6	0.6	0.15	0.07	0.6	0.12	0.6	
500	500	500	500	500	50.0	500	500	250.0	
500	500	5	2.5	2.5	5.0	5.0	0.15	12.5	
5.0	2.5	0.3	0.6	0.6	0.6	0.6	0.3	0.6	
5.0	5.0	0.6	0.6	0.3	0.6	1.2	0.12	0.3	
500	—	125	250	50.0	100	100	—	250.0	
2.5	0.3	0.3	0.15	10.0	0.6	2.5	50.0	2.5	
2.5	0.6	0.3	0.15	10.0	0.15	0.07	25.0	5.0	
2.5	0.3	0.6	0.07	10.0	0.15	0.07	25.0	1.2	
100	25.0	25.0	50.0	50.0	50.0	12.5	25.0	12.5	0.5

According to TLC, m.p. and IR investigations, the product was identical with an authentic sample prepared by acylation with the corresponding acyl chloride (64%).

$C_{10}H_{11}N_2O_4SCl$ (291.0). Calcd. S 11.01; N 9.62; Cl 12.19. Found S 11.05, 11.23; N 9.51, 9.40; Cl 12.22, 12.44%.

IR (KBr): νNH(amide) 3301; νC=O (β-lactam) 1765; νC=O (amide I) 1679; νC=O (COOH) 1710 cm^{-1}.

8-Quinolyl esters of (heteroaryl-thio)acetic acids (VIIIc,l,p)

(a) A solution of **VII** (1.1 g; 0.005 mole), the appropriate mercapto compound **III** (0.005 mole) and triethylamine (0.7 ml) in *N*,*N*-dimethylformamide (15 ml) was allowed to stand at room temperature for 3 h. The reaction mixture was diluted to 60 ml with water and

Table III

In vivo antituberculotic activities of semisynthetic deacetoxycephalosporanic acids on mice infected i.v. by Mycobacterium tuberculosis (RAVENEL)

Compound	Dose	Average survival (days)
IVb	12.5	18 (15—22)
	50.0	19.5 (17—22)
	0	22.0 (16.5—30)
IVd	10	23.0 (21—25)
	50	23.0 (21—25)
	200	18.0 (17—19)
	0	20.0 (17—23)
IVh	25	18.5 (17—20.5)
	100	20.5 (18.5—23)
	0	22.0 (16.5—30)
IVi	10	20 (17—23)
	50	23 (21—25)
	200	23 (21—25)
	0	20 (17—23)
IVj	25	19.0 (15—23)
	100	20.5 (17.5—24)
	0	22.0 (16.5—30)
IVk	25	20 (17—23.5)
	100	17 (15—19.5)
	0	22 (16.5—30)
Cefaloridin	50	21.5 (20—24)
	200	19.5 (18—22)
	0	21.0 (19—25)
Kanamycinsulfate	2	27 (22—34)
	10	34 (20—41)
	50	43 (34—52)
	0	22 (20—24)

extracted with ethyl acetate. The organic layer was washed with water, dried over $MgSO_4$ and evaporated to dryness. In the case of **VIIIc** the residue was crystallized from ether-petroleum ether and in the case of **VIIIl,p** from ether.

VIIIc: 1.37 g (78.5%), m.p. 100—102 °C.

$C_{18}H_{12}N_2O_2S_2$ (352.43). Calcd. S 18.21; N 7.96. Found S 18.18, 18.20; N 7.64, 8.13%.

VIIIl: 1.25 g (63.3%), m.p. 130°C.

$C_{19}H_{15}N_5O_2S$ (377.35). Calcd. S 8.49; N 18.57. Found S 8.49, 8.46; N 18.10, 18.06%.

VIIIp: 1.65 g (83.1%), m.p. 133 °C.

$C_{18}H_{12}N_5O_2SCl$ (397.87). Calcd. S 8.05; N 17.61; Cl 8.91. Found S 7.99; 7.83; N 17.23, 16.99; Cl 8.98, 9.01%.

(b) A solution of **VI** (0.005 mole), 8-hydroxyquinoline (0.73 g) and *N,N'*-dicyclohexylcarbodiimide (1.06 g) in dichloromethane (30 ml) was allowed to stand at room temperature for 1 h. After removal of *N,N'*-dicyclohexylurea by filtration, the filtrate was evaporated and the residue recrystallized as described above (method *a*).

VIIIl: 1.65 g (87.7%), m.p. 130 °C, mixed m.p. 130 °C.

7-[(Heteroaryl-thio)acetamido]-3-deacetoxy-3-cephem-carboxylic acids (IVa-t)

Method A

To a solution of **II** (1.45 g; 0.005 mole) and triethylamine (0.7 ml) in *N*,*N*-dimethylformamide (10 ml) a solution of **IIIa—t** (0.005 mole) in *N*,*N*-dimethylformamide (10 ml) and triethylamine (0.7 ml) were added. After standing at room temperature for 12 h, the reaction mixture was diluted with water to 100 ml and acidified with 5% hydrochloric acid to pH 2. The solid product which precipitated was isolated by filtration. In the cases when no precipitate was formed, the mixture was extracted with ethyl acetate.

Method B

To a solution of 7-ADCA (1.07 g; 0.005 mole) and triethylamine (0.7 ml) in *N*,*N*-dimethylformamide (20 ml) 0.005 mole of the 8-quinolyl ester of the heteroaryl-thioacetic acid (**VIIIc,l,p**) was added and the mixture allowed to stand at room temperature for 12 h. Work-up of the resulting mixture was carried out as described above (method A).

In the IR spectra of compounds **IVa—t** the following bands were assigned: νC=O (β-lactam) 1767—1780; νC=O (amide I) 1660—1681; νC=O (COOH) 1712—1730; νNH (amide) 3260—3300 cm^{-1}. The yields and physical data of the products are summarized in Table I.

When both the preparation of esters **VIIIc, l** and the acylation of 7-ADCA with the former compounds was effected as a one-spot process without the isolation of the crystalline esters, the yields of **IVc** and **IVl** were 70 and 45%, respectively.

Potassium salt of 6-chloroacetamidopenicillanic acid (X)

A solution of **VII** (1.1 g; 0.005 mole), 6-APA (1.09 g; 0.005 mole) and triethylamine (0.67 ml) in dichloromethane (20 ml) was stirred at room temperature for 12 h. The reaction mixture was then extracted with water and the aqueous layer acidified with 2*N* HCl to pH 2 at 0— +3 °C. The resulting penicillin derivative was extracted with ether. The combined organic layer was dried over $MgSO_4$ and the potassium salt **X** was isolated after the addition of α-ethylcapronic acid potassium salt. Yield: 0.63 g (39%); m.p. 203 °C (dec.);

R_f(B) = 0.37. According to TLC, m.p. and IR examination, the product was identical with those prepared by acylation with an acyl chloride (62%).

$C_{10}H_{12}N_2O_4SClK$ (330.5). Calcd. S 9.70; N 8.47; Cl 10.73. Found S 9.57, 9.56; N 8.51, 8.27; Cl 10.74, 10.54%.

6-Chloroacetamidopenicillanic acid-S-sulfoxide (XI)

To a solution of **X** (3.7 g; 0.011 mole) in water (50 ml) 3 g of potassium periodate was added (pH 6.5—6.7), and the mixture was stirred at room temperature for 2.5 h. The reaction mixture was acidified to pH 2 and extracted with ether to remove the colouring, and starting materials. The aqueous layer was extracted with ethyl acetate, the organic layer dried over $MgSO_4$ and evaporated to dryness. The residue was crystallized from acetone-petroleum ether to obtain **XI** (1.7 g; 47.2%), m.p. 157 °C (dec.).

$C_{10}H_{13}N_2ClS$ (308.84). Calcd. S 10.37; Cl 11.48. Found S 10.29, 10.22; Cl 11.70, 11.75%.
$[\alpha]_D^{20}$ + 238° (c = 0.5, $CHCl_3$).

IR (KBr): νC=O (β-lactam); 1800 νC=O (amide I) 1693; νC=O (COOH) 1750; νNH(amide) 3360 cm^{-1}, ν(S → O) 1078 cm^{-1}.

Earlier ENEBÄCK and NOPONEN [20] described the preparation of **XI** by the oxidation of **X** with peracetic acid. However, their reported data correspond to those calculated for an incorrect formula which does not contain sulfur, and the m.p. is not given. Nevertheless, the reported value of optical rotation $[\alpha]_D^{20}$ + 244° (c = 0.5, $CHCl_3$) is in good agreement with that observed by us for **XI**.

6-[(Benzoxazole-2-yl-thio)acetamido]-penicillanic acid-sulfoxide (XIIe)

XIIe was synthesized from **XI** (3.08 g; 0.01 mole) and 2-mercaptobenzoxazole (1.51 g; 0.01 mole) according to the procedure described above for the preparation of **VIIIc, l, p.**

The crude product was recrystallized from acetone-petroleum ether to give 3.5 g (82.9%) of **XIIe**, m.p. 170 °C (dec.).

$C_{17}H_{16}N_3O_6S_2$ (422.45). Calcd. S 15.14; N 9.91. Found S 15.06, 14.99; N 9.47, 9.42%.

6-[(Benzoxazole-2-yl-thio)acetamido]penicillanic acid-sulfoxide acetoxymethyl ester (XIIIe)

A solution of **XIIe** (1.26 g; 0.003 mole), bromomethyl acetate (0.42 ml) and triethylamine (0.42 ml) in *N*,*N*-dimethylformamide (10 ml) was allowed to stand at room temperature for 2. The reaction mixture was then diluted with water and extracted several times with ethyl acetate. The combined organic layer was dried over $MgSO_4$ and evaporated to dryness. The residue was purified by column chromatography on Kieselgel G using the eluant system A. Yield: 0.75 g (51%). $R_f(A) = 0.2$.

7-[(Benzoxazole-2-yl-thio)acetamido]-3-deacetoxy-3-cephem-4-carboxylic acid acetoxymethyl ester (XVe)

A mixture of **XIIIe** (2.0 g; 0.004 mole), polyphosphoric acid (0.5 g), pyridine (0.5 ml) and calcium oxide (1 g) in abs. dioxane (60 ml) was refluxed for 12 h. The mixture was filtered and the filtrate evaporated to dryness. The residue was chromatographed on a Kieselgel G column using the eluant system A. Fractions containing **XVe** were combined and petroleum ether was added until turbidity appeared. The resulting crystals were filtered off to obtain pure **XVe** (0.3 g; 15.8%), m.p. 170 °C. The physical data (R_f, m.p., and IR spectrum) of the product was completely identical with that of **XVe** synthesized by the direct esterification of **IVe** (29.4%).

$C_{20}H_{19}N_3O_7S_2$ (477.5). Calcd. S 13.43; 8.80. Found S 13.47, 13.55; N 8.45, 8.33%.

IR (KBr): νC=O (β-lactam) 1770; νC=O (amide I) 1675; νC=O (ester) 1730; νNH-(amide) 3260 cm^{-1}.

6-Chloroacetamidopenicillanic acid-sulfoxide trichloroethyl ester (XIV)

A solution of **XI** (3.08; 0.01 mole), trichloroethanol (1.5 g), pyridine (0.9 ml) and *N*,*N*'-dicyclohexylcarbodiimide (2.06 g) in dichloromethane (100 ml) was allowed to stand at room temperature for 12 h. After removal of *N*,*N*'-dicyclohexylurea, the filtrate was washed with 5% aqueous sodium hydrogen carbonate and then with water. After drying over $MgSO_4$, the solution was evaporated to dryness and the residue was crystallized from acetone-water to obtain 3.6 g (81.8%) of **XIV**, m.p. 173—174 °C.

$C_{12}H_{14}O_5N_2SCl$ (440.14). Calcd. S 7.28; N 6.36; Cl 32.22%. Found S 7.39, 7.49; N 6.36, 6.40; Cl 32.23, 32.63%.

IR (KBr): νC=O (β-lactam) 1800; νC=O (amide I) 1685; νC=O (ester) 1770; νNH (amide) 3360; ν(S → O) 1090 cm^{-1}.

6-[(Heteroaryl-thio)acetamido]penicillanic acid-sulfoxide trichloroethyl esters (XIIIp,r)

Preparation of **XIIIp, r** from **XIV** (3.3 g; 0.0075 mole) and the corresponding mercapto compounds (**IIIp, r**) was effected as described above for the synthesis of **VIIIc, l, p**. The reaction mixture was diluted with water to 100 ml, the precipitate was filtered off and washed with water. Crystallization from acetone-ether gave crystalline **XIIIp**, whereas **XIIIr** was isolated as an amorphous powder.

XIIIp: 3.4 g (73.53), m.p. 165 °C.

$C_{19}H_{18}N_6O_5S_2Cl_4$ (616.34). Calcd. S 10.40; N 13.63; Cl 23.01. Found S 10.00, 9.95; N 13.62, 13.72; Cl 23.57, 23.68%.

IR (KBr): νC=O (β-lactam) 1800; νC=O (amide I) 1685; νC=O (ester) 1770; νNH (amide) 3360; ν(S → O) 1015 cm^{-1}.

XIIIr: 4.5 g (97.9%), m.p. 85 °C (melting), 140 °C (dec.).

$C_{20}H_{21}N_6O_6S_2Cl_3$ (611.91). Calcd. S 10.48; N 13.73. Found S 10.57, 10.70; N 13.67, 13.82%.

IR (KBr): νC=O (β-lactam) 1800; νC=O (amide I) 1685; νC=O (ester) 1770; νNH (amide) 3350; ν(S → O) 1060 cm^{-1}.

7-Chloroacetamido-3-deacetoxycephalosporanic acid trichloroethyl ester (XVI)

A solution of 7-ADCA-trichloroethyl ester (3.81 g; 0.01 mole), triethylamine (1.4 ml), chloroacetic acid (0.95 g) and *N,N'*-dicyclohexylcarbodiimide (2.06 g) in dichloroethane (100 ml) was allowed to stand at room temperature for 2 h. The precipitated *N,N'*-dicyclohexylurea was filtered off and the filtrate was washed with water. The organic layer was dried over $MgSO_4$ and evaporated to dryness. The residue was crystallized from ether to give 2.4 g (57.14%) of **XVI**, m.p. 120 °C.

$C_{12}H_{12}N_2O_4SCl_4$ (422.13). Calcd. S 7.59; N 6.63; Cl 33.60%. Found S 7.82, 7.97; N 6.59, 6.70; Cl 33.89, 34.10%.

IR (KBr): νC=O (β-lactam) 1780; νC=O (amide I) 1680; νC=O (ester) 1735; νNH (amide) 3300 cm^{-1}.

7-(1-*p*-Chlorophenyltetrazole-5-yl-thio)acetamido-3-deacetoxycephalosporanic acid trichloroethyl ester (XVp)

Compound **XVp** was prepared from 1.05 g (0.0025 mole) of **XVI** according to the procedure described above for the preparation of **VIIIc, l, p**. After dilution of the reaction mixture with water 1.0 g (67.1%) of amorphous **XVp** was obtained, m.p. non-characteristic, R_f(A) 0.80.

The product was identical (TLC) with the main product of the ring enlargement react on of **XIIp**.

Ring enlargement and de-esterification of XIIIp and XIIIr (Method C)

The ring enlargement reaction of **XIIIp, r** (0.005 mole) was effected by means of the procedure given for the preparation of **XVe**. The residue obtained on evaporation was dissolved in *N,N*-dimethylformamide (45 ml) and treated with zinc dust (3 g) and acetic acid (9 ml), with stirring, for 1.5 h at 0 °C. The reaction mixture was then filtered, the filtrate diluted with water and extracted with ethyl acetate. The combined organic layer was washed with water, dried over $MgSO_4$ and evaporated to dryness. Crystallization of the residue from methanol gave the pure product.

IVp: 0.82 g (35.4%), m.p. 185 °C (dec.), R_f(B) 0.28.

IVr: 0.65 g (28.13%), m.p. 178 °C (dec.) R_f(B) 0.27.

On TLC examination both **IVp** and **IVr** proved to be identical with the compounds prepared from **IIp** and **IIr**, respectively.

In vitro and in vivo antibacterial investigations

The susceptibility (MIC) of the microorganisms to the antibiotic analogues **IVa—p**, shown in Table II, was determined by a 2-fold broth dilution method using PENASSAY BROTH (DIFCO B-243) liquid medium. In the experiments with strains belonging to the *Pneumococcus* and *Streptococcus* groups, the medium was completed with 0.1 ml of defibrinated cow blood per 3 ml of the medium. The inoculed amount of bacteria from a 18 h culture was 10^{-4} ml per 3 ml of medium.

The MIC values are expressed in μg/ml and denote the antibiotic concentration inhibiting the reproduction of the microorganisms after incubation at 37 °C for 72 h. In the experiments with *Mycobact. tuberculosis* strain a DUBOIS liquid medium [21] was used, and the inoculed amount of the bacteria from a 14-day Dubois-culture was 0.01 ml per 5 ml of broth in 15×150 mm test tubes. The MIC of the products was determined after incubation at 37 °C for 14 days.

The *in vivo* antituberculotic activities of the antibiotic analogues were determined in mice. To groups of mice, consisting of 10 animals, there was administered (*i.v.*) a 0.2 ml portion of a ten-fold diluted Dubois-culture of *Mycobact. tuberculosis typ. bovinus* (RAVENEL) incubated for seven days. Comparison of the average survival of mice belonging to the same

group (Table III) was made according to the method of DONOVICK [22]. The freshly prepared aqueous solutions of the antibiotics were administered after a 48-h period as of the infection. The solutions of the antibiotic analogues were administered 10 times, with a break of 2 days after the 5th day. The number of the killed animals was recorded every day.

*

The authors are indebted to Dr. István KOCZKA and Dr. Gábor KULCSÁR for the microbiological investigations, to the Hungarian Academy of Sciences, as well as to the Chinoin Pharmaceutical and Chemical Works (Budapest) and Biogal Pharmaceutical Works (Debrecen) for support of this research.

REFERENCES

[1] VAJDĚLEK, Z. J., NĚMEČEK, O., ŠIMEK, A.: Coll. Czechoslov. Chem. Commun. **28,** 2618 (1963)
[2] RABINOVICH, M. S., LEVITOV, M. M., KULIKOVA, G. N., BUYANOVSKAYA, I. S., SHNEERSON, A. N.: Antibiotiki **9,** 392 (1964)
[3] SJÖBERG, B., EKSTRÖM, B., GRONOWITZ, S., MOSES, B.: Acta Pharm. Suecica **2,** 65 (1965)
[4] NAKANO, H., YANAGISAWA, H., SHIMIZU, B., KANEKO, M., NAGANO, M., SUGAWARA, S.: J. Antib. **29,** 554 (1976)
[5] DEMARINIS, R. M., HOOVER, J. R. E., DUNN, G. L., ACTOR, P., URI, J. V., WEISBACH, J. A.: J. Antib. **28,** 463 (1975)
[6] DEMARINIS, R. M., URI, J. V., WEISBACH, J. A.: J. Antib. **29,** 973 (1976)
[7] NANNINI, G., MOLGORA, G., COZZI, P., CASABUONA, F., GALLI, G., SEVERINO, D., SALA, L., CONFALONIERI, C., GIRALDI, P. N., VITA, G., DECARNERI, I., MEINARDI, G., MONTI, G., BIANOMI, A.: Arzneim. Forsch. **27,** 343 (1977)
[8] CRAST, Jr. L. B., GRAHAM, R. G., CHENEY, L. C.: J. Med. Chem., **16,** 1413 (1973)
[9] DEMARINIS, R. M., HOOVER, J. R. E., LAM, L. L., URI, J. V., GUARINI, J. R., PHILLIPS, L., ACTOR, P., WEISBACH, J. A.: J. Med. Chem. **19,** 754 (1976)
[10] DEMARINIS, R. M., BOEHM, J. C., DUNN, G. L., HOOVER, J. R. E., URI, J. V., GUARINI, J. R., PHILLIPS, L., ACTOR, P., WEISBACH, J. A.: J. Med. Chem. **20,** 30 (1977)
[11] NIGHTINGALE, C. H., GREENE, D. S., QUINTILIANI, R.: J. Pharm. Sci. **64,** 1899 (1975)
[12] MISIEK, M., PURSIANO, T. A., CRAST, L. B., LEITNER, F., PRICE, K. E.: Antimicrob. Agents. Chemoth. **1,** 54 (1972)
[13] MISIEK, M., MOSES, A. J., PURSIANO, T. A., LEITNER, F., PRICE, K. E.: J. Antib. **26,** 737 (1973)
[14] SZTARICSKAI, F., MISKOLCZI, I., R. FARKAS, E., BOGNÁR, R.: Acta Chim. Acad. Sci. Hung. **94,** 169 (1977)
SZTARICSKAI, F., MISKOLCZI, I., BOGNÁR, R., R. FARKAS, E.: Hung. Pat. Appl. (June 25, 1976)
[15] HO, T-L.: Synth. Commun. **7,** 393 (1977)
[16] MORIN, R. B., JACKSON, B. G., MUELLER, R. A., LAVAGNINO, E. R., SCANLON, W. B., ANDREWS, S. L.: J. Am. Chem. Soc. **85,** 1896 (1963)
[17] JÁSZBERÉNYI, J. Cs., FARKAS, R. E., GUNDA, E. T., BOGNÁR, R., SZTARICSKAI, F., PERIKOVICS, I.: Hung. Pat. Appl. (June 25, 1976)
[18] BEHERA, B., RATH, P. C., ROUTH, M. K.: J. Ind. Chem. Soc. **44,** 119 (1967)
[19] German Pat. 24.42661 (C. A. **83,** 43355a); 24.42663 (C. A. **83,** 43356a); 24.42687 (C. A. **83,** 43312j)
[20] ENEBÄCK, C., NOPONEN, A.: Finn. Chem. Lett. **1976,** 146
[21] DUBOS, R. J., MIDDLEBROOK, G.: Am. Rev. Tuberc. **56,** 334 (1947)
[22] DONOVICK, R., MCKEE, C. M., JAMBOR, W. P., RAKE, G.: Am. Rev. Tuberc. **60,** 109 (1949)

Ferenc SZTARICSKAI
Rezső BOGNÁR } H-4010 Debrecen, Pf. 20.

István MISKOLCZI H-4042 Debrecen, Pallagi út 13—15.

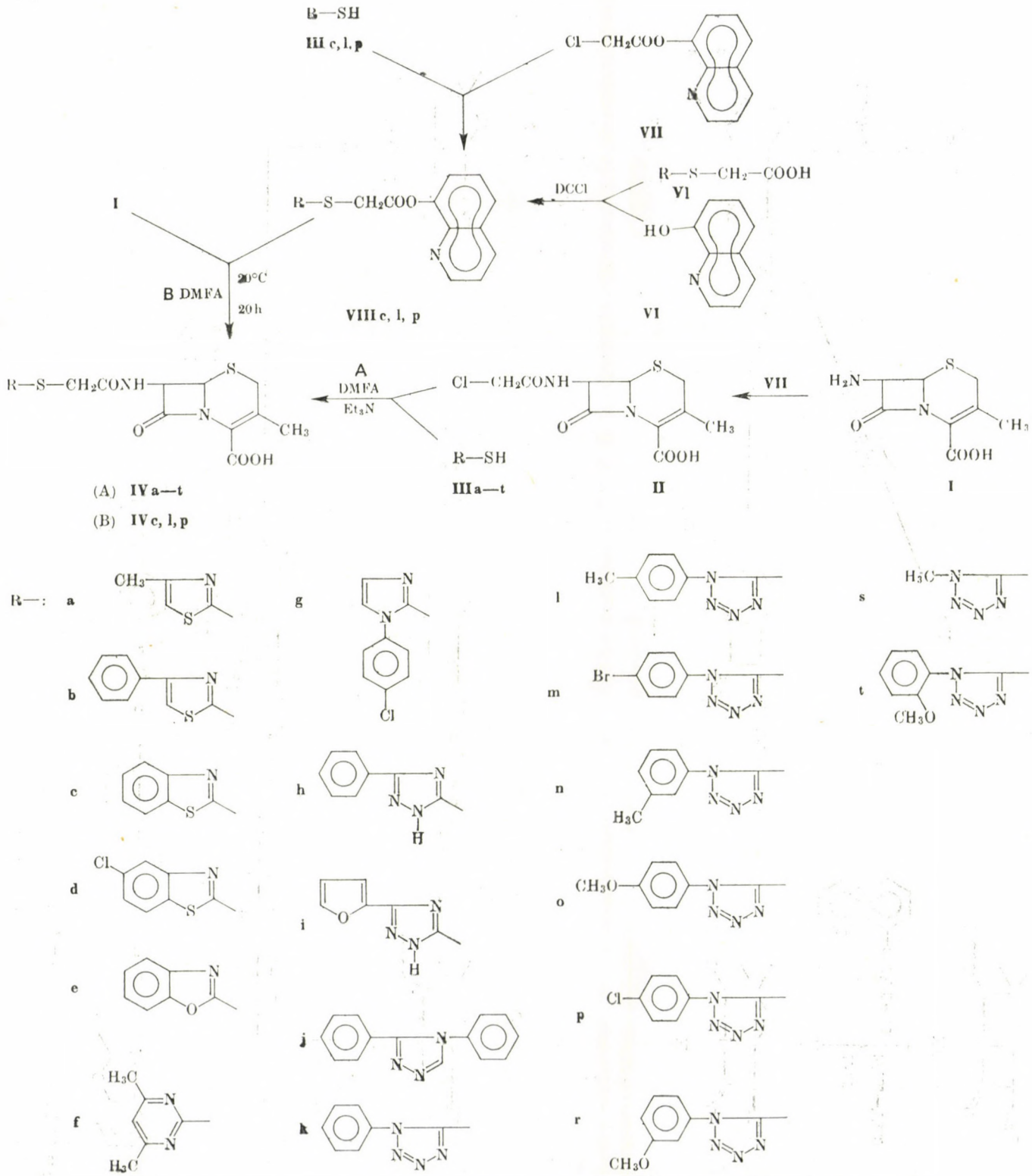

Fig. 1. Synthesis of 7-[(heteroaryl-thio)acetamido]-3-deacetoxycephalosporanic acids

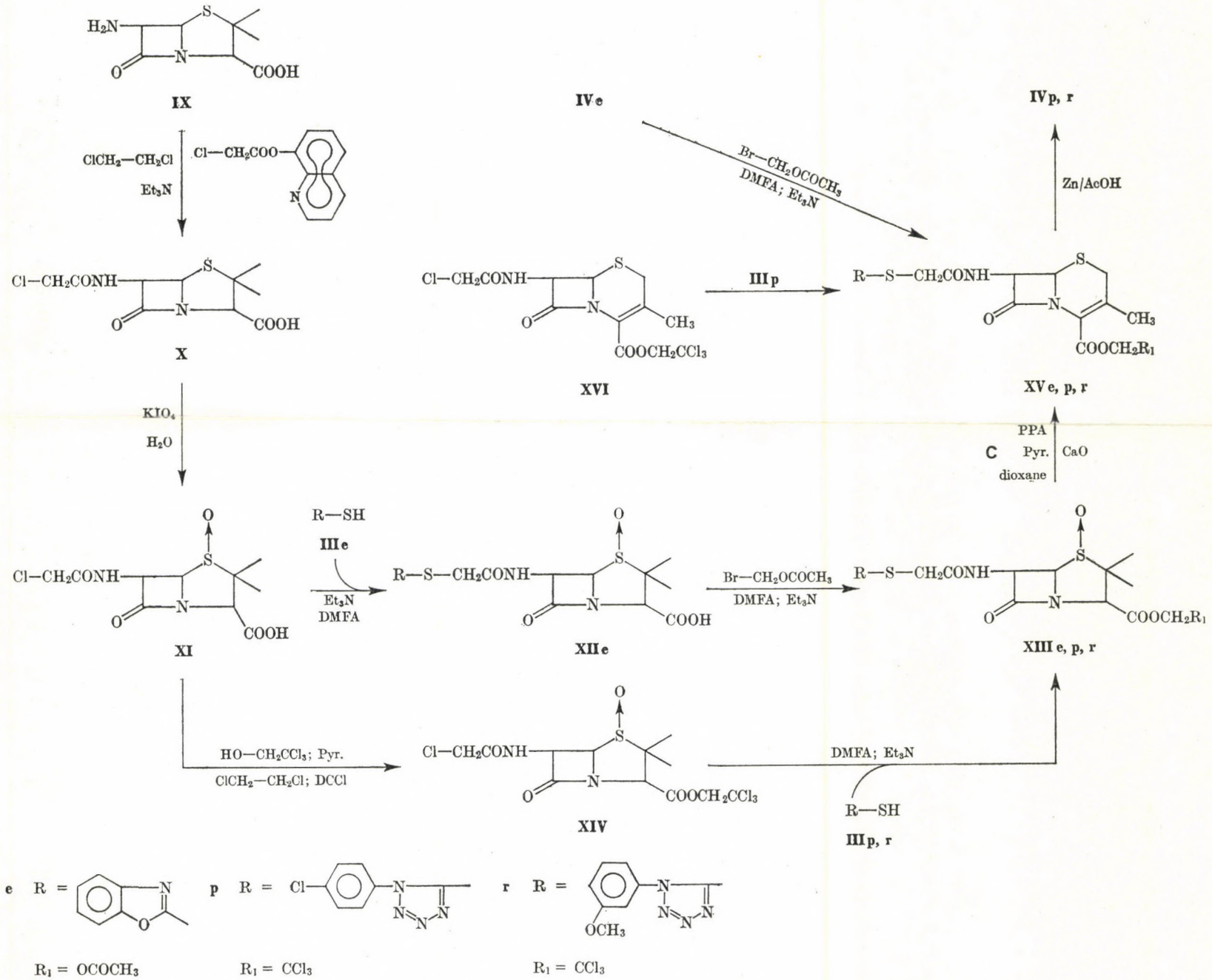

Fig. 2. Synthesis of 7-[(heteroaryl-thio)acetamido]-3-deacetoxycephalosporanic acid derivatives from 6-APA by ring expansion

Acta Chimica Academiae Scientiarum Hungaricae, Tomus 100 (1—4), pp. 377—382 (1979)

ANALYSIS OF STEROIDS, XXXIII*

SIMULTANEOUS DETERMINATION OF THE REDUCTION PRODUCTS OF NORETHISTERONE ACETATE**

S. Görög, A. Laukó, B. Herényi, G. Czira, É. Csizér and Z. Tuba

(Chemical Works of Gedeon Richter Ltd., and Central Research Institute for Chemistry, Hungarian Academy of Sciences, Budapest)

Received July 11, 1978

Accepted for publication September 4, 1978

During the reduction of norethisterone acetate by complex metal hydrides, in addition to the main reduction product (4-ene-3β-hydroxy derivative), two by-products are formed (4-ene-3α-hydroxy and 4,5-dihydro-3β-hydroxy derivatives). The epimers were determined by high performance liquid chromatography, and the determination of the saturated derivative was carried out by gas chromatography after the transformation of the thermally unstable unsaturated derivatives to 3,5-dienes. The use of other analytical techniques (volumetry, thin-layer chromatography and UV spectrophotometry) is also discussed.

Reduction of the 4-ene-3-keto group in steroid hormones and their intermediates with complex metal hydrides is a very important reaction [1]. This is a basic reaction in preparation of the pharmaceutically important 4-ene-3β-hydroxy steroids, and the difference spectrophotometric determination of 4-ene-3-keto steroids [2, 3, 4], as well as the spectrophotometric determination of traces of oestrogens in the latter [5, 6, 7], is also based on this process.

As shown in Scheme 1 the main reduction product is a 4-ene-3β-hydroxy derivative, which is accompanied by its 3α-epimer and the 4,5-dihydro derivative. The yield of the preparation of the main reaction product is determined by the ratio of the main reaction and the side reactions, the latter being a function of the composition of the reducing agent, solvent, additives, temperature, *etc.* Rapid and reliable analytical methods were required for the simultaneous determination of the three products in order to permit optimalization of the reduction.

This paper reports an approach to solving this analytical problem by means of chromatographic techniques. The model compound chosen was norethisterone acetate (17α-ethynyl-17-hydroxy-4-oestrene-3-one acetate — NA); the reduction product was 17α-ethynyl-4-oestrene-3β,17-diol 17-acetate-(β-EODA) accompanied by its 3α-epimer (α-EODA) and 17α-ethynyl-oestran-3β, 17-diol 17-acetate (dihydro-EODA).

* Part XXXII: Analyst *104*, 196 (1979).
** Presented at Euroanalysis III, Dublin, August, 1978.

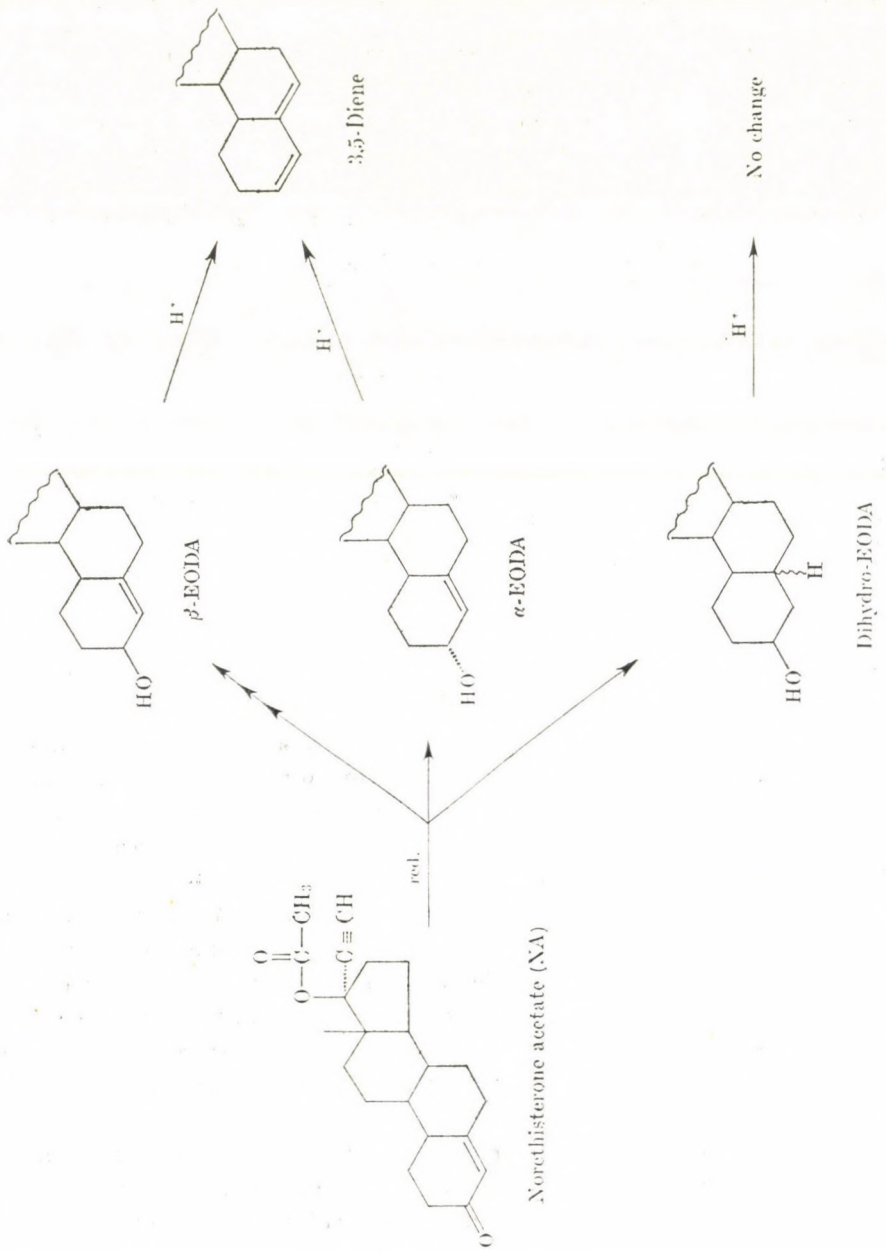
3,5-Diene
H·
H·
No change
H·
β-EODA
α-EODA
Dihydro-EODA
HO
HO
HO
H
red.
O
O—C—CH₃
C ≡ CH
O
Norethisterone acetate (NA)

Scheme 1

Experimental

Crude reduction products of NA were investigated.

High performance liquid chromatography

A Hewlett—Packard 1010B instrument was used, equipped with HP 1030 variable wavelength UV detector set to 210 nm and HP 3380 digital integrator. Column: 30 cm×4 mm μ-Bondapak C_{18} (Waters). Eluent: 7 : 3 mixture of methanol and water at a flow rate of 1.0 ml/min. Temperature: ambient.

25 μl of the methanolic test solution containing about 25 μg of reduced NA was injected into the chromatograph using a Valco loop injector.

The relative quantities of β and α-EODA were calculated from their integrator readings related to the total area, taking into account that the signal of β-EODA at 210 nm is 1.15 times greater than that of the α-epimer. When necessary, the absolute quantity of β-EODA was calculated from its integrator reading using a calibration graph prepared by the external standard technique.

Gas chromatography

A Hewlett—Packard 5750 instrument was used, equipped with FID and HP 3380 digital integrator. Column: a 1.8 m×2 mm glass column packed with 4% UCC-W-982 on Anachrom ABS 90/100 mesh. Temperatures: column 220 °C, injector 240 °C, FID 250 °C. Nitrogen flow rate: 30 ml/min.

Reduced NA (0.02 g) was dissolved in 2 ml of ethanol. A freshly prepared mixture (2 ml) of equal volumes of ethanol and *conc.* hydrochloric acid was added. The mixture was allowed to stand at room temperature for 15 min. Water (15 ml) was added, and the steroids were extracted with two 2-ml portions of chloroform. Two-μl aliquots of the extract were injected into the chromatograph.

Gas chromatography — mass spectrometry

A Micromass 12 FIA mass spectrometer was used coupled with a Pye 104 gas chromatograph. Ionizing voltage: 20 eV; current: 10 μA; accelerating voltage: 3 kV; temperature of EI source: 200 °C; carrier gas: helium.

Results and Discussion

Figure 1 shows the high performance liquid chromatogram of reduced NA. The chromatographic system is a slightly modified version of the system used in this laboratory for the separation of the 3β and 3α epimers of ethynodioldiacetate [8]. The separation of the epimers is excellent, but it is noteworthy that the elution sequence is here β, α whereas in the case of ethynodioldiacetate an α, β sequence was found.

Since dihydro-EODA has no isolated double bond, it could not be detected by the UV detector under the given experimental conditions; only indirect evidence could be found for the presence of the saturated derivative. Namely, the quantity of total steroids as determined by the argento-acidimetric titration of the ethynyl group [9] was always higher than the sum of the quantities of EODA epimers determined either by HPLC as described above, or by spectrophotometry at 236 nm after transformation by hydrochloric acid catalysis to the spectrophotometrically active 3,5-diene derivative [10, 11],

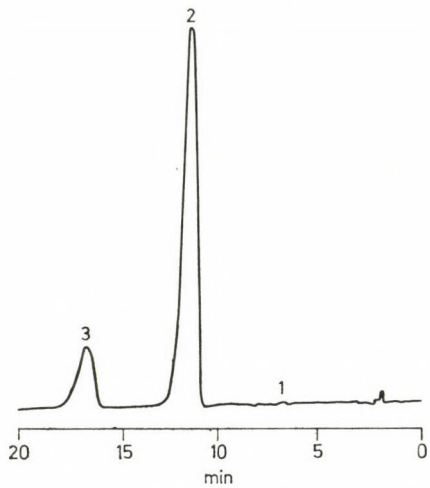

Fig. 1. High performance liquid chromatogram of reduced NA. 1: NA; 2: β-EODA; 3: α-EODA

(see Table I). The difference between these results has been attributed to the presence of dihydro-EODA. Direct evidence for the presence of the saturated derivative was provided by gas chromatography combined with mass spectrometry. Gas chromatography is suitable to furnish quantitative data for the concentration of the saturated by-product.

Direct injection of the solution of reduced NT would lead to chromatograms of poor quality, because 4-ene-3-hydroxy derivatives are thermally unstable [12]. For this reason, the above mentioned hydrochloric acid catalyzed transformation of the EODA epimers to 3,5-diene derivatives (see Scheme 1) was carried out prior to gas chromatography. As shown in Fig. 2, the 3,5-diene derivative gives a sharp peak in the chromatogram. The peak with the longer retention time was presumed to be due to dihydro-EODA, which is not affected by the treatment with hydrochloric acid, as proved by GC-MS. The base peak is that of the molecular ion (*m/e* 344), which is usually the case with 3-OH steroids having saturated skeleton, at low ionization electron voltages. The main fragmentation peaks at *m/e* 329, 270, 268 and 267 can also be derived from the structure of dihydro-EODA by the loss of the angular methyl and acetoxy groups, as well as water.

The GC-MS investigation of the small peak eluted before the main peak showed that it was 17α-ethynyl-3,5-oestradiene-17-ol, an artefact formed by hydrolytic deacetylation during the treatment of the sample with hydrochloric acid. For this reason, the integrator reading of this peak was added to those of the other two peaks when the quantity of dihydro-EODA was calculated by relating its peak area to that of the main reduction product. Although owing to the lack of standard dihydro-EODA the difference between the relative

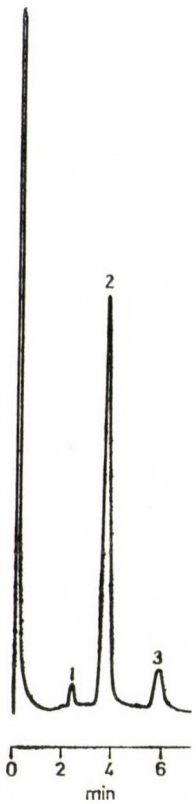

Fig. 2. Gas chromatogram of reduced NA after treatment with hydrochloric acid. 1: 17α-ethynyl-3,5-oestradiene-17-ol; 2: 17α-ethynyl-3,5-oestradiene-17-ol acetate; 3: Dihydro-EODA

detector responses had to be neglected, the results obtained by direct gas chromatography for dihydro-EODA are in good agreement with the indirect results (see Table I).

Table I

Analytical results of some typical reduced NT samples

Sample	$\frac{100 \cdot \alpha\text{-EODA,}}{\alpha + \beta\text{-EODA,}}$ % (HPLC)	$\alpha + \beta$ + Dihydro--EODA, % Titration (T)	$\alpha + \beta$ - EODA, % Spectrophotometry (S)	Dihydro-EODA, %	
				indirect (T—S)	direct (GC)
Std.	0	99.8	100.0	—	0
1	10.4	97.6	67.3	30.3	26.8
2	8.7	98.2	82.6	15.6	14.0
3	11.2	96.5	90.2	6.3	6.5
4	9.6	97.1	96.0	1.1	1.3

The principle described above has also proved useful in the thin-layer chromatographic detection of dihydro-EODA. Using silica gel layer and a 8 : 2 mixture of benzene and acetone, no separation of the epimers of EODA and dihydro-EODA could be achieved. On treatment of the sample with hydrochloric acid the EODA epimers were dehydrated and the resulting 3,5-diene migrated much faster than the parent compounds, while the R_f of the unchanged dihydro-EODA remained unaltered permitting detection.

*

The authors thank Mrs. M. EGERVÁRI and Mrs. M. MELEGH for technical assistance.

REFERENCES

[1] WHEELER, D. M. S., WHEELER, M. M.: in "Organic Reactions in Steroid Chemistry" (Ed. FRIED, J., EDWARDS, J. A.) Vol. **1**, pp. 61—110, Van Nostrand Reinhold Co., New York, 1972
[2] GÖRÖG, S.: Steroids **11**, 93 (1968)
[3] GÖRÖG, S.: J. Pharm. Sci. **57**, 1737 (1968)
[4] CHAFETZ, L., TSILIFONIS, D., RIEDL, J. M.: J. Pharm. Sci. **61**, 148 (1972)
[5] LEGRAND, M., DELAROFF, V., SMOLIK, R.: J. Pharm. Pharmacol. **10**, 683 (1958)
[6] BASTOW, R. A.: J. Pharm. Pharmacol. **19**, 41 (1967)
[7] GÖRÖG, S., CSIZÉR, É.: Acta Chim. Acad. Sci. Hung. **65**, 41 (1970)
[8] GÖRÖG, S., HERÉNYI, B.: J. Chromat. **152**, 240 (1978)
[9] GÖRÖG, S.: Acta Chim. Acad. Sci. Hung. **47**, 7 (1966)
[10] GÖRÖG, S., CSIZÉR, É.: Z. Anal. Chem. **254**, 119 (1971)
[11] CSIZÉR, É., GÖRÖG, S.: Anal. Chim. Acta **86**, 217 (1976)
[12] WOTIZ, H. H., CLARK, S. J.: Gas Chromatography in the Analysis of Steroid Hormones, pp. 84—85, Plenum Press, New York, 1966

Sándor GÖRÖG
Anna LAUKÓ
Bulcsu HERÉNYI
Éva CSIZÉR
Zoltán TUBA
H-1103 Budapest, Gyömrői út 19/21.

Gábor CZIRA
H-1025 Budapest, Pusztaszeri út 59/67.

Acta Chimica Academiae Scientiarum Hungaricae, Tomus 100 (1—4), pp. 383—389 (1979)

MOLAR VOLUME OF PERDEUTEROBENZENE AND -CYCLOHEXANE

I. KISS, Zs. KOVÁCS and Gy. JÁKLI[1]

(National Office of Measures, Budapest,
[1] Central Research Institute for Physics, Budapest)

Received July 12, 1978

Accepted for publication July 24, 1978

The molar volumes of benzene, cyclohexane and of their completely deuterated analogues have been measured between 15 and 70 °C. The isotope effect on the molar volume of benzene may be expressed by the equation

$$(V_H - V_D)/V_H = 2.687 \times 10^{-3} - 3.014 \times 10^{-6}\, t - 6.05 \times 10^{-8}\, t^2$$

and that for cyclohexane by

$$(V_H - V_D)/V_H = 2.954 \times 10^{-3} - 2.408 \times 10^{-5}\, t - 1.62 \times 10^{-7}\, t^2$$

Results are compared with earlier measurements.

Introduction

Condensed phase isotope effects have received considerable attention in the last decade with the most extensive studies being carried out in the field of vapour pressure isotope effects [1—3]. It is well established that properly evaluated potential functions to a good approximation are independent of isotopic substitution, so measured isotope effects can serve as probes in investigation of certain details of the nature of a given potential energy surface. The theoretical interpretation of experimental isotope effects is mainly based on BIGELEISEN's formalism [4] ; this author, by introducing the so-called "reduced partition function ratios", related the condensed phase isotope effects to external and internal molecular vibrational frequencies.

Recently, within the framework of a collaboration project with the Chemistry Department, University of Tenessee, we carried out a comprehensive vapour pressure isotope effect investigation on different deuterobenzenes, deuterocyclohexane and on their mixtures [5]. The measurements on the C_6H_6—C_6D_6 and C_6H_{12}—C_6D_{12} mixtures have proved that even isotopic mixtures show deviations from the ideal behaviour. From the excess vapour pressure isotope effect of the mixtures, both the excess free energy and the excess free enthalpy of mixing could be evaluated and the theoretical analysis showed that the molar volume isotope effect plays an important role in the interpretation of the above properties [6, 7].

Since the few data on the molar volume isotope effect of benzenes and cyclohexanes available in the literature show a large scatter both in their magnitudes and temperature dependences, we decided to carry out new measurements.

Experimental

Materials: Benzene and cyclohexane were analytical reagents. The deuterated compounds were obtained from Merck and Co., Canada.

The supplied mass-spectral analysis gave for the deuterium content of benzene-d_6 99.5% and for cyclohexane-d_{12} 99.0%. All samples were dried over freshly cut sodium, then subjected to purification by preparative scale gas-liquid chromatography. The column was packed with chromosorb-supported didecyl phthalate (30 wt.%).

Apparatus and Procedure: For the density determination an Anton Paar oscillating tube density meter was used with an external measuring cell, type DMA 601. This instrument includes a small (1 cm^3) U-tube oscillator which contains the investigated liquid at atmospheric pressure. Its frequency is measured with a 6-digit frequency meter. The tube is thermostated by the water-circuit of an ultrathermostate, its temperature is measured to ± 0.01 °C with a calibrated 100 ohm Pt resistance thermometer. Such types of density meters are suitable mainly for relative density measurements because the frequency meter has to be calibrated with standard reference materials. In the temperature range 15—40 °C we used distilled water, whereas between 45—70 °C toluene was used, the density of which was determined previously by the pycnometric method [8]. Although this procedure does not give such a high degree of accuracy of the absolute values of density as do some other methods (0.003% at 15—40 °C and 0.01 % at 45—70 °C); we preferred it because on the one hand, it requires but a small amount of material, on the other hand, our main purpose was to determine the isotope effect and not the absolute densities (here most of the systematic errors cancel out).

Results and Discussion

The density and molar volume data are presented in Table I. In the case of C_6D_6 and C_6D_{12} we listed the extrapolated values for 100% deuteration. In the extrapolation process, the molar volumes of the actual samples (with incomplete deuteration) were calculated first and these were then extrapolated linearly. We note this because in some cases in the earlier literature not the molar volumes but the densities were extrapolated linearly, although in an ideal mixture the molar volume is the additive property. The data in Table I were least-squared to a 3-constant equation, which gave the following results:

$$\varrho_{C_6H_6} = 9.00230 \times 10^2 - 1.0564\,t - 2.0939 \times 10^{-4} t^2 \quad (1)$$

$$\varrho_{C_6D_6} = 9.72422 \times 10^2 - 1.1447\,t - 2.7043 \times 10^{-4} t^2 \quad (2)$$

$$\varrho_{C_6H_{12}} = 7.96920 \times 10^2 - 9.0612 \times 10^{-1} t - 5.6105 \times 10^{-4} t^2 \quad (3)$$

$$\varrho_{C_6D_{12}} = 9.13966 \times 10^2 - 1.0627\,t - 7.3746 \times 10^{-4} t^2 \quad (4)$$

$$V_{C_6H_6} = 8.67839 \times 10^1 + 1.0076 \times 10^{-1} t + 1.6663 \times 10^{-4} t^2 \quad (5)$$

$$V_{C_6D_6} = 8.65513 \times 10^1 + 1.0071 \times 10^{-1} t + 1.7281 \times 10^{-4} t^2 \quad (6)$$

Table I

Densities and molar volumes of benzene and cyclohexane and of their deuterated analogues

Temperature (°C)	$\varrho_{C_6H_6}$ (kg/m³)	$\varrho_{C_6D_6}$ (100%) (kg/m³)	$\varrho_{C_6H_{12}}$ (kg/m³)	$\varrho_{C_6D_{12}}$ (100%) (kg/m³)	$V_{C_6H_6}$ (cm³/mol)	$V_{C_6D_6}$ (100%) (cm³/mol)	$V_{C_6H_{12}}$ (cm³/mol)	$V_{C_6H_{12}}$ (100%) (cm³/mol)
15	884.38	955.22	783.29	897.97	88.327	88.096	107.447	107.171
20	879.04	949.45	778.59	892.45	88.864	88.632	108.096	107.834
25	873.67	943.64	773.88	886.90	89.410	89.178	108.754	108.508
30	868.30	937.78	769.16	881.31	89.963	89.735	109.421	109.197
35	862.93	931.96	764.40	875.70	90.523	90.295	110.103	109.896
40	857.62	926.16	759.59	870.04	91.083	90.861	110.800	110.611
45	852.20	920.30	755.23	864.91	91.662	91.439	111.440	111.267
50	847.04	914.67	750.33	859.14	92.221	92.002	112.167	112.014
55	841.56	908.73	745.45	853.40	92.821	92.603	112.902	112.768
60	836.09	902.78	740.55	847.56	93.429	93.214	113.649	113.545
65	830.62	896.82	735.60	841.74	94.044	93.833	114.413	114.330
70	825.24	890.94	730.69	835.86	94.657	94.452	115.182	115.134

Table II

Comparison of benzene and cyclohexane densities with the earlier literature

	$\varrho_{C_6H_6}$ (kg/m³)							$\varrho_{C_6H_{12}}$ (kg/m³)				
Temperature (°C)	This work Eq. (1)	Land.-Borns. Tab. [17] (1971)	HALES [9] (1970)	SHRAIBER *et al.* [10] (1965)	HARRIS *et al.* [11] (1970)	BARTELL *et al.* [12] (1965)	SANNI *et al.* [13] (1971)	This work Eq. (3)	Land.-Borns. Tab. [17] (1971)	IUPAC [8] (1976)	SANNI *et al.* [13] (1971)	BARTELL *et al.* [12] (1965)
15	884.34	883.91						783.20	783.45			
20	879.02	878.54	878.98	878.88		879.01		778.57	778.68	778.58		778.55
25	873.69	873.18	873.63		873.68		873.40	773.92	773.92	773.90	774.30	
30	868.35	867.81	868.20	868.23				769.23	769.16	769.17		
35	863.00	862.45						764.52	764.39	764.41		
40	857.64	857.08	857.47	857.47			857.30	759.78	759.63	759.62	760.10	
45	852.27	851.72						755.01	754.86	754.81		
50	846.89	846.35	846.66	846.67				750.21	750.10	749.96		
55	841.50	840.99						745.39	745.34			
60	836.09	835.62	835.78	835.72			835.60	740.53	740.57		740.60	
65	830.68	830.26						735.65	735.81			
70	825.26	824.89	824.77	824.71				730.74	731.04			

$$V_{C_6H_{12}} = 1.05633 \times 10^2 + 1.1809 \times 10^{-1} t + 2.5976 \times 10^{-4} t^2 \quad (7)$$

$$V_{C_6D_{12}} = 1.05323 \times 10^2 + 1.2006 \times 10^{-1} t + 2.8375 \times 10^{-4} t^2 . \quad (8)$$

In Eqs (1)—(8) the variances of the fits were as follows: 6.30×10^{-3}, 5.72×10^{-3}, 1.52×10^{-2}, 2.52×10^{-2}, 7.11×10^{-5}, 6.92×10^{-5}, 3.71×10^{-4}, and 4.77×10^{-4}, respectively.

In Table II the density data of the normal compounds are compared with some from the latest literature. They are in reasonably good agreement except for the high temperature (45—70 °C) benzene data, which might be 0.04—0.05% high.

Figures 1 and 2 show the isotope effects on the molar volumes of benzene and cyclohexane together with the available earlier data (where necessary, these were recalculated on the ^{12}C atomic weight scale). Unlike the earlier data, the present measurements establish the temperature dependences for both systems satisfactorily. To represent the temperature dependence of the molar volume isotope effect for benzene we obtained

$$(V_H - V_D)/V_H = 2.687 \times 10^{-3} - 3.014 \times 10^{-6} t - 6.05 \times 10^{-8} t^2 \quad (9)$$

and for cyclohexane

$$(V_H - V_D)/V_H = 2.954 \times 10^{-3} - 2.408 \times 10^{-5} t - 1.62 \times 10^{-7} t^2 . \quad (10)$$

The variances of the fits were 2.88×10^{-10} and 1.39×10^{-9}.

We mentioned earlier that the above results were needed for model-calculations on the excess free energy of benzene and cyclohexane isotopic

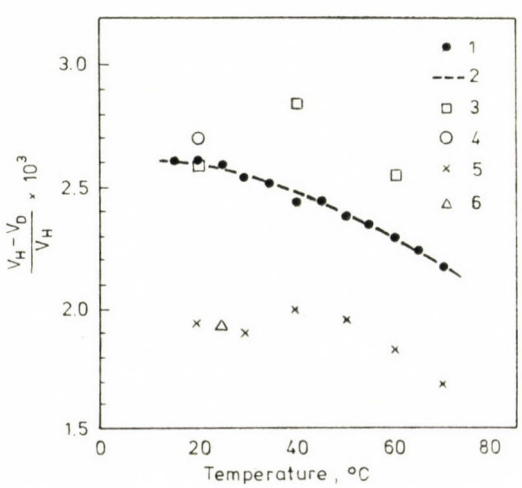

Fig. 1. Isotope effect on the molar volume of benzene. (1) this work; (2) Eq. (9); (3) DIXON—SCHIESSER [14]; (4) BARTELL—ROSKOS [12]; (5) RABINOVICH [16]; (6) INGOLD—RAISIN [15]

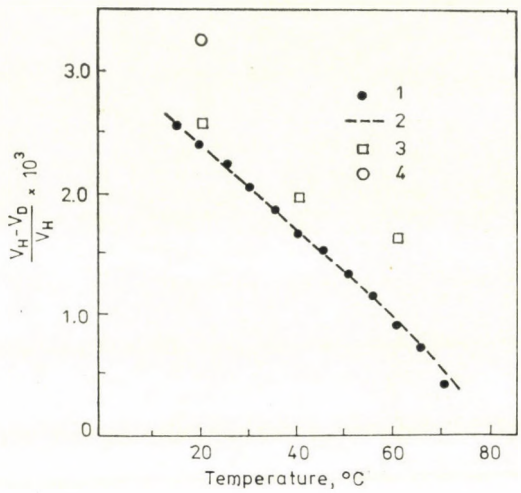

Fig. 2. Isotope effect on the molar volume of cyclohexane. (1) this work; (2) Eq. (10); (3) DIXON—SCHIESSER [14]; (4) BARTELL—ROSKOS [12]

mixtures. This analysis [6] has shown that in the nonideality of the isotopic mixture the internal degrees of freedom play a much more important role than the external translations and rotations.

So far the molar volume has received very little attention in isotopic studies, the theory of its origin is by no means so well developed as, for example, that of the vapour pressure isotope effect. All the available data show that deuterated compounds have molar volumes which are lower than those of the corresponding hydrocarbons. BARTELL and ROSKOS, in connection with their study of the molar volume isotope effect of benzene, cyclohexane and toluene [12], discussed the probable origins of the isotope effects observed. They found that their experimental results, which were restricted only to 20 °C, can be accounted for quantitatively by a simple steric effect having its origin in the anharmonic zero-point motions of the C—H bonds. It is clear from our data that this simple model, which is actually based on the fact that the C—H bonds are longer than the C—D bonds by about 0.005 Å, would not work at higher temperatures. The difference between the molar volumes of isotopic benzenes and cyclohexanes decreases considerably, although the C—D and C—H bond-length vary little with temperature. This also shows that more precise measurements over a wide temperature range are needed to understand the complex nature of the molar volume isotope effect.

REFERENCES

[1] BIGELEISEN, J., LEE, M. W., MANDEL, F.: Ann. Rev. Phys. Chem., **24,** 407 (1973)
[2] JANCSO, G., VAN HOOK, W. A.: Chem. Rev., **74,** 689 (1974)
[3] KISS, I., JANCSO, G., JAKLI, GY.: A kémia újabb eredményei, Vol. **32** (Advances in Chemistry), Akadémiai Kiadó, Budapest, 1976
[4] BIGELEISEN, J.: J. Chem. Phys., **34,** 1485 (1961)
[5] JAKLI, GY., TZIAS, P., VAN HOOK, W. A.: J. Chem. Phys., **68,** 3177 (1978)
[6] JANCSO, G., VAN HOOK, W. A.: J. Chem. Phys., **68,** 3199 (1978)
[7] JANCSO, G., VAN HOOK, W. A.: Physica, **91** A, 619 (1978)
[8] IUPAC Recommended Reference Materials: Pure and Appl. Chem., Vol. **45,** pp. 1—9. Pergamon Press, 1976
[9] HALES, J. L.: Sci. Instr. **3,** 833 (1970)
[10] SCHRAIBER, L. S., PECHENYUK, N. G., KUKOLENKO, O. V.: Russ. J. Phys. Chem., **39,** 219, 281 (1965)
[11] HARRIS, K. R., DUNLOP, P. J.: J. Chem. Thermodyn. **2,** 813 (1970)
[12] BARTELL, L. S., ROSKOS, R. R.: J. Chem. Phys., **44,** 457 (1966)
[13] SANNI, S. A., TELL, C. J., HUTCHISON, H. P.: J. Chem. Eng. Data, **16,** 424 (1971)
[14] DIXON, J. A., SCHIESSLER, R. W.: J. Am. Chem. Soc., **76,** 2197 1(954)
[15] INGOLD, C. K., RAISIN, C. G., WILSON, C. L.: J. Chem. Soc., **1936,** 915
[16] RABINOVICH, I. B.: "Influence of Isotopy on the Physico-chemical Properties of Liquids", Consultants Bureau, New York 1970
[17] Landolt—Bornstein, Tabellen, II/1 (Springer, Berlin—Heidelberg—New York, 1971), p. 639

István KISS, Zsuzsa KOVÁCS } H-1531 Budapest, P.O. Box 19.
György JÁKLI H-1525 Budapest, P.O. Box 49.

Acta Chimica Academiae Scientiarum Hungaricae, Tomus 100 (1—4), pp. 391—408 (1979)

THERMAL DECOMPOSITION OF PROPANE IN A HYDROGEN PLASMA JET

P. STEINGASZNER, L. VAJTA, É. DUDÁS and I. SZEBÉNYI

(Department of Chemical Technology, Technical University of Budapest)

Received July 12, 1978

Accepted for publication August 1, 1978

The authors made an investigation of propane decomposition in an atmospheric pressure hydrogen plasma jet. It has been found that the product composition is a sole function of propane conversion, and that propane conversion in turn depends on the adiabatic mixing temperature of the hot hydrogen plasma with cold propane gas. Substituting pure deuterium for hydrogen, interaction of the plasma gas with the decomposition products was shown to occur. Based on deuterium content and distribution found in the products a dual mechanism for explaining the formation of different products is suggested.

Introduction

Acetylene and ethylene are among the most important starting materials for the petrochemical industry. They are manufactured mainly by the thermal decomposition of hydrocarbons. Hydrocarbon pyrolysis in the temperature range of 1000—1200 K in the presence of steam is a widely used process for the production of ethylene and propylene. Its basic mechanism and kinetics have been studied extensively; individual reactions are generally attributed to radical chain initiation, propagation and termination [1]. Several models have been developed for ethane and propane pyrolysis [2, 3, 4, 5, 6]. Under these conditions acetylene formation is only in the range of a few tenths of a per cent. In order to attain high yields of acetylene temperatures over 1400 K must be used. To reach these high temperatures special techniques have been developed, such as partial oxydation [7], recuperative use of the heat content of alternately heated refractories [8], use of high temperature flue gases obtained by burning hydrocarbons in oxygen [9], electric arc processes [10] and the use of the heat content of electrically heated reactive or non-reactive gases [11, 12].

The present article reports on the pyrolysis of technical propane in a hydrogen plasma jet.

Literature

In spite of the fact that already BERTHELOT [13] produced acetylene in 1866 by passing a stream of hydrogen through an electric arc struck between carbon electrodes, only a surprisingly small amount of papers appeared on reactions of hydrocarbons at temperatures higher than 1400 K.

Studies of different reactions of carbon and hydrogen have been made *e.g.* by SZABÓ [14] at 2300—2700 K, by BADDOUR *et al.* [15, 16] at 3500—4000 K ; the former found methane, ethylene and acetylene to be the main products, while the latter observed the formation of acetylene only, when high-speed cooling was used. For an excellent review on hydrogen — graphite reactions see CLARKE's work [17].

Several articles appeared on the pyrolysis of different hydrocarbons in plasma jets of argon or hydrogen (for a review see VENUGOPALAN [18]), however, the behaviour of propane was studied by only a few. MOGEL and EREMIN [19] investigated the hydrogen plasma induced pyrolysis of propane in an insulated cylindrical reactor made of graphite, which served also as the anode, by introducing propane tangentially into the hydrogen plasma jet. Experimental results were expressed empirically, by plotting electric power consumption *vs.* propane conversion, and yields of products (acetylene, ethylene, methane, propylene) *vs.* specific power input related to propane. At zero conversion all the compounds mentioned appeared simultaneously, while at higher conversion levels all hydrocarbon concentrations — with the exception of acetylene — decreased. No ethane has been detected. Based on observations the following reaction scheme was suggested :

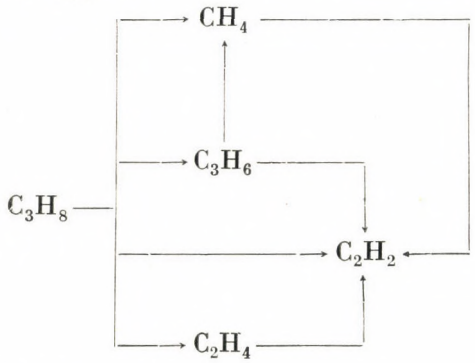

GLADISCH [11] described the hydrogen plasma process developed at the Chemische Werke Hüls : first, a high temperature hydrogen plasma is produced, and mixed with hydrocarbons to attain a temperature of 1400—1700 K, followed by a fast quench to freeze the reactions to obtain as high acetylene concentration, as possible. Using propane as feed, 48 wt% of acetylene and 22 wt% of ethylene was produced ; the gases leaving the reactor contained 13.7 vol% of acetylene and 5.8 vol% of ethylene. Ethylene was thought to be produced mainly during the quenching step. No details with respect to the mechanism of product formation were given.

DE VYNCK [20] studied the conversion of propane in an argon plasma jet. Electric power actually used was calculated by making a heat balance around the reactor. Products found were acetylene, ethylene and methane.

FEDOSEEV and ARTAMANOV [21] made an investigation of propane decomposition kinetics in an argon plasma jet and determined values of the frequency factors and activation energies for propane decomposition and acetylene formation rate equations.

Thermodynamic equilibrium calculations

DUFF and BAUER [22] published a set of constants for the calculation of thermodynamic functions from polynomial equations for temperature ranges of 300—2000 K, and 1500—6000 K for 71 hydrocarbon species. They also presented equilibrium calculations for hydrogen to carbon ratios of 3 to 10, and pressures of 0.1 to 3 atmospheres. Since under our experimental conditions higher hydrogen to carbon ratios were used, equilibrium calculations have been carried out with the data of DUFF and BAUER.

In order to limit the number of compounds of interest, preliminary equilibrium calculations have been made for an H/C ratio of 2 for 1 atm total pressure. The set of equations was solved by linear programing, using the data generating method of BENEDEK and VÁCZI [23]. Results of these calculations are summarized in Table I which show that in the temperature range of 1750 to 2500 K acetylene and hydrogen are the main components, whereas at temperatures above these hydrogen deficient species, such as C_4H, C_3H and C_2H appear in increasing concentrations.

Table I

Moles formed from **1** *atom of carbon and* **2** *atoms of hydrogen at thermodynamic equilibrium;* $P = 1$ *atm, no solid C present*
(Calculated by linear programming)

	Temperature (K)								
	1500	1750	2000	2250	2500	2750	3000	3250	3500
H_2	0.40500	0.46056	0.50000	0.49497	0.49497	0.58589	0.65179	0.62733	0.65335
H				0.01005	0.01005	0.02828	0.10656	0.23322	0.48961
C_2H_2	0.06333	0.48685	0.50000	0.50000	0.50000	0.36662	0.22657	0.11909	0.03777
CH_4	0.06333	0.02629							
C_6H_6	0.13500								
C_4H						0.06669	0.13671		
C_3H								0.25394	0.30815

Detailed thermodynamic equilibrium calculations have been carried out with a Wang Type 2200 desktop computer, with a simple program containing all the constants for the equations of free energy of formation, the equations

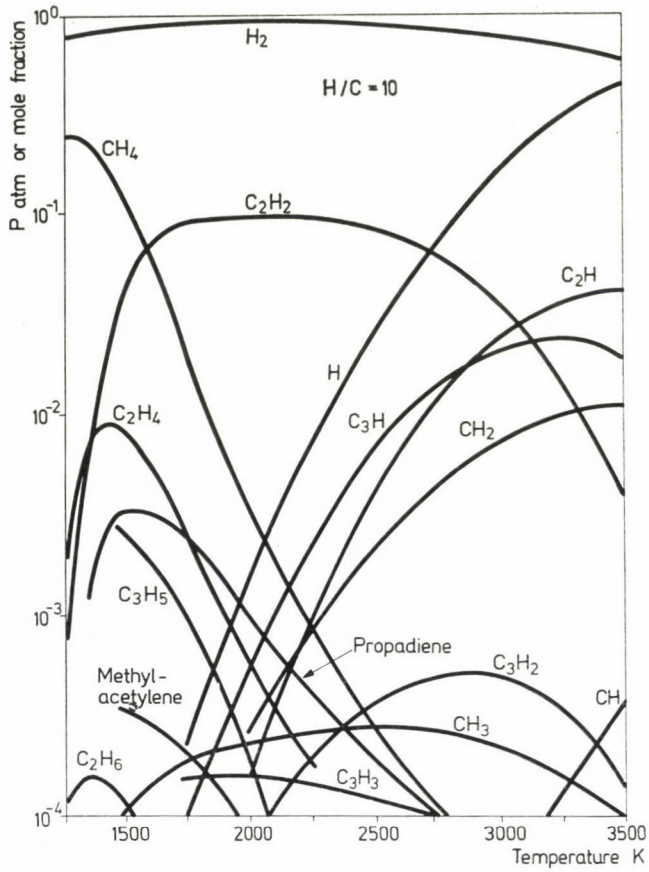

Fig. 1. Thermodynamic equilibrium composition at 1 atm pressure. Hydrogen to carbon ratio = 10

for calculating equilibrium partial pressures at any temperature, hydrogen-to-carbon ratio and total pressure. Results could be printed by a teletype or a Wang line printer.

Calculations have been carried out for the temperature range of 1250 to 3500 K, hydrogen to carbon ratios of 10 and 100 with the following compounds : hydrogen molecule, hydrogen atom, methane, ethane, ethylene, acetylene, propane, propylene, propadiene, methylacetylene, radicals CH_3, CH_2, CH, C_2H_3, C_2H, C_3H_5, C_3H_3, C_3H_2, and C_3H. Results for a hydrogen to carbon ratio of 10 are plotted in function of the temperature in Fig. 1. The effect of the hydrogen to carbon ratio for the temperature range of 1000—2000 K can be seen on Fig. 2.

Calculations show that methane concentration drops to very small values above 2250 K ; acetylene concentration maxima occur between 1750 and 2250

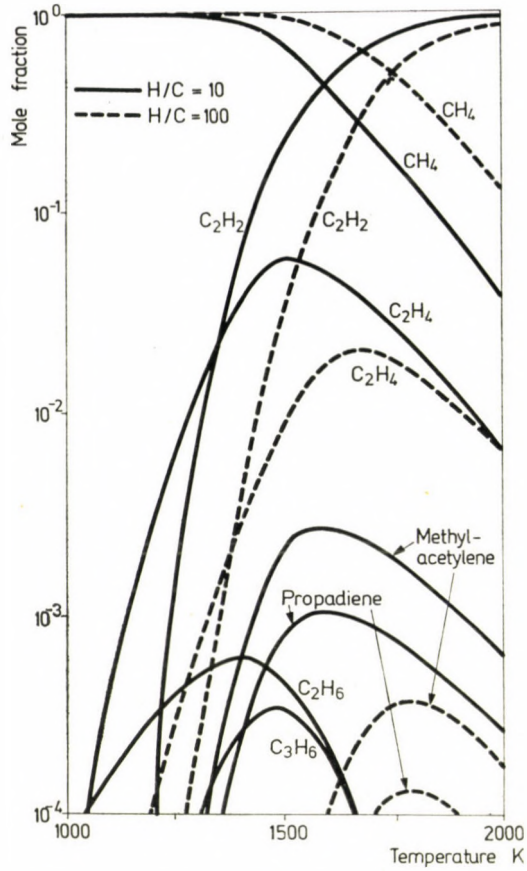

Fig. 2. Thermodynamic equilibrium composition at 1 atm pressure. Effect of hydrogen to carbon ratio. (Composition plotted on a hydrogen-free basis)

K, those of ethylene around 1500 K. Hydrocarbon radical species appear in considerable concentrations only above 2000 K. The concentration of the hydrogen atom reaches 1% at about 2250 K. Ethane and propylene concentrations are negligible in the range studied. Increasing the hydrogen to carbon ratio concentration maxima are shifted to higher temperatures. The only hydrocarbons appearing in higher concentrations above 1500 K are acetylene, ethylene and methane.

Experimental

Apparatus

The plasma jet microreactor previously described [24] was used with slight modifications inasmuch as hydrocarbon feed was not mixed to the hydrogen before the arc, but was introduced into the hot plasma jet leaving the anode bore. A detailed drawing of the plasma jet reactor is seen in Fig. 3.

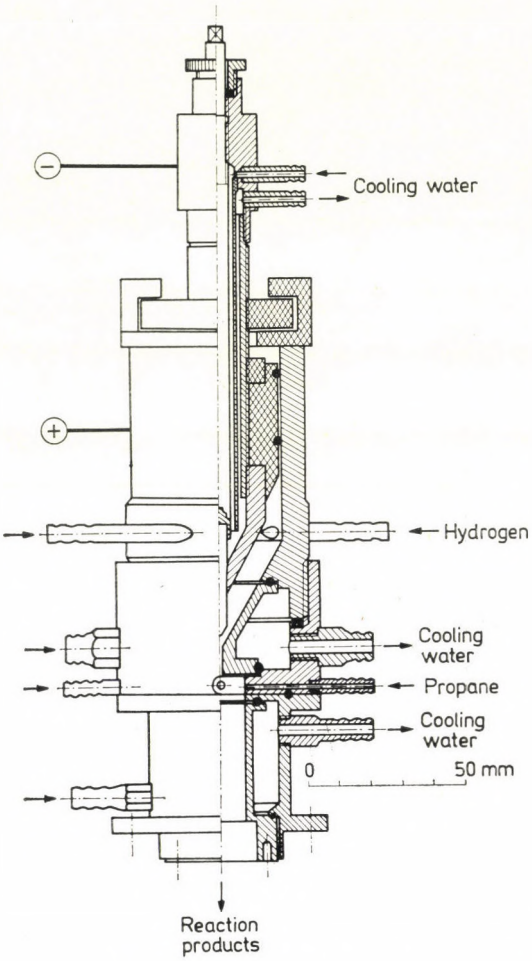

Fig. 3. Plasma jet microreactor

Analytical

Feed and product compositions were analyzed with a Hewlett—Packard Reporting Gas Chromatograph, Type 5830A, with a 2 m long, 1/8″ diameter GSC-120 alumina (Woelm) packing, using argon carrier gas at a rate of 30 ml/min and a flame ionization detector. The initial temperature, temperature programing and a typical chromatogram are shown in Fig. 4. For the determination of deuterium distribution a DuPont 21—490B MS has been used.

TEMP1	50 50
TIME1	1.0
RATE	20.00
TEMP2	180
TIME2	5.0
INJ TEMP	200 200
FID TEMP	200 200
OVEN MAX	200
CHT SPD	0.50

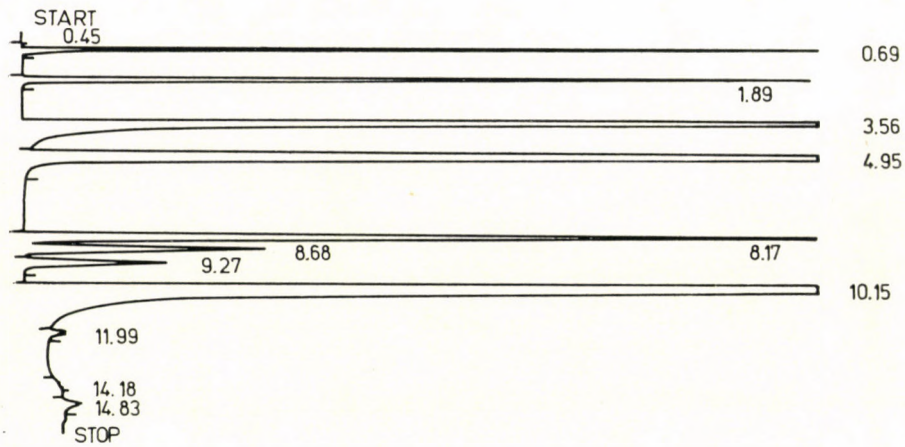

Fig. 4. Gas chromatographic program and a typical chromatogram

ATTN 2 ↑	8
FID SGNL	+B
SLP SENS	0.00
AREA REJ	1
FLOW A	23
FLOW B	29
OPTN	0

RT	AREA	AREA %	
0.45	30	0.000	
0.69	1228000	11.090	methane
1.89	177700	1.605	ethane
3.56	1613000	14.567	ethylene
4.95	3671000	33.152	propane
8.17	389900	3.521	propylene
8.68	131800	1.190	normal butane
9.27	76180	0.688	*iso*-butane
10.15	3761000	33.965	acetylene
11.99	13970	0.126	unknown
14.18	1009	0.009	unknown
14.83	9722	0.088	unknown
	XF: 1.0000 E+ 0		

Reagents

Propane: commercial grade propane (ÁFOR) with the following composition was used:

methane	trace
ethane	2.4 wt%
propane	93.0 ,,
isobutane	2.7 ,,
n-butane	1.9 ,,

Hydrogen: commercial bottled hydrogen was used without purification.

Deuterium: commercial deuterium (D-content over 99.4 atom-%) was used without further purification.

Results

Experiments covered hydrogen to carbon ratios from 10 to 120, net heat input to the reactants (hydrogen plus propane) from 20 to 40 kcal/mole. The feed rate of hydrogen was varied between 760 and 1520 Nl/hr, that of propane between 9 and 70 Nl/hr. In some runs deuterium was used instead of hydrogen.

Experimental results are summarized in Table II. No coke formation has been observed during the runs, only a wax-like deposit was formed on the walls of the product cooler, the amount of which was negligible and therefore does not appear in the material balances. Temperature of the plasma was calculated from heat balance around the plasma generator in the following way: electric power applied minus heat losses in anode and cathode cooling water was divided by number of moles of hydrogen introduced giving average plasma

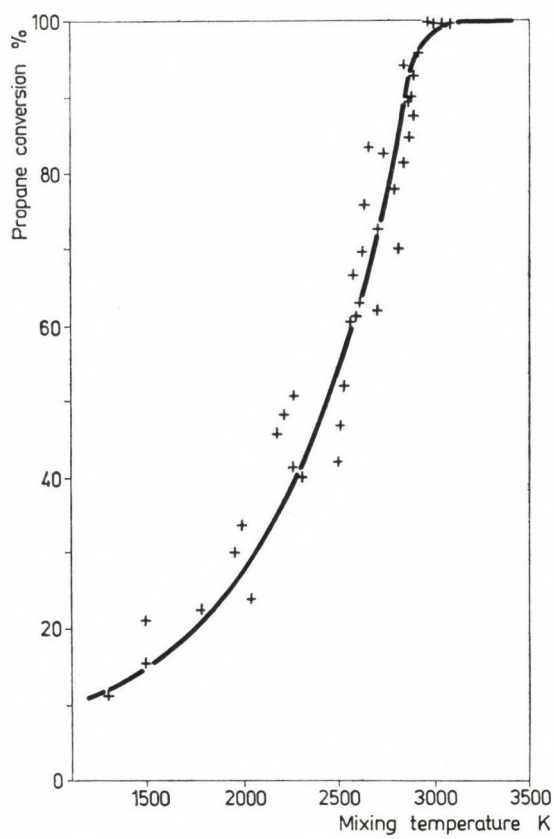

Fig. 5. Propane conversion *vs.* calculated adiabatic mixing temperature

enthalpy. Plasma average enthalpy was converted to plasma temperature by an iterative calculation using free energy of formation equations of DUFF and BAUER for atomic and molecular hydrogen.

Initial reaction temperature was calculated assuming adiabatic mixing and no heat loss during mixing. Both plasma jet temperature and adiabatic mixing temperature was calculated on a Wang 2200 desktop computer with input data for power and current, cooling water flow rates, inlet and outlet temperatures, hydrogen and propane flow rates, with a program containing equations for enthalpies with the appropriate constants of DUFF and BAUER.

On Fig. 5 propane conversion was plotted in function of calculated adiabatic mixing temperatures. Data show, that increasing the adiabatic mixing temperature, the conversion of propane increases, irrespective of other reaction parameters. All points could be joined by a common curve.

Selectivities for methane, ethane, ethylene, propylene and acetylene formation were plotted *vs.* propane conversion in Figures 6 to 10. Selectivity

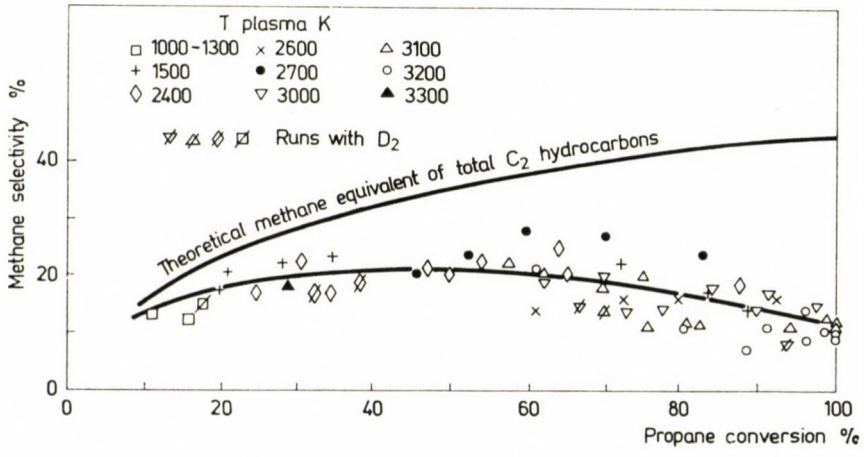

Fig. 6. Methane selectivity

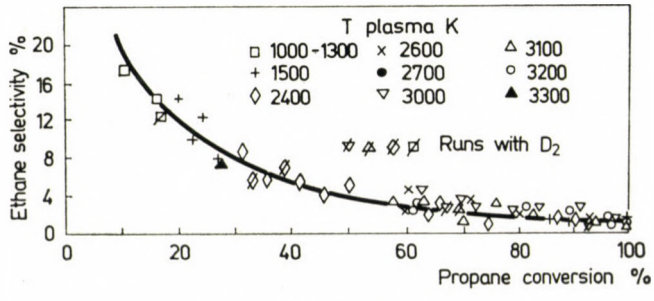

Fig. 7. Ethane selectivity

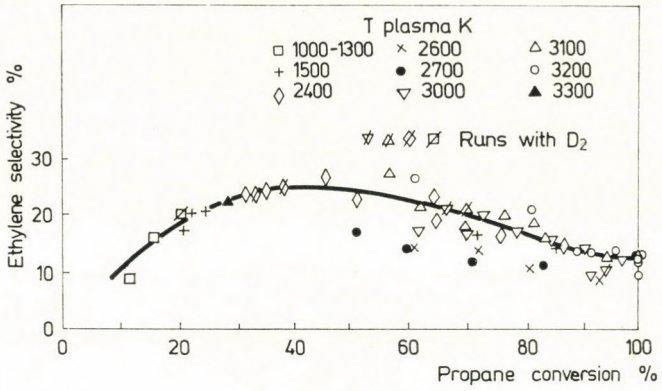

Fig. 8. Ethylene selectivity

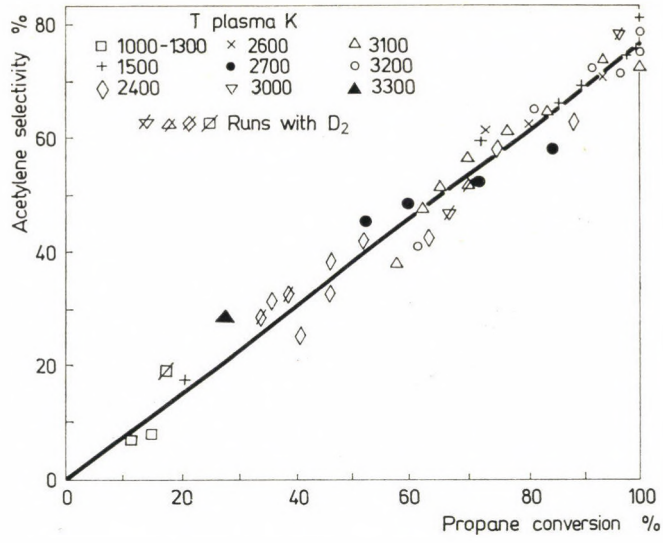

Fig. 9. Acetylene selectivity

for component "i" is defined as follows:

$$\text{Selectivity} = \frac{\text{moles of feed converted to compound "i"}}{\text{total number of moles of propane converted}} \times 100$$

Conversion is defined as follows:

$$\text{Conversion} = 100 - \frac{\text{moles of propane in product}}{\text{moles of propane in feed}} \times 100\,.$$

Methane selectivity (Fig. 6) goes through a slight maximum around 50% propane conversion. The methane equivalent to the C_2 hydrocarbons found in

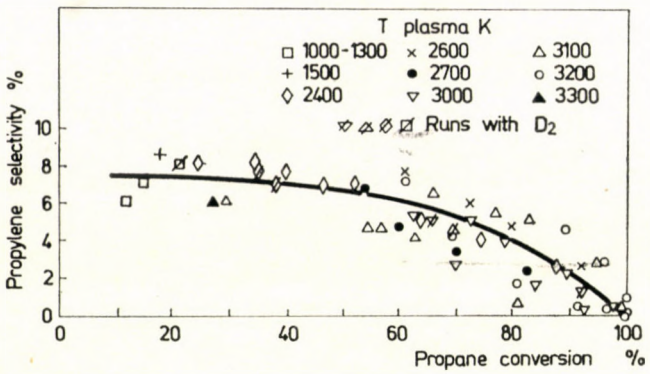

Fig. 10. Propylene selectivity

the products is also shown in the graph : there was far less methane in the products than could be expected on the assumption of splitting one molecule of propane into a C_1 and C_2 fragment, showing that *e.g.* the C_1 fragment so formed must have underwent fast secondary reactions leading to higher molecular weight compounds, such as ethylene and acetylene.

Ethane selectivity (Fig 7) appears to be high at low conversion levels and drops to very small values at conversions approaching 100%.

Ethylene selectivity (Fig. 8) shows a maximum in the function of propane conversion. At low conversion ethylene selectivity tends to very low values, whereas at high conversion around 10% of the propane molecules converted appears as ethylene.

Acetylene formation is a linear function of propane conversion, starting at zero per cent at zero propane conversion and reaching 75—80% at total propane conversion (Fig. 9).

Propylene selectivity (Fig. 10) extrapolated to zero propane conversion is around 8%, while at 100% propane conversion its value drops to practically zero per cent.

In order to gain more insight into the individual reactions in plasma pyrolysis of propane, also a deuterium plasma was produced into which propane was introduced.

As points on Figures 6 to 10 show, product selectivities *vs.* propane conversion fell on the same lines as with hydrogen. Deuterium distribution of some of the runs with deuterium are summarized in Table III.

Methane had a very high deuterium content, showing practically equilibrium distribution among d_0 to d_4 species.

Ethane in the product consisted mainly of the d_0 species, with 10—20% monodeuterated and 5—10% bideuterated ethane. Ethane molecules with deuterium atoms more than two were practically absent.

Table II

Pyrolisis of propane in a hydrogen plasma jet; experimental data. (Run numbers with asterics are deuterium plasma experiments.)

Run No.	Feed, moles/hr		Plasma temperature (K)	Adiabatic mixing temperature (K)	Propane conversion (%)	Selectivity (%) to					
	Hydrogen	Propane				CH_4	C_2H_6	C_2H_4	C_3H_6	C_2H_2	C_4H_{10}
1.	33.84	0.39	2240	2044	21	20.72	12.60	19.40	9.36	17.77	20.15
2.	33.84	0.39	2358	2266	31	22.20	9.80	23.30	7.77	24.19	12.74
3.	33.84	0.39	2696	2634	53	23.70	4.62	21.95	6.76	39.46	3.51
4.	33.84	0.39	2650	2600	93	15.94	1.19	9.39	2.58	70.90	0.00
5.	33.84	0.39	3050	3000	100	14.51	0.45	9.09	0.40	75.55	0.00
6.	33.84	0.39	3200	3050	100	10.14	0.36	9.53	0.00	79.97	0.00
*7.	33.84	1.17	2460	2217	38	19.04	8.13	22.73	6.88	34.61	8.61
8.	33.84	1.17	2650	2500	80	16.40	2.00	16.50	4.75	60.35	0.00
9.	33.84	1.17	3000	2850	93	11.05	0.84	13.77	2.85	71.49	0.00
*10.	33.84	1.17	3326	3240	96	10.85	0.70	9.87	1.40	76.96	0.22
11.	33.84	1.17	3100	3000	100	9.67	0.76	10.65	0.76	78.16	0.00
12.	33.84	1.17	3389	3306	100	8.15	0.53	10.68	0.40	80.24	0.00
*13.	33.84	1.96	2240	1844	33	17.47	5.20	24.17	7.50	30.70	14.96
14.	33.84	1.96	2549	2178	46	20.92	3.92	26.58	6.19	38.86	3.53
*15.	33.84	1.96	2862	2586	67	16.62	2.40	21.86	5.24	51.19	2.69
*16.	33.84	1.96	2908	2648	70	16.71	2.15	21.50	4.86	52.39	2.39
17.	33.84	1.96	2950	2707	78	15.67	1.22	20.97	4.19	56.68	1.27
18.	33.84	2.35	2700	2400	62	15.50	3.29	13.66	6.02	61.53	0.00
19.	33.84	2.35	3000	2750	83	11.80	2.06	16.36	5.10	64.68	0.00
20.	33.84	2.35	3200	2930	96	8.95	1.18	13.83	2.94	73.10	0.00
21.	33.84	3.14	2700	2300	61	13.85	4.52	13.65	7.53	60.45	0.00
22.	33.84	3.14	3000	2650	76	10.38	3.20	19.81	5.66	60.95	0.00
23.	33.84	3.14	3200	2875	89	7.79	2.11	13.63	4.64	71.83	0.00
24.	33.84	3.92	2107	1500	15	11.66	13.88	15.13	7.14	18.14	34.05
*25.	33.84	3.92	2107	1500	16	14.80	12.95	20.38	8.06	20.11	23.70
26.	33.84	3.92	2460	1785	18	15.93	9.73	22.12	9.29	21.25	21.68
27.	33.84	3.92	2549	1967	24	16.60	5.93	23.44	8.61	32.96	12.46
28.	33.84	3.92	3060	2610	61	19.58	3.03	26.26	7.18	40.69	3.26
29.	50.76	0.39	2420	2525	88	19.27	1.26	14.13	2.45	62.89	0.00
30.	50.76	0.39	3000	2925	97	14.50	1.06	13.23	0.37	70.84	0.00
31.	50.76	0.39	3200	3100	100	11.28	0.41	9.46	0.00	78.85	0.00
32.	50.76	1.17	2450	2400	74	20.15	1.72	15.81	4.16	58.16	0.00
33.	50.76	1.17	3000	2875	90	14.04	1.24	14.16	2.30	68.26	0.00
34.	50.76	1.17	3200	3050	100	10.97	0.81	12.46	0.24	75.52	0.00
35.	50.76	2.35	2450	2350	65	20.48	2.69	19.27	6.44	51.12	0.00
36.	50.76	2.35	3000	2800	78	14.21	2.10	17.65	4.05	61.99	0.00
37.	50.76	2.35	3200	3000	92	10.59	1.34	14.22	0.54	73.31	0.00
38.	50.76	3.14	2450	2275	51	20.61	5.14	24.50	8.53	41.22	0.00
39.	50.76	3.14	3000	2725	73	13.71	2.88	20.28	5.19	57.94	0.00
40.	50.76	3.14	3200	2950	81	10.08	2.36	20.39	1.71	65.45	0.00
41.	67.68	0.39	2700	2675	84	24.16	3.94	11.34	2.39	58.17	0.00
42.	67.68	0.39	3000	2900	93	17.86	2.06	9.94	0.33	69.81	0.00
43.	67.68	0.39	3100	3000	100	11.05	0.62	9.67	0.00	78.68	0.00
44.	67.68	1.17	2700	2650	70	26.34	4.84	12.59	3.56	52.67	0.00
45.	67.68	1.17	3000	2875	85	18.76	2.36	15.21	1.79	61.88	0.00
46.	67.68	1.17	3100	2975	100	11.40	0.93	12.12	0.00	75.55	0.00
47.	67.68	2.35	2700	2575	61	27.67	6.13	13.51	4.86	47.83	0.00
48.	67.68	2.35	3000	2825	70	20.29	3.06	16.94	2.65	57.07	0.00
49.	67.68	2.35	3100	2900	88	11.40	2.05	16.07	0.24	70.24	0.00
50.	67.68	3.14	2700	2550	52	23.35	7.99	16.27	6.83	45.56	0.00
51.	67.68	3.14	3000	2750	62	18.05	4.36	17.60	5.43	54.56	0.00
52.	67.68	3.14	3100	2850	82	10.11	2.64	18.33	0.81	68.11	0.00

Ethylene showed a higher deuterium content. The relative amounts of d_0, d_1, d_2, d_3 and d_4 species were 25—35, 25—30, 20—25, 10—15 and *cca.* 5%, respectively.

Acetylene consisted mainly of the d_0 species, with small amounts of d_1. The d_2 content was below the detection limit.

Unconverted propane contained practically no deuterium at all.

Propylene consisted of 10—60% d_0, 25—80% d_1 and less than 10% of d_2 and higher species.

Discussion

The plasma reactor used in our experiments was operated with calculated adiabatic mixing temperatures between 1500 and 3300 K, the residence time in the reactor part being in the order of a few thousandths of a second. Because neither temperature profiles, nor changes in composition along the reactor could be measured, formal kinetic evaluation of the results could not be made, and results were evaluated by comparing them with thermodynamic equilibrium data and possible reaction steps deduced by chemical reasoning.

It was found that propane conversion data could be plotted as a function of calculated adiabatic mixing temperature and all product distributions were solely a function of propane conversion, irrespective of reaction parameters. These observations point to the fact that most, if not all the reactions occuring during the plasma induced pyrolysis are practically unidirectional and their relative rates are independent of temperature. There was a certain scatter of data points inherent to high temperature work in small scale equipment [25], in spite of that however, agreement was good.

The relative selectivities of formation of the C_2-hydrocarbons (ethane, ethylene and acetylene) were plotted on Fig. 11. The lines extrapolated to zero

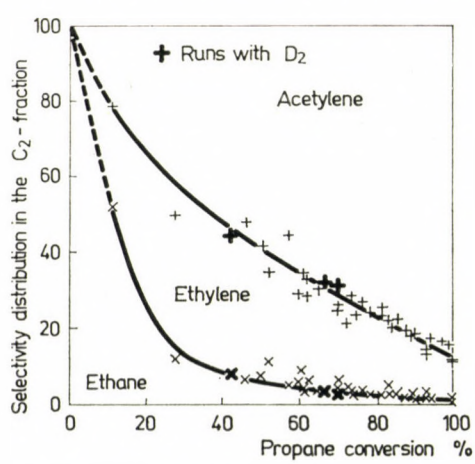

Fig. 11. Composition of the C_2-fraction

Table III

Deuterium distribution data from runs carried out in deuterium plasma jet

Run number	13	15	16
Propane conversion %	33	67	70
Methane			
d_0	4	23	25
d_1	29	35	34
d_2	27	23	21
d_3	24	12	12
d_4	16	7	8
Ethane			
d_0	75	72	70
d_1	10	15	17
d_2	8	7	7
d_3	4	4	4
d_{4+}	3	2	2
Ethylene			
d_0	34	32	24
d_1	26	28	31
d_2	21	24	26
d_3	14	12	15
d_4	5	4	4
Acetylene			
d_0	96	93	90
$d_1 + d_2$	4	7	10
Propane			
d_0	99	100	100
Propylene			
d_0	27	60	87
d_1	60	27	
d_2	8	8	8
d_{3+}	5	5	5

propane conversion clearly show, that ethane might be the primary product. In spite of the fact that the presence of ethane under the conditions of our experiments is not favoured thermodynamically, ethane concentrations several orders of magnitude higher than the equilibrium values have been found. This finding strongly supports that ethane might have been formed as a result of splitting of propane in a primary step.

The acetylene to ethylene ratio depends on propane conversion level.

Thermodynamic equilibrium at the calculated reaction temperatures shows much higher acetylene to ethylene ratios than found in our experiments; these two facts strongly support that ethylene might be the intermediate to acetylene formation, though direct formation of acetylene from propane can not be completely excluded. The picture is obscured by the fact, that methane formed in the primary step is also transformed to ethylene and acetylene [24].

As the conversion level of the propane increases, the percentage of propylene in the C_3 fraction increases to practically 100 per cent. This observation falls in line with observations made by others at lower pyrolysis temperatures and tendencies following from thermodynamic calculations.

Experiments carried out with a deuterium plasma showed that the stable hydrocarbon compounds as well as precursor radicals react with the plasma forming gas, since in most products considerable concentrations of deuterated compounds could be found (see Table III). Moreover, a close analysis of the deuterium content and deuterium distribution of the methane, ethane, ethylene, acetylene, propylene and propane showed, that the generally accepted mechanism of decomposition of hydrocarbons under plasma conditions is incorrect.

The three most striking facts with the experiments with deuterium were the following:

1. the methane consisted of all possible d_0 to d_4 compounds in an equilibrium distribution,
2. there was practically no deuterium in the acetylene formed, and
3. unconverted propane molecules did not contain deuterium at all.

These observations — along with other data from Table III — led to the conclusion that contrary to the generally accepted mechanism of KASSEL [26] acetylene cannot be the final product of the following reaction sequence

$$2\ CH_3^{\cdot} \rightarrow C_2H_6 \rightarrow C_2H_4 \rightarrow C_2H_2$$

since this sequence involves methyl radicals (as well as others) which according to our observation contain deuterium atoms in equilibrium distribution, therefore the acetylene so formed would contain deuterium too.

Since the acetylene formed from propane in a deuterium plasma is practically deuterium-free, only those reaction paths can account for the formation of C_2H_2 that do not involve any exchange of extraneous hydrogen (deuterium)

either from hydrogen (deuterium) atoms or molecules or from hydrocarbon species. In other words, the hydrogen atoms found in the acetylene produced must come from the parent propane molecule. On the other hand the reaction mechanism should be able to explain the other experimental findings too, such as equilibrium deuteration of methane, near-equilibrium deuterium distribution in ethylene and the occurrence of mostly d_1 species in ethane and propylene and the absence of deuterium in the starting propane.

To explain these facts, three parallel initial steps must be assumed. The *first* is the decomposition of propane into CH radicals, which upon recombination yield acetylene in a following step.

The *second* initiating step must be the same as found at low temperature pyrolysis, namely the decomposition of propane into a methyl and and ethyl radical:

$$C_3H_8 \rightarrow CH_3^{\cdot} + C_2H_5^{\cdot}$$

The radicals so formed may undergo reactions with hydrogen (deuterium) to yield deuterated radical species, such as $CH_2D^{\cdot}$, $CHD_2^{\cdot}$, $CD_3^{\cdot}$, $C_2H_4D^{\cdot}$ *etc.*, which on quenching will give in the presence of deuterium the corresponding stable deuterated methanes and ethanes.

Recombination of primary methyl radicals can yield C_2H_6. This, along with the probable smaller rate of deuterium exchange of the ethyl radicals could explain the relatively small deuterium content of the ethane.

Ethylene may be formed by the well-known recombination reaction

$$CH_3^{\cdot} + C_2H_5^{\cdot} \rightarrow CH_4 + C_2H_4$$

or by ethyl radical decomposition

$$C_2H_5^{\cdot} \rightarrow H^{\cdot} + C_2H_4$$

and if this reaction is preceeded by exchange reactions of the ethyl radical with deuterium, the formation of deuterated ethylenes can also be understood.

The *third* initiation step must be the formation of the propyl radical either by direct splitting of propane

$$C_3H_8 \rightarrow H^{\cdot} + C_3H_7^{\cdot}$$

or by hydrogen abstraction from propane by a radical *e.g.*

$$C_3H_8 + C_2H_5^{\cdot} \rightarrow C_3H_7^{\cdot} + C_2H_6$$

and the propyl radical so formed may decompose to propylene and a hydrogen atom. If this reaction proceeds by radical deuterium exchange, deuterated propylenes result.

Summarizing, the decomposition of propane under plasma conditions in the presence of hydrogen (or deuterium) proceeds by two distinct ways: one

is the direct formation of acetylene probably through CH intermediates, the other is a radical decomposition yielding methyl, ethyl and hydrogen radicals, which by different radical chain and termination reactions give ethane, ethylene, propylene and methane.

The rates of these two parallel reactions depend on temperature; at higher temperature the direct formation of acetylene is faster than the radical path, which explains the increase of acetylene to ethylene ratios at high conversion levels, *i.e.* at high temperatures.

The dual mechanism here proposed also explains the deficiency of methane relative to the C_2 hydrocarbons as illustrated *e.g.* on Fig. 6.

It is of course not excluded that acetylene formation may involve hydrogen exchange reactions as well, however, this accounts only for a fraction of the acetylene formed.

*

The authors gratefully thank to Prof. P. BENEDEK[1] for his many useful suggestions, to P. VÁCZI[1] for carrying out the preliminary thermodynamic equilibrium calculations by linear programing, to Mrs A. BÁLINT and J. BÁRKAI for their help in computations. Thanks are extended to Prof. L. GUCZI[2] and K. MATUSEK[2] for the mass spectrometric identification of some product compounds and the determination of isotope distribution of the individual hydrocarbons found in reaction products of experiments carried out in deuterium plasma. The technical assistance of Mr L. LIPOCZKY is kindly acknowledged.

REFERENCES

[1] RICE, F. O., HERZFELD, K. F.: J. Am. Chem. Soc. **54,** 284 (1934)
[2] SNOW, R. H.: J. Phys. Chem. **70,** 2780 (1966)
[3] CRYNES, B. L., ALBRIGHT, L. F.: Ind. Eng. Chem. Proc. Des. Develop. **8,** 25 (1969)
[4] HERRIOTT, G. E., ECKERT, R. E., ALBRIGHT, L. F.: AICHE **18,** 84 (1972)
[5] ZALOTAI, L.: Thesis, József Attila University, Szeged 1974
[6] LIFSHITZ, A., FRENKLACH, M.: J. Phys. Chem. **79,** 686 (1975)
[7] SACHSSE, H.: Chem.-Ing.-Techn. **26,** 245 (1954)
[8] BOGART, M. J. P., LONG, R. H.: Chem. Eng. Progress **58,** 90 (1962)
[9] AKIN, G. A., REID, T. F., SCHRADER, R. J.: Chem. Ing. Progress **54,** 41 (1958)
[10] BRACONIER, F.: Erdöl und Kohle **13,** 248 (1960)
[11] GLADISCH, H.: Chem-Ing.-Tech. **41,** 204 (1969)
[12] SITTIG, M.: Acetylene Processes and Products, p. 37, Noyes Development Corp., Park Ridge N. J. 1968
[13] BERTHELOT, M.: Ann. Chem. IV. **9.,** 445 (1866)
[14] SZABÓ, Z.: J. Am. Chem. Soc. **72,** 3497 (1950)
[15] BADDOUR, R. F., IWASIK, J. M.: Ind. Eng. Chem. Proc. Des. Develop. **1,** 169 (1962)
[16] BADDOUR, R. F., BLANCHET, J. L.: Ind. Eng. Chem. Proc. Des. Develop. **3,** 258 (1964)
[17] CLARKE, J. T.: "Reaction of Graphite and Hydrogen above 2000 K" in BADDOUR, R. F., TIMMINS, R. S.: The Applications of Plasmas to Chemical Processing, Pergamon, New York 1967
[18] VENUGOPALAN, M.: Reactions under Plasma Conditions, John Wiley, New York 1971
[19] MOGEL, G., EREMIN, E. N.: J. Phys. Chem. (in Russian) **44,** 43 (1970)
[20] DEVYNCK, I.: Ind. Chim. Belge, **32,** 861 (1967)
[21] FEDOSEEV, S. D., ARTAMANOV, E. V.: Kinetika i Kataliz (in Russian) XI, 1102 (1970)
[22] DUFF, R. E., BAUER, S. H.: J. Chem. Phys. **36,** 1754 (1962)

[1] Vegyipari Számítástechnikai Fejlesztési Társulás, Budapest
[2] Magyar Tudományos Akadémia Izotóp Intézet, Budapest

[23] BENEDEK, P., VÁCZI, P.: Magyar Kémiai Folyóirat **77,** 383 (1971)
[24] VAJTA, L., STEINGASZNER, P., SZEBÉNYI, I.: Periodica Polytechn. Chem. Eng. **22,** 37 (1978)
[25] HAPPEL, J., KRAMER, L.: "Acetylene and Hydrogen from the Pyrolysis of Methane" in Applied Kinetics and Chemical Reaction Engineering, Am. Chem. Soc., Washington, D. C., 1967
[26] KASSEL, J.: J. Am. Chem. Soc. **54,** 3949 (1932)

Pál STEINGASZNER
László VAJTA
Éva DUDÁS
Imre SZEBÉNYI

H-1521 Budapest, Budafoki út 8.

Acta Chimica Academiae Scientiarum Hungaricae, Tomus 100 (1—4), pp. 409—420 (1979)

IR INVESTIGATION OF CO CHEMISORPTION ON Pd/SiO_2

T. SZILÁGYI, A. SÁRKÁNY,* J. MINK and P. TÉTÉNYI

(Institute of Isotopes of the Hungarian Academy of Sciences, Budapest)

Received July 13, 1978

Accepted for publication July 24, 1978

IR spectra of CO as a function of the surface coverage have been investigated on a Pd/SiO_2 catalyst covered initially either with hydrogen or with oxygen. At low and medium coverages the CO stretching frequency varies from 1800 to 1850 cm^{-1}. Formation of a compressed, delocalized CO layer is suggested by the appearance of "linear" bands at 2050—2060 cm^{-1} (L_1) and at 2085—2098 cm^{-1} (L_2) and by the simultaneous increase of the B band frequency to 1890—1920 cm^{-1} (B_1) and to 1950—1967 cm^{-1} (B_2). Measurements on an oxidized surface suggest the formation of "compressed islands" of chemisorbed CO. The results can be interpreted on the basis of the slow reaction between chemisorbed oxygen and CO.

Introduction

The adsorption of CO on transition metal surfaces has been extensively investigated by means of IR spectroscopy in the past twenty years. The complexity of the observed spectra resulted in different interpretations. EISCHENS and PLISKIN [1] have suggested the formation of linear and bridged species by analogy to transition metal carbonyls. The multiplet structure of these bands on Pd has been explained [2] by surface heterogeneity. This concept has been generally accepted [5, 9—11, 16—18]. BLYHOLDER [3] has criticized the original assignment of EISCHENS. He expressed the opinion that CO is chemisorbed in a linear form only and the bands of different frequency in the CO stretching region represent different degrees of back-bonding from the metal atoms into the π^* orbital of CO. According to his view, the band above 2000 cm^{-1} can be attributed to CO chemisorbed on regular crystal faces, whereas the bands below 2000 cm^{-1} are due to CO adsorbed on edges, corners, *etc.* In a more recent paper PALAZOV [4] has ascribed the multiplicity of the observed bands on a Pd sample to CO—CO interactions.

The complexity of the observed bands on Pd has been reproduced in several laboratories [2, 4, 5, 16]. However, it is not perfectly clear whether the appearance of new bands or shifts in the CO stretching frequency can be attributed to dipole interactions [1, 4—7] or merely to differences in the surface environment [3,8]. Our recent paper deals with the adsorption of CO on a Pd/SiO_2 sample. Using the computer and the disc memory of the Digilab

FTS 14 spectrometer the small differences between two states of the adsorbed layer can be determined with reasonable accuracy. The measurements provide evidence that the multiplicity of the bands below 2000 cm^{-1} may originate from the variation of CO co-ordination.

Experimental

The Pd/SiO_2 catalyst was prepared by "total wetting" of silica (Cabosil HS5) with solution of $Pd(NH_3)_4Cl_2 \cdot H_2O$. The metal content of the batch was 5 wt.% Pd. The sample was dried to *ca.* 30 wt.% water content and pressed (1—1.5 t/cm^2) into self-supporting wafers, which weighed between 60—100 mg and were *ca.* 25 mm in diameter. One of the discs was placed into the cell described elsewhere [12]. The sample was reduced and oxidized at 150 °C several times; finally it was reduced at 400—450 °C for 4—5 hrs in a stream of hydrogen (1 atm) passed through a deoxo unit. All IR measurements were then performed on this stabilized sample.

Prior to CO adsorption, the sample was pretreated in different ways. The wafer was re-oxidized at 25 °C, reduced at 250 °C for 10 min, cooled to the temperature of the experiment and evacuated to a residual pressure of 10^{-5} Torr. Further on, it will be referred to as an initially hydrogenated Pd surface. The oxygen-pretreated sample was prepared by heating the reduced sample at 100 °C for 2—3 hrs in oxygen then keeping it in O_2 overnight at room temperature. Such a treatment [13] gives $PdO_{(S)}$, while the formation of bulk PdO and PdO_2 or Pd_2O_3 can be neglected. The diffusion of O into the bulk may proceed, however, at this moderate temperature. The sample was then evacuated for 1 hr at a dynamic pressure of 10^{-5} torr. Although we did not use a UHV system, grease- and mercury-free conditions were ensured.

CO was obtained from Fluka (*puriss.* grade). It was passed through a BASF-11 contact prior to use.

The infrared spectra were measured by means of a DIGILAB FTS-14 interferometer equipped with its own NOVA minicomputer. The computer has a 128K disc as mass storage memory for storing recorded spectra. Spectra were measured by collecting and signal averaging 200 scans at an original resolution of 2 cm^{-1} which was decreased by a factor of two in consequence of the subsequent smoothing procedure. This resulted in spectra with a reasonably high signal-to-noise ratio. All runs were made in the single-beam mode and the computed spectra were stored on the disc. The spectrum of the catalyst was taken prior to the admission of CO and used as background later. CO was introduced in small doses into the cell and the spectra were recorded for each step. Spectra were then rationed against the reference spectrum, thus all bands due to the adsorbent were eliminated. In order to monitor the developing of the bands and to be able to follow small changes in the structure of the bands the single-beam spectra were also ratioed against each other resulting in difference spectra.

Results

A) Adsorption of CO on an initially hydrogenated surface

An adsorption sequence of CO chemisorption, measured at room temperature, is depicted in Fig. 1. With increasing surface coverage, the CO stretching frequency apparently shifts continuously to higher frequencies and simultaneously with this the low frequency side decays. (Note that the numbering of the curves reversed at the low-frequency side) Figure 2 shows the difference spectra determined from the spectra of Fig. 1. It can be seen that, instead of a continuous shift of the CO stretching frequency, individual bands are discernible: B_0 at 1800—1850 cm^{-1} appears first after a few doses of CO.

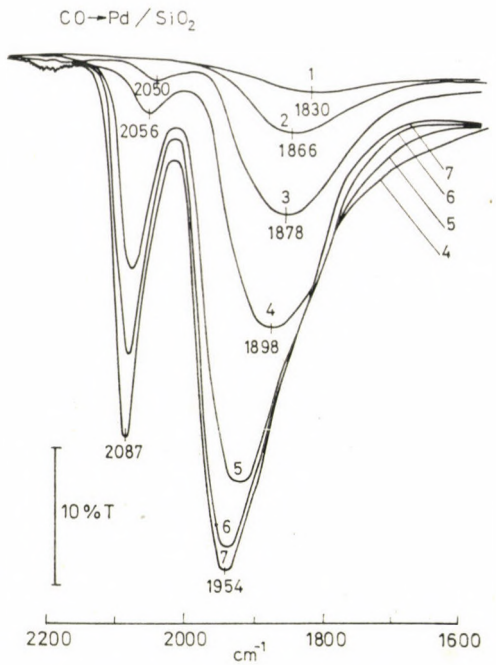

Fig. 1. Adsorption of CO at room temperature on a pre-hydrogenated Pd/SiO_2 sample: *1* — 0.01 Torr CO, *2* — 0.05 Torr CO, *3* — 0.12 Torr CO, *4* — 0.2 Torr CO, *5* — 0.3 Torr CO, *6* — 1.37 Torr CO and *7* — 3.87 Torr CO

This is followed by L_1 at 2050—2060 cm^{-1} and B_1 at 1890—1920 cm^{-1} but B_0 is still increasing (see 4/3 in Fig. 2) and finally bands L_2 and B_2 are formed at 2085—2098 cm^{-1} and 1950—1967 cm^{-1}, respectively (5/4, 8/7 and 9/8 in Fig. 2). According to the difference spectra, the appearance of the L_2 and B_2 bands is accompanied with the diminishing of the low-frequency side of B_0 (note the inverted bands in the difference spectra).

Figures 3 and 5 show spectra of the desorption sequence, while Figs 4 and 6 present the corresponding difference spectra. The desorption of CO can be divided into two main periods at room temperature. Physiosorbed CO can be readily removed by decreasing the pressure of CO from 27 Torr to 10^{-5} Torr. Desorption of physisorbed CO leads to the disappearance of the L_2 and B_2 bands, whereas the intensity on the low-frequency side of the B band is partly restored. These results are shown in Fig. 4. In contrast to EISCHENS's findings [21], the remaining "linear band" L_1, shown in Figs 3 and 5, cannot be removed by evacuation at room temperature. This observation permits to suggest that species L_1 is rather tightly bonded to the surface considering the strength of the CO—Pd interaction. Desorption measurements at 85 °C (Figs 5 and 6) show that the intensity of L_1 and simultaneously that

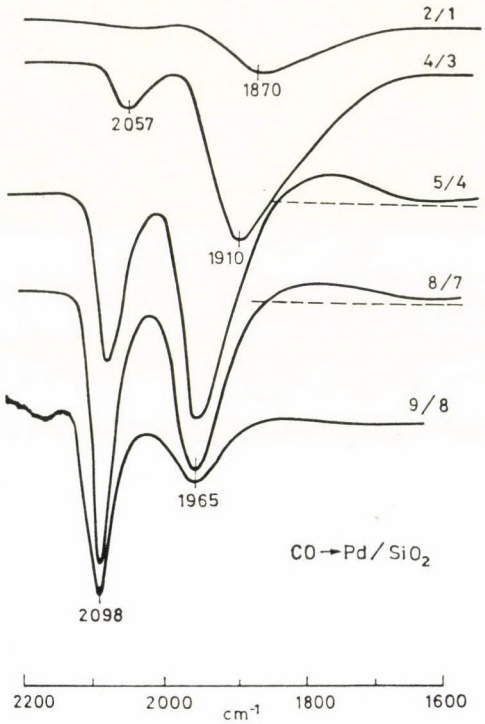

Fig. 2. Ratio-recorded spectra calculated from the spectra in Fig. 1. *8* — 8.00 Torr CO and *9* — 27 Torr CO (not shown in Fig. 1)

of the B_1 band decrease, while the low-frequency side of band B becomes more intense. Inspection of curves 4/10, 6/10 and 8/10 in Fig. 6 proves that while the intensity of the L_1 band decreases, the intensity of the B branch is only slightly influenced since apparently B_1 borrows intensity from the low-frequency side of the B_0 band. At the final stage (not reached at 85 °C), L_1 and B_1 are completely removed and the B band occupies its original position at 1830—1800 cm^{-1} (B_0).

Adsorption and desorption resulted in comparable spectra considering the position of the L_2, B_2, L_1, B_1 and B_0 bands. This observation rules out that the spectral changes are connected with the aging of the Pd/SiO_2 sample. It is noticeable, however, that in the adsorption run B_1 and L_1 appear before B_0 reaches saturation. One of the main reasons could be that the sample is not in equilibrium with the gas phase.

Prior to adsorption measurements at 150 °C, the sample was evacuated for a prolonged time, therefore, it can be assumed that the Pd surface contains but negligible amounts of hydrogen. As shown by Fig. 7, the sequence of events, *i.e.* the appearance of B_0 and then the L_1 and B_1 bands is analogous to that

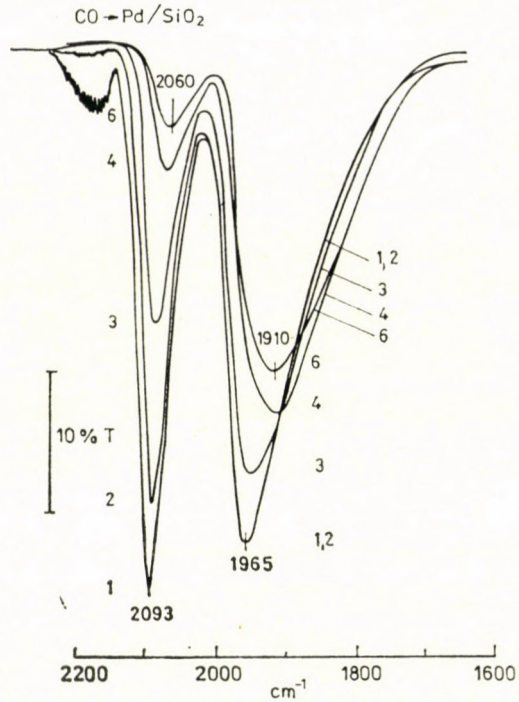

Fig. 3. Desorption of CO at room temperature: *1* — 27 Torr CO, *2* — 2.0 Torr CO, *3* — 0.13 Torr CO, *4* — after 2 min evacuation (10^{-5} Torr dynamic pressure), *5* — and *6* — measured after 20 and 50 min evacuation, respectively

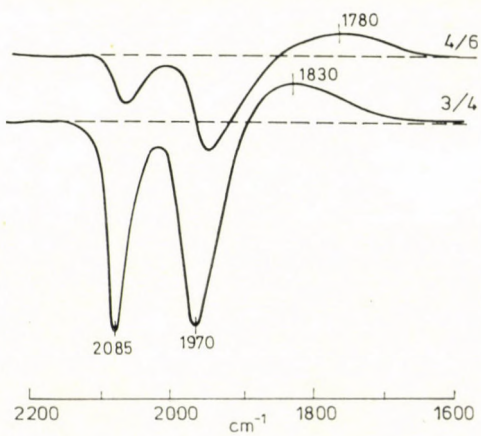

Fig. 4. Ratio-recorded spectra calculated from the spectra of Fig. 3

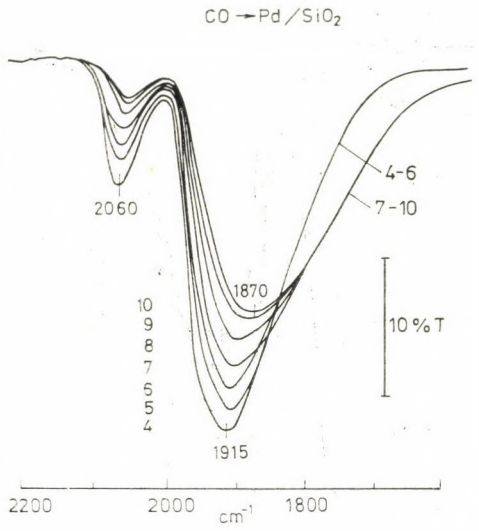

Fig. 5. Desorption of CO at 85 °C: *4*, *5* and *6* — are presented in Fig. 3, too, *7* — 76 min evacuation, *8* — 95 min, *9* — 125 min and *10* — 150 min evacuation (dynamic pressure 10^{-5} Torr)

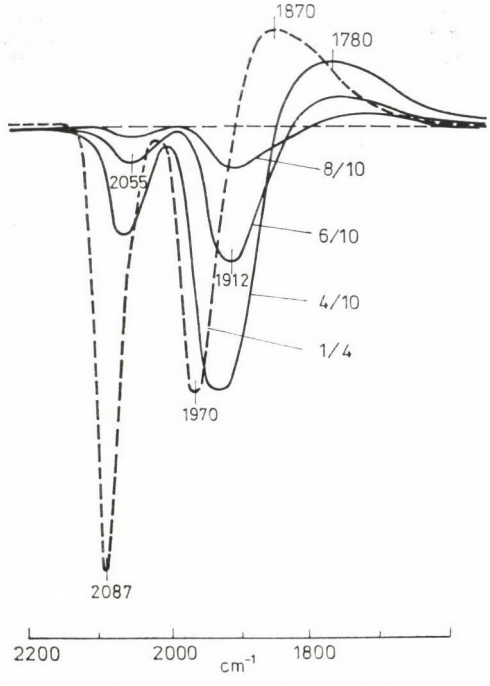

Fig. 6. Ratio-recorded spectra calculated from the spectra of Figs 3 and 5

measured at room temperature. The comparison of spectra in Figs 1 and 7 permits to suggest that chemisorbed or absorbed hydrogen does not influence the observed spectra. This conclusion has been confirmed in separate experiments with hydrogen-CO mixtures, too. At 150 °C the two mobile bands L_2 and B_2 are missing but they are formed after cooling the sample to room temperature. (In these experiments the background spectrum was recorded at room temperature. This explains the sloping baseline of the double-beam spectra recorded at 150 °C.)

Annealing experiments between 25 and 198 °C did not alter the Pd sample, in agreement with the low disproportionation activity of Pd. Upon enclosing 2 Torr of CO into the cell and gradually rising the temperature of the sample, L_2 and B_2 disappeared at 105 °C. At 198 °C the main band is B_0 but a trace of L_1 is still discernible.

B) Adsorption of CO on an initially oxygenated surface

$PdO_{(s)}$ was titrated by admitting successively small doses of CO. The first few doses of CO titrate the surface oxygen and lead to the formation of gaseous CO_2. Spectra from chemisorbed CO_2 cannot be measured because the desorption of CO_2 is rapid from the surface.

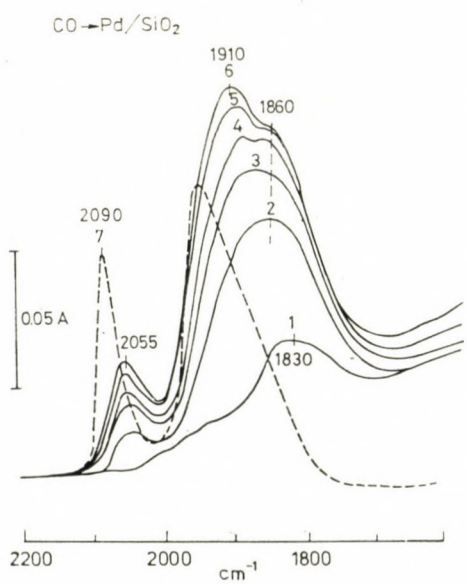

Fig. 7. Adsorption of CO at 150 °C. *1* — 0.01 Torr CO, *2* — 0.06 Torr CO, *3* — 0.26 Torr CO, *4* — 0.65 Torr CO, *5* — 1.55 Torr CO, *7* — sample cooled to 25 °C

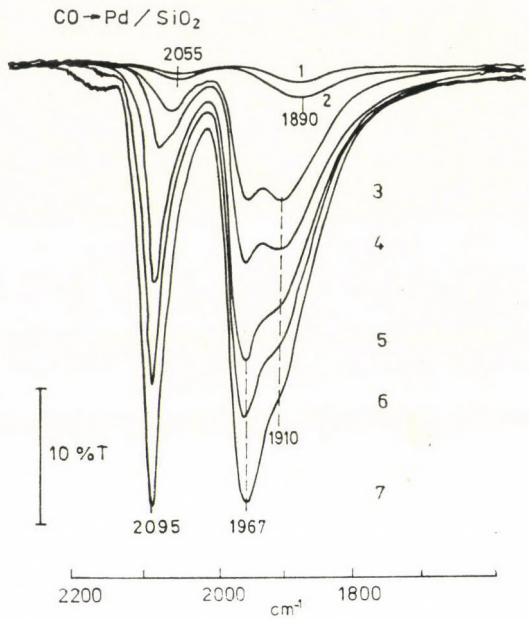

Fig. 8. Adsorption of CO on an oxidized surface at 25 °C: *1* — 0.01 Torr CO, *2* — 0.11 Torr CO, *3* — 0.19 Torr CO, *4* — 0.23 Torr CO, *5* — 0.52 Torr CO, *6* — 1.25 Torr CO and *7* — 4.4 Torr CO

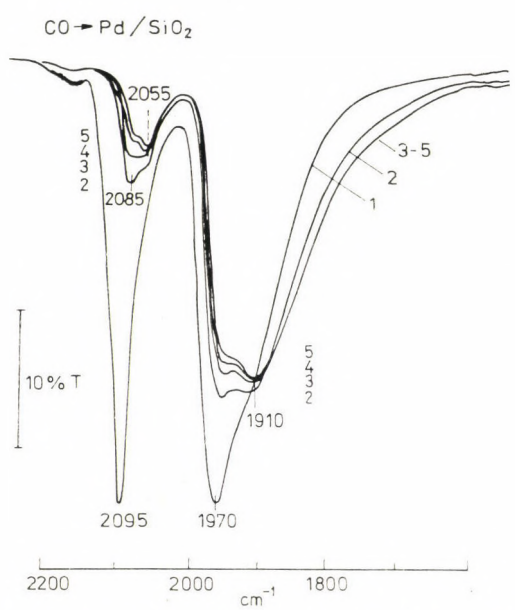

Fig. 9. Desorption of CO at room temperature from pre-oxidized surface: *1* — 4 Torr CO, *2* — after 8 min evacuation (dynamic pressure 10^{-5} Torr), *3* — after 30 min evacuation, *4* — and *5* — after 70 and 100 min evacuation

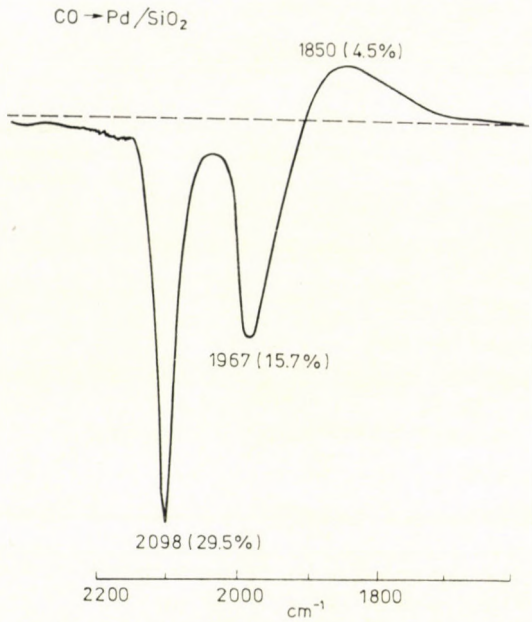

Fig. 10. Ratio-recorded spectrum calculated from spectra *1* and *2* in Fig. 9

An adsorption run at room temperature is presented in Fig. 8. Chemisorbed CO first gives broad bands at 1890 and at 2055 cm^{-1}. Tentatively we assign them as L_1 and B_1. Both B_1 and L_1 appear simultaneously. With increasing coverage (spectra 3—7 in Fig. 8) the band maxima shift to higher frequencies. Bands at 2095 cm^{-1} (L_2), 1967 cm^{-1} (B_2) and at 1915 cm^{-1} (B_1) are observable.

The desorption spectra (measured at room temperature) are shown in Fig. 9. Prior to desorption, 4 Torr of CO was admitted into the cell and the sample was kept in it overnight. Evacuation of the cell to 10^{-4} Torr resulted in the broadening of the low-frequency side of the curves. This observation is also confirmed by the difference spectrum computed from the first and the 5th curves. This spectrum is given in Fig. 10.

As shown by Figs 8 and 9, the adsorption-desorption sequences on a preoxidized surface do not give compatible spectra. The difference could be the result of changes in the chemisorbed layer (*i.e.* oxygen, which is initially present, is removed from the surface) or of the rearrangement (alteration) of the Pd catalyst. Reducing the sample in repeated measurements gave spectra identical to those presented in Fig. 1. On this basis the spectral changes cannot be attributed to the structural rearrangement of the catalyst.

Adsorption sequences at 85 and 150 °C agree with measurements on a reduced surface. It can be noted furthermore that the small shoulders at 2085 cm^{-1} and 1970 cm^{-1} (see curves 2—5 in Fig. 9) are absent at these temperatures.

Discussion

The position of the observed bands is greatly influenced by the surface coverage, as shown by adsorption, desorption and annealing experiments on reduced and oxidized surface. The multiplicity of the bands, *i.e.* the main features of the EISCHENS and PLISKIN spectra [2] are thus reproduced. The experimental results unambiguously prove, however, that the observed bands are "connected" with each other. It has been shown in the experimental section that bands B_1 and B_2 may originate from B_0 and their gradually increasing frequency is the result of gradually decreasing adsorption energy as a consequence of the rearrangement of the CO surface net. We tentatively suggest that band B_0 represents isolated CO in three- or four-fold coordination. With increasing coverage CO moves to sites of two-fold coordination (B_1). The compression permits also formation of linearly bonded CO (L_1) owing to the poor ordering of the domains. The final compression of admolecules results in delocalized CO chemisorption bands B_2 and L_2 are present at this stage. On this basis the complexity of the absorption bands cannot be ascribed to "surface heterogeneity" as was proposed originally by EISCHENS and PLISKIN [2]. On the other hand, the well defined frequencies of the bands rule out that a wide variety of surface sites is present [3], offering varying degrees of π- and σ-bonding.

Considering the strength of Pd—CO interaction as well as the position of the IR bands, three distinct states of CO adsorption are discernible. Band B_0 is observable at low coverages. The corresponding species (absorbing at B_0) is the most tightly bonded to the Pd sites. This band may be attributed to CO bonded in multicentered positions. The position of band B_0 is influenced probably by an a priori heterogeneity of the polycrystalline surface and at higher coverages by long-range [23] mutual interactions. An a priori heterogeneity of the polycrystalline surface can be ascribed to the presence of different oriented faces. As suggested by LEED results [21] on oriented crystals of Pd the arrangement of CO on different planes is not identical. The difference appears also in the initial energy of adsorption [21], which is 40, 36.5, and 34 kcal mol^{-1}, on 110, 100 and 111 planes, respectively. Recent results of BRADSHAW [24] on Pd single crystal surfaces give further evidence for surface specificity. The C—O stretch frequency on the (100) surface is measurable at 1895 cm^{-1} at low coverages, whereas on the (111) surface the initial absorption band appears at 1823 cm^{-1}. Considering the position of band B_0

the experimental results seem to prove that our silica supported palladium sample contains planes of (111) orientation in considerable fraction.

Both the position of the L_1 and L_2 bands and their stability on the surface suggest that L_1 and L_2 represent distinct states of CO. These bands appear during the rearrangement and the compression of the CO surface net. This process may also force CO molecules into sites permitting single co-ordination only.

The L_1 band can be tentatively assigned to linearly bonded CO located on the top (or in the vicinity of the top) of a Pd atom. Energy profile calculations [20] in fact show that the "top" of a Pd atom is energetically less favourable than the holes or the positions between two Pd atoms. Formation of L_2 represents probably the final compression of the surface structure. The flatness of CO adsorption isotherms proves that the intermolecular repulsive forces are significant.

The measurements on oxidized Pd surfaces can be rationalised assuming the simultaneous presence of CO and oxygen on the surface. We assume, that "compressed domains" of chemisorbed CO are formed on the reduced sites (bands L_1 and B_1 appear simultaneously, whereas B_0 band is missing) which is possible if the reaction between chemisorbed CO and oxygen is slow at room temperature. This suggestion is in agreement with the proposed mechanism of catalytic oxidation of CO on Pd since, according to kinetic investigations [22], this reaction proceeds between chemisorbed oxygen and gaseous CO mainly via an Eley—Rideal mechanism at room temperature. One also expects, that the C—O stretching frequency increases for CO molecules chemisorbing in the vicinity of Pd/Pd^{2+} interface owing to the decreased electron density of Pd atoms. (At the Pd/Pd^{2+} interface Pd is expected to donate electrons to Pd^{2+} to equilibrate the Fermi levels.) On this basis, the appearance of small shoulders at 2085 cm^{-1} and 1970 cm^{-1} (curves 2—5 in Fig. 9) can be attributed to the presence of chemisorbed (or dissolved) oxygen not removed in the adsorption sequence.

In summary, the experimental results presented in this paper provide further evidence, on the basis of the compound difference spectra, that the multiplicity of the observed bands in the B branch cannot be explained by heterogeneity of the surface. Apparently, the a priori heterogeneity of the polycrystalline surface influences mainly the broadness of the B_0 band. The multiplicity of the B bands (B_1 and B_2) originates from the variation of the CO co-ordination.

REFERENCES

[1] EISCHENS, R. P., PLISKIN, W. A.: Adv. Catal., **10,** 1 (1958
[2] EISCHENS, R. P., FRANCIS, S. A., PLISKIN, W. A.: J. Phys. Chem., **60,** 194 (1956)
[3] BLYHOLDER, G.: J. Phys. Chem., **68,** 2772 (1964)

[4] PALAZOV, A., CHANG, C. C., KOKES, R. J.: J. Catal., **36,** 338 (1975)
[5] PRIMET, M., MATHIEU, M. V., SACHTLER, W. M. H.: J. Catal., **44,** 324 (1976)
[6] HEYNE, H., TOMPKINS, F. C.: Trans. Faraday Soc., **63,** 1274 (1967)
[7] HOFFMANN, F. M., BRADSHAW, A. M.: J. Catal., **44,** 328 (1976)
[8] VANHARDEVELD, R., HARTOG, F.: Adv. Catal., **22,** 75 (1972)
[9] KAVTARADZE, N. N., BORESKOVA, E. G., LYGIN, V. I.: Kinet. Katal., **2,** 349 (1961)
[10] BADDOUR, R. F., MODELL, M., HEUSSER, V. K.: J. Phys. Chem., **72,** 3621 (1968)
[11] WENTRCEK, P., KIMOTO, K., WISE, H.: J. Catal., **33,** 279 (1974)
[12] SZILÁGYI, T., SÁRKÁNY, A., MINK, J., TÉTÉNYI, P.: Acta Chim. Acad. Sci. Hung., (In press)
[13] LAM, Y. L., BOUDART, M.: J. Catal., **47,** 393 (1977)
[14] ERTL, G., KOCH, J.: Proc 5th Int. Congr. Catal., Vol **2,** p. 969. North Holland, Amsterdam 1973
[15] BADDOUR, R. F., MODELL, M., GOLDSMITH, R. L.: J. Phys. Chem., **74,** 1787 (1970)
[16] SOMA-NOTO, Y., SACHTLER, W. M. H.: J. Catal., **32,** 315 (1974)
[17] RICE, R. W., HALLER, G. L.: J. Catal., **40,** 249 (1975)
[18] GARLAND, C. W., LORD, R. C., TROIANO, P. F.: J. Phys. Chem., **69,** 1195 (1965)
[19] NELSON, N. J., KIME, N. E., SHRIVER, D. F.: J. Amer. Chem. Soc., **91,** 5173 (1969)
[20] DOYEN, G., ERTL, G.: Surf. Sci., **43,** 197 (1974)
[21] CONRAD, H., ERTL, G., KOCH, J., LATTA, E. E.: Surf. Sci., **43,** 462 (1974)
[22] ERTL, G., KOCH, J.: Proc. 5th Int. Congr. Catal., Vol. **2,** p. 969. North Holland, Amsterdam 1973
[23] BLYHOLDER, G., ALLEN, M.: J. Am. Chem. Soc., **91,** 3158 (1969)
[24] BRADSHAW, A. M., HOFFMANN, F. M.: Surf. Sci., **72,** 513 (1978)

Tibor SZILÁGYI
Antal SÁRKÁNY
János MINK
Pál TÉTÉNYI

H-1525 Budapest, P.O. Box 77

Acta Chimica Academiae Scientiarum Hungaricae, Tomus 100 (1—4), pp. 421—432 (1979)

PROTONATION OF OXYGEN-CONTAINING ORGANIC COMPOUNDS

F. Joó and M. T. Beck

(Institute of Physical Chemistry, L. Kossuth University, Debrecen)

Received July 13, 1978

Accepted for publication July 28, 1978

The solubility of benzoic acid, benzyl alcohol and naphthalene was investigated in aqueous solutions of mineral acids of different acidities. Using these data, the protonation of benzoic acid in sulfuric acid was characterized by the parameters: $m = 0.87$ and $pK_{BH^+} = -6.23$ (half-protonation in 78.4% H_2SO_4). It is concluded that changes in the solubility of benzoic acid, benzyl alcohol and naphthalene in dilute aqueous solutions of mineral acids are not due to protonation but medium effects only. In the case of benzoic acid dissolved in sulfuric acid solutions, the contribution of protonation to the overall change in the solubility is negligible up to 70% concentration of sulfuric acid.

Introduction

In condensed phases the proton is always attached to some of the components as a consequence of its high polarizing ability. It is the aim of studies on protonation equilibria to determine the distribution of the total amount of protons among the different protonated compounds. Whether or not the protonated molecules can be experimentally detected depends on their stability and the total concentrations.

The response of slightly basic compounds to changing acidity cannot be characterized by only one parameter, pK_{BH^+} the thermodynamic measure of the interaction between a given base, B, and H^+ in a (usually aqueous) acid solution of infinite dilution [1]. Theoretically, the activity coefficient ratio y_B/y_{BH^+} in Eq. (1) defining the acidity function

$$H_0 = -\lg \frac{a_{H^+} y_B}{y_{BH^+}} = -\lg h_0 \tag{1}$$

may behave in a different way from compound to compound with increasing c_{H^+}, so it is not possible to define an H_0 scale applicable to compounds of different structure, using but a single set of indicators. The problem can be practically solved by applying the Bunnett—Olsen equation

$$\lg I + H_0 = \varphi(H_0 + \lg c_{H^+}) + pK_{BH^+} \tag{2}$$

or the relationship suggested by YATES and MCCLELLAND

$$\lg I = -mH_0 + pK_{BH^+}, \qquad (3)$$

where φ or m indicate the different behaviour of the above-mentioned activity coefficient ratios of the base under consideration and that of the indicator base, used to define the H_0 scale [2].

Oxygen-containing organic compounds are protonated only in rather concentrated acid solutions. It is surprising, therefore, that according to some investigations [3—9], carboxylic acids, ketones, alcohols, *etc.*, are protonated to a considerable extent in dilute mineral acid solutions.

We now present the results of investigations on the protonation of benzoic acid and benzyl alcohol, using spectrophotometric, solubility and quantum-chemical methods. Measurements were made both in dilute and concentrated solutions of mineral acids. Based on these results and literature data, suggestions regarding the protonation behaviour of oxygen-containing organic compounds in dilute mineral acids are critically evaluated.

Experimental

Benzoic acid was a Reanal *p.a.*, benzyl alcohol and naphthalene were Reanal *p.* products. Naphthalene was purified by sublimation before use. Solutions of mineral acids were diluted from *p.a.* concentrated solutions and standardized against $KHCO_3$. Spectra were recorded on a Beckman Acta III recording spectrophotometer, measurements at fixed wavelengths were carried out using a Hitachi—Perkin Elmer 139 single-beam spectrophotometer.

For solubility determinations, the mixtures of acid solutions and benzyl alcohol or benzoic acid in sealed ampoules were shaken in a constant temperature bath till reaching equilibrium. After separation of the phases, aliquots were diluted as required, and the concentrations of solutes were determined by measuring the absorbance at fixed wavelengths. For benzyl alcohol $\varepsilon_{257} = 211$, for benzoic acid $\varepsilon_{273} = 1000$ [10] for naphthalene $\varepsilon_{266} = 4660$ were used.

The acidities of the solutions were expressed by H_0 values given by JOHNSON, KATRITZKY and SHAPIRO [11]. Some H_0 values for dilute solutions of constant ionic strength were taken from the paper of PAUL and LONG [12].

Results and Discussion

1. *Properties of benzyl alcohol and benzoic acid in concentrated sulfuric acid solutions*

In *conc.* sulfuric acid, benzyl alcohol gives polybenzyl, which is insoluble in water. No irreversible reaction occurs with benzoic acid. Its solubility, however, is much higher than in water, and a saturated warm solution gives on cooling and adduct of the composition $C_6H_5COOH \cdot H_2SO_4$ in the form of long, white needles.

With increasing sulfuric acid concentration the bands in the UV spectrum of benzoic acid are shifted to higher wavelengths and the intensities increase considerably. HOSOYA and NAGAKURA have shown [10] that it is the carbonyl-

oxygen of the carboxylic group to which the proton is bonded. The Raman frequency of the CO group (1650 cm^{-1}) was found to be very weak in 85% sulfuric acid solution and could not be detected at all at 95%. The spectrum of benzoic acid solutions prepared in 95% H_2SO_4 thus can be assigned to the following structure:

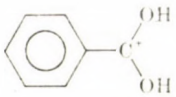

The results of our quantum-chemical studies [13] are also in agreement with this structure, as the energy and intensity values for the transitions of the benzoic acid cation close to those found experimentally (Table I).

Table I

Ultraviolet spectral data of neutral and protonated benzoic acid in H_2SO_4 solutions
(1) *Experimental data,* **(2)** *Calculated values*

Compound	E band		K band		B band	
	λ(nm)	lg ε	λ(nm)	lg ε	λ(nm)	lg ε
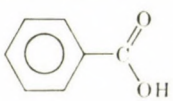	**(1)** 193	4.64	228	4.03	272	2.93
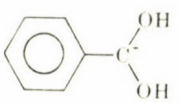	**(1)** 198	4.00	262	4.30	303	3.18
	(2) 205	3.71	261	4.40	303	3.51

On the whole, it can be stated that benzoic acid is protonated in concentrated sulfuric acid solutions on its carbonyl oxygen atom, and its solubility is greatly increased.

Based on the changes in the ultraviolet spectrum of benzoic acid, several authors have determined the protonation constant ($pK^*_{BH^+}$)* and values spanning the range −7.02— (−7.60) were obtained (corresponding sulfuric acid concentrations: 80.5—85.2%) [10, 14—18].

The protonation constant can also be estimated from the solubility of benzoic acid as a function of H_2SO_4 concentration in the range 1—95%. The results of our measurements are presented in Fig. 1.

The solubility of benzoic acid changes only slightly up to $-H_0 = 5.9$, however, in more concentrated acid solutions it increases very steeply. The acidity range up to $-H_0 = 8.4$ was also studied by FLEXSER, HAMMETT and

* $pK^*_{BH^+}$ denotes $-H_0$ corresponding to half protonation.

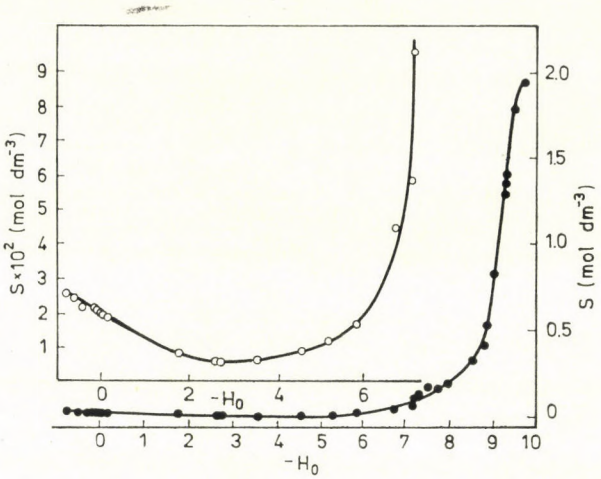

Fig. 1. Solubility of benzoic acid in sulfuric acid as a function of the acidity of the solvent ($T = 298.1$ K)

DINGWALL [14] and the solubilities reported are in good agreement with those determined in this work. At acidities higher than $H_0 = -9.5$, the solid phase transforms to $C_6H_5COOH \cdot H_2SO_4$. The highest solubility is about seventy times larger than that determined in a pure aqueous solution.

The increase of solubility is caused by the following protonation process:

$$Ba + H^+ \rightleftarrows BaH^+, \tag{4}$$

where Ba and BaH^+ denote neutral and protonated benzoic acid, respectively. The equilibrium constant of protonation is given by Eq. (5):

$$K = \frac{a_{BaH^+}}{a_{Ba}\, a_{H^+}}. \tag{5}$$

Considering Eq. (1), Eq. (4) becomes

$$K = \frac{c_{BaH^+}}{c_{Ba}\, h_0} \frac{y_{BaH^+}/y_{Ba}}{y_{BH^+}/y_B} = \frac{S - c_{Ba}}{c_{Ba}\, h_0} Y. \tag{6}$$

The crucial point of all the investigations of such kind is whether or not the second term (Y) on the right-hand side of Eq. (6) can be taken as unity in the given acidity range. This assumption holds only for compounds of very similar structure. As the solubility (S) is the sum of c_{BaH^+} and c_{Ba}, K can be determined only from those values of S, where c_{BaH^+} is much higher than c_{Ba}, a condition, which is met in the case of benzoic acid in the acidity range $-H_0 = 8.4-9.5$. With these approximations Eq. (6) is simplified to

$$K = \frac{S}{c_{Ba}\, h_0}. \tag{7}$$

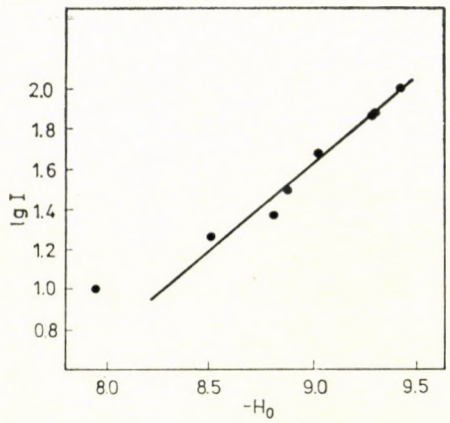

Fig. 2. Plot of lg I *vs.*-H_0 for benzoic acid protonation in sulfuric acid solutions

Even now, a good approximation of c_{Ba} is still needed. One of the possibilities is to take c_{Ba} constant throughout the range of extensive protonation. This choice is supported by the fact that S is only slightly changed in solutions of medium sulfuric acid concentration. For this constant (c_{Ba}) we have chosen the solubility determined at the highest sulfuric acid concentration, where the presence of protonated benzoic acid cannot be observed (70% H_2SO_4, $c_{Ba,min.} = 0.016$ M). The second possibility is to extrapolate the solubility changes observed in the $-H_0 = 2.6-5.9$ acidity range to $-H_0 = 9.5$ and to use the values given by this extrapolation for the point by point calculation of K. In every calculation the condition $S - c_{Ba} = 10\ c_{Ba}$ was fulfilled.

Using the solubility of benzoic acid in the acidity range $-H_0 = 8.4-$ $- 9.5$, $pK^*_{BH^+}$ can be calculated as -7.3 ± 0.4 (79% H_2SO_4, 6.8 ± 0.4 on the H_0 scale of PAUL and LONG). This value is slightly less than, but not too different from, the values determined spectrophotometrically.

The acidity range useful for the determination of I is too narrow to construct a good Bunnet—Olsen plot. However, the lg I *vs.* H_0 plot (Fig. 2) gives $m = 0.87$ and $pK_{BH^+} = -6.23$. The intercept on the H_0 axis at lg $I = 0$ (half protonation) gives $-pK^*_{BH^+} = 7.2 \pm 0.4$ (78.4% H_2SO_4). The relatively high value of m reflects easier charge delocalization and consequently less severe solvation demands of protonated benzoic acid as related to aliphatic acids [19].

It is important to point out that, despite the severe conditions and approximations needed for these calculations, the protonation constant proved to be the same as that determined spectrophotometrically. One can state, therefore, that by careful treatment of data, solubility measurements, which are very directly related to the protonation process, offer a reliable method for the determination of protonation constants of weak organic bases.

2. Properties of benzyl alcohol, benzoic acid and naphthalene in dilute solutions of mineral acids

We have investigated the effect of increasing acidity on the ultraviolet spectrum of benzyl alcohol in dilute aqueous perchloric acid solutions. No change in the transition energies or intensities was observed up to 1.0 M acid concentration at a constant ionic strength of $I = 3$. Possible protonation at higher acid concentrations cannot be investigated because of polymerization.

In UV spectrophotometric measurements on benzoic acid solutions in aqueous HCl, the ionic strength was kept constant up to $c_{HCl} = 4.5$ M (with NaCl), but at higher acid concentrations no NaCl was added. At constant ionic strength ($I = 4.5$), the spectrum was unchanged in the range $c_{HCl} =$ $= 1.0-4.5$. At higher hydrochloric acid concentrations the band at 273 nm shifted to a somewhat higher wavelength and its intensity increased. However, the changes amount to a few percent only. These observations are in accordance with the suggestion of FLEXSER, HAMMETT and DINGWALL [14] that changes in the UV spectrum of benzoic acid in dilute acid solutions should be attributed to medium effects.

In $NaClO_4-HClO_4$ solutions of constant ionic strength the solubility of both benzyl alcohol and benzoic acid increases considerably with increasing

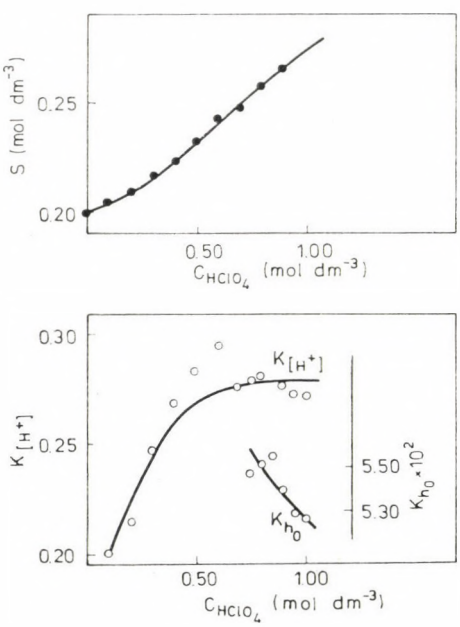

Fig. 3. Solubility and "protonation constant" of benzyl alcohol as a function of perchloric acid concentration ($I = 3$, $T = 2.98.1$ K)

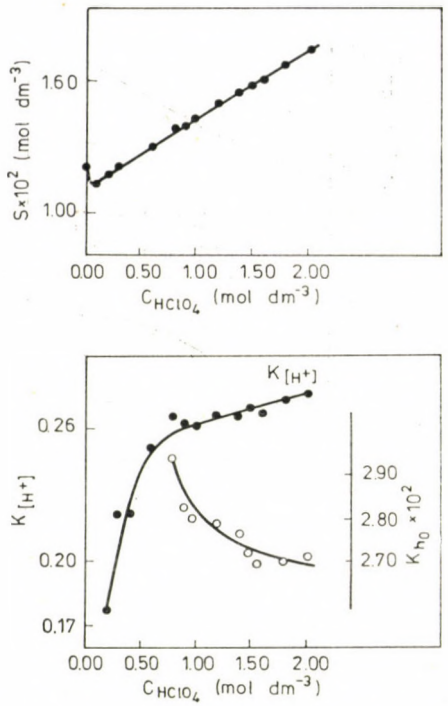

Fig. 4. Solubility and "protonation constant" of benzoic acid as a function of perchloric acid concentration ($I = 4$, $T = 298.1$ K)

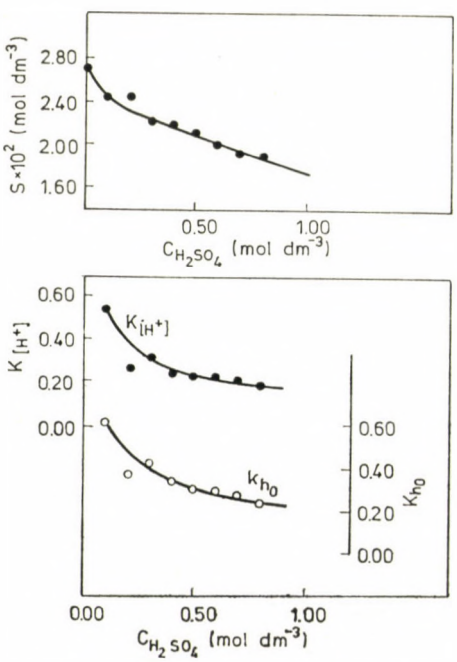

Fig. 5. Solubility and "protonation constant" of benzoic acid as a function of sulfuric acid concentration ($I \neq$ const., $T = 298.1$ K)

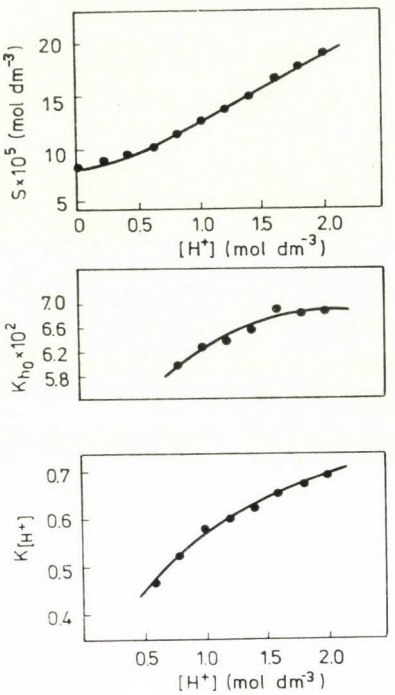

Fig. 6. Solubility and "protonation constant" of naphthalene as a function of perchloric acid concentration ($I = 4$, $T = 298.1$ K)

$HClO_4$ concentration. In contrast, in sulfuric acid solutions of changing ionic strength, a decrease of solubility was observed. Results are shown in Figs 3—5. For comparison, the solubility of naphthalene in $HClO_4/NaClO_4$ solutions ($I = 4$) was measured, too. With increasing $[H^+]$, it increases monotonously (Fig. 6) similar to the behaviour of benzyl alcohol and benzoic acid.

One can now calculate virtual protonation constants using either Eqs (5) or (7). In these calculations the solubilities belonging to 0.1 M acid concentration were chosen as c_{Ba}. For the calculations either $[H^+]$ or h_0 were taken into consideration. The corresponding concentration quotients referring to dilute mineral acid solutions are denoted as $K_{[H^+]}$ and K_{h_0}, respectively, and are shown in Figs 3—6.

In every case the "protonation constants" change monotonously with changing acid concentration. The K_{h_0} values for benzoic acid differ by an order of magnitude, depending on whether they were determined in H_2SO_4 or $HClO_4$ solutions. Besides this, the values of these "constants" are much higher than those determined in concentrated sulfuric acid solutions. These observations indicate that neither the slight spectral changes nor the changes of solubility are due to protonation processes.

3. *Comments on the theory of protonation of oxygen-containing organic compounds in dilute mineral acid solutions*

In the preceeding, we have calculated some concentration quotients based on the incorrect assumption that the solubility changes are caused by protonation. $K_{[H^+]}$ was found in all three cases to be of the same magnitude $[(3-5)\times 10^{-1}]$, whereas K_{h_0} for benzoic acid, benzyl alcohol and naphthalene in perchloric acid solutions was about $(3-7)\times 10^{-2}$, for benzoic acid in sulfuric acid solution about 3×10^{-1} dm^3 mol^{-1}.

However, these values are in agreement with "protonation constants" derived by WELLS and coworkers [3—9]. According to their explanation, the following process takes place between the solvated substrate and the proton in dilute mineral acid solutions:

$$S_{solv} + H^+(H_2O)_{4solv} \rightleftharpoons H^+(S)(H_2O)_{3solv} + H_2O\,, \qquad (8)$$

where S is the oxygen-containing organic base.

The experimental method of WELLS can be summarized as follows. Neutral *p*-nitroaniline exhibits an intensive electronic transition at $\lambda = 383$ nm. In acidic solutions this band almost completely vanishes. However, on adding bases to solutions of *p*-nitroaniline in dilute mineral acids, some absorbance can be observed at this wavelength, too. WELLS concluded that this absorbance indicates the decrease of hydrogen ion activity as a consequence of protonation of the oxygen-containing compounds. Based on this conclusion, he has determined protonation constants of 36 compounds, some of which are included in Table II. The values refer to $T = 298$ K, $I = 1$ and 5 vol. alcohol, carboxylic acid, *etc.*, concentration.

(For comparison, Table II contains the $pK^*_{BH^+}$ values of the same compounds, which were determined in concentrated sulfuric acid solutions.) Protonation constants of the same magnitude were determined by WELLS, based on the kinetic analysis of the acid-catalyzed hydrolysis of esters, too.

According to WELLS, the reaction studied is the incorporation of the organic base into the ordered structure of a tetrahydrated proton.* However, in our opinion, this could not lead to an independent chemical entity, S . . . H^+. $\cdot\, nH_2O$ distinguishable from solvated SH^+, formed in more concentrated acid solutions. Examination of the experiments and hypotheses supporting this theory, and the results derived from it reveal basic inconsistencies. This has been partly done already by WYATT and coworkers [20], who have mea-

* A similar view was developed by HALDNA and coworkers based on conductometric and calorimetric studies. These investigations were often cited by WELLS [8, 27] as supporting his theory. However, HALDNA has now revised this former opinion and concluded that the observed changes in the conductivity were not due to protonation but "reflect only the changes in solution structure around solute particles" [28].

Table II

Protonation constants of oxygen-containing organic compounds

$$K_c = \frac{[BH^+][H_2O]}{[B][P]}, \text{ where } P = (H_2O)_x H^+$$

Compound	K_c according to WELLS	Ref.	$-pK^*_{BH^+}$*	Ref.	$C^{1/2}_{H_2S_4}$* (%)
Ethanol	0.27	6	7.20	23	79
Acetic acid	0.14	7	6.2	24	74
n-Propionic acid	0.33	7	6.99	19	77.7
Diethyl ether	0.50	6	6.96	23	77.0
Ethyl acetate	0.78	9	7.1	25	78.4
Cyclohexanone	1.00	7	6.8	26	79
Phenol	0.26	6			
Benzoic acid	(0.3)	this work	7.2	this work	78.4

* As in the papers cited different acidity scales were used for the computation of $pK^*_{BH^+}$, only the sulfuric acid concentrations belonging to half-protonation are strictly comparable

sured the solubility of *p*-nitroaniline in solutions of the composition given by WELLS, and have found that the activity coefficient of the indicator itself changes considerably on the change of the medium. Besides this, they critically commented on the method of derivation of "protonation constants" (reply of WELLS in ref. [27]).

"Protonation constants" determined by WELLS in dilute mineral acids in every case fall in the range of 0—1 $dm^3\ mol^{-1}$, in the majority of cases amounting to 0.2—0.7 $dm^3\ mol^{-1}$. regardless of the chemical nature of the substance under consideration. According to these values, the basicity of phenol, and ethanol are approximately the same, and propionic acid is more basic than acetic acid!

Absorbance of *p*-nitroaniline is effected to a considerable extent even by minor changes of the medium [21]. Therefore, the changes of absorbance cannot be attributed exclusively to a single chemical process. It is also surprising that the calculated "protonation constants" are not affected by the change of the medium even when the concentration of organic compounds reaches 40—50 vol.%. It is very unlikely that values of the activity coefficients change in such a way that their product remains constant and just unity — a basic condition in the derivation of K_c [3] — despite the strong change of the medium.

One does not need extreme high values of protonation constants to explain the kinetics of the acid-catalyzed hydrolysis of esters. The rate constant of hydrolysis of ethyl acetate in 1.35 *M* sulfuric acid is $1.88 \times 10^{-4}\ s^{-1}$

[22]. The reaction proceeds through a protonated intermediate. Considering the basicity of ethyl acetate ($m = 0.51$, $pK_{BH^+} = 3.63$, [25]), the rate constant of the reaction of this intermediate should be 0.43 s^{-1}. The assumption of a rate constant of such magnitude is quite reasonable, *i.e.* consideration of another intermediate of higher concentration is not necessary. It should also be considered that this latter assumption is based on values of intercepts of linear functions drawn through points of kinetic data. The intercepts only slightly differ from zero, the case being similar to that criticized by WYATT, commenting on the spectrophotometric studies of WELLS.

Changes in the solubility of naphthalene on increasing acidity allow the calculation of a "protonation constant", the value of which is about the same as that of benzoic acid and benzyl alcohol, determined under the same conditions. It is clear, however, that in this case there is no possibility of substitution of a water molecule by the hydrocarbon, not containing any oxygen atom. These solubility changes should be attributed exclusively to medium effects.

According to our investigations in dilute and concentrated mineral acid solutions, the protonation of benzoic acid and benzyl alcohol does not take place at low acidities. Therefore, it would be incorrect to regard the concentration quotients $K_{[H^+]}$ and K_{h_0} as equilibrium constants for some kind of a protonation process. Changes in the electronic spectrum and the solubility of neutral, oxygen-containing organic bases in the 0.1—2.0 M range of proton concentration indicate only the change of activity coefficients of neutral molecules, as a consequence of changes in the medium.

REFERENCES

[1] SCORRANO, G.: Acc. Chem. Res., **6,** 132 (1973)
[2] L. P. HAMMETT: Physical Organic Chemistry, 2nd Ed., p. 275 McGraw-Hill Book Co., New York 1970
[3] WELLS, C. F.: Nature, **196,** 770 (1962)
[4] GILES, C. D., WELLS, C. F.: Nature, **201,** 606 (1964)
[5] WELLS, C. F.: Trans. Faraday Soc., **61,** 2194 (1965)
[6] WELLS, C. F.: Trans. Faraday Soc., **62,** 2815 (1966)
[7] WELLS, C. F.: Trans. Faraday Soc., **63,** 147 (1967)
[8] WELLS, C. F.: J. Phys. Chem., **77,** 1994 (1973)
[9] WELLS, C. F.: J. Phys. Chem., **77,** 1997 (1973)
[10] HOSOYA, H., NAGAKURA, S.: Spectrochim. Acta, **17,** 324 (1961)
[11] JOHNSON, C. D., KATRITZKY, A. R., SHAPIRO, S. A.: J. Am. Chem. Soc., **91,** 6654 (1969)
[12] PAUL, M. A., LONG, F. A.: Chem. Rev., **57,** 1 (1957)
[13] KISS, Á. I., JOÓ, F.: Int. J. Quant. Chem., **9,** 261 (1975)
[14] FLEXSER, L. A., HAMMETT, L. P., DINGWALL, A.: J. Am. Chem. Soc., **57,** 2103 (1935)
[15] YATES, K., STEWART, R.: Can. J. Chem., **37,** 664 (1959)
[16] YATES, K., SCOTT, B. F.: Can. J. Chem., **41,** 2320 (1963)
[17] YATES, K., STEWART, R.: J. Am. Chem. Soc., **82,** 4059 (1960)
[18] STEWART, R., GRANGER, M. R.: Can. J. Chem., **39,** 2508 (1961)
[19] LEE, D. G., SADAR, M. H.: Can. J. Chem., **54,** 3464 (1976)
[20] SIERRA, J., TEIXIDO, M., WYATT, P. A. H.: J. C. S. Faraday Trans. I, **68,** 290 (1972)
[21] KISS, Á. I., HORVÁTH, G.: Acta Chim. Acad. Sci. Hung., **42,** 15 (1964)
[22] BELL, R. P., DOWDING, A. L., NOBLE, J. A.: J. Chem. Soc., **1955,** 3106

[23] PERDONCIN, G., SCORRANO, G.: J. Am. Chem. Soc., **99,** 6983 (1977)
[24] GOLDFARB, A. R., MELE, A., GUTSTEIN, N.: J. Am. Chem. Soc., **77,** 6194 (1955)
[25] LEE, D. G., SADAR, M. H.: J. Am. Chem. Soc., **96,** 2862 (1974)
[26] CAMPBELL, H. J., EDWARD, J. T.: Can. J. Chem., **38,** 2109 (1960)
[27] WELLS, C. F.: J. C. S. Faraday Trans. I, **68,** 993 (1972)
[28] HALDNA, Ü., L., KARELSON, M., M., ORASTE, L. R.: Organic Reactivity (Tartu State University), **14,** 500 (1977)

Ferenc Joó
Mihály T. BECK } H-4010 Debrecen

Acta Chimica Academiae Scientiarum Hungaricae, Tomus 100 (1—4), pp. 433—448 (1979)

MECHANICAL STABILITY OF LIQUID BRIDGES IMMERSED IN A SECOND LIQUID

E. WOLFRAM* and J. PINTÉR

(Department of Colloid Science, Loránd Eötvös University, Budapest)

Received July 17, 1978

Accepted for publication September 12, 1978

The capillary force acting in, as well as the distribution of bridge liquid after breakdown of, polymer/(water/*n*-alkane)/glass type liquid bridges has been measured using the horizontally parallel plate geometry. At a given volume of bridge liquid, the force *vs.* separation curves go through a maximum, and so do the maximum force *vs.* bridge mass curves. The maximum of the latters occurs in the same region of bridge mass where the bridge becomes unstable. Surfactants affect the bridge stability in a complicated manner due to their influence upon both interfacial tension and contact angle resulting in changes of the fluid surface area and that of the bridge liquid/solid contact surface. A possible explanation is given to account for the configurational changes with surfactant concentration.

Introduction

Liquid bridges are four-phase systems consisting of two solids the surfaces of which are attracted by capillary forces due to the presence of a small amount of liquid within the (small) gap between the solid surfaces. The liquid is, of course, surrounded by a second fluid phase (vapour or another liquid being immiscible with the bridge liquid) and the liquid/fluid interface meets both of the solid surfaces, forming a finite contact angle on each of them. The solids can be of similar or dissimilar nature, and both their position and geometry can arbitrarily be chosen. However, a mathematical analysis requires some restrictions, as, *e.g.*, two spheres [1], a sphere and a plate [2], two parallel plates [3], *etc.*

Liquid bridge type interfacial systems are important in many practical fields like powder technology (drying of wet particulate matter), printing processes (transfer of printing ink from type on to paper), enhanced oil recovery, capillary condensation in porous media and many more. That is why there has recently been a continuously growing interest in these systems opening a new field in the area of classical capillarity [4].

Of major importance of the properties of a liquid bridge is its *mechanical* (or *Laplace*) stability, *i.e.* its resistance against perturbances in the geometrical configuration due to mechanical influences, *e.g.* changing the volume of the bridge liquid or varying the distance of separation or the mutual position of the solids. A liquid bridge is mechanically stable if, upon changing the above parameters, the system is able to get into another geometrical configuration

such that the Laplace equation for fluid interfaces is satisfied and the boundary conditions, as given by the contact angles at which the fluid interface meets the solids, are still met.

According to a classification due to PADDAY [5], the fluid interfaces of liquid bridges form axially symmetrical unbounded menisci, *i.e.* those with a meridian profile that do not intersect the rotational axis. So, from a pure

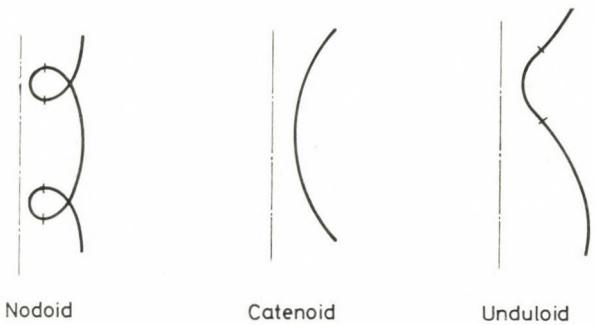

Fig. 1. Theoretical shapes of axisymmetric unbounded menisci

geometrical point of view, the meniscus shape in liquid bridges could, in principle, be a segment of a nodoid, catenoid, unduloid or toroid type surface of rotation, see Fig. 1. However, the boundary conditions and the influence of gravity results in that, contrarily to the above ideal surfaces with constant mean curvature, the actual curvature of a real meniscus varies from point to point along the fluid interface. Consequently, there is, as a rule, no possibility of getting an analytical expression for the meniscus shape even although this is the crucial point to describe the condition for the Laplace stability which, according to EVERETT and HAYNES [6], is given by

$$\mathrm{d}A_{\mathrm{eff}}/\mathrm{d}V = \mathrm{const}, \tag{1}$$

where V is the volume of the bridge liquid, and the *effective area*, A_{eff}, is defined as

$$A_{\mathrm{eff}} = A^{\mathrm{lv}} - A^{\mathrm{sl}} \cos \Theta ; \tag{2}$$

here A^{lv} and A^{sl}, resp., are the liquid/vapour (or liquid/liquid) and the solid/liquid interfacial areas, and θ is the equilibrium contact angle at the solid/liquid/fluid boundary line as given by the Young equation. A^{sl} is easily to be measured, for it is the area of the circle of contact. A^{lv}, on the other hand, can at best be obtained by a reasonable numerical approximation, *e.g.* by dividing the bridge into thin truncated cones as was shown previously [7]. Even then, however, the boundary conditions can not be given exactly because the Young equation disregards the practically always occurring hysteresis. (For an approximate solution of this problem see a recent work of this laboratory [8].)

Therefore, an operational way for studying experimentally the mechanical stability of liquid bridges appears to consist in determining the distribution of a given volume of the liquid between the two solid surfaces after rupture of the bridge, *i.e.* the most dramatic change in stability [9]. Detailed earlier studies of one of us revealed the principal stages of the breakdown of the bridge between horizontal surfaces [10] and it became clear that important information can be obtained by determining experimentally the dependence upon separation distance of the capillary force acting in the bridge [11—13].

So far, this was done on bridges with a single liquid phase. This paper deals with our recent work involving bridges of the solid/liquid-in-liquid/solid type where the solids are of dissimilar nature, having low and high energy surfaces, the bridge liquid is either water or an aqueous solution of a surfactant and the second liquid phase is a nonpolar organic liquid.

Experimental

Materials: Polyethylene (PE) and polytetrafluoroethylene (PTFE) plates as a bottom surface and pyrex glass plates as a top surface were used. The plates were purified in the usual manner as described elsewhere [14], and their cleanliness was checked by measuring advancing contact angle of water. This was found to be 93 $\pm$ 1 degrees for PE, 114 $\pm$ 2 degrees for PTFE and less than 5 degrees for the pyrex glass surface. Double distilled water ($\gamma = 72.6$ mN m^{-1}, tensiometric value) and aqueous solutions of sodium dodecyl sulfate (SDS) as well as dodecyl trimethyl ammonium bromide (DTAB) over the concentration range $c/c_M = 0.1$ to 5 were used; c_M (= critical concentration of micellisation) was found to be 8.15 mmol dm^{-3} for SDS and 15.25 mmol dm^{-3} for DTAB (mean values from specific conductance and surface tension data). No minimum in the surface tension *vs.* concentration curves was found. As a second liquid, *n*-hexane and *n*-octane (reagent grade) was employed.

Measuring procedure. Using a Hamilton microsyringe, drops of 10 to 500 mm^3 volume of the bridge liquid were placed on to one of the horizontally adjusted plates that were immersed prior to the measurement in the surrounding second liquid. In case of water bridges, the carrier surface was the bottom plate (the polymer) whereas the organic liquid, because of its lower

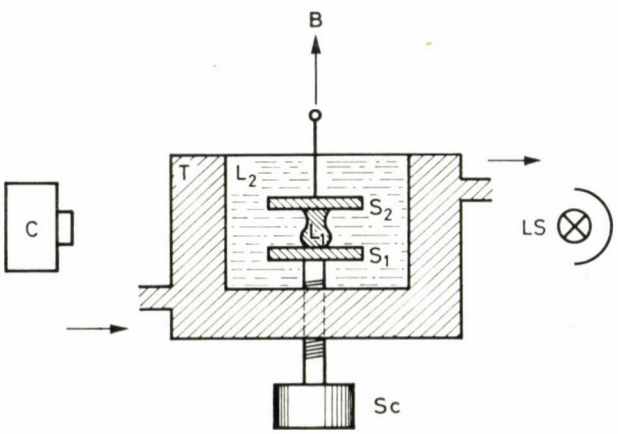

Fig. 2. Outline of experimental set up. L_1 bridge, L_2 immersing liquid, S_1 bottom surface, S_2 top surface, *B* balance, *Sc* screw for adjustment of separation, *T* constant temperature cell, *C* camera, *LS* light source

density, contacts first the top glass surface. The top plate is connected with the arm of a balance allowing for the actual force to be measured with an accuracy of 0.1 mN. The separation between the two surfaces was varied by means of a fine screw fixed to the bottom plate (Fig. 2). During the measurements, the system was observed through the viewer of a Practica Super TL type camera and photographs were taken of each position of the meniscus profile by varying the separation with an accuracy of 0.05 mm. The photographs were evaluated by means of a MWM 183 (PZO) type two-dimensional catetometer. All measurements were carried out at a temperature of 20 °C as follows. First, the carrier (for water the bottom) plate is raised until the drop contacts the other (for water the top) plate and the bridge forms. Then, by lowering the bottom plate with the screw, the separation is varied in chosen constant steps of say 0.1 or 0.2 mm. The actual separation is, of course, not identical with that calculated from the adjusted value, and the difference which varies over a broad range depends upon the force *vs.* separation relation.

Results

PTFE/ (water/n-hexane)/glass systems

In order to complete our earlier studies on free water (*i.e.*, water/air type) bridges between horizontal PTFE and glass surfaces, both water/*n*-hexane and *n*-hexane/water type bridges between the same surfaces were investigated. (The denotation is such that the first substance stands for the bridge liquid and the second one for the surrounding phase in which the bridge is immersed.) It is important that the two liquids be mutually saturated with each other in order to avoid the occurrence of nonequilibrium configurations that might arise if any mass transfer takes place apart from that due to the adsorption of the two components on the interfaces involved in the system.

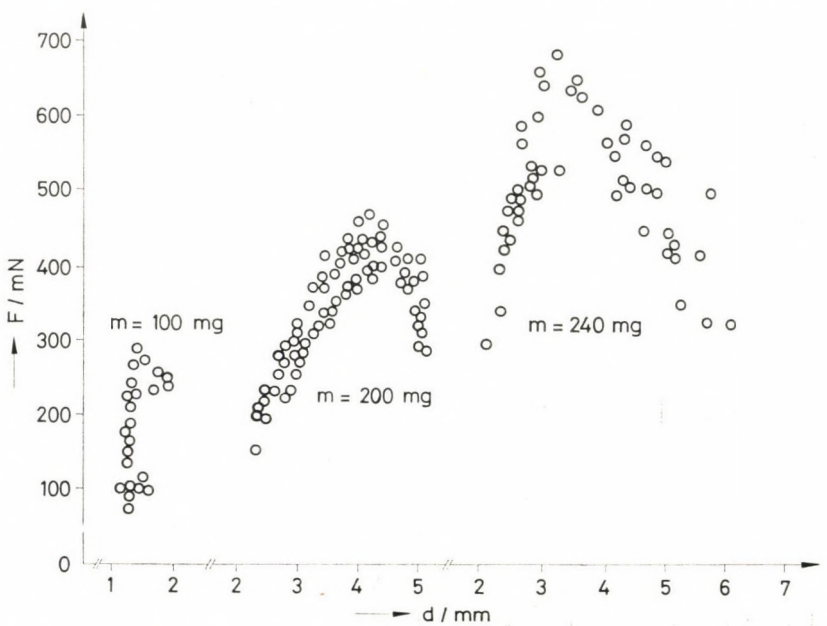

Fig. 3. F vs. d curves at various mass of water for PTFE/(water/*n*-hexane)/glass bridges

Even though the attainment of adsorption equilibrium is, as a rule, a rather quick process, the reproducibility of the experimental data depends upon the rate of separating the surfaces as was shown earlier for free water bridges [15] and also observed for the two-liquid systems in this work. This effect is, therefore, most likely to be due to hydrodynamical effects rather than to the finite rate of adsorption. In fact, the viscosity of the bridge liquid plays a role as was found in our laboratory in case of glycerol bridges [16].

The capillary force depends both upon the volume (exactly: the mass) of the bridge liquid and the separation. At a given mass, m, the actual force, F, that can be measured directly varies with separation, d, according to a maximum curve. As Fig. 3 shows, the smaller the mass of the bridge, the sharper the maximum and, at the same time, the smaller the separation at which it occurs. Hence, the maximum force, F_{max}, is a characteristic quantity being dependent only on the mass, and Fig. 4 shows this dependence.

The F_{max} *vs.* m graph is basically a maximum type curve but in the region of the local maximum the reproducibility of the points becomes rather poor and one observes a big scattering of the data. This indicates that there is a critical region of mass at which some uncertainty occurs and it was obvious to look at the *mass distribution* (MD) curve of the same system. One obtains these curve by measuring, after having suddenly ruptured the bridge, the mass of the portion of the liquid that rests on the top surface as a function of the

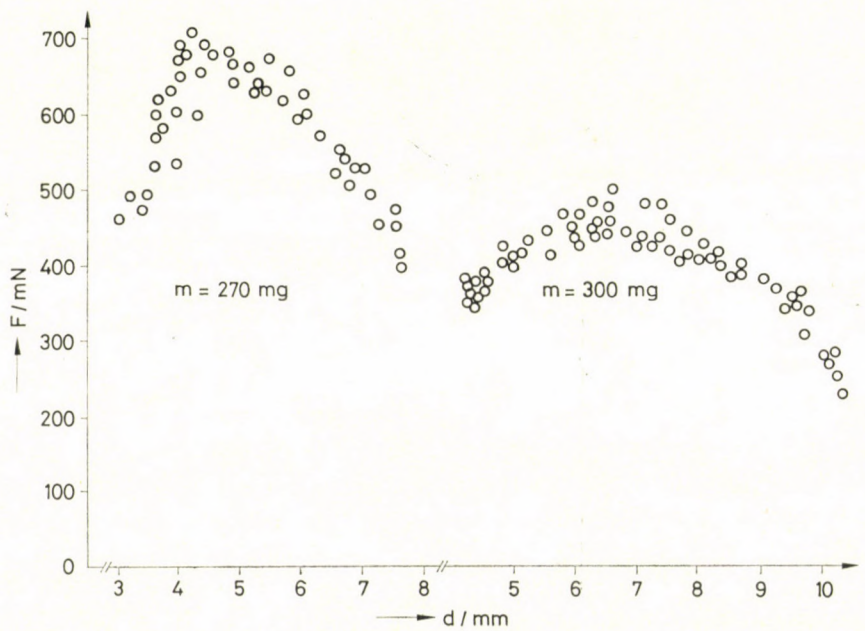

3a.

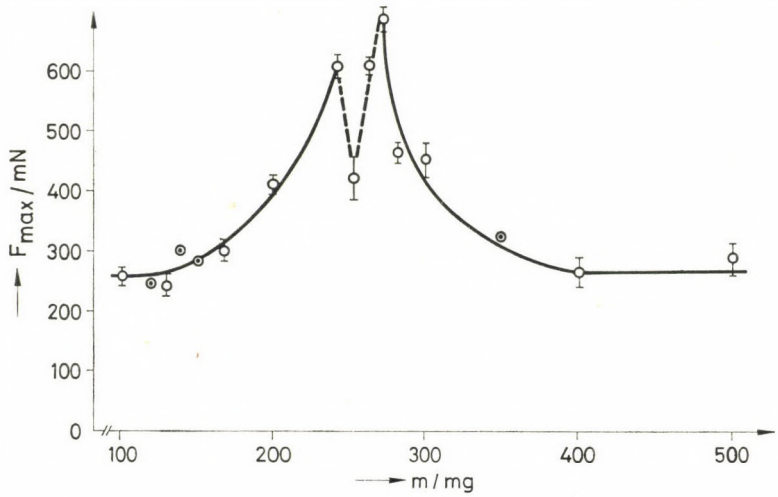

Fig. 4. F_{max} *vs. m* curves for PTFE/(water/*n*-hexane)/glass bridges

whole mass of the bridge liquid. As reported earlier [10], there are three main types of MD curves, see Fig. 5.

As Fig. 6 shows, the MD curve for the investigated systems is of type I, and it can be seen that the transient section of the MD curve occurs in the same region of the bridge mass where the measuring of the capillary force, too, becomes uncertain. It can, therefore, be concluded that the observed critical region is that of minimum Laplace stability.

PTFE/ (n-hexane/water)/glass systems

Formally, these systems can be considered (see Fig. 7) as the reverse of those discussed above, for they only differ in that the sign of the density difference between the two liquids is opposite. The wetting behaviour, on the

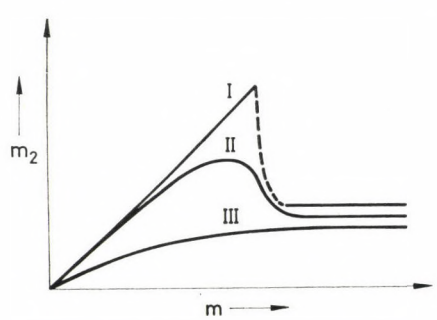

Fig. 5. **Types of mass distribution curves after breakdown of liquid bridges**

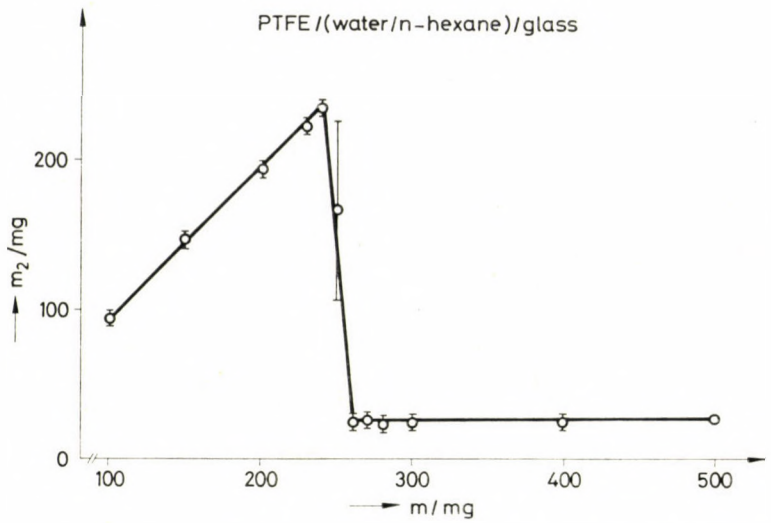

Fig. 6. Mass distribution curve for PTFE/(water/*n*-hexane)/glass bridges

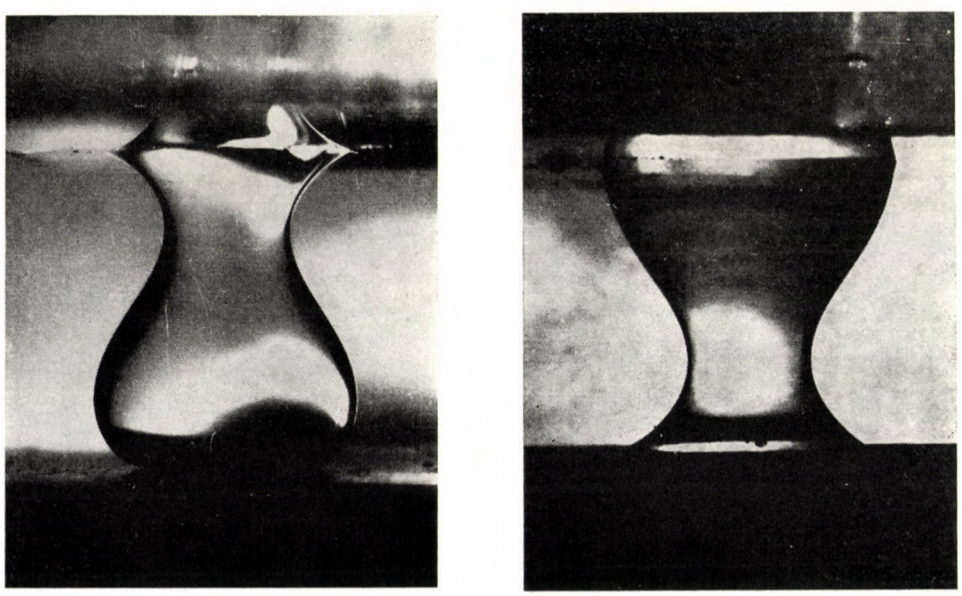

Fig. 7. Meniscus profile of *(a)* PTFE/(water/*n*-hexane)/glass, and *(b)* PTFE/*n*-hexane/water)/glass bridges. Volume of bridge liquid: 250 mm³

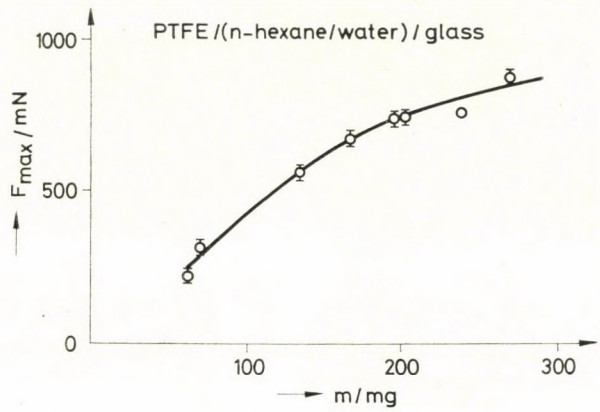

Fig. 8. F_{max} *vs. m* curves for PTFE/(*n*-hexane/water)/glass bridges

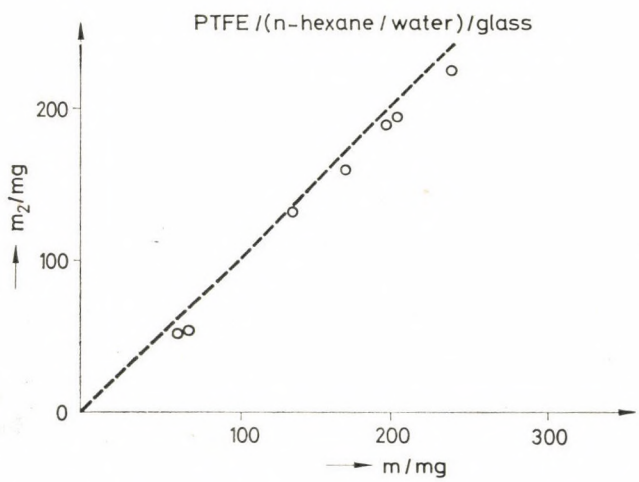

Fig. 9. Mass distribution curve for PTFE/(*n*-hexane/water)/glass bridges

other hand, is qualitatively different owing to the hysteresis which results in that the sum of the corresponding contact angles does not equal to 180 degrees but is found to be 188 degrees for PTFE and 136 degrees for the glass surface.

The essential dissimilarity of the "reverse" and the "normal" bridge manifests itself most clearly in the F_{max} *vs. m* curve (Fig. 8) showing that the maximum force increases monotonously with the bridge mass in contrary to the maximum type dependence found for the water/*n*-hexane bridge. Also, the mass distribution curve (Fig. 9) is different from that of the "normal" bridge. The transfer of the liquid occurs in this case obviously from the top to the bottom surface. The experimental data for both the F_{max} *vs. m* and the mass distribution curves are summarized in Table I.

Table I

Maximum force (F_{max}) and top transfer (m_2) as a function of the amount of a n-hexane bridge in water between PTFE and glass surfaces

V/mm³	m/mg	m_2/mg	F_{max}/mN
90±5	61.6±3.2	52.7±1.2	223±28
100±5	68.4±3.2	53.7±0.1	320±34
200±5	136.9±3.2	131.6±2.3	568±23
250±5	171.0±3.2	159.8±1.2	671±31
290±7	198.4±4.4	190.3±1.3	723±25
300±7	205.2±4.4	195.1±0.7	727±11
350±7	239.4±4.4	225.9±2.0	748±10
400±7	273.8±4.4	258.0±3.5	859±57

Effect of surfactants

To our knowledge, no experiments of this kind have as yet been carried out in liquid/liquid type bridges. Our earlier results obtained for the mass distribution in water/air bridges showed that there is rather a profound effect of surfactants [7] such that the MD curve is of type I for the pure water bridge, but it becomes type II and type III with increasing concentration of sodium dodecyl sulfate.

In the present work, we have been mainly interested in the influence upon capillary force of a surfactant solved in the aqueous phase of water/organic solvent type bridges. In these experiments, too, the surfactant was solved in water that had previously been saturated with the organic phase, and, *vice versa*, the latter was saturated with water. However, the interfacial tension was only very slightly affected by the lack of presaturation and even then solely in the region nearest the c_M (see Fig. 10).

Preliminary experiments have shown that the effect of surfactant on the stability of bridges discussed above is so pronounced, that the bridge breaks down at very low concentrations. This is likely to be due to the fact that the free surface energy of PTFE ($\sim$20 mJ m^{-2}) is too low with respect to that of the glass surface. Therefore, PTFE was replaced by PE having a free surface energy of about 30 mJ m^{-2}, and the bridge was immersed in *n*-octane.

The force *vs.* separation curves go, in these systems, too, through a maximum (Fig. 11), and so do the F_{max} *vs.* m curves (not shown here). The most important result is that demonstrated by Fig. 12. As can be seen, the maximum force varies with surfactant concentration according to a minimum-maximum

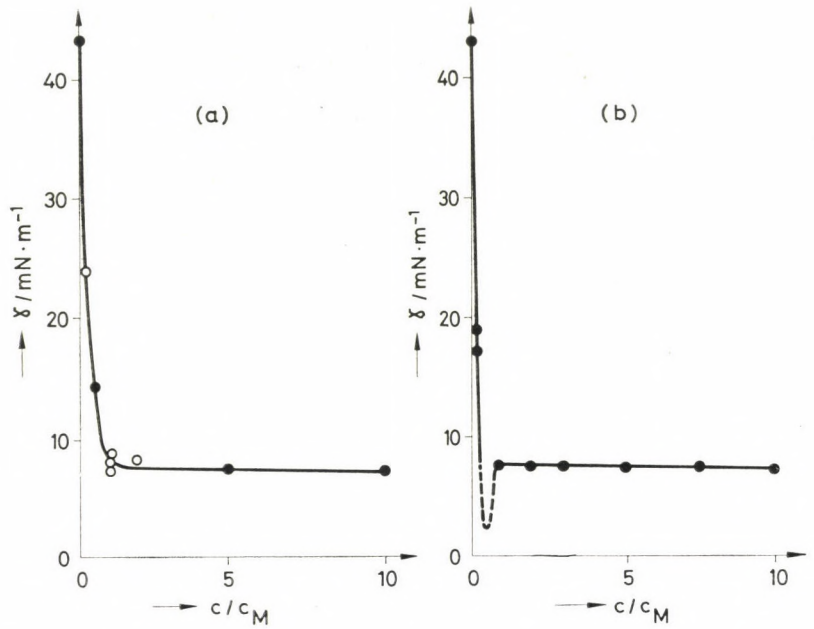

Fig. 10. Effect of *(a)* SDS and *(b)* DTAB on the interfacial tension water/*n*-octane

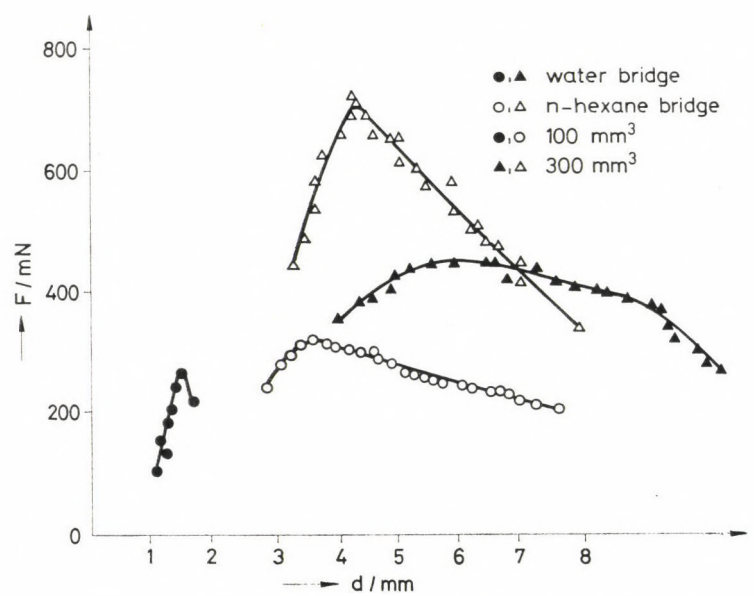

***Fig. 11. F vs. d* curves for bridges between PE and glass**

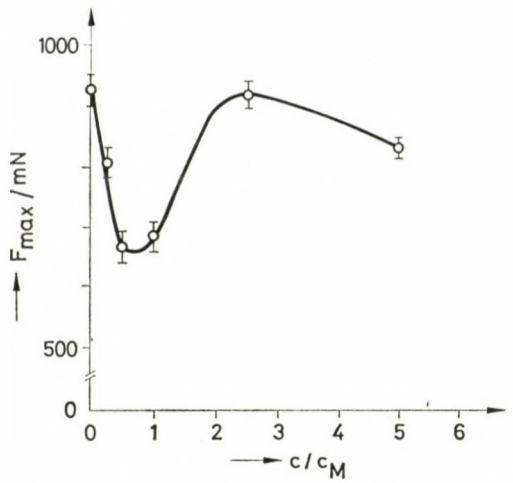

Fig. 12. Maximum force as a function of SDS concentration

type curve. The very pronounced minimum occurs at a concentration of about half the critical concentration of micellisation. The maximum force then increases rather rapidly and reaches at about $c/c_M = 5$ practically the same value as in pure water.

Discussion

The ideally simplest configuration of a liquid bridge is a fluid cylinder in zero gravity. As was shown by PLATEAU [17], it becomes unstable if the ratio of length to radius exceeds 2π, and this was experimentally confirmed with great precision recently by MASON [18]. In a detailed analysis, HAYNES [19] extended the treatment of capillary instability including the distortion of fluid cylinders into unduloids considering the constant volume condition. He pointed out that "although alternative stable configurations exist over a range of length/diameter ratios less then π, they are either less stable, then the cylinder, or are separated from it by a potential energy barrier". He concluded that "the surface formed from the cylinder at its stability limit cannot retain constant curvature for finite perturbations".

The situation becomes even more complicated if gravity effects cannot be neglected. It is customary to account for the gravity effect by using the Bond number $B = \varrho g R^2/\gamma$, where ϱ is the density difference between the liquid and the adjoining fluid phase, and CORIELL *et al.* have, by means of calculus of variation, computed the maximum stable value of the ratio of length to radius as a function of the Bond number [3]. This attempt, however, is restricted to a highly simplified situation, disregarding not only the real meniscus

shape, which is by far not a cylinder or an unduloid, but also the existence of finite contact angles.

In principle, every capillary surface can be described by the Laplace equation which relates the pressure jump across any point of the meniscus to the curvature of the surface at that particular point. In its most general form this equation reads in Cartesian co-ordinates

$$\Delta p/\gamma = C_1 + C_2 = 2H\,, \tag{3}$$

where Δp is the pressure difference at a point of the surface where the principal curvatures are C_1 and C_2, and H is the mean curvature defined as the arithmetic mean of the two curvatures.

For axially symmetrical surfaces, it is convenient to use cylindrical co-ordinates. Then eq. (3) becomes

$$2H = \frac{\mathrm{d}^2z/\mathrm{d}r^2}{[1 + (\mathrm{d}z/\mathrm{d}r)^2]^{3/2}} + \frac{\mathrm{d}z/\mathrm{d}r}{r\,[1 + (\mathrm{d}z/\mathrm{d}r)^2]^{1/2}}\,. \tag{4}$$

This is a non-linear equation which cannot be solved in closed form analytically only by using elliptic integrals. For the zero gravity case, this was done by SCRIVEN *et al.* [20] for both liquid bridges and pendular rings but only for the sphere-plate bridge geometry. These authors have also calculated the capillary force acting within the bridge. There has been a controversy in the literature as to this point. According to the classical treatment of FISHER [1], the force in a sphere-sphere or sphere-plate type bridge is given by

$$F = \pi R^2 p + 2\pi R\gamma \sin\theta\,, \tag{5}$$

where p is the pressure at the contact line and θ is the contact angle.

SCRIVEN *et al.* showed that the buoyancy, too, has to be taken into account. On this basis, we derived the following expression for the plate-plate bridge geometry (see Fig. 13):

$$F = 2\pi r_2^2 p_A + 2\pi r_2 \sin\theta_2 + (V - r_2^2\, d)\varrho_2 g - \pi d r_2^2 \varrho_1 + Mg \tag{6}$$

here M is the mass, V is the volume and d is the thickness of the top plate; g is the acceleration due to gravity.

The derived formula gave reasonable values as shown in Fig. 14. Application of Fisher's relation, on the other hand, has led to pronounced disagreement between measured and calculated force values. However, both formulas described the variation of force with separation qualitatively correctly, *i.e.* resulting in a maximum curve.

The stability criterion as given by eq. (1) has less operational value for several reasons. First, under the experimental circumstances of the force measurements $\mathrm{d}A_{\mathrm{eff}}/\mathrm{d}V$ is, because of the constant volume condition, invariantly zero although A_{eff} obviously varies while bringing the surfaces apart

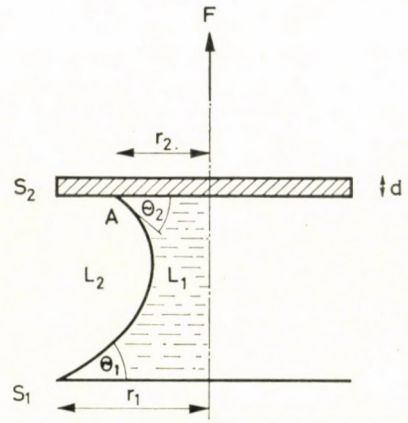

Fig. 13. Bridge geometry

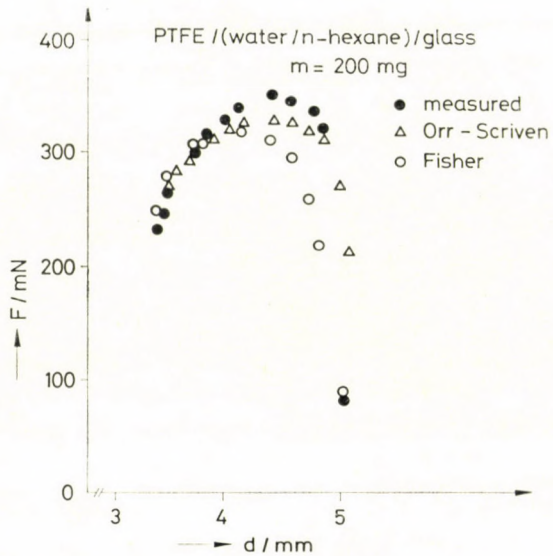

Fig. 14. Comparison of experimental and calculated force values

from each other. Second, it seemingly neglects the effect of gravity which results in a change of the potential energy of the system while changing the separation. More exactly, A_{eff} implicitly does account for the gravity effect since this manifests itself in the variation of the contact angles at various separations resulting in more or less sudden changes in the surface area of the fluid interface and that of the bridge/solid contact surfaces. This point will be discussed below.

The situation is, at least in principle, more favourable if the mass distribution curves are considered. In this case, V is no more constant and it is possible to prove whether eq. (1) is in fact at variance if the bridge is disrupted. One has, of course, to distinguish between the pseudo-instability of the bridge, *i.e.*, the total transfer of the bridge liquid from one surface to the other one, and the true instability when the bridge is in fact disrupted into two portions. If the MD curve is of type I, then both cases are encountered with increasing volume: the pseudo-instability corresponds to the initial linear section of (practically) unity slope and the second one to the sudden drop of the transferred amount.

Even in this situation, one obtains a realistic picture only by taking the gravity effect explicitly into account as was done in this laboratory for liquid/air type bridges [12]. Using a relatively simple numerical approximation for the fluid interfacial area, and calculating the total energy of the system, *i.e.* the sum of the interfacial free energy and the potential energy (the latter can be calculated from the shift of the mass center), it was possible to show that the total energy (related to a conveniently chosen reference state) is at minimum in the region where total transfer occurs and suddenly increases when the bridge breaks down.

This sudden change corresponds to the maximum of the F_{max} *vs.* m curves, for this occurs, as was demonstrated by Figures 4 and 6, nearly in the same region of m. On the other hand, it is clear that, at constant drop mass, the potential energy, being the derivate of the force with respect to distance, goes itself through an extreme value.

Closer consideration of possible changes with separation of the actual geometry reveals that, taking the constant volume condition into account, either the contact angle varies ("sticking by hysteresis") or the contact area does or else, what is the general case, both do (see Fig. 15). What really happens is dependent upon the energy change which is connected with the actual variation.

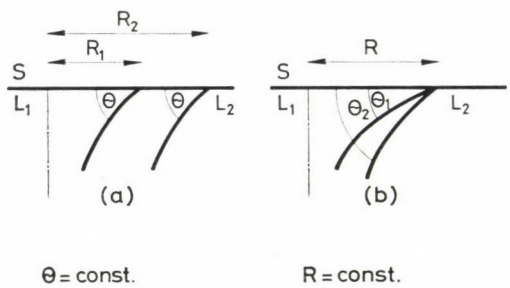

Fig. 15. Variation of the bridge profile near the solid surface for *(a)* constant contact angle, *(b)* constant contact area

The energy needed for the contact circle radius to vary from R_1 to R_2 at a constant contact angle is given by

$$E(R)_\theta = \pi(R_2^2 - R_1^2)\,(\gamma_{SL_2} - \gamma_{SL_1}) = \pi(R_2^2 - R_1^2)\,\gamma_{L_1L_2}\cos\theta\,. \qquad (7)$$

The energy connected with the change of the contact angle from θ_1 to θ_2 at a constant contact area is the difference of the works of adhesion:

$$E(\theta)_R = w_2 - w_1 = \pi R^2 \gamma_{L_1L_2}\,(\cos\theta_2 - \cos\theta_1)\,. \qquad (8)$$

The total energy change is clearly the sum of the two energies. If $E(R)_\theta \gg E(\theta)_R$ then variation of the contact angle is energetically more favourable, whereas for $E(\theta)_R \gg E(R)_\theta$ the contact area is likely to vary.

In order to prove whether the above treatment can be used to account for actual variations of the configurational changes, contact angle and contact radius values were measured on photographs taken of the menisci of water bridges in *n*-octane between PE and glass surfaces at different surfactant concentrations with various separation.

The overall picture was found to be rather complicated but some characteristic features are apparent. So, at concentrations less than about 0.2 of the c_M, the contact radius is approximately nonvariant on the polymer surface, and exactly constant on the glass surface as the separation is varied. At higher concentrations it decreases strongly with separation on both surfaces.

Contact angles, on the other hand, vary with separation over the whole concentration range according to a minimum curve on PE but irregularly fluctuate on glass. Table II contains data for the highest and lowest contact angles. It can be seen that the difference of the corresponding pairs of data, which is an approximate measure for the hysteresis, increases with concentration on PE but decreases on glass.

Table II

Effect of sodium dodecyl sulfate on extreme values of the contact angles of the water/n-octane interface against polyethylene (PE) and glass surfaces
c : actual concentration, c_M : critical concentration of micellisation

c/c_M	PE			Glass		
	Θ_{max}	Θ_{min}	$\Delta\Theta$	Θ_{max}	Θ_{min}	$\Delta\Theta$
	degrees			degrees		
0	117	84	33	42	18	24
0.5	135	91	44	50	28	22
1.0	148	88	60	48	35	13
5.0	150	82	68	38	30	8

Evaluation of the variation of individual θ and R data over small displacements of the meniscus near the solid surface showed that the energy conditions as given by eqs. (7) and (8) are indeed indicative for the direction of the actual changes. However, the above treatment is far from being exact due to the lack of detailed knowledge as to the molecular structure within the three-phase boundary region being different from that both in the fluid and solid/liquid interfaces. As is known, the specific state of this "one-dimensional" region manifests itself phenomenologically in the line tension and it is thought that important information will be obtained in future work by taking this parameter into account.

REFERENCES

[1] FISHER, R. A.: J. Agricult. Sci. **16,** 492 (1926)
[2] O'BRIEN, W. J., HERMANN, J. J.: J. Adhesion **5,** 91 (1973)
[3] CORIELL, S. R., HARDY, S. C., CORDES, M. R.: J. Colloid Interface Sci. **60,** 126 (1977)
[4] PRINCEN, H. M.: in "Surface and Colloid Science" (E. MATIJEVIC and F. R. EIRICH, Eds.), Vol. **2,** p. 1. Interscience, New York 1969
[5] PADDAY, J. F.: Pure and Appl. Chem. **48,** 484 (1976); Phil. Trans. Roy. Soc. (London) Ser. A **269,** 265 (1971)
[6] EVERETT, D. H., HAYNES, J. M.: Z. phys. Chem. (N. F.) **82,** 36 (1972), ibid. **97,** 301 (1975)
[7] WOLFRAM, E.: Croat. Chem. Acta **45,** 125 (1973)
[8] WOLFRAM, E., FAUST, R.: in "Wetting, Spreading and Adhesion" (ed. J. F. PADDAY), Pergamon Press, London 1978, p. 212
[9] WOLFRAM, E.: Kolloid-Z. **173,** 73 (1960), ibid. **182,** 75 (1962)
[10] WOLFRAM, E.: Ann. Sect. Chim. Univ. Budapestin. **6,** 77, 83, 95 (1964)
[11] WOLFRAM, E., BÁN, S., LACZKOVICH, L.: Proc. 6th Intern. Cong. Surf. Act. Subst. (Zürich, 1972), **2,** 761 (1973)
[12] BÁN, S.: Ph. D. Thesis, Budapest 1977
[13] WOLFRAM, E., PINTÉR, J., BÁN, S.: Proc. 7th Intern. Congress on Surface Active Substances (Moscow, 1976), **2,** 123 (1978)
[14] PINTÉR, J.: Ph. D. Thesis (to be submitted)
[15] WOLFRAM, E.: Lecture at the Symposium "Liquid menisci near solid surfaces", Bristol 1974
[16] FAUST, R.: M. Sc. Thesis, Budapest 1974
[17] PLATEAU, J. A. F.: "Statique expérimentale et théorique des liquids soumis aux seules forces moléculaires", Paris 1873
[18] MASON, G.: J. Colloid Interface Sci. **32,** 172 (1970)
[19] HAYNES, J. M.: ibid. **32,** 652 (1970)
[20] ORR, F. M., SCRIVEN, L. E., RIVAS, A. P.: J. Fluid Mech. **67,** 723 (1975)

Ervin WOLFRAM
János PINTÉR
} H-1445, Budapest P.O. Box 328

Acta Chimica Academiae Scientiarum Hungaricae, Tomus 100 (1—4), pp. 449—461 (1979)

CALORIMETRIC STUDIES ON THE BELOUSOV—ZHABOTINSKY OSCILLATORY CHEMICAL REACTION

E. KŐRÖS, M. ORBÁN and ZS. NAGY

(Institute of Inorganic and Analytical Chemistry, L. Eötvös University, Budapest)

Received July 18, 1978

Accepted for publication August 10, 1978

The heat output and the accumulation of bromomalonic acid (BrMA) were measured calorimetrically and polarographically, respectively, in the malonic acid—bromate—sulphuric acid—catalyst [Ce^{3+}, Mn^{2+}, $Fe(phen)_3^{2+}$] reacting systems. During the oscillatory period of the reaction both the rate of heat evolution and the rate of formation of BrMA are periodic. The heats of reaction of the preoscillatory period, that of the oscillatory period and of the uncatalyzed bromate-malonic acid reaction were approximately the same, about 650 kJ/mol bromate. The heats of some of the composite reactions of the Belousov—Zhabotinsky system [*e.g.* bromination of malonic acid, oxidation of catalysts with bromate, oxidation of malonic acid and BrMA, respectively, with cerium(IV)] were also determined.

Introduction

In our previous papers [1—3] we have reported that during the oscillatory phase of the Belousov—Zhabotinsky (BZ) reaction the rate of heat evolution is periodic. Our investigations revealed the character of heat change during chemical oscillations and it has been proved undoubtedly that temperature oscillation — which has been claimed by FRANCK and GEISELER [4], and by BUSSE [5] — does not occur. The periodicity in heat evolution, and the exothermicity of the overall process have been confirmed later also by other authors [6—8]. We have established previously that periodicity in the rate of heat evolution appears synchronized with oscillations in redox potential and bromide ion concentration, and that during the introductory (non-oscillatory) phase of the reaction considerable amount of heat is evolved. These are illustrated on Fig. 1.

In our present communication we give account of the results of our investigations directed to gain quantitative data on the heat of the BZ oscillatory chemical reaction. Alone from calorimetric measurements only qualitative considerations can be drawn and for this reason we attempted to follow quantitatively the progress of the reaction. With the material balance and the calorimetric data in hand the heat of the BZ reaction could be calculated.

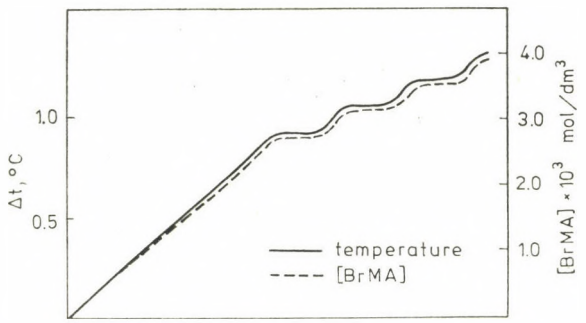

Fig. 1. The change of temperature, (a), redox potential (b) and bromide ion concentration (c) in time during the Belousov—Zhabotinsky reaction

The stoichiometry of the BZ reaction — early during reaction — is the following:

$$3CH_2(COOH)_2 + 2BrO_3^- + 2H^+ \rightarrow 2BrCH(COOH)_2 + 4H_2O + 3CO_2 \quad (a)$$

This means that in the early phase of the reaction (usually from the start of the reaction through 20—30 oscillations) the only organic bromo-compound is monobromomalonic acid (BrMA). During the later phase further reactions emerge and dibromoacetic acid appears in the reaction mixture [9]:

$$2BrO_3^- + 2CH_2(COOH)_2 + 2H^+ \rightarrow Br_2CHCOOH + 4CO_2 + 4H_2O \quad (b)$$

If only the early phase of the reaction is looked at, the progress of the reaction can be followed by determining the concentration of BrMA; therefore it was necessary to elaborate an analytical method which enabled us to determine BrMA — even in concentrations of 10^{-3}—10^{-4} mol/dm³ — in the presence of 100—500-fold excess of bromate.

Our further aim was to compare BZ systems of different catalysts. The catalysts used were cerium(III), manganese(II) and tris(1,10-phenanthroline)-iron(II). [The last is abbreviated further as $Fe(phen)_3^{2+}$].

Experimental

Reagents

$KBrO_3$, $Ce(NO_3)_3 \cdot 6H_2O$, $MnSO_4 \cdot 5H_2O$ and *cc.* H_2SO_4 were of analytical grade; malonic acid was purchased in purissimum grade. Tris(1,10-phenanthroline)iron(II) sulphate was freshly prepared from $(NH_4)_2Fe(SO_4)_2 \cdot 6H_2O$ and 1, 10-phenanthroline (both of analytical grade). BrMA was prepared as described by CONRAD and REINBACH [10].

Stock solutions:

2.0 mol/dm³ malonic acid
0.40 mol/dm³ potassium bromate
5.0 mol/dm³ sulphuric acid

0.10 mol/dm³ cerium(III) nitrate
0.10 mol/dm³ manganese(II) sulphate
0.025 mol/dm³ $Fe(phen)_3SO_4$

Methods

Determination of BrMA

The concentrations of BrMA in the presence of large excess of bromate were measured polarographically on a RADELKIS OH 102 polarograph, using a dropping mercury electrode and a saturated calomel reference electrode. By taking the polarogrammes at different BrMA concentrations the concentration dependence of the limit current was linear. The electron number *(n)* of the reduction of BrMA was determined coulombmetrically using a three-electrode setup (platinum anode, bottom mercury cathode and calomel reference electrode) in an acetate buffer of about pH 3.5. A value of 2.1 was obtained for *n*. This means that BrMA undergoes a two-electron reduction on the dropping mercury electrode:

$$\diagdown\!\!\diagup C-Br + H^+ + 2e^- \rightarrow \diagdown\!\!\diagup C-H + Br^-.$$

The electrode process is diffusion-controlled.

In strongly acid solutions of the oscillatory systems the reduction wave of bromate interferes with that of the BrMA. The two waves can be separated by the proper choice of the pH.

From the reaction mixtures, thermostatted to 25.0 ± 0.05 °C, aliquots were withdrawn in appropriate intervals and added to an acetate buffer of about pH 3.5 of the same volume. At this pH the oscillatory reaction was quenched. Then nitrogen was bubbled through the solutions for a few minutes, 0.002% Triton X was added as a maximum suppressor and the BrMA was recorded. The actual concentrations of BrMA were calculated from a calibration curve.

By the procedure described as low as 5×10^{-4} mol/dm³, BrMA could be determined with an accuracy of ±2%.

Calorimetry

The calorimetric experiments were performed in a calorimeter of constant temperature environment type. The measuring vessel was doubly jacketted, and thermostatted by an ultrathermostat. The initial temperature of reactants and environment were kept at 25.0 °C. In the calorimeter vessel the solutions of malonic acid, potassium bromate and sulphuric acid were mixed, and the reaction was started by adding the catalyst to the reaction mixture. The solution of the catalyst was introduced into the vessel from a calibrated burette with compressed air. The temperature change accompanying the reaction was sensed by a 6 kΩ thermistor forming one arm of a d.c. Wheatstone bridge. The change in its resistance was recorded continuously on a Kipp and Zonen BD9 recorder. The calorimeter was calibrated both electrically and chemically. This system allowed 0.2 joule to be detected, equivalent to about 1×10^{-4} °C temperature change in the reaction mixture of a total volume of 200 cm³.

Procedure

The BZ reactions were started by adding an appropriate amount of a catalyst solution to a mixture of malonic acid, potassium bromate and sulphuric acid, thermostatted to 25.0 ± ± 0.05 °C. The chemical oscillation was followed by a bromide selective electrode (ORION Model 94—35A); as a reference electrode a double junction calomel electrode was used, a 10% potassium nitrate solution making contact with the reaction mixture. The signal of the electrode was transferred to a recorder (RADELKIS Potentiometric Recorder, OH-814/1) through a pH-meter (RADELKIS Precision pH-meter, OP-205). From the oscillating reaction mixture aliquots were withdrawn at appropriate intervals, and analyzed for BrMA content.

Results and discussion

Calorimetric measurements

The calorimetric measurements were performed in systems composed of malonic acid, potassium bromate, sulphuric acid and a catalyst [cerium(III), manganese(II) and $Fe(phen)_3^{2+}$, respectively]. The initial concentration of malonic acid ($[MA]_0$) was 0.40 mol/dm³ in every run. The results are compiled in Table I.

Table I

$[MA]_0 = 0.40\ mol/dm^3$

Catalyst	$[BrO_3^-]_0$ mol/dm³	[catalyst] × 10⁴ mol/dm³	Heat evolved, J/dm³ reaction mixture			
			preoscillatory period	1	2	3
				oscillation		
Ce^{3+}	0.100	5.74	3010	106.5	100.5	98.5
	0.100	11.5	2910	195.0	190.5	186.0
$[H_2SO_4]$ =	0.100	46.0	2845	447.5	416.5	395.5
= 0.50 mol/dm³	0.050	11.5	1295	112.0	108.0	104.5
	0.163	11.5	4185	265.5	255.0	247.0
	0.100	1.15	1525	17.0	16.5	16.0
Mn^{2+}	0.100	4.60	1550	117.5	113.0	107.5
	0.100	11.5	1525	249.0	232.0	217.5
	0.100	46.0	1540	555.0	525.0	489.5
$[H_2SO_4]$ =	0.025	11.5	88.0	86.0	74.5	68.0
= 0.50 mol/dm³	0.050	11.5	485.5	172.5	154.5	147.5
	0.163	11.5	2290	311.5	288.5	274.0
	0.100	1.44	59.5	42.0	42.5	43.0
	0.100	5.74	185.5	139.0	141.0	150.0
$Fe(phen)_3^{2+}$	0.100	11.50	454	320.0	322.5	325.0
$[H_2SO_4]$ =	0.050	5.74	171.5	no osc. even after 60 min		
= 0.25 mol/dm³	0.130	5.74	190.5	144.0	148.5	154.0
	0.175	5.74	191.0	140.0	142.5	145.0

Measurement of BrMA and bromate

Parallel with the calorimetric measurements the accumulation of BrMA was followed by using the polarographic method described above. The results are given in Table II.

Table II

$[MA]_0 = 0.40\ mol/dm^3$

Catalyst	$[BrO_3^-]_0$ mol/dm³	[Catalyst] $\times 10^4$ mol/dm³	[BrMA] $\times 10^4$ mol/dm³	
			at the end of the preoscillatory period	in the first oscillation
Ce^{3+}	0.100	5.47	68.0	1.6
	0.100	11.5	68.0	3.0
$[H_2SO_4] =$	0.100	46.0	68.0	6.9
$= 0.50$ mol/dm³	0.050	11.5	30.0	1.75
	0.163	11.5	104.0	4.2
Mn^{2+}	0.100	1.15	34.0	0.26
	0.100	4.60	34.0	1.8
	0.100	11.5	34.0	4.0
$[H_2SO_4] =$	0.100	46.0	35.0	8.7
$= 0.50$ mol/dm³	0.025	11.5	1.50	1.35
	0.050	11.5	10.5	2.7
	0.163	11.5	59.5	4.8
$Fe(phen)_3^{2+}$	0.100	1.44	6.5	0.65
	0.100	5.74	10.6	2.0
$[H_2SO_4] =$	0.100	11.5	17.5	5.1
$= 0.25$ mol/dm³	0.130	5.74	13.5	2.0
	0.175	5.74	16.2	2.05

During the reaction the concentration of bromate was determined iodometrically after appropriate dilution. One series of measurements are shown in Table III.

Table III

$[BrO_3^-]_0 = 0.100\ mol/dm^3$, $[MA]_0 = 0.40\ mol/dm^3$, $[Ce^{3+}] = 5 \times 10^{-3}\ mol/dm^3$, $[H_2SO_4] = 0.50\ mol/dm^3$

The number of measurement, n	Oscillation number	$[BrO_3^-]_{n-1} - [BrO_3^-]_n$ mol/dm³	$[BrMA]_n - [BrMA]_{n-1}$ mol/dm³	$\frac{[BrMA]_n - [BrMA]_{n-1}}{[BrO_3^-]_{n-1} - [BrO_3^-]_n}$
1	5	3.41×10^{-3}	3.57×10^{-3}	1.11
2	7	1.62×10^{-3}	1.65×10^{-3}	1.02
3	10	2.17×10^{-3}	2.10×10^{-3}	0.97
4	15	2.90×10^{-3}	2.95×10^{-3}	1.01
5	21	2.53×10^{-3}	2.50×10^{-3}	0.99
6	31	4.89×10^{-3}	4.78×10^{-3}	0.98

The results confirmed our earlier finding that even after 20—30 oscillations practically BrMA was the only bromo-compound which formed in the oxidative bromination of malonic acid by bromate.

Heat of the BZ reaction

Heat of reaction of the oscillatory phase

The results of Tables I and II show that in every BZ system there exists a close parallelism between the amount of BrMA formed and the heat evolved. Figure 2 displays this fact expressively. Also it can be gathered from the same figure that the BZ reaction can be divided into two phases: a non-oscillatory phase and an oscillatory one. The non-oscillatory phase was mentioned in previous publications as induction period. This is, however, a misnomer since during the "induction period" the same overall process proceeds as during the oscillatory one. For this reason the non-oscillatory phase will be called henceforth the preoscillatory period.

Table IV

$[MS]_0 = 0.40\ mol/dm^3$

Catalyst	$[BrO_3^-]_0$ mol/dm³	[Catalyst]×10⁴ mol/dm³	Heat output J/dm³ (in the first oscillation)	[BrMA]×10⁴ mol/dm³ (in the first oscillation)	ΔH J/mol BrO_3^-
Ce^{3+}	0.100	5.74	106.5	1.6	665.6
	0.100	11.5	195.0	3.0	650.0
$[H_2SO_4]$ =	0.100	46.0	447.5	6.9	648.5
= 0.50 mol/dm³	0.050	11.5	112.0	1.75	640.0
	0.163	11.5	265.5	4.2	632.1
Mn^{2+}	0.100	1.15	17.0	0.26	653.8
	0.100	4.60	117.5	1.8	652.7
	0.100	11.5	249.0	4.0	622.5
$[H_2SO_4]$ =	0.100	46.0	555.0	8.7	637.9
= 0.50 mol/dm³	0.025	11.5	86.0	1.35	637.0
	0.050	11.5	172.5	2.7	638.8
	0.163	11.5	311.5	4.8	648.9
$Fe(phen)_3^{2+}$	0.100	1.44	42.0	0.65	645.2
	0.100	5.74	139.0	2.0	695.0
$[H_2SO_4]$ =	0.100	11.5	320.0	5.1	627.5
= 0.25 mol/dm³	0.130	5.74	144.0	2.15	669.8
	0.175	5.74	140.0	2.05	682.9

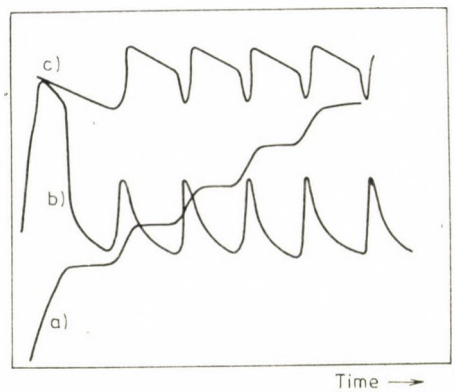

Fig. 2. Temperature and BrMA concentration vs. time plots of a Belousov—Zhabotinsky rection

With the calorimetric data and BrMA concentrations in hand the heat of reaction, ΔH, of the different BZ systems could be calculated. It is well known that the only irreplaceable component of the BZ systems is the bromate ion and therefore the heat of the BZ reaction is referred to 1 mol bromate.

In Table IV the amount of BrMA formed and the heat evolved during the first oscillation in reacting systems of different bromate — and catalyst concentrations, and the heat of reaction are given. From the data of the last column of Table IV the heats of reaction of the investigated BZ systems are the following:

Catalyst	Heat of reaction of the oscillatory phase kJ/mol bromate
Cerium(III)	647.2±5.0
Manganese(II)	641.7±3.8
$Fe(phen)_3^{2+}$	664.1±10

The results obtained with systems of different catalysts agree within the experimental error. The average value is:

$$651 \pm 6.2 \text{ kJ/mol bromate}$$

Heat of reaction of the preoscillatory period

The heat of reaction was calculated also for the preoscillatory period of the BZ reaction. At the calculations, however, correction was necessary. Namely the BZ reaction was started, after adjusting the temperature of the

reaction mixture to 25.0 °C, by the addition of a catalyst. Separate experiments, however, revealed that malonic acid is oxidized slowly by acid bromate even in the absence of a catalyst. Thus a considerable amount of BrMA is formed during the period of thermostation (about 30 min). By the polarographic method the total amount of BrMA was measured, calorimetrically, however, the heat output from the addition of a catalyst until the initiation of the oscillation was obtained. Therefore at the calculation of the heat of reaction the amount of BrMA formed until the addition of the catalyst was substracted from the total amount of BrMA accumulated during the preoscillatory period. The correction value was determined separately in uncatalyzed bromate-malonic acid reaction.

During the preoscillatory period of the $Fe(phen)_3^{2+}$-catalyzed BZ reaction very small amount of BrMA accumulated and the correction value was about 90—95% of the amount of BrMA formed until the start of the oscillation. Therefore in this system the heat of reaction of the preoscillatory period could not be determined with the required accuracy. With the cerium(III)- and manganese(II)-catalyzed BZ systems the correction values were 20—30% of the total BrMA concentrations.

The heat of reaction data for the preoscillatory period are given in Table V.

Table V

$[MA]_0 = 0.40\ mol/dm^3$; $[H_2SO_4] = 0.50\ mol/dm^3$

Catalyst	$[BrO_3^-]_0$ mol/dm³	[Catalyst]×10⁴ mol/dm³	Heat output of the preosc. per.	[BrMA]×10³ mol/dm³		[BrMA]×10³ corr. mol/dm³	ΔH kJ/mol BrO_3^-
				at the addition of the catalyst	at the start of oscil.		
	0.100	5.74	3010	2.25	6.80	4.55	661.5
Ce^{3+}	0.100	11.5	2910	2.40	6.80	4.40	661.4
	0.100	46.0	2845	2.40	6.80	4.40	646.6
	0.050	11.5	1295	1.00	3.00	2.00	647.5
	0.163	11.5	4185	4.05	10.40	6.35	659.1
	0.100	1.15	1525	1.10	3.40	2.30	663.0
	0.100	4.60	1550	1.05	3.40	2.35	659.6
Mn^{2+}	0.100	11.5	1525	1.10	3.40	2.30	663.0
	0.100	46.0	1540	1.20	3.50	2.30	669.6
	0.025	11.5	88.0	0.015	0.15	0.135	651.8
	0.050	11.5	485.5	0.30	1.05	0.75	647.3
	0.163	11.5	2290	2.51	5.95	3.44	665.7

The average values are the following:

Catalyst	Heat of reaction of the preoscillatory period kJ/mol bromate
Cerium(III)	655.4±6
Manganese(II)	633.0±8

These values are practically the same as those obtained for the oscillatory phase of the reaction.

Heat of the uncatalyzed malonic acid–bromate reaction

We found that the oxidative bromination of malonic acid by acid bromate proceeds even in the absence of a catalyst [11], and we measured the heat of reaction also of this process. The reaction is rather slow and for this reason separate runs were carried out in order to take the [BrMA] *vs.* time and heat *vs.* time plots.

The heat of reaction is

$$648 \pm 10 \text{ kJ/mol bromate.}$$

Discussion

Calorimetric and polarographic data indicate that the uncatalyzed and catalyzed reactions between malonic acid and acid bromate, and in the latter case both in the preoscillatory and the oscillatory periods proceed with the stoichiometry given in Eq. *(a)*.

The high value of the heat of reaction (about 650 kJ/mol bromate) can be explained and calculated approximately by the data obtained for the composite reactions. (See "Appendix".) The great heat output observed during the BZ reaction is first of all due to the total oxidation of malonic acid

$$CH_2(COOH)_2 + 2H_2O \rightarrow 3CO_2 + 8H^+ + 8e^-$$

which is a highly exothermic reaction. Also the bromination of malonic acid and the oxidation to water of the hydrogen in malonic acid substituted by bromine contribute considerably to the overall heat effect.

$$CH_2(COOH)_2 \xrightarrow{\text{bromination}} CHBr(COOH)_2$$

$$H \xrightarrow{\text{oxidation}} 1/2\ H_2O$$

ΔH for this latter reaction is 142 kJ/mol hydrogen atom.

RASTOGI, YAVADA and KUMAR [7], who performed calorimetric measurements on the cerium(III)-catalyzed BZ reaction and also on some composite reactions, claim that to the overall heat output the reaction between bromate and bromide contributes considerably. The named authors carried out the calorimetric experiments in a very simple apparatus and did not follow the heat evolution continuously. They made the temperature vs. time plots by measuring the temperature of the reaction mixture at appropriate intervals, and did not report on the large amount of heat, which evolves during the pre-oscillatory period. They did not measure the accumulation or the consumption either of the reactants or products and for this reason they could not draw any quantitative conclusion from their results.

The oxidation of bromide with bromate is an important reaction concerning the overall BZ process. Namely, by this reaction is bromide ion — the so-called control intermediate of the oscillatory reaction [12] — consumed. At a critical bromide ion concentration (which has a value of about 10^{-5} $[BrO_3^-]$ the reacting system changes from one kinetic state to the other [13]. However, the actual bromide ion concentration in the reaction mixture is very low. Even its highest value is below 10^{-4} mol/dm^3 [14]. For this reason, this reaction, as a respect to the overall heat output, is of little importance. This consideration is supported also by the fact that in the oscillatory phase of the BZ reaction when phases of high and low rates of heat evolution follow each other periodically (see Fig. 2) the bromate-bromide reaction proceeds in that phase when the rate of heat evolution is low.

Our calorimetric results indicate that in all the three cases of the bromate-malonic acid reaction: 1. uncatalyzed, 2. catalyzed, non-oscillatory and 3. catalyzed, oscillatory (in cases 2. and 3. irrespective of the chemical nature of the catalyst) the same stoichiometry prevails.

Appendix

Above we reported on the determination of the heat of the BZ reaction. We regarded as important to reveal which of the composite reactions are responsible for the high value of the heat of reaction. For this reason we carried out calorimetric measurements on many composite reactions of the BZ systems.

1. *The reaction between acid bromate and the catalyst* (Me^{n+})

The stoichiometry of the reaction is given by Eq. (1) [15, 16]:

$$BrO_3^- + 4Me^{n+} + 5H^+ \rightarrow HOBr + 4Me^{(n+1)+} + 2H_2O \qquad (1)$$

The calorimetric measurements were performed in dilute sulphuric acid. The following results were obtained:

Catalyst	Heat of reaction kJ/mol bromate	$[H_2SO_4]$ mol/dm³
Ce^{3+}	26.6	0.50
Mn^{2+}	−21.7	0.50
$Fe(phen)_3^{2+}$	40.7	0.25

It is rather peculiar that during the oxidation of manganese(II) by bromate heat is consumed.

2. *Bromination of malonic acid*

The bromination of malonic acid was carried out with different brominating agents and the stoichiometry of the reaction was established by determining the BrMA content of the reaction mixtures.

2.1. *The bromination* of an excess of malonic acid *with bromine* proceeds according to the following stoichiometry:

$$Br_2 + CH_2(COOH)_2 \rightarrow BrCH(COOH)_2 + Br^- + H^+ \qquad (2)$$

The heat of reaction is 66.0 ± 2.9 kJ/mol BrMA in 1 mol/dm³ sulphuric acid.

With an excess of bromine ΔH increases by increasing the bromine concentration which indicates that additional bromocompounds (mostly dibromoacetic acid) are formed. A strict stoichiometry, however, can not be obtained in this case.

2.2. *Bromination with a mixture of bromide and bromate.*

When $[MA] \gg [BrO_3^-] \gg [Br^-]$ the overall reaction is composed of the reactions between bromate and bromide, and between malonic acid and bromine:

$$BrO_3^- + 5Br^- + 6H^+ \rightarrow 3Br_2 + 3H_2O \qquad (3)$$

$$3Br_2 + 3CH_2(COOH)_2 \rightarrow 3BrCH(COOH)_2 + 3Br^- + 3H^+ \qquad (4)$$

$$BrO_3^- + 2Br^- + 3CH_2(COOH)_2 + 3H^+ \rightarrow 3BrCH(COOH)_2 + 3H_2O \qquad (5)$$

The heat of reaction (3) is 205.8 kJ/mol bromate, and that of reaction (5) 407.4 kJ/mol bromate. From this value the heat of reaction (4) was cal-

culated according to Hess's law:

$$\Delta H_4 = \frac{\Delta H_5 - \Delta H_3}{3} .$$

A value of 67.0 kJ/mol BrMA was obtained for ΔH_4, which agrees well with ΔH_2, which was measured directly.

2.3. *The bromination of malonic acid by hypobromous acid* proceeds according to Eq. (6):

$$HOBr + CH_2(COOH)_2 \rightarrow BrCH(COOH)_2 + H_2O \qquad (6)$$

if malonic acid is in large excess. The heat of reaction falls between 67 and 104 kJ/mol BrMA depending on the ratio of the reagents. At higher concentrations hypobromous acid acts also as an oxidizing agent.

3. *Oxidation of malonic acid and BrMA with cerium(IV)*

The stoichiometry of the reactions was established by volumetric titration of cerium(IV) with a standard iron(II)-solution using ferroin as a redox indicator.

3.1. *The oxidation of malonic acid with cerium(IV)* was performed with 2—10-fold excess of the oxidizing agent in 1 mol/dm^3 sulphuric acid solution. The redox reaction proceeds with six-electron change when bromide ions are absent:

$$CH_2(COOH)_2 + 6Ce^{4+} + 2H_2O \rightarrow 6Ce^{3+} + HCOOH + 2CO_2 + 6H^+. \qquad (7)$$

The heat of reaction is 535 kJ/mol malonic acid.

Bromide ions catalyze the oxidation of malonic acid with cerium(IV) and in their presence the reaction proceeds with eight-electron change [9]:

$$CH_2(COOH)_2 + 8Ce^{4+} + 2H_2O \rightarrow 8Ce^{3+} + 3CO_2 + 8H^+. \qquad (8)$$

Bromide ions are intermediates in the BZ oscillatory reactions and they are always present in the oscillating systems. For this reason we performed calorimetric measurements on the malonic acid-cerium(IV) reaction at 4.10^{-3}—$-1 \cdot 10^{-2}$ mol/dm^3 bromide concentrations. Under these conditions the redox reaction proceeds according to Eq. (8). The heat of the reaction is 857 kJ/mol malonic acid in 1 mol/dm^3 sulphuric acid solution.

We looked also at the $Br^- + Ce^{4+} \rightarrow 1/2Br_2 + Ce^{3+}$ reaction. This redox reaction is extremely slow and does not interfere reaction (8).

3.2. *The oxidation of BrMA with an excess of cerium(IV)* is a six electron redox process:

$$BrCH(COOH)_2 + 6Ce^{4+} + 2H_2O \rightarrow 6Ce^{3+} + 3CO_2 + Br^- + 7H^+$$

The heat of reaction in 1 mol/dm^3 sulphuric acid solution is 711 kJ/mol BrMA.

REFERENCES

[1] Kőrös, E., Orbán, M., Nagy, Zs.: Nature Phys. Sci., **242**, 30 (1973)
[2] Kőrös, E., Orbán, M., Nagy, Zs.: J. Phys. Chem., **77**, 3122 (1973)
[3] Kőrös, E., Burger, M., Friedrich, V., Ladányi, L., Nagy, Zs., Orbán, M.: Faraday Symposia Chem. Soc., No. 9. 28 (1974)
[4] Franck, U. F., Geiseler, W.: Naturwiss., **58**, 52 (1970)
[5] Busse, H. G.: Nature Phys. Sci., **233**, 137 (1971)
[6] Janjic, D., Stroot, Ph., Burger, U.: Helv. Chim. Acta, **56**, 266 (1974)
[7] Rastogi, R. P., Yadava, K. D. S., Kumar, A.: Ind. J. Chem., **12**, 1280 (1974)
[8] Bond, J. R.: Faraday Symposia Chem. Soc., No. 9. 97 (1974)
[9] Bornmann, L., Busse, H. G., Hess, B.: Z. Naturforsch., **28c**, 514 (1973)
[10] Conrad, M., Reinbach, M.: Ber., **35**, 1813 (1902)
[11] Kőrös, E.: Faraday Symposia Chem. Soc., No. 9. 92 (1974)
[12] Noyes, R. M., Field, R. J.: Ann. Rev. Phys. Chem., **25**, 95 (1974)
[13] Noyes, R. M., Field, R. J., Kőrös, E.: J. Am. Chem. Soc., **94**, 1394 (1972)
[14] Kőrös, E., Burger, M.: Ion-Selective Electrodes, Ed. E. Pungor, Akadémiai Kiadó, Budapest, 1973, 191. o.
[15] Thompson, R. C.: J. Am. Chem. Soc., **93**, 7315 (1971)
[16] Kőrös, E., Burger, M., Kis, Á.: Reaction Kin. Cat. Lett., **1**, 475 (1974)

Endre Kőrös
Miklós Orbán
Zsuzsanna Nagy
H-1088, Budapest, Múzeum krt 4/b.

Acta Chimica Academiae Scientiarum Hungaricae, Tomus 100 (1—4), pp. 463—479 (1979)

MESOMORPHIC POLYMERS*

F. CSER, K. NYITRAI and Gy. HARDY

(Research Institute for Plastics, Budapest)

Received July 18, 1978

Accepted for publication September 21, 1978

The conditions for the formation of mesomorphic mono-substituted vinyl polymers have been studied. Freezing of the mesomorphic state into a glassy phase may be attributed to the formation of a rigid, irregular, atactic polymer chain. The laminar smectic structure may be observed for polymers in the "herring-bone" arrangement. The structure is, from many aspects, related to the structure of polymers with elastic main chains. The molecular chain in the "herring-bone" arrangement may be observed in the case of polymers with a rigid group, bound to the main chain by elastic side chains (*min.* C_6-C_8) or at least four elastically attached atoms. The melting point of polymers is relatively sharp. Bulky polymers in the glassy state are optically anisotropic, rigid and brittle.

Helix polymers are formed if the bulky, rigid side group is bound to the main chain directly or by some elastically attached atomic chains. Polymer molecules may be considered as rigid cylinders, the close packing of which will form the nematic bulky polymer. Molecular size may be determined from maximum values of X-ray diffraction curves. Nematic polymers are workable by pressing, even at low temperatures. Their melting points are high, lying in a wide range often beyond the temperature of decomposition. Helix polymers with cylindrical symmetry, containing a chiral carbon atom are in the cholesteric state. The structure of mesomorphic polymers can be determined only by combining the results of several independent investigations on the texture and structure of the polymers.

Mesomorphic states

A peculiar feature of some organic compounds with anisotropic arrangements is that, on heating, the crystals melt into an anisotropic liquid and become isotropic at constant temperature only upon further heating. The range between the isotropic melting point and the crystalline state is called the mesomorphic state. The isotropic melting point is referred to in the literature as the clearing point.

The mesomorphic state cannot be considered as a single homogeneous state. It covers a collective term for several structurally well-definable states. Considering the structural arrangement of mesomorphic substances presented in Fig. 1, the following states may be distinguished.

The smectic states formed upon the destruction of crystals approaches best the crystalline state structurally. These are laminar structures (Fig. 2),

* Polymerization in Liquid Crystals, VII.

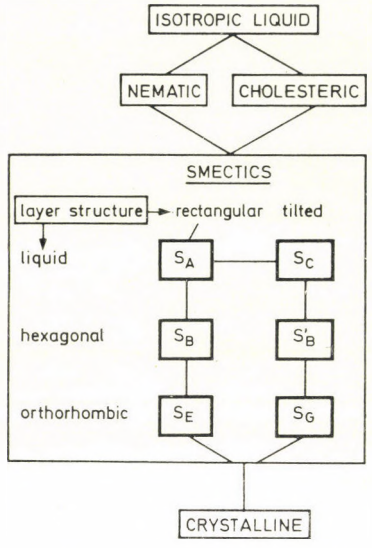

Fig. 1. Mesomorphous states

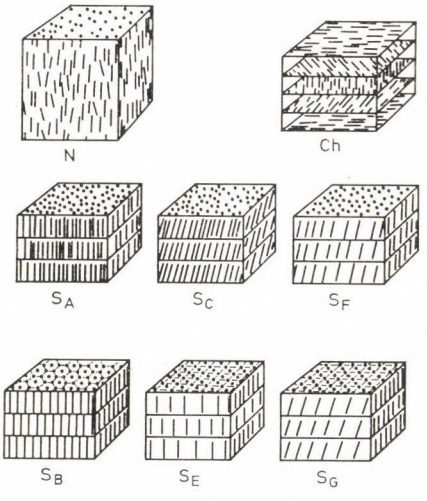

Fig. 2. Structural characteristics of the mesomorphous state

where the molecules in the layers are crystals (S_G, S_E), or two-dimensional liquids (S_A, S_C). The long axis of the molecules may be parallel to the layer normal (S_E, S_B, S_A), or makes an angle with it (S_G, S_F, S_C). Periodical recurrence of the mass center of the layer resembling a reciprocal lattice is characteristic of layer packing. Molecules within the layer, however, do not give direct translation parallel to the reciprocal lattice [1—4].

The common features of nematic and cholesteric states are as follows. The anisotropic molecules considered to have a cylindrical symmetry are approximately parallel to their axes. Nevertheless their mass centers are ordered statistically in two directions and the molecules are packed in parallel to their long axes by direct translational symmetry. This translation has, however, no reciprocal lattice character [1]. Nematic materials containing chiral atoms are in a cholesteric state. This manifests itself in a more or less regular arrangement of the long axes of molecules. Periodical occurrence of the long axes of the molecules results in a periodicity characteristic of the substance. Due to the cholesteric system, extremely large light scattering appearing as an iridescent colour can be observed at the wavelength corresponding to half periodicity.

Mesomorphic polymer solutions

Considering molecular structure, polymers have an anisotropic geometrical arrangement, where the main chain may be flexible and in this case the polymer melt has isotropic properties. The polymer chain may be, however, also rigid — or become rigid during formation of the helix — when the occurrence of anisotropic properties may be expected [5—7]. In fact, the formation of anisotropic (nematic or cholesteric) solutions could be observed in the dissolution of poly(*p*-benzamide), poly(*p*-phenylenephthalamide) [8—9], poly(γ-benzyl-L-glutamate) and different biopolymers [10—12].

Anisotropic polymer solutions have, however, often limited miscibility on the side of the polymer. Therefore, the polymer itself cannot be considered to be in a mesomorphic state because it crystallized from the solution upon increasing concentration.

The combination of spontaneous orientation and arrangement of the polymer molecules with the liquid crystalline state seems to be a very feasible method in technical procedures. The removal of the solvent from mesomorphic solutions is, however, a tedious procedure. Therefore, it seems particularly advantageous if the mesomorphic state develops thermotropically during thermal treatment of the polymers.

Thermotropic mesomorphic polymers

Several authors have aimed to demonstrate the thermotropic mesomorphic state of polymers [13—31]. This was mostly attained by polymerization in the mesomorphic state. According to previous experiences [13, 20, 23], the mesomorphic solution of traditional monomers did not produce any mesomorphic polymer after polymerization. When the monomers themselves

were in the mesomorphic state, the polymers formed showed mainly anisotropic properties.

Of the above mesomorphic states, the polymer was assumed by most authors to be in the state observed also for the monomer. PERPLIES *et al.* observed [31—33] a peak in the small-angle X-ray scattering of the product of polymerization of the nematogenic monomer in the nematic phase or in solution at —78 °C. During the polymerization of the monomers in smectic state, HARDY *et al.* [14, 15] found the polymers to be isomorphous with their monomers. Subsequent experiments based on X-ray diffraction measurements showed [36] the above polymer to be in the smectic B state. The polymer formed from the nematogenic monomer was found to be rigid with a mesomorphic structure in investigations carried out by TSVETKOV *et al.* [37, 39]. These authors [39] assumed the nematic state for the polymer as a consequence of the nematic state of the monomer. The structure of the polymers were identified by us [18, 41, 42] using the thermodynamic system of the polymer formed with a nematic or cholesteric monomer as well as via the law of full miscibility given by SACKMANN [40] for such systems. Although the phase conditions of polymer-monomer systems were found to be more complex than those of low molecular weight substances [43, 46], we did not find a fully miscible series between the nematic monomer and its polymer, it being limited on the monomer side [18, 41, 42]. The polymer phase was studied by small and wide angle X-ray diffraction, polarization microscopy and thermomechanic measurements. In spite of the different methods of investigations applied, the specific structure of the mesomorphic polymer could not be identified unambiguously. The method applied by several authors, who determined the mesomorphic phase of the polymer on the basis of a single experimental result (*e.g.*, small angle X-ray scattering, estimation of chain rigidity in solution, or DSC investigation of the polymer-monomer system), seems to be, therefore, rather superficial.

Recently, polymers prepared from the homologous series of *p*-alkoxyphenyl *p*-acryloiloxybenzoates have been studied by the following methods [47—49]: small and wide angle X-ray scattering, polarization microscopy (texture investigation, optical anisotropy), thermomechanics, DSC, scanning electron microscopy, density measurements, measurements of molecular size by GPC, *etc.* Further investigations (X-ray, NMR) were carried out in a magnetic field on softened systems. Evaluation of these independent methods verifies that the polymer has a rigid cylindrical shape, the mesomorphic phase of which shows the closest resemblance to the nematic state.

The above investigations also indicate that the nematic polymer cannot be isomorphous with the nematic phase of the monomer. These fundamental structural discrepancies offer an explanation of the fact that if the monomer molecules are forced (*e.g.* by means of a magnetic field), into an arrangement

parallel to their long axes, polymerization will lead to a smectic polymer [29, 32]. As the polymerization reaction is not complete, on the basis of our experience with polymer-monomer interaction, we can state that the vitrified polymer-monomer system is in an oriented smectic state.

Another difficulty in the identification of the mesomorphic phase is that polymers have molecular weights several orders of magnitude greater than traditional mesomorphic substances. The extremely high molecular weight considerably modifies the relaxation properties of the whole molecule. Therefore, upon going from well-known mesomorphic substances to mesomorphic polymers, the individual mesomorphic structures must be interpreted in terms of the specific features of the polymer. In other words the structure must be verified by unambiguous experimental evidence.

Our most recent experiments [47—49] allowed the reinvestigation of our polymers previously considered to be only mesomorphic, using relatively few specific measurements and closer determination of the mesomorphic state.

Polymers may be expected to be in the smectic state in the case of the so-called "herring-bone" geometrical arrangement [50]. The side chains on both sides of the main chain lie in one common plane and are perpendicular to the average direction of the main chain. The molecular strings formed in such a way are arranged in parallel forming a symmetrical layer.

The nematic state is expectable with molecules of cylindrical symmetry, therefore, in our assumption this state is characteristic for helical polymer chains. Completing published data with our own experimental results, we wish to give a comprehensive view of thermotropic mesomorphic polymer states in our present paper.

Experimental

The texture of the polymers was studied by the use of a polarization microscope (Zeiss Polmi A) [43]. Plasticity was tested by Höppler's consistometer [43]. Small angle diffractograms were recorded on a Rigaku Denki diffractometer and the results evaluated by GUINIER's method [51, 52]. Wide angle records were made on a wide angle Philips powder diffractograph, using Ni-filtered Cu Kα radiation. X-ray diffraction was carried out by the transmission method with pellets prepared at room temperature under 200 MN/m^2 pressure. The pellets were broken up and after treatment with Au, the surface of fracture was studied by scanning electron microscopy. X-ray diffractograms recorded for samples below room temperature were taken by the reflection method at a rate of 1°/min of 2Θ.

Syntheses of the polymers studied were described in our earlier publications [14—19; 41, 46].

Results and Discussion

Smectic polymers

Smectic polymers were expected to form in the course of homogeneous polymerization in the smectic phase [5, 14—19, 41]. Figures 3 and 4 show the X-ray diffractograms of poly(cetyl vinyl ether) and poly(cetyl methac-

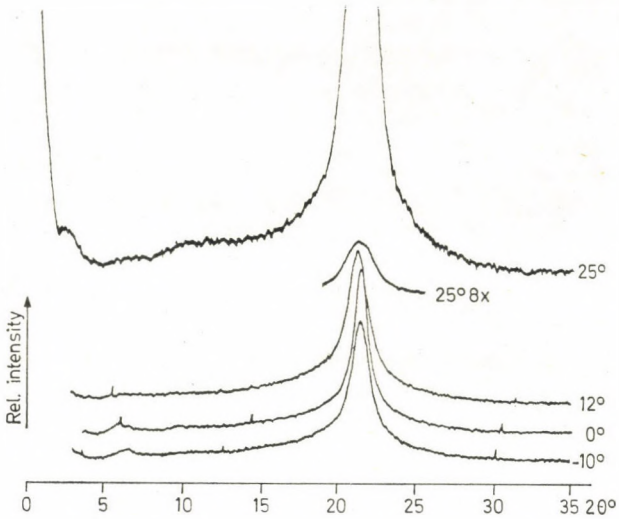

Fig. 3. X-ray diffractogram of poly(cetyl vinyl ether)

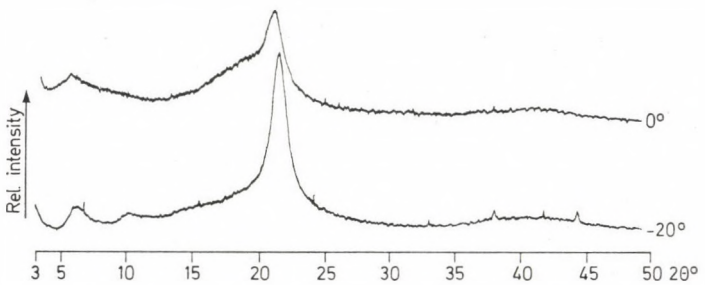

Fig. 4. X-ray diffractogram of poly(cetyl methacrylate)

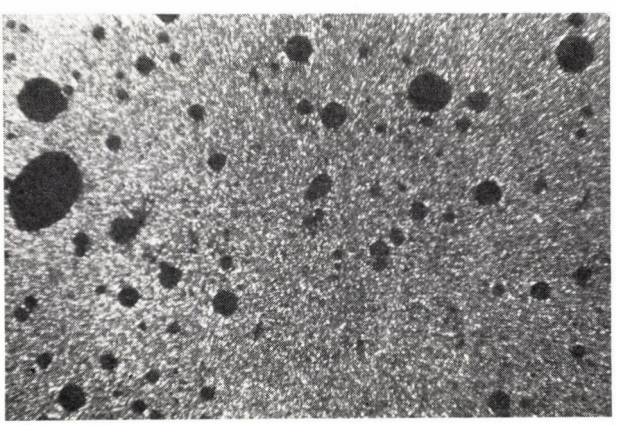

Fig. 5. Polarization micrograph of poly(cetyl vinyl ether)

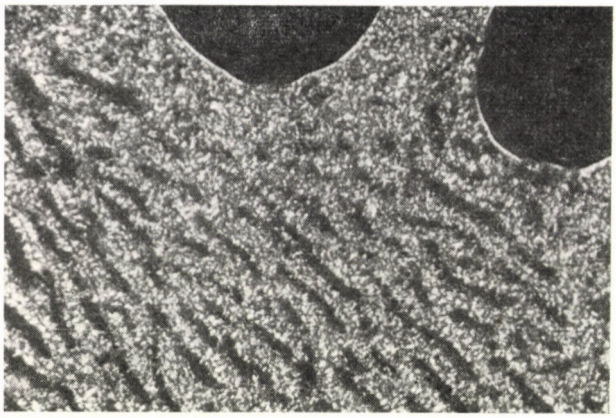

Fig. 6. Polarization micrograph of poly(cholesteryl vinyl succinate)

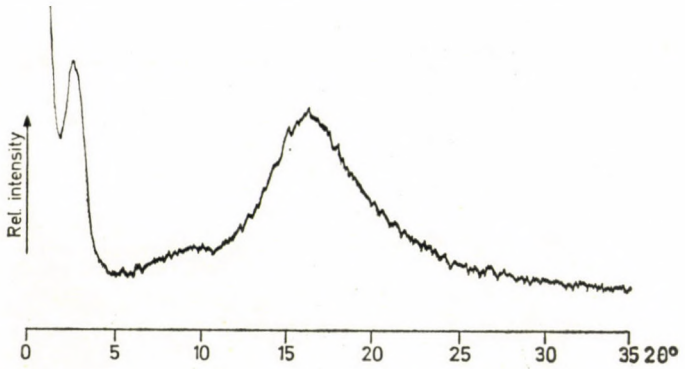

Fig. 7. X-ray diffractogram of poly(cholesteryl vinyl succinate)

rylate) at different temperatures, respectively. The peaks observed in the small angle range reflect the double length of the side chain and its 2nd and 3rd order reflections. The sharp peak in the wide angle range reflects „crystallization" of the hexagonal vide chain in the smectic B state [3]. As can be seen in the case of poly(cetyl vinyl ether), the intensity of the peak representing the packing of side chains decreases and the harmonics of the layer period disappear at higher temperatures. This phenomenon can be observed on transition from smectic B to smectic C or A, respectively [36]. Similar results were reported for vinyl polymers [50, 55] substituted by various long carbon chains. The polarized microphotograph of poly(cetyl vinyl ether) depicted in Fig. 5 shows a focal conic texture. A similar texture can be observed with poly(cetyl methacrylate) at −10 °C. Figure 6 presents the micrograph of poly-(cholesteryl vinyl succinate). Its X-ray pattern can be seen in Fig. 7 ; comparison of the possible interpretations of this diffractogram with the results

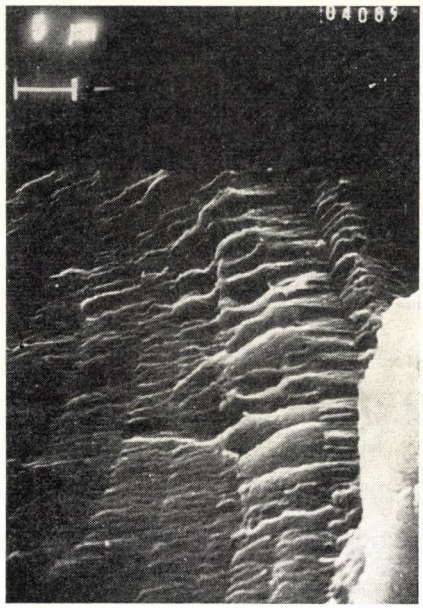

Fig. 8. SEM of poly(cholesteryl vinyl succinate); magnification: 6100×

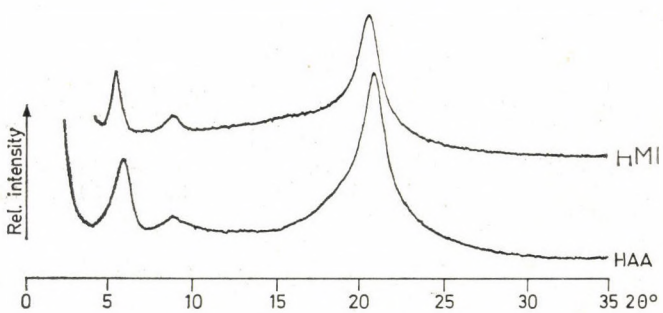

Fig. 9. X-ray diffractogram of poly(hexadecylacrylamide) and poly(hexadecylmethacrylamide)

of earlier investigations [19] points to the smectic structure of the polymer. No harmonics of the layer period can be seen in the diffractogram. Since the peak representing the packing of the side chain is diffuse (smectic C), the diffractogram does not essentially differ from that of polymers with cylindrical shape, as will be seen later. The laminar structure of poly(cholesteryl vinyl succinate) determined by SEM is well discernible in Fig. 8. Figure 9 displays diffractograms of hexadecylacrylamide and metacrylamide polymers in smectic B phase.

The smectic polymers studied were plastic under high pressure. The polymer blocks pressed from powder or prepared from solution were rigid, rather brittle, with a sharp and marked melting point (Table I).

Table I

Characteristics of the polymers studied

Polymer	T_m °C	D nm	$n(D)$ —	d nm	$n(d)$ —	Length of a monomer unit (nm)
Poly(cetyl vinyl ether)	38—40	3.33	2.7	0.417	21.5	2.63
Poly(cetyl methacrylate)						
at —20°	0—6	2.83	2.6	0.414	33.2	2.8
at 0°		2.95	1.9	0.419	?	
Poly(cholesteryl vinil succinate)	190	3.39	3.7	0.54	6.0	2.95
Poly(hexadecylacrylamide)	100	2.95	7.5	0.427	26.3	2.8
Poly(hexadecylmethacrylamide)	80—90	3.15	9.3	0.433	29.6	2.8
Poly(phenyl *p*-acryloiloxybenzoate)	200—220	2.52	2.9	0.46	4.9	1.65
Poly(*p*-butoxy phenyl-*p*-acryloiloxybenzoate)	300[d]	3.93	2.8	0.437	5.9	1.9
Poly(cholesteryl acrylate)	300[d]	3.05	2.9	0.568	5.1	2.7
Poly(cholesteryl vinyl fumarate)	300[d]	3.33	2.2	0.557	5.7	3.3
Poly(butyl ithaconate)	120—140	1.61	2.1	0.455	6.0	1.29
Poly(octyl ithaconate)	60—80	2.76	2.0	0.46	5.8	1.79

d = melting with degradation
n = periodicity number calculated from the line width of the reflexion peak

Vinyl polymers, where a bulky substituent was attached to the vinyl group through a soft, elastic alkyl chain, were found to be smectic [34, 35, 56]. In polymers with a soft main chain, the smectic structure could be detected for folded chains of polypropylene [57] and polyethylene, respectively. In the case of these polymers the smectic state appears macroscopically similar to the spherolite structure. The polymer of cholesteryl methacrylate was also found to be smectic [25].

Nematic polymers

The only structural feature to be expected for nematic polymers is that the molecules are approximately parallel with their long axes. In this respect they are similar to their oriented amorphous polymers. The most essential difference between oriented amorphous and nematic polymers is [49] that the orientation of molecules in the nematic polymer is spontaneous, therefore, the system is thermodynamically in the vicinity of minimum free energy, whereas the orientation of molecules in amorphous substances is a state artificially created under the effect of some field of force and is frozen, *i.e.* it is far from the minimum of the free energy. Therefore, this orientation is an unstable state of the substance, which ceases upon approaching equilibrium after the elapse of a certain period (possibly over several years).

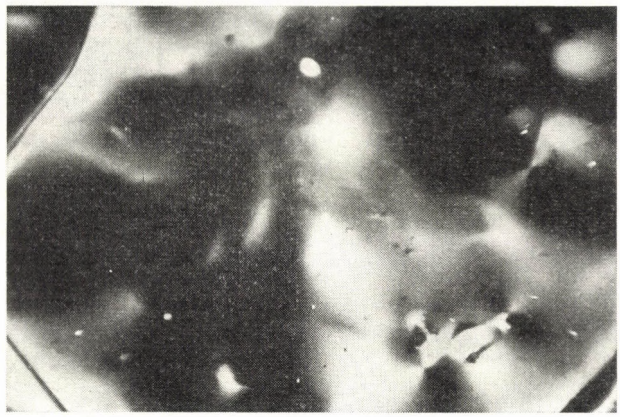

Fig. 10. Polarization micrograph of a poly(phenyl *p*-acryloiloxy benzoate)film

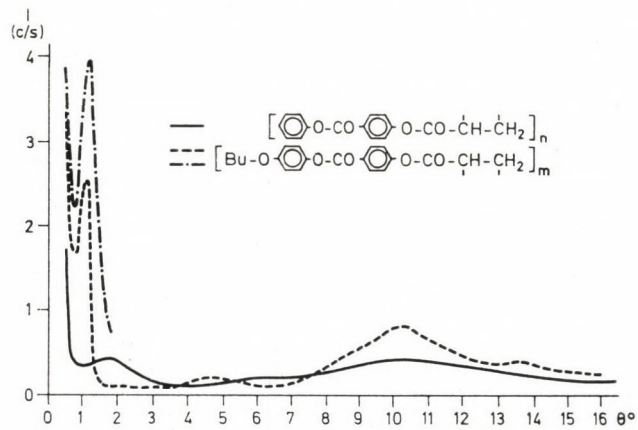

Fig. 11. X-ray diffractogram of poly(phenyl *p*-acryloiloxybenzoate) and poly(*p*-butoxyphenyl *p*-acryloiloxybenzoate)

The system with a cylindrical heterogeneous phase developed upon mechanical effects of ABA block copolymers cannot be considered as nematic polymers [58], though these substances show nematic properties and may be considered essentially as extrapolated macroscopic reflexions of such equilibrium systems.

Figure 10 presents the polarization micrograph of a polymer film prepared from a chloroform solution of poly(phenyl *p*-acryloiloxybenzoate). The mesomorphic structure has the Schlieren texture [59] characteristic of nematic substances. The range of singularities is, however, much larger than in the case of nematic substances with low molecular weight.

Figure 11 displays the X-ray diffractograms of poly(phenyl *p*-acryloiloxybenzoate) and poly(*p*-butoxy *p*-acryloiloxybenzoate). A broad maxi-

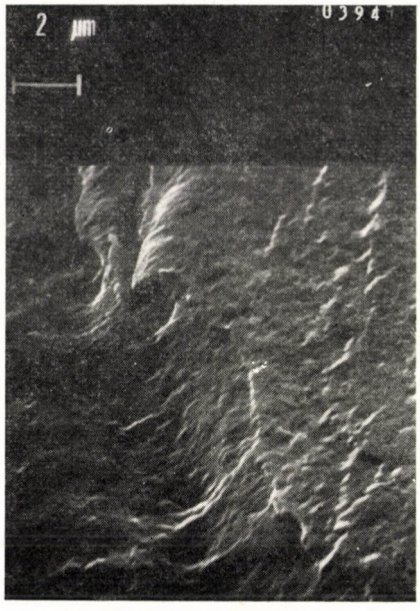

Fig. 12. SEM micrograph of poly(*p*-butoxy phenyl-*p*-acryloilhydroxybenzoate); magnification: 6100×

mum can be observed in the range of small angles. On the basis of the line width, periodicity extends, however, only as far as the 3rd or 4th neighbour. The value of periodicity is higher than the length of the side chain but lower than the double length of the molecule. A similar X-ray diffractogram can be observed for *p*-metoxy-, as well as for *p*-ethoxy- and *p*-propoxyphenyl *p*-acryloiloxybenzoate polymers. Small angle X-ray scattering shows the diameter of the cylinder of the rigid polymer molecule [47].

On the basis of GPC measurements as well as of the Guinier's plot of the small angle X-ray scattering of the polymer, its molecules can be considered as rigid cylinders with a length to diameter ratio of approximately 3–4.

Figure 12 shows the SEM pattern of poly(*p*-butoxyphenyl *p*-acryloiloxybenzoate). The thread-like texture can be readily observed in contrast to the lamellar texture of poly(cholesterylvinylsuccinate) shown in Fig. 8. The SEM pattern of the polymers obtained from other *p*-alkoxyphenyl *p*-acryloiloxybenzoates show also many similarities to that presented on Fig. 12 [47].

The nematic-phase polymer is described in the literature as a polymer prepared from a monomer having a nematic state. The nematic state has been determined mainly on the basis of whether or not a peak comparable with the length of the side chain could be detected in the X-ray diffractogram of the

optically anisotropic polymer. In the absence of this peak, the polymer was considered to be in the nematic state. Our investigations showed [47—48], however, the diameter of the enveloping surface of the polymer helix to appear in the diffractogram. In our opinion, if the diagram shows a reflexion whose d spacing corresponds to or is longer than the length of the monomer, this does not exclude the existence of the nematic polymer. The appearance of the harmonic of this line points, however, to the smectic state. The "sharpness" of the first reflexion is also relative, *i.e.* the identical line widths measured at different reflection peaks point to different distances of arrangements D [see Eq. (1)]:

$$n = \frac{R}{D} = \frac{K\lambda}{\beta \cos \Theta^0} \Big/ \frac{\lambda}{2 \sin \Theta^0} = \frac{K \operatorname{tg}(\Theta^0)}{2\beta}, \tag{1}$$

where β denotes the half line width (rad) at the half height of the peak, λ denotes wavelength, $K \sim 1$, D is the period assigned to the peak maximum (Θ^0) and R is the crystallite size assigned to line width.

The film or pellets prepared from nematic polymers are much more elastic and harder even in the glassy state than those obtained from polymers in the smectic phase. In the case of identical substituents, the clearing point of the nematic polymer is at a higher temperature than that of the smectic polymer (see Table I). In the smectic phase, the side chains along both sides of the main chain are in a two-dimensional crystalline state. The chain melting is expected to proceed, therefore, similarly to the process of crystal melting. The position of side chains in aperiodic helices corresponds to their position in glassy amorphous systems [47]. In melting, cylindrical symmetry ceases upon further destruction of the bulkier molecular blocks in disordered state due to the stretching effect of repulsion forces. Anisotropic rigid bodies tens of thousands in molecular weight cannot be expected to take statistically disoriented positions, for this would require an extremely great destruction of the packing. Further desctruction of the aperiodic helix usually takes place with the cleavage of chemical bonds.

Cholesteric polymers

As pointed out in the Introduction, the cholesteric state is characteristic of molecules containing chiral carbon atoms. Therefore, helical polymers are presumably in this state in the case of a parallel helical arrangement, provided the monomer is not racemic. In the course of vinyl polymerization, the configuration of subsequent asymmetric C atoms is identical in isotactic chain segments. This does not imply that the polymer is macroscopically capable of optical rotation because the probabilities for the formation of d and l chains are identical. In the unit cells of crystalline vinyl type helical

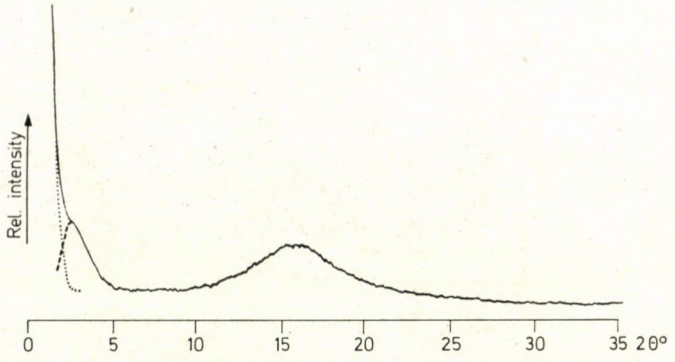

Fig. 13. X-ray diffractogram of poly(cholesteryl acrylate)

polymers, the right and left handed helices are simultaneously present. In other words, this means that the polymer is racemic [60]. Racemic substances have no cholesteric state while the mixture (1 : 1 ratio) of originally cholesteric *d* and *l* molecules is nematic.

This is not the case when the substituent of the vinyl chain contains an asymmetric atom. The nematic state of such polymers appears then as the cholesteric state [10—12].

Figure 13 presents the X-ray diffractogram of poly(cholesteryl acrylate). Similarly as in Fig. 11, a reflexion corresponding to the diameter of the molecule can be detected in the small angle range, which points to a cylindrical diameter of 3 nm. This value is higher than the length of the side chain but lower than the layer periodicity in the tilted, double, smectic monomer layer.

In Figure 14 we may see the SEM pattern of poly(cholesteryl acrylate). The fracture surface of the polymer pellet resembles that of a glassy amorphous polymer and no fine structure can be observed.

The polymerization of cholesteryl vinyl fumarate was described in a previous paper [41, 42]. It could be observed that the polymer in interaction with its monomer had a cholesteric phase. The X-ray diffractogram of the polymer is presented in Fig. 15. The diffractogram corresponds essentially to the patterns presented earlier. The diameter of enveloping surface of the polymer helix is 3.4 nm.

The clearing point of the polymer is 300 °C (with decomposition) its melting point is, however, 190 °C [41]. In the polymer-monomer phase diagram, the appearance of a cholesteric phase was observed at the side of the polymer, which becomes glassy upon cooling. The colour characteristic of the cholesteric state gradually shifts with the decrease of monomer content from the visible to the UV range. The cholesteric state freezes at 90 °C and the characteristic coloured light scattering persists at room temperature for years.

Fig. 14. SEM micrograph of poly(cholesteryl acrylate); magn.: 6100

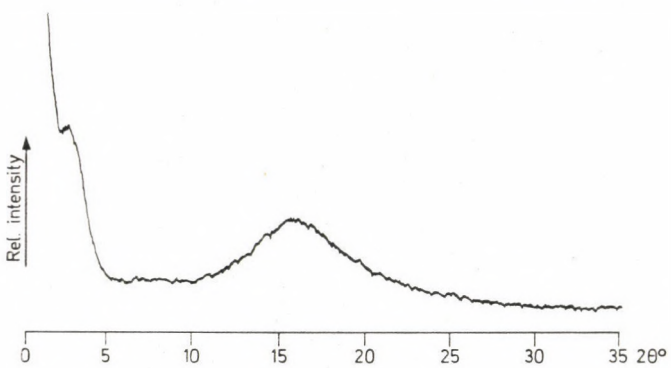

Fig. 15. X-ray diffractogram of poly(cholesteryl vinyl fumarate)

In the course of copolymerization of monomers containing a cholesteryl group, FINKELMANN [35] found the copolymer to be cholesteric in an extremely narrow range of composition, whereas in all other ranges the substance proved to be smectic. These states were determined on the basis of an X-ray diagram and the cholesteric state was identified by the polarization of circular light reflection.

Accordingly, it may be stated that under certain conditions which are not known yet, the diffractogram of smectic polymers shows a striking resemblance to those of nematic and cholesteric polymers.

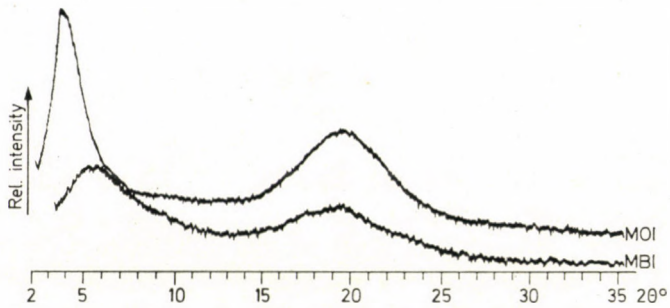

Fig. 16. X-ray diffractogram of poly(β-butyl ithaconate) and poly(β-octyl ithaconate)

Figure 16 shows the X-ray diffractogram of poly(β-monobutylithaconate) and poly(β-monocetylithaconate) [61]. In the small angle scattering range a relatively sharp peak can be observed. The corresponding spacing increases with growing length of side chains. The polymers are, however, isotropic. No other properties seem to justify the assumption of their mesomorphic states. In the case of *N*-substituted maleimide polymers, BARRALES RIENDA *et al.* [62] observed diffuse peaks shifted towards smaller reflexion angles inversely proportional to the length of the side chain. Reflections corresponding to the diameter of the enveloping surface of the helical molecule were shown earlier in the X-ray diffractogram of poly-acenaphthylene [63]. Thus, a diffuse peak with an identity period corresponding to the diameter of the molecular helix observed in the X-ray diffractograms is, in itself, not sufficient to justify the assumption of a mesomorphic polymer.

In the case of mesomorphic polymers, an enthalpy change of some 100 J/mol monomer unit may be discerned in the range of the clearing point. A similar enthalpy change can be recorded by the DSC method if measurements are carried out on an amorphous isotropic polymer with rapid scanning through the glass temperature. The fact that an enthalpy change can be measured during heat treatment of the polymer does not sufficiently support the assumption of the mesomorphic state of the polymer. The only reliable method is to determine the thermotropic anisotropy by the use of a polarization microscope. This is, namely, the most essential requirement of the mesomorphic state. The mesomorphic state cannot be identified, however, solely on the basis of polarization microscopic investigations. An unambiguous solution to the problem can be attained only by a series of complex parallel investigations performed by different methods.

The number of polymers in the thermotropic mesomorphic state reported in the literature is rather high. The general experience is that if the substituent of the vinyl monomer is relatively rigid and attached directly to the main chain, the formation of less bulky helices in the nematic (cholesteric) state

may be observed. In our experience, ambient conditions of polymer formation do not significantly affect the tacticity of the main polymer chain [34, 35] and have, consequently, no substantial effect on the polymer structure. Isotactic or syndiotactic polymer chains form crystallizing helices [60]. Smectic polymers are expected to form if the vinyl group is separated from the rigid bulky side chain by elastic carbon chains or if the substituent is entirely an elastic carbon chain [34, 56]. If the side chain is an alkyl chain, the smectic state may be expected in the presence of carbon chains longer than C_6 [50].

REFERENCES

[1] HERMANN, C.: Z. Kristallogr., **79,** 186 (1931)
[2] VRIES, A. D.: Mol. Cryst. Liquid Cryst., **10,** 219 (1970)
[3] DIELE, S., BRAND, P., SACKMANN, H.: Mol. Cryst. Liquid Cryst., **16,** 105 (1972)
[4] DIELE, S., BRANDT, P., SACKMANN, H.: Mol. Cryst. Liquid Cryst., **17,** 163 (1972)
[5] FLORY, P. J.: Proc. R. Soc. London, A **234,** 73 (1956)
[6] FLORY, P. J.: J. Polymer Sci., **49,** 105 (1961)
[7] FLORY, P. J.: Polym. Prepr., Am. Chem. Soc., **17,** 46 (1976)
[8] MORGAN, P. W., KWOLEK, S. L.: J. Polymer Sci., A **2,** 181, 209 (1964)
[9] MORGAN, P. W.: Macromolecules, **10,** 1381 (1977)
[10] ROBINSON, C.: Trans. Faraday Soc., **52,** 571 (1956)
[11] SAMULSKI, E. T., TOBOLSKY, A. V.: Macromolecules **1,** 555 (1968)
[12] PAPKOV, S. D., KULITSICHIN, V. G.: Zhidkokrystallicheskoe Sostoyanie Polimerov (Liquid Craystalline State of Polymers). Khimiya, Moscow 1977.
[13] SADRON, C.: Pure Appl. Chem., **4,** 347 (1962)
[14] HARDY, GY., NYITRAI, K., CSER, F., CSELIK, GY., NAGY, I.: European Polymer J., **5,** 133 (1964)
[15] HARDY, GY., CSER, F., KALLÓ, A., NYITRAI, K., BODOR, G., LENGYEL, M.: Acta Chim. Acad. Sci. Hung., **65,** 287 (1970)
[16] HARDY, GY., CSER, F., FEDOROVA, N., BÁTKY, M.: Acta Chim. Acad. Sci. Hung. **94,** 274 (1977)
[17] NYITRAI, K., CSER, F., SEYFRIED, É., HARDY, GY.: European Polymer J., **13,** 673 (1977)
[18] CSER, F., NYITRAI, K., SEYFRIED, É., HARDY, GY.: European Polymer J., **13,** 678 (1977)
[19] NYITRAI, K., CSER, F., CSERMELY, G., BUI DYC GNOC, HARDY, GY.: European Polymer J. **14,** 467 (1978)
[20] AMERIK, YU. B., KRENTSEL, B. A.: J. Polymer Sci, C **16,** 1383 (1967)
[21] AMERIK, YU. B., KONSTANTINOV, I. I., KRENTSEL, B. A.: J. Polymer Sci., C **23,** 231 (1968)
[22] BACON, W. E.: J. phys., **36,** C1 409 (1975)
[23] BLUMSTEIN, A., KITAGAWA, Y., Y., BLUMSTEIN, R.: Mol. Cryst. Liquid Cryst. **12,** 215 (1971)
[24] BLUMSTEIN, A., BLUMSTEIN, R., CLOUGH, S. B., HSU, E. C.: Macromolecules, **8,** 73 (1976)
[25] BLUMSTEIN, A., OSADA, Y., CLOUGH, S. B., HSU, E. C., BLUMSTEIN, R.: Polym. Prepr., Am. Chem. Soc. **18,** 14 (1977)
[26] HSU, E. C., BLUMSTEIN, A.: J. Polymer Sci., Polym. Lett. Ed., **15,** 120 (1977)
[27] LIEBERT, L., STRZELECKI, L.: Bull. Soc. Chim. Fr., **1973,** 603.
[28] LIEBERT, L., STRZELECKI, L.: Compt. Rend. Acad. Sci. C **276,** 647 (1973)
[29] LORKOWSKI, H. J., REUTHER, F.: Plaste und Kautschuk, **23,** 81 (1976)
[30] PALEOS, C. M., LABES, M. M.: Mol. Cryst. Liquid Cryst., **11,** 385 (1970)
[31] PERPLIES, E., RINGSDORF, H., WENDORFF, J. H.: Makromol. Chem., **175,** 385 (1970)
[32] PERPLIES, E., RINGSDORF, H., WENDORF, J. H.: J. Polymer Sci., Polym. Lett. Ed., **13,** 243 (1975)
[33] WENDORFF, J. H., PERPLIES, E., RINGSDORF, H.: Progr. Colloid Polym. Sci., **57,** 272 (1975)
[34] WENDORFF, J. H., FINKELMANN, H., RINGSDORF, A.: Polym. Prepr. Am. Chem. Soc., **18/2,** 5 (1977)

[35] FINKELMANN, H., RINGSDORF, H., WENDORFF, J. H.: Makromol. Chem., **179,** 273 (1978)
[36] HARDY, GY., CSER, F., NYITRAI, K., FEDOROVA, N.: Proc. IVth Tihany Symposium on Radiation Chemistry. Ed. P. HEDVIG and R. SCHILLER, p. 365. 1977. Akadémiai Kiadó
[37] TSVETKOV, V. N., RYUMTSEV, E., KONSTANTINOV, I. I., AMERIK, YU. B., KRENTSEL, B. A.: Vysokomol. Soedin., A **14,** 67 (1972)
[38] TSVETKOV, V. N.: Vysokomol. Soedin., A **11,** 132 (1969)
[39] TSVETKOV, V. N., SHTENNIKOVA, J. N., RYUMTSEV, E. I., KOLBINA, G. F., KONSTANTINOV, I. I., AMERIK, YU. B., KRENTSEL, B. A.: Vysokomol. Soedin., A **11,** 2528 (1969)
[40] SACKMANN, H., DEMUS, D.: Mol. Cryst. Liquid Cryst., **21,** 239 (1973)
[41] CSER, F., NYITRAI, K., HARDY, GY.: Polym. Prepr., Am. Chem. Soc., **18/2,** 21 (1977)
[42] CSER, F., NYITRAI, K., HARDY, GY.: J. Polymer Sci., C **61,** 9 (1977)
[43] HARDY, GY. CSER, F., KOVÁCS, G., SZATMÁRI, J., SAMAY, G.: Acta Chim. Acad. Sci. Hung., **79,** 143 (1973)
[44] HARDY, GY., KOVÁCS, G., KOSZTERSZITZ, G., FEDOROVA, N., CSER, F.: Proc. IIIrd Tihany Symposium on Radiation Chemistry, Ed. by J. DOBÓ and P. HEDVIG, p. 601. Akadémiai Kiadó, Budapest
[45] HARDY, GY., CSER, F., TAKÁCS, E.: J. Polymer Sci., C **42,** 663 (1973)
[46] NYITRAI, K., LAN, N. G., CSER, F., TAKÁCS, E., HARDY, GY.: Magyar Kém. Folyóirat, **82,** 76 (1976)
[47] HARDY, GY., CSER, F., NYITRAI, K., SAMAY, G., KALLÓ, A.: J. Crystal Growth, accepted for publication.
[48] CSER, F., PÓCSIK, I., TOMPA, K., MENCZEL, J.: unpublished data.
[49] CSER, F.: Main lecture, 7th Liquid Crystal Congress, Bordeaux France, July 1—5, 1978.
[50] PLATE, N. A., SHIBAEV, V. P.: Macromol. Rev., **8,** 117 (1974)
[51] GUINIER, A.: Compt. Rend. Acad. Sci., **204,** 1115 (1937)
[52] KRATKY, O.: Progr. Biophysics, **13,** 107 (1963)
[53] HARDY, GY., NYITRAI, K., KOVÁCS, G., FEDOROVA, N.: Acta Chim. Acad. Sci. Hung., **43,** 121 (1965)
[54] MOROSOFF, N., MORAWETZ, H., POST, B.: J. Am. Chem. Soc., **87,** 3035 (1965)
[55] PUTERMANN, M., FORT, T., LANDO, J. B., *Jr.:* J. Coll. Int. Sci. **47,** 705 (1974)
[56] SHIBAEV, V. P., FREYDZON, YA. S., PLATE, N. A.: Vysokomol. Soedin. A **20,** 82 (1978)
[57] SMIT, P. P. A.: Kolloid Z. Z. Polym., **250,** 27 (1972)
[58] SKOULIOS, A. S.: "Mesomorphic Properties of Block Copolymers", in Advances in Liquid Crystals. Ed. G. H. BROWN, Vol. **1.** p. 169. Academic Press, New York 1975.
[59] BROWN, G. H., SHAW, N. G.: Chem. Rev., **57,** 1049 (1957)
[60] NATTA, G., CORRADINI, P.: Industrie Chim. Belge, **1,** 1 (1964)
[61] NYITRAI, K., NGUYEN, NGOC LAN, HARDY, GY.: Acta Chim. Acad. Sci. Hung., **88,** 195 (1976)
[62] BALTA-CALEJA, F. J., RAMOS, J. G., BARRALES-RIENDA, J. M.: Kolloid Z., Z. Polym., **250,** 474 (1972)
[63] CSER, F., HARDY, GY.: Acta Chim. Acad. Sci. Hung., **84,** 297 (1975)

Ferenc CSER
Károly NYITRAI
Gyula HARDY
H-1950 Budapest, Hungária krt. 114.

Acta Chimica Academiae Scientiarum Hungaricae, Tomus 100 (1—4), pp. 481—498 (1979)

VIBRATIONAL SPECTRA OF *m*-DINITRO-BENZENE DERIVATIVES

G. VARSÁNYI[1,2], É. MOLNÁR-PAÁL[1], K. KÓSA[1] and G. KERESZTURY[2]

([1] Department of Physical Chemistry, Technical University, Budapest, [2] Central Research Institute for Chemistry of the Hungarian Academy of Sciences, Budapest)

Received July 22, 1978

Accepted for publication August 16, 1978

Of the vibrational spectra of 39 *m*-dinitrobenzene derivatives a detailed assignment of the infrared and Raman spectra of *m*-dinitrobenzene, 2,6- and 2,4-dinitrotoluene, 2,4-dinitrophenylacetic acid and its methyl ester is given. The correlation of nitro stretching frequencies with the Hammett sigma of other substituents has been studied. Only the frequencies of derivatives substituted in identical positions can be compared and the different kinds of substituents in *meta* position do not affect the frequencies. The frequency of the out-of-phase component of the symmetric stretching vibrations is anomalously low in the spectra of aniline derivatives. Hot bands joined to the $\nu_{as}NO_2$ band offer the conclusion that in the excited state of this vibration the frequency of the twisting mode is lower.

Introduction

Several authors have studied the influence of substituents on the frequencies and band intensities of the nitro group in infrared and Raman spectra of nitrobenzene derivatives [1]. We may mention *e.g.* the investigations of BROWN [2], KROSS and FASSEL [3], and VARSÁNYI, HOLLY and IMRE [4] into correlations of NO stretching frequencies with substituents, the observations of SHORYGIN and ILICHEVA [5] and NAKASHIMA [6] involving the effect of steric hindrance on the same frequencies, the findings of HORÁK and coworkers [7] on the strong overtones of nitro stretching vibrations in the infrared spectra of dinitrobenzene derivatives, and the remarks of KATRITZKY and SIMMONS [8] on scissoring frequencies depending on the position of the substituents. In spite of the many assigned spectra available, no systematic treatment of the vibrational spectra of *m*-dinitrobenzene derivatives has been published so far.

Classification of spectra

The vibrational spectra of 39 *m*-dinitrobenzene derivatives have been studied. The assignment or at least a comparative analysis of similar normal vibrations in the majority of spectra has been reported earlier, however some of these are first assigned in the present paper. The compounds investigated (nitro groups systematically in positions 1 and 3) were as follows:

	2	4	5	6	
1	—	—	—	—	[9], [10], [11], [12]
2	CH_3	—	—	—	
3	OH	—	—	—	[13]
4	NH_2	—	—	—	[13]
5	—	CH_3	—	—	[14]
6	—	CH_2COOH	—	—	
7	—	CH_2COOCH_3	—	—	
8	—	F	—	—	[15], [16]
9	—	OH	—	—	[13], [14]
10	—	OC_2H_4Br	—	—	[13]
11	—	NH_2	—	—	[13]
12	—	$NHNH_2$	—	—	[13]
13	—	Cl	—	—	[15], [16], [17]
14	—	Br	—	—	[17]
15	—	—	NO_2	—	[18], [19]
16	D	D	NO_2	D	[18], [19]
17	—	—	COCl	—	[13]
18	—	—	COOH	—	[13]
19	OH	—	CN	—	[20]
20	OH	—	OH	—	[20]
21	OCH_3	—	CN	—	[20]
22	OCH_3	—	OH	—	[20]
23	OH	—	$OCOCH_3$	—	[20]
24	OH	—	OSO_2CH_3	—	[20]
25	OCH_3	—	OSO_2CH_3	—	[20]
26	NHC_2H_5	—	CN	—	[20]
27	$N(CH_3)_2$	—	CN	—	[20]
28	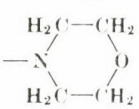	—	CN	—	[20]
29	OH	—	NO_2	—	[13], [20]
30	—	OH	COOH	—	[20]
31	—	CH_3	Br	—	[20]
32	—	CH_2OH	Br	—	[20]
33	—	$CONH_2$	Br	—	[20]
34	—	CN	Br	—	[20]
35	—	F	Br	—	[20]
36	—	NH_2	Br	—	[20]
37	—	Cl	$CONH_2$	—	
38	—	Cl	Br	—	
39	NH_2	NH_2	NO_2	NH_2	[21]

A detailed study has been made of the IR (60—3500 cm^{-1}) and Raman spectra of the following five compounds : *m*-dinitrobenzene (parent compound of the series, the detailed assignment of which was given earlier [11], but had to be partly modified according to our experiments), 2,6-dinitrotoluene (2), 2,4-dinitrotoluene (5), 2,4-dinitrophenylacetic acid (6) and methyl-2,4-dinitrophenyl acetate (7). No interpretation has been given, however, of the IR spectra of 2-chloro-3,5-dinitrobenzamide (37) and 1-bromo-2-chloro-3,5-dinitrobenzene (38) either. In the last wo cases we refer only to the characteristic frequencies of the nitro groups.

Detailed investigation of spectra

***m*-Dinitrobenzene.** Following the detailed assignment reported by GREEN and LAUWERS [11], BOBROV and coworkers [12] have studied the polarized Raman and infrared spectra of the crystal. In the IR spectrum of the crystal we succeeded in indentifying two vibrations of a_2 species (16a, 17a) at 572 and 952 cm^{-1}, yielding also some combinations, *e.g.* the latter the intense benzene finger component at 1767 cm^{-1}. GREEN and LAUWERS estimated two frequencies at 500 and 900 cm^{-1}, without taking into account, however, that the 16a frequency, was higher than 500 cm^{-1} in the cpectra of all *m*-disubstituted benzenes except *m*-xylene. The 16a frequency of *m*-difluorobenzene proved to be 591 cm^{-1} [22], whereas the 17a frequency was without exception higher in the spectra of all *m*-disubstituted benzenes than that of the 17b vibration of b_1 species. The C—H out-of-plane ($\gamma C_{Ar}H$) frequencies of nitrobenzenes were found to be the highest of all benzene derivatives, therefore, the 916 cm^{-1} 17b frequency is not surprising (assigned so also by GREEN and LAUWERS) and the 17a frequency must be above this value.

GREEN and LAUWERS assigned the 572 cm^{-1} band to the second rocking (β_{as}) mode of the nitro group. However, the diffuse appearance of the 514 cm^{-1} band indicates the coincidence of the two components. In the solution spectrum the 572 cm^{-1} band is hardly observable, which supports our assignment to an a_2 vibration.

It is very difficult to identify vibration 9a, the in-plane bending of both complete nitro groups [$\beta C_{Ar}—(NO_2)$]. GREEN and LAUWERS assign a Raman frequency at 180 cm^{-1}. In agreement with BOBROV and coworkers, no band was found, however, between 162 and 196 cm^{-1} in the Raman spectrum studied. On the high wavenumber side of the 161 cm^{-1} infrared band a shoulder could be discerned, which at higher resolution separated from the main band. At the same time in the Raman spectrum of the solution the 162 cm^{-1} band proved to be partly polarized, confirming the accidental degeneracy of vibrations 9a and 10b. In the infrared spectrum the shoulder frequency was found to be 167

cm^{-1}. The frequency of the combination band found similarly in the infrared spectrum (363 cm^{-1}) was the sum of 167 and 196 cm^{-1} the latter belonging to vibration 10a found in the Raman spectrum. This demonstrates that 167 cm^{-1} belongs to the 10b vibration of b_1 species because 10a of a_2 symmetry cannot combine in the infrared with a completely symmetric vibration.

GREEN and LAUWERS have assigned the strong infrared band at 725 cm^{-1} to an in-plane vibration of b_2 species. The infrared crystal spectrum investigations of BOBROV and coworkers have proved the in-plane character and the correctness of the assignment. This is noteworthy because the 725 cm^{-1} frequency of vibration 7b is anomalously low, while that of the b_2 symmetry scissoring ($\beta_s NO_2$) of opposite phase is anomalously high (909 cm^{-1}). Coupling of the vibrations belonging to the same species, particularly that of the opposite-phase C—N stretching 7b and the opposite-phase $\beta_s NO_2$ can considerably separate the frequencies.

2,6-Dinitrotoluene. Assuming a cylindrical symmetry of the methyl group (according to the spectrum this is not quite justified), also this molecule can be assigned to point group C_{2v}. Without taking into consideration the methyl hydrogens, the molecule has 16 atoms and $3 \times 16 - 6 = 42$ normal vibrations. These are completed by the nine normal vibrations of the methyl group. The distribution of normal vibrations belonging to the skeleton is the following :

15 a_1 : 2 C—H stretchings ($\nu C_{Ar}—H$, 2, 7a), 1C—H bending ($\beta C_{Ar}—H$, 18a), 2 ring stretchings ($\gamma—C_{Ar}$, 8a, 19a), 3 more ring vibrations, breathing vibration enclosed (1, 6a, 12), 2 ring-substituent stretchings ($\nu C_{Ar}—X$, 13, 20a), 1 substituent in-plane bending ($\beta C_{Ar}—X$, 9a), further-more, one symmetric, ($\nu_s NO_2$) one antisymmetric stretching, ($\nu_{as} NO_2$) one scissoring ($\beta_s NO_2$) and one rocking ($\beta_{as} NO_2$) mode of the nitro group ;

5 a_2 : 1 $\gamma C_{Ar}—H$ (17a), 1 skeleton ($\gamma C_{Ar}—C_{Ar}$, 16a), 1 substituent out-of-plane vibration ($\gamma C_{Ar}—X$, 10a) and the wagging ($\gamma_s NO_2$) and twisting ($\gamma^{as} NO_2$) vibrations of the nitro group ;

8 b_1 : 2 $\gamma C_{Ar}—H$ (5, 11), 2 $\gamma C_{Ar}—C_{Ar}$ (4, 16b), 2 $\gamma C_{Ar}—X$ (10b, 17b) and the other $\gamma_s NO_2$ and $\gamma_{as} NO_2$ modes, and finally,

14 b_2 : 1 $\nu C_{Ar}—H$ (20b), 2 $\beta C_{Ar}—H$ (3, 9b), 3 $\nu C_{Ar}—C_{Ar}$ (8b, 14, 19b) 1 $\beta C_{Ar}—C_{Ar}$ (6b), 1 $\nu C_{Ar}—X$ (7b), 2 $\beta C_{Ar}—X$ (15, 18b), and the opposite phase $\nu_s NO_2$ and $\nu_{as} NO_2$ $\beta_S NO_2$ and $\beta_{as} NO_2$ vibrations.

The 9 methyl vibrations can be assigned to the pseudo-species : 3 stretchings (a_1, b_1, b_2), 3 bendings δ_s and δ_{as}^{+} (a_1, b_1, b_2) 2 rockings δ_{as}^{-} (b_1, b_2) and the twisting vibration (internal rotation, τ, a_2).

The frequency assignment was rather unambigous on grounds of the spectrum assignment of numerous 1,2,3-trisubstituted benzenes, particularly of molecules of higher symmetry, supported by normal coordinate calculations [13]. From Raman polarization properties one can establish a symmetry

Table I

m-Dinitrobenzene

IR	Raman	Int.	Sym.	IR	Raman	Int.	Sym.
	24 s	lattice		1384 w		415 + 980	A_1
	38 vs	lattice		1420 sh		2×716	A_1
	61 w	γ_{as}	a_2	1439 w	1440 w	19a	a_1
80 vs	78 vs	lattice		1468 w	1472 vw	19b	b_2
98 w	100 sh	lattice		1491 sh		1530−4×10	B_2
161 vs	162 m	9a	a_1	1500 sh		1530−3×10	B_2
167 sh		10b	b_1	1510 sh		1530−2×10	B_2
	196 m	10a	a_2	1516 sh		572 + 952	A_1
303 w	306 vw	15	b_2	1520 sh		1530−10	B_2
353 s	354 m p	6a	a_1	1530 vs		ν_{as}	b_2
363 sh		167 + 196	B_2	1541 vs	1538 s ?	ν_{as}	a_1
404 s	406 vw	6b	b_2	1557 sh		655 + 909	B_2
415 m	416 vw	16b	b_1	1560 sh		729 + 839	B_2
514 m d	514 w d	β_{as}	a_1−b_2	1571 sh		761 + 819	B_2
572 w		16a	a_2	1603 s	1604 s ?	8a	a_1
655 s	651 m dp	1, 4	a_1−b_1	1617 s	1620 vw	8b	b_2
716 vs	713 vw	γ_s	b_1	1631 sh		729 + 909	A_1
729 s	726 vw	7b	b_2	1656 w		655 + 1004	A_1
	761 w	γ_s	a_2	1702 vw		161 + 1541	A_1
764 w		196 + 572	A_1	1767 m		819 + 952	B_2
819 s	819 w	11	b_1	1828 m		2×916	A_1
839 s	839 s p	β_s	a_1	1948 m		2×980	A_1
909 s	908 w	β_s	b_2	2000 m		655 + 1350	A_1
916 s		17b	b_1	2260 vw		909 + 1350	B_2
952 vw		17a	a_2	2440 vw		909 + 1541	B_2
1004 m	1003 vs p	12	a_1	2492 w	2496 vw	1149 + 1350	A_1
1070 s	1073 vw	18a	a_1		2648 vw	1275 + 1375	A_1
1095 m	1095 vw	18b	b_2		2685 vw	2×1350	A_1
1123 vw		404 + 729	A_1	2740 w		2×1375	A_1
	1130 vw	2×572	A_1	2762 vw		1149 + 1617	B_2
1149 m	1149 s p	13	a_1	2815 vw		1275 + 1541	B_2
1171 w	1172 w	9b	b_2	2872 m		1350 + 1530	B_2
1257 w		353 + 909	B_2	2945 vw	2952 vw	1350 + 1603	A_1
1275 s	1276 vw	14	b_2	3048 w	3045 vw	7a	a_1
	1310 w	3	b_2	3080 sh		20a	a_1
1328 sh	1328 vw	572 + 761	A_1	3095 vw	3095 s p	2	a_1
1350 vs	1356 vs p	ν_s	a_1	3108 s		20b	b_2
1375 sh	1373 w	ν_s	b_2				

Table II

2,6-Dinitrotoluene

IR	Raman	Int.	Sym.	IR	Raman	Int.	Sym.
	22 vw	lattice			1360 sh	1368—8	A_1
	41 w	lattice		1363 sh	1368 vs p	ν_s	a_1
	48 m	lattice		1384 vw		467+935	B_2
70 sh	65 vs	γ_{as}	a_2	1389 m	1387 m p	δ_s	a_1
84 m	76 sh	lattice		1424 s	1422 w	19b	b_2
101 m	98 m	17b	b_1	1443 sh	1448 w	δ_{as}^+	b_2
	108 sh	lattice (τCH_3?)		1458 s		δ_{as}^+	b_1
				1470 sh	1470 w p	19a	a_1
	124 sh	10a	a_2	1487 sh		1528—4×8	B_2
189 s	181 s dp	10b	b_1	1505 sh		1528—3×8	B_2
226 w	228 vw dp	15	b_2	1515 sh		1528—2×8	B_2
	242 m	2×124	A_1	1520 sh	1521 s	ν_{as}	a_1
292 w	297 vw p	9a	a_1	1528 vs	1531 w ?	ν_{as}	b_2
329 s	329 m p	6a	a_1	1540 sh	1540 sh	732 + 819	A_1
365 sh	364 w	18b	b_2	1547 sh	1550 sh	388 + 1164	A_1
380 sh		2×189	A_1	1559 vw		365 + 1207	B_2
388 s	387 w	6b	b_2	1563 sh		687 + 893	B_2
446 w	449 w	16a	a_2	1575 m	1581 m ?	8a	a_1
467 m	466 w	16b	b_1	1613 vs	1613 w dp	8b	b_2
514 m	514 vw	β_{as}	a_1	1709 w		732 + 988	A_1
579 m	578 s p	1	a_1	1749 m		819 + 935	B_2
630 w	631 vw	189 + 446	B_2	1803 w		819 + 988	A_1
687 sh	689 w	12	a_1	1860 m		2×935	A_1
712 vs	712 w dp	4	b_1	1914 m		935 + 988	B_2
732 vs	730 w	γ_s	b_1	1970 m		2×988	A_1
755 w	758 w	γ_s	a_2		2596 w	2×1300	A_1
791 w	797 vs p	β_s	a_1		2697 vw	2×1350	A_1
819 vs	822 w	11	b_1		2750 vw	2×1387	A_1
841 m	841 s p	β_s	b_2		2845 vw p	2×1422	A_1
893 vs	896 vw dp	7b	b_2	2858 m		1348 + 1520	A_1
988 m		5	b_1	2870 vw		1348 + 1528	B_2
1024 vw		δ_{as}^-	b_1		2878 vw	2×1448	A_1
1031 w	1028 w p	δ_{as}^-	b_2	2905 w		2×1458	A_1
1081 s	1084 s p	18a	a_1	2930 m	2942 s p	ν_s	a_1
1132 w	1137 m p	13	a_1		2987 w	ν_{as}	b_2
	1164 m dp	9b	b_2	3013 w		1470 + 1520	A_1
1207 s	1206 s p	20a	a_1		3028 w	7a	a_1
1220 w	sh dp	329 + 893	B_2	3052 sh	3053 sh	2×1528	A_1
	1232 w	388 + 841	A_1	3064 sh			
1270 sh		467 + 819	A_1	3074 m	3078 s p	2	a_1
1299 m	1300 w dp	14	b_2	3082 w	3088 vw	1520 + 1575	A_1
1333 sh	1336 sh	1348—14	B_2		3098 s	20b	b_2
1348 vs	1350 sh dp	ν_s	b_2		3152 w	2×1581	A_1

degradation in the surroundings of the three neighbouring substituents originating from the asymmetric positions of the methyl hydrogens. In the more stable position one of the hydrogens lies in the ring plane, the other two are out of it. This follows from the polarized character of both $\beta_s NO_2$ bands and of the $\delta_{as}^{-}CH_3$ band assignable in the Raman spectrum, which can be interpreted only by an overall C_s symmetry where all these vibrations are symmetric (*a'*). Consequently, it is possible that the Raman shoulder at 108 cm^{-1} does not belong to a lattice vibration but to the τCH_3 mode.

The infrared band of the puckering vibration (4) is very strong, like in the spectra of all 1,2,3-trisubstituted benzenes. On the low wavenumber side of the stretching bands of the nitro group hot bands are to be found, supposed originating from the *v-v* transitions of the $\gamma_{as}NO_2$ vibration [4]. The benzene finger region is characteristic, containing the combination and overtone bands of C—H out-of-plane vibrations. Out of 9 possible bands, five can be identified. The approximate frequency of vibration 17a (not only infrared-inactive but unassignable also in the Raman spectrum) can be established from combinations (935 cm^{-1}).

2,4-Dinitrotoluene. The highest symmetry of the molecule is C_s. Regardless of the vibrations of the methyl hydrogens, the molecule possesses 29 in-plane (*a'*) and 13 out-of-plane (*a''*) vibrations. On the basis of infrared and Raman intensities, polarization properties and mainly of comparison to the spectra of many similarly assigned 1,2,4-trisubstituted benzenes, the assignment can be made. According to Raman polarization ratios, the assignment of two bands seems to be contradictory. In the Raman spectrum a relatively strong depolarized band is to be found at 638 cm^{-1} and a much weaker but polarized band at 670 cm^{-1}. One can expect in this region the breathing vibration of the ring loaded by substituents (1) and the puckering mode (4). The band of vibration 1 is generally strong in the Raman spectrum while that of vibration 4 is always weak. From intensity considerations, 638 cm^{-1} has to be assigned to vibration 1 and 670 cm^{-1} to vibration 4, especially because vibrational frequency 4 of 1,2,4-trisubstituted benzenes never lies below 650 cm^{-1}. Depolarization ratios, however, are in contradiction to this. The anomaly may be perhaps interpreted by the accidental degeneracy of the 638 cm^{-1} band and an *A''* symmetry combination (160 + 479 = 639), and of the 670 cm^{-1} and an *A'* symmetry combination (281 + 390 = 671) · 638 cm^{-1} is accidentally degenerated also with an *A'* symmetry combination (282 + + 352 = 634) causing Fermi resonance in the infrared spectrum.

Depolarization ratios seem to contradict to the assignment in one more case. Both bands belonging to the δ_{as}^{-} vibration are polarized although one of them has an *a''* symmetry. An accidental degeneracy arises also in this case with the overtone of the $\beta_{as}NO_2$ vibration, which is naturally polarized like

all overtones (1035, $2 \times 520 = 1040$). The νNO_2 bands are very broad: only one hot band can be identified as a shoulder. The combination of the $\nu_{as}NO_2$ frequencies and the overtone of the stronger IR component yields relatively strong bands in the infrared, corresponding to the observations of HORÁK and coworkers [7].

2,4-Dinitrophenylacetic acid and methyl-2,4-dinitrophenyl acetate. The frequencies of the aromatic ring differ but slightly from those of 2,4-dinitrotoluene (Fig. 1) and if they do, the difference can be interpreted by the longer side chain instead of the methyl group. The frequency differences of the acid and the ester do not originate, however, from the different lengths of the side chains, but rather from the dimeric structure of the acid. The dimeric structure partly increases the $\beta C_{Ar}-X$ frequency of the whole substituent (9a), similarly as holding down a string increases its pitch, partly decreases the $C_{Ar}-C$ bond order. This latter effect prevails in the slightly higher frequencies of vibrations 7a and 13 and in the lower one of vibration 6a of the ester. 7a and 13 are mainly $\nu C_{Ar}-X$ modes while 6a denotes a radial vibration of the ring loaded by substituents coupling with $\nu C_{Ar}-X$ vibrations.

Frequencies that cannot be attributed to the ring or nitro groups in the acid spectrum are as follows: 147, 176, 353, 489, 588, 766, 905, 942, 1182, 1274, 1316 cm^{-1} and other characteristic methylene, carbonyl and OH frequencies. 766, 1182 and 1316 are characteristic of the methylene group. The very strong IR band at 905 cm^{-1} belongs to the γOH vibration of the dimeric acid. 588 and 1274 cm^{-1} can be considered as characteristic of the carboxy and 942 cm^{-1} of the C—C stretching in the side chain. Thus only the four lowest frequencies should be assigned. It is obvious that the two higher frequencies belong to in-plane bending vibrations, namely 489 cm^{-1} to the C—(OH) group and 353 cm^{-1} to the chain $C(H_2)-C(=O)-O(H)$. The two lower frequencies are probably due to out-of-plane vibrations of the same groups. These would be internal rotations in the monomeric acid but are real vibrations in the dimer. The νOH vibration appears in the dimeric structure in six separate strong bands consisting of two equidistant triplets between 2545 and 2998 cm^{-1}. Band separation of the first triplet is 90, that of the other 72 cm^{-1}. The band structure can be interpreted also by Fermi resonances, all six bands corresponding to combinations of skeletal or nitro group vibrations. The usually very strong band of the $\nu C=O$ vibration is to be found at 1692 cm^{-1} in the infrared, it does not appear, however, in the Raman spectrum. A very weak band belonging to the centro-symmetric $\nu C=O$ vibration of the dimer is observed instead at 1640 cm^{-1}, while 1692 cm^{-1} belongs to the antisymmetric mode.

The frequencies which cannot be assigned to the ring or the nitro groups in the acetate spectrum are the following: 177, 287, 599, 766, 987, 1166,

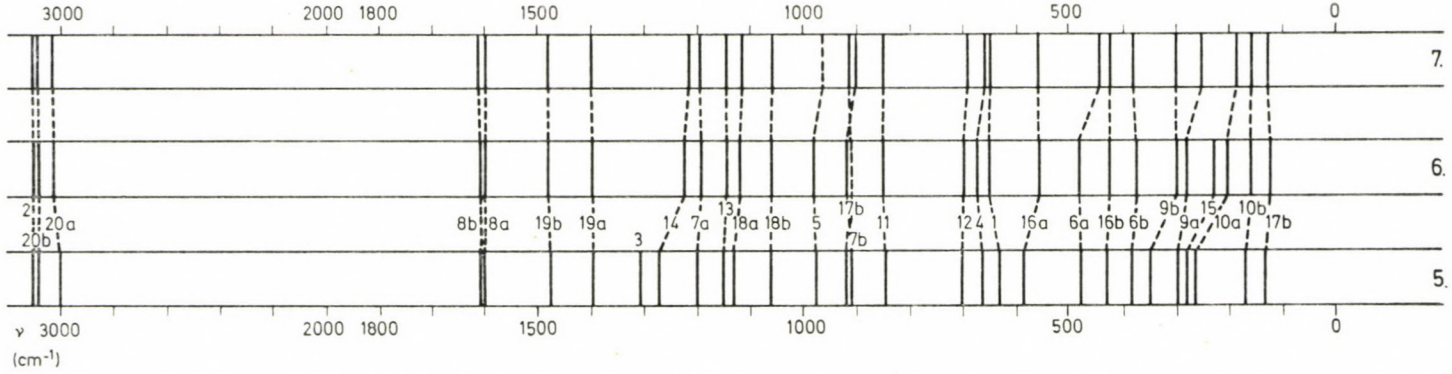

Fig. 1. Frequencies of the aromatic skeleton of 2,4-dinitrotoluene (5), 2,4-dinitrophenylacetic acid (6) and methyl-2,4-dinitrophenyl acetate (7)

Table III

2,4-Dinitrotoluene

IR	Raman	Int.	Sym.	IR	Raman	Int.	Sym.
	39 vs	lattice		1307 sh	1308 w ?	3	a'
	45 w	lattice		1345 vsd	1348 vs p	ν_s	a'
	58 m	γ_{as}	a''	1362 sh	1357 vs p	ν_s	a'
84 s	83 vs	γ_{as}	a''	1382 s	1382 w p	δ_s	a'
133 vw	130 vw	17a	a''	1394 w	1398 w p	19a	a'
168 s	160 m dp	10b	a''	1437 m	1441 vw	δ^+_{as}	a''
	265 vw	10a	a''	1454 m	1456 vw p	δ^+_{as}	a'
282 w	281 vw	15	a'		1468 vw ?	638 + 836	A'
296 m	297 w	9a	a'	1476 w	1480 vw p	19b	a'
341 w	340 sh	83 + 265	A'	1487 sh		296 + 1199	A'
352 s	355 w p	9b	a'		1490 vw	733 + 765	A'
387 m	390 vw	6b	a'	1503 sh		1528—24	A'
428 w	432 vw	16b	a''	1528 vsd	1529 m p	ν_{as}	a'
478 s	479 vw	6a	a'	1542 sh	1542 m ?	ν_{as}	a'
520 sh	518 sh	β_{as}	a'	1560 sh		586 + 973	A'
527 m	529 vw	β_{as}	a'	1600 sh	1610 s p	8a	a'
566 vw		133 + 428	A'	1607 vs	1612 ?	8b	a'
586 vw	590 vw	16a	a''	1686 w		2×843	A'
632 s } F	632 sh	282 + 352	A'		1700 vw	791 + 914	A'
638 s } F	638 m dp	1(160 + 479)	a'—A''	1737 vw		765 + 973	A'
666 m	670 vw p	4(281 + 390)	a''—A'	1754 vw		843 + 918	A'
706 s	706 vw p	12	a'	1814 m		843 + 973	A'
733 vs	732 vw	γ_s	a''	1870 vw		918 + 973	A'
765 w	765 vw	γ_s	a''	1943 m		2×973	A'
792 vs	791 w p	β_s	a'		2280 vw	2×1149	A'
836 vs	836 s p	β_s	a'		2490 vw	1149 + 1345	A'
843 s	842 sh	11	a''		2620 vw	1270 + 1357	A'
912 vs	914 w p	7b	a'		2688 vw	2×1345	A'
918 sh	920 sh	17b	a''	2728 vw		2×1362	A'
950 sh		2×478	A'		2748 vw	2×1382	A'
973 w		5	a''	2850 m		1270 + 1607	A'
1004 vw	1008 vw p	δ^-_{as}	a''		2895 vw	2×1454	A'
1033 m	1035 vw p	δ^-_{as}	a'		2935 m p	ν_s	a'
1066 s	1071 w p	18b	a'	2980 w	2978 vw	ν_{as}	a'
1088 vw	1095 vw	428 + 666	A'		3000 w	20a	a'
1128 m	1134 m p	18a	a'	3040 m	3052 vw	2×1528	A'
1149 s	1153 m p	13	a'	3067 m		1528 + 1542	A'
1199 m	1205 m p	7a	a'	3085 s	3082 m p	2	a'
1270 s	1271 w p	14	a'		3100 w	20b	a'

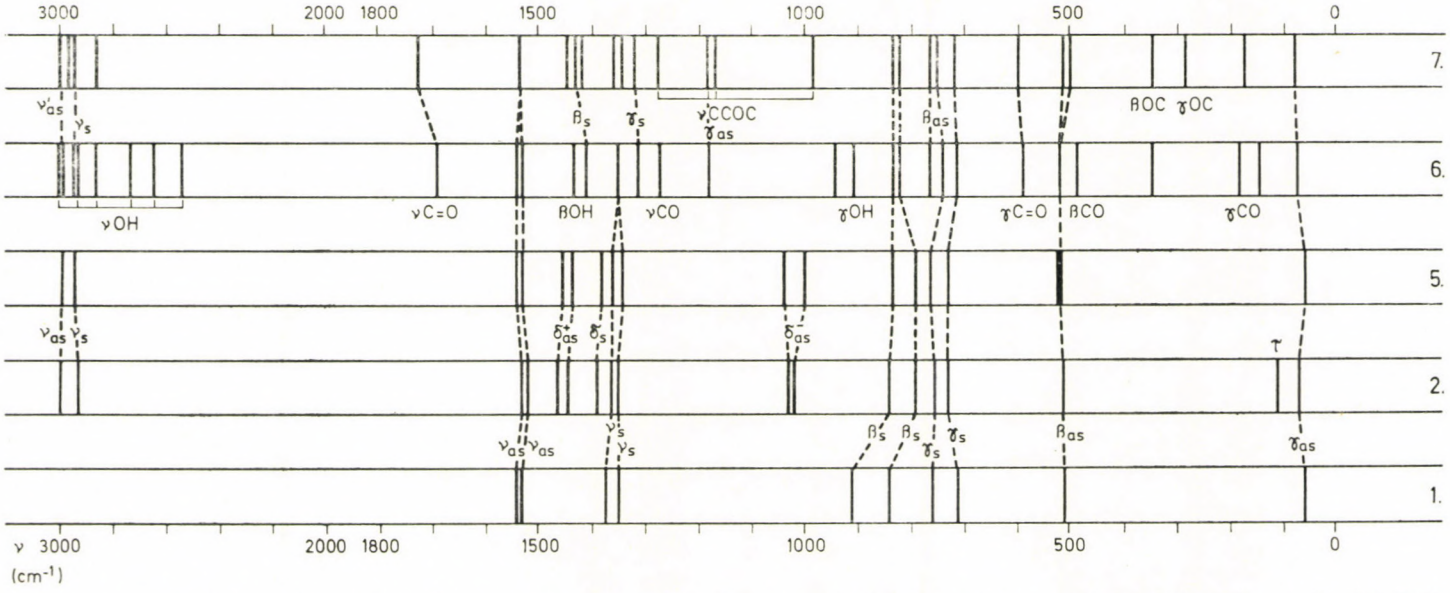

Fig. 2. Internal vibration frequencies of substituents of m-dinitrobenzene (1), 2,6-dinitrotoluene (2), 2,4-dinitrotoluene (5), 2,4-dinitrophenylacetic acid (6) and methyl-2,4-dinitrophenyl acetate (7). Symbols between the schemes of the spectra of compounds 1 and 2 refer to nitro groups, those between the spectra of compounds 2 and 5 to the methyl group and the symbols without group references between the spectra of compounds 6 and 7 pertain to the methylene group

1180, 1276, 1322 cm^{-1} and other characteristic methyl, methylene and carbonyl frequencies. 766, 1180 and 1322 cm^{-1}, present also in the acid spectrum, belong to the methylene group. 599 cm^{-1} may be attributed to the $\gamma C{=}O$ vibration (in the acid spectrum 588 cm^{-1}). Two strong and one weak IR bands appear as stretching vibrations of the chain $C(H_2){-}C(=O){-}O{-}C(H_3)$ at 987, 1166 and 1276 cm^{-1}. The two lowest frequencies can obviously be assigned to $\beta C{-}(CH_3)$ vibrations of the methyl group and $\beta C(=O){-}O{-}C(H_3)$, respectively. Out-of-plane vibrations of the side chain represent internal rotations, which cannot be assigned with certainty either in the far IR or in the low-frequency Raman spectrum.

The $\nu_s NO_2$ bands do not split in the spectra of both the acid and ester: in the latter also one component of the $\nu_{as} NO_2$ vibration gives only a weak shoulder. The overtones of the stretching vibrations are identified both in the IR and Raman spectra.

Frequencies belonging to internal vibrations of the substituents in the five interpreted spectra are shown in Fig. 2.

Some general remarks on nitro group frequencies

The frequency region of the $\nu_s NO_2$ vibration, excepting the aniline derivatives, is 1320—1375 cm^{-1}, with one amino or substituted amino group the lowest frequency limit is 1268 cm^{-1}, and in 1,3,5-triamino-2,4,6-trinitrobenzene 1229 cm^{-1}. The correlation of frequencies with Hammett sigmas [2], [3] is justified but only when different substitution types are separately studied. This is so because the νNO_2 vibrations couple more or less with other skeletal vibrations whose region depends on the number and position of the substituents. Figure 3 shows frequency *vs.* Hammett sigma curves for four substitution types. Hammett sigmas refer only to *para* and *ortho* positions because, in our experience, in *meta* position the stretching frequencies of the nitro groups are not affected even by different kinds of substituents.

A similar tendency can be established for the $\nu_{as} NO_2$ vibration. Except for the aniline derivatives, again the correlation of the frequency with Hammett sigmas may be linear. The amino or substituted amino group enhance the conjugation of the nitro group with the ring to such an extent that the stretching vibrations of the group couple much strongly with skeletal vibrations. Consequently the splitting of the in-phase and out-of-phase modes of both ν_s and ν_{as} vibrations increases. As the opposite-phase stretching vibration of the *meta*-substituent has a significantly lower frequency, the lower frequency component can be certainly assigned to the opposite-phase mode in the spectra of aniline derivatives.

Table IV

2,4-Dinitrophenylacetic acid

IR	Raman	Int.	Sym.	IR	Raman	Int.	Sym.
	28 sh	lattice		1348 vs	1351 vs	ν_s	a'
	42 vs	lattice		1395 m	1398 m	19a	a'
75 m	71 vw	γ_{as}	a''	1412 m	1417 vw	$\beta_s CH_2$	a'
	102 m	lattice		1434 vs	1440 vw	βOH	a'
126 w	120 sh	17a	a''	1478 vw	1483 vw	19b	a'
	147 vw	γCCO	a''	1503 sh		1532−32	A'
160 m	164 vw	10b	a''	1510 sh	1510 sh	1532−24	A'
181 s	176 w	γ C−O	a''	1518 sh		1532−16	A'
	206 vw	10a	a''	1532 vs	1533 s	ν_{as}	a'
228 wd		15	a'	1538 sh	1542 m	ν_{as}	a'
279 m	282 vw	9a	a'	1558 vw		716 + 852	A'
301 m	305 vw	9b	a'	1600 vs	1606 sh	8a	a'
	324 vw	2×164	A'	1606 sh	1611 s	8b	a'
346 s	353 vw	βCCO	a'	1692 vs	1640 vw	νC=O	a'
377 s	369 w	6b	a'	1803 vw		2×910	A'
427 m	430 vw	16b	a''	1820 vw		852 + 978	A'
478 w		6a	a'	1948 w		2×978	A'
489 m	498 vw	βC−O	a'	2172 vw		833 + 1348	A'
518 w	522 vw	β_{as}	a'	2230 w		2×1118	A'
554 vw	566 vw	16a	a''	2454 w		2×1237	A'
588 w		γC=O	a''	2497 w	2500 vw	1140 + 1348	A'
	653 m	1	a'	2545 m		νOH + 2×1274	A'
674 s		4	a''				
702 m	702 vw	12	a'	2592 w		1237 + 1348	A'
716 vs	716 vw	γ_s	a''	2638 mb	2628 vw	νOH + 2×1333	A'
742 s	742 w	γ_s	a''				
766 s	765 w	$\beta_{as} CH_2$	a''	2698 vw	2692 w	2×1348	A'
822 s	822 w	β_s	a'	2728 mb		νOH + 1140 + 1600	A'
833 s	837 s	β_s	a'				
852 s		11	a''	2745 vw		1140 + 1606	A'
905 vs	904 w	γOH	a''	2855 sb		νOH + 1333 + 1532	A'
922 m	922 w	7b	a'				
942 m	947 vw	νCC	a'	2927 sb		νOH + 1333 + 1600	A'
978 w	982 vw	5	a''				
1059s	1063 w	18b	a'	2940 sh	2945 m	$\nu_s CH_2$	a'
1118 m	1128 m	18a	a'	2958 vw		1274 + 1692	A'
1140 s	1148 s	13	a'		2978 w	$\nu_{as} CH_2$	a''
1182 sh	1189 w	$\gamma_{as} CH_2$	a''	2998 mb		νOH + 1478 + 1532	A'
1192 s	1198 m	7a	a'				
1237 vs	1239 w	14	a'	3038 m		20a	a'
1274 vs	1277 w	νC−O	a'		3058 vw	2×1532	A'
	1316 vw	$\gamma_s CH_2$	a'	3079 w		20b	a'
1333 vw	1335 sh	518 + 822	A'	3092 s	3092 s	2	a'

Table V

Methyl-2,4-dinitrophenyl acetate

IR	Raman	Int.	Sym.	IR	Raman	Int.	Sym.
	31 vs	lattice		1344 vs	1350 vs	ν_s	a'
	46 s	lattice			1356 sh	297 + 1067	A'
79 m	76 w	γ_{as}	a''	1360 sh	1367 sh	$\delta_s CH_3$	a'
106 w	103 vw	lattice		1401 w	1409 w	19a	a'
128 vw	130 m	17a	a''	1422 m	1426 m	$\beta_s CH_2$	a'
159 s	153 m	10b	a''	1431 s	1436 vw	$\delta^+_{as} CH_3$	a''
177 s	173 sh	βCOC	a'		1447 vw	$\delta^+_{as} CH_3$	a'
186 sh		10a	a''	1486 sh	1488 vw	19b	a'
250m	252 w	9a	a'	1502 sh		1533 − 4×8	A'
287 m		γOC	a''	1514 sh		1533 − 2×8	A'
298 m	297 m	9b	a'	1523 sh		1533 − 8	A'
345 s	354 m	βOC	a'	1533 vs	1540 s	ν_{as}	a'
351 m		2×177	A'	1536 sh	1544 sh	ν_{as}	a'
380 s	378 w	6b	a'	1552 sh		650 + 906	A'
427 w	427 w	16b	a''	1559 sh		345 + 1215	A'
444 m	446 w	6a	a'	1567 sh		659 + 917	A'
503 m	503 vw	β_{as}	a'	1602 vs		8a	a'
514 w	518 w	β_{as}	a'	1608 m	1613 vs	8b	a'
560 w		16a	a''	1633 vw		444 + 1194	A'
599 m	603 vw	γC=O	a''	1643 sh		818 + 833	A'
650 m	652 w	1	a'	1686 w		2×852	A'
659 sh	660 sh	4	a''	1727 vs	1730 w	νC=O	a'
691 s	692 w	12	a'	1772 vw		852 + 917	A'
722 vs	730 vw	γ_s	a''	1802 w		852 + 965	A'
751 m	753 w	γ_s	a''	1834 vw		2×917	A'
766 w	769 w	$\beta_{as} CH_2$	a''	1882 vw		917 + 965	A'
818 s	821 m	β_s	a'	1968 w		444 + 1533	A'
833 s	838 s	β_s	a'		2475 vw	1147 + 1344	A'
852 m	860 w	11	a''		2642 vw	2×1322	A'
906 s	907 m	7b	a'		2686 w	2×1344	A'
917 m	922 m	17b	a''	2745 vw		1344 + 1401	A'
938 w	944 w	298 + 650	A'	2825 vw		1344 + 1486	A'
987 s	997 m	νCCOC I	a'	2860 m	2840 w	$\nu_s CH_3$	a'
1059 m	1067 m	18b	a'	2939 m	2946 w	$\nu_s CH_2$	a'
1116 w	1126 m	18a	a'		2958 m	$\nu_{as} CH_3$	a'
1147 sh	1159 m	13	a'	2969 w		$\nu_{as} CH_3$	a''
1166 s	1176 w	νCCOC II	a'	2993 m	2985 w	$\nu_{as} CH_2$	a''
1180 m	1190 w	$\gamma_{as} CH_2$	a''		3012 vw	1486 + 1533	A'
1194 m	1203 w	7a	a'	3033 w		20a	a'
1215 vs	1221 m	14	a'	3059 m	3054 m	2×1533	A'
1276 w	1285 w	νCCOC III	a'	3079 m		20b	a'
	1322 vw	$\gamma_s CH_2$	a'	3093 sh	3088 m	2	a'

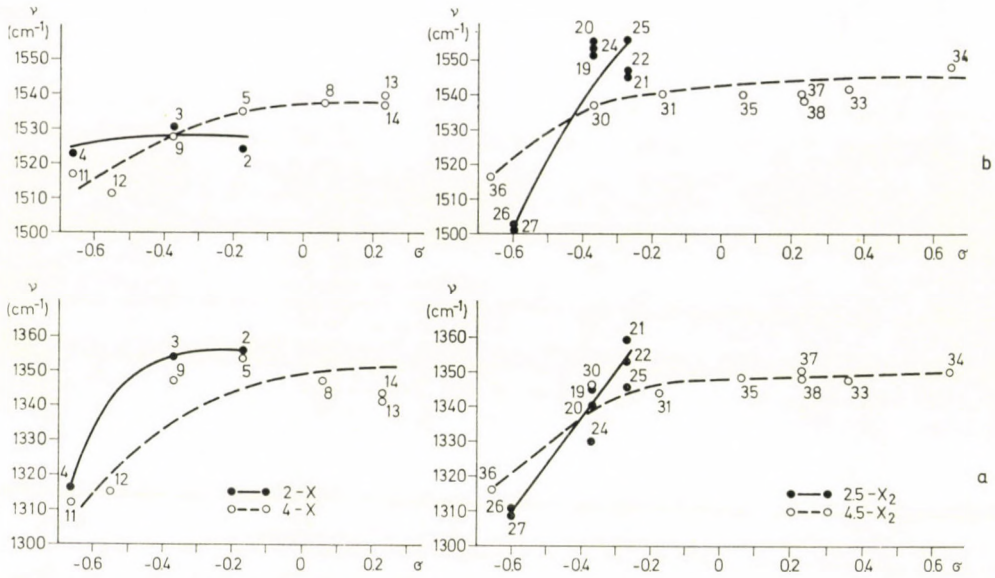

Fig. 3. a) Dependence of the average symmetric stretching vibration frequency on the Hammett sigma. *b)* Dependence of the average antisymmetric stretching vibration frequency on the Hammett sigma. Left-hand figures refer to 1,3-dinitrobenzenes substituted in 2- or 4-positions, right-hand figures to those twice substituted in 2,5- or 4,5-positions. Compound numbers are given at the experimental points

The correlation between the $\beta_s NO_2$ frequencies and the Hammett sigmas is very uncertain. On the one hand, the frequency is highly dependent on the properties and positions of other substituents, on the other hand, both components cannot always be identified. A tendency opposite to that of the stretching vibrations is probable: with increasing Hammett sigmas the frequency drops. Its region is 791—886 cm^{-1}.

Frequencies of the $\gamma_s NO_2$ vibration show, however, no such tendency. The $\gamma_s NO_2$ frequency of phenols is higher because of couplings with other out-of-plane vibrations, except for dinitrosalicylic acid (30), where the OH group forms a chelate with the *ortho*-carboxy group. It is a general rule that the lower frequency component corresponds to the in-phase mode and gives a stronger band in the infrared. Its frequency region is 721—749 cm^{-1}, and that of the opposite-phase component is 735—775 cm^{-1}. Because of multiple intramolecular hydrogen bonds, however, these bands appear at 786 and 819 cm^{-1} in the spectrum of triaminotrinitrobenzene.

The frequency of the $\beta_{as} NO_2$ vibration hardly depends on the substituents. Its frequency region is 504—547 cm^{-1} except for triaminotrinitrobenzene (430 and 445 cm^{-1}).

The twisting vibration has a low frequency. No reliable assignment can be given in the nitrobenzene spectrum either. According to RIBEAUD and co-

Table VI

	ν_s	ν_{as}	β_s	γ_s
1	1350—1375	1530—1541	839—909	716—764
2	1348—1363	1520—1528	791—841	732—755
3	1348—1360	1523—1538	860	748—763
4	1268—1364	1523	864	739
5	1345—1362	1528—1542	792—836	733—765
6	1348	1532—1538	822—833	716—742
7	1344	1533—1536	818—833	722—751
8	1347	1525—1551	813—835	743
9	1347	1514—1542	840	747—775
10	1342—1355	1519—1530	840	749
11	1286—1338	1500—1534	840	749—769
12	1291—1338	1498—1524	835	748—769
13	1341	1536—1543	841	737—751
14	1343	1533—1541	851	736
15	1345—1365	1520—1547	825	728—754
16	1345—1369	1545	830	725—754
17	1352	1546—1554	808	727—742
18	1337—1352	1540—1550	811	726—735
19	1323—1366	1552	832—890	737—763
20	1340	1555	832—886	743—772
21	1355—1364	1546	812	728—747
22	1353	1547	822—865	723—737
23	1320—1375	1542—1560	846	740—757
24	1320—1340	1546—1560	820—850	722—737
25	1334—1358	1556	804—850	717—728
26	1270—1350	1481—1523	830—873	723—739
27	1269—1349	1480—1521	829—873	721—738
28	1268—1353	1485—1536	830—868	725—756
29	1322—1348	1534—1555	836	734—741
30	1345	1537	839	720—745
31	1344	1540	855	732—739
32	1356	1533—1551	820—859	731—750
33	1348	1533—1550	864	739—749
34	1350	1544—1553	865	740
35	1348	1540	814—867	737
36	1290—1342	1516	824—850	734—742
37	1350	1540		721—745
38	1348	1538		732—739
39	1229—1303	1447	831—880	782—819

workers [23], the potential barrier of internal rotation in nitrobenzene is about 1000 cm^{-1} corresponding to 12 kJ/mol. Calculating with the harmonic potential

$$V_0 = \frac{8\pi^2 \nu^2 I}{n^2}$$

(in nitrobenzene $I = 4.36 \times 10^{-46}$ kg m^2/rad^2 and $n = 2$) one obtains 51 cm^{-1} for the twisting frequency. Considering anharmonicity, however, this value has to be regarded as the lowest limit. BOBROV and coworkers [12] assign one of the twisting frequencies to 61 cm^{-1} in the spectrum of *m*-dinitrobenzene. Considering the $\gamma_{as}NO_2$ mode to be independent of the other nitro group, one can calculate with a reduced moment of inertia of 5.8×10^{-46} kg m^2/rad^2 yielding as an upper potential barrier limit of internal rotation 23 kJ/mol. In a previous paper we have called attention to some hot bands on the low wavenumber side of the $\nu_{as}NO_2$ band [4] with a separation of 8—10 cm^{-1}. This would mean that in the excited state of the antisymmetric stretching vibration, where the two N—O distances and bond orders are mostly different, the twisting vibration has a frequency lower by 8—10 cm^{-1}.

Experimental

The near infrared spectra were recorded on Perkin—Elmer 225, UR-10 and Specord 75 IR spectrometers. All materials were investigated in KBr pellets: the spectra of *m*-dinitrobenzene, 2,4-dinitrotoluene and methyl-2,4-dinitrophenyl acetate were also studied in solution. The thickness of the benzene solution was 0.11 mm.

Far infrared spectra were recorded in the region of 10—450 cm^{-1} using an IS-3 Grubb—Parsons FT spectrometer. The spectral resolution, without apodization, was 6 cm^{-1}. Solid samples were studied in pellets in mixture with polyethylene powder.

The Raman spectra were obtained on a Cary 82 Laser-Raman spectrometer using the 514.5 nm exciting line of an argon ion laser. The spectra reported here were all recorded at room temperature with 50—100 mW laser power at sample point. A conventional 90° scattering geometry has been used. The spectral band width was constant (3 cm^{-1}) throughout the spectrum. Depolarization ratios were measured with unchanged orientation of the exciting vector, setting a Polaroid sheet analyzer at 0 and 90 degrees with respect to the electric vector of the exciting radiation.

REFERENCES

[1] VARSÁNYI, G.: Vibrational Spectra of Benzene Derivatives, pp 384—390. Akadémiai Kiadó, Budapest 1969
[2] BROWN, J. F.: J. Am. Chem. Soc., **77**, 6341 (1955)
[3] KROSS, R., FASSEL, V. A.: J. Am. Chem. Soc., **78**, 4225 (1956)
[4] VARSÁNYI, G., HOLLY, S., IMRE, L.: Spectrochim. Acta, **23A**, 1205 (1967)
[5] SHORYGIN, P. P., ILICHEVA, Z. F.: Izv. Akad. Nauk Fiz. Otd., **22**, 333 (1966)
[6] NAKASHIMA, R., WATARAI, S., KINUGASA, T.: Bull. Chem. Soc. Japan, **34**, 1740 (1961)
[7] HORÁK, M., SMOLIKOVÁ, J., PITHA, J.: Coll. Czech. Chem. Comm., **26**, 2391 (1961)
[8] KATRITZKY, A. R., SIMMONS, P.: Rec. Trav. Chim., **79**, 361 (1960)
[9] FUSON, N., GARRIGOU-LAGRANGE, C., JOSIEN, M. L.: Spectrochim. Acta, **16**, 106 (1960)
[10] SHUKLA, J. V., UPADHYA, K. N.: Ind. J. Pure Appl. Phys., **7**, 830 (1969)
[11] GREEN, J. H. S., LAUWERS, H. A.: Spectrochim. Acta, **24A**, 817 (1971)
[12] BOBROV, A. V., MATHIEU, J. P., POULET, H.: J. Raman Spec., **2**, 381 (1974)

[13] VARSÁNYI, G.: Assignments for Vibrational Spectra of 700 Benzene Derivatives. Akadémiai Kiadó, Budapest 1973
[14] SHUKLA, J., UPADHYA, K. N.: Ind. J. Pure Appl. Phys., **11,** 787 (1973)
[15] MEDHI, K. C.: Ind. J. Phys. **35,** 583 (1961)
[16] BENTLEY, F. F., SMITHSON, L. D., ROZEK, A. L.: Infrared Spectra and Characteristic Frequencies 700—300 cm^{-1}. Interscience Publishers, New York, London, Sydney 1968
[17] MOONEY, E. F.: Spectrochim. Acta, **20,** 1021 (1964)
[18] SHURVELL, H. F., FANIRAN, J. A., SYMONS, E. A.: Can. J. Chem., **45,** 117 (1967)
[19] SHURVELL, H. F., NORRIS, A. R., IRISH, D. E.: Can. J. Chem., **47,** 2515 (1969)
[20] VARSÁNYI, G., HORVÁTH, G., IMRE, L., SCHWARTZ, J., SOHÁR, P., SÓTI, F.: Acta Chim. Ac. Sci. Hung., **93,** 315 (1977)
[21] DECPURA, B. I., GUPTA, V. D.: J. Chem. Phys., **54,** 4013 (1971)
[22] GREEN, J. H. S.: Spectrochim. Acta, **26A,** 1523 (1970)
[23] RIBEAUD, M., BAUDER, A., GÜNTHARDT, H.: J. Mol. Phys., **23,** 235 (1972)

GYÖRGY VARSÁNYI
ÉVA MOLNÁR—PAÁL
KATALIN KÓSA
H-1521 Budapest, Budafoki út 8.

GÁBOR KERESZTURY
H-1025 Budapest, Pusztaszeri út 59—67.

ACTA CHIMICA

ТОМ 100

РЕЗЮМЕ

Влияние металлического лития на структуру окисно-дотированных вольфрамовых проволок

Р. ГРОХ, Т. МИЛНЕР и Л. БАРТА

Металлографические съемки полированных поверхностей, значения твердости по Викерсу, прочности на разрыв и остаточные сопротивления указывают на то, что первичная перекристаллизация вольфрамовых проволок, дотированных KSiAl (диаметр 0,6 мм), значительно облегчается диффузией атомов лития из жидкого лития в проволоку при 1100°C за 100 часов.

Синтез бензо[*a*]хинолизидиновых производных с противовоспалительной активностью без побочного язвенного эффекта

Л. САБО, К. НОГРАДИ, И. ТОТ, Ч. САНТАИ, Л. РАДИЧ, Ш. ВИРАГ и Э. КАНЬО

Был разработан новый метод получения производных бензо[а]хинолизидина. Стереохимия этих соединений была исследована с помощью методов ЯМР H^1 и C^{13}. Была определена структура спиртов **5a—f** и **6a—f**, полученных восстановлением кетонов **3b—d** и **3h—j** с помощью борогидрида натрия. Некоторые из полученных соединений обладают противовоспалительной активностью без побочного ульцерогенного эффекта.

Синтез 1-арил-1, 4-дигидро-2-карбамоил-3(2H)-изохинолинонов и их реакции с аминами

Новый метод получения *o*- {[α-(*N'*-фенилуреидо)]-бензил}-фенилацетамидов

Е. ЗАРА-КАЦИАН, ДЬ. ДЕАК, Л. ХАЗАИ, К. ГАЛЛ-ИШТОК и Й. ХАШКО-БРАЙЕР

В ходе исследований замещения 1-арил-1,4-дигидро-3(2*H*)-изохинолинонов, синтезированных впервые авторами, было найдено, что *N*-карбамоильные производные могут быть получены с хорошими выходами с помощью изоцианатов. Наблюдалось, что 2-карбамоил-1-фенил-1,4-дигидро-3(2*H*)-изохинолиноны, обладающие диациламиновой структурой, реагируют с аминами двумя путями, зависящими от условий (Схема 2, Таблица V): с первичными аминами с хорошими выходами были получены производные мочевины с открытым кольцом, а со вторичными аминами отщепляется боковая цепочка.

Автоматизированная система програмах для исследования механизма гомогенных газовых реакций

П. БЕНЕДЕК

На основе сообшения [1] анализируется общепринятый подход к составлению механизмов гомогенных реакций в газовой фазе. Соединяя выводы анализа с вожмостями вычислительной техники предлагается общий алгорифм распознавания. Метод соединяет в себе следующие основные действия: автоматический выбор элементарных реакций из совокупности, принимая во внимание методы химической кинетики, автоматическое составление и решение системы жёстких дифференциальных уравнений, расчёт веса отдельных реакций системы и отбор реакций с малым весом, сопоставление результатов, полученных на основе предпологаемого механизма с результатами измерения, анализ чувствительности в параметрах для обяснения значимых отклонений.

Синтез и определение структуры геометрических изомеров 1-арил-2-этил-1,2--дифенилэтиленов с помощью ЯМР—Н¹

П. ШОХАР, Г. АБРАХАМ, Г. ШНЕЙДЕР, Т. ХОРВАТ и Э. ФУГЕРТ

Изомеры *Z* и *E* производных 1,2-дифенил-1-арилэтилена были разделены и идентифицированы с помощью ЯМР—Н¹.

Экстракция европия из фазы расплавленной соли

Т. ЛЕНДЬЕЛ

Согласно экспериментальным данным, европий существует главным образом как двухвалентный ион в безводных средах и, в зависимости от используемого реагента, может быть экстрагирован с соответствующей эффективностью из фазы расплавленной соли в органическую фазу.

Исследованные бинарные системы растворителей проявляют антагонистическое, нормальное и синергическое поведение. Это может быть использовано при разделении главных продуктов распада редкоземельных металлов.

Математическая модель частичного окисления в пламенном реакторе

А. ЛАСЛО и А. НЕМЕТ

Получение ацетилена частичным окислением углеводородов является промышленным примером химических операций, основанных на реакциях в пламени. Исследование моделирования пламенных реакторов направлено на замену более ранних эмпирических и полуэмпирических моделей [1, 2] на теоретически обоснованную модель. Этим попыткам моделирования способствуют, с одной стороны, более детальные сведения относительно механизма химических реакций в процессе горения накопленные в литературе за последнее время, а с другой стороны, наличие мощных методов расчета на ЭВМ, позволяющих составление моделей пламенных реакторов, основанных на механизме химических реакций, и обращение с ними.

Синтез и исследование новых спиростероидов, I

Ш. ШОЙОМ, З. ЗУБОВИЧ и Л. ТОЛЬДИ

Некоторые 17*S*-спиро-оксираны, полученные из 17-кетостероидов, были обработаны метиламином. Из полученных 17α-метиламинометил-17β-гидроксистероидов были синтезированы производные мочевины и исследованы их реакции замыкания кольца в окисляющих и щелочных условиях. Былы получены 17-спиростероиды нового типа: спиро-пергидро--1,2,4-оксатиазины, спиро-(2'-иминооксазолидины), а также спиро-(2'-тиоксооксазолидины). Спиросоединения, содержащие пергидро-1,2,4-оксатиазиновое кольцо, являются новыми представителями такого типа цикла, приготовленные впервые нами. Химические и физические свойства этих соединений были изучены. Некоторые соединения обладают антиальдостеронным влиянием, но более слабым, чем спиронолактон.

Встраивание α-аминооксикислот в биологически активные пептиды

Л. КИШФАЛУДИ, М. ЛЁВ, И. ШЁН и О. НЬЕКИ

Было установлено, что включение α-аминооксикислот в молекулы биологически активных пептидов может вызвать значительное изменение их активности, в зависимости от того, где произошло замещение. У молекул пентагастрина наблюдалось качественное,

ценное и с практической точки зрения, изменение активности при замещении *N*-концевой аминокислоты: активность повышается и биологическое действие пептида ярко выражено при введении в тонкую кишку. При замещении *N*-концевой аминокислоты в молекуле ангиотензина-II также почулены аналоги, обладающие ценными антагонистическими свойствами. Замещение в обоих биологически активных молекулах *C*-концевой аминокислоты приводит к инактивным соединениям. В молекуле АКТГ изменение активности, вызванное различными замещениями, неоднозначно. Изменение сильно зависит от длины пептидной цепи.

Кинетика отщепления атома водорода от масляного альдегида *н*-пропильными радикалами

Ш. ФЁРГЕТЕГ, Т. БЕРЦЕШ, Ф. МАРТА и Ш. ДОБЕ

Отщепление атома водорода н-пропильными радикалами из различных положений молекулы масляного альдегида было исследовано в интервале температур 253—529°К. Пропильные радикалы были получены фотолизом *н*-C_3H_7CHO при 313 nm. Используя константу скорости рекомбинации радикалов, для которой было получено значение $10^{9,8}$, были определены выражения для констант скоростей отрыва водорода от формильной группы (1a) и от α- и β-углеродных атомов алкильной цепочки (1b и 1*c*, соответственно):

$$\log k_{1a} = (7{,}8 \pm 0{,}2) - (6300 \pm 300)/2{,}303\ RT$$
$$\log k_{1b} = (7{,}1 \pm 0{,}2) - (8100 \pm 300)/2{,}303\ RT$$
$$\log k_{1c} = 7{,}0 - 9000/2{,}303\ RT \text{ (полагая } A_{1c} = A_{1b}).$$

Исследование полимеризации ненасыщенных кардодиамидов с помощью полудинамического метода ДСК

Т. СЕКЕИ, В. В. КОРШАК, С. В. ВИНОГРАДОВА, М. ЛЕНДЬЕЛ, Я. С. ВЫГОДСКИЙ и Г. С. ГУРБИЧ

Было синтезировано бисметакриламиды четырех *кардо*диаминов и измерены некоторые важные физические свойства новых соединений.Ненасыщенные мономеры подвергались теромополимеризации и определялась растворимость полимеров. Полимеризация двух веществ 9,9-бис(4'-акрилоиламинофенил)фталида и 9,9-бис(4'-акрилоиламинофенил)флуорена была подвергнута тщательному калориметрическому исследованию на приборе Perkin—Elmer *DS* C-2. Были исследованы термомеханические свойства этих двух образцов. Были определены физические свойства — кристалличность, плавление и размягчение —, а также зависимость между процессом полимеризации и свойствами образующегося полимера.

О спонтанных процессах, происходящих на поверхности металлов под влиянием собственных ионов, III

Л. КИШ, Й. ФАРКАШ и И. МАТРАИ

Разработан метод определения констант скорости процессов, происходящих в системе $M - M^{z_1+} - M^{z_2+}$. Константы скорости определяются на основе данных, полученных с помощью дискового электрода с кольцом. Применение метода показано на примере системы $Cu - Cu^+ - Cu^{2+}$ в растворах HCl и $HClO_4$.

Новый метод различия механизмов S_N и S_{RN} 1. Реакция 2-галоген-2,2-дифенилацетамидов с метанольным метоксидом натрия. Исключение механизма $S_{RN}1$

ДЬ. ШИМИГ, К. ЛЕМПЕРТ, Г. ТОТ и Й. ТАМАШ

Под влиянием метанольного метоксида натрия α-галогенамиды **1a** и **1b** дают два *сине* продукта (**3a** и **3b**) наряду с обычным продуктом (**2a**). Отношение **3b**/**3a** не зависит от природы галогена в исходном соединении. Это указывает на то, что соединения **3***a* и **3b** вероятно образуются согласно механизму $S_{RN}1$ или S_N1/S'_N1 (рис. 2 и 3). Полученный независимым путем радикал **12**, являющийся ключевым промежуточным продуктом пути $S_{RN}1$, в присутствии метанольного метоксида не дает **2a**, **3***a* и **3b**, даже в следах, что, таким образом, исключает для данной реакции механизм $S_{RN}1$. Продукты, образующиеся из галогенамида **1a** под влиянием метанольного метоксида (**2c**, **3c**, **4**), могут быть интерпретированы также лишь на основе механизма S_N1/S'_N1.

Была исследована также реакция радикалов **12** с чистым метанолом и метанольным хлористым водородом; механизмы были предложены для объяснения образования продуктов, получаемых из **12** при различных условиях.

Фотокаталитические методы, I. Фотоокисление эриоглауцина-А, катализированное железом(III)

А. ПЕТЕР и Л. Й. ЧАНИ

Было найдено, что эриоглауцин-А — краситель с хорошей фотостабильностью — претерпевает значительное обесцвечивание при облучении его фотонами с $\lambda > 360$ nm и в присутствии железа(III). Было найдено, что обеспечивание вызвано радикалами OH, образующимися при возбуждении гидролизованных частиц железа(III) [особенно $Fe(OH)^{+2} \cdot aq$]. Обесцвечивание имеет максимум при pH = 2,7 и увеличивается с увеличением концентраций железа(III) и красителя. Обесцвечивание протекает как в присутствии, так и в отсутствии кислорода. При удалении кислорода прибл. 8,5 молей радикалов OH было израсходовано на одну молекулу красителя и образовалось эквивалентное количество железа(II). В присутствии кислорода, однако, почти в 8,5 раз больше красителя обесцвечивалось за счет O_2 без какого-либо образования железа(II).

Обесцвечивание красителя ингибируется галоидами (однако, хлорид оказался неэффективным) и псевдогалоидами, медью(II), ионами нитрита и арсенита.

Метод, основанный на фотокаталитическом эффекте железа (III), предложен для селективного определения железа в микроколичествах в присутствии других переходных металлов.

Превращение 2'-гидроксиизофлавонов и 11H-бензофуро[2,3-b](1)-бензопиран-11-оны

Ш. АНТУШ и М. НОГРАДИ

Окисление 2'-гидроизофлавона карбонатом серебра до хинолина дает соответствующий 11*H*-бензобуро [2,3-b] [1]бензопиран-11-он.

Метод исследования скорости коррозии, основанный на фарадеевском искажении

Й. ДЕВАИ и Л. МЕСАРОШ

Был разработан метод исследования кинетики процессов коррозии, основанный на использовании фарадеевского искажения, для тех случаев, когда как анодная, так и катодная ступени процесса обладают характеристиками типа Тафеля. Гармонические компоненты тока, протекающего под влиянием наложения синусоидального переменного на-

пряжения на прямое напряжение поляризации, были исследованы в зависимости от средней величины прямого напряжения поляризации во времени и от амплитуды переменного тока.

Было установлено, что ток коррозии и тафельный наклон анодной и катодной ступеней процесса могут быть определены измерением первых трех гармонических компонентов тока фарадея при двух анодных и катодных потенциалах, находящихся в области Тафеля. Был разработан также метод определения тока коррозии и наклона Тафеля с помощью гармонических компонентов тока, измеряемых при потенциалах коррозии. Выведенные зависимости значительно упрощаются в случае переменного напряжения с малой амплитудой.

Исследование превращений диолов и циклических эфиров, XLIV

Получение лактонов, насыщенных и ненасыщенных эфиров с помощью превращений диолов различной структуры на медных катализаторах. (Исследование структуры диолов и ее влияния на различные пути превращений)

М. БАРТОК и А. МОЛЬНАР

Были исследованы превращения шести различных дипервичных, первичных-вторичных и дивторичных диолов (**I**—**VI**) на трех различных медных катализаторах (Cu/Al, Cu/SiO_2, Cu). Объясняли каким образом характерные процессы (образование насыщенных и ненасыщенных циклических эфиров, лактонов) зависят от структуры исходных диолов, от реакционной способности и стабильности промежуточных продуктов, а также от свойств отдельных катализаторов.

Исследование способности платиновых катализаторов без носителей к сорбции H_2 различными экспериментальными методами

Ф. НАДЬ, Д. МОГЕР, М. ХЕГЕДЮШ, ДЬ. МИНК и Ш. САБО

С помощью электрохимических, волюметрических и термодесорбционных (TPD) методов была исследована сорбция H_2 на платиновых катализаторах без носителя при одинаковом спекании. Было установлено, что степень удельной сорбции водорода зависит от термических условий адсорбции. Если адсорбционное насыщение производится при 0—25°C, то отношение адсорбированных атомов к поверхностным атомам Pt, рассчитанное из количества адсорбированного H_2, равно обычному отношению 1 : 1. Если, однако, адсорбционное насыщение производилось медленным охлаждением от высоких температур катализатора до низких и в атмосфере H_2, то количество адсорбированного H_2 было в 4—6 раз больше, чем в предыдущей процедуре. На основе дополнительных исследований было найдено, что сорбирующийся за счет активированной хемосорбции водород располагается, вероятно, не на поверхности платинового катализатора.

Спектрохимическое исследование летучих компонентов в термохимических процессах, I

Аппаратура, системы и экспериментальные условия

Э. ГЕГУШ, Й. КРЕЙТЕР, Л. МЕРАИ и Й. ИНЦЕДИ

Был сконструирован микрореактор с электрическим обогревом для исследования деталей термохимических процессов, т. напр., процессов испарения и превращений, а также термохимических реакций, протекающих вплоть до температур 1350°C. Паровая фаза, полученная во время периода нагрева, вводилась с помощью аргонового газа-носителя источник излучения дуги прямого тока, стабилизированной внешним магнитным полем. Интенсивность излучения выбранного характерного элемента записывалась как функция времени и температуры. В первой части статьи описывается проект аппаратуры, а также характеристики и функции нагрева микрореактора, системы газа-носителя, внешнего магнитного поля, электрического детектора и самописца.

Влияние сильной хемосорбции на стационарное сосояние анодной поляризации простых органических соединений на электроде платинированной платины

ДЬ. ХОРАНИ и ДЬ. ИНЗЕЛЬТ

Изложены взгляды относительно роли сильно хемосорбированных частиц в электроокислении простых органических соединений. Для выяснения проблемы, вместо окисления метанола, была предложена модель окисления этиленгликоля и его окисленных продуктов. Было показано, что в данном случае хемосорбция играет второстепенную роль по сравнению с основными реакциями окисления. Несмотря на это, форма начального участка поляризационных кривых зависит от поведения сильно хемосорбированных частиц. Обоснованность механистических допущений подтверждалась экспериментальными результатами, полученными с помощью радиоактивной техники адсорбционного метода.

Исследование связи между электропроводностью и вязкостью водных и солянокислых растворов хлоридов металлов

Э. БЕРЕЦ и И. БАДЕР

В ходе систематических исследований с целью более глубокого познания подевения растворов систем типа MCl_x—H_2O и MCl_2—HCl—H_2O на основе экспериментальных результатов и функций активации($\Delta H^{\ddagger}\eta$, $\Delta H^{\ddagger}\lambda$, $\Delta H^{\ddagger}\eta/\Delta H^{\ddagger}\lambda$), а также некоторых других полезных функций ($\lambda\eta$, $k\eta$, $\lambda-\vartheta$), рассчитанных из предыдущих, были сделаны заключения относительно взаимосвязи электропроводности и вязкости, а также ее зависимости от концентрации. Авторами были сделаны попытки интерпретации и согласования результатов со структурными изменениями, происходящими под влиянием изменения концентраций в растворе исследованных систем.

Производные полиэтиленгликоля как комплексующие реагенты и катализ с переносом фазы, II

Комплексообразующее поведение полиэтиленгликоля и его производных

Л. ТЁКЕ, Г. Т. САБО и К. АРАНЬОШИ

Было произведено замещение конечной группы в полиэтиленгликолях. Каталитическая сила соединений полиоксиэтилена зависит от качества конечной группы и средней длины цепи.

Характеристика циклодекстриновых полимеров и изучение их хроматографического поведения

Б. ЖАДОН, М. СИЛАШИ, К. Х. ОТТА, Ф. ТЮДЁШ, Е. ФЕНЬВЕШИ и Й. СЕЙТЛИ

С помощью сшивки циклодекстринов (α-CD, β-CD и γ-CD) были получены полимеры (α-CDP, β-CDP и γ-CDP) в виде регулярных шариков. Эти полимеры были охарактеризованы их химическим составом, свойствами набужания и размерами зерен. Циклодекстриновые полимеры со средней степенью набухания и с хорошо определенным составом могут быть успешно использованы в качестве наполнителей колон в инклузинной хроматографии. Они быстро набухают, сохраняют форму и эластичны, содержатся без разложения и в набухшем состоянии, а также сохраняют свои исходные свойства и после нескольких регенераций. Хроматограммы, снятые на набухших гелях, хорошо воспроизводимы.

Используя в качестве моделей 20 природных аминокислот, подробно исследовалось хроматографическое поведение α-CDP, β-CDP и γ-CDP, их разрешающая способность, а также зависимость ее от условий. Приводятся данные удерживаемости аминокислот, а также многие данные относительно теоретической высоты тарелок (HETP). Согласно проведенным исследованиям, ароматические аминокислоты хорошо отделяются от других аминокислот, в первую очередь, на колоннах с β-CDP. В случае трипофана наилучшее разделение было получено на α-CDP. Результаты сравниваются с полученными для гелей Sephadex G. 25.

Новый метод определения констант протонирования полифункциональных лигандов

Эффект растворителя на протонирование функциональных групп молекулы Corticotropine

Б. НОСАЛ и К. БУРГЕР

Был разработан метод, использование которого позволяет одновременное определение величин констант протонирования, характеризующих функциональные группы и пары групп, образующих водородные связи, а также числа водородных связей. С помощью этого метода были определены группы и структурные константы $ACTH_{1-4}$ и $ACTH_{1-32}$ в 50%-ном растворе пропиленгликоля и, исходя из констант, были сделаны заключения относительно взаимодействий функциональных групп друг с другом и с растворителем.

Определение адсорбционной емкости из избыточных изотерм L/S ($Ж/Т$) разбавленных растворов

Г. ШАЙ, Л. ДЬ. НАДЬ и Г. ФОТИ

Демонстрируется полезность трансформации изотерм

$$\frac{x_1' x_2'}{\Delta n_2^{(n)}} = \frac{1}{S n_{1,0}^s} + \frac{x_2'}{n_{2,0}^s}$$

относящихся к разбавленным растворам сильно адсорбированных веществ. В благоприятных случаях они позволяют более надежное определение адсорбционной емкости, чем изотермы в их обычных формах, и содержат больше сведений относительно взаимодействий растворенное вещество-твердое вещество и природы адсорбированного слоя. Были исследованы следующие системы: стеариновая кислота из циклогексана на углеродной черни, бензойная кислота из воды, *н*-бутанол из воды и антрацен из циклогексана на активированном угле.

Непрерывный электролиз органических соединений

[illegible] ДЬ. КОРАНИ, Л. РЕДЕИ и Э. ГАДЬИ-ПАЛФИ

Была сконструирована электролитическая установка различного назначения типа фильтропресса для проведения электролитических реакций органических соеденений в непрерывном процессе. Опыты восстановления бензойной кислоты до бензилового спирта указывают на то, что этот процесс может быть осуществлен непрерывно с достаточной эффективностью восстановления и тока.

Новые использование аминалей в органическом синтезе. Селективное ядерное алкилирование и ара лкилирование ацетофенонов

Ф. КАЛЛАИ, Г. ЙАНЖО, И. ЕДЕД, Е. БАШИЗ-ГАЧ и Й. ТАМАШ

Бензолиден-бис-пиперидин (**2a**) влияет на ядерное аминоалкилирование 2', 4'-дигидрокси- (**1a**) и 2', 4', 6'-тригидроксиацетофенона (**1b**), давая 3'-(**3a**) и 3', 5'-(фенил-1-пиперидинометильные) (**3b**) производные, соответственно. Подобным образом, соединение **1a** с метилен-бис-пиперидином (**2b**) дает 2', 4'-дилидрокси-3'-(1-пиперидинометил)ацетофенон (**3c**). Восстановление аминометильных производных является селективному путем к *С*-бензил- и *С*-метилацетофенонов.

Влияние фотографических и фотометрических факторов на оценку спектрограмм, I

К. ЦИММЕР и ДЬ. ХЕЛТАИ

В первой статье этой серии обсуждаются проблемы, связанные с фотографическим проявлением спектрограмм, а в первую очередь, источники ошибок измерения интенсивности и факторы расширения интервала измерений. При сравнении различных типов микроденситометров было установлено, что интервал измерения интенсивности обычного микроденситометра типа C. Zeiss Jena G II может быть вдвое увеличен до $S = 4$, применяя современную систему детектирования с низким шумом, линейную в широком интервале, с одновременным уменьшением рассеянного света в зачительной мере.

Описание переходных потенциометрических сигналов, полученных в аналитических системах со вспрыскиванием

М. ГРАТЦЛ, Ж. ФЕХЕР, Г. НАДЬ, К. ТОТ и Э. ПУНГОР

Математически описываются кривые сигнала концентрации — время, снятые как с помощью кулонометрии, так и с помощью ручного вспрыскивания в непрерывный поток носителя в серийных аналитических аппаратурах. Хффект планируемых параметров на обоснованность выведенных математических моделей обсуждается в случае потенциометрического детектирования.

Ионная сольватация в среде с аномальным уравнением электрического состояния

И. РУФФ и З. Г. САБО

Исходя из приближения электрострикции диэлектрика вокруг иона, было выведено уравнение свободной энтальпии электростатической сольватации, содержащее зависимость плотности от относительной электропроницаемости растворителя. Для жидкостей с нелинейным отношением между электропроницаемостью и массовой плотностью (т. е. аномальным с точки зрения их уравнения электрического состояния), интеграл заряда Борна для ионов, погруженных в диэлектрик, умножаем на фактор $\mathrm{d} \ln \varepsilon / \mathrm{d} \ln g$, где g — массовая плотность. Совокупление этого результата с уравнением Грэхема, которое примает в учет диэлектрические «эффекты насыщения», указывает на то, что вышеупомянутый фактор дает наибольшую поправку в области высоких полей вокруг иона, где относительная проницаемость уменьшается до квадрата коэффициента внутренней рефракции, n^2. Расчеты зависимости n^2 от плотности, основанные на данных молярной рефракции, указывает на то, что наиболее полярные растворители ведут себя аномально. Численные расчеты для щелочных галоидов в диметилформамиде, 1-пропаноле и воде находятся в хорошем согласии с экспериментальными данными.

Синтез производных 7-[(гетероарилтио)-ацетамидо]-3-диацетоксицефалоспоранойной кислоты, I

Ф. СТАРИЧКАИ, И. МИШКОЛЬЦИ и Р. БОГНАР

Описывается получение 19 новых 7-[(гетероарилтио)-ацетамидо]-3-диацетоксицефалоспоранойных кислот (**IVa-t**) через нуклеофильное замещение 7-хлорацетамидо-3-диацетоксицефалоспоранойной кислоты (**II**) некоторым меркаптогетероарильными соединениями. Был разработан новый удобный метод синтеза этих соединений, заключающий в себе ацилирование 7-ADCA с помощью химически «активных» 8-хинолильных эфиров гетероарилтиоуксусных кислот (приготовление *in Situ* вр еакционной смеси). Были исследованы также реакции превращений соединений **XIIIe, p, r** — полученных из сульфоксида 6-хлорацетамидопенициллановой кислоты (**XI**) — в соответствующие производные дигидротиазинового эфира (**XVe, p, r**).

В *in vitro* и *in vivo* опытах, синтезированные соединения проявляют антибиотическую активность лишь на бактерий положительные по Грэму. Соединение **IV***n* оказалось более эффективным, чем цефалексин, в то время как **IVd** — проявляющее эначительную биологическую активность *in vitro* — оказалось неэффективным в опытах с крысами, зараженными *Mycobact. tuberculosis typ. bovinus* (RAVENEL).

Анализ стероидов, XXXIII

Одновременное определение продуктов восстановления ацетата норетистерона

Ш. ГЁРЁГ, А. ЛАУКО, Б. ХЕРЕНИ, Г. ЦИРА, Е. ЧИЗЕР и З. ТУБА

При восстанавлении ацетата норетистерона с помощью лидридов комплексов металлов, наряду с основным продуктом восстановления (4-ен-3β-гидроксильных производных), образуется два побочных продукта (4-ен-3α-гидрокси- и 4,5-дигидро-3β-гидроксипронзводные). Эпимеры были определены с помощью жидкостной хроматографии высокой чувствительности, в то время как определение насыщенных производных производилось с помощью газовой хроматографии после превращения термически нестабильных производных в 3,5-диены. Обсуждается также использование других аналитических методов (волюмометрия, тонкослойная хроматография и УФ спектрфотометрия).

Молярные объемы пердейтерированных бензола и циклогексана

И. КИШ, Ж. КОВАЧ и ДЬ. ЯКЛИ

Измерения молярных объемов бензола и циклогексана и их полностью дейтерированных аналогов проводились в интервале температур 15—70°С. Изотопный эффект молярного объема бензола может быть выражен следующим уравнением: $(V_H - V_D)/V_H = 2{,}687 \cdot 10^{-3} - 3{,}014 \cdot 10^{-6} \cdot t - 6{,}05 \cdot 10^{-8} \cdot t^2$ а для циклогексана:

$$(V_H - V_D)/V_H = 2{,}954 \cdot 10^{-3} - 2{,}408 \cdot 10^{-5} \cdot t - 1{,}62 \cdot 10 - 7 \cdot t^2.$$

Результаты сравниваются с полученными ранее.

Термическое разложение пропана в струе водородной плазмы

П. ШТЕЙНГАСНЕР, Л. ВАЙТА, Е. ДУДАШ и И. СЕБЕНИ

Было исследовано разложение пропана в струе атмосферной водородной плазмы. Было найдено, что состав продукта зависит только от степени превращения пропана, которая, в свою очередь, зависит от адибатической температуры смеси горячей струи водорода и холодного пропана. Исследования с дейтерийной плазмой показали, что газовая плазма реагирует с крекированными остатками углеводородов. На основе содержания и распределения дейтерия в продуктах предложен механизм, объясняющий образование различных продуктов.

ИК исследование хемосорбции CO на Pd/SiO_2

Я. МИНК, А. ШАРКАНЬ, Т. СИЛАДИ и П. ТЕТЕНИ

Были изучены инфракрасные спектры CO, в зависимости от покрытия поверхности катализатора Pd/SiO_2, покрытом вначале или водородом или кислородом. При низком и средних покрытиях частота валентного колебания изменяется от 1800 до 1850 $см^{-1}$. Исходя из появления «линейных» полос при 2050—2060 $см^{-1}$ (L_1) и при 2085—2098 $см^{-1}$ (L_2) и одновременного повышения частоты полосы B до 1890—1920 $см^{-1}$ (B_1) и до 1950—1967 $см^{-1}$ (B_2), предполагается образование сжатого, делокализованного слоя *CO*. Измерения на окисленной поверхности указывают на образование «сжатых островов» хемосорбированног CO. Результаты интерпретируются на основе медленной реакции между хемосорбированным кислородом и CO.

Протонирование кислородсодержащих органических соединений

Ф. ЙО и М. Т. БЭК

Растворимость бензойной кислоты, бензилового спирта и нафталина была исследована в водных растворах минеральных кислот различной кислотности. Используя эти данные, протонирование бензойной кислоты в серной кислоте было охарактеризовано следующими параметрами: $m = 0{,}87$ и $pK_{BH^+} = -6{,}23$ (полупротонирование в 78,4%-ой H_2SO_4). Было заключено, что изменения растворимости бензойной кислоты, бензолового спирта и нафталина в разбавленных водных растворах минеральных кислот вызваны не протонированием, а лишь эффектом среды. В случае бензойной кислоты, растворенной в сернокислой среде, вклад протонирования в суммарную растворимость пренебрежительно мал вплоть до концентрации серной кислоты, равной 70%.

Механическая стабильность мостиков из одной жидкости в другую

Э. ВОЛЬФРАМ и Й. ПИНТЕР

Капиллярные силы, в также распределение мостиков после разрыва, в случае жидкостных мостиков типа полимер) (вода/*н*-алкан)/стекло были измерены, используя геометрию с горизонтально параллельными пластинами. При данном объеме мостиковой жидкости кривая силы в зависимости от разделения проходит через максимум, и также выглядят кривые максимальной силы в зависимости от мостиковой массы. Максимум последней находится в той области мостиковой массы, где мостик становится нестабильным. Поверхностно-активные вещества влияют на стабильность мостиков сложным образом, вследствие их влияния на поверхностное натяжение, а также и на краевой угол, приводя к изменению площади поверхности жидкости и площади контакта мостиковая жидкость/твердое вещество. Приводится вероятное объяснение конфигурационных изменений с изменением концентрации поверхностно-активного вещества.

Калориметрическое исследование осциллирующих реакций Белоусова-Жаботинского

Э. КЁРЁШ, М. ОРБАН и Ж. НАДЬ

Выделение тепла и накопление бромомалоновой кислоты (BrMA) были измерены калориметрически и полярографически, соответственно, в реагирующей системе малоновая кислота — бромат — серная кислота — катализатор [Ce^{+3}, Mn^{+2}, $Fe(phen)_3^{+2}$]. В течение осциллирующего периода реакции, как скорость выделения тепла, так и скорость образования BrMA являются периодическими. Теплоты реакции преосциллирующего периода, осциллирующего периода и некатализированной реакции бромата с малоновой кислотой были приблизительно одинаковыми и равными 650 кдж/моль бромата. Были также определены теплоты некоторых составных реакций системы Белоусова—Жаботинского (т. напр., бромирование малоновой кислоты, окисление катализатора броматом, окисление малоновой кислоты и BrMA церием(IV)).

Мезоморфные полимеры

Ф. ЧЕР, К. НИТРАИ и ДЬ. ХАРДИ

Были изучены условия образования мезоморфных монозамещенных виниловых полимеров. Замораживание мезоморфного состояния в стекливидную фазу может быть приписано образованию жестких, нерегулярных, атактических полимерных цепей. Слоистая смектическая структура наблюдалась для полимеров и построением «рыбный скелет». Эта структура, со многих точек зрения, подобна структуре с гибкой основной целью. Молекулярная цепочка с построением «рыбный скелет» наблюдалась в случае полимеров с жесткими группами, присоединенными к основной цепи с помощью гибких боковых цепочек (ми. C_6—C_8) или, по крайней мере, четырьмя эластические соединенными атомами. Точка плавле-

ния полимеров относительно ярко выражена. Объемистые полимеры в стекловидном состоянии оптически анизотропны, являются жесткими и хрупкими.

Спиральные полимеры образуются, если объемистые жесткие боковые группы присоединены к основной цепи непосредственно или с помощью эластично соединенных боковых цепей. Полимерные молекулы могут быть рассмотрены как жесткие цилиндры, плотная упаковка которых образует жидкокристаллический объемистый полимер. Размеры молекул могут быть определены из максимальных величин кривых рентгенограмм. Жидкокристаллические полимеры могут быть обработаны прессованием даже после охлаждения. Их температура плавления высока, в широком интервале часто ниже температуры разложения. Спиральные полимеры с цилиндрической симметрией, содержащие хиральные атомы углерода, находятся в холестирическом состоянии. Структура мезоморфных полимеров может быть определена, комбинируя результаты некоторых независимых исследований структуры и текстуры полимеров.

Колебательные спектры производных м-динитробензола

Д. ВАРШАНИ, Е. МОЛЬНАР-ПАЛ, К. КОША и Г. КЕРЕСТУРИЬ

Среди колебательных спектров 38 производных *м*-динитробензола подробно ассигнировались ИК и Раман-спектры *м*-динитробензола, 2,6-динитротолуола, 2,4-динитротолуола, — фенилуксусной кислоты и ее метилового эфира. Была исследована зависимость частоты валентных колебаний нитрогруппы от констант Гаммета других заместителей. Было установлено, что можно сравнивать частоты производных, замещенных в одинаковых положениях, а качество прочих заместителей в положении *мета* безразлично с точки зрения частоты. Частота симметричного валентного колебания с противоположной фазой аномально мала в спектрах производных анилина. Исходя из горячих полос, присоединяющихся к полосе антисимметричных валентных колебаний, было установлено, что в состоянии возбуждения этого колебания частота вращательного колебания меньше.

Printed in Hungary

A kiadásért felel az Akadémiai Kiadó igazgatója — Műszaki szerkesztő: Zacsik Annamária

A kézirat nyomdába érkezett: 1979. I. 4. — Terjedelem: 43,75 (A/5) ív, 252 ábra 1 melléklet

79.6637 Akadémiai Nyomda, Budapest — Felelős vezető: Bernát György

A new volume in the successful series

ABSORPTION SPECTRA IN THE INFRARED REGION

Ed. by L. LÁNG

Volume 5

This is the fifth volume of the series which presents the infrared spectra of selected organic compounds over the range 400—4000 cm^{-1}, together with full details of sample and experimental conditions. The empirical formula, molecular weight and melting point of each substance is also given. The choice of the spectra has been made by a panel of experienced spectroscopists, who have given primary considerations to covering compounds which have been isolated or synthetized recently. More familiar materials have also been included, generally because the spectra presented for them are more detailed than those of other published sources, or because they refer to different experimental conditions.

The volumes of ABSORPTION SPECTRA IN THE INFRARED REGION provide a valuable source of reference which complements and extends existing sources. Organic chemists and biochemists in academic and industrial laboratories, particulary in the petrochemicals and pharmaceuticals industries, will find this series an easily accessible source of clearly presented infrared spectra of an interesting range of compounds.

In English — Approx. 320 pages — Spectra of 300 compounds — 21×29 cm — ISBN 963 05 1768 X — Cloth

AKADÉMIAI KIADÓ, Budapest **E. KRIEGER PUBLISHING CO. INC., Huntington**

Les Acta Chimica paraissent en français, allemand, anglais et russe et publient des mémoires du domaine des sciences chimiques.

Les Acta Chimica sont publiés sous forme de fascicules. Quatre fascicules seront réunis en un volume (4 volumes par an).

On est prié d'envoyer les manuscrits destinés à la rédaction à l'adresse suivante:

Acta Chimica
Budapest, P.O. Box 67, H-1450, Hongrie

Toute correspondance doit être envoyée à cette même adresse.

La rédaction ne rend pas de manuscript.

Le prix de l'abonnement: $36,00 par volume.

Abonnement en Hongrie à l'Akadémiai Kiadó (1363 Budapest, P. O. B. 24, C. C. B. 215 11488), à l'étranger à l'Entreprise du Commerce Extérieur « Kultura » (H-1389 Budapest 62, P. O. B. 149 Compte-courant No. 218 10990) ou chez représentants à l'étranger.

Die Acta Chimica veröffentlichen Abhandlungen aus dem Bereich der chemischen Wissenschaften in deutscher, englischer, französischer und russischer Sprache.

Die Acta Chimica erscheinen in Heften wechselnden Umfanges. Vier Hefte bilden einen Band. Jährlich erscheinen 4 Bände.

Die zur Veröffentlichung bestimmten Manuskripte sind an folgende Adresse zu senden:

Acta Chimica
Budapest, Postfach 67, H-1450, Ungarn

An die gleiche Anschrift ist jede für die Redaktion bestimmte Korrespondenz zu richten.

Manuskripte werden nicht zurückerstattet.

Abonnementspreis pro Band: $36,00.

Bestellbar für das Inland bei Akadémiai Kiadó (1363 Budapest, Postfach 24, Bankkonto Nr. 215 11488), für das Ausland bei »Kultura« Außenhandelsunternehmen (H-1389 Budapest 62, P.O.B. 149. Bankkonto Nr. 218 10990) oder seinen Auslandsvertretungen.

«Acta Chimica» издают статьи по химии на русском, английском, французском и немецком языках.

«Acta Chimica» выходит отдельными выпусками разного обектъка, 4 выпус составляют один том и за год выходят 4 тома.

Предназначенные для публикации рукописи следует направлять по адресу:

Acta Chimica
Budapest, P.O. Box 67, H-1450, ВНР

Всякую корреспонденцию в редакцию направляйте по этому же адресу.

Редакция рукописей не возвращает.

Подписная цена — $36,00 за том.

Отечественные подписчики направляйте свои заявки по адресу Издательства Академии Наук (1363 Budapest, P.O.B. 24, Текущий счет 215 11488), а иностранные подписчики через организацию по внешней торговле «Kultura» (H-1389 Budapest 62, P.O.B. 149. Текущий счет 218 10990) или через ее заграничные представительства и уполномеченных.

Reviews of the Hungarian Academy of Sciences are obtainable at the following addresses:

AUSTRALIA
C.B.D. LIBRARY AND SUBSCRIPTION SERVICE, Box 4886, G.P.O., *Sydney N.S.W. 2001*
COSMOS BOOKSHOP, 145 Ackland Street, *St. Kilda (Melbourne), Victoria 3182*

AUSTRIA
GLOBUS, Höchstädtplatz 3, *1200 Wien XX*

BELGIUM
OFFICE INTERNATIONAL DE LIBRAIRIE, 30 Avenue Marnix, *1050 Bruxelles*
LIBRAIRE DU MONDE ENTIER, 162 Rue du Midi, *1000 Bruxelles*

BULGARIA
HEMUS, Bulvar Ruszki 6, *Sofia*

CANADA
PANNONIA BOOKS, P.O. Box 1017, Postal Station "B", *Toronto, Ontario M5T 2T8*

CHINA
CNPICOR, Periodical Department, P.O. Box 50, *Peking*

CZECHOSLOVAKIA
MAD'ARSKÁ KULTURA, Národní třída 22, *115 66 Praha*
PNS DOVOZ TISKU, Vinohradská 36, *Praha 2*
PNS DOVOZ TLAČE, *Bratislava 2*

DENMARK
EJNAR MUNKSGAARD, Norregade 6, *1165 Copenhagen*

FINLAND
AKATEEMINEN KIRJAKAUPPA, P.O. Box 128, *SF-00101 Helsinki 10*

FRANCE
EUROPERIODIQUES S. A., 31 Avenue de Versailles, *78170 La Celle St.-Cloud*
LIBRAIRIE LAVOISIER, 11 rue Lavoisier, *75008 Paris*
OFFICE INTERNATIONAL DE DOCUMENTATION ET LIBRAIRIE, 48 rue Gay-Lussac, *75240 Paris Cedex 05*

GERMAN DEMOCRATIC REPUBLIC
HAUS DER UNGARISCHEN KULTUR, Karl-Liebknecht-Strasse 9, *DDR-102 Berlin*
DEUTSCHE POST ZEITUNGSVERTRIEBSAMT, Strasse der Pariser Kommüne 3—4, *DDR-104 Berlin*

GERMAN FEDERAL REPUBLIC
KUNST UND WISSEN ERICH BIEBER, Postfach 46, *7000 Stuttgart 1*

GREAT BRITAIN
BLACKWELL'S PERIODICALS DIVISION, Hythe Bridge Street, *Oxford OX1 2ET*
BUMPUS, HALDANE AND MAXWELL LTD., Cowper Works, *Olney, Bucks MK43 4BN*
COLLET'S HOLDINGS LTD., Denington Estate, *Wellingborough, Northants NN8 2QT*
WM. DAWSON AND SONS LTD., Cannon House, *Folkes-one, Kent CT19 5EE*
H. K. LEWIS AND CO., 136 Gower Street, *London WC1E 6BS*

GREECE
KOSTARAKIS BROTHERS, International Booksellers, 2 Hippokratous Street, *Athens-143*

HOLLAND
MEULENHOFF-BRUNA B.V., Beulingstraat 2, *Amsterdam*
MARTINUS NIJHOFF B.V., Lange Voorhout 9—11, *Den Haag*
SWETS SUBSCRIPTION SERVICE, 347b Heereweg, *Lisse*

INDIA
ALLIED PUBLISHING PRIVATE LTD., 13,14 Asaf Ali Road, *New Delhi 110001*
150 B-6 Mount Road, *Madras 600002*
INTERNATIONAL BOOK HOUSE PVT. LTD., Madame Cama Road, *Bombay 400069*
THE STATE TRADING CORPORATION OF INDIA LTD., Books Import Division, Chandralok, 36 Janpath, *New Delhi 110001*

ITALY
EUGENIO CARLUCCI, P.O. Box 252, *70100 Bari*
INTERSCIENTIA, Via Mazzé 28, *10149 Torino*
LIBRERIA COMMISSIONARIA SANSONI, Via Lamarmora 45, *50121 Firenze*
SANTO VANASIA, Via M. Macchi 58, *20124 Milano*
D. E. A., Via Lima 28, *00198 Roma*

JAPAN
KINOKUNIYA BOOK-STORE CO. LTD., 17-7 Shinjuku-ku 3 chome, Shinjuku-ku, *Tokyo 160-91*
MARUZEN COMPANY LTD., Book Department, P.O. Box 5050 Tokyo International, *Tokyo 100-61*
NAUKA LTD., IMPORT DEPARTMENT, 2-30-19 Minami Ikebukuro, Toshima-ku, *Tokyo 171*

KOREA
CHULPANMUL, *Phenjan*

NORWAY
TANUM-CAMMERMEYER, Karl Johansgatan 41—43, *1000 Oslo*

POLAND
WĘGIERSKI INSTYTUT KULTURY, Marszałkowska 80, *Warszawa*
CKP I W ul. Towarowa 28 *00-958 Warsaw*

ROUMANIA
D. E. P., *Bucureşti*
ROMLIBRI, Str. Biserica Amzei 7, *Bucureşti*

SOVIET UNION
SOJUZPETCHATJ — IMPORT, *Moscow*
and the post offices in each town
MEZHDUNARODNAYA KNIGA, *Moscow G-200*

SPAIN
DIAZ DE SANTOS, Lagasca 95, *Madrid 6*

SWEDEN
ALMQVIST AND WIKSELL, Gamla Brogatan 26, *101 20 Stockholm*
GUMPERTS UNIVERSITETSBOKHANDEL AB, Box 346, *401 25 Göteborg 1*

SWITZERLAND
KARGER LIBRI AG, Petersgraben 31, *4011 Basel*

USA
EBSCO SUBSCRIPTION SERVICES, P.O. Box 1943, *Birmingham, Alabama 65201*
F. W. FAXON COMPANY, INC., 15 Southwest Park, *Westwood, Mass, 02090*
THE MOORE-COTTRELL SUBSCRIPTION AGENCIES, *North Cohocton, N. Y. 14868*
READ-MORE PUBLICATIONS, INC., 140 Cedar Street, *New York, N. Y. 10006*
STECHERT-MACMILLAN, INC., 7250 Westfield Avenue, *Pennsauken* N.J. 08110

VIETNAM
XUNHASABA, 32, Hai Ba Trung, *Hanoi*

YUGOSLAVIA
JUGOSLAVENSKA KNJIGA, Terazije 27, *Beograd*
FORUM, Vojvode Mišiča 1, *21000 Novi Sad*

30. VIII. 1979 HU ISSN 0001—5407 Index: 26.007